29 October 2010 | $10

Science

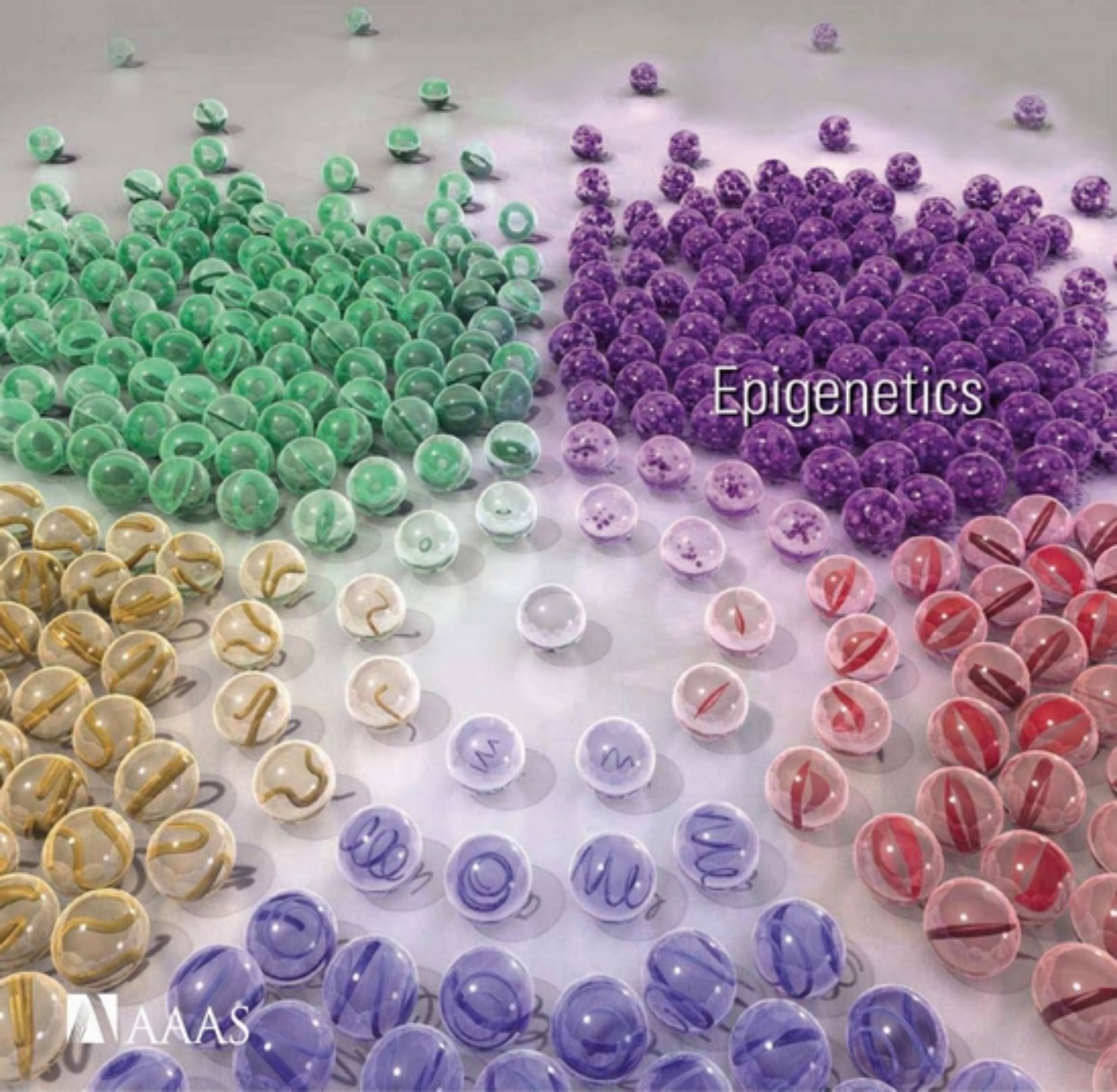

AAAS

SPECIAL SECTION

Epigenetics

INTRODUCTION

REVIEWS

PERSPECTIVES

>> News story p. 576; Perspective p. 598; Report p. 680; Science Translational Medicine; Science Signaling; Science Careers; Video; and Science *Podcast at www.sciencemag.org/special/epigenetics/*

page 568

EDITORIAL

NEWS OF THE WEEK

NEWS FOCUS

LETTERS

BOOKS *ET AL.*

POLICY FORUM

PERSPECTIVES

CONTENTS continued >>

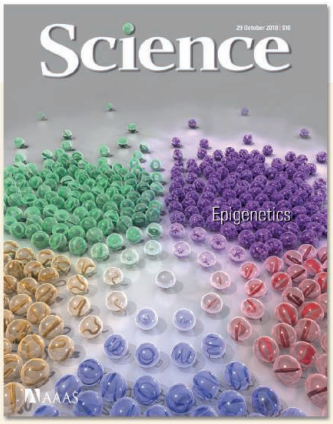

COVER

During development, a multicellular organism generates many different cell types (colored marbles) from a single progeny cell (clear marble in the center), yet all of the cells have nominally identical DNA sequences (and, therefore, the same genetic instruction sets). The maintenance and inheritance of these distinct cellular phenotypes is the basis of epigenetics (the prefix "epi-" is Greek for over or above), the subject of a special section beginning on page 611.

***Image: Chris Bickel*/Science**

DEPARTMENTS

Published by AAAS

SCIENCE PRIZE ESSAY

BREVIA

RESEARCH ARTICLES

REPORTS

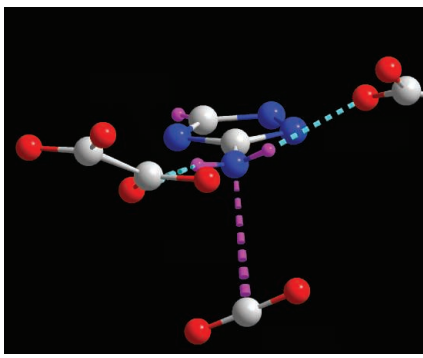

pages 595 & 650

page 683

CONTENTS continued >>

Published by AAAS

SCIENCEONLINE

SCIENCEXPRESS
www.sciencexpress.org

Probing the Ultimate Limit of Fiber-Optic Strain Sensing
G. Gagliardi et al.
The precisely spaced teeth of an optical frequency comb can be used as a highly accurate strain gauge.
10.1126/science.1195818

The Impact of Conservation on the Status of the World's Vertebrates
M. Hoffmann et al.
Though the threat of extinction is increasing, overall declines would have been worse in the absence of conservation.
10.1126/science.1194442

Scenarios for Global Biodiversity in the 21st Century
H. M. Pereira et al.
A range of measures predicts continuing declines of biodiversity, highlighting opportunities for policy development and action.
10.1126/science.1196624

Calcium-Permeable AMPA Receptor Dynamics Mediate Fear Memory Erasure
R. L. Clem and R. L. Huganir
The subunit composition of AMPA receptors at lateral amygdala synapses changes after the acquisition of associative fear.
10.1126/science.1195298

PML Regulates Apoptosis at Endoplasmic Reticulum by Modulating Calcium Release
C. Giorgi et al.
The promyelocytic leukemia protein likely influences apoptosis by influencing a calcium channel in the endoplasmic reticulum.
10.1126/science.1189157

SCIENCENOW
www.sciencenow.org
Highlights From Our Daily News Coverage

Robot 'Hands' Write Without Fingers
Grain-filled sacks help robots get a grip on cumbersome objects.

Attention Passengers: Please Keep Your Shoes On
New sensor array quickly sniffs out shoe-bomber explosive.

Malaria in India May Be 13 Times Worse Than Feared
New estimates of 200,000 deaths per year prompt shock and skepticism.

SCIENCESIGNALING
www.sciencesignaling.org
The Signal Transduction Knowledge Environment

RESEARCH ARTICLE: PI3K Signaling Through the Dual GTPase–Activating Protein ARAP3 Is Essential for Developmental Angiogenesis
L. Gambardella et al.

PODCAST
S. Vermeren and A. M. VanHook
The guanosine triphosphatase–activating protein ARAP3 may be a target for antiangiogenic therapies.

RESEARCH ARTICLE: Antagonistic Regulation of Actin Dynamics and Cell Motility by TRPC5 and TRPC6 Channels
D. Tian et al.
Coupling TRPC5 and TRPC6 calcium channels to different Rho GTPases allows calcium to both promote and inhibit cell migration.

RESEARCH ARTICLE: Regulation of 3-Phosphoinositide–Dependent Protein Kinase 1 Activity by Homodimerization in Live Cells
T. A. Masters et al.
Spatial and temporal regulation of the homodimerization of PDK1 modulates its activity.

PERSPECTIVE: Delivering the Lateral Inhibition Punchline—It's All About the Timing
J. D. Axelrod
New ways to understand lateral inhibition in patterning sensory bristles in the fruit fly are proposed.

REVIEW: Apoptosis, Stem Cells, and Tissue Regeneration
A. Bergmann and H. Steller
Cells undergoing stress- or injury-induced apoptosis can stimulate tissue regeneration by promoting stem or progenitor cell proliferation.

SCIENCECAREERS
www.sciencecareers.org/career_magazine
Free Career Resources for Scientists

Opening New Research Avenues in Epigenetics
E. Pain
Epigenetics provides a common theme to Spanish cancer researcher Manel Esteller's broad interests in basic and translational research.

Environmental Exposures Shape Human Health—and Careers
L. S. Chiu
Brown University scientist Carmen Marsit's unique training allows him to take an interdisciplinary and translational approach to epigenetics.
>> Epigenetics section p. 611 and www.sciencemag.org/special/epigenetics/

SCIENCETRANSLATIONAL MEDICINE
www.sciencetranslationalmedicine.org
Integrating Medicine and Science

RESEARCH ARTICLE: The Inducible Costimulator (ICOS) Is Critical for the Development of Human T_H17 Cells
C. M. Paulos et al.

PERSPECTIVE: ICOStomizing Immunotherapies with T_H17
J. Garaude and J. M. Blander
The inducible costimulator ICOS promotes the antitumor activity of human T_H17 cells.

RESEARCH ARTICLE: Thermal Enhancement with Optically Activated Gold Nanoshells Sensitizes Breast Cancer Stem Cells to Radiation Therapy
R. L. Atkinson et al.
Local heating with gold nanoshells sensitizes mouse and human breast cancer stem cells to radiation treatment.

SCIENCEPODCAST
www.sciencemag.org/multimedia/podcast
Free Weekly Show
Download the 29 October *Science* Podcast to hear about the distribution of exoplanets, cancer epigenetics, how people detect errors, and more.

SCIENCEINSIDER
news.sciencemag.org/scienceinsider
Science Policy News and Analysis

VIDEOFEATURE
video.sciencemag.org

Defining Epigenetics
Science Senior Editor Guy Riddihough taps experts for their definition of epigenetics.
>> Epigenetics section p. 611 and www.sciencemag.org/special/epigenetics/

SCIENCE (ISSN 0036-8075) is published weekly on Friday, except the last week in December, by the American Association for the Advancement of Science, 1200 New York Avenue, NW, Washington, DC 20005. Periodicals Mail postage (publication No. 484460) paid at Washington, DC, and additional mailing offices. The title SCIENCE is a registered trademark of the AAAS. Domestic individual membership and subscription (51 issues): $146 ($74 allocated to subscription). Domestic institutional subscription (51 issues): $910; Foreign postage extra: Mexico, Caribbean (surface mail) $55; other countries (air assist delivery) $85. First class, airmail, student, and emeritus rates on request. Canadian rates with GST available upon request, GST #1254 88122. Publications Mail Agreement Number 1069624. **Printed in the U.S.A.**

Change of address: Allow 4 weeks, giving old and new addresses and 8-digit account number. **Postmaster:** Send change of address to AAAS, P.O. Box 96178, Washington, DC 20090–6178. **Single-copy sales:** $10.00 current issue, $15.00 back issue prepaid includes surface postage; bulk rates on request. The identification code for *Science* is 0036-8075. *Science* is indexed in the *Reader's Guide to Periodical Literature* and in several specialized indexes.

AAAS
ADVANCING SCIENCE, SERVING SOCIETY

Published by AAAS

Bruce Alberts is Editor-in-Chief of *Science*.

Driving U.S. Energy Leadership

I HAVE JUST RETURNED FROM A TRIP TO CHINA, WHERE THERE IS A TREMENDOUS EMPHASIS on the importance of investing in science and technology for a sustainable future. For the Chinese, business as usual is not an option: It seems obvious to everyone that an economy that continues to expand using available technologies will choke on its own air pollution. Many nations share China's urgent need to shift away from an economy dominated by fossil fuels. Last month, Germany unveiled a bold proposal to move the country toward renewable "green" energies through aggressive policies, which may spur other European nations to follow suit. What about the United States?

Unfortunately, this year's attempt by the Obama Administration to produce a major climate-energy bill at the national level failed. But my home state of California has been more successful, attracting international attention when it passed the Global Warming Solutions Act of 2006 (also known as AB32). This law requires that California's emissions of greenhouse gases be reduced to 1990 levels by 2020, an approximate 30% reduction from those expected otherwise. As a large state with a population of 37 million, California is the second largest emitter of greenhouse gases in the United States. AB32 has therefore stimulated major private-sector investments in renewable energy technologies, aimed at markets that the new rules promise to generate.

But the entire fate of this bold plan, and of the investments in innovation that it stimulates, hinges on a popular vote that will take place in a few days. On 2 November, California voters will consider Proposition 23, a referendum sponsored by out-of-state oil interests that would suspend implementation of AB32 until unemployment in California, now at about 12%, drops to 5.5% or less for a full year. Because this level has been reached only three times in the past 40 years, Proposition 23 would effectively stop the new investments in renewable energy. As critics of California's AB32 are quick to point out, reducing the state's emissions will, by itself, do little to reduce the threat of global warming. But this badly misses the point. The legislation establishes the market opportunities that the entire United States urgently needs if it is to play a major part in reducing the cost of clean energy, and thereby remain a world leader in creating important new industries that boost the economy and benefit human welfare.

Consistent with AB32, in *A Business Plan for America's Energy Future*, seven of the most accomplished business leaders in the United States—Norman Augustine, Ursula Burns, John Doerr, Bill Gates, Chad Holliday, Jeff Immelt, and Tim Solso—call for policies that generate "clear, long-term market signals to create market pull for innovation." Arguing that "the economic, national security, environmental, and climate costs of our current energy system will condemn our children to a seriously constrained future," they also urge a federal investment of $16 billion per year in clean energy innovation, an increase of $11 billion over the current annual investment of about $5 billion.* Thus, for example, while commending the recent formation of the Advanced Research Projects Agency in the U.S. Department of Energy (ARPA-E), they urge that its budget be tripled, pointing out that ARPA-E was able to fund only 37 of the 3700 proposals that it received in its first year. As these 3700 proposals demonstrate, the United States has an immense innovation engine that is waiting to be unleashed to address the world's huge future needs for clean energy. Its scientists and engineers are noted for their ability to pioneer creative solutions, but they must be challenged and supported to do so at all levels of government.

The public and private investment in energy innovation now totals only about 0.3% of U.S. energy expenditures. California's Proposition 23 needs to be soundly defeated, sending a clear signal to Washington that the people of the United States are ready and willing to mobilize its considerable resources in the vital drive to a sustainable energy future.

– Bruce Alberts

10.1126/science.1199255

*www.americanenergyinnovation.org.

Published by AAAS

www.sciencemag.org

Science

1200 New York Avenue, NW
Washington, DC 20005
Editorial: 202-326-6550, FAX 202-289-7562
News: 202-326-6581, FAX 202-371-9227
Bateman House, 82-88 Hills Road
Cambridge, UK CB2 1LQ
+44 (0) 1223 326500, FAX +44 (0) 1223 326501

Subscription Services For change of address, missing issues, new orders and renewals, and payment questions: 866-434-AAAS (2227) or 202-326-6417, FAX 202-842-1065. Mailing addresses: AAAS, P.O. Box 96178, Washington, DC 20090-6178 or AAAS Member Services, 1200 New York Avenue, NW, Washington, DC 20005

Institutional Site Licenses please call 202-326-6755 for any questions or information

Reprints: Author Inquiries 800-635-7181
Commercial Inquiries 803-359-4578

Permissions 202-326-7074, FAX 202-682-0816

Member Benefits AAAS/Barnes&Noble.com bookstore www.aaas.org/bn; AAAS Online Store www.apisource.com/aaas/ code MKB6; AAAS Travels: Betchart Expeditions 800-252-4910; Apple Store www.apple.com/eppstore/aaas; Bank of America MasterCard 1-800-833-6262 priority code FAA3YU; Cold Spring Harbor Laboratory Press Publications www.cshlpress.com/affiliates/aaas.htm; GEICO Auto Insurance www.geico.com/landingpage/go51.htm?logo=17624; Hertz 800-654-2200 CDP#343457; Office Depot https://bsd.officedepot.com/portalLogin.do; Seabury & Smith Life Insurance 800-424-9883; Subaru VIP Program 202-326-6417; VIP Moving Services www.vipmayflower.com/domestic/index.html; Other Benefits: AAAS Member Services 202-326-6417 or www.aaasmember.org.

science_editors@aaas.org	(for general editorial queries)
science_letters@aaas.org	(for queries about letters)
science_reviews@aaas.org	(for returning manuscript reviews)
science_bookrevs@aaas.org	(for book review queries)

Published by the American Association for the Advancement of Science (AAAS), *Science* serves its readers as a forum for the presentation and discussion of important issues related to the advancement of science, including the presentation of minority or conflicting points of view, rather than by publishing only material on which a consensus has been reached. Accordingly, all articles published in *Science*—including editorials, news and comment, and book reviews—are signed and reflect the individual views of the authors and not official points of view adopted by AAAS or the institutions with which the authors are affiliated.

AAAS was founded in 1848 and incorporated in 1874. Its mission is to advance science, engineering, and innovation throughout the world for the benefit of all people. The goals of the association are to: enhance communication among scientists, engineers, and the public; promote and defend the integrity of science and its use; strengthen support for the science and technology enterprise; provide a voice for science on societal issues; promote the responsible use of science in public policy; strengthen and diversify the science and technology workforce; foster education in science and technology for everyone; increase public engagement with science and technology; and advance international cooperation in science.

Information for Authors
See pages 352 and 353 of the 15 January 2010 issue or access www.sciencemag.org/about/authors

EDITOR-IN-CHIEF **Bruce Alberts**
EXECUTIVE EDITOR **Monica M. Bradford**
NEWS EDITOR **Colin Norman**
MANAGING EDITOR, RESEARCH JOURNALS **Katrina L. Kelner**
DEPUTY EDITORS **R. Brooks Hanson, Barbara R. Jasny, Andrew M. Sugden**

Editorial senior editors/commentary Lisa D. Chong, Brad Wible; **senior editors** Gilbert J. Chin, Pamela J. Hines, Paula A. Kiberstis (Boston), Marc S. Lavine (Toronto), Beverly A. Purnell, L. Bryan Ray, Guy Riddihough, H. Jesse Smith, Phillip D. Szuromi (Tennessee), Valda Vinson, Jake S. Yeston; **associate editors** Kristen L. Mueller, Jelena Stajic, Sacha Vignieri, Nicholas S. Wigginton, Laura M. Zahn; **research associate** Alexis Wynne Mogul; **book review editor** Sherman J. Suter; **associate letters editor** Jennifer Sills; **editorial manager** Cara Tate; **senior copy editors** Jeffrey E. Cook, Cynthia Howe, Harry Jach, Lauren Kmec, Barbara P. Ordway, Trista Wagoner; **copy editor** Chris Filiatreau; **editorial coordinators** Carolyn Kyle, Beverly Shields; **publications assistants** Ramatoulaye Diop, Joi S. Granger, Emily Guise, Jeffrey Hearn, Michael Hicks, Lisa Johnson, Scott Miller, Jerry Richardson, Jennifer A. Seibert, Brian White, Anita Wynn; **editorial assistants** Emily C. Horton, Patricia M. Moore, Miriam Weinberg; **executive assistant** Alison Crawford; **administrative support** Maryrose Madrid; **editorial fellow** Melissa R. McCartney

Editorial director, web and new media Stewart Wills; **senior web editor** Tara S. Marathe; **web editor** Robert Frederick; **web development manager** Martyn Green; **web developer** Andrew Whitesell; **intern** Sophia Cai

News deputy news editors Robert Coontz, David Grimm (Online), Eliot Marshall, Jeffrey Mervis, Leslie Roberts; **contributing editors** Elizabeth Culotta, Polly Shulman; **news writers** Yudhijit Bhattacharjee, Adrian Cho, Jennifer Couzin, Jocelyn Kaiser, Richard A. Kerr, Eli Kintisch, Greg Miller, Elizabeth Pennisi, Lauren Schenkman, Robert F. Service (Pacific NW), Erik Stokstad; **web developer** Daniel Berger; **intern** Kristen Minogue; **contributing correspondents** Jon Cohen (San Diego, CA), Daniel Ferber, Ann Gibbons, Sam Kean, Robert Koenig, Andrew Lawler, Mitch Leslie, Charles C. Mann, Virginia Morell, Gary Taubes; **copy editors** Linda B. Felaco, Melvin Gatling, Melissa Raimondi; **administrative support** Scherraine Mack; **bureaus** San Diego, CA: 760-942-3252, FAX 760-942-4979; Pacific Northwest: 503-963-1940

Production senior manager Wendy K. Shank; **assistant manager** Rebecca Doshi; **senior specialists** Steve Forrester, Chris Redwood, Anthony Rosen; **Preflight director** David M. Tompkins; **manager** Marcus Spiegler; **specialist** Jason Hillman

Art director Yael Fitzpatrick; **associate art director** Laura Creveling; **senior illustrators** Chris Bickel, Katharine Sutliff; **illustrator** Yana Hammond; **senior art associates** Holly Bishop, Preston Huey, Nayomi Kevitiyagala; **art associates** Kay Engman, Matthew Twombly; **photo editor** Leslie Blizard

***Science* International**

Europe (science@science-int.co.uk) **editorial: international managing editor** Andrew M. Sugden; **senior editor/commentary** Julia Fahrenkamp-Uppenbrink; **senior editors** Caroline Ash, Stella M. Hurtley, Ian S. Osborne, Peter Stern; **associate editor** Maria Cruz; **locum editor** Helen Pickersgill; **editorial support** Rachel Roberts, Alice Whaley; **administrative support** John Cannell, Janet Clements, Louise Hartwell; **news: europe news editor** John Travis; **deputy news editor** Daniel Clery; **contributing correspondents** Michael Balter (Paris), John Bohannon (Vienna), Martin Enserink (Amsterdam and Paris), Gretchen Vogel (Berlin); **intern** Sarah Reed

Latin America contributing correspondent Antonio Regalado

Asia Japan Office: Asca Corporation, Tomoko Furusawa, Rustic Bldg. 7F, 77 Tenjin-cho, Shinjuku-ku, Tokyo 162-0808, Japan; +81 3 6802 4616, FAX +81 3 6802 4615, inquiry@sciencemag.jp; **asia news editor** Richard Stone (Beijing: rstone@aaas.org); **contributing correspondents** Dennis Normile [Japan: +81 (0) 3 3391 0630, FAX +81 (0) 3 5936 3531; dnormile@gol.com]; Hao Xin [China: cindyhao@gmail.com]; Pallava Bagla [South Asia: +91 (0) 11 2271 2896; pbagla@vsnl.com]

EXECUTIVE PUBLISHER **Alan I. Leshner**
PUBLISHER **Beth Rosner**

Fulfillment Systems and Operations (membership@aaas.org); **director** Waylon Butler; **customer service supervisor** Pat Butler; **specialists** Latoya Casteel, LaVonda Crawford, Vicki Linton, April Marshall; **data entry supervisor** Cynthia Johnson; **specialists** Shirlene Hall, Tarrika Hill, William Jones

Business Operations and Administration director Deborah Rivera-Wienhold; **business systems and financial analysis director** Randy Yi; **manager, business analysis** Eric Knott; **manager, business operations** Jessica Tierney; **financial analysts** Priti Pamnani, Celeste Troxler; **rights and permissions: administrator** Emilie David; **associate** Elizabeth Sandler; **marketing director** Ian King; **marketing managers** Allison Pritchard, Alison Chandler, Julianne Wielga; **marketing associates** Aimee Aponte, Mary Ellen Crowley, Wendy Wise; **senior marketing executive** Jennifer Reeves; **director, site licensing** Tom Ryan; **director, corporate relations** Eileen Bernadette Moran; **publisher relations, eresources specialist** Kiki Forsythe; **senior publisher relations specialist** Catherine Holland; **publisher relations, east coast** Phillip Smith; **publisher relations, west coast** Philip Tsolakidis; **fulfillment supervisor** Iquo Edim; **fulfillment coordinator** Carrie MacDonald; **marketing manager** Christina Schlecht; **marketing associate** Laura Tutino; **electronic media: manager** Lizabeth Harman; **project manager** Trista Snyder; **assistant manager** Lisa Stanford; **senior production specialists** Ryan Atkins, Christopher Coleman, **computer specialist** Walter Jones, Kai Zhang; **production specialists** Angela Forest, Nichele Johnston, Kimberly Oster; **director, web and new media** Will Collins

advertising director, worldwide ad sales Bill Moran
commercial editor Sean Sanders: 202-326-6430
assistant commercial editor Tianna Hicklin 202-326-6463
project director, outreach Brianna Blaser

Product (science_advertising@aaas.org); **midwest** Rick Bongiovanni: 330-405-7080, FAX 330-405-7081; **east coast/e. canada** Laurie Faraday: 508-747-9395, FAX 617-507-8189; **west coast/w. canada** Lynne Stickrod: 415-931-9782, FAX 415-520-6940; **uk/europe/asia** Roger Goncalves: TEL/FAX +41 43 243 1358; **japan** ASCA Corporation, Nanako Ide +81 (0) 3 6802 4616, FAX +81 (0) 3 6802 4615; ads@sciencemag.jp; **senior traffic associate** Deiandra Simms

worldwide associate director of *Science* Careers Tracy Holmes: +44 (0) 1223 326525, FAX +44 (0) 1223 326532

Classified (advertise@sciencecareers.org); **u.s.: midwest/west coast/south central/canada** Tina Burks: 202-326-6577; **east coast/industry** Elizabeth Early: 202-326-6578; **advertising operations manager** Kate Panganiban **sales coordinators** Rohan Edmonson, Shirley Young; **europe/row sales:** Susanne Kharraz, Dan Pennington, Alex Palmer; **sales assistant** Lisa Patterson; **japan** ASCA Corporation, Jie Chin +81 (0) 3 6802 4616, FAX +81 (0) 3 6802 4615; careerads@sciencemag.jp; **advertising support manager** Karen Foote: 202-326-6740; **advertising production operations manager** Deborah Tompkins; **senior production specialist/graphic designer** Amy Hardcastle; **production specialist** Yuse Lajiminmuhip; **senior traffic associate** Christine Hall

Carl Wieman on teaching science
572

Leaked documents spur casualty studies
575

Into the streets. Demonstrators led by Science is Vital hoist a banner outside the U.K. Treasury.

RESEARCH FUNDING

Campaign for U.K. Science Helps Deflect Budget Ax

British researchers had been expecting a budgetary bloodbath last week. The much-heralded Comprehensive Spending Review (CSR) from the United Kingdom's new Conservative–Liberal Democrat coalition government came with numerous warnings to expect funding cuts of 20%, 30%, or even 40%—all to reduce the budget deficit. Researchers mobilized by writing letters to newspapers, signing petitions, demonstrating outside government buildings, and—for the well-connected—having a quiet word with departmental officers and ministers about the importance of science to Britain's future. Something worked. Even though the CSR outlines average cuts of 19% across all government departments, the main part of civil research spending, the science budget, was fixed for the next 4 years at this year's amount, £4.6 billion ($7.2 billion). Inflation will chip away at that between now and 2015, possibly by as much as 10%, but many believe much worse scenarios were being considered until recently.

"It's better than most feared," says Astronomer Royal Martin Rees, president of the Royal Society. Scientists were shocked by the prospect of a 25% cut, says University of Oxford neuroscientist Colin Blakemore, former head of the Medical Research Council (MRC). "It brought people on to the streets. The government was impressed by the scale of the response and how responsible it was," he says.

But there are many issues yet to be resolved. One is how £2.75 billion of the science budget will be divided up between MRC and six other research councils that give grants to researchers, run national labs, and pay for international collaborations. The CSR documents say that funding for MRC will remain level in real terms—its budget will grow to compensate for inflation. That means that one or more of the other councils will have a real-terms cut. Few if any details on capital spending for research have been revealed, and it remains to be seen what impact a major funding reform will have on universities. "Our job is not done. There are continuing threats," says cell biologist Jenny Rohn of University College London, who in September launched the pressure group Science is Vital to campaign against cuts.

Knives come out

Soon after the coalition government took power after May's general election, the U.K.'s Treasury asked each department to prepare a range of draft budgets including cuts of 10%, 20%, and 30%. Throughout the summer and early autumn, departmental ministers negotiated with Treasury officials over the final level. Alarm bells started ringing in early September when Business Secretary Vince Cable, whose Department for Business, Innovation and Skills (BIS) is responsible for the science budget, said in a speech: "There is no justification for taxpayers' money being used to support research which is neither commercially useful nor theoretically outstanding." On a radio news program, he suggested that a cut of 45% in BIS's science budget was possible.

Many researchers were spurred into action. Rohn started a blog and was soon joined by others. Three weeks later, the Science is Vital campaign had an estimated 2000 researchers and students demonstrating outside the Treasury. "It was completely mad. I didn't do any lab work," Rohn says. An online petition drew 33,000 signatures and 110 members of parliament signed a motion supporting research. Well-known scientists wrote op-ed pieces for newspapers and appeared on TV news programs. "It was a very concerted effort," says Rees.

It's widely thought that David Willetts, the minister for universities and science at BIS, was instrumental in fending off cuts. "He was clearly won over to science," says Blakemore. On 20 October, the day of the CSR announcement, Willetts spoke to the press and was presented with a large bunch of flowers by William Bown, publisher of the *Research Fortnight* newsletter. "This is exceptionally good news for science," Willetts told reporters. "This is not a temporary stimulus package. It's a guaranteed ring-fenced package for 4 years."

In addition to the research council funding, BIS's annual science budget includes £1.6 billion for "quality-related" (QR) funding, given as block grants to the best-performing university departments as judged in periodic assessments; £150 million for technology-transfer projects; and £100 million for the Royal Society, Royal Academy of Engineering, and British Academy.

The overall research council funding is

CREDIT: JOE DUNCKLEY/COTCH.NET

Published by AAAS

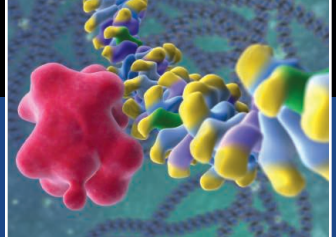

Cancer epigenetics 576

Paris's first rodents 582

guaranteed, but there is concern about how it will be divided over the next few weeks. The Science and Technology Facilities Council (STFC) is particularly nervous, having suffered deep cuts last year that forced it to withdraw from a number of international projects and reduce grant funding to researchers (*Science*, 1 January, p. 22). Much of the STFC budget is committed to large national labs (whose cost is hard to trim) and subscriptions to international facilities such as CERN, the European Southern Observatory (ESO), and the European Space Agency. (The declining pound-euro exchange rate has exacerbated the latter issue.) Any cuts to STFC would fall heavily on the grants it provides to astronomers, particle and nuclear physicists, and space scientists. The research council heads have collectively decided not to speak to the press before their budgets are decided. But STFC chief Keith Mason wrote in a letter to his research community: "We obviously cannot be certain of the impact on our programme, facilities or staff until we have a final budget. … [T]he CSR outcome isn't pain free. … The job's not finished."

Willetts said that CERN, ESO, and similar collaborations were safe for the moment: "We have no immediate plans to disengage from any international projects, though we will be working to keep costs down." He made no such promises over capital spending on research facilities, however. These are funded from the general BIS capital budget, which will be cut by 52% over the 4-year CSR period. "Capital spending is a loose end. We will be looking at it separately," says Willetts.

Still, several projects have been guaranteed funding: new beamlines for STFC's Diamond synchrotron near Oxford; redevelopment of the Institute for Animal Health at Pirbright, which was at the center of a foot-and-mouth disease outbreak 3 years ago; a new building for the Laboratory of Molecular Biology in Cambridge; and the new UK Centre for Medical Research and Innovation (UKCMRI), due to open in London in 2015. Completion of UKCMRI was made possible by the Department of Health chipping in £200 million. "Over the coming weeks we will identify other projects" to receive capital funding, Willetts says.

Willetts also suggested that research councils wouldn't feel the pain of inflation because BIS aims to find ways to use funds more efficiently, freeing up £324 million by 2014–15 that will be plowed back into research. Some feel such forecasts are too optimistic. "We've heard that all before," says Blakemore. BIS will also demand "efficiency savings" of more than 30% in the operating costs of the research councils' headquarters in Swindon and London.

By including QR funding within the ring fence, the government shows that it intends to keep the U.K.'s "dual-support" system of block grants to universities and competitively won grants for research teams or individual scientists. Yet major changes are afoot for higher education funding that could have an impact on research. At present, university undergraduates pay a maximum of £3290 per year in tuition fees, and the additional cost of teaching is provided to universities by BIS. But in the CSR, the ministry has slashed support for tuition by 40%. The cap on tuition fees will be raised or removed so that universities can try to make up for these cuts. "This is an enormous amount of money being withdrawn," says Blakemore. And, asks Rees, "Will the new funding scheme come in soon enough to compensate?"

This is a "ring-fenced package for 4 years."

—DAVID WILLETTS, U.K. SCIENCE MINISTER

Although these changes to tuition do not affect research directly, there could be indirect impacts. "Science depends on higher education to provide scientists," says Rohn. "If cuts mean an increased teaching load, scientists will have less time for research," adds Blakemore.

Apart from BIS's science budget, other U.K. departments also sponsor research, in particular the Ministry of Defence (currently £2 billion) and the Department of Health (£700 million). The CSR has already guaranteed that Health's research would stay level in real terms, but Defence has yet to reveal the fate of its R&D spending. Willetts said that he and the government's chief science adviser, John Beddington, have been campaigning to prevent departments achieving overall budget cuts by raiding their R&D funding. Willetts says, "We have a feeling that this issue has been understood."

The previous Conservative government in the 1980s and 1990s cut back severely on research spending, which caused a lengthy exodus of top scientists from Britain. Willetts says the current Conservative–Liberal Democrat coalition aims to prevent a similar brain drain with this research-friendly CSR. Key was convincing the coalition's top powers that science could help restore the hum to Britain's flagging economy. "One thing that has changed is the level of empirical evidence that the scientific community can generate about its own research activity—it's productivity and the economic return. That evidence really helped the debate," he says.

–DANIEL CLERY

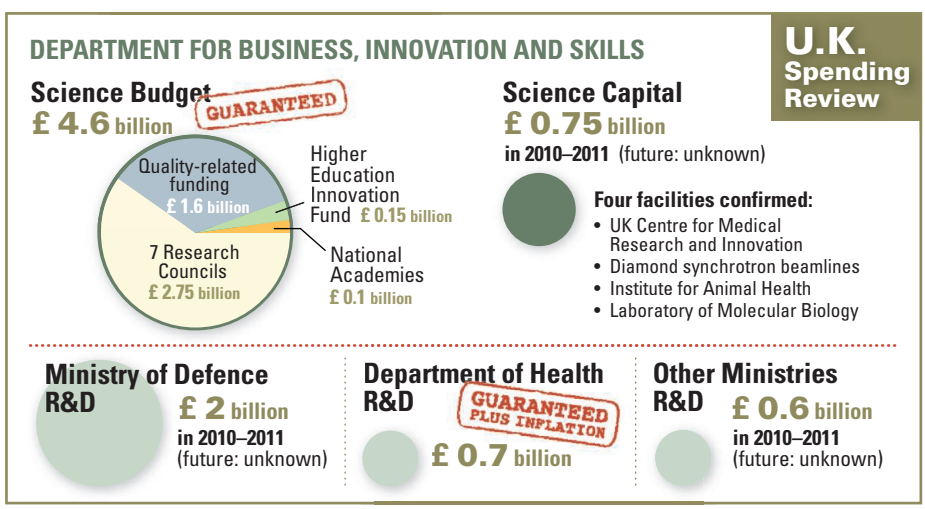

Published by AAAS

PLANETARY SCIENCE

Liquid Water Found on Mars, But It's Still a Hard Road for Life

Researchers appear to have finally achieved one of the Phoenix lander's primary goals. After digging through piles of data left from the mission to Mars more than 2 years ago, they've discovered signs that liquid water has lately flowed on the frigid planet.

In a paper in press in *Geophysical Research Letters*, Phoenix team members report that liquid water—probably only thin films of it—appears to have concentrated salts onto small patches of soil that Phoenix uncovered. The water may be liquid every martian spring or summer, or perhaps it only melted many millennia ago. Liquid water "seems plausible, quite reasonable," says planetary geochemist Sushil Atreya of the University of Michigan, Ann Arbor. If so, life might—just might—be holding out a bit beneath the surface of the martian arctic.

On the face of it, Phoenix team members are merely reporting a second detection of perchlorate salts by Phoenix. The lander's mass spectrometer had found the chlorine-containing salts uniformly distributed down through the soil, a pattern that suggested there had been no liquid water to move salts around. But planetary scientist Selby Cull of Washington University in St. Louis, Missouri, and her colleagues later used observations from Phoenix's Surface Stereo Imager to map the visible and near-infrared "color" of soils exposed by the lander's robotic arm.

Cull and colleagues found a simple spectroscopic signature of magnesium or calcium perchlorates, but only in centimeter-size patches where the perchlorates had been concentrated. The only way to concentrate perchlorates that way, the group says, would be for perchlorates at the soil surface—where they settle after the ultraviolet of sunlight forms them—to dissolve in liquid water and diffuse or flow downward.

It's not entirely clear just how water could melt at the 68°N-latitude Phoenix site, which never got warmer than –28°C. Perchlorates do take up water vapor from the atmosphere, and they powerfully lower the melting point of water, but something more may have been needed.

Cull and her colleagues offer the so-called solid-state greenhouse as a possible energy source for helping to melt Phoenix ice. Thirty centimeters of frozen carbon dioxide—dry ice—freezes out of the atmosphere each winter at the Phoenix site. That's on top of a thin layer of autumnal water frost. Come spring, the translucent dry ice can trap solar energy at its base the way a greenhouse built of glass does. Such a solid-state greenhouse is thought to fuel the carbon dioxide–driven black "spiders" that mark southern high latitudes each martian spring.

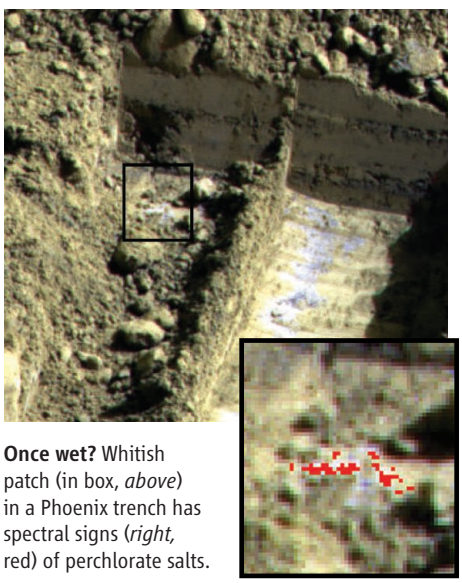

Once wet? Whitish patch (in box, *above*) in a Phoenix trench has spectral signs (*right*, red) of perchlorate salts.

But it's very hard for water to melt under dry ice that has to stay at –128°C, says planetary science consultant Hugh Kieffer of Celestial Reasonings in Genoa, Nevada. Kieffer originated the solid-state greenhouse explanation for martian spiders. It would be a stretch, Cull says, but today's summer heat might suffice. Alternatively, melting may have occurred during the warmer summers that prevailed millennia ago when Mars was tilted farther over on its axis.

Even if a briny dampness returns to the martian arctic every year, "it's not necessarily a good habitat for life," notes astrobiologist Christopher McKay of NASA's Ames Research Center in Mountain View, California. The problem is the perchlorate brine that helps lower water's melting point. On Earth, many extremophile microbes have evolved a tolerance for high concentrations of salt, he notes, but any liquid water at the Phoenix site would be even brinier than most Earth brines (http://scim.ag/salty-mars). Besides confirming the perchlorate patches, then, researchers may want to figure out just how briny the waters of Mars might get.

–RICHARD A. KERR

ScienceInsider

From the *Science* Policy Blog

A battle over a **prize in the life sciences** that honors Teodoro Obiang Nguema Mbasogo, president and longtime dictator of Equatorial Guinea, has ended with the effective **cancellation of the award**. The executive board of the United Nations Educational, Scientific and Cultural Organization has adopted a diplomatic compromise that would require "consensus," thus putting the award on indefinite hold. In an interview, an Obiang representative said the decision sends "the wrong message." http://scim.ag/prize_kibosh http://scim.ag/obiang_comment

Next week, citizens in Arizona will vote on Proposition 109, which includes language that gives "exclusive authority" to lawmakers over hunting, fishing, and "harvesting wildlife." The broad wording of the measure has some fearing that its passage would remove the central **role of government scientists in wildlife management** there. Others say the measure's requirement of "reasonable" rules will protect the process should it pass. http://scim.ag/AZ_prop109

An anonymous, self-described "**stem cell research** watch group" has sent e-mails to prominent stem cell researchers, scientific journals, and reporters raising spurious accusations of scientific misconduct in two papers. http://scim.ag/spurious-claims

The death of Bob Guccione, the founder of *Penthouse* magazine, invoked memories of his investments in **fusion energy research** and in *Omni*, a science and science-fiction magazine published in the 1980s and '90s. http://scim.ag/Gucc_fusion

The University of Virginia and Ken Cuccinelli, the state's attorney general, continue to wrangle over **documents related to Michael Mann**, a climate scientist who worked at the school until 2005. In the latest twist, the university has challenged a third request for documents—the first two were thrown out by a state judge—as too broad. Cuccinelli says the documents are needed to investigate possible fraud on grant proposals. http://scim.ag/Cuccinellis_saga

For more science policy news, visit **http://news.sciencemag.org/scienceinsider**.

NEWSMAKER INTERVIEW: CARL WIEMAN

Nobelist 'Coach' Takes On U.S. Science Education

When President Barack Obama spoke last week to students at the first-ever White House science fair, he likened them to star athletes. "We welcome championship sports teams to the White House to celebrate their victories," Obama said. "I thought we ought to do the same thing for the winners of science fair and robotic contests, and math competitions."

The comparison is apt, according to Carl Wieman, who in September took up the job of associate director for science in the White House Office of Science and Technology Policy. He says students become academic champions the same way as they excel on the field: through proper training that features repetition of the needed skills, incentives, and good coaching.

The 59-year-old Wieman, who received the 2001 Nobel Prize in physics for creating the first Bose-Einstein condensates, has spent more than a decade understanding how students learn. He began his work on improving undergraduate science instruction at the University of Colorado, Boulder, and in 2007 extended it to the University of British Columbia, Vancouver, in Canada. He's eager to apply that knowledge as part of his job coordinating research and education activities across the federal government.

Wieman sat down with *Science* on 21 October to discuss the state of science, technology, engineering, and math (STEM) education and how he became involved. His comments have been edited for length.

–JEFFREY MERVIS

Q: What are the key elements in improving science education?

C.W.: My own synthesis of a whole bunch of research is that you have to approach it as a brain-development process. You look at brain images and you have people learn something, and you see the brain is different afterwards. It's a changing of the brain, because of having to practice hard. So it's very analogous to a muscle. … You also have to think about motivation. You're not going to work hard to do something if you don't see a reason to do it. … Then you have to think of the right task to give students practice about thinking the right way … and then feedback on what they did right and wrong.

… It's very much like coaching. A good coach knows what it takes to perform at a high level and what drills are most effective. They are also good at motivating athletes and providing them with lots of feedback. It applies at all levels.

Q: How will you use this knowledge to improve federal STEM education programs?

C.W.: I hope to be able to help people realize what programs are more effective, to make better use of findings that come out of research. … When I meet with agency people, I act as an expert consultant and talk about how to design better evaluations to measure the effectiveness of what they are already supporting. At a higher, policy, level, I'll be talking with [White House budget officials] about how to design federal programs to be more effective.

Q: What's your reaction to a recent White House report [*Science*, 24 September, p. 1582] recommending bonuses for master STEM teachers and the creation of 1000 STEM-focused schools?

C.W.: I absolutely agree with their recommendation on the need for better coordination across STEM agencies. And we're already working to do that. Their recommendation to improve teacher training cites the importance of strong content knowledge. That's totally consistent with what I know about being a good coach. When you get into the area of master teachers, however, that's more of a process issue. If you don't understand the process of becoming a master teacher, then you can't do the job. So thinking about how to inject expertise into the equation is very important.

Q: Richard Ingersoll has argued for years [see p. 580] that the supply of math and science teachers is sufficient and that our primary focus should be to reduce turnover by improving working conditions rather than recruiting more teachers. What do you think?

C.W.: Well, I agree that if all you are going to say is more, then you'll still have a problem. But what's more important, I think, is not just more but better. If you have teachers who are more skilled, who understand better how students learn and can demonstrate that expertise in the classroom, you'll have fewer disciplinary problems, and more motivated students, and better outcomes. And then working conditions will improve, too. I think that education is more similar to a complicated physics experiment than people think. An experiment has an infinite number of failure modes, and if you focus on just one piece, it's not going to be successful.

Q: Why is it so hard for universities to improve undergraduate science instruction?

C.W.: I don't think that's the right question. The right question is, "Why isn't science instruction better?" A big reason is that the research we've been talking about is very recent. And when you've been doing something the same way for hundreds of years, it takes a while to be convinced that you need to change. There's also the problem of incentives. We don't have good metrics for measuring how to improve learning.

Q: When did you decide to devote your energy to science education?

C.W.: It began when I started to see common patterns among my graduate students in the way they were learning to become scientists. So I figured that there must be some underlying principles. Then I started dabbling in my own experiments. For several years I maintained two parallel research groups, one in atomic physics and one in physics education. Then I decided that there were incredible opportunities to make a difference in our current state of knowledge about how people learn. Of course, by then I also had the advantage of being a Nobel Prize winner.

Q: Is STEM a useful acronym?

C.W.: Not particularly. I don't understand what the T is, to be honest. But it's probably better than any of the alternatives.

CREDIT: MARTIN DEE/UBC

Published by AAAS

ScienceNOW

From *Science's* Online Daily News Site

A handheld sensor device.

Passengers, Keep Your Shoes On

A new device could spare air travelers a major annoyance: removing their shoes in the security line.

Triacetone triperoxide (TATP), the explosive of choice in footwear—"shoe bomber" Richard Reid tried to ignite his TATP-infused shoes aboard a flight in 2001—is notoriously difficult to detect directly. So chemist Kenneth Suslick of the University of Illinois, Urbana-Champaign, turned to colorimetric arrays, dots of chemicals deposited on a plastic square, and an acid catalyst called Amberlyst 15. When TATP vapor comes in contact with Amberlyst 15, TATP breaks down into acetone and peroxide, both of which alter an array's colors in predictable patterns that can be compared with an image database.

The method detects TATP concentrations of two parts per billion within seconds—making it sensitive enough to pick up explosives concealed in shoes, Suslick and colleagues report in the *Journal of the American Chemical Society.* A company is now developing a portable version of the device that security officials could wave near a passenger's shoes. http://scim.ag/shoes-on

Malaria in India Much Worse Than Feared

The number of people who die every year from malaria in India could be 13 times higher than current estimates, according to a new study.

Many malaria deaths occur outside of hospitals and thus aren't easily recorded. Malaria can also strike fast, making it even harder to track. To get a better estimate of malaria deaths in India, a team of international scientists led by Neeraj Dhingra of the National AIDS Control Organisation in New Delhi sent surveyors to randomly selected areas of the country; they asked families and other witnesses to describe deaths that had occurred there between 2001 and 2003.

When physicians reviewed the reports, they attributed 3.6% of roughly 75,000 deaths to malaria. That translates to 205,000 malaria deaths nationwide every year, the researchers report in *The Lancet*. Ninety percent occurred in rural areas, and 86% occurred outside of any sort of health facility. Previous World Health Organization (WHO) reports put the total at 15,000.

Robert Newman, the director of WHO's Global Malaria Programme, says such verbal autopsies are notoriously inaccurate. But other experts say that the new report's estimate could be legitimate, partly because so many deaths slip through the cracks and partly because, at least in terms of geography, the study's stats match up with state-reported malaria deaths. http://scim.ag/malaria-deaths

Unearthed. Paleontologists dig for primate fossils at Dur At-Talah in Libya.

New Clues to Higher Primate Origins

A new discovery in Libya of fossils from several types of tiny primates suggests that anthropoids—higher primates that include monkeys, apes, and humans—were well established in Africa earlier than previously believed.

Researchers had long thought that anthropoids arose in Africa, but in the past 16 years, tiny primates found in Asia—such as the 45-million-year-old *Eosimias*—have emerged as the strongest candidates for the earliest anthropoids. Now an international team led by paleontologist Jean-Jacques Jaeger of the University of Poitiers in France report in *Nature* that they've unearthed teeth from four new species of primates in central Libya. If the dates of the new fossils are good, this would make them just 1 million years younger than Africa's oldest potential anthropoid fossils. It is unlikely that so many new species evolved in such a short amount of time. So anthropoids either arose in Africa much earlier than thought or arose and diversified in Asia but quickly made their way to Africa. http://scim.ag/clues-origins

Exercise Boosts Muscle Stem Cells

Exercising can help you age gracefully by keeping you fit. But it turns out that endurance exercise, like running, doesn't just tone muscles, it enhances muscle stem cells, too. Lead author Gabi Shefer of Tel Aviv University in Israel and colleagues report in *PLoS ONE* that the number of muscle stem cells, called satellite cells, increased after rats spent 13 weeks running on a treadmill for 20 minutes a day. Younger rats showed a 20% to 35% increase in the mean number of stem cells per muscle fiber, whereas older rats showed a 33% to 47% increase. These cells regenerate muscles after injury or illness, so the boost could explain why human exercisers have better muscle function than nonexercisers as they age. Better muscle quality could also delay sarcopenia, the decline in muscle mass that occurs with aging. Better hit the gym! http://scim.ag/muscle-boost

Read the full postings, comments, and more at **http://news.sciencemag.org/sciencenow**.

CREDITS: (TOP, LEFT TO RIGHT) KENNETH SUSLICK; UTPAL BARUAH JSG/RCS/REUTERS; (BOTTOM) © MPFL

Published by AAAS

GENOMICS

1000 Genomes Project Gives New Map Of Genetic Diversity

Talk about inflation. A decade ago, one human genome was the goal. Now nothing less than 1000 will do. By sequencing hundreds of human genomes, the 1000 Genomes Project has produced the most detailed catalog of human variation ever: a compendium of millions of previously unknown single-nucleotide polymorphisms (SNPs) and other variants. This treasure chest of genetic data, which was generated by three pilot projects, is described in the 28 October issue of *Nature*. Researchers are already using those data to pinpoint DNA involved in both complex and inherited diseases. "The resource should have a large impact on medical genetics," says Sekar Kathiresan, a cardiovascular geneticist at Massachusetts General Hospital in Boston.

Also, on page 641 of this issue of *Science*, a second analysis describes an approach for determining another aspect of genetic variation that arises when genes and other stretches of DNA are duplicated. There is growing interest in these so-called copy number variants because of their potential ties to disease risk (*Science*, 7 September 2007, p. 1315).

Although all humans share 99% of their DNA, the relatively few differences among us matter—for disease, personality, and other traits. The first large-scale effort to identify these differences was the International HapMap Project, which identified 3.5 million SNPs, places on the genome where one base might vary from one individual to the next. Geneticists have since used those SNPs in so-called genome-wide association studies (GWAS) to home in on genes important to diabetes, heart disease, various cancers, and age-related macular degeneration, to name a few. But these GWAS covered only variants that existed in at least 10% of humans and often helped pinpoint a region but not the particular base causing the disease risk. The 1000 Genomes Project addresses these issues.

In 2008, spurred by rapid advances in sequencing technologies, the Wellcome Trust Sanger Institute in Hinxton, U.K.; the National Human Genome Research Institute in Bethesda, Maryland; and BGI in Shenzhen, China, embarked on the 1000 Genomes Project with the goal of identifying the SNPs that are present at 1% or greater frequency among humans, as well as other variants. To figure out how to do this, they set up the three pilot projects now being reported. Ultimately, the project will sequence to varying degrees 2500 samples from 27 populations around the world. The pilot data are already publicly available.

In one pilot, the researchers thoroughly sequenced the genomes of two families—mother, father, child trios—revealing that offspring inherit about 60 mutations that arose in their parents, with slightly more coming from the father. The second project involved sequencing in less detail the genomes of 179 people with ancestry from Europe, East Asia, or Africa. In the third, the consortium determined the sequences of 8140 exons—covering 906 genes—of 697 people. By testing different sequencing technologies and working out ways of preparing and analyzing samples, the nine-center group has come up with reliable methods of studying variation that are rapidly becoming the field's standard, says 1000 Genomes Project co-leader David Altshuler, a human geneticist at the Broad Institute in Cambridge, Massachusetts.

The pilot projects identified 15 million SNPs—including 8.5 million novel ones—as well as 1 million small insertions and deletions and 20,000 other structural variants. "It's a huge increase over what was [known] before," says Gilean McVean, a population geneticist at the University of Oxford in the United Kingdom, who is helping to coordinate the analysis of the 1000 Genomes Project. This total represents almost 95% of the variants that are found in at least 10% of humans.

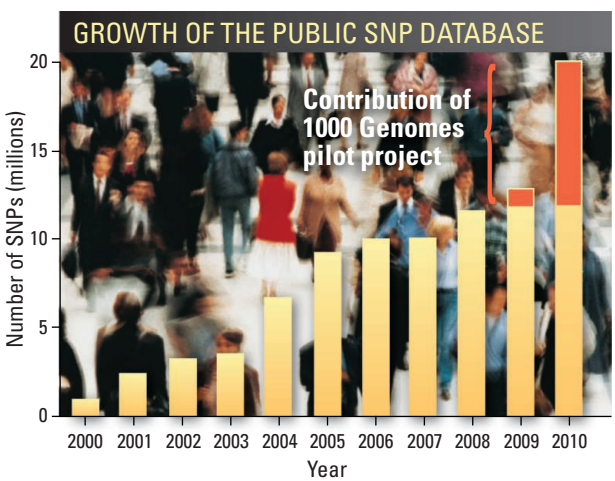

Pinning down differences. The 1000 Genomes Project has greatly increased the number of known single-base differences that can exist among people.

Using this new resource, researchers will be more likely to find the exact SNP linked to a disease, or at least will be able to get much closer to it in their GWAS. Working with 1000 Genomes data, researchers and companies are increasing the number of SNPs that can be evaluated. In the works are microarrays that will test for the presence of 5 million or more SNPs—quite an improvement over the 1 million typically assessed with current technology.

Researchers are already using the 1000 Genomes pilot to add missing SNPs to their maps of regions associated with disease. For instance, Oxford statistician Jonathan Marchini, GlaxoSmithKline, and other collaborators took this approach in a meta-analysis of 20 studies that had looked for genes linked in various ways to smoking. Those studies had implicated a cluster of genes on chromosome 15 that code for proteins that bind strongly to nicotine. As they reported in the May issue of *Nature Genetics*, the researchers used 1000 Genomes data to home in on a particular SNP that affects transcription of one of these genes. "The 1000 Genomes data set will allow many other groups to carry out fine-mapping experiments in the same way … and will help people focus in on the underlying causal variants," says Marchini.

The data can also help track down genes involved in rare genetic diseases. Kathiresan and his colleagues wanted to find the faulty gene in a family with very low cholesterol levels, in the hope that the gene could provide clues about new cholesterol-lowering strategies. "Our analysis relied on an assumption: the causal variant in this family is private to this family and therefore, the causal variant would not be present in any [existing] public databases of variation," Kathiresan explains. With the help of the new data, they narrowed their search from thousands to 481 SNPs, eventually tagging two in a gene called *ANGPTL3*, they reported 13 October in the online edition of *The New England Journal of Medicine*.

But even the 1000 Genomes Project has limitations, as its searches for genetic variation tend to skip over variation in large stretches of highly duplicated DNA. About 1000 genes lie in regions of the genome that have been duplicated. That realization prompted Evan Eichler of the University of Washington, Seattle, and

CREDITS: (SOURCE) MARK A. DEPRISTO/BROAD INSTITUTE OF MIT AND HARVARD; (PHOTO) GETTY IMAGES

his colleagues to come up with a way to analyze this previously impenetrable DNA.

As described on page 641, Eichler and his colleagues have developed a technique for counting the number of copies of a gene in any duplicated region. The genes can vary in copy number among people. The number can affect how much of that gene's protein is produced, and consequently, the function of that protein.

Eichler's team has also come up with a way of distinguishing near-identical copies. Over time, copies tend to develop slight sequence differences that could also affect how that gene—or its protein product—works. Eichler's team has cataloged these telltale variant bases for about 70% of the duplicated genes. "It's opened up a whole new area of genetic diversity that we have not been able to tap previously," says Eichler.

Surprisingly, analysis of the 1000 Genomes data showed quite large differences in the copy number of certain genes between the African, European, and Asian populations, Eichler reports. "Humans are more different than we would have ever thought," says Eichler.

"Once all this variation is revealed, it changes the way you can think about [doing] genetics," notes 1000 Genome Project co-leader Richard Durbin of the Sanger Institute. For most of the history of genetics, researchers have been fishing out variation without knowing what was there. Now, "we are right on the cusp where we do genetics in the light and [see] exactly what it is that we are studying."

–ELIZABETH PENNISI

IRAQ WAR

Leaked Documents Provide Bonanza for Researchers

The Pentagon is fuming after last week's release of a huge cache of classified Iraq War data by the organization WikiLeaks. But researchers struggling to build an accurate picture of the death toll in post-invasion Iraq are thrilled. "It is hard to overstate the significance of this development for the conflict field," says Michael Spagat, an economist at Royal Holloway, University of London, U.K.

Within the nearly 400,000 leaked documents is a stream of raw data called SIGACTS—for Significant Activities—that chronicles the casualties directly observed by U.S. soldiers in Iraq. In late summer, WikiLeaks passed a copy of these data to Iraq Body Count (IBC), a London-based organization that has tallied the war's death toll using media reports of casualties. Their numbers do not include insurgents or soldiers. And because not every violent death is reported in the media, IBC's numbers are known to be an underestimate of the true number of war dead. But how much higher the true number is has been a source of intense debate, with surveys of Iraqi households yielding a wide spread of casualty estimates (*Science*, 20 October 2006, p. 396). As *Science* went to press, the IBC toll for Iraqi civilians stood at 98,585 to 107,594 violent deaths.

According to the IBC analysis of the leaked SIGACTS data, published online on 25 October, more than 109,000 violent deaths in Iraq were logged by the U.S. military between January 2004 and December 2009. Of these, over 79,000 were civilian deaths comparable to those logged by IBC, which recorded about 91,000 over the same period. By extrapolating from a sample of the data, IBC estimates that at least 27,000 civilian deaths went unrecorded by the U.S. military, while the military observed 15,000 comparable deaths that the media missed. Most of these unreported deaths were from small incidents of violence, with between one and three casualties. This confirms a widely assumed bias in media reporting in favor of larger incidents, such as suicide bombings. "But with such a huge overlap, it does not seem very likely that there are a large number of civilian deaths missed by both sources," says Spagat, who helped IBC with its analysis.

Buried data. WikiLeaks' Julian Assange at a briefing on the release of classified Iraq war records.

CREDIT: JOHN STILLWELL/PA PHOTOS/LANDOV

Taking the WikiLeaks data into account, IBC now estimates that at least 150,000 have died violently during the war, 80% of them civilians. That falls within the range produced by an Iraq household survey conducted by the World Health Organization—and further erodes the credibility of a 2006 study published in *The Lancet* that estimated over 600,000 violent deaths for the first 3 years of the war (*Science*, 18 January 2008, p. 273).

The leaked data are sure to keep researchers busy for months to come. Besides the number of casualties, the SIGACTS release includes geographic locations of the violence and other information that has not been available until now. But there could be serious challenges to those hoping to publish an analysis, says Gary King, director of the Institute for Quantitative Social Science at Harvard University. "I have had a couple of students asking [Harvard] for permission to use the previous WikiLeaks data release, and last I heard they still weren't allowed to touch it." But others are more optimistic. "As long as the data is stripped of information that could be used to identify anyone, it shouldn't be a problem," says Christian Davenport, a political scientist at the University of Notre Dame in Indiana who studies conflict mortality. "What's important is that people appreciate the complexity." For example, he says, "we don't know exactly how these data were gathered." It represents the results of an experiment, "but we don't know the methods."

–JOHN BOHANNON

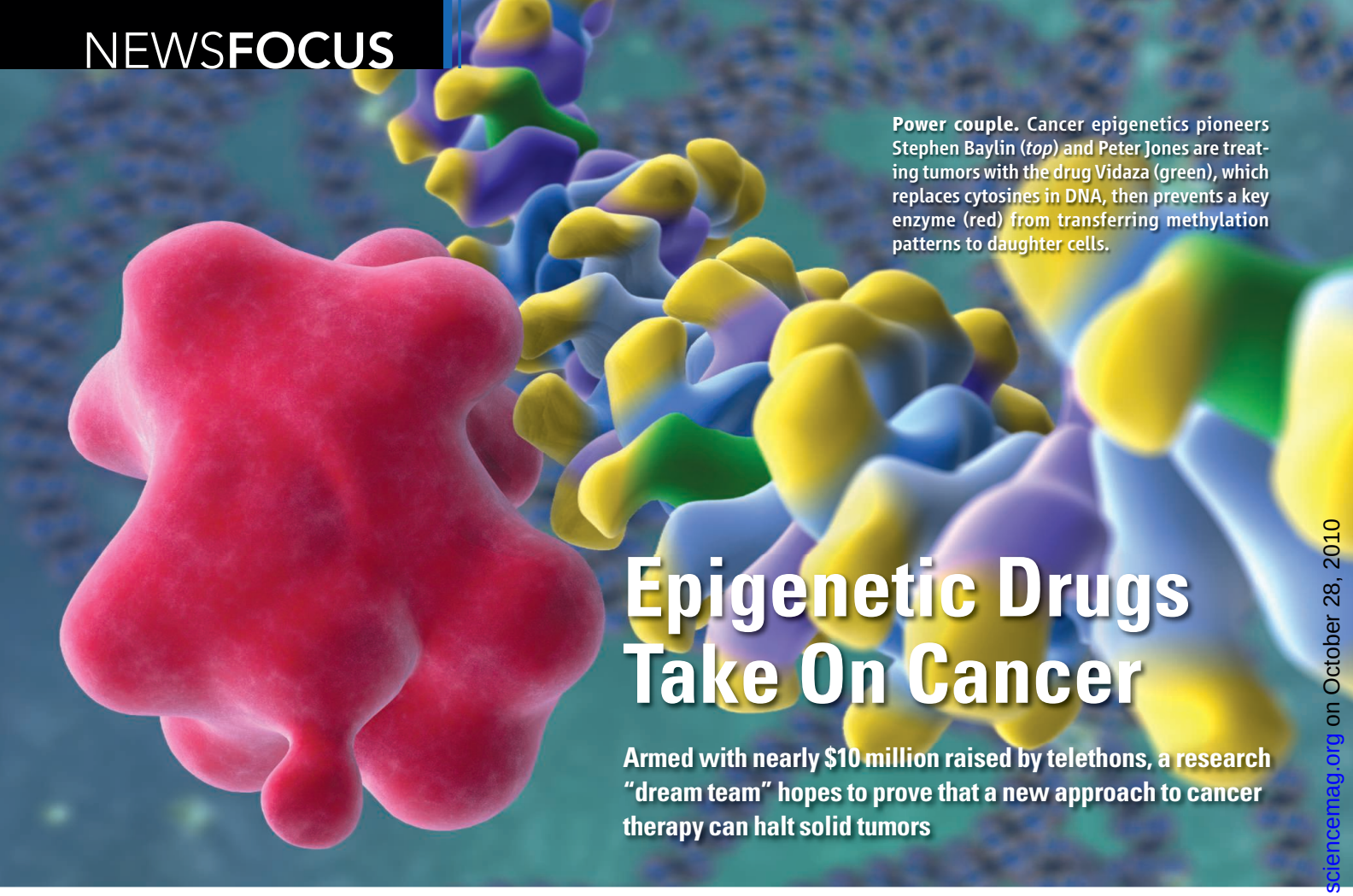

Power couple. Cancer epigenetics pioneers Stephen Baylin (*top*) and Peter Jones are treating tumors with the drug Vidaza (green), which replaces cytosines in DNA, then prevents a key enzyme (red) from transferring methylation patterns to daughter cells.

Epigenetic Drugs Take On Cancer

Armed with nearly $10 million raised by telethons, a research "dream team" hopes to prove that a new approach to cancer therapy can halt solid tumors

WHEN STEPHEN BAYLIN AND PETER JONES began their research careers about 3 decades ago, they found themselves challenging the cancer establishment. Tumor cells are typically riddled with genetic mutations, and most cancer biologists suspected that these altered DNA sequences were driving the uncontrolled cell growth. But Baylin and Jones—initially rivals and later collaborators—suggested that another factor was a suite of chemical modifications to DNA and its accessory proteins that determines whether genes are turned on.

For years, they were virtually ignored at meetings. "There would be a sort of glaze in people's eyes," says Jones, who is at the University of Southern California in Los Angeles. But today, many cancer biologists agree that DNA methylation, a process in which enzymes tack methyl groups onto genes and block their activity, and other so-called epigenetic changes might be as important as genetic mutations in causing cancer. Last year, Baylin and Jones received an award from the American Association for Cancer Research (AACR); the presenter noted that "The two of us worked sort of like salmon swimming upstream," recalls Baylin wryly, in his sunny fifth-floor corner office at Johns Hopkins University overlooking downtown Baltimore, Maryland.

AACR has also helped select Baylin and Jones, as leaders of a so-called epigenetics dream team, to receive more than $9 million from Stand Up To Cancer, a glitzy Hollywood campaign that has raised nearly $200 million for research with star-laden telethons. The 3-year grant has helped fund the first phase II clinical trials to test DNA demethylating drugs—already used successfully to treat a blood cancer—for solid tumors such as lung cancer. The idea is not to kill cancer cells but to correct their DNA methylation and thereby "reprogram" them to behave more normally, Baylin says: "It really is a different way of looking at therapy."

Online
sciencemag.org
Podcast interview with author Jocelyn Kaiser.

The two are again running into skepticism in the cancer community. Some scientists worry that instead of resetting epigenetic patterns, the primary drug Baylin and Jones are testing simply kills cells, whether cancerous or healthy ones, and therefore has toxic side effects. Precisely how the treatment works isn't yet known. And because drugs that remove methyl groups from DNA can potentially switch on hundreds of genes in healthy cells, including known oncogenes, there is concern that the drugs could cure one kind of cancer but cause another. "From a scientific point of view, you would like to know why these drugs sometimes work and develop more specific agents," says Johns Hopkins cancer geneticist Bert Vogelstein, whose lab neighbors Baylin's.

More specific versions of the drugs being tested by the epigenetics dream team are in fact in the pipeline. But molecular biologist Phillip Sharp of the Massachusetts Institute of Technology (MIT), who chaired the AACR committee that selected the Baylin and Jones–led effort for the Stand Up To Cancer funding, says the project seemed worth the investment to gauge the promise of cancer epigenetic therapies. Raising money to test the key drug was particularly important, Sharp says, because the U.S. patent will soon expire, dulling the interest of pharmaceutical companies: "Very few companies will want to put serious money into this until someone shows it works."

Muffled genes

The field of cancer epigenetics took off in the 1970s, when Jones's lab was experimenting

CREDIT: DAVID RAITT/PLASTICMILK/CELGENE

Published by AAAS

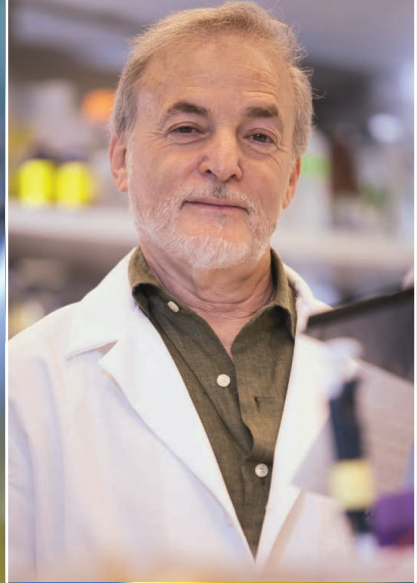

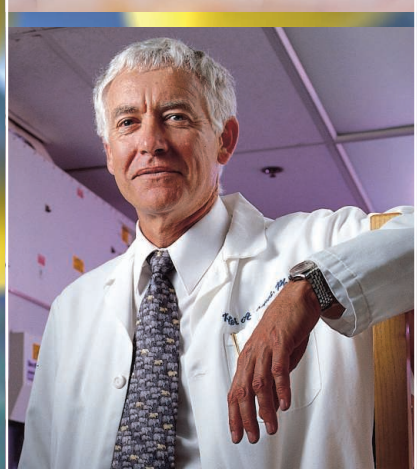

CREDITS (TOP TO BOTTOM): JOE RUBINO; PHOTO COURTESY OF USC

with a potent cancer cell–killing compound developed in Czechoslovakia. Jones noticed that this compound, azacitidine, could turn embryonic mouse cells into muscle and did so without mutating DNA. He showed that the compound was turning on a muscle-development gene that had been shut off by methylation. From this work, Jones suggested that changes in DNA methylation might be linked to aberrant gene expression in cancer.

Not long after, researchers began to document abnormal DNA methylation in most kinds of cancer cells. Some at Johns Hopkins, including Vogelstein, reported in 1983 that in colon cancer, much of a tumor cell's genome is stripped of these methyl groups. Yet Baylin noticed that certain genes in cancers tended to have too much methylation, particularly so-called tumor suppressor genes that normally check cell growth. Baylin's lab eventually showed that methylating such genes could be as effective at silencing genes as mutating them.

The growing understanding of epigenetics suggests a new way of treating cancers, because, unlike mutations, changes to a gene's methylation can be reversed. For example, silenced tumor suppressor genes might be turned back on. In theory, this might be done with compounds that lead to the loss of the methyl groups from DNA by interfering with the enzyme DNA methyltransferase (DNMT). As it happens, azacitidine, the DNMT inhibitor that sparked Jones's interest in methylation, and a similar compound, decitabine, did undergo early clinical testing for cancers in the 1970s and 1980s, but both were abandoned at the time because they were too toxic.

Partly through "serendipity," says Jean-Pierre Issa of MD Anderson Cancer Center in Houston, Texas, he and a few other clinical researchers revisited these drugs in the 1990s. While searching for a treatment for myelodysplastic syndrome (MDS), a preleukemia condition, the investigators discovered that the two compounds could safely slow the cancer. The key, notes Issa, was to ignore the conventional practice of giving patients as much of a cancer drug as they can safely tolerate. A medical oncologist named Lewis Silverman at Mount Sinai School of Medicine in New York City was treating elderly MDS patients and found that relatively low doses of azacitadine improved health and extended survival in 30% to 60% of those treated and sent a few into remission.

Meanwhile, Issa followed up on lab observations suggesting that at low doses, decitabine might stop cancer cells from dividing by reactivating tumor suppressor genes. That, he and others realized, could offer a way to stop tumor growth that is gentler than killing cells outright. Issa started clinical trials of low-dose decitabine for MDS patients and was soon having success similar to Silverman's. Their trials led the U.S. Food and Drug Administration (FDA) to approve azacitidine (marketed as Vidaza) in 2004 and decitabine (Dacogen) in 2006 for treating MDS.

It makes sense, researchers say, that these two drugs help cancer patients only at low doses given the way they work. In structure, they mimic cytosine, one of the four bases of DNA. During cell replication, the fake cytosine swaps places with real cytosine in growing strands of DNA, then traps DNA methyltransferases, interfering with the ability of these enzymes to reproduce the cell's existing methylation in the new DNA of the daughter cell. If the drug dose is too high, the cells simply die. At low doses, the cells survive but with less DNA methylation.

Building on success

With the money from Stand Up To Cancer, the epigenetics dream team is now extending the clinical trials of DNMT inhibitors to lung, breast, and colon cancers. There's no reason why such drugs should not work on solid tumors as well, Baylin and Jones say.

The team is combining the DNMT inhibitors with histone deacetylase (HDAC) inhibitors, another class of compounds that target epigenetic changes in cancer cells. Within the cell's nucleus, DNA is wound around proteins called histones that are packed together to form a package called chromatin. Somewhat like DNA, these histones can also get chemically tagged by methyl groups and acetyl groups. These tags determine the chromatin's structure, influencing whether certain genes are on, and scientists have found abnormal histone acetylation patterns in various types of cancer cells. Indeed, a compound that in cell studies appeared promising as an anticancer drug ultimately turned out to be an

Genes Link Epigenetics and Cancer

Despite abundant evidence that most kinds of tumor cells carry so-called epigenetic changes, scientists haven't yet worked out exactly whether such glitches are a cause or a consequence of disease. That's one reason for skepticism about cancer treatments that target epigenetic features such as DNA methylation and chromatin structure (see main text). But recent reports that genes affecting the latter are mutated in several types of solid tumors could help resolve this conundrum. The discoveries bolster the notion that epigenetics can drive cancer, says Jean-Pierre Issa of MD Anderson Cancer Center in Houston, Texas.

In the past 2 years, projects in the United States and Europe that are systematically cataloging genetic changes in cancer have turned up mutations in genes whose encoded proteins modify chromatin, DNA's packaging structure. These genes include *JARID1C*, mutated in 3% of 407 kidney cancer tumors, according to a report early this year in *Nature*; and *ARID1A*, which two separate teams last month found mutated in roughly 50% of about 160 samples of a type of ovarian cancer (***Science***, 8 October, p. 228). Mutations in a gene called *BRG1* have also been found in 24% of 59 lung cancer cell lines.

Exploring the function of these mutations may enable researchers to trace the exact pathways by which epigenetic changes trigger cancer, says Andrew Futreal of the Wellcome Trust Sanger Institute in Hinxton, U.K.: "There's a complicated story developing here." **–J.K.**

Published by AAAS

HDAC inhibitor. This drug, known as SAHA (Zolinza), like other HDAC inhibitors, blocks the removal of acetyl groups from histones. It was approved in 2006 by FDA for treating a rare immune system cancer called cutaneous T-cell lymphoma.

Cell studies by Baylin's group have shown that the two types of epigenetic therapies should synergize, which is why the Stand Up To Cancer team is venturing ahead with a combination approach, initially testing Vidaza and the HDAC inhibitor Entinostat for advanced non–small cell lung cancer in a trial at Johns Hopkins. The unpublished results, says Baylin, are promising for patients with cancer that had spread despite several chemotherapy treatments. The drug combo has slowed or stopped tumor growth in 30% of 28 patients and has produced "very robust and durable responses" in four people, he adds, shrinking or even eliminating their tumors for at least 1.5 years.

Two-thirds of the people in the trial were not helped by the treatment, however. Baylin and others offer several explanations. Not enough of the drug may be getting into the lung tumor cells, the researchers suggest, noting that a more stable DNMT inhibitor, which the team will use in a future trial, may help. Another possibility is that, because they have received chemotherapy, these advanced cancer patients may have already developed "resistance" to nucleus-targeting drugs (including the epigenetic treatment). Mutations in their tumor cells may have closed off the drugs' access points to the nucleus, Issa says. To test this idea, the Stand Up To Cancer team plans to try the epigenetic drugs on cancer patients who have had surgery but no chemotherapy.

Yet another explanation is that only some patients' tumors are driven by epigenetic changes (see sidebar). Indeed, the team is examining the DNA methylation and gene expression of each patient in their trials, with the hope of finding a pattern that predicts whether a person will respond to the drug combo. Others are also taking this approach. In the 20 October issue of *Science Translational Medicine*, researchers at the U.S. National Cancer Institute report that they have used epigenetic and gene-expression signatures to classify liver cancer cell lines into two distinct types: one that dies when treated with a DNMT inhibitor and one that does not.

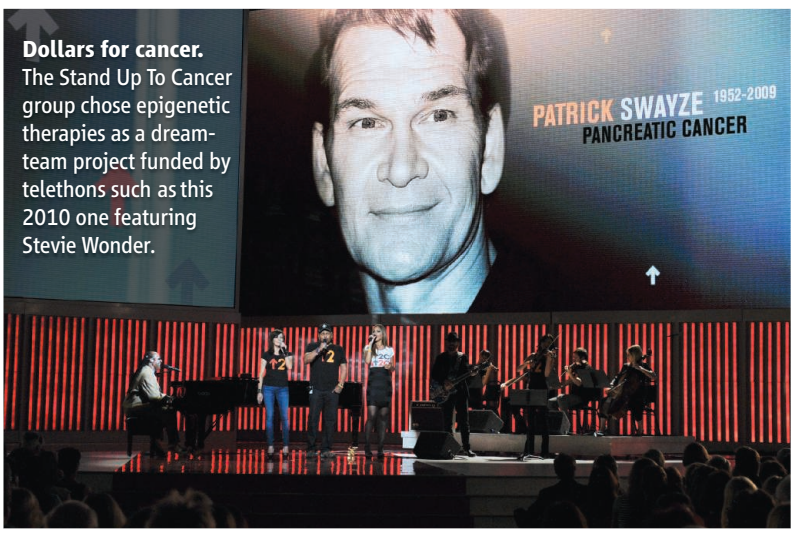

Dollars for cancer. The Stand Up To Cancer group chose epigenetic therapies as a dream-team project funded by telethons such as this 2010 one featuring Stevie Wonder.

Room for improvement?

As the Stand Up To Cancer team pushes ahead with its solid-tumor trials, skepticism continues about the drugs being tested, most of it centering on questions about the mechanism. "The drugs do work at low doses, and they do change epigenetic modification patterns, but it is not clear whether the clinical benefits are due to the epigenetic changes," says molecular biologist Frank Lyko of the German Cancer Research Center in Heidelberg. DNA-demethylating drugs such as azacitidine and decitabine may simply be killing cells, he suggests. And HDAC inhibitors, which act on many cell pathways, may be changing some that have nothing to do with epigenetics, such as acetylation patterns in proteins in cytoplasm. Paul Marks of Memorial Sloan-Kettering Cancer Center in New York City, who developed the first HDAC inhibitors, agrees: "We're still in the very early stages of trying to understand how best to use these inhibitors in a clinical setting."

And even if DMNT inhibitors do epigenetically reprogram cancer cells, they could also turn on genes that cause cancer. Rudolf Jaenisch, a developmental biologist at MIT, has conducted mouse studies that illustrate this potential problem. He and his colleagues have shown that if they disable the gene for a DNA methyltransferase, the mice eventually develop a type of lymphoma (*Science*, 18 April 2003, p. 489). "One has to be cautious playing with a mechanism that could have several potential effects," he says.

Jaenisch says his group's mouse results may not be relevant to adult cancer patients undergoing treatment with DNMT inhibitors because the clinical doses don't seem high enough to match knocking down the gene for a methylating enzyme. Still, Jaenisch lauds efforts by researchers such as Lyko, a former postdoc in his lab, to develop drugs that demethylate DNA by blocking one or more of the DNA methyltransferase enzymes rather than globally suppressing methylation by incorporating a fake cytosine into DNA. Such specific enzyme inhibitors should demethylate fewer genes and perhaps reduce the potential for side effects.

Baylin and other members of the epigenetics dream team are quick to respond to such criticisms. They say there is plenty of evidence that the drugs they're testing aren't mere cell killers. "You see things in the clinic that you never see with cytotoxic drugs," says Issa. He points to MDS patients' slow response time—some show no change in cancer growth for months—and he notes that people can stay on the drugs a long time without serious toxicity. Jones says that because most normal cells aren't dividing and don't have messed-up methylation patterns, they should be little affected. The drugs "are targeting an abnormal chromatin state not present in normal cells," Jones says.

Whether more specific drugs will work better is debatable, says Baylin, who calls himself "agnostic" on the issue. The wide-ranging effects of the older drugs may actually make them more effective, he and Jones suggest.

Baylin says that how DNMT inhibitors stymie cancer should soon become clearer. His own lab hopes to publish a study showing that when very low doses of decitabine and azacitidine—similar to those given to MDS and lung cancer patients—are added to cultured leukemia and breast cancer cells, the cells don't die right away. Instead, the cells die days or weeks later, perhaps because they act more like normal cells and can't survive in the foreign environment in a tumor. Most intriguing, says Baylin, is that his experiments suggest that the drugs reprogram cancer stemlike cells, a much-debated type of tumor-initiating cell that resists traditional cancer drugs.

Nonetheless, he and Jones may still have a long way to go to convince colleagues that low doses of DNA-demethylating drugs can control cancer in people. "This is not going to be easy," Baylin says. "Maybe we'll continue to swim upriver." **–JOCELYN KAISER**

CREDIT: RICHARD HARBAUGH/ABC

PHARMACOGENOMICS

Gene Variants Affect Hepatitis C Treatment, But Link Is Elusive

Genome scans have turned up single nucleotide polymorphisms associated with different responses to treatment, but efforts to uncover the mechanism have drawn a blank

Ever since researchers identified the hepatitis C virus (HCV) almost 3 decades ago, they have known that individuals differ in their ability to fend off the virus and in their responses to treatment. But what lies behind those individual differences has been a mystery. A year ago, three groups independently came up with part of the answer: Patients with a particular variant of a gene called *IL28B* tend to fare better than others in battling the virus. The finding promised new insights into the complex interplay between the immune system and HCV, which is estimated to infect 4 million people in the United States and 170 million worldwide.

A diagnostic test for the *IL28B* variants recently became available. It is helping to guide decisions on whether, and when, patients begin treatment with the current therapy, a combination of pegylated interferon-α and the antiviral drug ribavirin. And there are hints that the *IL28B* polymorphisms may play a similar role in responses to treatment with two new drugs that are expected to be approved early in 2011. So far, however, research to determine why different versions of the gene provide different levels of protection against HCV and different responses to treatment have "hit a brick wall at every turn," says geneticist David Goldstein of Duke University in Durham, North Carolina, a lead investigator for one of the groups that made the initial finding.

Last year's findings came from whole-genome scans that looked for associations between genetic variants known as single-nucleotide polymorphisms (SNPs) and treatment outcomes. They pointed to three SNPs, CC, CT, and TT, that are very close to *IL28B*. Patients with the CC genotype tend to respond well to treatment and also have higher rates of eradicating the virus without drug intervention—a phenomenon known as spontaneous clearance, observed in about 30% of HCV patients. By contrast, those with the CT and TT alleles tend to fare poorly. Treatment is often ineffective and poorly tolerated, and spontaneous clearance is unlikely.

The finding explained one baffling hallmark of hepatitis C: The treatment is less effective for African Americans than for patients of European and Asian ancestry. The CT and TT alleles, it turns out, are far more common among African Americans, while the CC allele is more common among Europeans and Asians. The polymorphism accounts for at least half the difference in treatment response between these groups.

Several labs immediately turned their attention to uncovering the mechanism linking the *IL28B* polymorphisms and treatment responses, in the hope that it might point the way to better treatments. The implications could extend beyond HCV. "It's such a big effect, I would imagine it's not completely exclusive to hepatitis C," says Goldstein, who theorizes that the CC allele might be protective against other infectious agents more common in Asia than in Africa. Early results of these studies are now coming in, and they are mostly disappointing, defining no clear route from polymorphism to patient outcome.

According to a recent publication by Goldstein's group in *Hepatology*, the three SNPS don't seem to affect the level of expression of the *IL28B* gene itself, which would have been perhaps the most direct pointer to new therapies. The Duke group and researchers at Kanazawa University in Japan and the University of Basel in Switzerland separately found that the CC allele is associated with lower baseline expression of genes in the liver that are stimulated by interferon. The finding is puzzling, considering that interferon blocks viral reproduction. "Somehow this must be connected to the mechanism," says Goldstein, who theorizes that the higher baseline expression associated with the CT and TT alleles might weaken the pathway by which the body responds to interferon treatment. The exact connection between the *IL28B* alleles and interferon-stimulated genes remains a mystery, however.

While researchers are exploring the biology behind the polymorphisms, physicians are beginning to use the associations to help guide treatment. In July, the U.S. Food and Drug Administration approved LabCorp's test for the three SNPs, which costs $300 to $350. As David Thomas of Johns Hopkins University School of Medicine in Baltimore, Maryland, another lead investigator on the initial *IL28B* studies, explains, the test can help patients and physicians decide whether to initiate, delay, or skip treatment, which can have debilitating side effects. "This test has obvious implications because it gives you very important information about the likelihood of response," says Thomas.

That information may also apply to the next generation of anti-HCV treatment. Early next year, FDA is expected to approve two proteasome inhibitors, telaprevir and boceprevir, which would be added to the current interferon and ribavirin combination. A study published in the August issue of *Hepatology*, in which 81 Japanese HCV patients were given the triple combination therapy, hints at the same association between the *IL28B* alleles and treatment response. Of the 42 patients with the CC allele, 84% experienced a long-lasting response to the triple combination therapy. By contrast, only 32% of those with the CT and TT alleles had the same benefit.

The work indicates the potential benefits of including genetic studies as a component of drug trials. Goldstein, for one, thinks this is an area that is ripe for academic-industrial collaboration. "There are many trials with high-quality data," he says, "but the careful genetics just haven't been done." **–JESSICA WAPNER**

Jessica Wapner is a science writer in New York City.

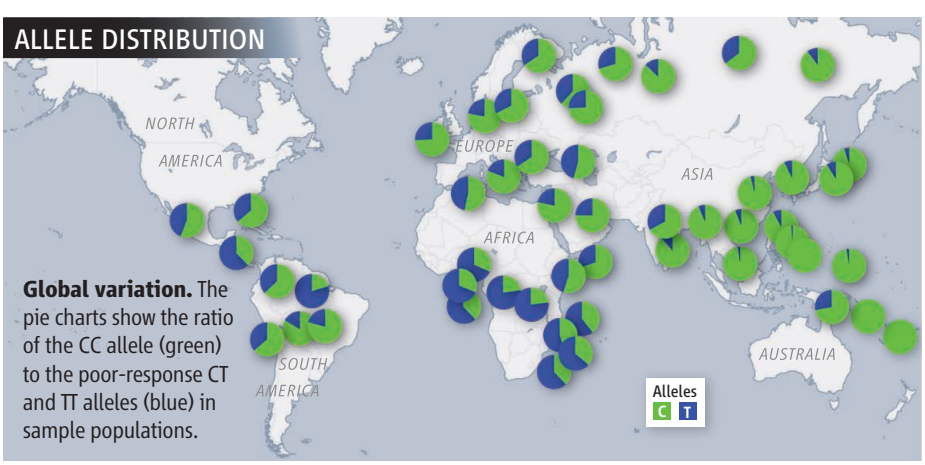

Global variation. The pie charts show the ratio of the CC allele (green) to the poor-response CT and TT alleles (blue) in sample populations.

CREDIT: ADAPTED FROM D. L. THOMAS *ET AL.*, *NATURE* **461** (8 OCTOBER 2009)

Published by AAAS

U.S. SCIENCE EDUCATION

Data Say Retention Is Better Answer To 'Shortage' Than Recruitment

Most efforts to improve STEM education start with recruitment. But working with those teachers already in the classroom may yield a bigger payoff

Finding science teachers who want to teach at Henninger High School has never been a problem, says Mickey Grosnick. Grosnick should know: She graduated from the Syracuse, New York, public school in 1967, returned there 16 years later to teach biology, and spent almost 2 decades as chair of the science department before retiring in June after a 37-year career as a secondary school science teacher in the district.

But keeping them is another story. Grosnick remembers a year earlier in the decade when a wave of retirements at Henninger required the hiring of five new science teachers at the same time. (The school typically has a fairly low turnover rate.) Within a few years, however, all of them were gone. "There were a lot of reasons. They didn't like the setting, the large classes, the confrontations with students, the lack of resources," says Grosnick. "I guess they just weren't comfortable teaching in a large, urban district."

Conventional wisdom has it that the dismal performance of U.S. students on international math and science tests can be blamed in large part on an inadequate supply of good teachers. That assumption has fueled initiatives by several higher education and business groups aimed at eliminating the shortage by pumping up the supply. And the White House has applauded the effort. In his 2006 State of the Union address, President George W. Bush announced that his Administration would strive to "bring 30,000 math and science professionals to teach in classrooms." President Barack Obama has talked repeatedly of "preparing 100,000 STEM [science, technology, engineering, and mathematics] teachers over the next decade." And last week, at a White House science fair, Obama reiterated his belief that training more STEM teachers is the key to meeting his goal "to move [the country] from the middle to the top in math and science education over the next decade."

But what if the conventional wisdom is wrong? Is there really a national shortage of STEM teachers?

A new analysis by Richard Ingersoll, an education policy researcher at the University of Pennsylvania who has tracked teacher workforce issues for 2 decades, suggests that the problem lies further down the pipeline. The title of his article in the September issue of the *American Educational Research Journal* poses the provocative question, "Is the Supply of Mathematics and Science Teachers Sufficient?" And his answer, unambiguously, is yes. "The problem is retention, not recruitment," says Ingersoll. "In the same year that Bush called for recruiting 30,000 STEM teachers, we had 26,000 quit. That's a terrible waste of talent."

That conclusion, he admits, "is heresy" to most science educators and advocates. It also has important policy implications (see sidebar, p. 581). "When I started this work I assumed, like everybody else, that we have a critical shortage," he says. "And it was only slowly that I came to these contrarian views. Now I'm getting hate mail from people saying that I'm undermining their arguments to politicians and college presidents about the need to train more STEM teachers."

There are approximately 3.6 million public school teachers working in 90,000 school districts across the 50 states. Almost 500,000 are classified as math and science teachers. (That number represents only secondary schools—grades 7 through 12. Elementary school teachers are generally certified to teach all subjects, and there are no reliable figures for how many concentrate on science or math.) And every year, the media report that some school districts are struggling to find enough math and science teachers.

Ingersoll wanted to get a better handle on the supply side and to replace anecdotes with hard data. So he examined teacher flows, that is, the number of teachers hired for any particular school year and the number who leave, for whatever reason, at the end of the year. Ingersoll combined data from three federal education surveys to paint a much more complete, and nuanced, picture than ever before of those joining and leaving the STEM teacher workforce.

One discovery was that newly certified teachers fresh out of education schools—the usual metric for whether the country is producing "enough" STEM teachers—were only a small part of the overall hiring pool. The single biggest source of new staff members is what he calls reentrants: teachers with math and science degrees who are not currently in the classroom (see pie chart). The next biggest group is those with STEM content degrees (biology or chemistry rather than education, for example), followed by those who delayed their entry into the pro-

GRAPH: ADAPTED FROM R. INGERSOLL *ET AL.*, *AMERICAN EDUCATION RESEARCH JOURNAL*, **47**, 3 (SEPTEMBER 2010)

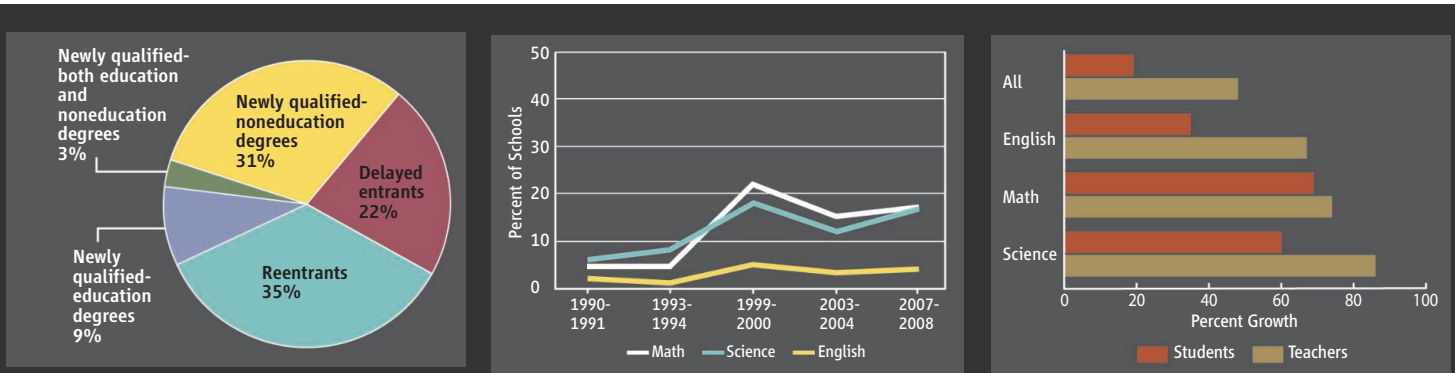

Data, at last. This pie chart (*left*) shows the backgrounds of math and science teachers hired in 1999, which was a peak year for schools having trouble filling vacancies (*middle*). The bar graph (*right*) shows that the teacher supply has grown faster than enrollments over the past 20 years.

Published by AAAS

fession after becoming qualified to teach in a STEM field. Only one in eight is a newly minted teacher with either an undergraduate degree in education or both content and education degrees.

Ingersoll's analysis also shows that, despite burgeoning student populations and more required math and science courses, the supply of math and science teachers actually increased at a faster rate between 1988 and 2008 than did enrollments in those courses. (Of course, schools don't have the option of leaving a classroom vacant, as a company might leave a position unfilled until it finds the right person.) The widespread perception that math and science are "shortage" areas, he surmises, comes from the attention given to a relatively small percentage of schools that must scramble to fill their teaching rosters. Turnover among STEM teachers isn't any higher than for other fields, he finds, but there's less of a cushion of candidates in math and science than in, say, English or social studies.

In a second paper, from the Consortium for Policy Research in Education (CPRE), Ingersoll and consortium colleague Henry May examine the factors leading to staff turnover. For math teachers, the lack of classroom autonomy, weak professional development, and student discipline are the primary reasons for leaving. Professional development and discipline are also important for science teachers, although low salaries are their biggest gripe. (Math teachers don't cite salary as a major concern.)

The CPRE paper reports that "high poverty, high minority, and urban public schools have among the highest mathematics and science [teacher] turnover levels." But it's lousy working conditions, not bad students, that contribute to high mobility, says Ingersoll: "Teachers aren't fleeing poor kids. They are fleeing poor jobs." The solution is to address the reasons teachers are leaving rather than continually trying to refill a leaky pipeline, says Ingersoll, adding that the solutions to many of the problems wouldn't involve a lot of money.

Not surprisingly, some researchers have raised questions about some of Ingersoll's assumptions. Jennifer Presley, head of science and mathematics education policy at the Association of Public and Land-Grant Universities (APLU), thinks Ingersoll has exaggerated the reserve pool of teachers. She argues that many more teachers than he assumes drop out for good once they leave a job, and others with degrees never enter the classroom. She also points out that data Ingersoll relies on are nearly 10 years old and may not reflect current conditions. Others accept his overall conclusion but maintain that a shortage does exist in some areas, especially physics.

Much of the data in both papers are drawn from 1999–2000 because all three federal surveys, done periodically, were conducted during that academic year. (The Schools and Staffing Survey is based on a random national sample of teachers, principals, and school districts. The Teacher Follow-Up Survey tracks a representative sample of those teachers 1 year later. And the Baccalaureate and Beyond Longitudinal Survey polls a representative sample of new bachelor's-degree recipients.) That year was also a peak for schools reporting serious difficulties in filling teacher vacancies, Ingersoll notes, meaning that the data should capture any purported shortage at its worst.

Presley, who's working with 125 of APLU's member institutions on an initiative to train more science and math teachers, acknowledges that "I have a bit of a conflict because we're trying to encourage our institutions to provide the type of teacher preparation that the country so desperately needs. And I feel that those efforts will definitely raise the quality of the teacher workforce."

But she's not letting that conflict cloud her professional judgment. "I think that it's quite a thoughtful paper," Presley says about Ingersoll's work, "and I actually agree with most of it."

–JEFFREY MERVIS

What's in a Number?

Ingersoll's research does more than just question whether teacher recruitment should be the top priority for improving science, technology, engineering, and math (STEM) education in the United States. It also casts doubt on the key number President Barack Obama uses to promote his education policy. The source is *Rising Above the Gathering Storm* (*RAGS*), a 2005 National Academies' report that recommends offering 4-year, government-funded STEM scholarships to "annually recruit 10,000 of America's brightest students into the teaching profession." Obama's self-proclaimed "ambitious goal" of preparing 100,000 new STEM teachers, for example, would continue that level of output for a decade.

To be fair, the academies' report also talked about the need to improve the quality of the STEM teaching force. But policymakers overwhelmingly mention its emphasis on boosting the number of teachers when they cite the report.

But how does that number compare to current levels of production? And how far would training 10,000 more STEM teachers a year go toward achieving Obama's goal of making the country No. 1 in math and science education?

At the wheel. President Obama tests a device to combat distracted driving at the White House science fair.

Michael Allen, an educational consultant who's working with the Association of Public and Land-Grant Universities (APLU) on an initiative at 125 member institutions to train more science and math teachers, conducted a futile search for what would be the first logical step toward specifying the number of new teachers needed. "I find it totally incredible that no agency collects data on how many math and science teachers are credentialed each year," he says. "I think that the number in the *RAGS* report was taken out of thin air."

Ellen Lagemann, an education historian at Bard College in Annandale-on-Hudson, New York, and former dean of the Harvard Graduate School of Education who co-chaired a recent study by the National Academies on teacher preparation programs, believes that "the number is essentially meaningless." Her report, which focused on reading, math, and science, found that "there have been no systematic efforts to collect the necessary data" to know who's being trained for what, much less the quality of the instruction. Even its seemingly innocuous description of the type of research needed to determine what needs to be improved provoked a dissent from one panelist who complained that the literature is too sparse to even design such studies.

"Until we get better baseline data on how many teachers are being trained and the nature of that preparation," says Lagemann, "it's just plain silly" to try to quantify what's needed. **–J.M.**

CREDIT: OFFICIAL WHITE HOUSE PHOTO BY PETE SOUZA

Published by AAAS

Rattled snake. This tiger rattlesnake's habitat in Arizona may shrivel as Earth warms.

CREDIT: JESSE M. MEIK

Going Back to the Future To Understand Climate Change

Paleontology is often seen as a time machine that allows scientists to reconstruct events that happened millions and millions of years ago. But several speakers at the meeting turned that notion on its head: They used paleontological data to predict the future, drawing on species' behavior during past episodes of climate change to predict how they will fare—and how to help them—as greenhouse gases warm the planet.

Many researchers have expected species ranges to shift toward the poles or up mountain slopes as the world warms. But independent paleontological data on several different animals suggest more complicated scenarios, says paleoecologist Anthony Barnosky of the University of California, Berkeley. "Some ecological niche models, commonly used in predicting future response, can be refined to give better predictions when fossil data are incorporated," he says.

In a study in the Great Basin, paleoecologist Rebecca Terry and colleagues at Stanford University in Palo Alto, California, studied 24 species of rodents by collecting owl pellets in two caves in Nevada and Utah. Owls regurgitate the remains of the critters they eat, and the caves preserved evidence of owl meals over 8000 years. They compared the abundance of species with climate data from lake cores and other sources. They were able to track how owl-prey populations fluctuated as climate changed and to spot trends in the way species responded, such as whether southern species moved north into the cave regions as climate warmed. "We focus on small mammals because they're known as bellwethers of climate change," Terry explains.

Researchers had expected that when climate became hotter and drier, all the southern species of rodents—presumably already accustomed to arid conditions—would fare better than northern ones, perhaps even expanding their range. But that's not what Terry found. Instead, what mattered most was what the rodents ate: Those that dined on plants, such as chisel-toothed kangaroo rats, suffered most when the climate dried. But seed-eating rodents, such as pocket mice, fared well because they could rely on seeds as a source of water in dry times.

As the Great Basin becomes warmer and drier over the next 50 years, Terry and her colleagues predict that southern species of seed eaters will fare better than herbivorous rodents from the north or the south. The work "is important in giving us some nice predictions on what kinds of species are apt to move where in response to climate change, and why," says Barnosky.

It's not just mammals that have exhibited complex responses to climate change. Michelle Lawing and David Polly of Indiana University, Bloomington, studied 11 species of rattlesnakes, which are good indicators of climate change because they depend on ambient conditions to regulate their body temperatures. Lawing and Polly used a paleontological database to create a track record of how the snakes' ranges expanded and contracted during the past 320,000 years, a time of dramatic climate change when glaciers waxed and waned. Overall, the snakes shifted their range by an average of only 2.3 meters per year in that time period.

Then the researchers applied the current climate model predictions, which range from a warming of 1.1°C to 6.4°C by 2100. They found that the warming was both so large and so fast that rattlesnakes would be displaced between 430 and 2420 meters a year, suggesting that the snakes won't be able to move fast enough to stay in a suitable habitat. "No one comes out ahead; they all do poorly," says Lawing. As with rodents, southern species don't fare much better than northern ones. For example, the timber or canebreak rattlesnake has a particularly large range on the East Coast today, from Florida to the Canadian border. But it would be hit hardest because its environment will become both warmer and wetter, says Lawing. "I would predict this is going to happen with a number of species," she says. "It's not just the rattlesnake; it's the habitat it lives in and all the other species associated with it."

If many species are at risk, is there a way to target conservation efforts? Here again, data from the past may offer insight, say Elizabeth Hadly and Malin Pinsky of Stanford University. They study northern fur seals, whose populations were decimated not by climate but by overhunting off the west coast. In a genetic study, they expected to find that the surviving seals had low diversity and were at risk of extinction. But instead they found that seals had managed to retain genetic diversity by retreating to their historic breeding grounds in the Bering Strait, where the remnant populations mix their genes thoroughly. Given their resilience, says Hadly, these seals would be ideal candidates for assisted migration to new habitats if they become endangered. Says Terry: "This type of predictive framework lets us prioritize our conservation efforts." **–A. G.**

Published by AAAS

Snapshots From the Meeting >>

Digging dinosaur. Researchers have long puzzled over how the large, fleet-footed, meat-eating dinosaurs called abelisaurids used their stubby arms, which were even shorter than those of tyrannosaurids. Now paleontologist Paul Sereno of the University of Chicago may have unearthed an important clue with the skeleton of a more primitive, smaller abelisaurid relative—a 110-million-year-old noasaurid theropod in Niger (right). The wolverine-sized African dinosaur used its short but fully functional arms, with their flat claws, to dig prey out of burrows the way wolverines do today, Sereno said in his talk. As later abelisaurids grew larger and even more adept at chasing prey, they may have retained this primitive forelimb but lost the ability to dig because they no longer had to burrow for food.

Flooding the Rift. Researchers often cite changes in climate as the forcing factor behind the evolution of new adaptive traits and species, including the appearance of new hominins in Africa. But it's often hard to understand how factors like more rainfall altered ancient communities. In a talk, Yale University paleoanthropologist Andrew Hill linked a boost in rainfall to ecological change at key ancient hominin sites. By analyzing the siliceous skeletons of blue-green algae called diatoms, his team found that freshwater lakes once filled parts of the Rift Valley of Kenya. As rainfall increased in response to cyclical changes in the tilt of Earth's axis, huge lakes formed repeatedly in the past 6 million years, leaving behind diatomites (white band, above) that reveal the lakes' size and composition. Graduate student Emily Goble's modeling of the elevation of the lakes shows that five large lakes filled Kenya's Baringo Basin between 2.7 million and 2.5 million years ago, unsettling animal communities just before our genus, *Homo*, arrived there. Hill and his colleagues think the climatic shifts had a "kaleidoscopic" effect, breaking up communities of animals that then reassembled in new patterns after the lakes shrank. If so, early *Homo* was part of a wave that recolonized the lakebed. **–A.G.**

PASCALE GOLINVAUX, IRSNB-KBIN; FLORENCE QUESNEL, BRGM (INSET)

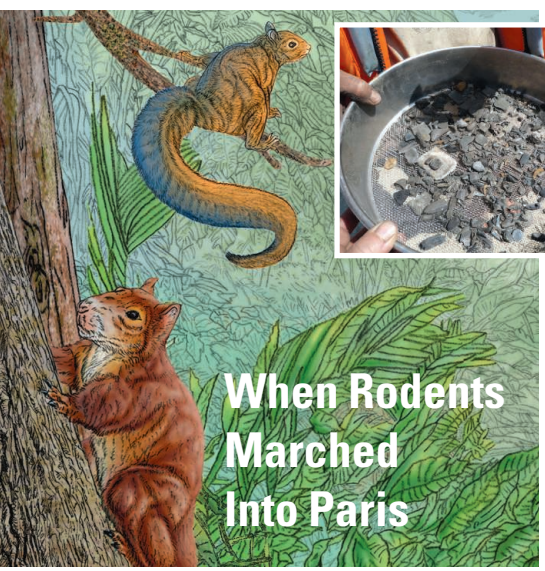

Headed for Paris. Fossils (*inset*) of early rodents turned up in Paris.

When Rodents Marched Into Paris

Walk around Paris and you will see plaques honoring the many famous people who were born there, from Monet to Voltaire. But it's a safe bet that Parisians won't commemorate the home of some of their city's first settlers: chipmunk-sized mammals that are among the world's oldest rodents, and the oldest in Europe. It was a Belgian member of a French-Belgian team, in fact, who at the meeting announced the discovery of fossil teeth of the squirrel-like rodents on the grounds of a quarry in northern Paris.

The discovery of two definitive rodent teeth, as well as part of a primitive carnivore's jaw, is an important clue to the mystery of how the first modern mammals spread around the globe, replacing archaic animals and ushering in the age of modern mammals, says Thierry Smith of the Royal Belgian Institute of Natural Sciences in Brussels. His team's finds show that the first modern rodents appeared in Europe at about the same time as in North America, some 57 million years ago. "It has long been assumed that these animals did not reach Europe until well after their first appearance in North America," says paleontologist Kenneth Rose of Johns Hopkins University in Baltimore, Maryland, who wasn't part of the study. "The new evidence suggests there was no substantial time lag between their arrival." Researchers have long looked for the earliest rodents in Europe, because rodents are the leading edge of a wave of modern mammals that colonized the world starting about 57 million years ago. Most modern orders, such as hoofed animals and primates, don't appear until almost 56 million years ago, when the climate warmed markedly.

Researchers think the first rodents arose in Asia, because several different kinds of rodentlike mammals lived there for millions of years before modern rodents replaced them. But the first true rodents were found in America, in 57-million-year-old fossil beds in Wyoming, so researchers thought rodents had dispersed rapidly from Asia to the Americas over the Bering Strait land bridge. As for Europe, most thought rodents arrived later but were unsure because few fossil sites date back to the right time period.

That is why Smith was so delighted to find two rodent teeth, plus a bit of jaw from a marten-like miacid carnivore, another early member of a modern order. "There is absolutely no doubt" that one tiny curved incisor belonged to a modern rodent, he says, because it shows a pattern of continuous growth seen in all rodents today. Like a squirrel, the early rodent used its incisor to detach seeds from plants.

The Parisian fossils suggest that from the start, rodents and other early mammals "went right and left, east and west," perhaps moving in two directions across a land bridge connecting Europe to Greenland and America, says Smith. At that time, "Greenland was green," with enough plants and trees to provide food and cover for this first wave of migrating rodents and small carnivores, says Smith. All this traffic happened before the dramatic warming event 56 million years ago. However, unpublished studies of carbon and oxygen isotopes in fossil teeth hint at an even earlier pulse of warming, about when rodents reached America, says vertebrate paleontologist Ross Secord of the University of Nebraska, Lincoln. Kicking up the temperature a notch might have been enough to allow intercontinental travel for a rat pack of small mammals. **–ANN GIBBONS**

CREDITS (TOP TO BOTTOM): JOHN KINGSTON; DIDIER DUTHEIL;

Published by AAAS

LETTERS

edited by Jennifer Sills

Mass Fruiting in Borneo: A Missed Opportunity

Dipterocarp tree seedlings. Many endangered Indonesian trees rarely produce seeds.

LARGE-SCALE RESTORATION OF tropical forest is increasingly recognized as a credible option for climate change mitigation and biodiversity conservation (*1*–*3*). To implement this strategy, we must collect and nurture vast numbers of tree seeds. Yet, in conservation priority areas such as Indonesia—discussed by D. Normile in his News Focus story "Saving forests to save biodiversity" (10 September, p. 1278)—many tree species (such as the dipterocarps) rarely produce seeds (*4*). In 2010, we witnessed the first large mass fruiting event in Borneo since 1998, both in geographic extent and species involved. Unfortunately, forestry departments, funding agencies, and most research institutes were unprepared for this rare opportunity. These seeds cannot be stored, even in state-of-the-art seed banks (*5*). To contribute to the restoration efforts, they must be collected and planted immediately. We have much of the scientific and botanical knowledge required to achieve successful restoration [discussed in E. Pennisi's News Focus story "Tending the global garden" (10 September, p. 1274) and in (*6*)], but we lack the financial and infrastructural resources for seed collection, propagation, and restoration.

Substantial financial support must be dedicated to enable Southeast Asian countries to respond quickly to these critical but rare opportunities for conservation and restoration. We must prepare now to provide funding, planning, and infrastructure for the next major fruiting event. This may be the last opportunity to collect sufficient seeds from many endangered tree species for conservation and forest restoration.

CHRIS J. KETTLE,[1]* JABOURY GHAZOUL,[1] PETER S. ASHTON,[2] CHARLES H. CANNON,[3,4] LUCY CHONG,[5] BIBIAN DIWAY,[5] ENY FARIDAH,[6] RHETT HARRISON,[3] ANDREW HECTOR,[7] PETE HOLLINGSWORTH,[8] LIAN PIN KOH,[1] EYEN KHOO,[9] KANEHIRO KITAYAMA,[10] KUSWATA KARTAWINATA,[11] ANDREW J. MARSHALL,[12] COLIN R. MAYCOCK,[13] SATOSHI NANAMI,[14] GARY PAOLI,[15] MATTHEW D. POTTS,[16] DOUGLAS SHEIL,[17] SYLVESTER TAN,[5] ICHIE TOMOAKI,[18] CAMPBELL WEBB,[2] TAKUO YAMAKURA,[14] DAVID F. R. P. BURSLEM[13]

[1]Ecosystem Management, Institute of Terrestrial Ecosystems, Department of Environmental Sciences, ETH Zürich, Zurich 8092, Switzerland. [2]The Arnold Arboretum of Harvard University, Harvard University Herbaria, Cambridge, MA 02138, USA. [3]Chinese Academy of Sciences, Xishuangbanna Tropical Botanic Garden, 666303 Yunnan, China. [4]Department of Biological Sciences, Texas Tech University, Lubbock, TX 79409, USA. [5]Botanical Research Centre (Sarawak Forestry Corporation), 93250 Kuching, Sarawak, Malaysia. [6]University of Gadjah Mada, Bulaksumur, Yogyakarta 55281, Indonesia. [7]Institute of Evolutionary Biology and Environmental Studies, University of Zurich (Irchel), CH 8057 Zurich, Switzerland. [8]Royal Botanic Garden, Inverleith Row, Edinburgh EH3 5LR, UK. [9]Forest Research Centre, Sabah Forest Department, Sabah, Malaysia. [10]Graduate School of Agriculture, Kyoto University, Kitashirakawa Oiwake-cho, Sakyo-ku, Kyoto 606-8502, Japan. [11]UNESCO, Jakarta Office, Regional Science Bureau for Asia and the Pacific, Jakarta, Indonesia. [12]Department of Anthropology, Graduate Group in Ecology, Animal Behavior Graduate Group, University of California, Davis, CA 95616–8522, USA. [13]Institute of Biological and Environmental Sciences, University of Aberdeen, Aberdeen AB24 3UU, UK. [14]Graduate School of Science, Osaka City University, Japan. [15]Daemeter Consulting, Jalan Tangkuban Perahu No. 6, Bogor, Indonesia. [16]Department of Environmental Science, Policy, and Management, University of California, Berkeley, CA 94720, USA. [17]Institute of Tropical Forest Conservation, Kabale, Uganda. [18]International Field Science Course, Faculty of Agriculture, Kochi University, B200, Monobe, Nankoku 783-8502, Japan.

*To whom correspondence should be addressed. E-mail: chris.kettle@env.ethz.ch

References

1. R. L. Chazdon, *Science* **320**, 1458 (2008).
2. O. Venter *et al.*, *Science* **326**, 1368 (2009).
3. D. Edwards *et al.*, *Conserv. Lett.* **3**, 313 (2010).
4. P. S. Ashton, *Annu. Rev. Ecol. Syst.* **19**, 347 (1988).
5. D. Z. Li, H. W. Pritchard, *Trends Plant Sci.* **14**, 614 (2009).
6. C. J. Kettle, *Biodivers. Conserv.* **19**, 1137 (2010).

Asian Water Towers: More on Monsoons

W. W. IMMERZEEL *ET AL*. ("CLIMATE CHANGE will affect the Asian water towers," Reports, 11 June, p. 1382) overlooked two features of monsoon influence on the future of Asian water resources: Regional climate models disagree on whether monsoon precipitation will increase or decrease in the 21st century, and the resulting changes in precipitation seasonality will affect snowmelt characteristics.

Using data from five global general circulation models (GCMs), Immerzeel *et al*. conclude that a rise in precipitation will partly or entirely offset the reduction in glacial meltwater. Monsoon precipitation, however, is known to be difficult to capture in GCMs (*1*).

Because of their higher horizontal resolution, regional climate models can better represent the important effects on precipitation of moist air climbing over the mountains in the Himalaya region. Experiments in which the regional climate models based on the IPCC Special Report on Emissions Scenarios are used disagree on whether monsoon precipitation will rise or fall (*2*, *3*). The reliability of an impact study built on the sole

CREDIT: CAMPBELL WEBB

assumption of rising monsoon precipitation thus seems questionable.

Immerzeel *et al*. argue that their basin-scale approach justifies the assumption of a constant linear relationship between positive daily mean temperatures and melt, because characteristics of different glaciers would equal out. However, this does not apply if important features of the melt process change over time. It has been shown that changes in precipitation seasonality, such as a late beginning of the monsoon season, strongly affect the surface albedo and thus snow and ice melt on Himalaya glaciers (*4*).

Lower surface albedos caused by a lack in summer snowfall would lead to higher melt rates for the same temperature scenarios. Immerzeel *et al*.'s use of a constant degree-day factor for the calculation of future glacier extent thus risks a severe underestimation of glacier retreat.

FELIX PITHAN

Matzenbergstrasse 99, 46145 Oberhausen, Germany. E-mail: felix.pithan@gmx.net

References

1. I. Kang *et al*., *Clim. Dyn*. **19**, 383 (2002).
2. R. Kumar *et al*., *Curr. Sci*. **90**, 334 (2006).
3. M. Ashfaq *et al*., *Geophys. Res. Lett*. **36**, 1704 (2009).
4. K. Fujita, Y. Ageta, *J. Glaciol*. **46**, 244 (2000).

Response

PITHAN RAISES TWO VALID CONCERNS. WE agree that future precipitation is highly uncertain and that general circulation models (GCMs) have difficulty in capturing monsoon precipitation (*1*, *2*), and we stress that in our Report. For all five of the river basins we analyzed, the multimodel average (MMA) of future precipitation shows limited changes both in total quantity and temporal shifts. The Yellow river basin is an exception, and the MMA shows a positive offset in total winter precipitation. However, there is considerable variation between the different GCMs. Therefore, we do not conclude that a reduction in melt water is offset by an increase in precipitation, but by an increase in rainfall. Given the projected increase in temperature, which is less uncertain than precipitation projections, more precipitation will fall in the form of rain. Because the melt season coincides with the rain season in most regions, this compensates the reduced melt.

Pithan disagrees with our use of a constant degree-day factor. His argument pertains to the spatial variation in melt rates within a basin. We agree in principle that this would be an important factor to consider in projections, and we did not consider it explicitly, due to lack of information about local albedo trends. However, we did implicitly account for uncertainty about the degree-day factor by using an uncertainty analysis around snow and ice degree-day factors (described in the supporting online material of our Report). The case for which melt rates would be higher because of lower albedo would be in the higher regions of our uncertainty envelopes. Moreover, we point out that our extreme case (without any glaciers) results in similar conclusions as our best-guess case.

WALTER W. IMMERZEEL[1,2]* AND MARC F. P. BIERKENS[2,3]

[1]FutureWater, Costerweg 1G, 6702 AA Wageningen, Netherlands. [2]Department of Physical Geography, Utrecht University, Utrecht, Netherlands. [3]Deltares, 3508 TC Utrecht, Netherlands.

*To whom correspondence should be addressed. E-mail: w.immerzeel@futurewater.nl

References

1. H. Annamalai, K. Hamilton, K. R. Sperber, *J. Clim*. **20**, 1071 (2007).
2. S. Yang *et al*., *J. Clim*. **21**, 3755 (2008).

Letters to the Editor

Letters (~300 words) discuss material published in *Science* in the previous 3 months or issues of general interest. They can be submitted through the Web (www.submit2science.org) or by regular mail (1200 New York Ave., NW, Washington, DC 20005, USA). Letters are not acknowledged upon receipt, nor are authors generally consulted before publication. Whether published in full or in part, letters are subject to editing for clarity and space.

The Best Test of Ph.D. Student Success

IN THEIR EDUCATION FORUM "PERFORMANCE-based data in the study of STEM Ph.D. education" (16 July, p. 282), D. F. Feldon, M. A. Maher, and B. E. Timmerman suggest that graduate education could be improved by the implementation of performance-based assessments. They do not acknowledge that a performance-based system already exists in graduate work: quality (not quantity) of publications. Feldon, Maher, and Timmerman downplay publication as an indicator of student performance because of the involvement of mentors and peers, but input from multiple parties is a necessary and productive aspect of collaborative research. Collaboration benefits individual success and leads to innovation. Failing to recognize published work as a predictor of effectiveness as a researcher trivializes employers' ability to distinguish poor research from quality research, and by extension, the graduate student's ability to conduct research and collaborate effectively.

Adding standardized testing to the graduate curriculum neither benefits research nor serves as an accurate indicator of an individual's problem-solving ability. Recently, Hazari *et al*. (*1*) found that being "learning-oriented" rather than "performance-oriented" predicted success at the graduate level. This research implies that—if assessments were added to the curriculum (a move I discourage)—assessments of student interest in learning would be a better indicator of program effectiveness than the performance-based assessments advocated by Feldon, Maher, and Timmerman.

GUNNAR NEWQUIST

Department of Biology, University of Nevada, Reno, Reno, NV 89557, USA. E-mail: newquist280@gmail.com

Reference

1. Z. Hazari, G. Potvin, R. Tai, J. Almarode, *Phys. Rev. Spec. Top. Phys. Educ. Res*. **6**, 010107 (2010).

Response

NEWQUIST SUGGESTS THAT STUDENTS' PUBlications are important predictors of post-degree research effectiveness, due in part to the importance of collaboration in innovative research. We agree that publication record is important and helpful, but the collaborative aspects of writing render publications a noisy metric by which to assess individual growth on specific skills (*1*). The variable time lags between the execution of an experiment, analysis of its data, and publication of findings [e.g., (*2*)] further limit the ability to identify direct relationships between experiences in a doctoral program and scholarly growth. Doctoral education's overarching goal is to develop competent researchers capable of performing independent research (*3*–*6*). To determine how effectively doctoral programs—and specific features of those programs—prepare individual students for independent scholarship, we suggest the implementation of measures reflecting individual growth in requisite skill sets identified by a discipline [e.g., (*7*)].

Newquist also infers that we advocate some form of standardized testing. This is not the case. The mechanism we do suggest, the rubric, represents a performance-based assessment that faculty at the program or department level can tailor to evaluate localized, authentic student research products (*8*, *9*). Rubrics may also be useful in conceptualizing and operationally defining necessary competencies that represent the consensus of a larger field or discipline at the local level. Far from constraining research creativity or inhibiting problem-solving in graduate students, an effective rubric makes transparent a faculty's expectations of excellence in research. This can help students to align the products of their innovative work with the quality indicators valued by faculty and the larger field to which they wish to contribute.

Newquist then cites findings from a recent study (*10*) that identifies a correlation between doctoral students' goal orientations ("learning-oriented" or "performance-oriented") and their subsequent professional productivity as measured by grants and publications. The definition of "performance-orientation" in this study refers to their indication on a survey that their sole motivation for attending graduate school was either having "received good grades in science" previously or being "awarded [a] scholarship or fellowship." In contrast, those classified as having a "learning-orientation" indicated a sole motivation of "enjoyed thinking about science." These results do not conflict with our position. Certainly, someone who is driven by an inherent interest in scientific inquiry will be more motivated to acquire necessary skills at the Ph.D. level and find productive research opportunities. We merely suggest that assessing those skills in a manner able to meaningfully inform the improvement of doctoral education requires measures that are well defined through faculty consensus, suitable for identifying longitudinal growth, and precisely targeted to measure students as individual learners.

DAVID F. FELDON,[1]*
BRIANA CROTWELL TIMMERMAN,[2]
MICHELLE MAHER[3]

[1]Department of Curriculum, Instruction, and Special Education, University of Virginia, Charlottesville, VA 22904–4261, USA. [2]South Carolina Honors College, University of South Carolina, Columbia, SC 29208, USA. [3]Educational Leadership and Policies, University of South Carolina, Columbia, SC 29208, USA.

*To whom correspondence should be addressed. E-mail: dff2j@virginia.edu

References and Notes

1. P. D. Isaac, S. V. Quinlan, M. M. Walker, *J. Higher Educ.* **63**, 241 (1992).
2. J. Ioannidis, *JAMA* **279**, 281 (1998).
3. Association of American Universities, *Committee on Graduate Education Report and Recommendations* (AAU, Washington, DC, 1998).
4. Committee of Vice-Chancellors and Principles, *The British PhD* (CVCP, London, 1988).
5. B. E. Lovitts, *Stud. Higher Educ.* **30**, 137 (2005).
6. C. Pole, *Res. Pap. Educ.* **15**, 95 (2000).
7. J. H. Nagel, D. W. Slaaf, J. Barbenel, *IEEE Eng. Med. Biol. Mag.* **26**, 18 (2007).
8. B. Lovitts, *Making the Implicit Explicit: Creating Performance Expectations for the Dissertation* (Stylus, Sterling, VA, 2007).
9. B. E. Timmerman, D. C. Strickland, R. L. Johnson, J. R. Payne, *Assess. Eval. High. Educ.*, in press (available 10.1080/02602930903540991).
10. Z. Hazari, G. Potvin, R. Tai, J. Almarode, *Phys. Rev. Spec. Top. Phys. Educ. Res.* **6**, 010107 (2010).
11. This work is supported by a grant from the NSF to the authors (NSF-0723686). The views expressed do not necessarily represent the views of the supporting funding agency.

Published by AAAS

QUANTUM PHYSICS

Exploiting Entanglement

Jeremy L. O'Brien

Dance of the Photons
From Einstein to Quantum Teleportation
by Anton Zeilinger
Farrar, Straus, and Giroux, New York, 2010. 313 pp. $26. ISBN 9780374239664.

Ever since the inception of the theory of quantum mechanics at the start of the previous century, debate has raged about how to interpret what the theory tells us about the fundamental workings of nature. For example, what is the origin for the seemingly impossible correlations between two entangled particles? What happens to a quantum particle in a superposition of two locations during a measurement of that location? The debates have often impinged on philosophy and religion. Einstein famously objected to the inherent randomness of the theory, remarking that "God does not play dice." He nevertheless made great contributions to our understanding of quantum physics (perhaps most notably through his questioning of the completeness of quantum mechanics), contributions that highlighted the strangeness of entanglement. Despite such intense questioning of the interpretation of quantum mechanics, its utility is beyond doubt: its predictive power is unmatched by any other scientific theory.

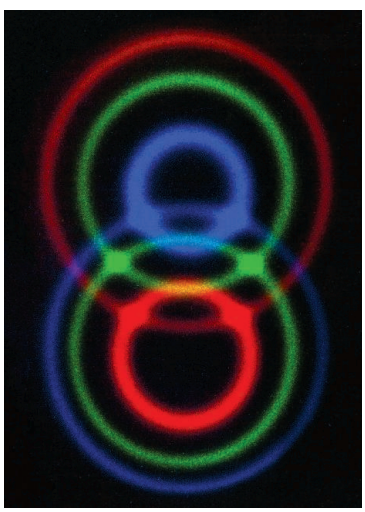

Anton Zeilinger's *Dance of the Photons* begins in a tunnel underneath the Danube. There, scientists are harnessing the strange quantum properties of superposition and entanglement for something useful—secure communication via the transmission of single particles of light (photons) in optical fibers running through the tunnel. The security comes from the fact that encoding information in a quantum system enables two legitimate parties, typically designated Alice and Bob, to detect the presence of an eavesdropper because any information the latter gains necessarily results in a detectable disturbance of the quantum system. And so we begin an exploration of this fascinating scientific field that lays the foundations for technologies designed specifically to employ quantum effects to gain new functionality and power in information processing, communication, and measurement.

Early in the book, Zeilinger (a physicist at the University of Vienna) introduces his Alice and Bob—two undergraduate physics students. Wanting to know more about quantum mechanics than Physics 1.01 has taught them, they approach Professor Quantinger (the author's fictionalized alter ego). Rather than recommending a few books, he gets them involved in an experiment set up by one of his graduate students. Working in separate labs connected by optical fibers to a source of (what they later learn are) pairs of entangled photons, they observe firsthand the bizarre "nonclassical" correlations. This narrative style gets the reader involved and excited to learn more. As Alice and Bob experience the strangeness of quantum physics firsthand, the reader feels like they are there with them as they work in the lab, attend lectures, and have informal conversations with the professor and his graduate student. Interleaved with this narrative are sections in Zeilinger's own voice, which work extremely well to complete the story.

Alice and Bob discover that when they each measure the polarization (the horizontal, vertical, etc. direction of the electric field) of their photon from an entangled pair, the correlations they see cannot be explained by any "classical" physics theory. More precisely, these correlations violate local realism. [This was what was bothering Einstein in the 1935 "EPR" paper, "Can quantum-mechanical description of physical reality be considered complete?" (*1*)] Zeilinger comments, "Some of the predictions of quantum physics question central cherished aspects of our view of the world." But "people were happy that quantum mechanics gave such an exact description of nature, and they were busy applying it to all kinds of phenomena." But this all changed dramatically in 1964, when Irish physicist John Bell "showed that it is not possible to understand the phenomenon of entangled systems if one starts from rather 'reasonable' assumptions of how the world should work, assumptions that one might even be tempted to call self-evident." Zeilinger asserts that Aristotle could have derived "Bell's inequality" had he known that it was an interesting problem.

As Zeilinger notes, when French physicist Alain Aspect thought about testing these ideas, Bell's first question was "Do you have a permanent position?" Only after Aspect's affirmative answer did Bell encourage him to carry out the experiment. Confirmation of Bell's ideas by Aspect, Philippe Grangier, and others forces us to abandon at least one of these cherished views. Whereas most physicists hold that quantum mechanics is nonlocal (the "spooky" property that Einstein objected to), Zeilinger argues that it is just as logical to "give up the picture of a world that exists in all its properties independent of us." Either way, nature is far stranger than we typically assume. Remarkably, John Clauser, who teamed with Stuart Freedman to carry out the earliest tests of Bell's inequality, expected that the inequality would not be violated. He didn't consider it at all possible "that the world could be so crazy that local realism could be wrong."

In recent years, some researchers have put aside philosophical concerns to explore the possibilities of technologies that take advantage of quantum features such as entanglement. Perhaps one of the most surprising and powerful of such applications is quantum teleportation. By making a joint entangling measurement of a photon in an unknown state and one of two photons in an entangled state, it is possible to teleport the unknown state to the third photon in the entangled state. Zeilinger and co-workers carried out the original experiment in 1997, and they have continued to push the distance over which such experiments are performed.

Zeilinger concludes by highlighting the path to quantum technologies: the fundamental curiosity of Einstein and others, the coincidence of the discovery of Bell's inequality with the invention of the laser, and finally, beginning in the 1990s and still unfolding, the ideas about new ways to transmit and process information. In a broad perspective, he notes, "all teleportation experiments are part of a research program to realize quantum computers." Of the various approaches to developing

The reviewer is at the Centre for Quantum Photonics and the Department of Electrical and Electronic Engineering, University of Bristol, Bristol BS8 1UB, UK. E-mail: Jeremy.OBrien@bristol.ac.uk

CREDIT: ANTON ZEILINGER/COURTESY FARRAR, STRAUS, AND GIROUX

such a device (*2*), using photons as quantum bits (or qubits) is particularly promising (*3*): "[I]n principle, it should be possible to build future quantum computers that are based on photons, that is, quantum light only," and there are great prospects for doing this in a silicon chip (*4*–*6*).

Those seeking an accessible popular account of this fascinating field will find their search over. No one has thought longer or harder about the fundamental science and practical applications of superposition and entanglement than Zeilinger. It is clear that he has also thought long and hard about how to give lucid and entertaining expositions of these challenging concepts. Readers should not be fooled by the simple cartoon diagrams. They reflect the beauty of *Dance of the Photons*: Taking some of the most complex ideas from cutting-edge science, Zeilinger provides simple and clear explanations that in no way compromise the fundamental concepts.

References

1. A. Einstein, B. Podolsky, N. Rosen, *Phys. Rev.* **47**, 777 (1935).
2. T. D. Ladd et al., *Nature* **464**, 45 (2010).
3. J. L. O'Brien, *Science* **318**, 1567 (2007).
4. A. Politi, M. J. Cryan, J. G. Rarity, S. Yu, J. L. O'Brien, *Science* **320**, 646 (2008).
5. A. Politi, J. C. Matthews, J. L. O'Brien, *Science* **325**, 1221 (2009).
6. A. Peruzzo et al., *Science* **329**, 1500 (2010).

10.1126/science.1196975

NEUROPHILOSOPHY

Unbounding the Mind

Erik Myin

Where is the mind? "In the head" or "in the brain," most people might respond. The philosopher Gilbert Ryle gave a different answer:

> The statement "the mind is in its own place," as theorists might construe it, is not true, for the mind is not even a metaphorical "place." On the contrary, the chessboard, the platform, the scholar's desk, the judge's bench, the lorry, the driver's seat, the studio and the football field are among its places. (*1*)

Recently, this idea of the mind not being confined to the head has been reinvigorated by philosophers and cognitive scientists, who see the mind as "spreading out" or "extending" into the world. "How do you know the way to San José?" philosopher John Haugeland has famously asked (*2*). Chances are you don't have some inner analog of a printed map. Rather, you know where you should enter the highway, and then you get there by following the road signs. Your knowledge seems to be partially "implemented" in the environment. There is now a blooming field of research into "situation cognition," which explores how cognitive or mental phenomena such as problem solving or remembering can be strongly dependent on interactions between subjects and their environments.

The Extended Mind
Richard Menary, Ed.
MIT Press, Cambridge, MA, 2010. 390 pp. $40, £29.95. ISBN 9780262014038.

The possible far-reaching implications of a situated view of cognition were brought into sharp focus by Andy Clark and David Chalmers in their 1998 paper "The extended mind" (*3*). There they defend the idea that the mind "extends" into the environment in cases in which a human organism and the environment become cognitively coupled systems. Their by now iconic illustration of cognitive coupling involves "Otto," a "slightly amnesic" person, who uses a notebook to write down important facts that he is otherwise likely to forget. Unlike a person who remembers the address of the Museum of Modern Art by relying on natural memory, Otto recalls it by accessing his notebook. If one supposes that the notebook is constantly available to Otto and that what is written in it is endorsed by Otto, it becomes plausible—so Clark and Chalmers argue—that Otto's memory extends to include the notebook. After all, they notice, Otto's notes seem to play exactly the same role as memory traces in other people. Wouldn't it be chauvinistic to restrict the mind's extent to what's natural and inner?

Clark and Chalmers's paper has triggered a vigorous and continuing debate. Nonbelievers concede that numerous tight causal couplings between minds and environments exist, but they deny that it therefore makes sense to speak of an extended mind instead of a mind

The reviewer is at the Centre for Philosophical Psychology, Department of Philosophy, University of Antwerp, 2000 Antwerpen, Belgium. E-mail: erik.myin@ua.ac.be

in a person that closely interacts with an environment. All things considered, they argue, thoughts remain in persons—never in objects like notebooks, however closely dependent a person could become on them.

Enthusiasts for the extended mind thesis insist that a close causal coupling between persons and environments can license the conclusion that the mind spreads into the environment. Some follow the argument in Clark and Chalmers that infers extendedness from the fact that external elements can play a role that would be considered as cognitive if played by something internal to a person.

Other supporters of the idea are suspicious of this argument from parity. They note that the most interesting cases of causal coupling are those in which the environment does not simply function as some ersatz internal milieu—when the involvement of external means makes possible forms of cognition that were not possible without them. For example, when pen and paper, symbolic systems, or computers make possible calculations, computations, and, ultimately, scientific theories. Those taking this position hold that it is when the environment becomes a necessary factor in enabling novel cognitive processes that the mind extends.

In *The Extended Mind*, philosopher Richard Menary (University of Wollongong) brings together the Clark and Chalmers paper and several responses to it. The collection, lucidly introduced by Menary, will neither definitively prove nor deal the deathblow to the idea that "the place of the mind" is the world—nor even establish that there really is such a question about "the place of the mind" that needs to be answered. Rather, the volume provides carefully drawn arguments for and against different interpretations of the extended mind thesis, often with extensive reference to empirical material. Several of the papers in the collection are excellent.

To take one fascinating idea, consider Susan Hurley on "variable neural correlates." We are comfortable with the correlation between types of experience and types of brain states, and undoubtedly such variation is one important source for the idea that the mind is in the head. Hurley notes, however, that there is also a dependence of experience on type of interaction with the environment, one not aligned to strictly neural properties. For example, when blind people haptically read Braille text, activity in the visual cortex seems to correlate with tactile experience. In people who are not blind, tactile experience correlates with activity in the tactile cortex. What explains the common enabling of tactile experience by the different kinds of cortex seems to be tactile causal coupling with the environment, rather than strictly neural type. According to Hurley, and others, the same kind of correlation-tracking reasoning that convinces us, in standard cases, that the mind is in the brain should here lead to the conclusion that the mind is not in the head.

References

1. G. Ryle, *The Concept of Mind* (Hutchinson, London, 1949).
2. J. Haugeland, *Having Thought: Essays in the Metaphysics of Mind* (Harvard Univ. Press, Cambridge, MA, 1998).
3. A. Clark, D. J. Chalmers, *Analysis* **58**, 7 (1998).

10.1126/science.1197367

EXHIBITION

Six-Legged Fun

Insectos em Ordem [Insects in Order]
Patrícia Garcia Pereira and Eva Monteiro, Curators
National Museum of Natural History and Centre for Environmental Biology, University of Lisbon. At the Old Riding School of the College of Nobles, the Polytechnical Museums. Through 28 November 2010. http://bioeventos2010.ul.pt/bioevento/expo_insectosemordem.html

Insects, the most diverse class of organisms on Earth, have a profound impact on our lives. We recognize the value of many—bees, for example, pollinate flowers and crops and provide us with food. Many other insects, however, are considered (deservedly or not) pests to be repelled or destroyed. To dispel myths, Lisbon's National Museum of Natural History invites visitors to explore the diversity and characteristics of Portuguese insects. One of the celebrations of the International Year of Biodiversity, the exhibition "Insects in Order" sets an irresistible challenge for children and adults alike: to become an entomologist for an hour by identifying insects according to their taxonomic order.

At the entrance, visitors are given an insect preserved in a resin block. The specimen may be any one of more than 100 species (from 16 orders). Insects, which represent more than half the known species of extant organisms, are hexapod (six-legged) arthropods. The class is divided into about 30 different orders. For example, beetles, the most diverse group of insects, are classified as Coleoptera. They have two pairs of wings. Their forewings are hardened and used not for flight but for abdominal protection—hence the order's name, which means sheathed wing. In contrast, adults of the order Neuroptera (which includes lacewings, mantidflies, owlflies, and antlions) have two pairs of membranous wings with a fine network of veins.

Neuropteran from Portugal. The striking thread-winged lacewing (*Nemoptera bipennis*).

To begin to classify their specimen, visitors must first carefully examine it and determine whether it has "delicate and membranous forewings with clearly visible veins" or "strong and hard forewings with no visible veins." Their choice leads them to enter the main exhibition room through one of two doors. The layout of that large room, organized as a labyrinth, sets the task ahead. Visitors proceed along a series of benches (each with an embedded magnifying glass), where they are challenged to closely look at some aspect of the specimen and pick one of a pair of answers to particular questions: Does the insect have a pair of wings or two? Are there pincers at the end of the abdomen or not? Etc. Each answer guides one to the next bench, via a trail marked on the floor. The choices are not always clear-cut, but with persistence, some practice, and occasionally trial and error, visitors should be able to correctly classify their insect and arrive at an illustrated panel that offers a description of its order.

Without becoming overtly explicit, the exhibition leads visitors through the dichotomous key method traditionally used by scientists to identify organisms. The experience transmits the enjoyment and excitement of discovery in science. And it is fun to identify insects. I, for one, could not stop after one specimen and repeated the process again another four times. What are you waiting for?

–Maria Cruz

10.1126/science.1199047

RESEARCH FUNDING

Sustaining the Data and Bioresource Commons

Globalization of biomedical research requires sustained investment for databases and biorepositories.

Paul N. Schofield,[1,2]* Janan Eppig,[2] Eva Huala,[3] Martin Hrabe de Angelis,[4] Mark Harvey,[5] Duncan Davidson,[6] Tom Weaver,[7] Steve Brown,[8] Damian Smedley,[9] Nadia Rosenthal,[10] Klaus Schughart,[11] Vassilis Aidinis,[12] Glauco Tocchini-Valentini,[13] John M. Hancock[8]

Development of powerful, high-throughput technologies, together with globalization of scientific research, presents the biomedical research community with unprecedented challenges for the management, archiving, and distribution of data and bioresources (*1*). We need a social contract between funding agencies and the scientific community to accommodate "bottom-up" integration and "top-down" financing of databases and biorepositories on an international scale.

The biological commons is evolving away from a traditional differentiated structure to one in which origination, ownership, and distribution of data and materials are subsumed by the same community (*2*). Scientific progress depends on efficient and open sharing to generate maximum value (*3*–*5*). The traditional paradigm of sharing scientific data and results through the published literature is no longer effective where new technologies produce large volumes of diverse types of data and biological materials. Critical to the maintenance, distribution, and archiving of these data and materials, therefore, are stable public databases and repositories. Provision of public funding for these long-term repositories does not fall into the traditional model of science funding, yet financial support is vital if we are to maximally exploit the investment into experimental science. Although funding agencies may exhort their experimental investigators to develop a "dissemination plan" for the data and bioresources they develop, in reality, such requirements are often not fulfilled, and noncompliance has little or no consequence. This often means that funders are effectively washing their hands of responsibility for future accessibility and reuse of the data and bioresources whose generation they have financed. Instead, funding for data and bioresource repositories needs to be ring-fenced from hypothesis-driven research and supported sufficiently to ensure preservation and maintenance of its outputs.

The contents of the new generation of data and bioresources are continuously being enhanced and augmented by the community of user-producers. There is not a sequential phase of research, followed by storage and use. Databases need continually to revise their data models to accommodate new data types. The associated bioontologies and other informatics tools need to continue to be developed, maintained, and applied to data to standardize and maximize access, retrieval, and exploitation for discovery. Repositories also need to innovate and respond to emerging disruptive technologies. Consequently, any distinction between time-delimited research projects and long-term, relatively static infrastructures is being eroded. The traditional distinction between "infrastructure" and "research" is even less appropriate, presenting a challenge to those funders who continue to think in these terms. The additional value created by manual data curation and integration in databases like Mouse Genome Informatics (MGI) or the *Arabidopsis* Information Resource (TAIR) is enormous, yet this activity does not fall into the recognized domain of "research activity" for many agencies.

The scale of investment required across the life sciences may be estimated from current funding of large community databases and bioresources. For 2009, MGI's core activity funding was U.S.$6.3 million including overhead, and for TAIR was $1.6 million. Curation activities alone of EMAGE, the embryonic mouse in situ gene expression database (*6*) based in the United Kingdom, currently cost roughly $0.7 million per year. The range represented here reflects the scope, as well as amount and complexity, of data.

The amount of investment in databases worldwide is a disproportionately small fraction of overall research budgets. For example, as little as a 5% allocation of the U.S. National Institutes of Health spending of $20.9 billion that constituted research grant awards in 2009 (*7*) would provide $1 billion toward biological data resources and huge added value for the community. Although some large public databases have survived rounds of competitive renewal, others have failed, often as a result of funding policy decisions rather than poor projects. Among high-profile databases, the one with the most recent funding crisis

[1]Department of Physiology, Development and Neuroscience, University of Cambridge, Cambridge, CB2 3EG, UK. [2]The Jackson Laboratory, Bar Harbor, ME 04609, USA. [3]Carnegie Institution for Science, Stanford, CA 94305, USA. [4]Institute of Experimental Genetics, Helmholtz Zentrum München, D-85764, Munich, Germany. [5]Department of Sociology, University of Essex, Colchester, CO4 3SQ, UK. [6]Medical Research Council (MRC), Human Genetics Unit, Western General Hospital, Edinburgh, EH4 2XU, UK. [7]MRC Mary Lyon Centre, Harwell, Didcot, Oxfordshire, OX11 0RD, UK. [8]MRC Harwell, Mammalian Genetics Unit, Oxfordshire, OX11 0RD, UK. [9]European Bioinformatics Institute, Hinxton, Cambridge, CB10 1SD, UK. [10]European Molecular Biology Laboratory, Monterotondo, I-00015, Rome, Italy. [11]Department of Infection Genetics, Helmholtz Centre for Infection Research, and University of Veterinary Medicine, Braunschweig, D-38124, Germany. [12]Biomedical Sciences Research Center Alexander Fleming, GR-16672, Vari, Athens, Greece. [13]Istituto di Biologia Cellulare, CNR, I-00015 Monterotondo Scalo (Rome), Italy.

*Author for correspondence. E-mail: ps@mole.bio.cam.ac.uk

Published by AAAS

is the *Arabidopsis* TAIR database (*8*), with other important databases, such as Eurexpress or Euregene, currently facing crises at the end of their existing funding cycles. Pressure will continue to grow as new community projects come to fruition and new data types (such as magnetic resonance images) without a dedicated public archive, need to be in the public domain.

Most biological stock centers have begun charging for products and services to meet their costs, but still require subsidy for long-term sustainability. For example, the annual operating costs of the European Mutant Mouse Archive network, including the repository and associated database (*9*), are €5 million (~U.S.$7 million), of which €2 million (U.S.$ 2.8 million) are provided by the European Commission. U.S. repositories receive NIH subsidies; for example, in 2009 the Knockout Mouse Project (KOMP) repository received $3.4 million and the Jackson Laboratory Mouse Mutant Resource received $1.5 million (*7*).

Various models for financial and scientific sustainability have been tried and discussed. "Recover costs from users" is a frequent exhortation from funding agencies. Experience shows that the viability of such strategies for databases is illusory (*10*). Public databases depend on the community's contributing freely to the commons, the quid pro quo being open and free access. No example of a successful fee-for-service model organism database exists.

In a recent online survey conducted by TAIR (*11*), users were strongly against the possibility of having to pay for access. Exclusion of investigators from access to data and resources, disadvantaging those most unable to pay (especially investigators in developing economies), was the primary reason cited. Second, data integration, increasingly an essential aspect of data sharing, would be crippled by the inability to integrate data between databases which did and did not charge for access. The seamless network of data (*12*) would be fragmented and disabled.

We have already seen bottom-up initiatives for data standardization and sharing on a global scale and acknowledgement of the importance of the commons (*3*–*5*, *13*). The challenges for funding agencies are those of coordination and strategy: how to adequately recognize the transnational nature of data and bioresources in funding instruments and how to sustainably fund core international resources when funding sources are likely to remain predominantly national.

An example of the advantages of international cooperation can be seen in the International Knockout Mouse Consortium (IKMC) (*14*), which is generating knockouts of protein-coding genes and distributing vectors, embryonic stem cells, and knockout mice. It involves centers in Europe, the United States, and Canada. International coordination has promoted efficiency and more rapid delivery of resources to investigators and has avoided duplication. Another is the International Nucleotide Sequence Database Collaboration, an action supported by the National Center for Biotechnology Information (NIH), European Molecular Biology Laboratory, and the Japanese National Institute of Genetics.

Funded nationally, required internationally, whose responsibility is it to fund future access to data and resources produced by projects such as the IKMC at the end of project funding? This generic problem is recognized by the European Council and Commission, which established the European Strategy Forum on Research Infrastructures (ESFRI) program (*15*, *16*), designed to identify strategic research road maps needed across the sciences and to build international organizations to coordinate and receive national funding. One of these projects, Infrafrontier (*17*), has as its goal the large-scale systematic phenotyping and archiving of mouse models to support not only the European, but also the international, biomedical research community. The success of this innovative program depends on the willingness of national agencies to support novel transnational organizations. Negotiations between the partners are under way, and Canada has recently joined the Infrafrontier project as the first full non-European partner.

We propose that national funding agencies should initiate infrastructure coordination programs, analogous to the European ESFRI process, from which support of internationally important databases and repositories might be sought. These funding opportunities should be restricted to data and bioresource-sharing infrastructures. The programs would implement the shared national research priorities of the agencies and would reflect strengths or needs in particular fields. This model already has fledgling examples. For example, in plant biology, the International Steering Committee on Plant Genomics (ISCPG) (*18*) includes representatives from funding agencies in Australia, Brazil, Canada, China, Japan, European Union, Consultative Group on International Agricultural Research, United States, and United Kingdom. The mission statement of the ISCPG could be taken as a model for international infrastructure coordination activity.

In this proposal, representatives of the national funding agencies and the scientific community would consult on research infrastructure priorities and needs in a particular area, and agencies whose policy priorities match those needs would cooperate on shared international funding calls. A stumbling block to universal participation in this model is that many national agencies are currently legally unable to provide funds to researchers in other countries. The adoption of a legal framework providing an international legal identity, such as the recently developed European Research Infrastructure Consortium (ERIC) (*19*) for internationally integrated projects, would solve this and could facilitate the mobilization of national funds.

International harmonization of data sharing and intellectual property policy could be both necessary and highly advantageous. Intellectual property right considerations can be addressed through negotiation and agreements between individual national funding organizations; these are now common and do not present insuperable problems. Interagency cooperation, for example on material transfer agreements, may accelerate the adoption of common policies to the great advantage of the scientific community.

References and Notes

1. F. S. Collins, *Science* **327**, 36 (2010).
2. M. Harvey, A. McMeekin, *Public or Private Economies of Knowledge* (Edward Elgar, Cheltenham, 2007).
3. Creative Commons, sciencecommons.org.
4. Toronto International Data Release Workshop Authors, *Nature* **461**, 168 (2009).
5. P. N. Schofield *et al.*, *Nature* **461**, 171 (2009).
6. EMAGE, www.emouseatlas.org/emage.
7. Research Portfolio Online Reporting Tools, report.nih.gov/.
8. A. Abbott, *Nature* **462**, 258 (2009).
9. P. Wilkinson *et al.*, *Nucleic Acids Res.* **38** (Database issue), D570 (2010).
10. C. Chandras *et al.*, *Database* **2009**, bap017 (2009) (Oxford).
11. Survey results, arabidopsis.org/doc/about/tair_survey/411.
12. R. W. Williams, *Front. Neurosci.* **3**, 154 (2009).
13. D. Field *et al.*, *Science* **326**, 234 (2009).
14. International Mouse Knockout Consortium, *Cell* **128**, 9 (2007).
15. I. W. Mattaj, *Nature* **465**, 1005 (2010).
16. ESFRI, ec.europa.eu/research/infrastructures/index_en.cfm?pg=esfri.
17. Infrafrontier, www.infrafrontier.eu/.
18. ISCPG, www.iscpg.com/index.htm.
19. Directorate-General for Research, *Legal Framework for a European Research Infrastructure Consortium (ERIC): Practical Guidelines* (European Commission, Brussels, 2010); ec.europa.eu/research/infrastructures/pdf/eric_en.pdf.
20. This Policy Forum is based on discussions at a meeting of the Coordination and Sustainability of International Mouse Informatics Resources (CASIMIR) consortium held 11 and 12 November 2009 in Rome and supported by the European Commission, contract no. LSHG-CT-2006-037811. A list of participants is available at *Science* Online.

Supporting Online Material

www.sciencemag.org/cgi/content/full/330/6004/592/DC1

10.1126/science.1191506

Published by AAAS

IMMUNOLOGY

Innate Lymphoid Cell Relations

A common progenitor cell gives rise to distinct lineages of innate lymphoid cells in the gastrointestinal tract.

Marc Veldhoen[1] and David R. Withers[2]

The immune response against invading pathogens involves many cell types, including rare immune cells whose roles are being teased out. These include the ambiguously named innate lymphoid cells (ILCs), which lack markers of mature lymphoid cells yet bear receptors commonly found on lymphoid progenitors. Their strategic position in the gastrointestinal tract and their capacity to secrete large amounts of immune response mediators (cytokines) make them a force to be reckoned with. But the diverse nature of the many ILC subtypes raises questions about their origin. On page 665 of this issue, Sawa *et al*. explore the developmental relationship of ILCs that express the transcription factor retinoic acid receptor–related orphan receptor γt (RORγt) (*1*) and report that distinct subsets do derive from a common precursor cell, but themselves do not give rise to further progenitors.

Adaptive immune responses initiate in highly organized lymphoid tissues where there is an increased chance for antigen-specific lymphoid cells to encounter antigen. These tissues include lymph nodes and gut-associated lymphoid tissue such as Peyer's patches, cryptopatches, and hundreds of solitary isolated lymphoid follicles (*2*). Lymphoid tissue inducer (LTi) cells and stromal organizer cells are crucial for the development of these lymphoid structures. LTi cells are a subtype of ILC. They derive from hematopoietic progenitor cells in the fetal liver, seed the developing lymphoid tissue during embryogenesis, and initiate the signals that recruit lymphocytes to these sites during development.

Throughout the length of the mammalian adult intestine, cells resembling embryonic LTi cells ("LTi-like" cells) are found mainly in cryptopatches and isolated lymphoid follicles (*3*). LTi-like cells (that express the nuclear receptor RORγt), cryptopatches, and lymph nodes can develop in the intestine in the absence of gut microbes (bacteria), whereas isolated lymphoid follicles form only after such colonization (*2*, *4*, *5*). These particular LTi-like cells support the production of antibodies by B cells and thus prevent bacteria from attaching to and damaging the epithelial cell lining of the intestine. A similar cluster of ILCs in the gut connective tissue also maintains B lymphocytes (*6*). Because these mesenteric ILCs produce large amounts of interleukin-5 (IL-5), IL-6, and IL-13 [cytokines also produced by effector T helper 2 (T_H2) cells], they resemble some of the ILCs found in the intestine (*7*, *8*). However, mesenteric ILCs are distinct from other ILCs because they do not rely on the transcription factor RORγt for development. Yet the colon contains other ILCs that express RORγt and secrete cytokines produced by T helper cells as well [such as interferon-γ (also produced by T_H1 cells) and IL-17 and IL-22 (also produced by T_H17 cells)] (*9*). Although these cytokine-secreting cells of the intestine are collectively called ILCs, their developmental relationship to each other has not been clear.

Within the adult small intestine, both LTi-like cells and a type of lymphocyte that is phenotypically similar to natural killer (NK) immune cells ("NK-like" cells), but lack cytotoxic function, express RORγt and secrete IL-22 (*5*, *10*, *11*). This suggested that these NK-like cells might be derived from LTi cells in the embryo. To investigate this possibility, Sawa *et al*. used an elegant cell fate–mapping approach in mice that can be kinetically controlled by the antibiotic doxycycline. Although the progeny of fetal precursor cells (that express RORγt) in the embryonic intestine have a uniformly LTi cell phenotype, Sawa *et al*. report that this rapidly changes after birth with the appearance of two other phenotypically distinct cell types, including the NK-like cells (the other subtype is not yet named) (see the figure). However, no precursor-progeny relationship among LTi-like cells, NK-like cells, or the third cell subtype (from either fetal liver or adult bone marrow) could be detected. A potential limitation of the cell fate–mapping approach used is that there is a lag time between the expression (and thus detection) of a reporter gene used to track cells and activation of the mechanism that turns on its expression (Cre-LoxP system). This may prevent identification of the earliest progenitor cells. However, the result was confirmed by other approaches including in vivo cell transfers, in vitro cultures of highly purified cells, and the targeted deletion

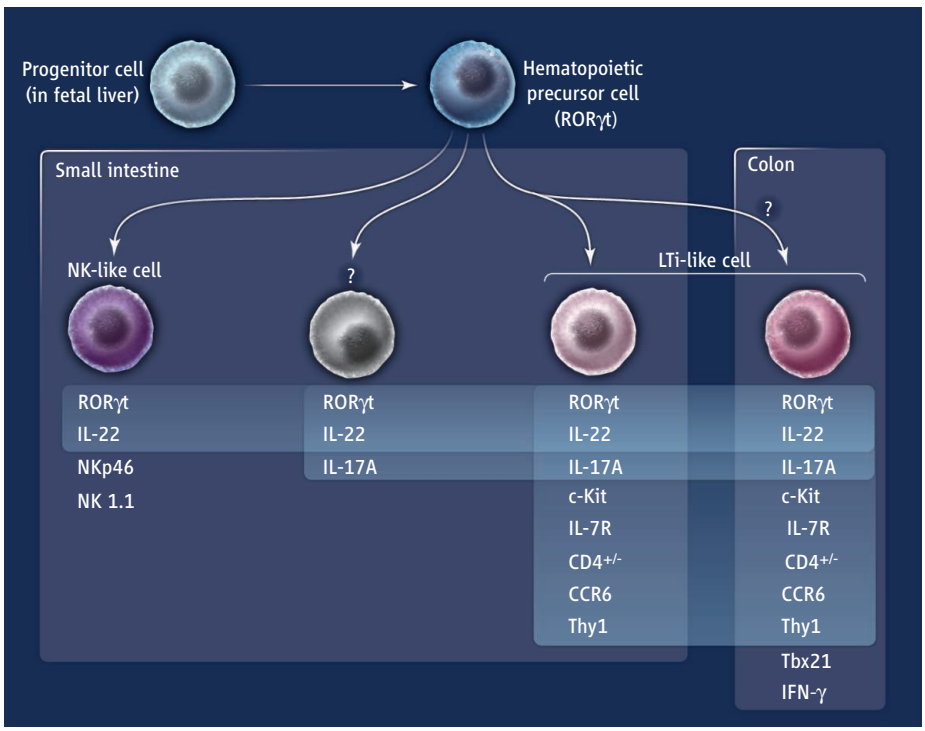

Lymphoid cell lineages. Innate lymphoid cells (that express the transcription factor RORγt) in the gastrointestinal tract display very different profiles. Some characteristic markers are shown. Three (perhaps four) distinct lineages appear to derive from a common progenitor. All secrete cytokines produced by T helper cells.

CREDIT: Y. HAMMOND/*SCIENCE*

[1]Laboratory of Lymphocyte Signalling and Development, Babraham Institute, Cambridge CB22 3AT, UK. [2]MRC Centre for Immune Regulation, Institute for Biomedical Research, Medical School, University of Birmingham, Birmingham B15 2TT, UK. E-mail: marc.veldhoen@bbsrc.ac.uk

Published by AAAS

of an LTi-like cell subset in mice. The result also agrees with the recent finding that development of mature NK and LTi cells, but not NK-like cells, depends on the transcription factor TOX (*12*).

Sawa *et al*. further show that RORγt expression in three progeny cell subtypes of the fetal hematopoietic precursor cell is very stable, so it is unlikely to give rise to ILCs that do not express this nuclear receptor. Likewise, ILCs that do not express this transcription factor do not seem to give rise to ILCs that express RORγt (*6*). However, a common progenitor population for all currently known ILCs does seem to exist in the mouse fetal liver and adult bone marrow. This population is currently defined only as a "classical" lymphoid progenitor cell (lineage expressing the cell surface proteins CD45, IL-7Rγ, c-Kit, and Sca-1) and the transcriptional regulator DNA-binding protein inhibitor 2 (ID2).

It is noteworthy that transcription factors such as RORγt, Gata3, and Tbx21, which regulate the differentiation of effector T lymphocytes (T_H17, T_H2, and T_H1, respectively), are also differentially expressed in ILCs. This suggests a division of labor among ILCs as seen with the effector T cells, with the potential to influence and skew adaptive immunity. The differential expression of cytokines by ILCs, together with their localization within tissues, may hold clues about their functions. The idea that different ILC populations (of the RORγt lineage) have different functions is supported by the finding that only populations with an LTi-like cell phenotype express the chemokine receptor CCR6, consistent with the requirement for LTi cells in the formation of isolated lymphoid follicles (*1*, *4*). This receptor may be instrumental in assembling LTi and stromal cells upon bacterial-induced expression of its ligand, CCL20 (*2*).

The NK-like cells lacking CCR6 are scattered within the connective tissue of the intestine (*5*). Their presence in the intestine only after birth indicates that their appearance may result from bacterial colonization of the gut. Surprisingly, Sawa *et al*. report similar numbers of NK-like cells in germ-free mice, suggesting a preprogrammed generation of these cells in preparation of the intestine for its impending bacterial colonization. However, this is at odds with another report showing that fewer NK-like cells are present in germ-free mice (*5*).

The identification of numerous immune cell types within the intestine demonstrates a previously unappreciated level of complexity among the non-B and non-T lymphocyte populations located there. The degree to which these different cell types share developmental relationships remains to be determined. Because at least some of the ILC family members also reside outside of the intestine, it is of particular interest to know how their local environment influences their function and how this affects adaptive immunity.

References

1. S. Sawa *et al*., *Science* **330**, 665 (2010); 10.1126/science.1194597.
2. M. Tsuji *et al*., *Immunity* **29**, 261 (2008).
3. G. Eberl *et al*., *Nat. Immunol.* **5**, 64 (2003).
4. D. Bouskra *et al*., *Nature* **456**, 507 (2008).
5. S. L. Sanos *et al*., *Nat. Immunol.* **10**, 83 (2008).
6. K. Moro *et al*., *Nature* **463**, 540 (2010).
7. D. R. Neill *et al*., *Nature* **464**, 1367 (2010).
8. S. A. Saenz *et al*., *Nature* **464**, 1362 (2010).
9. S. Buonocore *et al*., *Nature* **464**, 1371 (2010).
10. T. Cupedo *et al*., *Nat. Immunol.* **10**, 66 (2008).
11. C. Luci *et al*., *Nat. Immunol.* **10**, 75 (2008).
12. P. Aliahmad, B. de la Torre, J. Kaye, *Nat. Immunol.* **11**, 945 (2010).

10.1126/science.1198298

CHEMISTRY

Caging Carbon Dioxide

Christian Lastoskie

A better understanding of amine-CO_2 interactions may be pivotal in functionalizing novel adsorbents for carbon capture.

A transition to a portfolio of renewable energy, nuclear power, and biofuels may yet mitigate the perceived calamities of global climate change. In the meantime, the global abundance of accessible, inexpensive coal, combined with incessant pressure for economic growth among developed and developing nations, will ensure that present-day investments in fossil energy are not casually abandoned. Many more gigatons of carbon dioxide are thus slated for discharge into the atmosphere in the coming decades. Given this reality, technology advancements that address global climate change through carbon capture and sequestration (CCS) are equally important as innovations that spur the adoption of wind power, photovoltaics, and other generation assets with small carbon footprints. On page 650 of this issue, Vaidhyanathan *et al*. (*1*) report theoretical and experimental studies that impart a better understanding of a chemical interaction that appears central to improving CCS technology—the interaction of carbon dioxide with amine functional groups.

Aqueous amine solutions are the cheapest method currently available to remove CO_2 from combustion gas. In amine absorption, flue gas passes through a column containing a solvent such as monoethanolamine (MEA) that selectively absorbs CO_2. The CO_2-rich solution is then pumped to a tower where the temperature is raised, or the pressure lowered, to regenerate the solvent. CO_2 separation with MEA has been used in the chemical industry for more than 60 years (*2*), but it is not without problems. Recovery of CO_2 requires heating the MEA solvent to 100° to 120°C with process steam, imposing a parasitic demand on plant output; an 81% increase in the cost of electricity has been estimated for a medium-sized pulverized coal plant that uses MEA absorption to capture 90% of its flue gas CO_2 (*3*). Solvent disposal, water use, and corrosive interactions of oxygen and acidic components of combustion gas with absorber equipment pose additional environmental concerns.

Alternative methods to separate CO_2 from flue gas have therefore been suggested, including the use of physical adsorbents. Solid adsorbents could be particularly effective for CO_2 separation from synthesis gas, a mixture of hydrogen, carbon monoxide, and CO_2 formed by exposing coal to steam and controlled amounts of oxygen at elevated temperatures and pressures in integrated gasification combined-cycle configurations proposed for next-generation "clean coal" power plants. Conventional adsorbents such as activated carbons, however, have disappointingly low selectivity for CO_2 capture from combustion gases. This has spurred interest in porous coordination frameworks (PCFs) such as metal-organic frameworks (MOFs) for application to carbon capture. Many PCFs, including MOF-177 (zinc oxide-1,3,5-benzenetribenzoate) (*4*), have large CO_2 sorption capacities due to their high specific surface areas and low densities. Because MOF pore size and connectivity can be tuned by selection of the metal cluster and organic cross-link, a bewildering matrix of combinations confronts the nano-architect seeking to

Department of Civil and Environmental Engineering, University of Michigan, Ann Arbor, MI 48109, USA. E-mail: cmlasto@umich.edu

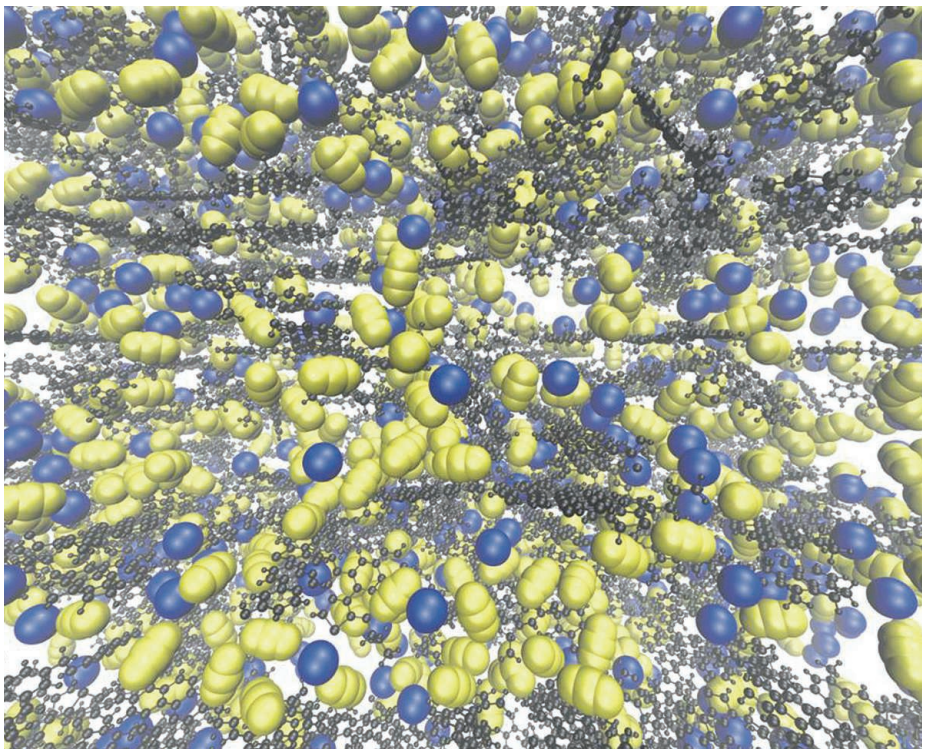

Get in there. Carbon dioxide adsorption in a model coal micropore, with displacement of methane, in a molecular simulation of enhanced coalbed methane recovery for geological CO_2 storage. CO_2 molecules are shown in yellow and methane molecules in blue. Similar atomistic modeling methods are used by Vaidhyanathan *et al*. to investigate carbon capture by amine-modified metal-organic framework adsorbents.

design a MOF optimally suited for CO_2 separation. Computational methods have thus been brought to bear on this problem to identify structure motifs in MOFs that better suit them for carbon capture, thereby reserving the time-consuming tasks of material synthesis and experimental verification for only the most promising candidates. Similar modeling strategies have been adopted to investigate carbon storage in complex, inaccessible, and chemically heterogeneous geological media such as saline aquifers and unmineable coal seams (see the figure).

A suite of scale-spanning computational methods have been used to this end, most notably grand canonical Monte Carlo (GCMC) atomistic simulations to obtain MOF sorption capacities and heats of adsorption, and quantum mechanical density functional theory (DFT) investigations of specific adsorption sites, binding energies, and interaction mechanisms (*5*). GCMC simulations require a force field to describe interactions of adsorbate molecules with each other and with the adsorbent. The most frequently used generic force fields were developed for simulations of organic or biological systems, and they often lack parameters for the new atom combinations encountered in MOFs. Nonbonded (*6*) or hybrid (*7*) force fields informed by first-principles calculations were thus recently introduced to represent, for example, the ZnO_4 metal cluster building block found in many MOF adsorbents.

Along these same lines, the GCMC simulations reported by Vaidhyanathan *et al*. use a force field for an amine-functionalized MOF [Zn_2(3-amino-1,2,4-triazole)$_2$ oxalate] with partial atomic charge parameters derived from periodic DFT calculations (*8*, *9*). The authors demonstrate exceptional agreement between predicted and experimentally determined physisorbed CO_2 positions in this MOF, allowing for analysis of the nature of the binding interaction with an unusually high level of detail. Interestingly, Vaidhyanathan *et al*. observe that appropriately oriented CO_2 molecules mutually enhance their binding by essentially the same amount as having an amine group protruding into the pore. So, although amine functionalization has been a common route to enhance CO_2 uptake (*10*–*12*), a strategically designed PCF that maximizes dispersion and electrostatic interactions between adsorbed CO_2 molecules through cooperative guest binding might achieve high CO_2 uptake with a much lower enthalpy penalty for CO_2 desorption than is incurred in more tightly bound CO_2-amine structures.

Some MOFs have a sufficiently high CO_2 capacity and a sufficiently low heat of adsorption to play a useful role in large-scale carbon capture (*13*). Nonetheless, much remains to be done to ascertain whether these materials fulfill their promise. In this regard, molecular modeling tools continue to play an important role in the screening and design of new MOF adsorbents, and in calculations of MOF properties not easily determined by experiment, such as CO_2 sorption selectivity from binary post-combustion gas mixtures of CO_2-N_2, CO_2-H_2, and CO_2-CH_4. Permeability selectivity for membrane-based CO_2 separation using MOFs or other porous materials can be calculated from Monte Carlo and molecular dynamics (MD) simulations (*14*). The features that give rise to gated CO_2 adsorption in elastic layered MOFs (*15*), and that yield isotherms exceptionally well suited for CO_2 capture and recovery using vacuum swing adsorption, can be examined by hybrid MD methods. Molecular modeling can help to answer the all-important question of whether MOFs maintain their structural integrity and function when subjected to the harsh environment of combustion gases, which contain moisture and acidic oxides (NO_x and SO_x) that can destabilize frameworks (*16*). Lastly, molecular simulations of model systems can provide helpful insights into CO_2 sorption and transport properties within media that are prospective geologic repositories for carbon storage, such as unmineable coal seams (*17*) and shale cap rocks (*18*).

References

1. R. Vaidhyanathan *et al*., *Science* **330**, 650 (2010).
2. D. Aaron, C. Tsouris, *Sep. Sci. Technol.* **40**, 321 (2005).
3. J. M. Klara, *Cost and Performance Baseline for Fossil Energy Plants* (DOE/NETL-2007/1281, National Energy Technology Laboratory, 2007; www.netl.doe.gov/energy-analyses/pubs/Bituminous%20Baseline_Final%20Report.pdf).
4. A. R. Millward, O. M. Yaghi, *J. Am. Chem. Soc.* **127**, 17998 (2005).
5. Z. Xiang, D. Cao, J. Lan, W. Wanga, D. P. Broom, *Energy Environ. Sci.* **3**, 1469 (2010).
6. J. A. Greathouse, M. D. Allendorf, *J. Phys. Chem. C* **112**, 5795 (2008).
7. D. Dubbeldam, K. S. Walton, D. E. Ellis, R. Q. Snurr, *Angew. Chem. Int. Ed.* **46**, 4496 (2007).
8. C. Campana, B. Mussard, T. K. Woo, *J. Chem. Theory Comput.* **5**, 2866 (2009).
9. D.-L. Chen, A. C. Stern, B. Space, J. K. Johnson, *J. Phys. Chem. A* **114**, 10225 (2010).
10. E. M. Mindrup, W. F. Schneider, *ChemSusChem* **3**, 931 (2010).
11. A. Torrisi, R. G. Bell, C. Mellot-Draznieks, *Cryst. Growth Des.* **10**, 2839 (2010).
12. W. Morris *et al*., *J. Am. Chem. Soc.* **132**, 11006 (2010).
13. S. Keskin, T. M. van Heest, D. S. Sholl, *ChemSusChem* **3**, 879 (2010).
14. R. Krishna, J. M. van Baten, *J. Membr. Sci.* **360**, 323 (2010).
15. H. Kanoh *et al*., *J. Coll. Interf. Sci.* **334**, 1 (2009).
16. A. O. Yazaydın *et al*., *Chem. Mater.* **21**, 1425 (2009).
17. C. M. Tenney, C. M. Lastoskie, *Environ. Prog.* **25**, 343 (2006).
18. D. R. Cole *et al*., *Philos. Mag.* **90**, 2339 (2010).

10.1126/science.1198066

CREDIT: CRAIG TENNEY AND CHRISTIAN LASTOSKIE

CELL BIOLOGY

Forced to Be Unequal

Stephan W. Grill

The distribution of a motor protein generates an unequal contractile force that controls the asymmetric division of eukaryotic cells.

A prominent way for an organism to develop many different cell types is to have cells divide unequally, generating daughter cells that differ in composition and fate, and often also in size. The importance of this process, called asymmetric cell division, for the development of multicellular organisms is undisputed (*1*). On page 677 of this issue, Ou *et al*. (*2*) describe a mechanism for generating unequal-sized daughter cells that is based on contracting one cell half by the action of the cytoskeletal motor protein myosin.

Much of our understanding about asymmetric cell division comes from studying developing embryos of the nematode *Caenorhabditis elegans* and the developing nervous system of the fruit fly *Drosophila melanogaster* (*3*, *4*). Generally, a cell divides along an axis that is determined by the orientation of the mitotic spindle to ensure that this microtubule-based structure properly segregates chromosomes. The position of the spindle can thus determine the size of the resulting two daughter cells. When the mitotic spindle is positioned off center in a dividing cell, the constriction ring (or cleavage furrow) is usually redirected to bisect the eccentrically positioned spindle. This generates daughter cells of unequal size. Lopsided positioning can occur if extra force is exerted from one side of the dividing cell, pulling the spindle toward it (*5*). Other mechanisms that direct the position of the cleavage furrow involve signaling from the pathway that controls cell polarity, as recently observed in *Drosophila* neuroblasts (*6*). This includes a polarized distribution of myosin. Now, Ou *et al*. also report that the uneven distribution of nonmuscle myosin II in directing asymmetric division. Myosins comprise a large family of motor proteins that walk along cytoskeletal actin cables. As the motor protein moves along actin, it slides filaments along each other to generate a contractile force through cycles of ATP hydrolysis and conformational changes.

Ou *et al*. discovered that a cell of the Q neuroblast lineage in *C. elegans* divides asymmetrically because of the polarized activity of cortical myosin. During division, half of the neuroblast accumulates more cortical myosin (compared to the other half) and as a result, contracts due to the forces generated by these motor proteins. Using live cell imaging, the authors observed that in one member of the Q neuroblast lineage (called the QR.a cell), the cleavage furrow does not bisect the mitotic spindle right in its center, but rather in a slightly off-center position in the spindle (but still between the paired chromosomes).

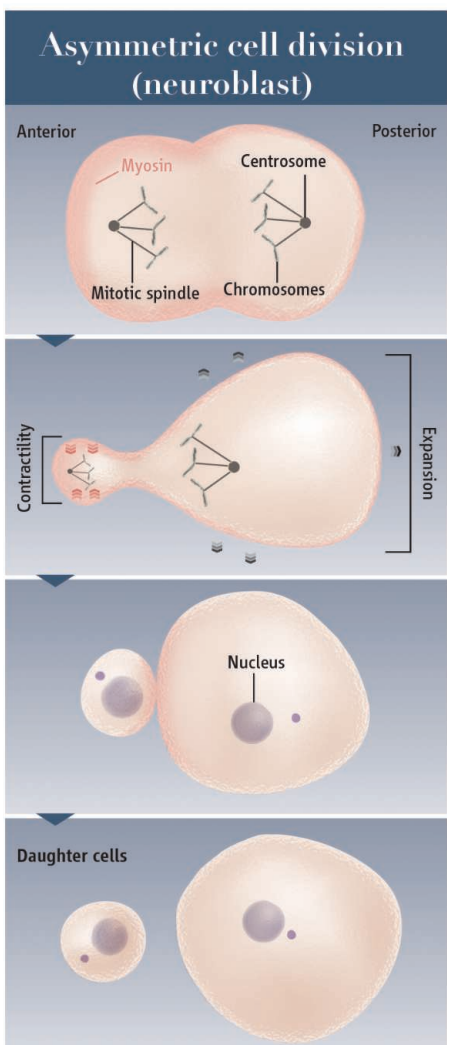

Putting on the squeeze. Asymmetric cell division occurs by having one (future) daughter cell contract more than the other, a process driven by myosin. Because the cytosol and cellular contents have to go somewhere, contraction of the anterior half of the dividing cell causes the expansion of the posterior half. This results in an unequal division.

CREDIT: N. KEVITIYAGALA/*SCIENCE*

Max Planck Institute for Molecular Cell Biology and Genetics and Max Planck Institute for the Physics of Complex Systems, Dresden 01307, Germany. E-mail grill@mpi-cbg.de

This is in addition to ecentric positioning of the spindle within the cell, similar to that seen in *Drosophila* neuroblast asymmetric division. Thus, a spindle-independent mechanism might control the asymmetric division in *C. elegans* neuroblasts.

Myosin is involved in several aspects of asymmetric cell division, most prominently in the establishment and maintenance of cellular polarity (*1*, *7*, *8*). Uneven distribution of myosin has been observed in asymmetric cell division (*6*, *7*, *9*), but only for extremely asymmetric meiotic divisions have they been made responsible for creating unequally sized daughter cells in a direct mechanical sense (*10*). Ou *et al*. observed that myosin is unevenly distributed in neuroblast daughter cells, with more myosin in the furrow region and within the smaller anterior daughter cell (see the figure). The authors propose that by causing the anterior half of the dividing neuroblast to contract more than the posterior half, myosin drives asymmetry in division. Indeed, the membrane of the posterior half of the dividing neuroblast appears to expand outward as the membrane of the anterior half shrinks, which is consistent with mechanical squeezing to drive asymmetry.

Perturbing the distribution and activity of myosin further confirmed that contraction at one end of the dividing cell underlies the asymmetry. This approach included chromophore-assisted laser inactivation (CALI) of myosin II (which was tagged with green fluorescent protein) to locally reduce myosin contractile activity (*11*). CALI of myosin in the anterior half of a dividing neuroblast not only diminished anterior contraction, but it resulted in a more symmetric cell division, which altered the fate of the anterior daughter cell (it avoided programmed cell death). By contrast, CALI of myosin at the posterior half of the dividing cell did not appreciably affect the ratio of daughter cell sizes that is normally observed.

Although much work on asymmetric cell division has focused on understanding how the mitotic spindle is positioned, Ou *et al*. reveal a simple mechanism that is entirely based on the differential regulation of actin-myosin (actomyosin) contractility. It will be interesting to see if asymmetric cell divisions in other cell types also use this mechanism. For example, the asymmetric distribution of

Published by AAAS

myosin in *Drosophila* neuroblasts (*6*) might function similarly to that in *C. elegans* neuroblasts, in addition to those mechanisms already known to control asymmetric division in these cells. It will also be important to examine the precise relationship between the mitotic spindle and actomyosin network (*12*, *13*) in the neuroblast (QR.a) cells. It may be that spindle-dependent mechanisms are acting in addition to the mechanical squeezing. Might biophysical measurements confirm that actomyosin-imparted cortical tension is different in the two halves of the dividing cell (*10*)? One might also expect a flow of cytosol through the constriction zone that accompanies the shrinking of the anterior daughter cell, and this flow could affect the position of the mitotic spindle. Understanding the biophysical implications of the findings in conjunction with the cell biological observations of asymmetric cell division will be an intriguing next step in understanding what drives this process.

References

1. J. Betschinger, J. A. Knoblich, *Curr. Biol.* **14**, R674 (2004).
2. G. Ou *et al.*, *Science* **330**, 677 (2010).
3. D. St Johnston, J. Ahringer, *Cell* **141**, 757 (2010).
4. P. Gönczy, *Nat. Rev. Mol. Cell Biol.* **9**, 355 (2008).
5. S. W. Grill, P. Gönczy, E. H. Stelzer, A. A. Hyman, *Nature* **409**, 630 (2001).
6. C. Cabernard, K. E. Prehoda, C. Q. Doe, *Nature* **467**, 91 (2010).
7. E. Munro, J. Nance, J. R. Priess, *Dev. Cell* **7**, 413 (2004).
8. M. Mayer, M. Depken, J. S. Bois, F. Jülicher, S. W. Grill, *Nature* **467**, 617 (2010).
9. C. S. Barros, C. B. Phelps, A. H. Brand, *Dev. Cell* **5**, 829 (2003).
10. S. M. Larson *et al.*, *Mol. Biol. Cell* **21**, 3182 (2010).
11. B. Monier, A. Pélissier-Monier, A. H. Brand, B. Sanson, *Nat. Cell Biol.* **12**, 60, 1 (2010).
12. C. Kozlowski, M. Srayko, F. Nedelec, *Cell* **129**, 499 (2007).
13. S. Redemann *et al.*, *PLoS ONE* **5**, e12301 (2010).

10.1126/science.1198343

STEM CELLS

Epigenome Disruptors

What can stem cells tell us about epigenetic perturbations?

Myriam Hemberger[1] and Roger Pedersen[2]

The "epigenome" comprises a range of modifications that are imposed on the genome (DNA) and ensure the stable transmission of gene expression patterns without changes to the DNA sequence. "Epigenetic disruptors" could change gene activity and in the case of stem cells, alter cell fate or number, causing, for example, an increased risk of cancer (*1*). "Epimutations" arising in this way may even pass through the germ line to the gametes, thereby affecting subsequent generations. Due to their inherent developmental plasticity, stem cells may be an ideal reporter system for epigenetic perturbations. This could be achieved by studying loci (such as imprinted genes) that undergo epigenetic alterations in normal development, and monitoring their response to potentially disruptive agents. Are such screens feasible, and would they provide a systematic and reproducible readout?

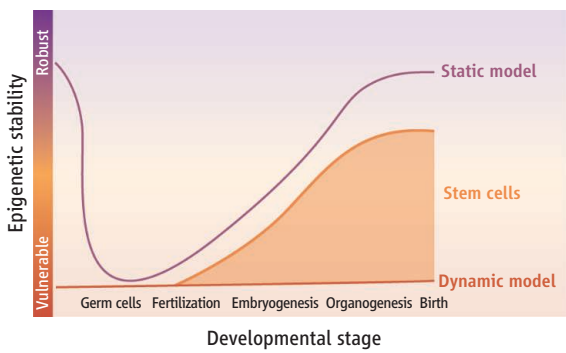

Epigenetic stability during development. In the conventional, static model, epigenetic stability is proportional to the amount of DNA methylation and histone modifications. In the dynamic model, the steady turnover of epigenetic modifications makes the epigenome persistently vulnerable. The contribution of stem cells to an organism's overall epigenetic vulnerability diminishes progressively with development as their proportion in tissues decreases. Vulnerability of individual stem cells could approach either the static or dynamic levels, depending on the actual state of their epigenome.

Early mammalian development (from fertilization) is characterized by progressive restriction of cellular plasticity and is accompanied by the acquisition of epigenetic modifications (such as DNA methylation). These impose a cellular memory that accompanies and enables stable differentiation. The unspecialized cells of the early (preimplantation) mouse embryo can give rise to "pluripotent" embryonic stem cells that exhibit the widest developmental potency and can colonize all tissues when combined with a mouse embryo to form a chimera. Epiblast stem cells derived from the postimplantation mouse embryo are also pluripotent but contribute poorly if at all to chimeras (*2*, *3*). Stem cells with progressively declining developmental plasticity can be derived from later embryonic stages or even the adult (such as neural and hematopoietic stem cells). In normal development, the epigenetically imposed restrictions to cellular plasticity are erased only in the germ line, where profound epigenetic reprogramming events lead to the formation of a new set of gametes (see the figure). However, fully differentiated cell types can be experimentally reprogrammed into induced pluripotent stem (iPS) cells by the temporary overexpression of key pluripotency factors. Human iPS cells hold therapeutic promise, as they are readily accessible from any individual (*4*).

Intense investigations of mouse and human pluripotent stem cells have established genome-wide profiles of DNA methylation, histone modifications, and DNA occupancy patterns of important chromatin-modifying enzymes (*5*). These analyses reveal fundamental epigenetic principles of pluripotency including hypomethylation of many gene promoters (versus hypermethylation in differentiated tissues) and a characteristic "bivalent" pattern of histone modifications that poise genes for activation at later stages.

However, pluripotency is inherently labile, and embryonic stem cells are epigenetically heterogeneous and dynamic. Perhaps as a consequence, they are prone to undergo epigenetic alterations during their derivation from early mouse embryos and in subsequent cell culture. Analysis of DNA methylation patterns reveals that they undergo extensive culture-induced alterations that persist throughout embryonic stem cell differentiation (*6*, *7*). DNA methylation is a key mediator of genomic imprinting, and perturbed expression of imprinted genes frequently accompanies epigenetic perturbations involving DNA methylation in mouse embryonic stem cells. However, human

[1]Laboratory for Developmental Genetics and Imprinting, The Babraham Institute, Babraham Research Campus, Cambridge CB22 3AT, UK. [2]The Anne McLaren Laboratory for Regenerative Medicine, University of Cambridge, Cambridge CB2 0SZ, UK. E-mail: myriam.hemberger@bbsrc.ac.uk

embryonic stem cells do not show the same vulnerability, possibly reflecting a more mature developmental state (*2*, *3*, *8*).

Recent findings shed some light on the mechanistic basis of this epigenetic vulnerability and may challenge the current view of DNA methylation as a stable epigenetic modification. DNA methylation appears subject to constant and dynamic turnover—for example, through conversion of 5-methyl cytosine into 5-hydroxymethyl cytosine—highlighting the possibility that DNA methylation patterns have to be actively maintained during each cell division cycle (*9*–*11*). In addition, individual embryonic stem cell lines (mouse and human) differ to some extent in their epigenome as well as in their precise differentiation potential (*7*, *12*). This variability is even more pronounced in iPS cells that exhibit some epigenetic memory, which biases their differentiation toward the cell type from which they were derived (*13*, *14*).

These issues raise several important questions that need to be addressed when considering stem cells as a screening tool of epigenetic disruptors. For example, what is the normal spectrum of epigenetic variability in stem cells, tissues, and organisms and how much of it is genetically determined (as opposed to environmentally induced)? And how can a baseline for normality be defined? Important progress on the fundamental characterization of stem cell and tissue type–specific DNA methylation patterns is anticipated from the Human Epigenome Project (HEP) and the High-throughput Epigenetic Regulatory Organisation In Chromatin (HEROIC) project (*15*, *16*). Another question concerns the choice of stem cell type for such screens. An ideal type should provide sufficient plasticity to monitor epigenetic changes without excessively high background fluctuation. Additionally, what sex of stem cells should be used? Male and female mouse embryonic stem cells can exhibit dramatic epigenomic differences (*17*), and sex differences also exist in the vulnerability to environmentally induced epigenetic changes. Further, which epigenetic modifications should be screened to deduce epigenetic perturbations, and on what scale? The known types of epigenetic modifications are still increasing, and their functional consequences for gene expression are still being established. Finally, it is necessary to determine when the cumulative acquisition of epigenetic changes becomes detrimental. Can a "point of no return" be defined when pathological outcomes become irreversible at the cellular, organismal, and transgenerational, levels?

Answers to these questions are instrumental for understanding the dynamics of the epigenome in stem cells, development, and aging. They are also integral to establishing meaningful stem cell models for screening chemicals and environmental compounds for epigenetic effects.

References

1. L. B. Hesson, M. P. Hitchins, R. L. Ward, *Curr. Opin. Genet. Dev.* **20**, 290 (2010).
2. I. G. Brons *et al.*, *Nature* **448**, 191 (2007).
3. P. J. Tesar *et al.*, *Nature* **448**, 196 (2007).
4. S. Yamanaka, *Cell Stem Cell* **7**, 1 (2010).
5. M. Hemberger, W. Dean, W. Reik, *Nat. Rev. Mol. Cell Biol.* **10**, 526 (2009).
6. W. Dean *et al.*, *Development* **125**, 2273 (1998).
7. C. Allegrucci *et al.*, *Hum. Mol. Genet.* **16**, 1253 (2007).
8. P. J. Rugg-Gunn, A. C. Ferguson-Smith, R. A. Pedersen, *Nat. Genet.* **37**, 585 (2005).
9. S. Kangaspeska *et al.*, *Nature* **452**, 112 (2008).
10. R. Métivier *et al.*, *Nature* **452**, 45 (2008).
11. M. Tahiliani *et al.*, *Science* **324**, 930 (2009).
12. O. Adewumi *et al.*, *Nat. Biotechnol.* **25**, 803 (2007).
13. K. Kim *et al.*, *Nature* **467**, 285 (2010).
14. J. M. Polo *et al.*, *Nat. Biotechnol.* **28**, 848 (2010).
15. F. Eckhardt *et al.*, *Nat. Genet.* **38**, 1378 (2006).
16. www.epigenome.org and www.heroic-ip.eu
17. I. Zvetkova *et al.*, *Nat. Genet.* **37**, 1274 (2005).

10.1126/science.1199006

CHEMISTRY

A Little Chemistry Helps the Big Get Bigger

The coarsening of small metal particles can be enhanced when metal atoms are transported between particles as part of larger complexes.

James W. Evans[1] and Patricia A. Thiel[2]

What is the common denominator between the geologic formation of gemstones, the degradation of pharmaceutical suspensions, and the manufacture of structural steels? They all can involve a process called coarsening, in which a group of objects of different sizes transforms into fewer objects with larger average size (*1*), such that "the big get bigger." The atoms that occupy boundary locations between different phases tend to be less energetically stable, and coarsening stabilizes the overall system by decreasing the number of such atoms. A fundamental scientific question in coarsening is identifying how the requisite transport of atoms occurs. New answers to this question are being revealed by studies of nanoscale particles that are grown on surfaces

In the case of gemstones, the end result of coarsening is easy to see, even though the process is not, because it occurs under extreme conditions of temperature and pressure over geological time scales. In the vast majority of cases, the objects that coarsen are microscopic and not readily discerned, but the ramifications can be clear. For example, in pharmaceutical suspensions, the effectiveness of an antibiotic may decrease from coarsening (coagulation), and the strength of a surgical tool made from hard martensitic steels can be reduced if tiny embedded particles coarsen during its fabrication. Alternatively, coarsening can be manipulated in such a way that it leads to a sharp, narrow distribution of particle sizes—an objective that is paramount in some nanotechnologies (*2*).

Since the mid-1990s, the scanning tunneling microscope (STM) has revealed a wealth of information about coarsening from studies of two-dimensional (2D) structures, or "islands," grown on single-crystal substrates (*3*, *4*). In the simplest of these systems, the islands are grown from the same material as the substrate (homoepitaxy). The classic mechanism for coarsening, Ostwald ripening (OR), was often observed in these studies. Discovered by Ostwald around 1900, in this mechanism, the particles are essentially immobile, but they exchange material by virtue of little "messengers" that constantly detach and reattach at their edges.

The default candidate for messengers on a metal surface would be single adsorbed metal atoms, or "adatoms" (*3*, *4*). The equilibrium vapor pressure of adatoms is higher at the periphery of smaller particles, which causes net transfer of mass from smaller to larger

[1]Department of Physics and Astronomy, Ames Laboratory–U.S. Department of Energy, Iowa State University, Ames, IA 50011–3020, USA. [2]Department of Chemistry, Ames Laboratory–U.S. Department of Energy, Iowa State University, Ames, IA 50011–3020, USA. E-mail: evans@ameslab.gov; thiel@ameslab.gov

particles. Lifshitz-Slyozov-Wagner (LSW) theory quantifying OR was developed around 1960 (*1*). Subsequently, coarsening dynamics for OR has been explored within the statistical physics community in many simulation studies of generic models (*5*).

However, another coarsening mechanism was also observed in the STM studies wherein the particles themselves can move, collide, and combine via coalescence (*3*, *4*). This process is now referred to as Smoluchowski ripening (SR) after Smoluchowski's coagulation equations. SR was rarely discussed in earlier statistical physics studies, but recent modeling has recognized the importance of a realistic treatment of kinetics in describing particle diffusion and nanostructure reshaping and in controlling the competition between OR and SR (*4*). Actually, this competition was also recognized long ago in studies of the degradation of metal catalyst nanoclusters on oxide surfaces (*6*).

The above paradigms usually explain coarsening of homoepitaxial islands either for single-element materials, such as silicon (*7*) and silver (*3*, *4*), or for compound materials, such as titanium nitride (*8*). However, refinements are needed to account for anisotropy (e.g., in surface diffusion), strain for growth of one material on another (heteroepitaxy), and other complexities. The situation is even more complicated for nanostructures in operating environments where they are exposed to "additives," such as oxygen or sulfur (S). In these cases, dramatic enhancements of coarsening have been observed.

What is the nature of the enhancement mechanism and of the messengers when additives alter OR-mediated coarsening? One possibility, suggested long ago for sulfur-enhanced transport of Ag, is that diffusion of a single-atom messenger is enhanced on additive-covered terraces (*9*). A more interesting possibility is that the messenger itself changes, in the presence of additives, into a metal-additive complex or cluster (see the figure). We focus on the latter scenario, but why would enhancement occur in the first place? For OR, three key factors affect the overall coarsening rate, namely the mobility of the messenger; the population of messenger on the terraces between islands; and the possibility of a barrier for attachment to islands (*1*, *3*, *4*).

Generally, a "bulky" complex is expected to be less mobile than its constituent metal adatoms, although the opposite can occur through the "sky-hook" effect, in which strong additive-metal adatom bonding weakens adatom-substrate bonding (*10*). For slower complexes, OR should be inhibited, not enhanced. However, stable complexes could potentially have a very high population if they have a low formation energy relative to that for adatoms, thus overcompensating the lower mobility. This key observation was emphasized recently in describing enhanced decay of copper (Cu) islands on the atomically flat Cu(111) surface caused by sulfur (*11*). The potentially favorable thermodynamics of complex formation has been recognized in earlier catalysis studies (*6*).

What are the mechanistic details of complex-enhanced coarsening? One might imagine the entire complex detaching and reattaching from island edges, but then it is difficult to rationalize why it should have a low formation energy relative to adatoms. At the other extreme, these complexes could form entirely on terraces from detaching adatoms by combining with terrace additives in a process driven by the energy reduction caused by bond formation (*12*). Sufficient coupling of adatoms detaching from islands to these complexes is needed; otherwise, the complexes may be passive bystanders in the coarsening process even if they are present in large numbers (*12*). Subtleties of transport and coupling require a generalized LSW theory. A simplified but elegant linear two-species (adatom plus complex) model was developed by Ling *et al*. (*12*) that captured different regimes of coupling observed in experiments for S/Cu/Cu(111). A quantitative theory requires coupled nonlinear reaction-diffusion equations (*13*), together with input on energetics from density functional theory.

Elucidation of the mechanisms for additive-enhanced coarsening will be important for improved durability of functional nanostructures, for example, avoiding the growth of larger metal particles that have lower surface area and are less effective as catalysts. For complex-mediated mass transport, there are challenges in identifying the complex and suitably extending LSW theory. It is likely that other mechanisms for coarsening could exist in which additives enhance messenger mobility (*9*) or reduce an attachment barrier (*4*). These mechanisms still await discovery and analysis.

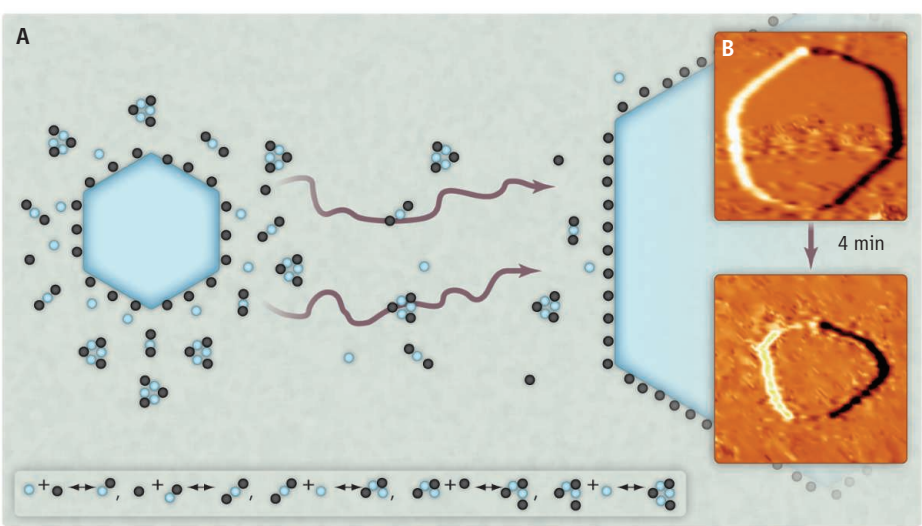

Additives accelerate change. Although coarsening processes happen in many settings, the advent of probes such as the scanning tunneling microscope (STM) allows such processes to be followed in detail on surfaces. (**A**) This schematic shows the shrinking of a hexagonal metal (M) island on a flat surface of the same metal, specifically the (111) surface termination of a face-centered cubic crystal. Transport to a larger island or extended surface step is assisted by the formation of metal-sulfur complexes, MS_2 and M_3S_3 (M shown in blue, S in black). Reaction steps in complex formation are indicated at the bottom. (**B**) STM images (90 nm by 90 nm) of the decay of a ~30,000-atom silver (Ag) island on Ag(111) in the presence of 11 millimonolayers of S at 300 K. Complete island decay takes 7 min (*13*) versus ~30 hours on a S-free Ag surface.

CREDIT: P. HUEY/*SCIENCE*

References and Notes

1. L. Ratke, P. W. Voorhees, *Growth and Coarsening* (Springer-Verlag, Berlin, 2002).
2. H. Zheng *et al*., *Science* **324**, 1309 (2009).
3. K. Morgenstern, *Phys. Status Solidi, B Basic Res.* **242**, 773 (2005).
4. P. A. Thiel, M. Shen, D.-J. Liu, J. W. Evans, *J. Phys. Chem. C* **113**, 5047 (2009).
5. A. J. Bray, *Adv. Phys.* **43**, 357 (1994).
6. P. J. F. Harris, *Int. Mater. Rev.* **40**, 97 (1995).
7. W. Theis, N. C. Bartelt, R. M. Tromp, *Phys. Rev. Lett.* **75**, 3328 (1995).
8. S. Kodambaka, S. Khare, I. Petrov, J. Greene, *Surf. Sci. Rep.* **60**, 55 (2006).
9. J. Perdereau, G. E. Rhead, *Surf. Sci.* **7**, 175 (1967).
10. G. L. Kellogg, *Phys. Rev. B* **55**, 7206 (1997).
11. P. J. Feibelman, *Phys. Rev. Lett.* **85**, 606 (2000).
12. W. L. Ling *et al*., *Phys. Rev. Lett.* **93**, 166101 (2004).
13. M. Shen, D. J. Liu, C. J. Jenks, P. A. Thiel, J. W. Evans, *J. Chem. Phys.* **130**, 094701 (2009).
14. This work was supported by NSF grant CHE-0809472.

10.1126/science.1191665

Published by AAAS

STRUCTURAL BIOLOGY

The Tao of Chloride Transporter Structure

A protein structure from a heat-loving alga offers insight into the diverse family of CLC chloride channels and transporters.

Joseph A. Mindell

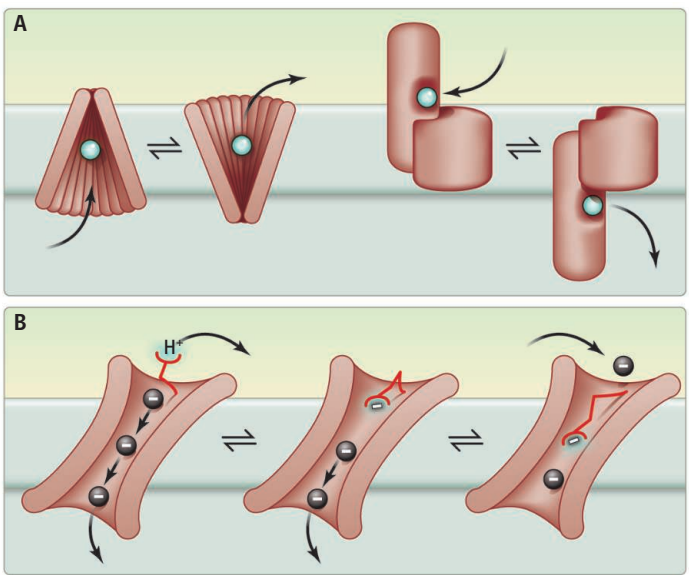

Into the pore. (**A**) Current models of CLC transporter function envision either "rocking bundles" (*12*) of transmembrane α helices (left) that change their tilt with respect to the membrane, shifting the exposure of a substrate binding site and allowing an ion (white sphere) to pass through; or a "sliding piston" (right) (*11*), in which a protein domain slides a large distance perpendicular to the membrane to enable ion transport. (**B**) Feng *et al*. propose that movements of a single side chain (the "gating glutamate") are central to the transport process. A prominent feature of this model is the "open" channel-like state (left), during which only an energetic barrier prevents fast downhill Cl^- flux through the protein. In two other states (center and right), the negatively charged glutamate side chain displaces Cl^- from two different binding sites along the ion pathway.

Lao Tzu's *Tao Te Ching*, a central text of Asian philosophy dating to the 6th century B.C.E., offers paths to enlightenment, in part by considering apparent paradoxes. "We put thirty spokes together and call it a wheel," it notes. "But it is on the space where nothing is that the usefulness of the wheel depends" (*1*). Such thinking applies equally well today—not only to the hole in the center of a wheel, but also to holes in proteins that move ions across cell membranes. Indeed, on page 635 of this issue, Feng *et al.* (*2*) present a new structure of a chloride (Cl^-) transporter that reveals the mechanistic importance of an aqueous hole through the center of the protein: a space where nothing is. This new structure clarifies several paradoxical features of the unusually diverse CLC family of Cl^--transporting proteins.

The CLCs contribute to a wide range of physiological processes, from maintaining the electrical stability of the resting muscle membrane, to regulating salt secretion in kidney cells, to facilitating acidification in endosomes and lysosomes (*3*). The CLCs possess a functional diversity unprecedented among membrane transport proteins: About half of the mammalian members of this family function as ion channels, whereas the others are transporters, coupling movement of Cl^- in one direction to an opposite flux of protons. This functional diversity is particularly surprising in light of current models for both transporter types: Ion channels are expected to form continuous aqueous pores across the membrane; transporters, in contrast, must provide means to alternately expose their substrate binding sites to both external and internal solutions, to avoid decoupling the movements of their various substrates (see the figure).

Membrane Transport Biophysics Section, Porter Neuroscience Research Center, National Institute of Neurological Disorders and Stroke, National Institutes of Health, Bethesda, MD 20892, USA. E-mail: mindellj@ninds.nih.gov

All mammalian CLCs have two functional parts, or domains; a transmembrane (TM) domain that spans the cell's lipid bilayer membrane is coupled to a carboxyl-terminal domain that extends into the cytoplasm. Investigators have previously reported structures for bacterial CLCs, which contain only the integral membrane domain (*4*), and for isolated mammalian cytoplasmic domains (*5*, *6*), but never for the two parts together in a single protein. Feng *et al*. sought to address this by determining the structure of a eukaryotic CLC that contains both domains, but they found that none of the mammalian candidates were sufficiently stable to make the crystals necessary for structural studies. Instead, they pursued an alternate approach, paralleling one that has been extremely successful for bacterial proteins. They isolated a protein (called CmCLC) from an alga that thrives at relatively high temperatures. This protein was amenable to crystallization, and the authors determined its structure at 3.5 Å resolution, enough to visualize the overall fold of the protein as well as some molecular detail.

The most striking feature that emerges upon first examining the new structure is the intimate contact between the two domains. Each domain is similar to structures previously described. It was expected that, like many ion channel structures, the cytoplasmic domains would be suspended almost like baskets below hot air balloons (*7*, *8*). Surprisingly, however, the CmCLC cytoplasmic domain is intimately nestled onto the inner surface of the TM domain. Highlighting this intimacy, the characteristics of the interface are similar to those of an antibody-antigen binding surface, with adjacent surfaces fitting into each other like adjacent pieces of a jigsaw puzzle. In mammalian CLCs, many disease-causing mutations occur in the amino acids lining the interaction surface between the two domains, suggesting that even minor perturbations of this interface can disrupt the protein's normal function. Given evidence that binding of ligands to these cytoplasmic domains can regulate CLC function (*9*), the close interaction between the domains provides clear paths for modulatory signals to influence the membrane transport process. The few known cytoplasmic domain ligands, however, have little or no effect on function, which has to be reconciled with the new evidence about structure—there may yet be much to learn in this area.

The second major insight provided by the structure is also a surprise, but one that perhaps sheds light on the fundamental duality of the CLC family. It concerns a critical residue for the function of both CLC channels and transporters. Referred to as the "gating glutamate," the acidic side chain of this residue is essential for coupling between protons

and Cl^- in CLC transporters, and for voltage-dependent gating in CLC channels. Part of the evidence for the role of the gating glutamate comes from a series of structures of the *Escherichia coli* CLC (*4*, *10*). They show that the side chain of the gating glutamate alternately occludes ion access to the ion permeation pathway, or swings out of the way to be replaced by a Cl^- ion (*4*, *10*). In the new structure, the gating glutamate occupies a new position, projecting into the core of the protein to displace Cl^- from a different, deeper binding site (see the figure).

On the basis of this observation, Feng *et al*. propose a novel mechanism; instead of the protein undergoing a large conformational change to enable transport, the movements of the gating glutamate alternately allow access to one side of the membrane or the other. This effectively makes it a "plunger" to expel bound Cl^- to the cytoplasm and to deliver (or accept) the transported proton well into the translocation pathway. This mechanism would require only minimal conformational change, certainly compared with the dramatic movements currently being described for other families of transporters (see the figure) (*11*, *12*). In CLC transporters, there is also evidence of transport-associated conformational changes (*13*, *14*), but the magnitude of those changes is unknown. Other data, however, do support a minimal change, most notably the low activation energy of CLC transporters compared with other transporters (*15*).

Another remarkable property of the model proposed by Feng *et al*. is that it predicts a state that has been considered forbidden for a transporter protein: an "open" channel-like state in which the protein contains a continuous aqueous pathway spanning the membrane. In a first-order approximation, such a pathway couldn't exist because it would allow the transported substrates to "slip," or move independently of each other down their concentration gradients, thereby wasting the work of the transporter. The new model avoids this slippage by invoking a kinetic barrier to movement: Cl^- ions encounter an energetic "hill" that prevents their rapid permeation. Such an energy barrier could bypass the need for a physical barrier to prevent unwanted "downhill" Cl^- flux. As the authors point out, an occasional Cl^- ion sneaking through the transporter (on the order of 1/1000 ions) would have minimal effects on coupled transport. This open state is predicted to occur while the gating glutamate is protonated and rotated away from the ion path—it should thus be favored at low pH. The model therefore predicts that coupling might be weaker at low pH than at high pH, a phenomenon not yet observed for ClCec1, a well-studied CLC transporter from *E. coli* (*16*). Yet uncoupling at low pH has been suggested for a mammalian CLC transporter, ClC-3, providing early support for the new mechanism (*17*).

Perhaps the most compelling aspect of the new transport model is that it offers a natural explanation of the relationships between the transporter and channel branches of the CLC family. By postulating an open aqueous pathway as an essential feature of the CLC transport mechanism, Feng *et al*. make it possible to imagine an evolutionary path to a channel that might involve a change only in the kinetic barrier to Cl^- movement. As this barrier is reduced, uncoupled (but not coupled) transport rates would increase dramatically. Indeed, a combination of two mutations along the transport path (including the gating glutamate) is sufficient to raise uncoupled transport rates by almost a factor of 20 (*18*). Thus, Feng *et al*.'s model accounts for a large number of the confusing, paradoxical features of the CLC family and, to paraphrase Lao Tzu, reveals that it is on the space where nothing is that the mechanism of the CLC depends.

References and Notes

1. A. Waley, *The Way and Its Power: Lao Tzu's Tao Te Ching and Its Place in Chinese Thought* (Grove Press, New York, 1994).
2. L. Feng, E. B. Campbell, Y. Hsiung, R. Mackinnon, *Science* **330**, 635 (2010); 10.1126/science.1195230.
3. T. J. Jentsch, *Crit. Rev. Biochem. Mol. Biol.* **43**, 3 (2008).
4. R. Dutzler, E. B. Campbell, M. Cadene, B. T. Chait, R. MacKinnon, *Nature* **415**, 287 (2002).
5. S. Meyer, S. Savaresi, I. C. Forster, R. Dutzler, *Nat. Struct. Mol. Biol.* **14**, 60 (2007).
6. S. Meyer, R. Dutzler, *Structure* **14**, 299 (2006).
7. A. Miyazawa, Y. Fujiyoshi, M. Stowell, N. Unwin, *J. Mol. Biol.* **288**, 765 (1999).
8. S. B. Long, E. B. Campbell, R. Mackinnon, *Science* **309**, 897 (2005).
9. B. Bennetts *et al*., *J. Biol. Chem.* **280**, 32452 (2005).
10. R. Dutzler, E. B. Campbell, R. MacKinnon, *Science* **300**, 108 (2003).
11. N. Reyes, C. Ginter, O. Boudker, *Nature* **462**, 880 (2009).
12. L. R. Forrest, G. Rudnick, *Physiology (Bethesda)* **24**, 377 (2009).
13. S. M. Elvington, C. W. Liu, M. C. Maduke, *EMBO J.* **28**, 3090 (2009).
14. S. P. Bell, P. K. Curran, S. Choi, J. A. Mindell, *Biochemistry* **45**, 6773 (2006).
15. A. Accardi, personal communication.
16. A. Accardi, C. Miller, *Nature* **427**, 803 (2004).
17. J. J. Matsuda, M. S. Filali, M. M. Collins, K. A. Volk, F. S. Lamb, *J. Biol. Chem.* **285**, 2569 (2010).
18. H. Jayaram, A. Accardi, F. Wu, C. Williams, C. Miller, *Proc. Natl. Acad. Sci. U.S.A.* **105**, 11194 (2008).

10.1126/science.1198306

IMMUNOLOGY

Infection Protection and Natural Selection

On an island off Scotland, variation in sheep immune response imposes fitness costs and benefits.

Lynn B. Martin and Courtney A. C. Coon

Why are infectious diseases still the major causes of animal mortality, despite the strong and ever-present evolutionary pressure to eliminate traits that make individuals susceptible to infection? Why hasn't natural selection weeded out weak immune systems? An emerging and rapidly growing field, known as ecological immunology or ecoimmunology, is trying to answer these questions by investigating how variation in immune response in free-living animal populations affects fitness. On page 662 of this issue, Graham *et al*. (*1*) provide an illuminating answer for feral sheep living on the Scottish island of Hirta in the St. Kilda archipelago. The sheep have varying blood levels of antibodies, and individuals with higher levels appear to confront a fitness trade-off: Although a strong immune response helps adult females survive harsh winters, it also reduces reproduction.

One journal (*2*) has dedicated a special issue to ecoimmunology, another special issue (*3*) is forthcoming, and the U.S. National Science Foundation recently funded a Research Collaborative Network (www.ecoimmunology.org) to help shape the field. Some of the first papers in the area (published just ~20 years ago) have been cited more than 1000 times (*4*, *5*). Recently, investigators have also begun to develop the study of human ecoimmunology (*6*–*8*), which may augment another nascent disci-

Department of Integrative Biology, University of South Florida, Tampa, FL 33620, USA. E-mail: lmartin@cas.usf.edu

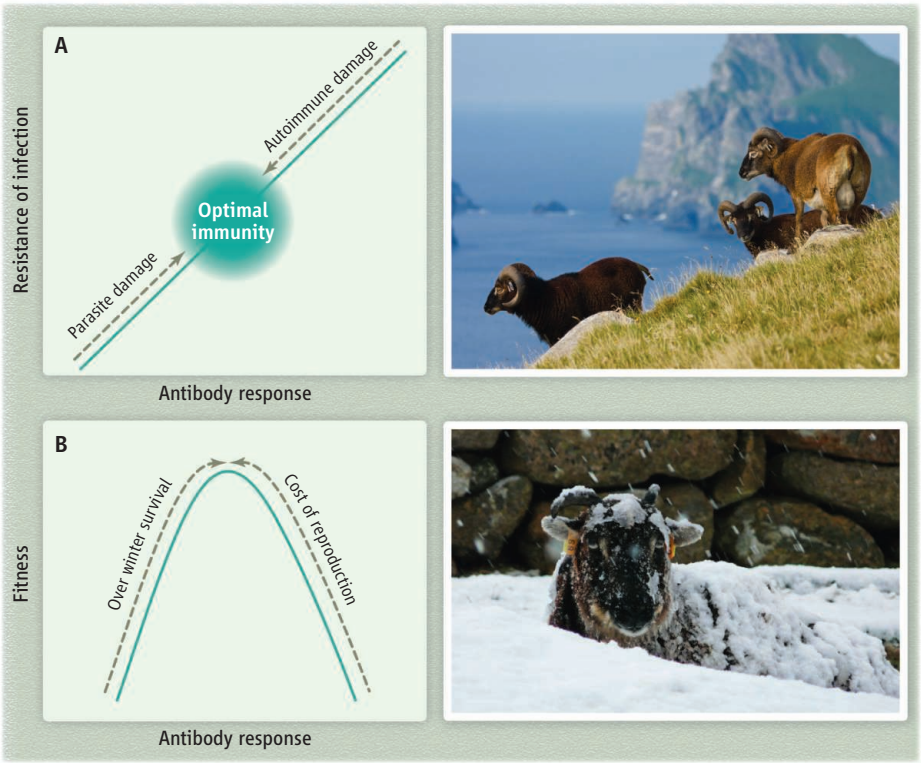

Fitness in the flock. Immune response in Soay sheep carries costs and benefits for survival and reproduction. (**A**) Increasing parasite pressure (upward black arrow) should favor strong infection resistance mechanisms, such as an active immune system. But an immune system that produces high levels of antibodies that attack the body's own cells extracts a cost that favors weaker immune response (downward-pointing black arrow). The opposing trends suggest that animals should evolve optimal, not maximal, immunity. (**B**) In Soay sheep, the costs and benefits of immune defenses appear to drive variation in levels of antibody response. Females had greater antibody responses than males, and females with the greatest antibody response (green curve) had the highest probability of surviving over the winter (upward black arrow on left), when exposure to parasites promotes mortality. But individuals of both sexes that had the highest antibody responses did not breed in the previous year (upward black arrow on right).

pline known as Darwinian medicine (*9*, *10*).

Perhaps the most important contribution of ecoimmunology to date has been to explicitly incorporate the costs of immune function into studies of how animals defend against parasites (*5*). Investigators have long known that immune defenses are expensive in terms of calories and proteins (*11*), lost opportunities (i.e., sickness preventing reproductive behavior) (*12*), and self-damage due to misdirected or overactive immune responses (*13*). These costs can be important from an evolutionary perspective, as populations selected for robust defenses often exhibit comparatively slow growth or reproductive output (*14*). Ecoimmunologists have brought these costs to the forefront and emphasized that the "best" immune system—the one expected to emerge from most evolutionary processes—is not the strongest one; rather, it is the one that maximizes or maximized fitness in light of constraints (*14*).

Graham *et al*. provide one of the best examples so far of such "optimal immunity" in a free-living animal population. They found that antibody responses were related to fitness in wild sheep, but in a complex way (see the figure). Antibodies help control parasites by interfering with their movement or replication or by targeting them for elimination by other immune cells. Given these functions, one might expect that "more is better," because more antibodies should mean faster elimination of more parasites. Some antibodies, however, can target the body's own cells and proteins for destruction, making them progenitors of disease. In humans, autoimmune diseases, including lupus and type 1 diabetes, are associated with overactive immune cells. This double-edged sword may explain why, for some Soay sheep, less was more. Specifically, sheep that maintained the highest concentrations of antibodies suffered costs to fitness in the form of lower reproductive output: Male and female sheep with high antibody concentrations in the fall, after the breeding season, were unlikely to have produced offspring in the previous season. But there were also benefits to antibody responses: Females with high levels were more likely to survive harsh winters that are associated with high parasite burdens, and produced offspring more likely to survive the neonatal period. The key discovery, however, was that an intermediate immune response may often be advantageous in wild animals.

Graham *et al*. also considered whether these "collateral damage" costs promoted some variation in antibody response. However, the response they measured—levels of antinuclear antibodies (ANAs) that bind to proteins released from dying cells—did not provide a clear answer; high ANA levels also correlated with antibody responsiveness to nonself proteins, meaning that the immune system was also primed to oust invaders. As a result, the direct relevance of autoimmunity to fitness in wild animals remains unclear, and future investigations of this issue could prove useful, especially since many human ailments involve immune dysregulation (*15*).

Other questions would also benefit from collaboration among eco- and traditional immunologists. What levels of antibodies, for instance, are needed to provide wild animals with protection against specific parasites? What factors besides genes explain why antibody responsiveness varies with age and among individuals? Ecoimmunology is poised to make novel contributions to immunology (*16*), but collaborations between bench and field researchers are needed to reveal and explain the gamut of natural immunological variation.

References and Notes

1. A. L. Graham *et al*., *Science* **330**, 662 (2010).
2. Theme Issue on Ecological Immunology, *Philos. Trans. R. Soc. London Ser. B* **364**, 3–142 (2009).
3. *Functional Ecology* will publish a special issue on ecoimmunology in 2011.
4. I. Folstad, A. J. Karter, *Am. Nat.* **139**, 603 (1992).
5. B. C. Sheldon, S. Verhulst, *Trends Ecol. Evol.* **11**, 317 (1996).
6. T. W. McDade, V. Reyes-García, S. Tanner, T. Huanca, W. R. Leonard, *Am. J. Phys. Anthropol.* **136**, 478 (2008).
7. S. C. Segerstrom, *Curr. Dir. Psychol. Sci.* **16**, 326 (2007).
8. J. Trotter, A. Liebl, E. Weeber, L. Martin, *Funct. Ecol.;* published online 8 October 2010; 10.1111/j.1365-2435.2010.01780.x.
9. R. M. Nesse *et al*., *Proc. Natl. Acad. Sci. U.S.A.* **107** (suppl. 1), 1800 (2010).
10. S. C. Stearns, R. M. Nesse, D. R. Govindaraju, P. T. Ellison, *Proc. Natl. Acad. Sci. U.S.A.* **107** (suppl. 1), 1691 (2010).
11. R. L. Lochmiller, C. Deerenberg, *Oikos* **88**, 87 (2000).
12. J. Adelman, L. Martin, *Integr. Comp. Biol.* **49**, 202 (2009).
13. A. Graham *et al*., *Funct. Ecol.;* published online 23 September 2010; 10.1111/j.1365-2435.2010.01777.x.
14. P. Schmid-Hempel, *Proc. R. Soc. Lond. B Biol. Sci.* **270**, 357 (2003).
15. C. E. Finch, *Proc. Natl. Acad. Sci. U.S.A.* **107** (suppl. 1), 1718 (2010).
16. I. Friberg, J. Bradley, J. Jackson, *Trends Parasitol.;* published online 14 July 2010; 10.1016/j.pt.2010.06.010.

10.1126/science.1198303

RETROSPECTIVE

Georges Charpak (1924–2010)

A generous Nobel laureate had a passion for particle detectors and reforming science education.

Yves Quéré

Georges Charpak was 7 years old in 1931 when his parents, Maurice and Anna, decided to leave their village in Poland and move to Paris. "I have a wonderful memory of my primary school," he often said, "where French quickly began to take over from the Polish of my youth, and where I set about indiscriminately devouring everything that came my way: mathematics, history, science, literature…Very soon, I felt that I had a debt to an education system that had given me so much." Brilliant studies, then war, the German occupation, and the French Resistance (he had a false identity card, and was arrested and deported to the Dachau concentration camp). All this made his youth an adventure worthy of a novel, in which conviction and courage went face to face with tragedy.

Then there is Georges after the war, beginning his research at the Fréderic Joliot-Curie laboratory in Paris, where he was soon gripped by a passion for particle detectors. It never left him. Drawn to the European Organization for Nuclear Research (CERN) in Geneva by the American physicist Leon Lederman, he would spend most of his career there as an impassioned physicist and an inspired experimenter. He built his multiwire proportional chambers for electronically tracking the particles created by accelerators; they deposed bubble chambers, creating his fame and earning him the Nobel Prize in Physics in 1992. On his return to Paris, he was invited to join the École supérieure de physique et de chimie industrielle de Paris, by Pierre-Gilles de Gennes, then the director. There, he continued his work, this time in radiology, developing detectors that cut the exposure time needed for radiography by several orders of magnitude. At the same time, he was a prominent campaigner against the proliferation of nuclear weapons, and in favor of nuclear power stations.

Georges was then seized by another passion. In 1995, while visiting schools in Chicago that his friend Lederman had helped save from violence and ruin through science taught "hands-on," Georges decided—with a faith that would have moved mountains—to reform the teaching of the natural sciences in French primary schools. With the support of a few teachers who were already working in that direction, and backed by a unanimous vote of the French Academy of Sciences in 1996, he launched La main à la pâte ("hands in the dough"). At first, several hundred schoolteachers embarked upon the adventure, and then several thousand, with the full backing of the French Ministry of Education. It involved teaching so that children learned science by doing it, and not just by reading about it on the blackboard or on a screen. Soon, Georges was joined by fellow members of the French Academy, and by a group of teachers and enthusiastic scientists. Fruitful contacts were made with other pioneers, such as Jerry Pine at the California Institute of Technology and Karen Worth of the Educational Development Center, headquartered in Boston.

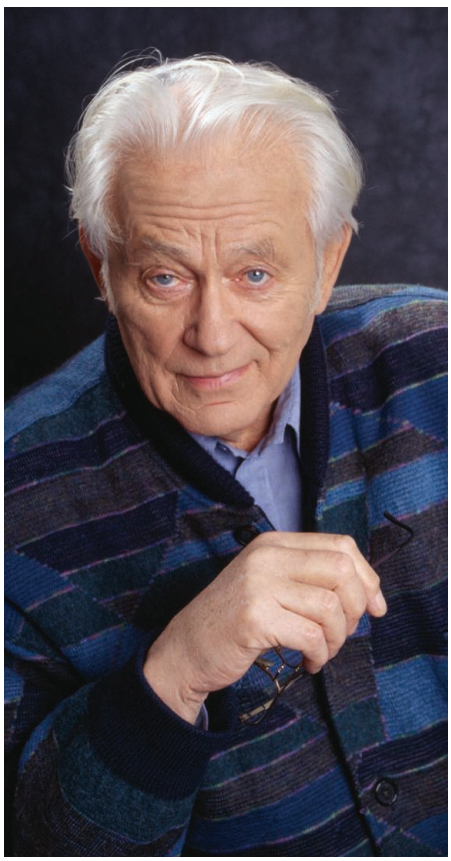

A team formed under the aegis of the French Academy, and it soon defined a strategy and tactics. The strategy was founded on a single priority: to use science to support the child's mental development. This meant inculcating a taste for questioning, a sense of observation, intellectual rigor, practice with reasoning, modesty in the face of facts, an ability to distinguish between true and false, and an attachment to logical and precise language. The tactics involved creating and organizing support for a major Web site, now consulted by a vast number of teachers, creating "pilot centers" around the country where La main à la pâte was rolled out on a model basis, and creating a prize for the best classes, to be presented annually by the minister at the French Academy's hall of honor. Today, Georges Charpak's scheme is officially endorsed by the ministry, and about 40% of French primary school teachers have adopted the approach.

Far beyond France, however, a similar trend was seen in the years around the turn of the millennium. Academies—such as the U.S. National Academy of Sciences, led by the determined action of its president, Bruce Alberts (now editor-in-chief of *Science*), the Swedish Academy, and a number of others—followed parallel paths. Networks formed, and an increasing number of international meetings and colloquia took place. La main à la pâte appeared in Colombia, Brazil, Argentina, Chile, and also, among many others, in China, Malaysia, Turkey, Afghanistan, and Cameroon. As for Europe, it has begun to organize itself around the Pollen and Fibonacci projects, funded by the European Commission, while the IAP, the global network of science academies, has made the teaching of science to children a sort of flagship for its international action.

At the heart of this national and international blossoming was the smiling but inflexible Georges, acting in favor of the children of the world. His enthusiasm, his strength of persuasion, his humor, and his charm were determining factors. His death, on 29 September in Paris, has deprived us of an outstanding man; a man who abhorred sectarian mindsets, compromise, bad faith, intolerance, the taste for power, and lies; a man who returned 100-fold the debt he believed he owed; a man who loved life, music, culture, friendship, science, action, and always going that bit further. Georges Charpak has left an indelible mark on all those who approached him, through his generosity, his youthfulness, and his passion.

10.1126/science.1198962

Académie des Sciences, Délégation à l'Enseignement et à la Formation, 23 quai de Conti, 75006 Paris, France. E-mail: yves.quere@academie-sciences.fr

CREDIT: ERIC FOUGÈRE/CORBIS

SPORE* SERIES WINNER

Physical Phenomena in Real Time

The use of videos allows teachers to tame the vagaries of experimentation while engaging students in the process of physics.

David Brookes† and Eugenia Etkina‡

There is a growing realization that nurturing scientists for the 21st century requires engaging students in the processes of doing science (*1*). For students to be engaged in the process of doing physics, they need to learn to think like a physicist. Physics is more than the final content that we assess in a traditional exam. Much of its richness is the process through which physicists acquire knowledge and those specific "habits of mind" that are necessary to practice physics. For example, when solving an experimental problem, a physicist needs to decide what features of the problem are relevant and which features can be ignored, how to represent the problem in different ways, including mathematical expressions, how to use available equipment to collect necessary data, how to analyze the data, and how to evaluate the results (*2*, *3*). Investigations are subject to the variability of experimental conditions and unanticipated complications. What if we could guide students so that they can make progress in a short amount of class time, yet still be engaged in the process of doing physics?

The Rutgers Physics Teaching Technology Resource (http://paer.rutgers.edu/pt3/) engages students from middle school to college in the process of physics. It contains more than 200 videos of real-life physics experiments that students can view and analyze as they learn new material, perform labs, carry out independent projects, or do homework. Videos allow them to see physical phenomena in real time and then again in slow motion for data collection. The videos do not contain tools for quantitative analysis. Instead, students need to decide themselves what data to collect and how to collect them. The goal is to engage students in actions and decisions similar to those of real physicists by working with simple experiments.

Physicists observe physical phenomena, collect data, find patterns in the data, and devise multiple explanations or mechanisms behind the patterns, test those explanations with more experiments, and apply their theories to solve real-world problems (*4*). Although it is a complex and nonlinear process, its logic can be used in physics instruction. A physics learning system called Investigative Science Learning Environment (ISLE) models this process for the students (*4*). In ISLE, all experiments that students encounter can be placed into one of three categories according to their roles: observational (experiments that are used to generate explanations), testing (used to test explanations), or application (experimental problems to solve for which one needs to synthesize multiple explanations and/or relations). The video Web site follows this scheme, helping an instructor form a learning progression that mirrors the process of doing physics.

To learn a new concept, students can start with a carefully selected set of observational experiment videos. They do not make any predictions of their outcomes before viewing but describe what they see or collect data. Students then use such representations as motion diagrams, force diagrams, and ray diagrams to analyze collected data to find patterns. If possible, students can then devise explanations or mechanisms for these patterns. Next, students can test their explanations by using them to predict the outcomes of new experiments, through a testing experiment video (sometimes there are multiple testing experiments), with the goal of ruling out the explanation instead of proving it. Finally, students can apply their new knowledge to solve real-world problems through an application experiment video.

Many application experiments are also reprised in a special section titled "Surprising data and puzzles." Each puzzle has a video that contains two experiments from which a particular quantity can be determined. Students must reconcile different outcomes by analyzing experimental uncertainties and theoretical assumptions. For example, one puzzle requires students to determine the height of a table in two different ways (see the first figure). Both experiments use many of the advantages afforded by a video format—such as the lack of markers, measuring instruments, and peripheral technology—and few instructions beyond the statement "find the height of the table in two different ways." Students have to decide what to measure, how to measure it, and what assumptions to make, while the camera frame helps constrain their attention and focus on the table, the falling ball, and the swinging pendulum. Additionally, students can step through the video frame by frame to measure how long it took for the orange ball to hit the floor and the period of the pendulum's oscillation, as both would be difficult to record in real time. Finally, having the falling ball and the swinging pendulum next to each other encourages students to compare their two methods. After finding that the height results obtained from the two experiments are not exactly the same, students can identify and estimate sources of instrumental uncertainty and then compare

A screen shot from the "table height" experiment. The orange ball rolls off the table and falls to the ground. The small metal ball on the right is attached to a string that is connected to a bar resting on the tabletop. The resulting pendulum swings back and forth, exhibiting simple harmonic motion. The length of the pendulum is roughly the height of the table.

Graduate School of Education, Rutgers University, New Brunswick, NJ 08901, USA.

*SPORE, *Science* Prize for Online Resources in Education; www.sciencemag.org/special/spore/. †Present address: Department of Physics, Florida International University, Miami, FL 33199, USA. ‡Author for correspondence. E-mail: eugenia.etkina@gse.rutgers.edu

Published by AAAS

A series of screen shots of E. Etkina on in-line skates being pulled by D. Brookes. Students are asked to observe Eugenia's motion, draw a motion diagram, and decide if she is moving at a constant rate or at an increasing rate.

the two height results taking those uncertainties into account. If the two numbers still do not match, they may think about sources of systematic uncertainty and how they might affect calculations.

"Surprising data" experiments have situations whose outcomes are difficult to predict correctly if one does not examine auxiliary assumptions. These experiments help students understand the role of assumptions in physics. For example, a traditional physics projectile problem may admonish students to "ignore air resistance." Correspondingly, students should predict that a projectile launched at 30° would fly the same distance as a projectile launched at the same speed at 60°. However, in one of our testing experiment videos in the "surprising data" section, a projectile launched at 60° falls roughly 8 cm shorter than the distance traveled by the same projectile launched at the same speed at 30°. Students need to decide if this is just random variation, or if air resistance has a different effect on the two projectiles despite student's calculations suggesting that both projectiles should fly the same distance.

To help instructors, the Web site explains how to use the videos, describes the underlying teaching philosophy, and provides examples of how students can work with the videos. All videos work with any curriculum and with any textbook and are supported by questions, all of which allow students to work independently at their own pace. In addition, there is a teacher component only available for registered teachers (registration is free) and invisible for the students. These pages explain why a particular experiment is important, how to analyze data, and so forth.

The Rutgers Physics Teaching Technology Resource receives feedback from active users, which helps illustrate the variety of ways in which the videos can be adapted and used in different instructional settings. A high school teacher from Nebraska uses some of the videos as an introductory demonstration to stimulate a discussion. For example, the video titled "David Hits a Ball so That It Travels in a Circle" leads to a discussion on what type of force is necessary to achieve circular motion, whereas the "Eugenia on Rollerblades" video usually results in students bringing in their Rollerblades to do a demonstration for the class. The videos also support struggling students and those who have missed a laboratory session.

A professor at the Physics Department at Oregon State University uses the videos for an in-class demonstration (see the second figure). Students record data directly from the videos, providing "buy-in" that they are investigating real scientific phenomena. These easily implemented videos lay the groundwork for student-generated explanations of physics laws.

A professor in the Department of Biology and Physics at Kennesaw State University uses the videos for assessment. For example, when a wand is rubbed with fur, it initially attracts a pith ball toward it. However, when the two touch, the pith ball is suddenly repelled. After watching this video, students need to explain what happened using previously learned physics concepts. Students first talk to their neighbors before discussing the video as a class. Many students comment that the videos make things clearer and bring everything together.

Those who prepare teachers have commented that the Web site allows them to share many experiments regardless of the amount of equipment available at schools. In districts with limited funds, videos become great free resources. In addition, electrostatics experiments help students observe phenomena when the weather is not cooperating.

In summary, the Web site allows access to a rich experimental environment free of cost and safety concerns. It helps students engage in practices similar to those of scientists where they have to make decisions on data collection and analysis and want to explore phenomena in slow motion. It simplifies some of the distracting complexity of real-world experimentation. It can be used to help students of all ages learn physics in a way that reflects the process of doing physics.

About the authors

David Brookes is an assistant professor of Physics at Florida International University, where he conducts research in physics education. He views his teaching and research as two dimensions of the same activity: learning. His research informs his classroom practice and what he learns from his students informs his research.

Eugenia Etkina is a professor of science education at Rutgers University. She spent 13 years teaching physics to 7th- through 12th-grade students and now runs one of the largest programs on physics teacher preparation in the country. She is engaged in teaching reforms for introductory physics and her research focuses on how students and future teachers learn physics through ISLE.

References and Notes

1. P. Chin *et al.*, in *Reconsidering Science Learning*, E. Scanlon *et al.*, Eds. (Routledge Falmer, London, 2004), pp. 118–134.
2. E. Etkina *et al.*, *Phys. Rev. ST Phys. Educ. Res.* **2**, 020103 (2006).
3. Also see http://paer.rutgers.edu/scientificabilities.
4. E. Etkina, A. Van Heuvelen, in *Research-Based Reform of University Physics*, E. F. Redish and P. J. Cooney, Eds. (American Association of Physics Teachers, College Park, MD, 2007); www.compadre.org/per/per_reviews/media/volume1/isle-2007.pdf.
5. We thank A. Van Heuvelen, S. Murthy, M. Lawrence, M. Gentile, L. Largo, Y. Sakano, A. Warren, D. Maiullo, and many others who provided ideas and technical assistance for our project. This work would be impossible without the funds from the U.S. Department of Education and the NSF.

10.1126/science.1186992

SCIENCE CAREERS

Obstacles for Women Scientists Could Slow Global Innovation

SAN JUAN, PUERTO RICO—Women scientists and students are still confronted by a "chilly" climate at many U.S. universities, and unless conditions improve, their departure from science and technology fields could hinder the nation's strength in a competitive global economy, said AAAS President Alice S. Huang.

Speaking at the AAAS Caribbean Division's 25th annual conference, the accomplished virologist and educator said it is imperative that the United States identify and support science talent wherever it is found. And she urged universities and colleges to lead those efforts.

"We've actually had marvelous changes in society in the past 20 years or so," Huang told the audience at the 25 September talk. "There has been much more acceptance of women…. But there is still a great deal that needs to be done. We're not there yet—and we're losing out on a lot of individuals who could contribute."

Huang's talk was one of several recent AAAS reports and events—including one on Capitol Hill—to explore the challenges faced by women in science, engineering, and technology fields. While women still report problems ranging from overt bias to a lack of social support, there is an increasing recognition that they must be crucial players in the global drive for innovation.

Campus challenge. AAAS President Alice S. Huang urged more systematic support for women in science and engineering.

A new survey of more than 1000 researchers, commissioned by AAAS/*Science* for L'Oreal USA (see www.aaas.org/go/loreal) found that more than half of the women who responded said they had experienced gender bias. More than half cited difficulties with child care as a major career barrier.

"We need to be more imaginative about how one can have a successful career in science as well as a life," said Shirley Malcom, director of Education and Human Resources at AAAS. "It will be necessary to reorient the expectations so that women scientists face fewer hurdles and can play on a level field with their male counterparts."

Support for women scientists has taken on new prominence as policy-makers promote innovation and technology development as economic necessities. Unless the United States can tap into the skill and experience of women and underrepresented minorities, Huang said, the nation may become less competitive.

Huang advised women to seek out mentors, join professional associations, and promote their own work. The AAAS survey found that women are lacking such support: Nearly one-third lacked career role models, and a quarter of the women said teachers and advisors could have helped them overcome career obstacles, compared to 14% of the men surveyed.

To remedy these deficits, policy-makers and employers are searching for new ways to support women scientists and engineers, speakers said at a 23 September Capitol Hill panel discussion of the survey. U.S. Representative Eddie Bernice Johnson (D–TX), who delivered opening remarks, has introduced legislation to promote gender parity among university faculty in science, technology, engineering, and mathematics fields.

"We need to keep the attention on getting rid of those barriers as much as we can," Johnson said.

Programs to remove career barriers for women scientists and engineers globally are the focus of renewed attention and funding by the U.S. State Department, the World Bank, and an array of other development agencies, speakers said at a regional meeting of the International Network of Women Engineers and Scientists (INWES). The meeting, held 25 to 26 August and hosted by Education and Human Resources and the AAAS International Office, featured scientists, educators, and policy experts from 11 nations.

Many of Joshua Mandell's clients at the World Bank "have expressed a demand" for science and technology programs that include a significant role for women, the program officer noted at the meeting, because the programs "can have strong impacts on economic growth."

—Edward W. Lempinen, Ginger Pinholster, Tina Adler, and Becky Ham

AAAS Council Reminder

The next meeting of the AAAS Council will take place during the AAAS Annual Meeting and will begin at 9 a.m. on 20 February 2011, in Washington, D.C., in the Congressional A&B Ballrooms of the Renaissance Hotel.

Individuals or organizations wishing to present proposals or resolutions for possible consideration by the council should submit them in written form to AAAS Chief Executive Officer Alan I. Leshner by 26 November 2010. This will allow time for them to be considered by the Committee on Council Affairs at its winter meeting.

Items should be consistent with AAAS's objectives and be appropriate for consideration by the council. Resolutions should be in the traditional format, beginning with "Whereas" statements and ending with "Therefore be it resolved."

Late proposals or resolutions delivered to the AAAS Chief Executive Officer in advance of the February 2011 open hearing of the Committee on Council Affairs will be considered, provided that they deal with urgent matters and are accompanied by a written explanation of why they were not submitted by the November deadline. The Committee on Council Affairs will hold its open hearing at 2:30 p.m. on 19 February 2011 in Room 147A of the Walter E. Washington Convention Center. Summaries of the council meeting agenda will be available during the Annual Meeting at the AAAS information desk and in the AAAS headquarters office in the Convention Center. A copy of the full agenda will be available for inspection in the headquarters office.

Published by AAAS

ELECTIONS

AAAS Annual Election: Preliminary Announcement

The 2010 AAAS election of officers will be held in November. All members will receive a ballot for election of the president-elect, members of the Board of Directors, and members of the Committee on Nominations. Members will receive ballots for elections for each section they are enrolled in.

Additional names may be placed in nomination by petition submitted to the Chief Executive Officer no later than 12 November. Petitions for president- elect, the Board, or Committee on Nominations must be signed by at least 100 Association members; petitions for any section office must be signed by at least 50 section members. Petitions must be accompanied by the nominee's C.V. and statement of acceptance of nomination. Biographical information for the candidates will arrive with ballots mailed in November.

Slate of Candidates

GENERAL ELECTION

President: William H. Press, Univ. of Texas, Austin; Linda P. B. Katehi, Univ. of California, Davis

Board of Directors: Raymond L. Orbach, Univ. of Texas, Austin; Inder M. Verma, Salk Institute for Biological Studies; Cynthia M. Beall, Case Western Reserve Univ.; Priscilla P. Nelson, New Jersey Institute of Technology

Committee on Nominations: Rosina M. Bierbaum, Univ. of Michigan; Wayne Clough, Smithsonian Institution; Francisco J. Ayala, Univ. of California, Irvine; John E. Burris, Burroughs Wellcome Fund; May R. Berenbaum, Univ. of Illinois, Urbana-Champaign; Thomas D. Pollard, Yale Univ. Jo Handelsman, Yale Univ.; Roger Beachy, U.S. Department of Agriculture

SECTION ELECTIONS

Agriculture, Food, and Renewable Resources

Chair Elect: Deborah Delmer, Univ. of California, Davis; Donald R. Ort, Univ. of Illinois, Urbana-Champaign

Member-at-Large of the Section Committee: Cynthia Rosenzweig, NASA Goddard Institute for Space Studies; Rodney A. Hill, Univ. of Idaho

Electorate Nominating Committee: Leon V. Kochian, USDA-ARS Robert W. Holley Center for Agriculture & Health; Peter R. Grace, Queensland Univ. of Technology, Australia; Richard T. Sayre, Donald Danforth Plant Science Center; Harry J. Klee, Univ. of Florida

Anthropology

Chair Elect: John H. Relethford, SUNY-Oneonta; Leslie C. Aiello, Wenner-Gren Foundation for Anthropological Research

Member-at-Large of the Section Committee: Susan Antón, New York Univ.; George R. Milner, Pennsylvania State Univ.

Electorate Nominating Committee: Lynnette Leidy Sievert, Univ. of Massachusetts, Amherst; Arlen F. Chase, Univ. of Central Florida; Daniel E. Brown, Univ. of Hawaii; Dawnie Wolfe Steadman, Binghamton Univ.

Astronomy

Chair Elect: Charles Alcock, Harvard-Smithsonian Center for Astrophysics; Jean L. Turner, Univ. of California, Los Angeles

Member-at-Large of the Section Committee: Chris Impey, Univ. of Arizona; Amy J. Barger, Univ. of Wisconsin, Madison

Electorate Nominating Committee: Eileen D. Friel, Boston Univ.; Scott J. Kenyon, Smithsonian Astrophysical Observatory; Elizabeth Barton, Univ. of California, Irvine; Heidi B. Hammel, Space Science Institute

Atmospheric and Hydrospheric Sciences

Chair Elect: Susan K. Avery, Woods Hole Oceanographic Institution; Thomas E. Graedel, Yale Univ.

Member-at-Large of the Section Committee: Michael E. Mann, Pennsylvania State Univ.; Sally A. McFarlane, Pacific Northwest National Laboratory

Electorate Nominating Committee: Ronald G. Prinn, Massachusetts Institute of Technology; James R. Luyten, King Abdullah University of Science & Technology; Randall M. Dole, National Oceanic and Atmospheric Administration; L. Ruby Leung, Pacific Northwest National Laboratory

Council Delegate: Anthony J. Broccoli, Rutgers Univ.; Nominee to be announced

Biological Sciences

Chair Elect: Michael Lynch, Indiana Univ.; Gary Felsenfeld, National Institute of Diabetes and Digestive and Kidney Diseases/NIH

Member-at-Large of the Section Committee: Nancy J. Cox, Univ. of Chicago; Charles F. (Chip) Aquadro, Cornell Univ.

Electorate Nominating Committee: Jay A. Tischfield, Rutgers Univ.; Deborah E. Goldberg, Univ. of Michigan; Anna Marie Skalka, Fox Chase Cancer Center; Charles D. Laird, Univ. of Washington

Chemistry

Chair Elect: Alison Butler, Univ. of California, Santa Barbara; Bruce C. Garrett, Pacific Northwest National Laboratory

Member-at-Large of the Section Committee: Joseph A. (Joe) Gardella, Univ. at Buffalo; Bruce A. Parkinson, Univ. of Wyoming

Electorate Nominating Committee: Debra Rolison, Naval Research Laboratory; Peter C. Ford, Univ. of California, Santa Barbara; Robin L. Garrell, Univ. of California, Los Angeles; Hilary A. Godwin, Univ. of California, Los Angeles

Dentistry and Oral Health Sciences

Chair Elect: Floyd E. Dewhirst, Harvard School of Dental Medicine, The Forsyth Institute; Barbara D. Boyan, Georgia Institute of Technology

Member-at-Large of the Section Committee: Janet Moradian-Oldak, Univ. of Southern California School of Dentistry; Susan Kinder Haake, Univ. of California, Los Angeles School of Dentistry

Electorate Nominating Committee: Gill Diamond, Univ. of Medicine and Dentistry of New Jersey; Susan Reisine, Univ. of Connecticut School of Dental Medicine; Bjorn Steffensen, Univ. of Texas Health Science Center at San Antonio; David K. Ann, City of Hope Hospital, Univ. of Southern California

Council Delegate: Maria Emanuel Ryan, Stony Brook Univ.; Jacques E. Nör, Univ. of Michigan

Education

Chair Elect: Judith A. Ramaley, Winona State Univ.; John R. Jungck, Beloit College

Member-at-Large of the Section Committee: Susan Rundell Singer, Carleton College; Robert L. DeHaan, Emory Univ.

Electorate Nominating Committee: Min Li, Univ. of Washington; Anne E. Egger, Stanford Univ.; Troy M. Livingston, Museum of Life and Science, Durham, NC; Gerald R. Van Hecke, Harvey Mudd College

Council Delegate: Arthur Eisenkraft, Univ. of Massachusetts, Boston; Larry Bell, Museum of Science

Engineering

Chair Elect: John L. Anderson, Illinois Institute of Technology; Nicholas A. Peppas, Univ. of Texas, Austin

Member-at-Large of the Section Committee: J. Gary Eden, Univ. of Illinois, Urbana-Champaign; Tomás Díaz de la Rubia, Lawrence Livermore National Laboratory

Electorate Nominating Committee: John L. Hudson, Univ. of Virginia; Sarah A. Rajala, Mississippi State Univ.; William E. Bentley, Univ. of Maryland, College Park; Margaret Murnane, Univ. of Colorado, Boulder

General Interest in Science and Engineering

Chair Elect: Sharon Dunwoody, Univ. of Wisconsin, Madison; Lynn Timpani Friedmann, Friedmann Communications

Member-at-Large of the Section Committee: Chase Huntley, The Wilderness Society; Katarina Nordqvist, Nobel Museum

Electorate Nominating Committee: Kathleen M.B. Boomer, Smithsonian Environmental Research Center, Edgewater, MD; Kathryn E. Perez, Univ. of Wisconsin, La Crosse; Mary K. Miller, Exploratorium, San Francisco; Steve Miller, Freelance Science Writer

Council Delegate: Assad Panah, Univ. of Pittsburgh, Bradford; JoAnn M. Valenti, Brigham Young Univ.

Geology and Geography

Chair Elect: Glen M. MacDonald, Univ. of California, Los Angeles; Kenneth Nealson, Univ. of Southern California

Member-at-Large of the Section Committee: Ronald F. Abler, International Geographical Union; Paul H. Glaser, Univ. of Minnesota
Electorate Nominating Committee: Robert K. Peet, Univ. of North Carolina, Chapel Hill; Patrick J. Bartlein, Univ. of Oregon; Ester Sztein, National Academy of Sciences; Kenneth P. Kodama, Lehigh Univ.

History and Philosophy of Science
Chair Elect: Joseph E. Pitt, Virginia Polytechnic Institute and State Univ.; Jed Z. Buchwald, California Institute of Technology
Member-at-Large of the Section Committee: Anne-Marie Carroll Mazza, The National Academies; Sandra D. Mitchell, Univ. of Pittsburgh
Electorate Nominating Committee: Jason Scott Robert, Arizona State Univ.; Hanne Andersen, Aarhus Univ., Denmark; Carl Mitcham, Colorado School of Mines; Alan E. Shapiro, Univ. of Minnesota

Industrial Science and Technology
Chair Elect: Cammy R. Abernathy, Univ. of Florida; Gary E. Marchant, Arizona State Univ.
Member-at-Large of the Section Committee: Daniel J.C. Herr, Semiconductor Research Corporation; François Coallier, École de Technologie Supérieure, Canada
Electorate Nominating Committee: Wen-li Wu, National Institute of Standards and Technology; Gordon D. Jarvinen, Los Alamos National Laboratory; Derek Hook, Univ. of Minnesota; Richard Broglie, Pioneer/DuPont

Information, Computing, and Communication
Chair Elect: Tony Hey, Microsoft Research; Francine Berman, Rensselaer Polytechnic Institute
Member-at-Large of the Section Committee: Christine L. Borgman, Univ. of California, Los Angeles; Eric S. Roberts, Stanford Univ.
Electorate Nominating Committee: Christopher R. Johnson, Univ. of Utah; Eugene H. Spafford, Purdue Univ.; W. Richards (Rick) Adrion, Univ. of Massachusetts, Amherst; Barbara Simons, Retired, IBM Research
Council Delegate: Julia Gelfand, Univ. of California, Irvine; Michael R. Nelson, Georgetown Univ.

Linguistics and Language Science
Chair Elect: Joseph E. Aoun, Northeastern Univ.; John A. Goldsmith, Univ. of Chicago
Member-at-Large of the Section Committee: Claire Bowern, Yale Univ.; Joan A. Sereno, Univ. of Kansas
Electorate Nominating Committee: Hans Henrich Hock, Univ. of Illinois; Maria Polinsky, Harvard Univ.; Jonathan David Bobaljik, Univ. of Connecticut; Karen Emmorey, San Diego State Univ.
Council Delegate: D. Terence Langendoen, National Science Foundation; Brian D. Joseph, Ohio State Univ.

Mathematics
Chair Elect: Philippe Tondeur, Univ. of Illinois, Urbana-Champaign; Jill P. Mesirov, Broad Institute of MIT and Harvard
Member-at-Large of the Section Committee: Joceline Lega, Univ. of Arizona; Reinhard Laubenbacher, Virginia Polytechnic Institute and State Univ.
Electorate Nominating Committee: Linda Petzold, Univ. of California, Santa Barbara; Robert E. Megginson, Univ. of Michigan; James Crowley, Society for Industrial and Applied Mathematics; William Yslas Vélez, Univ. of Arizona

Medical Sciences
Chair Elect: Nancy H. Ruddle, Yale Univ. School of Medicine; Ann M. Arvin, Stanford Univ. School of Medicine
Member-at-Large of the Section Committee: Arturo Casadevall, Albert Einstein College of Medicine; Rafi Ahmed, Emory Univ. School of Medicine
Electorate Nominating Committee: Jonathan D. Gitlin, Vanderbilt Univ. School of Medicine; Douglas D. Richman, Univ. of California, San Diego; Guy A. Zimmerman, Univ. of Utah School of Medicine; Richard Ransohoff, Cleveland Clinic Foundation

Neuroscience
Chair Elect: Ted M. Dawson, Johns Hopkins School of Medicine; David M. Holtzman, Washington Univ. St. Louis
Member-at-Large of the Section Committee: Amita Sehgal, Univ. of Pennsylvania School of Medicine; Yehuda Ben-Shahar, Washington Univ. St. Louis
Electorate Nominating Committee: Jeanne M. Nerbonne, Washington Univ. St. Louis School of Medicine; Joe Henry Steinbach, Washington Univ. St. Louis; Karen Hsiao Ashe, Univ. of Minnesota; John Huguenard, Stanford Univ. School of Medicine

Pharmaceutical Science
Chair Elect: Sidney D. Nelson, Univ. of Washington; Alice M. Clark, Univ. of Mississippi
Member-at-Large of the Section Committee: John R. Cashman, Human BioMolecular Research Institute; Charles D. Smith, Medical Univ. of South Carolina
Electorate Nominating Committee: Murali Ramanathan, Univ. of Buffalo; Maria Croyle, Univ. of Texas, Austin; Salomon A. Stavchansky, Univ. of Texas, Austin; Barbara E. Hayes, Texas Southern Univ.
Council Delegate: Jeanette M. Roberts, Univ. of Wisconsin, Madison; Courtney V. Fletcher, Univ. of Nebraska Medical Center

Physics
Chair Elect: Lynn A. Boatner, Oak Ridge National Laboratory; Allen Goldman, Univ. of Minnesota
Member-at-Large of the Section Committee: Megan Donahue, Michigan State Univ.; Edmund Bertschinger, Massachusetts Institute of Technology
Electorate Nominating Committee: David K. Campbell, Boston Univ.; Malcolm R. Beasley, Stanford Univ.; Harold C. Craighead, Cornell Univ.; Roberto Peccei, Univ. of California, Los Angeles

Psychology
Chair Elect: Richard J. Davidson, Univ. of Wisconsin, Madison; Emanuel Donchin, Univ. of South Florida
Member-at-Large of the Section Committee: Janice K. Kiecolt-Glaser, Ohio State Univ. College of Medicine; Niels Birbaumer, Univ. of Tübingen, Germany
Electorate Nominating Committee: Hill Goldsmith, Univ. of Wisconsin, Madison; Nora S. Newcombe, Temple Univ.; Michael Rugg, Univ. of California, Irvine; William G. Iacono, Univ. of Minnesota

Social, Economic, and Political Sciences
Chair Elect: Henry E. Brady, Univ. of California, Berkeley; Craig Calhoun, Social Science Research Council
Member-at-Large of the Section Committee: Julia Lane, National Science Foundation; David L. Featherman, Univ. of Michigan
Electorate Nominating Committee: Cecilia L. Ridgeway, Stanford Univ.; Robert A. Pollak, Washington Univ. St. Louis; Peter J. Burke, Univ. of California, Riverside; Wendy Baldwin, Population Council

Societal Impacts of Science and Engineering
Chair Elect: Peter D. Blair, National Academy of Sciences; William Bonvillian, Massachusetts Institute of Technology
Member-at-Large of the Section Committee: Mahmud Farooque, Consortium for Science, Policy & Outcomes; Anne Fitzpatrick, U.S. Dept. of Energy
Electorate Nominating Committee: Robert Margolis, National Renewable Energy Laboratory; Christopher Hill, George Mason Univ.; Jay Gulledge, Pew Center on Global Climate Change; Dena Plemmons, Univ. of California, San Diego
Council Delegate: Michael Imperiale, Univ. of Michigan; Additional nominee to be announced

Statistics
Chair Elect: James Berger, Duke Univ.; Mitchell H. Gail, National Cancer Institute/NIH
Member-at-Large of the Section Committee: James L. Rosenberger, Pennsylvania State Univ.; Alan F. Karr, National Institute of Statistical Sciences
Electorate Nominating Committee: Larry Wasserman, Carnegie Mellon Univ.; Emery N. Brown, Massachusetts Institute of Technology, Harvard Medical School; Xuming He, Univ. of Illinois, Urbana-Champaign; Charmain Dean, Simon Fraser Univ., Canada
Council Delegate: John Lehoczky, Carnegie Mellon Univ.; Paul P. Biemer, Research Triangle Institute International

Published by AAAS

INTRODUCTION

What Is Epigenetics?

THE CELLS IN A MULTICELLULAR ORGANISM HAVE NOMINALLY IDENTICAL DNA sequences (and therefore the same genetic instruction sets), yet maintain different terminal phenotypes. This nongenetic cellular memory, which records developmental and environmental cues (and alternative cell states in unicellular organisms), is the basis of epi-(above)–genetics.

The lack of identified genetic determinants that fully explain the heritability of complex traits, and the inability to pinpoint causative genetic effects in some complex diseases, suggest possible epigenetic explanations for this missing information. This growing interest, along with the desire to understand the "deprogramming" of differentiated cells into pluripotent/totipotent states, has led to "epigenetic" becoming shorthand for many regulatory systems involving DNA methylation, histone modification, nucleosome location, or noncoding RNA. This is to be encouraged, but the labeling of nongenetic systems as epigenetic by default has the potential to confuse (see the related video at www.sciencemag.org/special/epigenetics/).

So what is epigenetics? An epigenetic system should be heritable, self-perpetuating, and reversible (Bonasio *et al.*, p. 612). Whether histone modifications (and many noncoding RNAs) are epigenetic is debated; it is likely that relatively few of these modifications or RNAs will be self-perpetuating and inherited. Looking beyond DNA-associated molecules, prions (infectious proteins) are clearly epigenetic, perpetuating themselves through altered folding states. These states can act as sensors of environmental stress and, through the phenotypic changes they promote, potentially drive evolution (Halfmann and Lindquist, p. 629).

Some metazoans undergo genome-wide reprogramming of DNA methylation and histone modifications during gametogenesis and embryogenesis (Feng *et al.*, p. 622), which may suppress the activity of potentially deleterious DNA sequences. Furthermore, the activity of various populations of small noncoding RNAs (Bourc'his and Voinnet, p. 617) probably act as tags for these deleterious sequences. These small RNAs may also be involved in assessing parental compatibility at fertilization. Similar RNAs are likely to be important determinants in paramutation, where homologous DNA sequences communicate in trans to establish heritable expression states (Chandler, p. 628). Reprogramming is also critical for developmental phenomena such as imprinting in both plants and mammals, as well as for cell differentiation, and is linked to the establishment of pluripotency in gametes and zygotes.

A News Focus story by Kaiser (p. 576) examines efforts to treat cancer patients with drugs that reverse the abnormal epigenetic patterns found in tumors, and a paper in *Science Translational Medicine** describes the use of epigenetic markers to predict which liver cancer patients will respond to an anticancer drug that blocks DNA methylation. Papers in *Science Signaling* discuss signaling pathways that alter epigenetic patterning, posttranscriptional regulation of signaling molecules by microRNAs, and transcriptional networks. Articles on *Science* Careers trace careers embracing a translational approach to epigenetics.

– GUY RIDDIHOUGH AND LAURA M. ZAHN

*J. B. Andersen *et al.*, *Sci. Transl. Med.* **2**, 54ra77 (2010).

Epigenetics

CONTENTS

See also News Focus story p. 576; Perspective p. 598; Report p. 680; Science Translational Medicine, Science Signaling, Science *Careers, Video, and* Science *Podcast at www.sciencemag.org/special/epigenetics/.*

Published by AAAS

REVIEW

Molecular Signals of Epigenetic States

Roberto Bonasio,* Shengjiang Tu,* Danny Reinberg†

Epigenetic signals are responsible for the establishment, maintenance, and reversal of metastable transcriptional states that are fundamental for the cell's ability to "remember" past events, such as changes in the external environment or developmental cues. Complex epigenetic states are orchestrated by several converging and reinforcing signals, including transcription factors, noncoding RNAs, DNA methylation, and histone modifications. Although all of these pathways modulate transcription from chromatin in vivo, the mechanisms by which epigenetic information is transmitted through cell division remain unclear. Because epigenetic states are metastable and change in response to the appropriate signals, a deeper understanding of their molecular framework will allow us to tackle the dysregulation of epigenetics in disease.

Adaptation to environmental changes and cell specialization in multicellular organisms require a complex orchestration of the transcriptional output of the genome. From the simplest prokaryote to the most sophisticated human neuron, cells have evolved forms of molecular memory of past stimuli that can often be transmitted through cell division. The maintenance of cell identity in multicellular organisms constitutes a classic example of such inheritable cellular memory: Starting from the same zygotic genome, subsets of progeny cells become engaged in distinct programs of gene expression that dictate their developmental trajectory and specific functions. Typically, cell identities are maintained for a lifetime, even when the differentiation signal was experienced only once, during embryonic development (*1*). This is no trivial achievement, as a complex pattern of gene expression must be faithfully transmitted to each progeny cell upon division.

We use the term epigenetics to classify those processes that ensure the inheritance of variation ("-genetic") above and beyond ("epi-") changes in the DNA sequence (Box 1). Unlike genetic alleles, epi-alleles do not differ in their DNA sequence; the epigenetic information resides in self-propagating molecular signatures that provide a memory of previously experienced stimuli, without irreversible changes in the genetic information. The nature of these molecular signatures and the manner by which they initiate, maintain, and reverse epigenetic states is the subject of this Review.

Epigenetic Signals in cis and trans

As long as a transcriptional response is self-sustaining in the absence of the originating stimulus, it can be categorized as epigenetic. This can be achieved by self-propagating, trans-acting mechanisms or by cis-acting molecular signatures physically associated with the DNA sequence that they regulate (Fig. 1).

Self-propagating transcriptional states that are maintained through feedback loops and networks of transcription factors (TFs) (*2*) are the most common type of trans epigenetic states (Fig. 1A). These are often the system of choice for cellular memory in simple organisms, such as prokaryotes and single-cell eukaryotes. If a TF activates its own transcription (or represses antagonistic networks), it yields an epigenetic state that is self-sustaining after the originating stimulus is removed. After each cell division, inherited TFs resume their trans function on regulatory DNA sequences. Some small RNAs (sRNAs) can also act as trans epigenetic signals (*3*–*5*).

In contrast, cis epigenetic signals are physically associated and inherited along with the chromosome on which they act (Fig. 1B)—for example, as a covalent modification of the DNA itself, such as DNA methylation, or as changes in histones, which constitute the protein backbone of chromatin. Histones can carry information in their primary sequence (histone variants), in post-translational modifications often present on their N- and C-terminal tails, or in their position (remodeling) relative to the DNA sequence (*6*–*8*). Cis epigenetic information might also be encoded in chromatin through stable association of non-histone proteins, higher-order chromatin structure, and nuclear localization.

It is often difficult to distinguish experimentally between trans and cis epigenetic signals. For example, initial observations implicated SWI/SNF chromatin remodelers in transcriptional memory at the *Saccharomyces cerevisiae GAL1* locus (*9*), but cell-fusion experiments rigorously demonstrated that the site of memory was the cytosol (*10*), a case of trans epigenetics. However, if two identical DNA sequences are differentially regulated in the same nucleus, cis epigenetic mechanisms must be responsible. This is observed for mono-allelic gene expression in diploid cells,

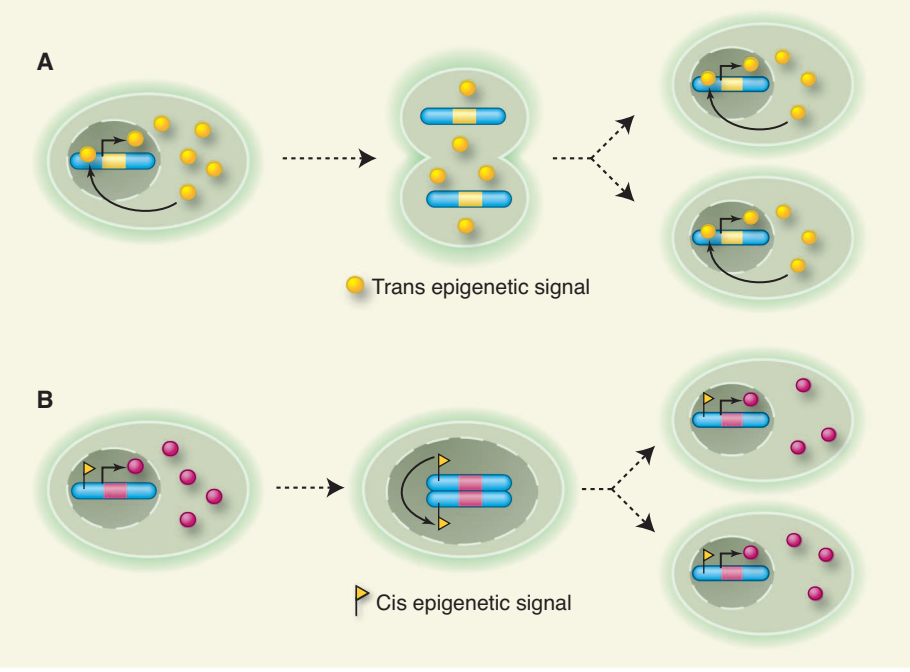

Fig. 1. Cis and trans epigenetic signals. (**A**) Trans epigenetic signals (yellow circles) are transmitted by partitioning of the cytosol during cell division and maintained by feedback loops. As an example, a simple regulatory loop in which the epigenetic signal induces its own expression is shown here. (**B**) Cis signals (yellow flags) are molecular signatures physically associated with the DNA and inherited via chromosome segregation during cell division.

Howard Hughes Medical Institute and Department of Biochemistry, School of Medicine, New York University, New York, NY 10016, USA.

*These authors contributed equally to this work.
†To whom correspondence should be addressed. E-mail: reinbd01@nyumc.org

Box 1. Epigenetics, What's in a Name?

The term "epigenetics" was coined by C. H. Waddington in the 1940s, fusing the word "genetics" with "epigenesis," the latter indicating the theory by which the adult form develops from the embryo through gradual steps, as opposed to being fully pre-formed in the zygote. Waddington intended to found a discipline to study the genetic control of developmental processes, merging the fields of embryology and genetics (*82*). More than a decade later, D. L. Nanney defined "epigenetic systems" as "auxiliary mechanisms … involved in determining which specificities [genes] are to be expressed in any particular cell." Nanney also warned that "[c]ellular memory is not an absolute attribute" and that using inheritance to define epigenetics might undermine the full understanding of the molecular pathways involved, which may also stabilize transcription patterns in nondividing cells (*83*). With the discovery of inheritable patterns of DNA methylation, the idea that epigenetic traits were inherited as regulatory signals in addition to genetic information quickly took hold, and the definition of epigenetics became "the study of mitotically and/or meiotically heritable changes in gene function that cannot be explained by changes in DNA sequence" (*84*).

The discovery of the regulatory role of histone posttranslational modifications and their correlation with transcriptional states promoted a looser use of epigenetics, to mean any molecular signature found on chromosomes (especially histone marks) and broadly defined as "the structural adaptation of chromosomal regions so as to register, signal or perpetuate altered activity states" (*85*). At the same time, a more narrow definition has been proposed as "a stably heritable phenotype resulting from changes in a chromosome without alterations in the DNA sequence" (*86*).

Here, we intend epigenetics to signify "the inheritance of variation (-genetics) above and beyond (epi-) changes in the DNA sequence." Rather than altering this basic definition, we prefer to append to it appropriate modifiers. The chromosome-dependent definition given in (*86*) corresponds to what we call cis epigenetics, as opposed to self-propagating patterns that operate in trans. We convey the distinction between transgenerational inheritance and cellular memory by referring to meiotic versus mitotic epigenetics, both cases of vertical epigenetics, as opposed to the RNA-mediated horizontal transmission of epigenetic states observed in plants (*53*).

imprinting, and X inactivation in mammals, wherein large portions of one X chromosome are inheritably silenced while its homolog continues to transcribe in the same nucleus (*11*). In fact, X chromosome inactivation involves many putative epigenetic signals and provides an excellent experimental and didactical model to study epigenetics.

If trans-acting transcriptional memory systems were readily available during evolution, why did the appearance of multicellularity expand the repertoire of cis epigenetic signals? One possibility is that trans mechanisms were simply inadequate for tackling the increased complexity and number of transcriptional networks in a large multicellular organism. Epigenetic states that are encoded in cis need to be set only once, and many transcriptional patterns can be maintained by a relatively small number of common molecular pathways, without having to deploy trans-acting feedback loops for each gene network.

Establishment

Most epigenetic states are established by transiently expressed or transiently activated factors that respond to environmental stimuli, developmental cues, or internal events (e.g., the reactivation of a transposon). These establishment signals converge on chromatin to shape the transcriptional landscape and are then converted into cis epigenetic signatures.

TFs orchestrate lineage-specification programs and are leading candidates as establishment signals (*12*). In addition to recruiting factors that modulate transcription transiently, TFs also influence cis epigenetic states. In *Drosophila*, TFs encoded by the segmentation genes establish cellular fate during early embryo development, and, although they disappear after only a few hours, cell identities are maintained into adulthood by the Polycomb group (PcG) of proteins that are associated with transcriptional repression, and the trithorax group (trxG) of proteins that are associated with transcriptional activation. Many members of both groups possess chromatin-modifying activities (*13*), and, given that *Drosophila* contains little DNA methylation, the PcG/trxG system is likely to be directly involved in the transmission (maintenance) of epigenetic states.

It is not clear how the transition from TF-driven regulation to a cis epigenetic state takes place. One possibility is that TFs directly recruit chromatin-modifying enzymes to their genomic targets. For example, sequence-specific DNA-binding proteins are required for PcG-mediated memory in *Drosophila* and recruit PcG complexes to regulatory regions called Polycomb response elements (PREs) (*14*), but recruitment does not always translate into repression of the downstream locus (*15*), suggesting that PRE localization of PcG and trxG complexes is necessary but not sufficient for the maintenance of transcriptional memory. Similarly, several TFs physically interact with DNA methyltransferases and recruit them to target genes (*16*).

In addition, TFs might establish epigenetic states through the process of transcription itself. Transcription of *Nesp* is required for the establishment of DNA methylation at the imprinted *Gnas* locus downstream, suggesting a cis mechanism (*17*), and transcription of the noncoding PREs induces an inheritable active state (*18*). Transcription also guides the deposition of histone posttranslational modifications, including H3K4me3, H3K36me3, H3K79me, and H2BK123ub (*19*), but these modifications have yet to pass the maintenance test for bona fide epigenetic signals (see below).

The transcription process affects chromatin structure, but it is often difficult to ascribe this effect to the physical passage of RNA polymerase II (RNAPII) or to the synthesis of noncoding RNAs (ncRNAs). Noncoding regions of the genome are heavily transcribed, giving rise to a constellation of ncRNAs that often have regulatory functions (*20*). Although early investigations focused on posttranscriptional gene silencing by microRNAs and other sRNAs, pioneering work in *Schizosaccharomyces pombe* and *Arabidopsis thaliana* established that sRNAs also affect epigenetic states (*3*). In particular, plants use sRNAs to repress transposable elements and regulate gene expression through the process of RNA-dependent DNA methylation (*21*). Other sRNAs with proposed effects on cis epigenetic states are PIWI-interacting RNAs (piRNAs) (*22*) and sRNAs that bind to (and perhaps mediate the recruitment of) PcG proteins (*23*). Even more classes of sRNAs may be involved in chromatin regulation, although a functional link has not yet been demonstrated; these include promoter- and termini-associated RNAs, tiny RNAs, and endo–small interfering RNAs (*20*).

Small ncRNAs are well suited for a role in bridging chromatin modifiers with the genome (*5*), but to fulfill this function they must interact in sequence-specific fashion with chromatin. We envision three modes of sequence recognition: (i) RNA:RNA interactions with nascent transcripts (Fig. 2A) (*3*), (ii) RNA:single-stranded DNA (ssDNA) heteroduplex (Fig. 2B), and (iii) RNA:double-stranded DNA (dsDNA) triplex (Fig. 2C) (*24*). These recognition modes are not mutually exclusive: piRNAs guide PIWI to *Drosophila* chromatin by both RNA:RNA and RNA:DNA interactions (*25*). Recruitment of chromatin modifiers might occur directly or via adaptor proteins, as in the case of Stc1, an *S. pombe* LIM domain–containing protein, that bridges Ago1 and its associated sRNAs to the H3K9 methyltransferase complex CLRC (*26*).

Long ncRNAs (lncRNAs) may also function as establishment signals for epigenetic states (*27*). Because of their size, these molecules can fold into complex structures with molecular surfaces dedicated to protein binding, while retaining the ability to recognize nucleotide sequences by base-pair interactions as described above for

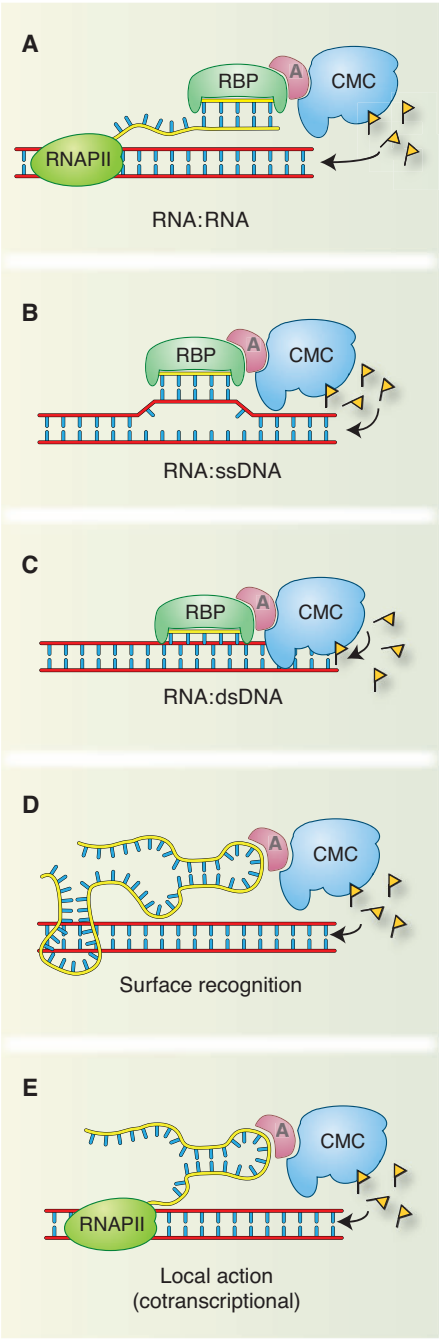

Fig. 2. RNA-directed deposition of epigenetic signals. (**A** to **C**) Sequence-specific recognition models for both sRNAs (shown here) and lncRNAs. (A) Interaction of an sRNA with complementary sequences on a nascent transcript. (B) Interaction of an sRNA with ssDNA to form a heteroduplex. (C) Recognition of sequence motifs by sRNA in a closed dsDNA duplex. (**D** and **E**) Additional recruitment models for lncRNAs. (D) A folded lncRNA recognizes a DNA sequence via complex surface-mediated interactions. (E) A lncRNA acting locally in a cotranscriptional fashion by being anchored to chromatin by RNAPII. RBP, RNA binding protein; A, hypothetical adaptor protein; CMC, chromatin-modifying complex.

sRNAs (*28*), although their tertiary structure may also allow for recognition modes that do not involve direct base-pair interactions (Fig. 2D). Some lncRNAs, such as *HOTAIR*, appear to act globally to recruit chromatin modifiers to target loci (*29*). Other lncRNAs act locally and establish cis epigenetic states on the genomic region from which they are transcribed. This second category includes lncRNAs involved in the classic epigenetic phenomena of parental imprinting and X chromosome inactivation, and their localized effect may be explained by two mechanisms: (i) The 5′ terminus may fold and interact with chromatin-modifying complexes, while the 3′ terminus is still tethered to the encoding locus by a transcribing RNAPII (Fig. 2E), and (ii) antisense transcription of a lncRNA might interfere with transcription of a neighboring gene or create double-stranded RNA species that are processed locally and establish cis epigenetic signal(s) to silence the locus.

Reinforcement and Spreading

Cis epigenetic states, such as those presumably encoded by histone posttranslational modifications and DNA methylation, can be reinforced locally or spread to adjacent areas to form larger chromatin domains. Feedback loops exist, in which enzymes responsible for the installment of a histone modification also interact with factors that bind to it. Examples of such histone modifier/binder pairs are SUV39H1 and HP1 for H3K9me, PR-SET7 and L3MBTL1 for H4K20me1, and EZH2 and EED for H3K27me (*30*–*32*). The local reinforcement may be necessary, because histone modifications are not permanent and may be removed by dedicated enzymes or histone turnover.

On the other hand, spreading in cis may be required to extend the reach of epigenetic regulation beyond the confined area in which establishment took place. Spreading of chromatin domains is the basis of classical epigenetic phenomena such as position-effect variegation in *Drosophila* and formation of silent domains in *S. cerevisiae* (*11*), and it was also observed for artificially established H3K27me3 domains in human cells (*33*).

Epigenetic states can also be reinforced by cross talk among histone modifications and DNA methylation (*34*). De novo DNA methyltransferases and associated factors bind to unmethylated H3K4 (*35*), whereas the H3K4 methyltransferase MLL preferentially binds to unmethylated DNA (*36*), providing a molecular explanation for the anti-correlation between H3K4me and DNA methylation levels (*37*). H3K9me is a prerequisite for all DNA methylation in *Neurospora crassa* and CHG DNA methylation in *A. thaliana* (*38*). In mice, the H3K9 methyltransferases SUV39H1/2 and EHMT2 (G9A) can direct de novo DNA methylation to certain loci, although the catalytic activity of G9A is not always necessary (*39*–*41*). This interplay suggests that, when present, DNA methylation may serve as a reinforcing signal for preexisting but less stable epigenetic signatures such as histone modifications.

Transmission

Three independent criteria should determine whether a certain molecular signal is indeed epigenetic: (i) mechanism for propagation; that is, pathways that explain how the molecular signature is faithfully reproduced after DNA replication/cell division; (ii) evidence of transmission; i.e., the demonstration of self-sustaining transmission to the progeny; and (iii) effect on gene expression; that is, a bona fide epigenetic signal should be sufficient to cause a transcriptional outcome reminiscent of that caused by the establishing stimulus (*42*).

DNA methylation satisfies all three requirements: (i) Because of the semiconservative nature of DNA replication, a DNA sequence carrying symmetrical methylation marks on both strands gives rise to two hemi-methylated double strands, which can be restored to fully methylated status by maintenance methyltransferases (*38*) (Fig. 3A); (ii) in vitro methylated DNA remains methylated after several rounds of DNA replication in vivo (*43*); and (iii) methylation regulates transcription.

The case for histone posttranslational modifications is less clear, and each mark should be considered separately. Some modifications exhibit strong correlation with transcriptional states (*7*); however, correlation does not imply causation, and experimental evidence for the epigenetic inheritance of histone modifications remains scarce.

Propagation mechanisms (criterion i) have been proposed for several histone modifications in the form of the same histone modifier/binder interactions involved in signal reinforcement and spreading (Fig. 3B). This model assumes that the information to re-establish chromatin domains is transferred from the parental nucleosomes containing such modifications to those deposited on the two daughter strands. However, it remains unclear whether and how parental histones (and their associated modifications) are reassembled after DNA replication in vivo. Alternatively, domains of histone modifications could be propagated via an intermediary (secondary) epigenetic signal. This appears to be the case for H3K9me in *S. pombe* heterochromatin, where S-phase–restricted transcription of repetitive sequences generates sRNAs that direct the re-establishment of H3K9me after replication (Fig. 3C) (*44*).

Whether histone posttranslational modifications are transmitted (criterion ii) remains largely unknown. This question can be addressed by artificially recruiting a histone modifier to chromatin using the GAL4/upstream activation sequence (UAS) system and then measuring the persistence of the resultant histone modification through cell division after terminating the expression of the histone modifier. The GAL4/UAS system can also be used to demonstrate that histone

modifications cause (not only correlate with) a transcriptional response (criterion iii) (*31*). To date, only short-term (4 days) transmission of H3K27me3 in cultured human cells has been observed (*33*, *45*), but doubts remain regarding incomplete repression of the GAL4-fused histone modifier. In addition, Polycomb repressive complex 1 remains bound to chromatin (independently of histone modifications) during DNA replication in vitro (*46*), and MLL (a trxG protein) appears to associate with mitotic chromosomes (*47*), suggesting that some chromatin modifiers may also function directly as cis epigenetic signals.

Some epigenetic information is transmitted through meiosis and gamete formation in multicellular organisms, giving rise to transgenerational inheritance. Many epigenetic signals appear capable of meiotic transmission, including maternally deposited TFs and piRNAs (*48*), RNAs involved in paramutation in mice (*49*), histone modifications in sperm chromatin (*50*), and DNA methylation in plants (*51*).

Finally, epigenetic signals are also transmitted from cell to cell in a horizontal fashion (*5*). This phenomenon is at the basis of the inheritance of RNA interference in *Caenorhabditis elegans* and occurs in plants, both in the germ line and in the soma (*52*, *53*), two cases in which sequence information is transmitted across cells to silence transposable elements. As no genomic DNA is exchanged between these cells, the epigenetic information must be transmitted in trans. In fact, it takes the form of sRNAs that direct DNA methylation of genomic sequences, converting a trans epigenetic signal into a cis epigenetic state (*53*).

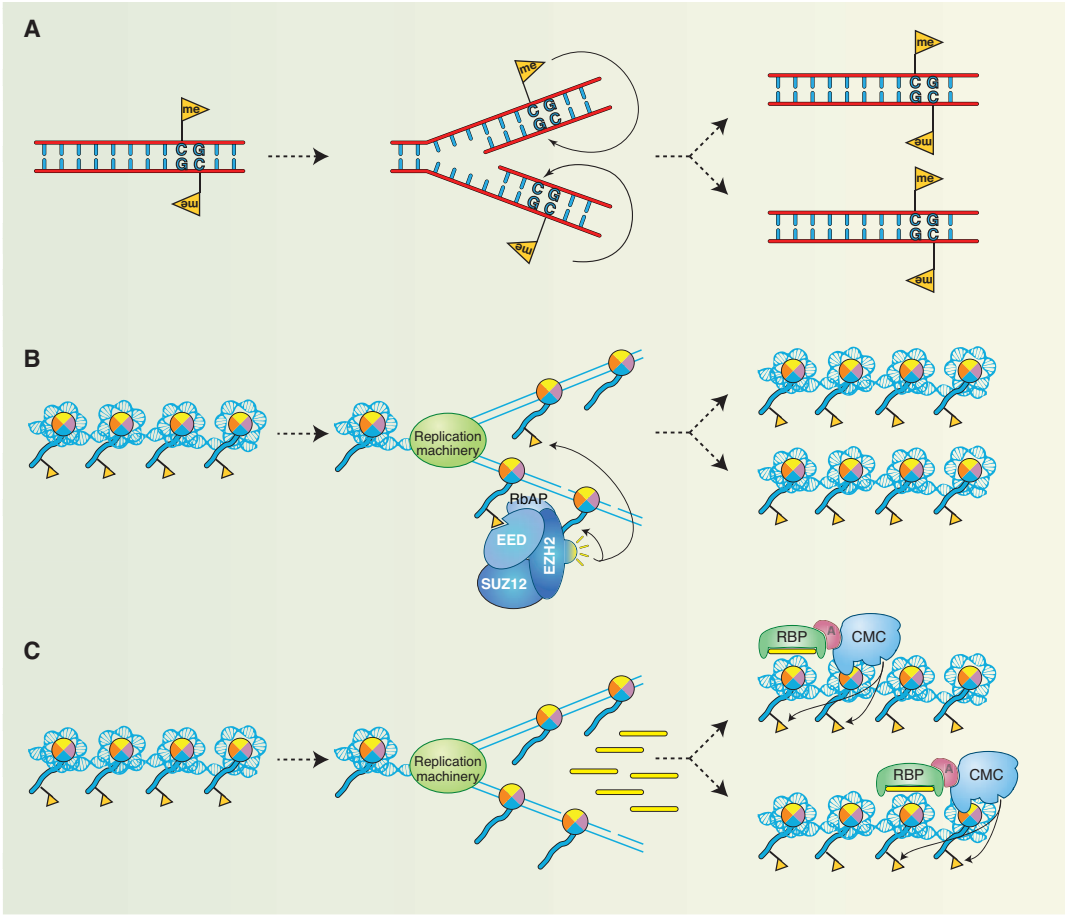

Fig. 3. Transmission of epigenetic states. (**A**) Transmission of DNA methylation patterns after DNA replication. (**B**) Hypothetical model for the maintenance of a histone-associated epigenetic signal, using H3K27me3 (yellow flags) as an example. H3K27me3 is diluted during DNA replication by the deposition of unmodified octamers. Binding of EED to H3K27me3 stimulates the enzymatic activity of EZH2, which places more H3K27me3 marks on neighboring nucleosomes, thus restoring a full epigenetic signature on both chromatids (*32*). (**C**) Maintenance of a chromatin domain via a secondary signal. S-phase transcription of heterochromatic repeats in *S. pombe* generates sRNA species that recruit chromatin-modifying complexes to reestablish heterochromatic signatures at the target loci.

Reversal

Epigenetic regulatory mechanisms are conservative in that no information is lost, and, given the appropriate signal, an epigenetic state can transition to a different one, as exemplified by the generation of induced pluripotent stem (iPS) cells from mouse embryonic fibroblasts (MEFs) by transient overexpression of cocktails of TFs (*54*). Although embryonic stem (ES) cells and MEFs have very different gene expression profiles, H3K4me and H3K27me distribution, and DNA methylation patterns, MEF-derived iPS cells closely resemble ES cells, both at the transcriptional and epigenetic levels (*55*). These observations not only demonstrate the plasticity of epigenetic signals, but also confirm the interdependence between cell identity and epigenetic states.

Reversible chromatin changes and antagonism between TFs provide the basis for cellular plasticity. Opposing TF networks reinforced by feedback loops direct the specification of hematopoietic and embryonic lineages (*12*, *56*). Histone modification profiles are also the result of a delicate balance between antagonistic pairs of histone-modifying enzymes—for example, histone acetyl-transferases versus deacetylases and histone methyl-transferases versus demethylases (*7*).

Nonetheless, the forced transition between two metastable epigenetic states requires a considerable "activation energy," as evidenced by the poor efficiency of epigenetic reprogramming by nuclear transfer or overexpression of pluripotency factors. Cells that fail to fully overcome this barrier are trapped in an intermediate state, probably because of a failure in resetting epigenetic signatures (*55*). For example, improper silencing by DNA hypermethylation and histone hypoacetylation of the imprinted *Dlk1-Dio3* cluster correlates with the failure of many iPS cell lines to generate chimeras (*57*). Thus, small-molecule inhibitors of histone modifiers and DNA methyl-transferases that stimulate reprogramming may do so by facilitating the creation of an "epigenetic tabula rasa" (*58*).

The most dramatic epigenetic plasticity is observed during early embryo development and germline specification in mammals. At fertilization, the condensed paternal genome is hypermethylated, until a wave of DNA demethylation restores it to an active state (*59*). Notably, some imprinted genes are not affected, suggesting that they must be marked with a different epigenetic signal (*60*). During development, germ cells undergo a second wave of DNA methylation (*61*), possibly in response to environmental cues in the

gonads, demonstrating that even the most stable epigenetic signal can be reversed by the appropriate stimuli.

These two cases in which genome-wide DNA methylation is rapidly lost likely involve the most elusive mode of epigenetic plasticity: DNA demethylation (*62*). Two mechanisms for DNA demethylation appear possible: (i) active demethylation through oxidation and (ii) base excision repair (BER). Hydroxylation of 5-methylcytosine by TET1-3 (*63*, *64*) argues in favor of the first mechanism, although the resulting 5-hydroxymethylcytosine must be further converted to unmethylated cytosine via presently unknown mechanisms. In plants, genetic evidence supports DNA demethylation via BER (*65*), but the importance of this pathway in animals is unclear. Activation-induced deaminase is involved in DNA demethylation in mammalian cells (*66*, *67*), yet its inability to act on dsDNA (*68*) and the lack of developmental defects in *Aid*$^{-/-}$ mice argue against a central role in DNA demethylation and development (*69*, *70*).

Thus, epigenetic states are stable enough to maintain cell identity, but they are also reversible enough to allow, when the proper signals are delivered, transitions among states. For example, the epigenetic plasticity of germ cells allows for cell specialization during gamete development, while retaining the potential for returning to the ground state of totipotency after fertilization.

Future Directions

Epigenetic signals have traditionally been studied in the context of development and transposon control, but we believe that epigenetic mechanisms will be the crux of many other biological processes. For example, brain function and memory formation may involve epigenetic signals (*71*, *72*). Although most neurons do not divide, they are very long-lived and must maintain a defined transcriptional state for an extremely long time. By our own definition, this phenomenon is not truly epigenetic, yet signals that evolved to maintain epigenetic states through cell divisions might have been co-opted by neurons to stabilize transcriptional profiles after the establishing stimulus has disappeared (*72*).

Another area in which a better understanding of epigenetic signals may benefit research is that of stem cell function. Stem cells divide asymmetrically, giving rise to one self-renewing cell and one cell committed to differentiate (*73*). This is usually attributed to external cues and asymmetric partitioning of trans-acting factors, but evidence suggests that chromatids (and any cis epigenetic signal they may carry) can also be segregated asymmetrically (*74*). Thus, asymmetric partitioning of epigenetic signals may participate in cell-fate decisions, as proposed in the "silent sister" hypothesis (*75*).

Epigenetics is also likely to affect aging, given that epi-mutations, especially in DNA methylation, may contribute to the aging phenotype (*76*). Epigenetic transmission is more error prone than DNA replication (*43*) and probably accumulates large amounts of inheritable errors over a lifetime. Pathways that impinge on chromatin states are also implicated in aging (*77*), but we are far from understanding the molecular mechanisms involved in this process.

Conserved molecular machineries manage genetic information in all organisms, yet different epigenetic signals predominate in different species. For this reason, epigenetic research has been conducted on an unusually broad spectrum of model organisms. If we had studied only *Drosophila*, we would know little about DNA methylation. Extending our studies to additional model organisms will undoubtedly be beneficial. Two emerging models appear to be very promising: (i) the planarian *Schmidtea mediterranea*, which displays incredible epigenetic flexibility in regenerating a complete adult from small patches of dissected tissue (*78*), and (ii) social insects, in which a single genome gives rise to epigenetically distinct castes that display dramatic physiological, morphological, and behavioral differences (*79*, *80*).

References and Notes

1. L. Ringrose, R. Paro, *Annu. Rev. Genet.* **38**, 413 (2004).
2. U. Alon, *An Introduction to Systems Biology: Design Principles of Biological Circuits* (Chapman & Hall/CRC Press/Taylor & Francis, Boca Raton, FL, 2006).
3. D. Moazed, *Nature* **457**, 413 (2009).
4. J. Brennecke *et al.*, *Cell* **128**, 1089 (2007).
5. D. Bourc'his, O. Voinnet, *Science* **330**, 617 (2010).
6. P. B. Talbert, S. Henikoff, *Nat. Rev. Mol. Cell Biol.* **11**, 264 (2010).
7. T. Kouzarides, *Cell* **128**, 693 (2007).
8. B. R. Cairns, *Nature* **461**, 193 (2009).
9. S. Kundu, P. J. Horn, C. L. Peterson, *Genes Dev.* **21**, 997 (2007).
10. I. Zacharioudakis, T. Gligoris, D. Tzamarias, *Curr. Biol.* **17**, 2041 (2007).
11. C. D. Allis, T. Jenuwein, D. Reinberg, *Epigenetics*, M. Caparros, Ed. (Cold Spring Harbor Laboratory Press, Cold Spring Harbor, NY, ed. 1, 2007).
12. T. Graf, T. Enver, *Nature* **462**, 587 (2009).
13. J. A. Simon, R. E. Kingston, *Nat. Rev. Mol. Cell Biol.* **10**, 697 (2009).
14. L. Ringrose, R. Paro, *Development* **134**, 223 (2007).
15. B. Papp, J. Müller, *Genes Dev.* **20**, 2041 (2006).
16. E. Hervouet, F. M. Vallette, P. F. Cartron, *Epigenetics* **4**, 487 (2009).
17. M. Chotalia *et al.*, *Genes Dev.* **23**, 105 (2009).
18. S. Schmitt, M. Prestel, R. Paro, *Genes Dev.* **19**, 697 (2005).
19. B. Li, M. Carey, J. L. Workman, *Cell* **128**, 707 (2007).
20. R. J. Taft, K. C. Pang, T. R. Mercer, M. Dinger, J. S. Mattick, *J. Pathol.* **220**, 126 (2010).
21. M. Matzke, T. Kanno, B. Huettel, L. Daxinger, A. J. Matzke, *Curr. Opin. Plant Biol.* **10**, 512 (2007).
22. A. A. Aravin *et al.*, *Mol. Cell* **31**, 785 (2008).
23. A. Kanhere *et al.*, *Mol. Cell* **38**, 675 (2010).
24. C. Escudeé *et al.*, *Nucleic Acids Res.* **21**, 5547 (1993).
25. B. Brower-Toland *et al.*, *Genes Dev.* **21**, 2300 (2007).
26. E. H. Bayne *et al.*, *Cell* **140**, 666 (2010).
27. J. T. Lee, *Genes Dev.* **23**, 1831 (2009).
28. M. J. Koziol, J. L. Rinn, *Curr. Opin. Genet. Dev.* **20**, 142 (2010).
29. J. L. Rinn *et al.*, *Cell* **129**, 1311 (2007).
30. M. D. Stewart, J. Li, J. Wong, *Mol. Cell. Biol.* **25**, 2525 (2005).
31. N. Kalakonda *et al.*, *Oncogene* **27**, 4293 (2008).
32. R. Margueron *et al.*, *Nature* **461**, 762 (2009).
33. K. H. Hansen *et al.*, *Nat. Cell Biol.* **10**, 1291 (2008).
34. H. Cedar, Y. Bergman, *Nat. Rev. Genet.* **10**, 295 (2009).
35. S. K. T. Ooi *et al.*, *Nature* **448**, 714 (2007).
36. M. Birke *et al.*, *Nucleic Acids Res.* **30**, 958 (2002).
37. A. Meissner *et al.*, *Nature* **454**, 766 (2008).
38. M. G. Goll, T. H. Bestor, *Annu. Rev. Biochem.* **74**, 481 (2005).
39. B. Lehnertz *et al.*, *Curr. Biol.* **13**, 1192 (2003).
40. S. Epsztejn-Litman *et al.*, *Nat. Struct. Mol. Biol.* **15**, 1176 (2008).
41. K. B. Dong *et al.*, *EMBO J.* **27**, 2691 (2008).
42. More generally, any phenotypic change may be transmitted epigenetically. For the sake of simplicity, we only discuss epigenetic control of gene expression in this Review. For an example of epigenetic transmission of altered protein function, see (*81*).
43. M. Wigler, D. Levy, M. Perucho, *Cell* **24**, 33 (1981).
44. E. S. Chen *et al.*, *Nature* **451**, 734 (2008).
45. K. Sarma, R. Margueron, A. Ivanov, V. Pirrotta, D. Reinberg, *Mol. Cell. Biol.* **28**, 2718 (2008).
46. N. J. Francis, N. E. Follmer, M. D. Simon, G. Aghia, J. D. Butler, *Cell* **137**, 110 (2009).
47. G. A. Blobel *et al.*, *Mol. Cell* **36**, 970 (2009).
48. J. Brennecke *et al.*, *Science* **322**, 1387 (2008).
49. M. Rassoulzadegan *et al.*, *Nature* **441**, 469 (2006).
50. S. S. Hammoud *et al.*, *Nature* **460**, 473 (2009).
51. H. Saze, *Semin. Cell Dev. Biol.* **19**, 527 (2008).
52. R. K. Slotkin *et al.*, *Cell* **136**, 461 (2009).
53. A. Molnar *et al.*, *Science* **328**, 872 (2010); published online 22 April 2010 (10.1126/science.1187959).
54. K. Takahashi, S. Yamanaka, *Cell* **126**, 663 (2006).
55. T. S. Mikkelsen *et al.*, *Nature* **454**, 49 (2008).
56. S. J. Arnold, E. J. Robertson, *Nat. Rev. Mol. Cell Biol.* **10**, 91 (2009).
57. M. Stadtfeld *et al.*, *Nature* **465**, 175 (2010).
58. D. Huangfu *et al.*, *Nat. Biotechnol.* **26**, 795 (2008).
59. W. Mayer, A. Niveleau, J. Walter, R. Fundele, T. Haaf, *Nature* **403**, 501 (2000).
60. W. Reik, W. Dean, J. Walter, *Science* **293**, 1089 (2001).
61. P. Hajkova *et al.*, *Mech. Dev.* **117**, 15 (2002).
62. S. K. Ooi, T. H. Bestor, *Cell* **133**, 1145 (2008).
63. M. Tahiliani *et al.*, *Science* **324**, 930 (2009); published online 16 April 2009 (10.1126/science.1170116).
64. S. Ito *et al.*, *Nature* **466**, 1129 (2010).
65. J. K. Zhu, *Annu. Rev. Genet.* **43**, 143 (2009).
66. N. Bhutani *et al.*, *Nature* **463**, 1042 (2010).
67. C. Popp *et al.*, *Nature* **463**, 1101 (2010).
68. R. Bransteitter, P. Pham, M. D. Scharff, M. F. Goodman, *Proc. Natl. Acad. Sci. U.S.A.* **100**, 4102 (2003).
69. M. Muramatsu *et al.*, *Cell* **102**, 553 (2000).
70. S. Feng *et al.*, *Science* **330**, 622 (2010).
71. K. Si, S. Lindquist, E. Kandel, *Cold Spring Harb. Symp. Quant. Biol.* **69**, 497 (2004).
72. C. Dulac, *Nature* **465**, 728 (2010).
73. S. J. Morrison, J. Kimble, *Nature* **441**, 1068 (2006).
74. T. A. Rando, *Cell* **129**, 1239 (2007).
75. P. M. Lansdorp, *Cell* **129**, 1244 (2007).
76. S. Gravina, J. Vijg, *Pflugers Arch.* **459**, 247 (2010).
77. G. Pegoraro, T. Misteli, *Aging (Albany NY)* **1**, 1017 (2009).
78. A. Sánchez Alvarado, *Cell* **124**, 241 (2006).
79. Honeybee Genome Sequencing Consortium, *Nature* **443**, 931 (2006).
80. R. Bonasio *et al.*, *Science* **329**, 1068 (2010).
81. R. Halfmann, S. Lindquist, *Science* **330**, 629 (2010).
82. C. Waddington, *Endeavour* **1**, 18 (1942).
83. D. L. Nanney, *Proc. Natl. Acad. Sci. U.S.A.* **44**, 712 (1958).
84. A. Riggs, R. Martienssen, V. Russo, in *Epigenetic Mechanisms of Gene Regulation*, V. Russo, R. Martienssen, A. Riggs, Eds. (Cold Spring Harbor Laboratory Press, Cold Spring Harbor, NY, 1996), vol. 32, p. 1.
85. A. Bird, *Nature* **447**, 396 (2007).
86. S. L. Berger, T. Kouzarides, R. Shiekhattar, A. Shilatifard, *Genes Dev.* **23**, 781 (2009).

87. We thank L. Vales for critical reading of this manuscript. Work in the Reinberg laboratory is supported by HHMI and NIH grants GM064844 and GM037120. R.B. is a fellow of the Helen Hay Whitney Foundation.

10.1126/science.1191078

REVIEW

A Small-RNA Perspective on Gametogenesis, Fertilization, and Early Zygotic Development

Déborah Bourc'his[1]* and Olivier Voinnet[2,3]*

Transient populations of cis- and trans-acting small RNAs have recently emerged as key regulators of extensive epigenetic changes taking place during periconception, which encompasses gametogenesis, fertilization, and early zygotic development. These small RNAs are not only important to maintain genome integrity in the gametes and zygote, but they also actively contribute to assessing the compatibility of parental genomes at fertilization and to promoting long-term memory of the zygotic epigenetic landscape by affecting chromatin. Striking parallels exist in the biogenesis and modus operandi of these molecules among diverse taxa, unraveling universal themes of small-RNA–mediated epigenetic reprogramming during sexual reproduction.

Protecting the sperm and oocyte, assessing their compatibility at fertilization, and safeguarding the progeny are key stages of sexual reproduction during which genome integrity must be monitored and preserved from the effects of potentially harmful genomic parasites including transposons. A major, pan-eukaryotic safeguard mechanism during this important time window is RNA silencing, whereby 20- to 35-nt-long RNA species guide transcriptional (TGS) or posttranscriptional gene silencing (PTGS) of complementary DNA or RNA, respectively. Silencing small RNAs fall into three categories [reviewed in (*1*)]. Small interfering RNA (siRNA) populations are produced from long double-stranded RNAs (dsRNAs) arising from converging or overlapping transcription; inverted gene duplication; or, in some organisms, through RNA-dependent RNA polymerases (RDRs) acting on single-stranded RNA. Discrete micro-RNA (miRNA) species, by contrast, are excised from stem-loop precursors transcribed from genetically defined loci. siRNAs and miRNAs accumulate in both soma and germline, are processed as 20- to 24-nt species by ribonuclease III–like Dicer enzymes, and are loaded into Argonaute (AGO) effector proteins that often display endonucleolytic ("slicer") activity on target RNA. A third small-RNA class, about 30 nt long, is made up of PIWI-associated RNAs (piRNAs), which are mostly germline-specific and Dicer independent, and are effected through AGO-like PIWI proteins (Fig. 1A).

This review examines recent evidence supporting central roles for transposon-derived siRNAs and piRNAs during pre- and postzygotic reproduction stages. The amplified nature, noncell autonomy and trans-targeting capacity of these molecules not only allow protection of gametes' genomes (preparation phase) but also might actively contribute to assessing parental compatibility at fertilization (confrontation phase) in *Drosophila*, *Arabidopsis*, and ciliates. Remarkably, when they are translocated into the nucleus, these small RNAs may also guide retrograde mechanisms, which allow chromatin-based reinforcement and potential memory of these events in the zygote and developing embryo (consolidation phase). We discuss further the possible impact of potentially related phenomena in mammalian reproduction.

Preparation

During preparation, small-RNA–based mechanisms monitor and enforce gametic genome integrity, which is required for successful fertilization. A double-layer piRNA system protects the *Drosophila* female germline against two distinct threats (Fig. 2A). First, Gypsy-like long terminal repeat (LTR) retroviruses proliferating in surrounding, somatic follicle cells can infect the oocyte as follicle cells feed the growing germline. Follicle cells are able to capture de novo integrating transposons (*2*, *3*) through genomic clusters epitomized by the FLAMENCO locus, whose transcription produces antisense, PIWI-bound piRNAs that guide degradation of complementary Gypsy-like mRNAs (Fig. 2A, top). Second, the female germline itself, composed of the haploid oocyte and polyploid nurse cells, faces the threat of many endogenous transposon types. These are silenced through the amplified "ping-pong" mechanism initiated in piRNA clusters, such as the 42AB locus, which display a wider transposon-trapping spectrum than FLAMENCO (Fig. 1A and Fig. 2A, bottom) (*4*). Ping-pong piRNAs are likely produced in nurse cells and fed to the quiescent meiotic oocyte through cytoplasmic bridges; their biogenesis within the germline-specific "Nuage" compartment requires, in addition to PIWI, the PIWI-like proteins Ago3 and Aubergine (*4*). Mutations in any of these components cause transposon mobilization and female sterility. Comparatively, maintenance of gametic genome integrity is more enigmatic in the male germline, where the piRNA pathway seems less specialized for transposon targeting (*5*). It notably controls the male germ cell–specific *Stellate* gene amplified on the X chromosome; Stellate protein aggregation into crystals is thought to compromise male gamete integrity (*6*).

Plant genomes lack PIWI proteins and adaptive piRNA genomic clusters. Consequently, revealing transposons' presence in gametophytes paradoxically entails their reactivation in accessory or nursing cells by overcoming two independent, yet often overlapping, mechanisms for transposon silencing (*7*). A first, innate TGS process involves the activities of MET1, which maintains DNA methylation at symmetric CG sites, and of DDM1, a SWI-SNF chromatin-remodeling factor with intrinsic affinity for transposons and/or repeats (Fig. 1B, top). Second, a plant-specific polymerase, PolIV (p4), can back up MET1-DDM1 action at some loci, owing to a presumed affinity for methylated or heterochromatic DNA. RDR2 converts PolIV transcripts into dsRNAs, which are further processed by Dicer-like protein DCL3 into 24-nt-long "p4" siRNAs. The p4 siRNAs guide AGO4 back onto the DNA, in cis, by recruiting a second plant-specific polymerase, PolV. AGO4-PolV complexes then attract de novo DNA methyltransferases, which target cytosines in all sequence contexts (CG, CHG, and CHH) (H = A, T, or C) (Fig. 1B, middle). Non-CG methylation, notably, provides a diagnostic signature of this back-up system. Only its combined loss with that of MET1-DDM1 allows PolII-dependent transcription and mobilization of transposons (*8*, *9*). As an ultimate back-up process, highly accumulating transposons may undergo posttranscriptional gene silencing, presumably by means of the RDR6-DCL4-AGO1–dependent pathway that normally silences transgenes through 21-nt-long siRNAs (Fig. 1B, bottom) (*7*, *10*). Both p4 and 21-nt siRNAs are mobile in *Arabidopsis*, which allows TGS and PTGS transmission not only between neighboring cells—for instance, those found in gametophytes (see below)—but also between distant organs, through the vascular system (*11*, *12*).

During female gametogenesis in angiosperm plants, such as *Arabidopsis*, the haploid egg cell and the homodiploid central cell—respectively precursors of the diploid embryo and triploid endosperm—are formed. Owing to MET1 downregulation during gametogenesis (*13*), a first wave of p4 siRNA production uncovers the presence and identity of transposons. Strictly restricted to the central cell is the additional and coincident induction of DEMETER (DME), a DNA glycosylase that erases cytosine methylation in all

[1]Institut Curie, CNRS UMR 3215, INSERM U934, 75248 Paris cedex 05, France. [2]Institut de Biologie Moléculaire des Plantes, CNRS UPR2357, Université de Strasbourg, 67081 Strasbourg, France. [3]Swiss Federal Institute of Technology (ETH-Z), 8092 Zurich, Switzerland.

*To whom correspondence should be addressed. E-mail: Deborah.Bourchis@curie.fr (D.B.); olivier.voinnet@ibmp-ulp.u-strasbg.fr or olivier.voinnet@ipw.biol.ethz.ch (O.V.)

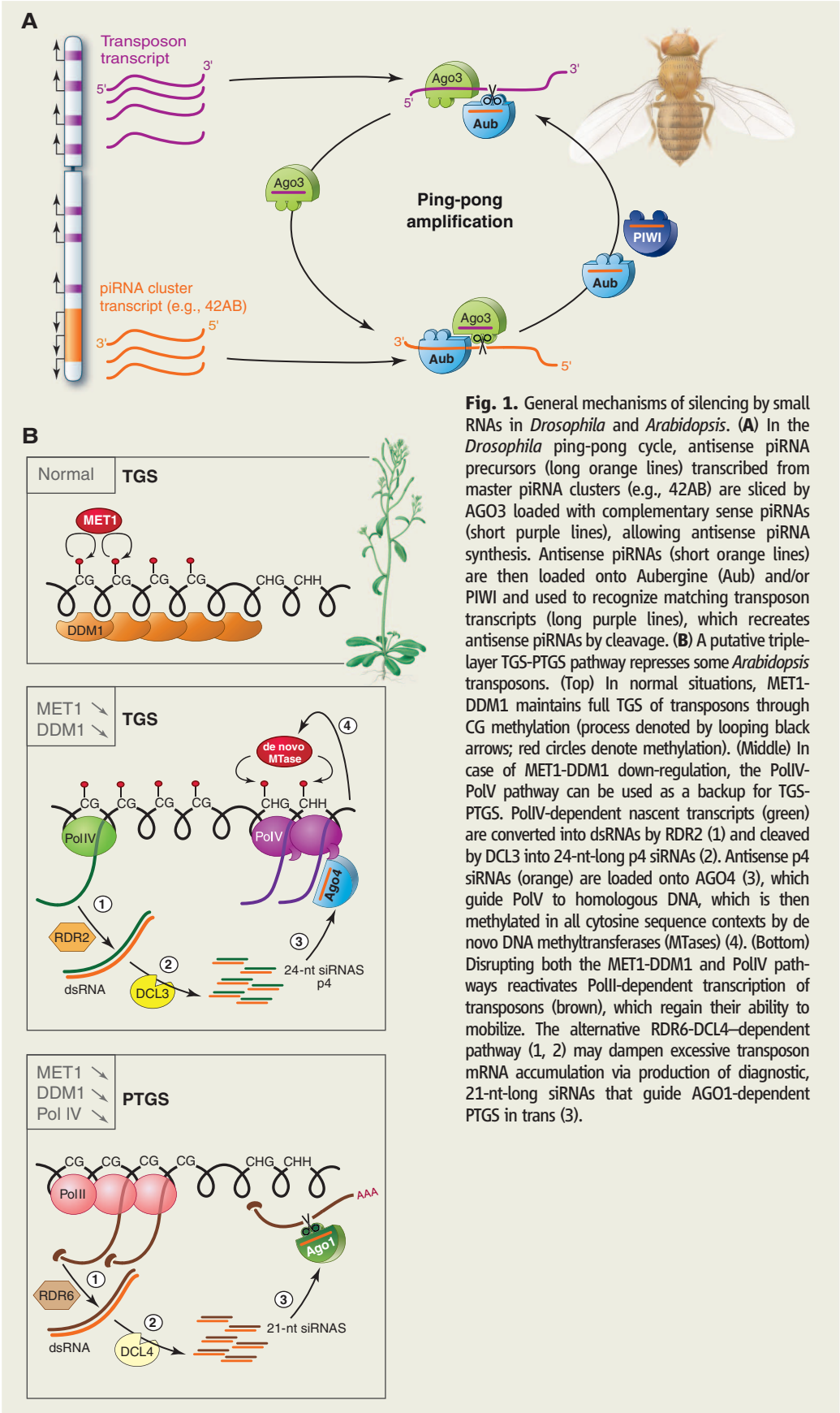

Fig. 1. General mechanisms of silencing by small RNAs in *Drosophila* and *Arabidopsis*. (**A**) In the *Drosophila* ping-pong cycle, antisense piRNA precursors (long orange lines) transcribed from master piRNA clusters (e.g., 42AB) are sliced by AGO3 loaded with complementary sense piRNAs (short purple lines), allowing antisense piRNA synthesis. Antisense piRNAs (short orange lines) are then loaded onto Aubergine (Aub) and/or PIWI and used to recognize matching transposon transcripts (long purple lines), which recreates antisense piRNAs by cleavage. (**B**) A putative triple-layer TGS-PTGS pathway represses some *Arabidopsis* transposons. (Top) In normal situations, MET1-DDM1 maintains full TGS of transposons through CG methylation (process denoted by looping black arrows; red circles denote methylation). (Middle) In case of MET1-DDM1 down-regulation, the PolIV-PolV pathway can be used as a backup for TGS-PTGS. PolIV-dependent nascent transcripts (green) are converted into dsRNAs by RDR2 (1) and cleaved by DCL3 into 24-nt-long p4 siRNAs (2). Antisense p4 siRNAs (orange) are loaded onto AGO4 (3), which guide PolV to homologous DNA, which is then methylated in all cytosine sequence contexts by de novo DNA methyltransferases (MTases) (4). (Bottom) Disrupting both the MET1-DDM1 and PolIV pathways reactivates PolII-dependent transcription of transposons (brown), which regain their ability to mobilize. The alternative RDR6-DCL4–dependent pathway (1, 2) may dampen excessive transposon mRNA accumulation via production of diagnostic, 21-nt-long siRNAs that guide AGO1-dependent PTGS in trans (3).

sequence contexts (Fig. 2B) (*14*). ROS3, a protein required for DME-like protein action, binds small RNAs in vitro and in vivo (*15*); it is therefore tempting to speculate that the first wave of p4 siRNAs might direct the DME-dependent genome-wide demethylation typically observed in the central cell and, after fertilization, in the endosperm (*16*, *17*). The ensuing transposon reactivation is likely to stimulate strongly the PolIV back-up pathway (*8*, *9*), and this probably explains the massive central cell– and endosperm-specific accumulation of p4 siRNAs seen in female gametophytes (*18*). These abundant p4 siRNAs are then potentially available to enforce transposon silencing through non-CG methylation in the egg cell and future embryo (Fig. 2B). Similarly, in the male gametophyte (pollen), which is composed of two haploid sperm cells and one accessory vegetative cell, only the vegetative cell relaxes transcriptional gene silencing of transposons, through the simultaneous down-regulation of DDM1 and dampening of the PolIV pathway (Fig. 2C) (*19*). As a backup, the vegetative cell uses PTGS to degrade the now highly abundant transcripts from mobilizing transposons, generating 21-nt-long siRNAs with intrinsic trans-activity (*19*). Should transposons escape the robust TGS set in sperm cells, these mobile 21-nt siRNAs can potentially provide an additional protection layer through PTGS and, perhaps, TGS via non-CG methylation (Fig. 2C). Therefore, accessory or nursing cells of plant gametophytes apparently lose their genome integrity in order to supply gametes with protective siRNAs.

In unicellular ciliates such as *Tetrahymena* and *Paramecium*, the diploid micronucleus (mic) fulfils germline functions, whereas the polyploid macronucleus (mac) ensures gene expression during vegetative growth. Although they occur post-zygotically, mechanisms for maintenance of genome stability in ciliates are conceptually similar to those observed in pollen, except that the germline equivalent (mic) is here involved in ensuring the integrity of the somatic genome (mac) (*20*). In the preparation phase, the meiotic mic exits quiescence to produce

DICER-dependent "scan" RNAs (scnRNAs), which map to all germline sequences, including transposons, whereas the mac transcribes longer, noncoding RNAs (ncRNAs), which represent an RNA "cache" of the somatic genome (Fig. 2D). After loading into meiosis-specific PIWI-like proteins (*21*), trans-acting scnRNAs then confront the mac-derived ncRNAs, as detailed below.

Confrontation

During confrontation, the genomic compatibility of gametes and/or nuclei is "assessed" through RNA-RNA interactions, preventing parental genomes' toxicity to the zygote. Confrontation in *Drosophila* primarily relies on ping-pong piRNAs that have accumulated in the oocyte (Fig. 3A). In the embryo, maternally deposited antisense piRNAs can initiate novel ping-pong cycles against any matching, sperm-delivered sense transposon (*22*). Although not formally demonstrated, a similar scenario of parental RNA confrontation may apply in plants. Double fertilization of the egg and the central cells by each sperm cell produces the embryo and the nurturing endosperm, respectively. Abundant maternal p4 siRNAs that have accumulated in the central cell could predictably direct non-CG methylation of matching, paternal transposons brought by the sperm into the endosperm. Conversely, sperm-derived 21-nt siRNAs could prevent excessive maternal transposition in the hypomethylated endosperm. In the embryo, these paternal 21-nt siRNAs could degrade transposon RNAs that have potentially escaped TGS (Fig. 3B). In ciliates, confrontation proceeds through a subtractive hybridization, where mic-derived scnRNAs are neutralized by annealing to complementary, mac-derived ncRNAs (Fig. 3C) (*20*). Noncomplementary scnRNAs originating from the mic genome escape this filtering and are thus singularized as nonself sequences,

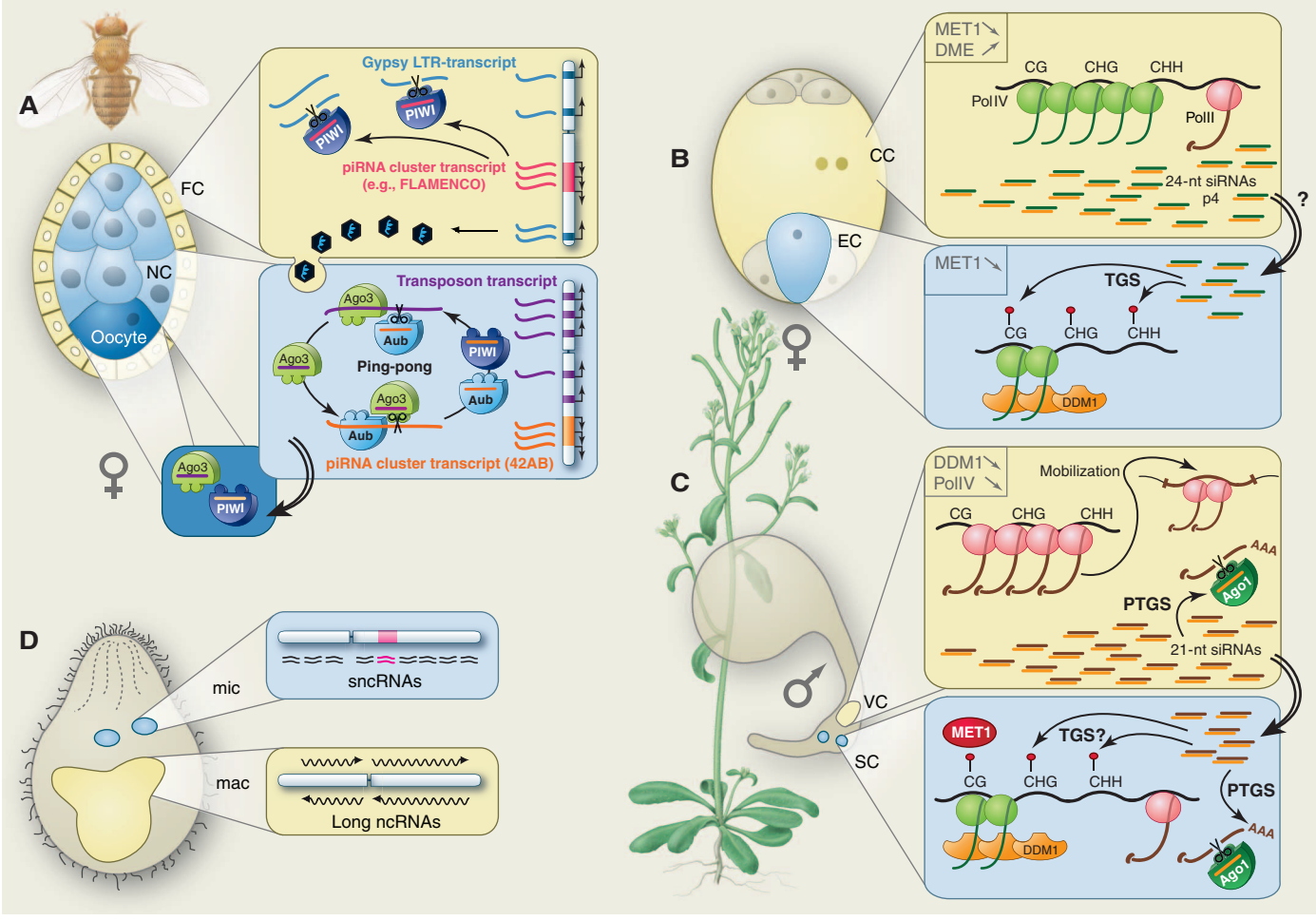

Fig. 2. Preparation phase in *Drosophila*, *Arabidopsis*, and ciliates. Accessory or nursing cells are depicted in yellow; germline cells, in blue. Molecular components are represented with the same color codes as in Fig. 1. (**A**) In *Drosophila* ovarioles, FLAMENCO-like piRNA clusters (red) in follicle cells (FC) feed a PIWI-dependent linear piRNA pathway that silences Gypsy-like retroviruses (blue), which can otherwise form infectious particles and invade the germline. A ping-pong–based piRNA pathway (Fig. 1A) operates in the germline nurse cells (NC) surrounding the haploid oocyte (darker blue), in which PIWI-Aub– and AGO3-bound piRNAs are likely deposited (double-line arrow). NC polyploidy may further enhance the ping-pong potency against transposons. (**B**) In the *Arabidopsis* female gametophyte, loss of MET1 occurs both in the diploid central cell (CC) and the haploid egg cell (EC). Simultaneous DME activation in the CC causes genome-wide demethylation only in this cell type, incurring strong production of PolIV-dependent, 24-nt-long p4 siRNAs (green and orange lines as in Fig. 1B) and, potentially, some PolII-dependent transcription. p4 siRNAs may move into the EC (double-line arrow) to enforce TGS through CG and non-CG methylation (CHG and CHH). The repressive state is potentially maintained by DDM1. (**C**) In the *Arabidopsis* male gametophyte, combined loss of DDM1 and PolIIV strongly reactivates PolII-dependent transcription and mobilization of transposons in the vegetative cell (VC). Excessive transposon levels promote massive production of 21-nt siRNAs (brown and orange lines) and PTGS via AGO1 (as in Fig. 1B). In the two sperm cells (SC), MET1 and DDM1 are present to provide full TGS of transposons. Nonetheless, in case of relaxation, 21-nt siRNAs delivered by the VC (double-line arrow) can enforce transposon silencing by PTGS, and maybe TGS through CG and non-CG methylation. (**D**) In *Paramecium*, scnRNAs and long ncRNAs are produced from the entire genome of the germline-like mic and somatic mac nuclei, respectively. The two nuclei may differ in their DNA content (pink chromosomal region in the mic nucleus and pink lines denoting scnRNAs from this region).

which will require elimination in the new zygotic mac (*23*).

Consolidation

To consolidate the outcome of preparation and confrontation, RNA-based information, labile by nature, is converted into chromatin-based information, which allows long-term perpetuation of embryonic and adult epigenetic landscapes. In *Drosophila*, piRNAs guide PTGS in the cytoplasmic Nuage structure, but PIWI also interacts in the nucleus with a variant of heterochromatin protein–1 (HP1α) (*24*). Disruption of piRNA biogenesis or function promotes a shift in transposon chromatin states from inactive to active (*25*), which suggests that PIWI-bound piRNAs guide the process of heterochromatinization and long-term TGS of at least some target loci (Fig. 3A). This process could, in principle, unfavorably silence master ping-pong piRNA clusters (e.g., 42AB) and ultimately compromise the pathway's adaptive potential, but a distinct HP1 homolog, Rhino, apparently prevents this by competing with HP1α at the 42AB locus (Fig. 3A) (*26*). In plants, the endosperm feeds the embryo with nutrients, and so p4 siRNAs may conceivably also use this path to reinforce silencing in the embryo, which indeed displays characteristic non-CG methylation at transposons or repeats (Fig. 3B) (*16*). The ultimate consolidation scheme appears to function in ciliates, where unwanted DNA is physically eliminated at once. Hence, mic-derived, PIWI-bound scnRNAs that have previously escaped subtractive hybridization guide repressive histone marks at homologous loci in the zygotic mac (*27*), from which DNA is excised (Fig. 3C).

When the System Fails: Hybrid Incompatibilities

Postfertilization barriers between distant strains or species often cause sterility or lethality in hybrid offspring. Given the processes discussed above, hybrid incompatibility might sometimes entail qualitative and/or quantitative inadequacies between transposon RNAs and transposon-derived small RNAs contributed by each confronting gamete or nucleus. In support of this view, transposons are reliable markers of genetic distance and speciation (*28*). In *Drosophila*, maternal ping-pong piRNAs can, in principle, accommodate infinite quantities of matching transposon RNAs delivered by the sperm (Figs. 1A and 3A). The system fails, however, if paternal transposons are too sequence-divergent to be recognized by the maternal piRNA reservoir (Fig. 4A). This incurs "hybrid dysgenesis," where transposons invading the developing embryonic germline cause genome instability and, ultimately, sterility in the offspring (*22*, *29*). A related mechanism may partly explain phenotypes of hybrid seed abortion observed in interspecific *Arabidopsis* crosses, which were indeed correlated with the massive activation of paternal ATHILA transposons (*30*). Here, hybrid failure could result

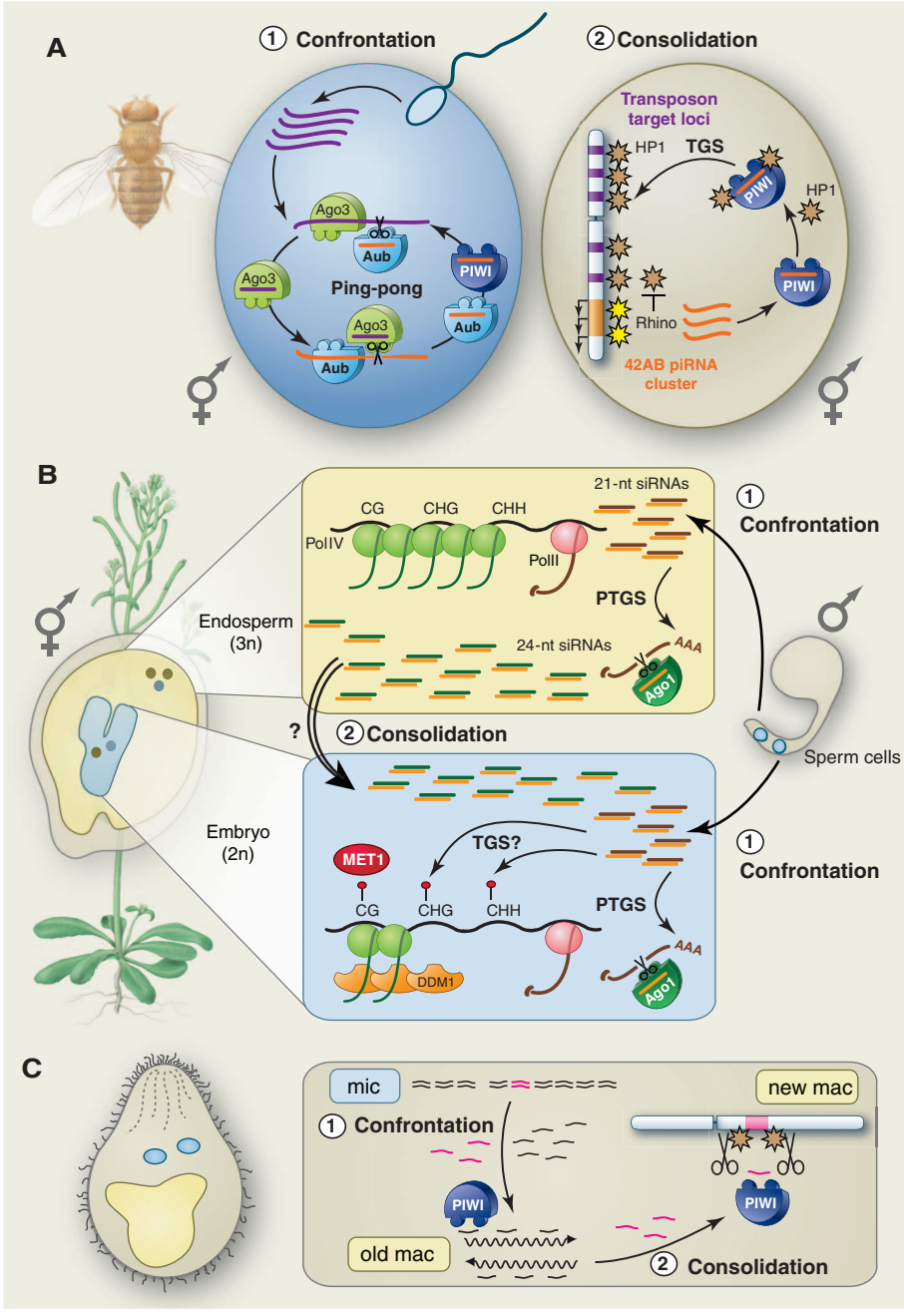

Fig. 3. Mechanisms for confrontation and consolidation. (**A**) In the *Drosophila* confrontation phase (1), Aub-PIWI- and Ago3-bound piRNAs deposited in the oocyte before fertilization protect the zygote against any matching, sperm-delivered transposon (purple), through the adaptive ping-pong pathway. During consolidation (2), PIWI-bound piRNAs can further direct heterochromatinization and TGS of target transposon loci (purple) via HP1 (brown stars). The HP1 homolog Rhino (yellow stars) prevents TGS of master ping-pong piRNA clusters of the 42AB type (orange), thereby preserving primary piRNA production. (**B**) In *Arabidopsis*, confrontation (1) might occur at fertilization through putative delivery of 21-nt siRNAs by the sperm cells into the CC (yellow) and the EC (blue), giving rise, respectively, to the triploid endosperm and diploid embryo. These 21-nt siRNAs can potentially direct PTGS (via AGO1) of complementary transposon RNAs escaping silencing, and they may also trigger transposon TGS by recruiting the DNA methylation machinery (as in Fig. 1B). TGS in the embryo (blue) can be potentially consolidated (2) by delivery of p4 siRNAs previously produced in the CC and fed by the endosperm (double-line arrow). (**C**) In ciliates, confrontation (1) consists in the filtering of most PIWI-bound mic-derived scnRNAs by long mac-derived ncRNAs (as in Fig. 2D). In the consolidation phase (2), remaining scnRNAs (pink) target heterochromatinization (brown stars) and excision of complementary sequences in the new zygotic mac.

either from excessive divergence between sequences of paternal transposon RNAs and maternal transposon-derived siRNAs or from an inadequate dosage of each protagonist at fertilization (Fig. 4A) (*31*). Consistent with the latter proposal, increasing maternal ploidy can override parental incompatibility in *Arabidopsis* (*30*). Similarly, one could envision that precise stoichiometry between confronting RNAs from the mic and the mac nuclei might influence ciliates' reproductive success (Fig. 4A). Hence, crucial portions of the mac genome may be erroneously eliminated in case of overrepresentation of mic-derived scnRNAs or underrepresentation of mac-derived ncRNAs. Conversely, overaccumulating ncRNAs may prevent elimination of unwanted sequences in the mac genome.

What About Mammals?

Are some of the above concepts applicable to mammals? As in *Drosophila*, the mammalian germline produces amplifiable piRNAs (*32*), and similarly to plants, genome-wide demethylation unmasks transposons (*33*), although mammalian gametes do not rely on accessory or nursing cells for this. Although impairing piRNA biogenesis or function reactivates transposons and compromises fertility in males (*33*), any similar function in oocytes is less evident. Nonetheless, dysgenesis-related phenomena are common among hybrid mammals, and we anticipate that some may involve inadequacies between transposon RNAs and silencing small RNAs brought by one or both parents into the zygote. In support of this view, transposon RNA can be carried over from parents to embryo in LINE1 transgenic mice (*34*), and amplification of endogenous retroelements occurs in hybrid progenies of distant kangaroo species (*35*). Moreover, crosses between females of the DDK inbred mouse strain and non-DDK males incur early embryonic lethality (DDK syndrome), owing to incompatibility between a maternally deposited factor and a paternal locus (*36*). Remarkably, the DDK susceptibility locus is strongly enriched in LTR and long interspersed nuclear element (LINE) repeats (*37*). Perhaps the DDK syndrome results from paternal transposon expansions that cannot be qualitatively or quantitatively matched by the female DDK factor, which might be small RNAs. Consistent with this idea, siRNAs and moderate amounts of piRNAs are detected in mammalian oocytes (*38*). Recent evidence suggests that the quiescent mammalian sperm also contains small RNAs (*39*), although whether they can be transmitted during fertilization is unknown. Nonetheless, ectopic miRNAs delivered by mouse sperm were shown to promote gene expression changes that, remarkably, persist in progenies (*40*).

Conclusions and Perspectives

RNA cross talk between nuclei or cells might thus represent widely used mechanisms for gametic or zygotic genome integrity and hybrid compatibility. Although presented merely from the standpoint of genome protection, the processes evoked here may also implicate non-transposon small RNAs with regulatory rather than defensive functions, such as miRNAs and trans-acting siRNAs. In *Brassica*, small RNAs produced during gamete preparation can overcome inbreeding barriers and therefore expand mating possibilities (*41*); specific to the diploid phase of heterozygous pollens, a dominant allele produces small RNAs that mediate in trans DNA methylation and repression of the recessive allele of a key locus involved in pollen or pistil recognition. Expression or sequence polymorphisms between regulatory small RNAs in one parent and their targets in the other could also influence hybrid compatibility during the confrontation phase. How hypothetical, maternal mRNAs encoding toxic products could act as fertilization gateways through their specific inactivation by matching paternal siRNAs or miRNAs is depicted in Fig. 4B. Excessive phylogenetic distance between the two parents would, this way, be strongly counterselected. Recent evidence for miRNA-directed DNA methylation in plants (*42*) further suggests a possible zygotic or embryonic consolidation of such putative events. Finally, in *Arabidopsis*, stress-responsive loci produce mobile small RNAs with the potential to invade the germline (*43*), whereas in *Drosophila*, aging and temperature influence female sterility in nonmendelian ways reminiscent of piRNA action (*44*). It is thus conceivable that environmental cues perceived in parents might not only affect epigenetic transgenerational memory (*43*), but also the mere capacity to pass their genome to subsequent generations.

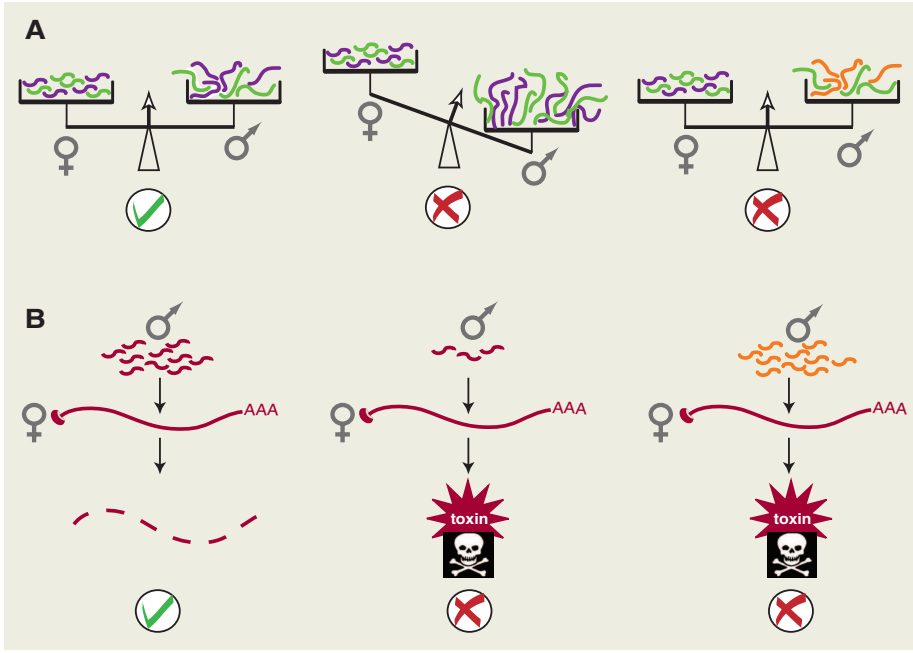

Fig. 4. Possible mechanisms underlying hybrid incompatibility. (**A**) Compatibility is fulfilled when appropriate levels of female small-RNA pools match transposon RNAs delivered by the male (left). Incompatibility may occur because of quantitative (middle) or qualitative (right) inadequacies between these two parental RNA populations. (**B**) Compatibility checking might also hypothetically involve maternal mRNAs (capped and polyadenylated), for instance, encoding a lethal toxin, that act as sentinels of features of sperm-delivered siRNAs or miRNAs. Degradation of maternal toxic mRNAs by paternal small RNAs would allow further development (left), while quantitative (middle) or qualitative (right) inadequacies would incur incompatibility. Schemes in (A) to (B) could apply to crosses in both parental directions.

References and Notes

1. M. Ghildiyal, P. D. Zamore, *Nat. Rev. Genet.* **10**, 94 (2009).
2. C. D. Malone *et al.*, *Cell* **137**, 522 (2009).
3. C. Li *et al.*, *Cell* **137**, 509 (2009).
4. J. Brennecke *et al.*, *Cell* **128**, 1089 (2007).
5. K. M. Nishida *et al.*, *RNA* **13**, 1911 (2007).
6. V. V. Vagin *et al.*, *Science* **313**, 320 (2006).
7. F. K. Teixeira, V. Colot, *Heredity* **105**, 14 (2010).
8. M. Mirouze *et al.*, *Nature* **461**, 427 (2009).
9. S. Tsukahara *et al.*, *Nature* **461**, 423 (2009).
10. F. K. Teixeira *et al.*, *Science* **323**, 1600 (2009).
11. P. Dunoyer *et al.*, *Science* **328**, 912 (2010).
12. A. Molnar *et al.*, *Science* **328**, 872 (2010).
13. P. E. Jullien *et al.*, *PLoS Biol.* **6**, e194 (2008).
14. Y. Choi *et al.*, *Cell* **110**, 33 (2002).
15. X. Zheng *et al.*, *Nature* **455**, 1259 (2008).
16. T. F. Hsieh *et al.*, *Science* **324**, 1451 (2009).
17. M. Gehring, K. L. Bubb, S. Henikoff, *Science* **324**, 1447 (2009).
18. R. A. Mosher *et al.*, *Nature* **460**, 283 (2009).
19. R. K. Slotkin *et al.*, *Cell* **136**, 461 (2009).
20. S. Duharcourt, G. Lepère, E. Meyer, *Trends Genet.* **25**, 344 (2009).
21. K. Mochizuki, M. A. Gorovsky, *Genes Dev.* **19**, 77 (2005).
22. J. Brennecke *et al.*, *Science* **322**, 1387 (2008).
23. G. Lepère, M. Bétermier, E. Meyer, S. Duharcourt, *Genes Dev.* **22**, 1501 (2008).

24. B. Brower-Toland *et al.*, *Genes Dev.* **21**, 2300 (2007).
25. M. Pal-Bhadra *et al.*, *Science* **303**, 669 (2004).
26. C. Klattenhoff *et al.*, *Cell* **138**, 1137 (2009).
27. S. D. Taverna, R. S. Coyne, C. D. Allis, *Cell* **110**, 701 (2002).
28. A. Böhne, F. Brunet, D. Galiana-Arnoux, C. Schultheis, J. N. Volff, *Chromosome Res.* **16**, 203 (2008).
29. S. Chambeyron *et al.*, *Proc. Natl. Acad. Sci. U.S.A.* **105**, 14964 (2008).
30. C. Josefsson, B. Dilkes, L. Comai, *Curr. Biol.* **16**, 1322 (2006).
31. R. A. Martienssen, *New Phytol.* **186**, 46 (2010).
32. A. A. Aravin, R. Sachidanandam, A. Girard, K. Fejes-Toth, G. J. Hannon, *Science* **316**, 744 (2007).
33. N. Zamudio, D. Bourc'his, *Heredity* **105**, 92 (2010).
34. H. Kano *et al.*, *Genes Dev.* **23**, 1303 (2009).
35. R. J. O'Neill, M. J. O'Neill, J. A. Graves, *Nature* **393**, 68 (1998).
36. C. Babinet, V. Richoux, J. L. Guénet, J. P. Renard, *Dev. Suppl.* **1990**, 81 (1990).
37. T. A. Bell *et al.*, *Genetics* **172**, 411 (2006).
38. T. Watanabe *et al.*, *Nature* **453**, 539 (2008).
39. W. Yan *et al.*, *Biol. Reprod.* **78**, 896 (2008).
40. V. Grandjean *et al.*, *Development* **136**, 3647 (2009).
41. Y. Tarutani *et al.*, *Nature* **466**, 983 (2010).
42. L. Wu *et al.*, *Mol. Cell* **38**, 465 (2010).
43. P. Dunoyer *et al.*, *EMBO J.* **29**, 1699 (2010).
44. X. Dramard, T. Heidmann, S. Jensen, *PLoS ONE* **2**, e304 (2007).
45. We are indebted to J. Brennecke, S. Duharcourt, and A. Pélisson for valuable discussions and advice. D.B. is supported by a European Young Investigator award and the Fondation Schlumberger pour l'Enseignement et la Recherche. O.V. is supported by a European Research Council starting grant (210890) "Frontiers of RNAi" and an award from the Bettencourt Foundation.

10.1126/science.1194776

REVIEW

Epigenetic Reprogramming in Plant and Animal Development

Suhua Feng,[1] Steven E. Jacobsen,[1]* Wolf Reik[2]*

Epigenetic modifications of the genome are generally stable in somatic cells of multicellular organisms. In germ cells and early embryos, however, epigenetic reprogramming occurs on a genome-wide scale, which includes demethylation of DNA and remodeling of histones and their modifications. The mechanisms of genome-wide erasure of DNA methylation, which involve modifications to 5-methylcytosine and DNA repair, are being unraveled. Epigenetic reprogramming has important roles in imprinting, the natural as well as experimental acquisition of totipotency and pluripotency, control of transposons, and epigenetic inheritance across generations. Small RNAs and the inheritance of histone marks may also contribute to epigenetic inheritance and reprogramming. Reprogramming occurs in flowering plants and in mammals, and the similarities and differences illuminate developmental and reproductive strategies.

Epigenetic marks are enzyme-mediated chemical modifications of DNA and of its associated chromatin proteins. Although they do not alter the primary sequence of DNA, they also contain heritable information and play key roles in regulating genome function. Such modifications—including cytosine methylation, posttranslational modifications of histone tails and the histone core, and the positioning of nucleosomes (histone octamers wrapped with DNA)—influence the transcriptional state and other functional aspects of chromatin. For example, methylation of DNA and certain residues on the histone H3 N-terminal tail [e.g., H3 lysine 9 (H3K9)] are important for transcriptional gene silencing and the formation of heterochromatin. Such marks are essential for the silencing of nongenic sequences—including transposons, pseudogenes, repetitive sequences, and integrated viruses—that could become deleterious to cells if expressed and hence activated. Epigenetic gene silencing is also important in developmental phenomena such as imprinting in both plants and mammals, as well as in cell differentiation and reprogramming.

DNA methylation occurs in three different nucleotide sequence contexts: CG, CHG, and CHH (where H = C, T, or A). In both mammals and plants, CG methylation is maintained by the maintenance DNA methyltransferase, termed DNMT1 [DNA (cytosine-5)-methyltransferase 1] in mammals and MET1 (DNA METHYLTRANSFERASE 1) in *Arabidopsis*, and by a cofactor that recognizes hemimethylated DNA at replication foci, called UHRF1 (ubiquitin-like containing PHD and RING finger domains 1) in mammals and VIM (VARIATION IN METHYLATION) family proteins in *Arabidopsis* (*1*). In addition, the mammalian de novo DNA methyltransferases DNMT3A and Dnmt3b are required for the maintenance of CG methylation at some loci (*2*). CHG methylation is common in *Arabidopsis* and other plant genomes and is maintained by a feedforward loop that is formed by a plant-specific DNA methyltransferase, CMT3 (CHROMOMETHYLASE 3), and a histone methyltransferase, KYP (KRYPTONITE) (*1*, *3*, *4*). CHH methylation is also abundant in plants and is maintained by the RNA-directed DNA methylation (RdDM) pathway, which actively targets the DNA methyltransferase DRM2 (DOMAINS REARRANGED METHYLTRANSFERASE 2; a homolog of Dnmt3) to DNA by means of 24-nucleotide (nt) small interfering RNAs (siRNAs) bound by AGO4 (ARGONAUTE 4) (*1*) (Fig. 1). CHG and CHH methylation are also present at detectable levels in mammals, especially in stem cells, and this methylation is likely introduced by DNMT3A and DNMT3B (*5*, *6*). De novo methylation of DNA in all of these sequence contexts is generally established by the DNMT3 (mammals) and DRM2 (*Arabidopsis*) methyltransferases. Mammals do not have an *Arabidopsis*-like RNA-directed DNA methylation pathway, but in germ cells, PIWI-associated RNAs (piRNAs) are thought to guide DNMT3 activity (*7*). Mammals have a noncatalytic paralog of de novo methyltransferase, DNMT3L, which interacts with DNMT3A and unmethylated H3K4 (as does DNMT3A and DNMT3B) (*8*–*10*); these findings imply a targeting mechanism of these methyltransferases to chromatin. Unmethylated CpG islands are specifically bound by CFP1 (CXXC finger protein–1), which in turn recruits the histone H3K4 methyltransferase SETD1 (SET domain containing–1) (*11*); this suggests that H3K4 methylation, and therefore exclusion of DNMT3 from CpG islands, could help to explain how promoters remain unmethylated. Consistent with this idea, demethylation of H3K4 has been shown to be important for the acquisition of DNA methylation in imprinted genes in oocytes (*12*). Additionally, transcription can also help to establish de novo DNA methylation at imprinted regions (*13*). Earlier this year, it was shown that the nucleosome landscape also influences the methylation patterning in both plant and animal genomes (*14*).

Some histone modifications are also thought to be actively maintained during DNA replication, in part facilitated by the association of the histone modification enzymes with the DNA replication machinery. For example, the mammalian histone H3K9 methyltransferases G9A and SETDB1 (SET domain bifurcated–1), the mammalian H4K20 methyltransferase SETD8 (SET domain containing–8), and the plant histone H3K27 monomethyltransferases ATXR5 (ARABIDOPSIS TRITHORAX-RELATED PROTEIN 5) and ATXR6 interact with the replication protein PCNA (proliferating cell nuclear antigen) (*15*, *16*). However, histone methylation can also be very dynamic and is controlled

[1]Howard Hughes Medical Institute and Department of Molecular, Cell and Developmental Biology, University of California, Los Angeles, CA 90095, USA. [2]Laboratory of Developmental Genetics and Imprinting, Babraham Institute, Cambridge CB22 3AT, UK, and Centre for Trophoblast Research, University of Cambridge, Cambridge CB2 3EG, UK.

*To whom correspondence should be addressed. E-mail: jacobsen@ucla.edu (S.E.J.); wolf.reik@bbsrc.ac.uk (W.R.)

by the combined action of both histone methyltransferases and histone demethylases, as well as by the proteins that read these histone marks (*16*).

Through the developmental regulation of these epigenetic mechanisms, both plants and animals undergo epigenetic reprogramming in various cell types and developmental stages, which serve either to transmit epigenetic information between cells or between sexual generations, or to reset epigenetic marks to reduce the risk of perpetuating dangerous epigenetic alleles.

DNA Methylation Throughout the *Arabidopsis* Life Cycle

To maintain genome integrity from generation to generation, transposons and repetitive DNA elements must be kept under tight regulation in reproductive cells. One of the ways that plants achieve this is through the stable inheritance of DNA methylation. Plants frequently show meiotic inheritance of gene silencing (*1*). Furthermore, plants are not known to undergo genome-wide waves of demethylation in germ cells, as occurs in animals. However, large-scale reprogramming occurs in non–germ line reproductive cells, and this reprogramming may function to reinforce silencing of transposable elements in germ cells (see below).

One way to actively reprogram the epigenome is to remove methylated cytosines. The *Arabidopsis* genome encodes four bifunctional helix-hairpin-helix DNA glycosylases and AP lyases—ROS1 (REPRESSOR OF SILENCING 1), DME (DEMETER), DML2 (DEMETER-LIKE 2), and DML3 (DEMETER-LIKE 3)—which recognize and remove methylated cytosines, resulting in a 1-nt gap in the DNA double strand. Subsequently, as yet unidentified DNA repair polymerase and DNA ligase enzymes are thought to fill in the gap with an unmethylated cytosine (*1*, *17*). ROS1, DML2, and DML3 mainly function in vegetative tissues, and genomic studies suggest that they demethylate hundreds of specific loci across the genome with a bias toward genes (*1*, *18*). Knocking out all three genes does not markedly affect the overall levels or patterns of methylation in the *Arabidopsis* genome (*18*, *19*). Instead, these enzymes appear to be acting as a counterbalance to the RNA-directed DNA methylation system to quantitatively fine-tune methylation levels at particular genomic locations.

By contrast, DME functions to cause global hypomethylation in the endosperm (the extra-embryonic tissue of flowering plants) of *Arabidopsis* (*20*, *21*), and thus contributes to large-scale epigenetic reprogramming (Fig. 1). In *Arabidopsis*, female gametogenesis begins when a somatically derived megaspore mother cell undergoes meiosis to give rise to a haploid megaspore, which subsequently develops into a mature female gametophyte (embryo sac) that contains one egg cell, one central cell (two nuclei), and several other accessory cells. During double fertilization (which is common in plants), the egg cell fuses with a sperm cell from the male gametophyte (pollen grain) to form an embryo, and the central cell fuses with the other sperm cell from pollen to form the triploid endosperm, which nourishes the embryo, and thus bears a function similar to that of the placenta in mammals. DME is expressed primarily in the central cell before fertilization, and thus only the maternal genome is demethylated by DME. This leads to maternal allele–specific gene expression (imprinting) in the endosperm (*22*). Until recently, only six imprinted *Arabidopsis* genes were known, but recent genomic studies of endosperm have revealed genome-wide differences in DNA methylation, including a substantial reduction of CG methylation; hence, many additional genes are likely to be imprinted in *Arabidopsis*, some of which have been verified by single-gene studies (*20*, *21*) (Fig. 1). Demethylation by DME may also reactivate transposon expression, which shunts transposon transcripts into the RNAi pathway, producing additional siRNAs that can guide DNA methylation to non-CG sites whose methylation is high in wild-type endosperm but decreased in *dme* mutant endosperm (Fig. 1). Curiously, there are even higher levels of non-CG methylation in the wild-type embryo that could be explained by movement of siRNAs produced in the central cell into the egg cell; this attractive idea awaits experimental support (*20*). Because the endosperm genome does not contribute to the next generation, mild reactivation of transposons in endosperm may not be deleterious and may reinforce the silencing of transposons in the egg cell and later embryo, contributing to the genome integrity of offspring. Indeed, there is a class of RNA polymerase IV (Pol IV)–dependent siRNAs that only accumulates in flowers and young siliques, likely originating from the endosperm (*23*). Notably, these siRNAs are derived from maternal alleles only, which suggests that they may be produced in part during female gametogenesis and then retained after karyogamy. However, these siRNAs are expressed more highly after fertilization, and therefore imprinted maternal expression of siRNA loci may also occur as the endosperm develops (*23*). It is tempting to speculate that the maternal Pol IV–dependent siRNAs are the "messenger" that mediates communication between endosperm and embryo (Fig. 1); however, these siRNAs were detected only in the endosperm, not in the embryo (*23*). Nonetheless, the possibility that they exist in low abundance in the embryo, or are ephemeral, cannot be ruled out.

The idea that siRNAs move from the endosperm to the embryo is consistent with the model put forth in an earlier study on paternal genome reprogramming in *Arabidopsis* (*24*). The male gametophyte of *Arabidopsis* (a pollen grain) contains two sperm cells, which fertilize the egg cell and central cell, respectively, and a vegetative nucleus (Fig. 1). Transposon expression is generally up-regulated in pollen, and certain transposons even become mobile in pollen, unlike the situation in most other tissues (*24*). Reduction of transposon methylation followed by transposon reactivation appears to occur in the vegetative nucleus; this is supported by the finding that transposon reactivation and movement are not inherited by the next generation (*24*). It has been shown that several key RdDM pathway proteins (RDR2 and DCL3) and CHG methylation maintenance pathway proteins (CMT3 and KYP) have reduced expression levels in pollen; in addition, DDM1 (DECREASE IN DNA METHYLATION 1), an important chromatin remodeler required for DNA and histone methylation and transposon silencing, is exclusively localized in sperm cells but not in the vegetative nucleus (*24*). These results suggest a model in which hypomethylation of the vegetative cell may reactivate transposons that could serve to reinforce transposon silencing in the adjacent sperm cells (Fig. 1) (*24*).

Small RNAs may be involved in this communication between the vegetative cell and the sperm cells. A class of siRNAs that is 21 nt in length and corresponds to *Athila* retrotransposons, the largest transposon family, is detected in sperm cells. Because *Athila* retrotransposons remain silenced in sperm cells but are activated in the vegetative nucleus, it is possible that the 21-nt siRNAs are produced in the vegetative nucleus and then travel to their site of action—sperm cells—where they mediate the silencing of transposons through an unknown mechanism (Fig. 1) (*24*). A common theme is that both male and female gametophytes contain nurse cells in which massive epigenetic reprogramming may serve to reinforce transposon silencing in the germ line (Fig. 1).

Another example of small RNAs silencing transposons at a distance occurs when the megaspore mother cell differentiates from somatic tissues (*25*). Mutations in AGO9 (ARGONAUTE 9), a member of the *Arabidopsis* Argonaute family of proteins, result in the reactivation of transposons in the ovule (including the egg cell) (Fig. 1). Remarkably, *AGO9* is not expressed in the reproductive cells themselves (megaspore mother cell, megaspore, or developing female gametophyte), but is expressed in the companion cells surrounding the female gametophyte. The transposon targets of AGO9 are similar to those reactivated in pollen, and evidence suggests that AGO9-mediated transposon silencing uses components of known silencing pathways, including the 24-nt RNA-directed DNA methylation pathway (*25*). Whether the AGO9-associated 24-nt siRNAs are the mobile signal remains to be tested.

Resetting of Histone Modifications in *Arabidopsis*

In addition to DNA methylation, plants also reprogram histones and their associated marks;

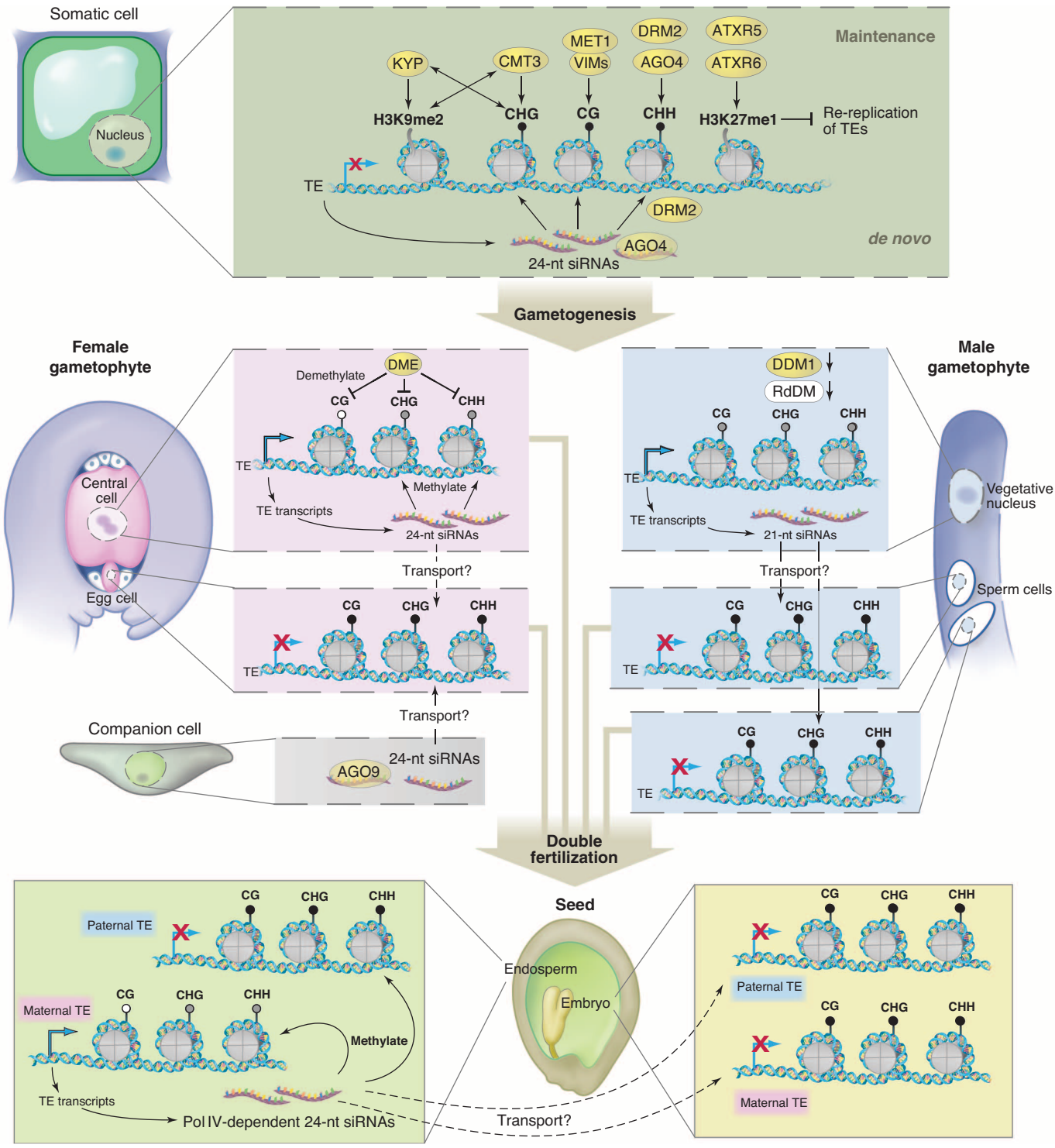

Fig. 1. Model of epigenetic silencing dynamics during the *Arabidopsis* life cycle. In somatic cells, three different mechanisms are responsible for repressing transcription from transposable elements (TEs), DNA methylation (in all three sequence contexts), histone H3K9 dimethylation (H3K9me2), and histone H3K27 monomethylation (H3K27me1). Methyltransferases and proteins regulating these epigenetic marks are shown. See text for details. In the female gametophyte, the central cell is demethylated by DME, which leads to TE activation and up-regulation of RdDM. The siRNAs produced from TEs not only direct non-CG methylation in the central cell, but also might travel to the egg cell and enhance the silencing of TEs there. In addition, AGO9-associated siRNAs produced in somatic companion cells also contribute to the silencing of TEs in the egg cell. In the male gametophyte, the vegetative nucleus does not express DDM1 and has reduced RdDM, which leads to TE activation and mobilization. A new class of 21-nt siRNAs, produced from TEs in the vegetative nucleus, travels to sperm cells to reinforce TE silencing. After double fertilization, maternal TEs in the endosperm stay activated and produce Pol IV–dependent siRNAs, which could function to silence the paternal TEs in the endosperm. The methylation levels in the embryo are elevated, possibly as a result of the siRNA signals transmitted from the endosperm. Different shadings indicate the level of DNA methylation (high, black; medium, gray; low, white).

as opposed to DNA methylation (which is typically inherited), some histone modifications are known to be reset in each generation. Because plants do not set aside a germ line early in development (germ cells are differentiated from adult somatic cells), some type of "reprogramming" process is likely needed to erase the effects of epigenetic marks caused by external stimuli (such as development or stress). For example, PCG (Polycomb group) proteins mediate the silencing of *FLC* (*FLOWERING LOCUS C*) in *Arabidopsis*, which controls flowering time (*26*). In winter-annual accessions of *Arabidopsis*, *FLC* is expressed at high levels to repress the initiation of flowering. During vernalization (prolonged exposure to cold, such as during winter), *FLC* becomes modified by H3K27 trimethylation, which helps to turn off *FLC* expression epigenetically. When winter passes and temperatures become warmer, trimethylation and silencing of *FLC* persists, and therefore *Arabidopsis* can flower in response to environmental cues such as photoperiod. When gametes are formed through meiosis, H3K27 trimethylation marks on *FLC* are removed by an unknown mechanism and *FLC* becomes reexpressed in the seeds. Thus, flowering is inhibited by *FLC* until the next-generation plants encounter cold weather.

Resetting of histone marks may involve, in part, global replacement of histones (*27*). The histone variant H3.3 can be incorporated in the absence of DNA replication, and thus is a candidate for the "replacement" histone H3 during reprogramming. HTR10 (HISTONE THREE RELATED 10) is exclusively expressed in male reproductive cells, but after karyogamy of sperm and egg cell nuclei, the paternal HTR10 signal disappears within a matter of hours before S phase of the first zygote division (*27*). This suggests that HTR10 is actively removed from the chromatin in a replication-independent manner specifically in the sperm cell that fertilizes the egg. Unlike DNA methylation reprogramming, which occurs in accessory cells, histone reprogramming takes place in the zygote and thus can transmit information to the next generation. These results raise a number of questions. How does the reprogramming system differentiate between the two sperm cells? Does similar reprogramming happen in the female genome as well? What types of histone H3 replace the parental histone H3 in the zygote, and where do they come from?

Recently a new transposon silencing mark was described in *Arabidopsis* that does not appear to involve the well-studied DNA methylation or histone H3K9 dimethylation marks. This mark, H3K27 monomethylation, is needed to suppress excessive replication of heterochromatin in which transposons reside (*15*). Overreplication of transposons might lead to transposon reactivation and copy number propagation, and the H3K27 monomethylation system may have evolved to suppress excessive replication and to ensure genome stability (Fig. 1). If true, this would suggest that histone marks not only get reprogrammed but also reprogram the genome, in the case of H3K27 monomethylation, by keeping the replication of transposons in check. This presumably is important for actively cycling plant cells, for reproductive cells undergoing meiosis, and perhaps for early stages of embryo development.

Mechanisms of Epigenetic Reprogramming in Mammalian Development

Genome-wide epigenetic reprogramming occurs in mammalian development at two distinct stages: in primordial germ cells (PGCs) primarily once they have reached the embryonic gonads (embryonic day E10.5 to E13.5), and in the early embryo beginning in the zygote immediately after fertilization and extending to the morula stage of preimplantation development (Fig. 2) (*28*–*30*). This reprogramming entails erasure of DNA methylation and loss of histone modifications (as well as loss of histones and histone variants); here we focus on demethylation of DNA. The loss of DNA methylation by E13.5 (the developmental endpoint of reprogramming) is truly global; in mouse female PGCs, only 7% of CpGs remain methylated [versus 70 to 80% in embryonic stem (ES) cells and somatic cells], and most promoters and genic, intergenic, and transposon sequences are hypomethylated at this stage (*31*). The only clear exception to global erasure is intracisternal A particles (IAPs), an active family of retrotransposons that have only recently been acquired in the rodent lineage, which only show partial demethylation in PGCs (*31*). Promoters of germ cell–specific genes (such as *Dazl* or *Vasa*) are methylated in early PGCs and become demethylated and expressed during reprogramming (*32*). Imprinted genes have allele-specific methylation in early PGCs and the *Xist* promoter is methylated, and this methylation is all erased in PGCs by E13.5 (Fig. 2) (*33*, *34*). Although most of the genome-wide demethylation appears to occur in E11.5 to E13.5 PGCs, it remains possible that some loci become demethylated at slightly earlier stages (*35*); hence, demethylation is not necessarily coordinated timewise throughout the genome. Nothing is currently known about the possible occurrence or erasure of non-CG methylation in PGCs.

DNA deaminases and the base excision repair pathway have recently been implicated in erasure, which suggests that active demethylation is involved at least in part (*31*, *36*). The cytosine deaminases AID and APOBEC1 are capable in vitro of deaminating 5-methylcytosine (5mC) as well as cytosine and are expressed, albeit at a low level, in PGCs (*36*, *37*). Notably, AID deficiency in PGCs results in a deficit in demethylation of 20% of all CpGs if it is assumed that early PGCs have methylation levels similar to those of ES cells or somatic cells (*31*). Because of this partial effect of AID deficiency on erasure, the potential redundancy with other DNA deaminases needs to be examined. The 5mC hydroxylases TET1 and TET2 are also expressed in PGCs (*36*), suggesting the possibility that 5mC could be modified by different mechanisms (deamination, hydroxylation) in order to initiate active demethylation. It is also possible that a combination of passive (resulting in hemimethylated substrates in G_2 phase of the cell cycle) and active demethylation could be involved. Finally, it is possible that the genome-wide nature of the demethylation process and its relatively coordinate timing require different mechanisms and different modifications of 5mC to join forces in order to achieve such large-scale reprogramming.

Initial modification of 5mC would require further modification or DNA repair in order to achieve demethylation. DNA repair pathways that might be involved in resolving mismatches or in excising 5-hydroxymethylcytosine (5hmC) are nucleotide excision repair, mismatch repair, and especially base excision repair (BER), which is also involved in demethylation during reprogramming in plants (*1*). BER components such as PARP1, APE1, and XRCC1 are all up-regulated at E11.5 in PGCs, together with enhancement of chromatin-bound XRCC1; thus, it is possible that BER is activated at this time point (Fig. 2) (*36*). Global losses of several histone modifications (e.g., H3K27me3, H3K9ac) as well as the linker histone H1 are observed after demethylation of DNA, indicating that widespread DNA repair might be associated with global remodeling of nucleosomes in PGCs (*38*). It is also possible that specific histone modification or demodification enzymes (deacetylases, demethylases) are in part responsible for erasure of histone marks in PGCs, but none have been identified so far.

Base excision repair also appears to be involved in demethylation in the zygote immediately after fertilization (Fig. 2). The added complication here is that it is specifically the paternal, sperm-derived, genome that is demethylated, whereas the maternal one is not; the maternal genome may be specifically protected from demethylation (*39*–*42*). Differentially methylated regions in imprinted genes are also specifically protected from demethylation, and so again are IAPs. Nonetheless, there appear to be substantial losses of methylation in the zygote, potentially of a similar scale to those occurring in PGCs (*39*, *43*, *44*). Notably, demethylation of the paternal genome may occur in two phases, one before DNA replication and one associated with the S and G_2 phases (*44*). The first phase might involve modification of 5mC but only partial demethylation (*44*). Demethylation might then continue at replication or afterward. BER components are also present at these stages with an

enhancement of chromatin-bound XRCC1 in the paternal pronucleus (*36*). Both phases show evidence of DNA strand breaks, indicating that repair may be involved in both of them, and inhibition of BER components partly interferes with demethylation (*36*, *44*). Whether AID or TETs are involved in zygotic demethylation is not yet known, but components of the Elongator complex (Elongator complex proteins, ELPs) have been implicated in demethylation of the paternal genome (Fig. 2) (*45*); Elongator is involved in diverse aspects of transcriptional regulation and can also modify tRNAs. Could Elongator catalyze an as yet unknown modification of 5mC that makes it a substrate for BER? After zygotic demethylation, the embryonic genome continues to be demethylated during the following few cleavage divisions until the blastocyst stage, with DNMT1 protein being largely excluded from the nucleus by an unknown mechanism (Fig. 2). Nonetheless, the maintenance of methylation in differentially methylated regions of imprinted genes does depend on DNMT1 (*46*), so it will be important to understand how DNMT1 might be targeted during this reprogramming phase to key regions in the genome, such as imprinted genes (*47*).

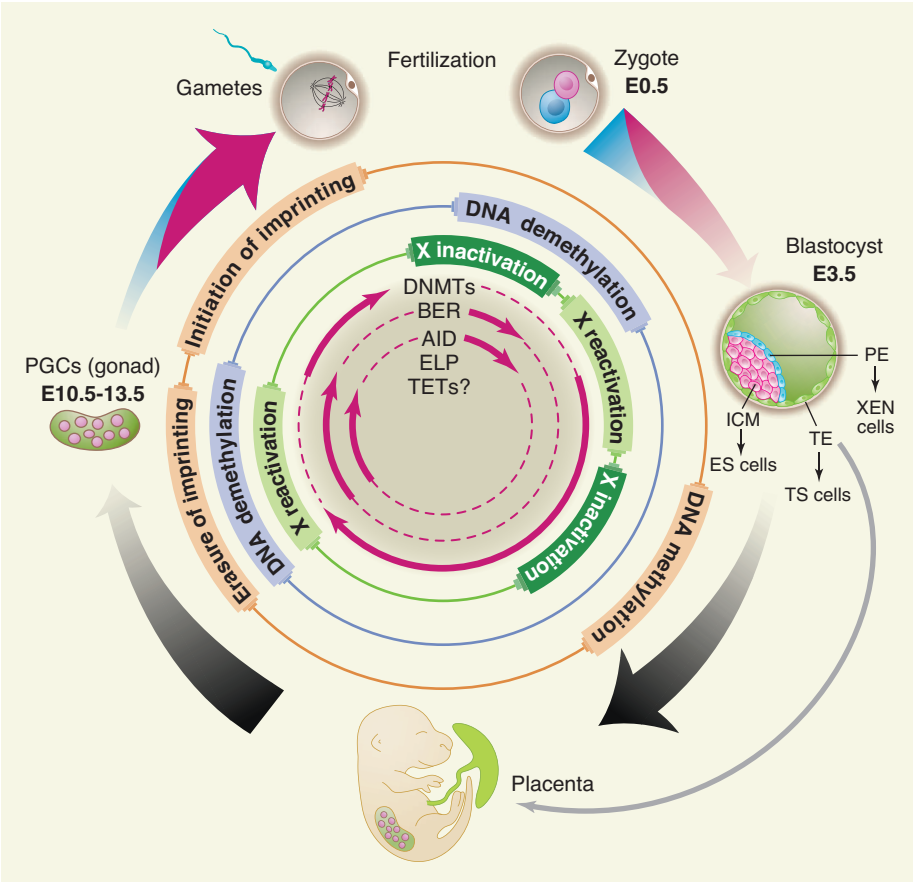

Fig. 2. The two major phases of genome-wide erasure of DNA methylation in the early embryo and in primordial germ cells (PGCs) of the mouse. Thickness of the outer arrows indicates levels of DNA methylation. Red, maternal genome; blue, paternal genome. After fertilization, the paternal genome is more rapidly demethylated than the maternal one. During gametogenesis, de novo methylation in spermatogenesis occurs earlier than in oogenesis. The inner circle shows factors or candidate factors that are implicated in de novo methylation, the maintenance of methylation, and demethylation, respectively. Solid arrows in the inner circle show at what developmental time these epigenetic regulators are thought to act. ES cells, TS cells, and XEN cells are stem cell lines that are derived from the inner cell mass (ICM), trophectoderm (TE), and primitive endoderm (PE) of the blastocyst, respectively.

Hence, the current evidence for the initiation and regulation of genome-wide erasure of DNA methylation in PGCs and the zygote points to initiating events that modify 5mC (such as deamination and hydroxylation), which would trigger a BER response. Of course, it is still possible that bifunctional DNA glycosylases of the type that excise 5mC in plants also exist in animals (although none have been found so far); conversely, homologs of APOBEC deaminases and TET and ALKBH-type hydroxylases have yet to be described in plants.

Experimental Reprogramming in Mammals

Experimental reprogramming to a pluripotent state can be achieved, albeit inefficiently, by fusion of somatic cells and pluripotent cells, by cloning, and by direct reprogramming using core transcription factors (*48*). With all three methods, there is evidence that epigenetic reprogramming is a central component of achieving the goal of an embryonic or ES cell–like (iPS) state. In cell fusion experiments between somatic cells and ES cells, key pluripotency genes such as *Oct4* and *Nanog* need to be demethylated; AID also seems to be important for demethylation in this system (*49*). Generation of iPS cells from somatic cells by the transduction of core transcription factors (such as OCT4, SOX2, KLF4, and C-MYC) probably requires multiple epigenetic reprogramming steps while the cells that undergo reprogramming divide (*50*). DNA demethylation is clearly critical because incompletely reprogrammed iPS cells can become completely reprogrammed by treatment with the methylation inhibitor azacytidine (*48*). Inhibitors of histone deacetylases and histone methyltransferases are also beneficial, showing in general that repressive epigenetic modifications acquired during differentiation and somatic development need to be reversed to achieve the pluripotent state (*48*). Notably, reprogramming by cloning apparently results in better resetting of the epigenome than can be achieved by direct reprogramming with transcription factors, indicating perhaps that true totipotency requires passage through germ cells or zygotes (*51*). Direct applications to regenerative medicine will result from unraveling the role of AID, hydroxymethylation, and the TETs, and of the base excision repair pathway as well as the methyltransferases in this process, and from knowledge of how the reprogramming network is connected with the pluripotency network.

Comparative Biology of Epigenetic Reprogramming

Whether genome-scale epigenetic reprogramming has a unified purpose is not clear; some aspects of reprogramming are clearly conserved (or have been reinvented) in animals and plants with their contrasting, although sometimes surprisingly similar, reproductive and biological strategies. In mammals, zygotic reprogramming is broadly conserved, although there may be some differences in timing or extent; by contrast, *Xenopus* does not appear to show demethylation of the paternal genome (*52*). Hypomethylation of PGCs is also seen in human and pig fetal development but has not been studied in non-mammalian organisms. Global DNA demethylation in PGCs and paternal demethylation in the

zygote may occur primarily in mammals (and in the central cell in seed plants) that also have imprinting whose mechanism is based on DNA methylation. Clearly, demethylation in PGCs is necessary for erasure of imprints so that new imprints can later be established properly, according to the sex of the germ line (Fig. 2). Plants do not seem to erase imprints; instead, they establish them by demethylation of the maternal genome in the endosperm after fertilization (with the endosperm being comparable to the placenta) (Fig. 1). Perhaps there are as yet undiscovered imprinted genes that acquire parent-specific methylation patterns by (paternal) zygotic demethylation, in analogy to plants.

A second group of genes where demethylation in PGCs seems important are the germ line–specific genes (e.g., *Dazl*, *Vasa*) that have specialized functions, for example, in meiosis and germ cell differentiation. These genes are generally demethylated and expressed in germ cells, but in early PGCs they are methylated and silenced. Genes that are demethylated in PGCs include those with a role in transposon control; *Tex19.1*, for example, silences members of the ERVK transposon family (*53*). Hence, global demethylation, which in principle would lead to transcriptional activation and potentially to transposition of active transposon families, at the same time activates defense mechanisms against transposons that are not needed in somatic cells where transposons are methylated. An extreme view of this scenario is the possibility that demethylated transposons produce small RNAs, which in turn lead to de novo methylation and renewed silencing of transposons (Fig. 1) (*24*). Although it may sound paradoxical, reprogramming may have an important role in resetting the permanent silencing program for transposons across generations. Also, the fact that AID has a role in the erasure of methylation in PGCs is interesting in connection with roles of APOBEC deaminases in innate immunity and transposon control, establishing another potential link between the two.

The extent of methylation reprogramming in PGCs is substantial, and this limits the potential in mammals for epigenetic transgenerational inheritance. By contrast, in plants where epigenetic reprogramming may not occur to such an extent in the germ line, examples of stable inheritance of epialleles over multiple generations are more common (*54*). In *Caenorhabditis elegans*, histone demethylation in the germ line is needed to prevent accumulation of aberrant epigenetic marks that interfere with normal physiology and limit life span (*55*). By analogy, epigenetic reprogramming in mammalian PGCs or early embryos may be important to prevent the accumulation of potentially detrimental epialleles, which could otherwise cause chronic diseases and limit life span in human populations. The inheritance of histone marks and of small RNAs potentially through both oocyte and sperm might also contribute to epigenetic inheritance and to reprogramming across generations in animals and in plants (*24*, *25*, *56*–*59*).

Finally, epigenetic reprogramming is linked to regaining pluripotency and, following that, lineage commitment. Early PGCs and cells in the early embryo are pluripotent, and these cells as well as the stem cell lines that can be isolated from them [ES and EG (embryonic germ) cells] have unique epigenetic signatures, which are at least in part the outcomes of reprogramming. For example, some of the key pluripotency transcription factors (such as *Nanog*) are methylated in sperm but not in ICM (inner cell mass) or ES cells, so their demethylation is important for the acquisition of pluripotency (*43*); in the absence of the highly expressed gene encoding TET1 (which hydroxylates 5mC), the *Nanog* gene is repressed and its promoter becomes methylated (*60*).

One final epigenetic parallel between mammals and plants is worth highlighting. After demethylation in the early mammalian embryo, selective de novo methylation occurs in ICM cells and their descendants, which is important for the identity and stability of embryonic lineages (*28*), whereas the placenta remains hypomethylated at the genome-wide level (*31*). Similarly, genome-wide demethylation in the plant endosperm but not the embryo (*20*, *21*) indicates that epigenetic regulation between the two primary lineages (embryonic, extraembryonic) is fundamentally different, with this difference apparently being conserved—or reinvented—in plants and animals.

References and Notes

1. J. A. Law, S. E. Jacobsen, *Nat. Rev. Genet.* **11**, 204 (2010).
2. T. Chen, Y. Ueda, J. E. Dodge, Z. Wang, E. Li, *Mol. Cell. Biol.* **23**, 5594 (2003).
3. S. Feng *et al.*, *Proc. Natl. Acad. Sci. U.S.A.* **107**, 8689 (2010).
4. A. Zemach, I. E. McDaniel, P. Silva, D. Zilberman, *Science* **328**, 916 (2010); published online 15 April 2010 (10.1126/science.1186366).
5. B. H. Ramsahoye *et al.*, *Proc. Natl. Acad. Sci. U.S.A.* **97**, 5237 (2000).
6. R. Lister *et al.*, *Nature* **462**, 315 (2009).
7. A. A. Aravin, G. J. Hannon, *Cold Spring Harb. Symp. Quant. Biol.* **73**, 283 (2008).
8. D. Jia, R. Z. Jurkowska, X. Zhang, A. Jeltsch, X. Cheng, *Nature* **449**, 248 (2007).
9. S. K. Ooi *et al.*, *Nature* **448**, 714 (2007).
10. Y. Zhang *et al.*, *Nucleic Acids Res.* **38**, 4246 (2010).
11. J. P. Thomson *et al.*, *Nature* **464**, 1082 (2010).
12. D. N. Ciccone *et al.*, *Nature* **461**, 415 (2009).
13. M. Chotalia *et al.*, *Genes Dev.* **23**, 105 (2009).
14. R. K. Chodavarapu *et al.*, *Nature* **466**, 388 (2010).
15. Y. Jacob *et al.*, *Nature* **466**, 987 (2010).
16. R. Bonasio, S. Tu, D. Reinberg, *Science* **330**, 612 (2010).
17. J. K. Zhu, *Annu. Rev. Genet.* **43**, 143 (2009).
18. J. Penterman *et al.*, *Proc. Natl. Acad. Sci. U.S.A.* **104**, 6752 (2007).
19. R. Lister *et al.*, *Cell* **133**, 523 (2008).
20. T. F. Hsieh *et al.*, *Science* **324**, 1451 (2009).
21. M. Gehring, K. L. Bubb, S. Henikoff, *Science* **324**, 1447 (2009).
22. J. H. Huh, M. J. Bauer, T. F. Hsieh, R. L. Fischer, *Cell* **132**, 735 (2008).
23. R. A. Mosher *et al.*, *Nature* **460**, 283 (2009).
24. R. K. Slotkin *et al.*, *Cell* **136**, 461 (2009).
25. V. Olmedo-Monfil *et al.*, *Nature* **464**, 628 (2010).
26. D. H. Kim, M. R. Doyle, S. Sung, R. M. Amasino, *Annu. Rev. Cell Dev. Biol.* **25**, 277 (2009).
27. M. Ingouff, Y. Hamamura, M. Gourgues, T. Higashiyama, F. Berger, *Curr. Biol.* **17**, 1032 (2007).
28. M. Hemberger, W. Dean, W. Reik, *Nat. Rev. Mol. Cell Biol.* **10**, 526 (2009).
29. M. A. Surani, K. Hayashi, P. Hajkova, *Cell* **128**, 747 (2007).
30. H. Sasaki, Y. Matsui, *Nat. Rev. Genet.* **9**, 129 (2008).
31. C. Popp *et al.*, *Nature* **463**, 1101 (2010).
32. D. M. Maatouk *et al.*, *Development* **133**, 3411 (2006).
33. P. Hajkova *et al.*, *Mech. Dev.* **117**, 15 (2002).
34. J. Lee *et al.*, *Development* **129**, 1807 (2002).
35. Y. Seki *et al.*, *Development* **134**, 2627 (2007).
36. P. Hajkova *et al.*, *Science* **329**, 78 (2010).
37. H. D. Morgan, W. Dean, H. A. Coker, W. Reik, S. K. Petersen-Mahrt, *J. Biol. Chem.* **279**, 52353 (2004).
38. P. Hajkova *et al.*, *Nature* **452**, 877 (2008).
39. J. Oswald *et al.*, *Curr. Biol.* **10**, 475 (2000).
40. W. Mayer, A. Niveleau, J. Walter, R. Fundele, T. Haaf, *Nature* **403**, 501 (2000).
41. F. Santos, B. Hendrich, W. Reik, W. Dean, *Dev. Biol.* **241**, 172 (2002).
42. T. Nakamura *et al.*, *Nat. Cell Biol.* **9**, 64 (2007).
43. C. R. Farthing *et al.*, *PLoS Genet.* **4**, e1000116 (2008).
44. M. Wossidlo *et al.*, *EMBO J.* **29**, 1877 (2010).
45. Y. Okada, K. Yamagata, K. Hong, T. Wakayama, Y. Zhang, *Nature* **463**, 554 (2010).
46. R. Hirasawa *et al.*, *Genes Dev.* **22**, 1607 (2008).
47. X. Li *et al.*, *Dev. Cell* **15**, 547 (2008).
48. S. Yamanaka, H. M. Blau, *Nature* **465**, 704 (2010).
49. N. Bhutani *et al.*, *Nature* **463**, 1042 (2010).
50. J. Hanna *et al.*, *Nature* **462**, 595 (2009).
51. K. Kim *et al.*, *Nature* **467**, 285 (2010).
52. I. Stancheva, O. El-Maarri, J. Walter, A. Niveleau, R. R. Meehan, *Dev. Biol.* **243**, 155 (2002).
53. R. Öllinger *et al.*, *PLoS Genet.* **4**, e1000199 (2008).
54. F. K. Teixeira *et al.*, *Science* **323**, 1600 (2009); published online 29 January 2009 (10.1126/science.1165313).
55. D. J. Katz, T. M. Edwards, V. Reinke, W. G. Kelly, *Cell* **137**, 308 (2009).
56. U. Brykczynska *et al.*, *Nat. Struct. Mol. Biol.* **17**, 679 (2010).
57. S. S. Hammoud *et al.*, *Nature* **460**, 473 (2009).
58. O. H. Tam *et al.*, *Nature* **453**, 534 (2008).
59. T. Watanabe *et al.*, *Nature* **453**, 539 (2008).
60. S. Ito *et al.*, *Nature* **466**, 1129 (2010).

61. We thank J. A. Law for reading and commenting on the manuscript, and F. Santos for help with figures. S.F. is a Special Fellow of the Leukemia & Lymphoma Society. Supported by NIH grant GM60398 (S.E.J.) and by grants from the UK Biotechnology and Biological Sciences Research Council, UK Medical Research Council, and European Union (W.R.). S.E.J. is an investigator of the Howard Hughes Medical Institute.

10.1126/science.1190614

PERSPECTIVE

Paramutation's Properties and Puzzles

Vicki L. Chandler

Paramutation refers to the process by which homologous DNA sequences communicate in trans to establish meiotically heritable expression states. Although mechanisms are unknown, current data are consistent with the hypothesis that the establishment and heritable transmission of specific chromatin states underlies paramutation. Transcribed, noncoding tandem repeats and proteins implicated in RNA-directed transcriptional silencing in plants and yeast are required for paramutation, yet the specific molecules mediating heritable silencing remain to be determined.

Alleles interact to establish heritable expression states in classic examples of paramutation, such as the well-studied *b1* locus in maize, which affects variation in coloration (Fig. 1). Paramutation-like interactions also can occur between transgenes or transgenes and endogenous genes and have been observed in multiple species [see (*1*–*3*) for recent reviews].

The nature of the interaction that leads to paramutation is unknown, but several lines of evidence suggest a role for RNA. The strongest evidence is that genetic screens for mutants unable to undergo paramutation identified several genes with homology to proteins that mediate RNA-directed transcriptional silencing (*3*). In *Arabidopsis*, transcriptional silencing of endogenous genes or transgenes can be mediated by 24-nucleotide (nt) siRNA (short interfering RNA) that target homologous sequences for silencing, which correlates with DNA cytosine methylation and histone modifications characteristic of heterochromatin (*4*). This pathway in *Arabidopsis* is referred to as RNA-directed DNA methylation (RdDM) or RNA-directed transcriptional silencing (*4*). In *Schizosaccharomyces pombe*, transcriptional silencing of mating-type loci and genes within centromeres is mediated by an RNA interference (RNAi)–heterochromatin pathway that shares several protein components with the RdDM pathway in *Arabidopsis* (*5*).

Additional data consistent with a role for RNA in paramutation is that the sequences mediating paramutation are transcribed noncoding tandem repeats (*1*, *3*). In both cases where the key sequences required for paramutation have been identified, they are either contiguous tandem repeats (Fig. 1) or direct repeats flanking unrelated sequences (*3*). These repeats contain enhancer sequences and are transcribed (*1*, *3*). At the *b1* locus, paramutation strength is correlated with the number of tandem repeats (*1*) because alleles with five to seven repeats exhibit strong paramutation, alleles with three repeats are intermediate, and alleles that do not participate in paramutation have only one copy. It is intriguing that repeats are also present within centromeres, transposons, and transgenes, which are also subject to RNA-directed transcriptional silencing (*4*, *5*), suggesting that underlying mechanisms regulating these elements may be shared with paramutation.

The *b1* tandem repeats are transcribed on both strands and generate 24-nt siRNAs (*3*, *6*). Given the *Arabidopsis* RdDM pathway (*4*), these *b1* repeat siRNAs are candidates for a direct role in paramutation, yet they are not sufficient to establish silencing, as evidenced by the fact that 24-nt siRNAs are produced from the single repeat unit in *b1* alleles that cannot induce silencing (*6*). The observation that a transgene, which produces *b1* repeat hairpin RNA and 24-nt siRNAs independently of *B′*, can change *B-I* into a *B′*-like allele (*6*) suggests that either double-stranded hairpin RNA or 24-nt siRNAs from the repeats are somehow mediating paramutation. One spec-

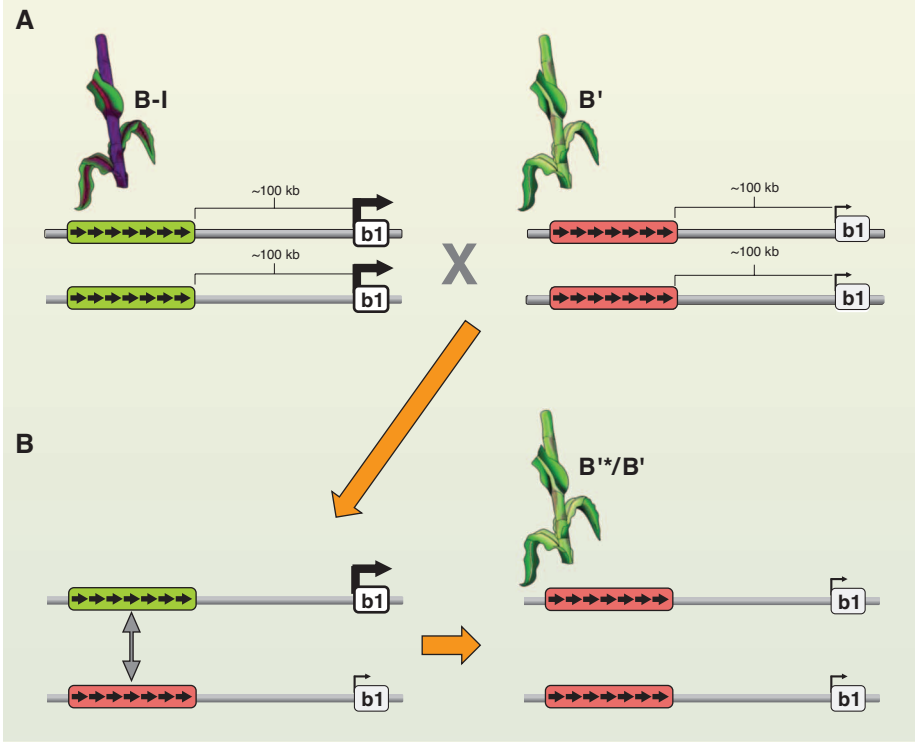

Fig. 1. Properties of *b1* paramutation. (**A**) *B-I* and *B′* phenotypes (dark and light colored plants, respectively) and diagrams of the *b1* locus and associated regulatory regions; because maize is diploid, the two diagrams for each plant represent the two alleles. The *b1* locus (white box labeled *b1*) encodes a transcription factor that activates the anthocyanin biosynthetic pathway, which produces purple coloration. When *b1* is highly transcribed (*B-I*, thick arrow above white box), a dark purple plant is observed. When transcription is low (*B′*, thin arrow above white box), a lightly pigmented plant is observed. *B-I* and *B′* have identical DNA sequences, including seven tandem copies of an 853–base pair (bp) repeat unit, located ~100 kb upstream of the *b1* coding region [indicated by seven black arrows within green (*B-I*) or red (*B′*) blocks]. The green and red blocks symbolize the distinct chromatin structures within the repeats (*7*) in *B-I* and *B′*, respectively. Extensive data demonstrate that the tandem repeats are required for *b1* paramutation and the high expression in *B-I* (*1*, *3*). The repeats have not been found elsewhere in the maize genome and are transcribed noncoding sequences that produce 24-nt siRNAs in both alleles (*3*, *6*). (**B**) The result of crossing *B-I* and *B′* is that *B-I* is always changed into *B′* by unknown mechanisms. The diagram portrays a two-step process (orange arrows), such that before establishment of paramutation both *B-I* and *B′* epigenetic states exist (left). Paramutation is established between early embryogenesis and the formation of 10 leaf primordia (*8*) through unknown mechanisms mediated by the repeats (symbolized by the double-headed gray arrow), resulting in *B-I* being changed into *B′* (right). The new *B′* allele (*B-I* in the previous generation) is denoted *B′**, is mitotically and meiotically stably silenced, and is as capable as *B′* at changing *B-I* into *B′* in subsequent generations (not diagrammed). [Modified from a drawing by M. Arteaga-Vazquez and J. E. Arteaga-Vazquez (*3*)]

BIO5 Institute, Department of Plant Sciences, University of Arizona, Tucson, AZ 85719, USA. E-mail: chandler@ag.arizona.edu

ulation is that repeat RNAs are the targeting signal, but whether the RNA signal (either siRNAs or larger RNAs) is received depends on the chromatin state of the alleles, which has been shown to differ between *B-I, B′*, and the single-copy repeat alleles that do not undergo paramutation (*7*). Another hypothesis that is not mutually exclusive is that differential production of paramutation-associated RNAs occurs in developing embryos (*6*), where paramutation is established (*8*) and where RNAs have not yet been examined. This latter hypothesis is exciting given that cis- and trans-acting small RNAs regulate epigenetic changes during gametogenesis, fertilization, and early zygotic development in multiple species (*9*).

Although the above evidence supports a role for RNA, other factors, such as protein-DNA interactions, could also be involved. For example, interactions between proteins that bind to the *b1* tandem repeats might mediate communication between alleles. Data consistent with that idea are that a transgene overexpressing a protein that binds to the *b1* tandem repeats and forms multimers, inducing a *B′*-like state in *B-I* (*10*). Another possible model, frequently discussed, is that the alleles communicate through DNA pairing (*1*, *2*). Although there is no experimental evidence demonstrating a role for DNA pairing, there is no evidence eliminating it either. It is of course possible that RNA, DNA, and protein interactions are all required for paramutation.

Why are repeats required for paramutation? Tandem repeats create a characteristic sequence at their junctions relative to single-copy sequences; the *b1* tandem repeat junctions have distinct chromatin structures, which have been hypothesized to affect silencing (*7*), potentially through specific proteins or RNAs that associate with these sequences. It has also been suggested that RNAs synthesized from repeats, but not a single-copy sequence, trigger silencing (*6*). A model proposed to explain how centromeric tandem repeats maintain heterochromatin silencing (*11*) offers an hypothesis for how tandem repeats could generate a distinct pool of RNAs relative to nonrepeats. That model suggests a mechanism by which multiple cycles of amplification of RNAs from tandem repeats [as outlined in (*9*)] results in distinct populations of RNA that span the full repeat sequence, as compared to RNA amplification from dispersed copies or single-copy sequences that have reduced sequence complexity (*11*).

Once paramutation is established (*8*), it is maintained through mitotic and meiotic cell divisions. Although the nature of the heritable molecule(s) is unknown, it is unlikely to be *b1* tandem repeat siRNAs, as mitotic silencing is maintained when a mutation dramatically reduces these siRNAs in juvenile and adult tissues (*3*). Analyses of cytosine methylation and histone modifications in *B-I* and *B′* revealed more cytosine methylation within the *b1* tandem repeats in *B′* relative to *B-I* (*7*), whereas histones associated with the *b1* repeats in both alleles did not carry modifications characteristic of silent chromatin. Future studies on the paramutation properties of mutants impaired in DNA methylation and various histone modifications should shed light on the potential role for these marks in paramutation. The observations that RdDM in *Arabidopsis* is associated with cytosine methylation and heterochromatin histone modifications (*4*), yet paramutation does not occur between RdDM silenced alleles (see below), leads to the speculation that paramutation involves additional mechanisms, such as RNA or proteins that remain associated with the *b1* repeats during mitosis and meiosis.

It is puzzling that RNAi-mediated heterochromatin in *S. pombe* and RdDM-silenced genes in *Arabidopsis* do not undergo paramutation (*4*, *5*). For example, specific alleles of *b1* and *FWA* in *Arabidopsis* are both silent when cytosine residues of the respective tandem repeats are methylated and active when hypomethylated. In both systems, the tandem repeats required for silencing are transcribed and produce small RNAs regardless of whether the alleles are active or silent. The methylated, silenced *FWA* allele can initiate trans methylation of an unmethylated transgene, yet, unlike the maize paramutation system, the unmethylated allele segregates normally and is active and unchanged (*12*). It is unclear whether the "natural" active *FWA* allele is protected from silencing, or the transgene is hypersensitive to silencing, or both (*12*). Additionally, the mechanism that makes *B-I* in maize highly sensitized to silencing is also unknown, although several hypotheses have been proposed (*13*).

The relationship with other RNA silencing pathways suggests that paramutation, despite being rare, may underlie fundamental mechanisms for gene regulation (*2*). Speculations on potential roles and consequences include that paramutation provides an adaptive mechanism through the transfer of favorable expression states to progeny, that paramutation could be a mechanism for establishing functional homozygosity in polyploids, and that it might function in inbreeding depression and hybrid vigor or inheritance associated with complex human diseases (*13*).

Independent of paramutation's function or frequency, our understanding of its mechanisms should shed light on potentially novel mechanisms for transmitting epigenetic information across generations.

References

1. M. Stam, *Mol. Plant* **2**, 578 (2009).
2. C. M. Suter, D. I. K. Martin, *Trends Genet.* **26**, 9 (2010).
3. M. A. Arteaga-Vazquez, V. L. Chandler, *Curr. Opin. Genet. Dev.* **20**, 156 (2010).
4. M. Matzke, T. Kanno, L. Daxinger, B. Huettel, A. J. M. Matzke, *Curr. Opin. Cell Biol.* **21**, 367 (2009).
5. S. I. S. Grewal, *Curr. Opin. Genet. Dev.* **20**, 134 (2010).
6. M. Arteaga-Vazquez *et al.*, *Proc. Natl. Acad. Sci. U.S.A.* **107**, 12986 (2010).
7. M. Haring *et al.*, *Plant J.* **63**, 366 (2010).
8. E. H. Coe Jr., *Genetics* **53**, 1035 (1966).
9. D. Bourc'his, O. Voinnet, *Science* **330**, 617 (2010).
10. K. Brzeska, J. Brzeski, J. Smith, V. L. Chandler, *Proc. Natl. Acad. Sci. U.S.A.* **107**, 5516 (2010).
11. R. A. Martienssen, *Nat. Genet.* **35**, 213 (2003).
12. I. R. Henderson, S. E. Jacobsen, *Nature* **447**, 418 (2007).
13. V. L. Chandler, *Cell* **128**, 641 (2007).

10.1126/science.1191044

PERSPECTIVE

Epigenetics in the Extreme: Prions and the Inheritance of Environmentally Acquired Traits

Randal Halfmann[1,2] and Susan Lindquist[1,2,3]*

Prions are an unusual form of epigenetics: Their stable inheritance and complex phenotypes come about through protein folding rather than nucleic acid–associated changes. With intimate ties to protein homeostasis and a remarkable sensitivity to stress, prions are a robust mechanism that links environmental extremes with the acquisition and inheritance of new traits.

In its modern usage, "epigenetics" encompasses all mechanisms for the inheritance of biological traits that do not involve alterations of the coding sequence of DNA (*1*). Considered elsewhere in this issue are well-known epigenetic mechanisms that control access to DNA by modifying nucleotides or associated histones, or involve the transmission of information through RNA. Here, we discuss an extreme case of epigenetic inheritance with a mechanism that is not based on heritable changes in nucleic acid. Instead, it is based on robust self-propagating changes in the folding of certain proteins known as prions.

Prions operate outside the canonical steps of molecular biology's central dogma. As protein-

based elements of inheritance, prions perpetuate not by changing the way that genetic information is transcribed or translated but rather by co-opting the final step in the decoding of genetic information—protein folding. A key feature of prion-forming proteins is their ability to exist in very different stable conformational states. In addition to a "native" nonprion conformation, they occasionally fold into a prion conformation that then replicates itself by templating the conformational conversion of other molecules of the same protein. These changes in conformation profoundly alter the functions of the proteins involved, resulting in phenotypes specific to each determinant protein.

The idea that proteins could transmit information in a manner analogous to nucleic acids was first conceived to explain baffling infectious neurodegenerative diseases (such as Kuru and mad cow disease) (*2*). As evidence accumulated that these diseases did not require nucleic acids for transmission, the infectious agent was postulated to be a self-replicating protein. It is now clear that the prion does not synthesize itself from individual amino acids. Rather, it is a host-encoded protein in a conformation that is profoundly different from normal. The prion "replicates" simply by templating that conformation to other molecules of the protein. The initially mysterious and controversial nature of infectious prions created a stir that even today sometimes overshadows what we believe is a far more interesting aspect of prion biology: the ability of proteins to serve as elements of heredity.

In the baker's yeast *Saccharomyces cerevisiae*, prions create dominant cytoplasmically transmitted traits that are, in contrast to the original disease-causing prion in mammals, often advantageous to the organism (*3*). Most biochemically characterized prion proteins have a modular prion-forming domain that is highly disordered in its native state (*4*, *5*). The extreme flexibility of these domains facilitates their occasional conversion to a self-propagating conformer, which for most prions is a well-ordered fibrillar protein polymer, or amyloid. De novo prion formation appears to proceed through a high-energy oligomeric nucleus that is stabilized by interacting with, and converting, other prion proteins to the same conformation (Fig. 1A) (*4*, *6*, *7*). The elongating prion polymer is then severed into smaller, actively growing pieces by the action of protein remodeling factors such as the disaggregase Hsp104 (*8*). Lastly, the resulting fragments are disseminated to daughter cells, ensuring the stable inheritance of the self-perpetuating prion template through round after round of cell division. Indeed, prions are stable even during mating and meiosis, allowing their transmission through the germ line. Prion states are not irreversible, however. Random fluctuations in prion dissemination to daughter cells, as well as changes in the activities of remodeling proteins and other factors, can generate daughter cells with the original nonprion state (Fig. 1B).

To date, at least nine different proteins are known to form prions in *S. cerevisiae* (*3*, *9*), and an additional 18 have experimentally verified prion-forming domains (*5*). The best understood prion protein, Sup35, is a translation termination factor whose ability to form prions has been conserved for hundreds of millions of years of fungal evolution (*10*). When Sup35 switches to a prion state, its ability to function in translation is compromised, leading to increased stop codon read-through and ribosome frame-shifting (Fig. 2) (*11*, *12*). The resulting changes in gene expression have diverse phenotypic effects, including alterations in cell-adhesion, nutrient use, and resistance to various toxins and antibiotics (*12*, *13*). Importantly, these phenotypes differ in different strain backgrounds, presumably because of genetic

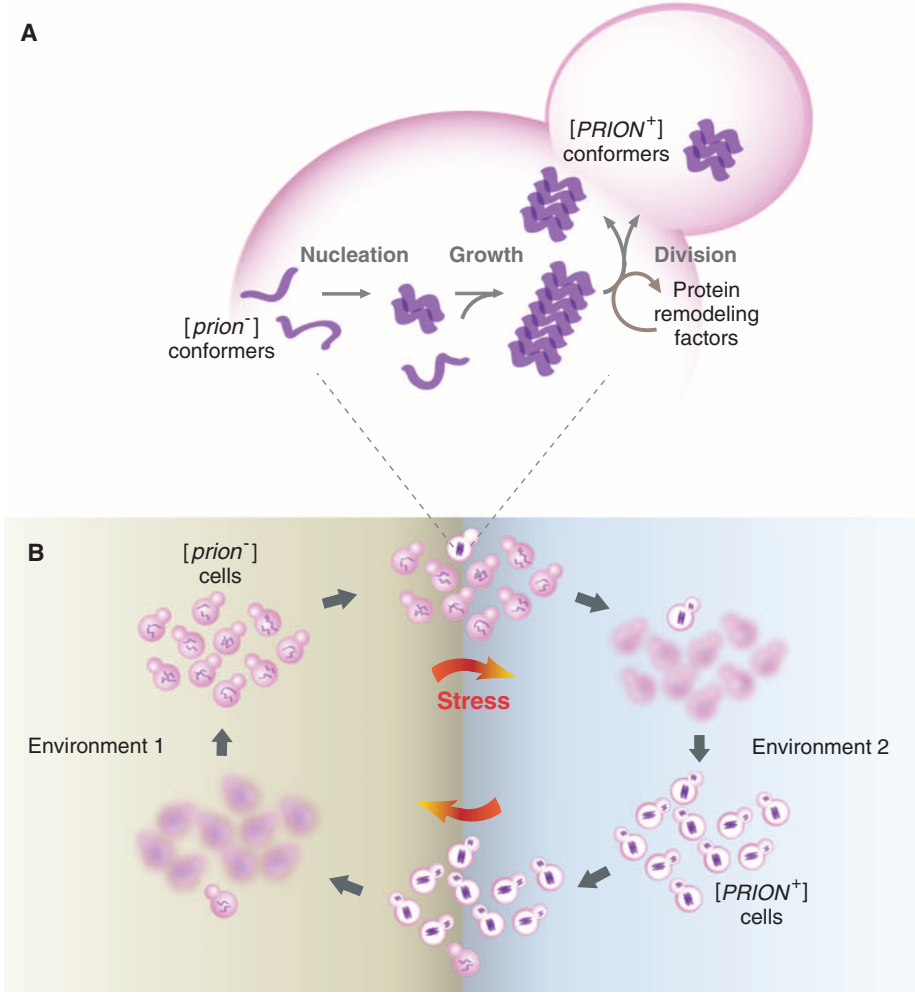

Fig. 1. Prion epigenetics. (**A**) The "life cycle" of a yeast amyloid prion. Soluble nonprion conformers in [*prion*$^-$] cells occasionally fold into an oligomeric amyloid nucleus, which then grows by sequestering additional nonprion conformers and templating their conformational conversion. The resulting prion particle divides into smaller transmissible pieces through the action of protein-remodeling factors such as Hsp104. The prion particles are disseminated to daughter cells during cell division. (**B**) Prion formation and loss are promoted by stress, and this provides a mechanism for the acquisition of heritable phenotypes in response to environmental changes. [*prion*$^-$] cells are well adapted to environment 1, but are poorly adapted to environment 2. When the environment changes, stress-induced changes in protein homeostasis result in an increased frequency of prion appearance ([*PRION*$^+$] cells) and consequently the exploration of new phenotypes. Some phenotypes revealed by prions provide a fitness advantage in environment 2, so that [*PRION*$^+$] cells survive and proliferate. The occasional loss of prion states—a process that is also increased by stress—ensures that [*prion*$^-$] cells will be available when conditions return to normal (environment 1).

[1]Whitehead Institute for Biomedical Research, Cambridge, MA 02142, USA. [2]Department of Biology, Massachusetts Institute of Technology, Cambridge, MA 02139, USA. [3]Howard Hughes Medical Institute, Cambridge, MA 02139, USA.

*To whom correspondence should be addressed. E-mail: lindquist_admin@wi.mit.edu

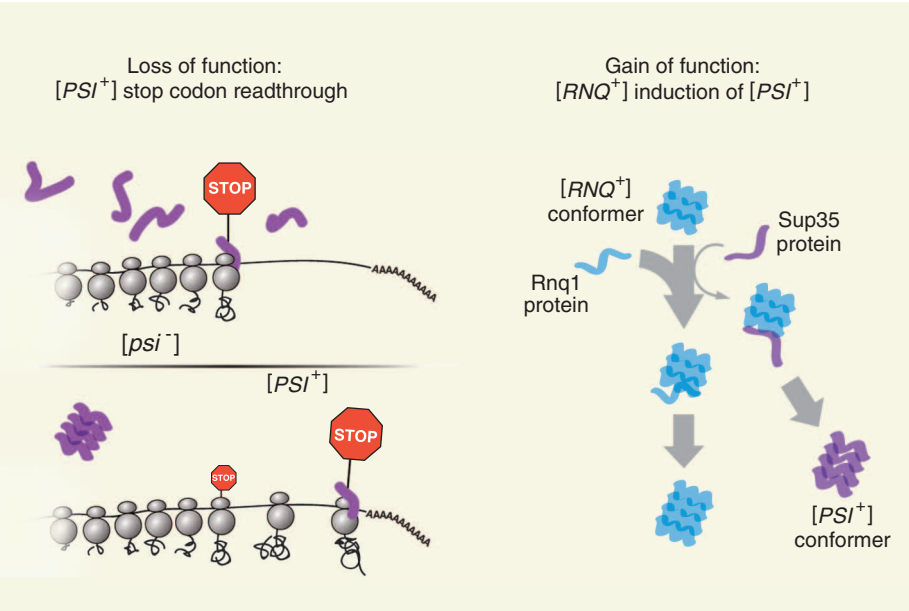

Fig. 2. Prion phenotypes can result from either a loss of function or a gain of function when the prion protein acquires its prion conformation. (**Left**) The [*PSI*$^+$] prion conformation of the translation termination factor Sup35 prevents it from associating with ribosomes. This results in the translational read-through of stop codons and corresponding C-terminal extensions that alter the activities of newly synthesized proteins. (**Right**) The Rnq1 protein, in its prion state, acquires the ability to induce other proteins, such as Sup35, to convert to their own prion states.

variation in sequences downstream of stop codons that are silent in the absence of the prion.

Prions Diversify Protein Function

Many prion phenotypes result from qualitative changes in protein function. Because function is dictated by structure, the refolding of a polypeptide into its prion form can dramatically alter the nonprion function and can even create gains of function. Aside from the ability to template their own conformational changes through homotypic interactions, some prion conformers form new interactions with other proteins. For example, the prion form of the HET-s protein in the filamentous fungus *Podospora anserina* interacts with an allelic variant of the same protein that is itself incapable of forming prions. This interaction is the basis of a self-/nonself-discrimination system that reduces the spread of parasitic cytoplasmic elements (*14*). Likewise, the prion form of the *S. cerevisiae* Rnq1 protein has the ability to interact with other prion-forming proteins. In this case, the interaction stimulates those proteins to convert to their own prion states (Fig. 2) (*8*). Another example of functionality gained in the prion state is that of the *S. cerevisiae* transcriptional regulator Sfp1. In this case, prion formation causes resistance to translation inhibitors and, remarkably, increases the cells' growth rate on rich media—phenotypes distinct from those of the nonprion state and opposite those of the genetic knockout of Sfp1 (*9*).

Prions Respond to Environmental Extremes

The way that proteins fold and interact with other proteins is very sensitive to environmental stress and the status of the protein-folding machinery. Abrupt changes in temperature, pH, and intracellular metabolites can have immediate consequences for protein folding and the regulation of protein chaperones and protein-remodeling factors. Not surprisingly then, environmental stresses also dramatically increase rates at which prions appear and disappear (*13*). The more extreme the stress, the greater the frequency of prion switching—hence, a second meaning invoked by this Perspective's title: "epigenetics in the extreme." In this way, prions connect environmental stresses with an unusual type of phenotypic plasticity that could improve an organism's ability to adapt to altered environments. When organisms experience protein homeostatic stress—which will commonly occur when they are poorly adapted to their environment—increases in protein "misfolding" and concomitant prion formation will facilitate the exploration of alternative phenotypes (Fig. 1). Indeed, we postulate that the accelerated appearance of prions in response to stress constitutes an evolved bet-hedging strategy: It allows a fraction of cells to try new phenotypes that, with reasonable frequency, prove beneficial (*3*, *15*). The self-sustaining nature of prions ensures that successful strategies are immediately heritable to subsequent generations. Prions, then, are a quasi-Lamarckian (*1*, *16*) mechanism that connects environmental conditions to the acquisition and transgenerational inheritance of new traits.

Prions Allow for the Sudden Appearance of Complex Traits

Complex evolutionary adaptations are the product of multiple interacting genetic loci (*17*). A plausible mechanism for the appearance of complex adaptations is phenotypic capacitance. Phenotypic capacitance is a property of certain biological systems that allows for the accumulation of genetic variation in a silent form, followed by its sudden stepwise release to create new phenotypes (*18*). Because prions allow cells to switch between two distinct and heritable physiological states, they provide one of the clearest examples for the reversible expression of natural genetic variation. In contrast to other mechanisms for genetically encoded stochastic phenotypic variation, such as Hsp90-buffered protein folding and variably methylated CpG islands (*19*), newly revealed prion-based phenotypes are immediately and robustly heritable. These traits can ultimately become hardwired by subsequent genetic changes, as demonstrated for phenotypes revealed by Sup35 prion formation (*12*). This observation provides experimental validation for the conjecture of West-Eberhard that in some cases genes may be followers rather than leaders in evolution (*20*, *21*).

Yeast prions are well-positioned to alter the phenotypic effects of genetic variation. The approximately two dozen prionogenic proteins discovered to date in yeast are enriched for proteins with information-processing functions, including transcription factors and RNA-binding proteins (*3*, *5*). Some, such as Swi1, Cyc8, and Sfp1, are globally acting transcriptional regulators of a large fraction of the yeast genome (*9*, *22*, *23*). Others, such as Puf2, Ptr69, and Pub1, act posttranscriptionally on the stabilities of hundreds of functionally diverse mRNAs (*24*). Because of the large number of regulatory targets of these proteins, reductions or alterations in their activities resulting from their conversion to a prion conformation can have large, and complex, phenotypic effects. Importantly, these effects also change the strength of the selective pressures that act on prion targets, resulting in these target sequences diverging at different rates when expressed under the prion versus nonprion states. As a consequence, prion-revealed phenotypes will tend to differ between genetic backgrounds (*12*). Thus, prions create phenotypic diversity on two levels: Within isogenic populations, they create distinct physiological states (prion versus nonprion), and within genetically diverse populations, they enhance the effects of genetic variation between lineages.

A Wider Range of Prion Phenomena?

In multicellular organisms, developmental signals trigger the epigenetic switches that drive cell differentiation. These switches parallel prions in

that both respond (directly or indirectly) to changes in the extracellular environment. In *S. cerevisiae*, chromatin-remodeling factors such as Swi1 and Cyc8 participate in epigenetic decisions that govern, for example, whether the cells grow as unicellular or as cohesive multicellular forms (*25*). That Swi1 and Cyc8 also form prions suggests a possible functional link between chromatin-based and prion-based regulatory strategies. In higher eukaryotes as well, prion-like switches may be involved in cell-remodeling processes. During memory formation, individual synapses must acquire a durable molecular "mark" that establishes—among the many hundreds of such marks most neurons carry—the individual long-term maintenance of that synapse. One protein contributing to this mark, neuronal cytoplasmic polyadenylation element–binding protein (CPEB), appears to undergo a prion-like conformational switch that can activate translation of synaptic mRNAs while simultaneously creating a nondiffusable self-sustaining aggregate that can act as a molecular memory (*26*). We fully expect that many such prion-like physiological switches await discovery as our abilities to characterize protein complexes and protein aggregates in vivo continue to improve.

A large array of regulatory strategies influences protein folding and may in the future prove to blur distinctions between prions and other epigenetic mechanisms for perpetuating phenotypes. Covalent modifications, including disulfide formation, phosphorylation, ubiquitination, and glycosylation, as well as protein-protein interactions (such as chaperone binding and prion templating), can all profoundly change protein-folding landscapes and/or the activity of folded proteins. All of these forms of regulation can theoretically give rise to self-sustaining heritable—that is, epigenetic—states. In fact, examples of these types of heritable factors now include an autoactivatable kinase, an autoactivatable protease, and a prion that appears to result from the interaction of two separate proteins involved in glucose signaling (*21*, *27*).

The Origins of Prions

The propensity of proteins to misfold and aggregate is probably as ancient as protein-based life forms themselves. Indeed, most polypeptides have an inherent tendency to form self-templated amyloid structures (*28*). Prion-forming proteins are unusual in having a conformational flexibility that allows access to the amyloid fold under physiological conditions (*5*, *29*). This property derives in part from a greatly reduced amino acid complexity as compared with that of globular proteins (*5*, *30*). We suggest that primordial proteins would have had similarly simple sequences, resulting in an elevated tendency to form self-perpetuating structures. Further, early biological systems would have lacked elaborate protein-folding machinery whose primary modern role is the prevention of protein aggregation. Without strong control over the important final step in the processing of gene-encoded information—protein folding—ancient polypeptides would have unencumbered access to self-perpetuating prion states. We speculate that prion formation by ancient proteins may have played a central role in the molecular evolution of early biological systems.

Our increasing awareness of prion phenomena highlights the fact that protein folding is not always uniquely specified by an amino acid sequence but instead provides a rich substrate for epigenetic determination of the map between genotype and phenotype. Beyond our speculative thoughts about early life, we suggest that prions are not simply elements of disease transmission but make distinct contributions to the flow of genetic information that are likely to profoundly influence the adaptive success, and therefore the evolution, of prion-containing organisms.

Note added in proof: The study by Derdowski *et al*. (*31*) adds another temporal dimension to the phenotypic heterogeneity conferred by prions. That the numbers of prion particles and the strength of their associated phenotypes increase as cells age suggests an accelerated exploration of alternative phenotypes among cells that have little left to lose.

References and Notes

1. O. J. Rando, K. J. Verstrepen, *Cell* **128**, 655 (2007).
2. A. Aguzzi, A. M. Calella, *Physiol. Rev.* **89**, 1105 (2009).
3. R. Halfmann, S. Alberti, S. Lindquist, *Trends Cell Biol.* **20**, 125 (2010).
4. T. R. Serio *et al*., *Science* **289**, 1317 (2000).
5. S. Alberti, R. Halfmann, O. King, A. Kapila, S. Lindquist, *Cell* **137**, 146 (2009).
6. M. Eigen, *Biophys. Chem.* **63**, A1 (1996).
7. M. M. Patino, J. J. Liu, J. R. Glover, S. Lindquist, *Science* **273**, 622 (1996).
8. I. S. Shkundina, M. D. Ter-Avanesyan, *Biochemistry (Mosc.)* **72**, 1519 (2007).
9. T. Rogoza *et al*., *Proc. Natl. Acad. Sci. U.S.A.* **107**, 10573 (2010).
10. Y. O. Chernoff *et al*., *Mol. Microbiol.* **35**, 865 (2000).
11. O. Namy *et al*., *Nat. Cell Biol.* **10**, 1069 (2008).
12. H. L. True, I. Berlin, S. L. Lindquist, *Nature* **431**, 184 (2004).
13. J. Tyedmers, M. L. Madariaga, S. Lindquist, *PLoS Biol.* **6**, e294 (2008).
14. S. J. Saupe, *Prion* **1**, 110 (2007).
15. A. K. Lancaster, J. P. Bardill, H. L. True, J. Masel, *Genetics* **184**, 393 (2010).
16. E. V. Koonin, Y. I. Wolf, *Biol. Direct* **4**, 42 (2009).
17. D. B. Weissman, M. M. Desai, D. S. Fisher, M. W. Feldman, *Theor. Popul. Biol.* **75**, 286 (2009).
18. J. Masel, M. L. Siegal, *Trends Genet.* **25**, 395 (2009).
19. A. P. Feinberg, R. A. Irizarry, *Proc. Natl. Acad. Sci. U.S.A.* **107** (suppl. 1), 1757 (2010).
20. M. J. West-Eberhard, *Developmental Plasticity and Evolution*. (Oxford Univ. Press, Oxford, New York, 2003).
21. E. Jablonka, G. Raz, *Q. Rev. Biol.* **84**, 131 (2009).
22. Z. Du, K. W. Park, H. Yu, Q. Fan, L. Li, *Nat. Genet.* **40**, 460 (2008).
23. B. K. Patel, J. Gavin-Smyth, S. W. Liebman, *Nat. Cell Biol.* **11**, 344 (2009).
24. D. J. Hogan, D. P. Riordan, A. P. Gerber, D. Herschlag, P. O. Brown, *PLoS Biol.* **6**, e255 (2008).
25. A. B. Fleming, S. Pennings, *EMBO J.* **20**, 5219 (2001).
26. K. Si, Y. B. Choi, E. White-Grindley, A. Majumdar, E. R. Kandel, *Cell* **140**, 421 (2010).
27. J. C. Brown, S. Lindquist, *Genes Dev.* **23**, 2320 (2009).
28. F. Chiti, C. M. Dobson, *Annu. Rev. Biochem.* **75**, 333 (2006).
29. V. N. Uversky, *Front. Biosci.* **14**, 5188 (2009).
30. P. Romero *et al*., *Proteins* **42**, 38 (2001).
31. A. Derdowski, S. S. Sindi, C. L. Klaips, S. DiSalvo, T. R. Serio, *Science* **330**, 680 (2010).

32. We thank members of the Lindquist laboratory for their insightful comments on the manuscript. S.L. is an Investigator of the Howard Hughes Medical Institute (HHMI).

10.1126/science.1191081

Magnitude of the 2010 Gulf of Mexico Oil Leak

Timothy J. Crone[1]* and Maya Tolstoy[2]

The Deepwater Horizon well was sealed on 15 July 2010 after flowing oil at the seafloor for approximately 84 days. A full accounting of the oil released will be required in order to fully understand the environmental and ecological impacts of this disaster. One method for determining this volume is to measure the flow at the discharge sites and integrate these measurements over time. We used optical plume velocimetry (OPV) to estimate the mean velocity of fluids issuing from the well with videos from before and after the removal of the collapsed riser pipe from the blowout preventer. We analyzed two short (20 to 30 s) high-resolution video sequences (*1*) representing each regime. We focused our analyses on flow near the nozzle, where momentum forces are dominant and velocities scale linearly with the average nozzle rate (*2*). In this part of the flow, differences between the image velocity and the average flow rate at the nozzle can be accounted for with a constant "shear layer" correction factor (*2*), and the median image velocity can be used to determine flow rate.

In the study of fluid dynamics, spatial cross-correlation methods (e.g., particle image velocimetry) are often used to calculate the image velocity field. However, such methods can yield velocities that are significantly lower than expected with this kind of flow (*2*). OPV was developed for measuring flow rates in seafloor hydrothermal systems (*3*) and uses temporal instead of spatial cross-correlation. Interpolated temporal cross-correlation functions of image intensity are calculated across the entire region of interest for pixel pairs separated by some distance horizontally and vertically. The distance is chosen on the basis of the direction of flow, the frame rate, and the resolution of the imagery. To increase accuracy, the separation is then refined so that the distance is maximized while ensuring that the signals still correlate (*2*). The lag value corresponding to the maximum of each cross-correlation function defines the time (in frames) required for flow features to traverse the distance defined by the pixel separation. In this way, a velocity (in pixels/frame) can be calculated at every pixel within the region of interest (Fig. 1A).

After the riser was removed, the flow was separated into two flows, one lighter and one darker in color (Fig. 1A and fig. S1), which we analyzed separately. Figure S2, A and B, shows the distribution of the image velocity magnitudes for the lighter and darker colored flows, which have median values of 13.6 and 9.43 pixels per frame, respectively. Assuming the smaller lighter-colored flow comprised 10% of the cross-sectional area of the riser pipe (*4*), we calculated an effective image velocity magnitude of 9.85 pixels/frame for the entire flow.

With a spatial resolution of 3.85 pixels/cm (fig. S1), a video frame rate of 30 frames/s, and a shear layer correction factor of 2.10 (*5*), we contoured the volumetric flow rate from this leak over a range of image velocities and effective flow diameters (Fig. 1B and fig. S3). Assuming the fraction of liquid oil in this fluid was 0.4 (*6*), we estimated the average flow rate after riser removal to be 9.3×10^3 and 5.8×10^4 barrels/day (1.7×10^{-2} and 1.1×10^{-1} m^3/s) for the lighter and darker flows, respectively, or 6.8×10^4 barrels/day (1.2×10^{-1} m^3/s) total. Our analysis from before riser removal (figs. S4 to S7) yielded a flow rate of 5.6×10^4 barrels/day (1.0×10^{-1} m^3/s). Because leaks at the kink above the blowout preventer were not included, this total is likely an underestimate. Thus, we cannot say with certainty that flow rates increased after riser removal.

Aside from temporal variability, we estimated the total combined uncertainty to be about 19 and 21% for the flows before and after riser removal (*6*). It was not possible to quantify temporal variability with the available data; however, changes were likely. Temporal variability may have been induced by variations in the gas content of the fluid, changes in the well integrity or abrasion of components within the system, changes in the formation pressure, or changes in the size and number of openings in the riser wall at the kink. Assuming a constant flow rate and subtracting the 804,877 barrels of oil (127,965 m^3) collected at the seafloor (*7*), we estimated that the total oil released from the Deepwater Horizon leak was $4.4 \times 10^6 \pm 20\%$ barrels (7.0×10^5 m^3). This estimate may be refined if additional video allows the temporal variability to be assessed or the flow from the secondary leaks to be added. Despite the uncertainties, it is clear that this oil release exceeds the Exxon *Valdez* spill by about an order of magnitude, with flow rates at least one order of magnitude higher than initially reported.

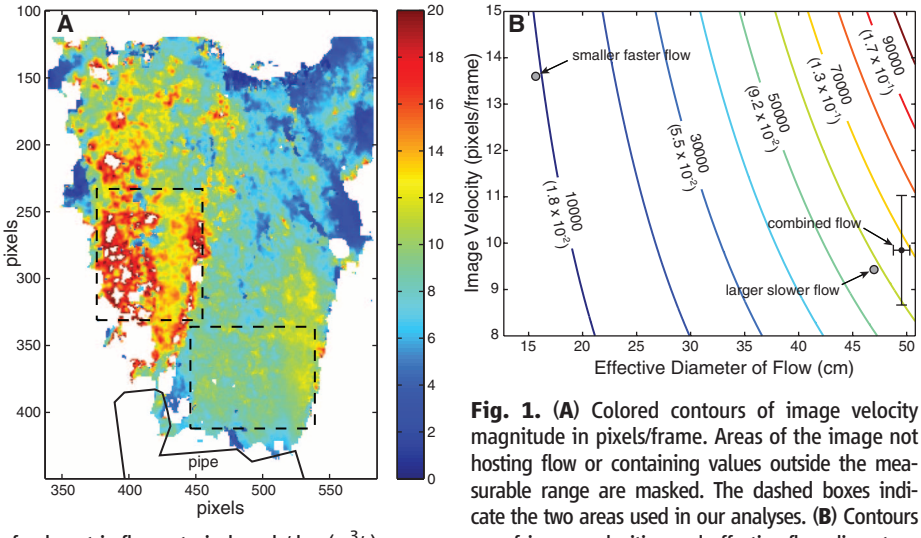

Fig. 1. (**A**) Colored contours of image velocity magnitude in pixels/frame. Areas of the image not hosting flow or containing values outside the measurable range are masked. The dashed boxes indicate the two areas used in our analyses. (**B**) Contours of volumetric flow rate in barrels/day (m^3/s) over a range of image velocities and effective flow diameters. Values associated with the lighter and darker flows are indicated with gray dots. The value calculated for the combined flow is shown with a black dot. Vertical error bars indicate the 12% combined uncertainty associated with the image resolution, the median image velocity, and the shear layer correction factor, and horizontal error bars indicate the 3% uncertainty associated with the area estimate (*6*). For a more detailed version, see fig. S3.

References and Notes

1. High-resolution video data was provided by the office of Senator Bill Nelson and by the Senate Committee on Environment and Public Works.
2. T. J. Crone, R. E. McDuff, W. S. D. Wilcock, *Exp. Fluids* **45**, 899 (2008).
3. T. J. Crone, W. S. D. Wilcock, R. E. McDuff, *Geochem. Geophys. Geosyst.* **11**, Q03012 (2010).
4. www.bp.com/genericarticle.do?categoryId=2012968&contentId=7062328
5. We analyzed original data from the laboratory experiments to obtain this correction factor.
6. A full discussion of all uncertainties is available as supporting material on *Science* Online.
7. www.energy.gov/open/oilspilldata.htm
8. This research was supported by the Lamont–Doherty Earth Observatory and by NSF under grants 0623285 and 0917955.

Supporting Online Material

www.sciencemag.org/cgi/content/full/science.1195840/DC1
SOM Text
Figs. S1 to S7
References

29 July 2010; accepted 14 September 2010
Published online 23 September 2010;
10.1126/science.1195840
Include this information when citing this paper.

[1]Lamont-Doherty Earth Observatory, Columbia University, Palisades, NY 10964, USA. [2]Department of Earth and Environmental Sciences, Columbia University, Palisades, NY 10964, USA.

*To whom correspondence should be addressed. E-mail: crone@ldeo.columbia.edu

Structure of a Eukaryotic CLC Transporter Defines an Intermediate State in the Transport Cycle

Liang Feng, Ernest B. Campbell, Yichun Hsiung, Roderick MacKinnon*

CLC proteins transport chloride (Cl^-) ions across cell membranes to control the electrical potential of muscle cells, transfer electrolytes across epithelia, and control the pH and electrolyte composition of intracellular organelles. Some members of this protein family are Cl^- ion channels, whereas others are secondary active transporters that exchange Cl^- ions and protons (H^+) with a 2:1 stoichiometry. We have determined the structure of a eukaryotic CLC transporter at 3.5 angstrom resolution. Cytoplasmic cystathionine beta-synthase (CBS) domains are strategically positioned to regulate the ion-transport pathway, and many disease-causing mutations in human CLCs reside on the CBS-transmembrane interface. Comparison with prokaryotic CLC shows that a gating glutamate residue changes conformation and suggests a basis for 2:1 Cl^-/H^+ exchange and a simple mechanistic connection between CLC channels and transporters.

CLC proteins form a large family of membrane proteins that transfer chloride ions across cell membranes. Present in all kingdoms of life, existing in both surface and intracellular membranes, CLCs mediate a wide range of physiological processes (*1*, *2*). In muscle, they govern resting membrane potential; in kidneys, they facilitate transepithelial fluid flow; and in intracellular compartments, they control pH through coupled Cl^-/H^+ exchange (*2*–*5*). Mutations of CLC proteins underlie numerous inherited diseases including myotonia congenita, Bartter's syndrome, Dent's disease, osteopetrosis, retinal degeneration, and lysosome storage diseases (*2*, *5*).

CLCs are divisible into two subgroups, Cl^- channels and secondary active transporters (*6*). The channels catalyze passive diffusion down the Cl^- electrochemical gradient, whereas the transporters (Cl^-/H^+ exchangers) actively couple Cl^- movement in one direction to H^+ movement in the opposite direction (*6*–*10*). Thus, in the transporters, "downhill" movement of one ion can drive "uphill" movement of the other. Even though channels and transporters catalyze energetically different reactions, conservation of specific amino acids informs us that these functionally distinct CLC subgroups must share the same basic architecture (*11*–*13*).

CLC proteins are homodimers with a separate ion pathway within each subunit (*14*, *15*). The two pathways act largely independently, but in some channels, they cooperate to turn on and off simultaneously (*16*). Each subunit of the dimer consists of a transmembrane (TM) component, which forms the ion pathway, and, in eukaryotic CLCs, a cytosolic cystathionine beta-synthase (CBS) domain component, which affects membrane localization and regulates the TM component (*17*–*22*).

Crystal structures of two closely related prokaryotic CLC-transporter proteins have been determined (*15*, *23*). These have defined the protein architecture within the membrane, including Cl^- binding sites along the ion-transport pathway, but they have not yet provided a clear mechanism for Cl^-/H^+ exchange, an explanation for the exchange stoichiometry of two Cl^- ions for one H^+, or a plausible hypothesis for understanding how CLCs can encode both channels and secondary active transporters. Moreover, the prokaryotic transporters of known structure do not contain the CBS domains found in all eukaryotic CLCs (*2*). The many disease-causing mutations discovered within the CBS domains and the effects of site-directed mutations will gain a more mechanistic interpretation in light of a eukaryotic CLC structure (*2*, *21*, *24*–*28*).

CmCLC is a Cl^-/H^+ exchange transporter. To overcome the instability of eukaryotic CLCs, we took an approach similar to that used in the study of prokaryotic voltage-dependent K^+ channels (*29*) and identified CmCLC from a thermophilic red alga *Cyanidioschyzon merolae* (fig. S1) (*30*, *31*), which migrated as a monodisperse peak on a size-exclusion column. On the basis of limited proteolysis, a final construct excluding 86 N-terminal and 7 C-terminal amino acids was expressed in *Trichoplusia ni* insect cells and purified for functional and crystallographic studies.

CmCLC was reconstituted into lipid vesicles and studied initially with a fluorescence assay (Fig. 1A) (*32*). Vesicles loaded with 450 mM KCl (pH 7.4) were diluted 20-fold into an assay buffer containing 450 mM K^+ gluconate (pH 7.5). Under these conditions, if CmCLC is a Cl^-/H^+ exchanger, Cl^- efflux will drive H^+ influx against its concentration gradient and cause quenching of the fluorophore 9-amino-6-chloro-2-methoxyacridine (ACMA). This reaction is initiated by the addition of the K^+ selective ionophore valinomycin, which collapses the electrical gradient built up by an electrogenic transporter. On the other hand, if CmCLC is a Cl^- channel, H^+ transport and, thus, a fluorescence change should not be observed. We first validated this assay with a known Cl^-/H^+ exchanger, EcCLC (*7*). The robust fluorescence decrease observed upon addition of valinomycin reflects H^+ influx into the vesicles driven by Cl^- efflux (Fig. 1B). Control experiments with empty vesicles and vesicles containing EcCLCs with a mutation of the "gating glutamate" [$Glu^{148} \rightarrow Ala^{148}$ (E148A) (*33*)], which are known to transport Cl^- without H^+ exchange activity, showed little fluorescence change (Fig. 1B). However, in assays with vesicles containing CmCLC, a clear fluorescence reduction was observed (Fig. 1C). When the gating glutamate of CmCLC was mutated (E210A), the fluorescence signal was minimized (Fig. 1C). Thus, CmCLC is a secondary active transporter, and Cl^-/H^+ exchange depends on the presence of the gating glutamate.

The exchange stoichiometry in EcCLC and other CLC transporters was shown to be two Cl^- ions to one H^+ (*7*, *9*, *10*, *34*, *35*). To estimate the exchange stoichiometry in CmCLC, we directly measured the Cl^- concentration change and pH change in a flux assay developed by Miller *et al.* for EcCLC (*6*). We determined the initial rate of Cl^- increase and H^+ decrease upon valinomycin addition in parallel under identical conditions. From the initial rates, the average Cl^-/H^+ flux ratio for CmCLC is 2.25 ± 0.22 (Fig. 1D).

Structure determination. CmCLC was crystallized in space group *C2* with two copies of the CmCLC dimer in each asymmetric unit. The crystals were grown in the presence of 150 mM Cl^- and diffracted x-rays to 3.5 Å resolution (fig. S2). The experimental phases were derived from single- and multiwavelength diffraction experiments on selenomethionine-containing crystals (table S1). The initial experimental map after solvent flattening allowed tracing of most of the main chain. After several rounds of model rebuilding and refinement, most of the TM component and part of the CBS component could be built with the aid of 16 selenomethionine markers. The remaining segments were built initially as polyalanine chains. To improve the model, we replaced 30 amino acids throughout the protein with methionine in 20 CmCLC mutants and crystallized them with selenomethionine labels. Anomalous difference analysis with the selenium edge identified 24 out of 30 mutation sites to aid in model building (Fig. 2A). Native plus mutant methionines provided one or more selenomethionine markers on almost every helix and strand and on some loops (Fig. 2A). By establishing the register and allowing the building of most of the side chains, this extensive labeling improved the accuracy and completeness of the model, which is refined

Laboratory of Molecular Neurobiology and Biophysics, Rockefeller University, Howard Hughes Medical Institute, 1230 York Avenue, New York, NY 10065, USA.

*To whom correspondence should be addressed. E-mail: mackinn@rockefeller.edu

to working and free residuals (R_{work}/R_{free}) = 0.259/0.284 (table S1).

Molecular architecture. Each monomer of the CmCLC dimer contains 24 α helices and 6 β strands (Fig. 2, B and C, Fig. 3A, and fig. S1). The TM monomer of CmCLC has an antiparallel architecture similar to that of EcCLC (fig. S3A) (*15*). The cytoplasmic CBS domains share the fold characteristics of other CBS-containing proteins (fig. S3B) (*36*). Two CBS subdomains on each subunit (CBS1 and CBS2) are related by a pseudo–twofold-symmetry axis and are tightly packed against each other through β sheets (Fig. 3, A and B). A long and ordered linker following the last TM helix, αR, makes sharp turns, crosses over CBS2, and reaches CBS1 (Fig. 3B). This arrangement brings CBS2 in close proximity to the TM and places CBS1 farther away from the membrane. As a result, the C-terminal end of the protein is positioned closest to the membrane.

The two subunits in the CmCLC dimer are related by a dyad perpendicular to the membrane and bury an extensive interface: 3200 Å^2 in the TM components and 1830 Å^2 in the CBS-domain components (Fig. 2B). The CBS interface is similar to that observed in the isolated domain structures from CLC-5 and CLC-Ka and is consistent with extensive mutagenesis studies on other members of the CLC family (*21*, *22*, *36*, *37*).

Although CmCLC and EcCLC have modest sequence identity (<25%), the structure of the CmCLC TM superimposes well onto EcCLC with a main-chain root mean square deviation (RMSD) of 1.7 Å over a range of 366 aligned residues (fig. S3A and fig. S4A). Helices forming the dimer interface superimpose best (1.2 Å main-chain RMSD for αH, αI, αP, and αQ), whereas helices on the perimeter farthest from the interface, particularly αJ and αK, superimpose worst (3.2 Å main-chain RMSD for αK and the C-terminal half of αJ and αM) (fig. S4, B and C). The larger deviations on the perimeter are mainly due to differences in the tilt angle of the helices. At present, we do not know whether these deviations reflect a true structural difference of equivalent conformational states or different conformations.

Interface between the TM and the CBS. In some membrane proteins, for example, eukaryotic voltage-dependent channels of the Kv1 class, regulatory, or structural domains in the cytoplasm are loosely attached to the TM component through extended polypeptide chains (*38*). In contrast, in CmCLC we observe an extensive protein-protein interface burying 3600 Å^2 between the CBS and TM components. The shape complementarity index is 0.69, similar to an antibody-antigen interface (*39*). This area and complementarity index suggest a highly specific interaction.

Three structural features of the interface seem relevant to the role of the CBS domains in regulating TM function. First, the polypeptide linker between the TM and CBS not only connects the two together, but also makes multiple contacts with TM helix αR (Fig. 4A). Helix αR extends

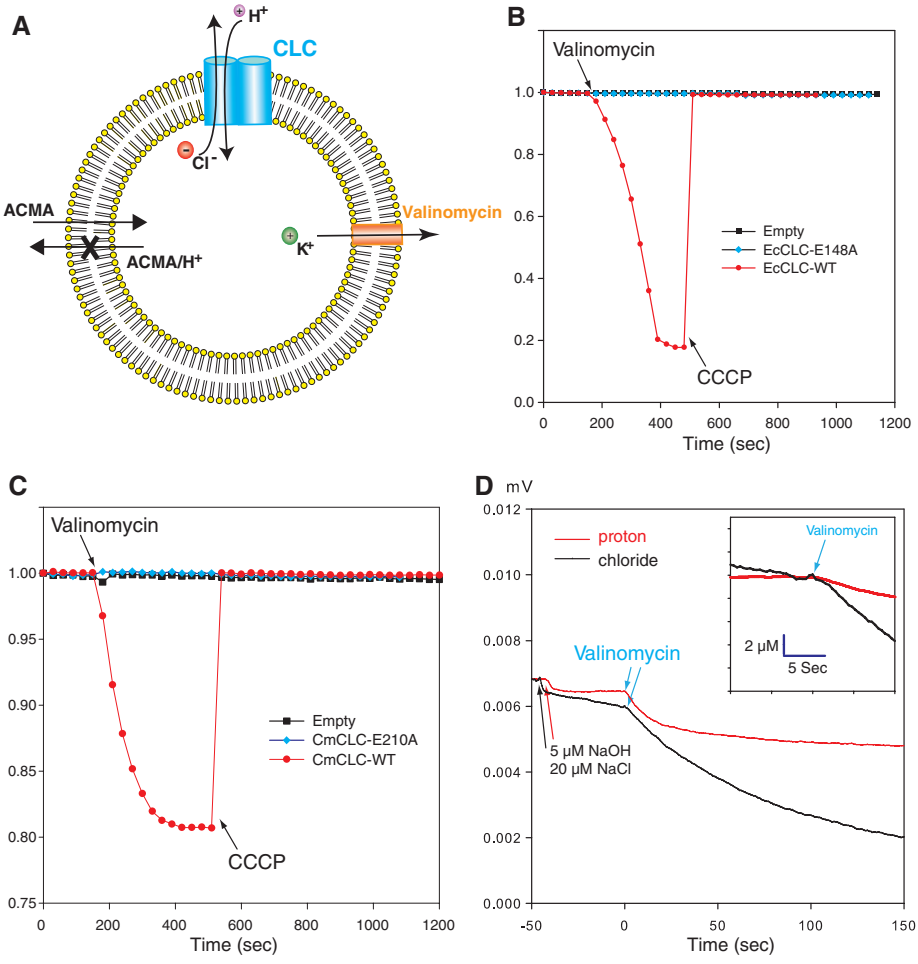

Fig. 1. Analysis of CmCLC transport activity. (**A**) Depiction of the fluorescent-based flux assay. Vesicles (yellow) were loaded with a high concentration of KCl and then diluted into the flux buffer with a low concentration of Cl^- and ACMA. Flux was initiated by addition of valinomycin. The X indicates that protonated ACMA does not exit. (**B**) Fluorescence changes for WT (red) and E148A mutant (blue) EcCLCs compared with empty (black) vesicles. CCCP, carbonyl cyanide *m*-chlorophenyl hydrazone. (**C**) Fluorescence changes for WT and E210A mutant CmCLCs and empty vesicles. (**D**) Recordings of pH (red) and [Cl^-] (black) over time in response to the addition of valinomycin to a solution of Cl^--loaded vesicles. Electrode response was calibrated by the addition of 5 μM NaOH and 20 μM NaCl before each experiment. The initial rates of Cl^- efflux and H^+ influx provide an estimate of the exchange ratio (inset).

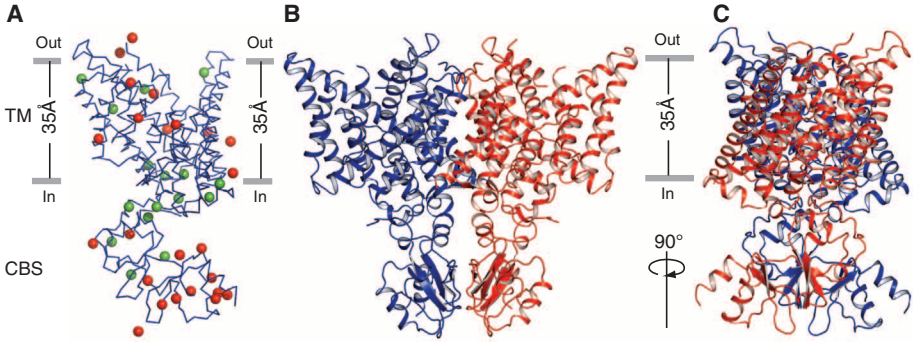

Fig. 2. Structure of CmCLC. (**A**) Selenium sites identified by single-wavelength anomalous dispersion. Wire representation of a CmCLC monomer is shown in blue. The selenium sites of the selenomethionine-labeled WT protein are shown as green spheres, and those corresponding to "marker mutants" are red. (**B** and **C**) Ribbon representation of a CmCLC dimer from the side of the membrane with the extracellular solution above. The two subunits are colored in blue and red, respectively.

into the ion pathway and holds Y515 in place to form part of the central Cl^- binding site (*23*, *40*, *41*). Second, the CBS domain contacts helix αD, which also extends into the ion pathway and contains another important amino acid, S165, that is involved in Cl^- ion coordination and selectivity (Fig. 4A) (*23*, *34*, *35*, *42*, *43*). This explains how conformational changes within the CBS domains could be transmitted directly to the ion pathway of the TM domain (fig. S6). Third, the loop connecting αH to αI, which forms part of the TM dimer interface, comes in direct contact with the CBS domains (fig. S5, A and B), raising the possibility that the CBS domains could influence cooperative interactions between the two TM components (*44*).

Several disease-causing mutations in human CLCs localize to the TM-CBS interface (Fig. 4B). Studies have shown that H835R mutations in hCLC-1 and H736A and E763K in the ortholog CLC-0 alter the "common gating" process that affects both subunits in unison (*25*). These amino acids localize to the surface of the CBS that faces the TM (Fig. 4B, green spheres). Several hCLC-1 mutations that underlie Thomsen's disease exist on the TM-dimer interface (*44*, *45*). We find that several other mutations causing this disease exist on the TM-CBS interface (Fig. 4B). More than 30 osteopetrosis-related mutations have been identified in a Cl^-/H^+ exchanger hCLC-7 (*2*). Although mutations involved in recessive osteopetrosis tend to be spread throughout the structure (*46*), most dominant mutations are located on the TM-CBS interface (Fig. 4B, yellow and pink spheres) (*46*–*49*). It appears that altering communication between CBS and TM domains may be a common mechanism underlying many CLC-related diseases.

Truncations of the hCLC-1 C terminus affect gating of the channel (*50*, *51*), and several disease-causing mutations are known to occur in this region. Because CLCs vary in the length of the unstructured C terminus following CBS2, the importance of this region to channel function was puzzling. The crystal structure offers a possible explanation; the C terminus is in close proximity to the TM and participates in the TM-CBS interface (Figs. 3A and 4A). Hence, it is possible that the C-terminal peptide affects transport function through its interaction with helix αR or other regions of the TM component.

Ion-transport pathway. The Cl^--transport pathway of CmCLC is shaped like an hourglass with aqueous vestibules on the extracellular and intracellular surfaces leading up to a narrow segment (Fig. 5A, blue mesh). In between the vestibules, the transport pathway narrows into a selectivity filter or transport region where ions become dehydrated as they cross the membrane. The α helices αN, αF, and αD are oriented with their N termini pointed toward the transport region, making amide nitrogen atoms available for anion coordination. Overall, the transport region of CmCLC is very similar to that of EcCLC with respect to the positioning of the oriented α helices and the locations of residues Y515 and S165, which are known to play an important role in Cl^- transport (*23*, *34*, *35*, *40*, *42*).

One major difference exists between the transport regions of CmCLC and EcCLC. In EcCLC, three Cl^- ion–binding sites were identified: S_{ext}, S_{cen}, and S_{int}, from the extracellular to the intracellular side (*23*). In a mutant of EcCLC in which the gating glutamate E148 (corresponding to E210 in CmCLC) was mutated to a glutamine residue, the Cl^- analog Br^- occupied all three sites in difference Fourier maps, and the glutamine side chain was located in the extracellular solution, directed away from the transport region (Fig. 6A) (*23*). In wild-type (WT) EcCLC, the gating glutamate was bound to the outermost site, S_{ext}, and Br^- was excluded from that position (Fig. 6A) (*23*). Thus, the gating glutamate appeared to compete with the halogen anion for the extracellular site. However, in CmCLC, a new conformation is observed: The gating glutamate occupies the central site, and Br^-, as demonstrated in an anomalous-difference Fourier experiment, occupies S_{ext} and S_{int} (Fig. 5, A and B). This new conformation is achieved mainly through a reorientation of the gating glutamate side chain. The carboxylate group in the central site interacts with the same hydrogen bond donor groups that interact with the halogen anion at that site in the other structures (Fig. 5C).

Two amino acids are known to affect the movement of H^+ through CLC transporters: the externally located gating glutamate and an internally located "proton glutamate," E203 in EcCLC (*7*, *52*). In EcCLC, mutations at either position can abolish coupled H^+ movement and convert the transporter into a Cl^- channel with a small conductance (*7*, *52*–*54*). In CmCLC, a threonine

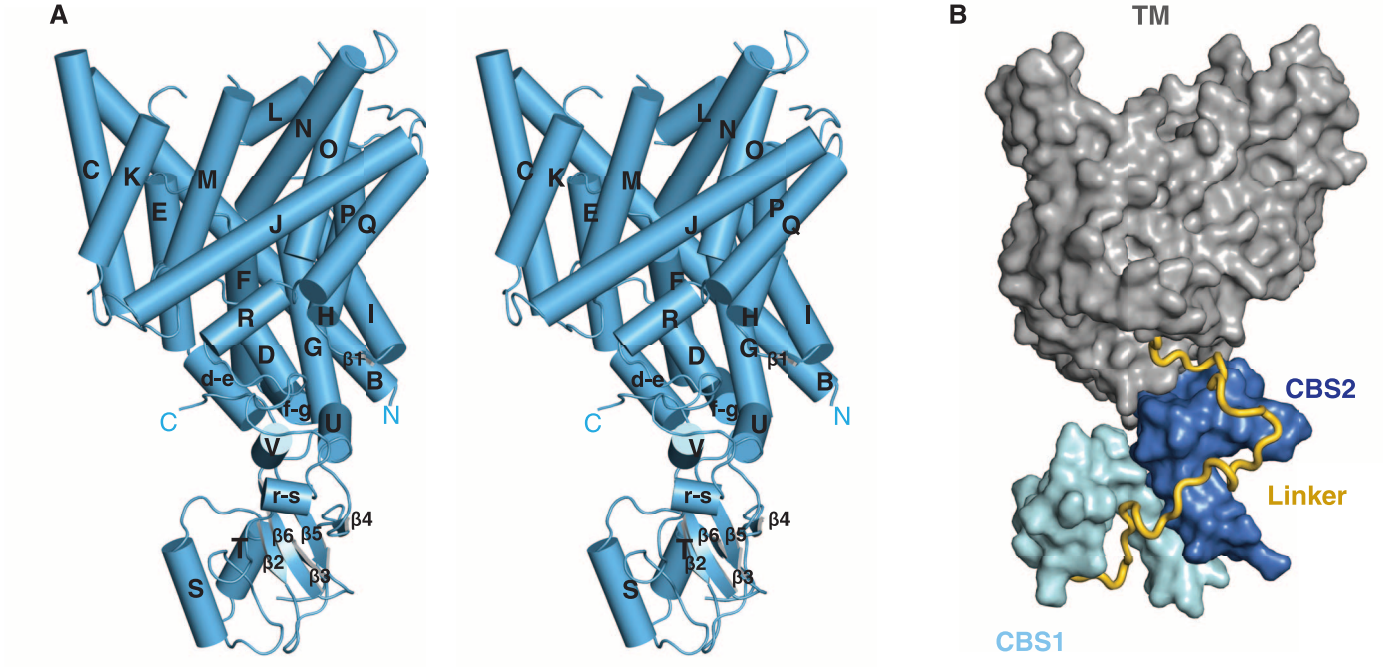

Fig. 3. Structure of CmCLC subunit. (**A**) Stereo view of a CmCLC subunit from the side of the membrane with the extracellular solution above. The black capital letters indicate elements of secondary structure; the blue C and N denote the C and N termini, respectively. d-e, f-g, and r-s correspond to secondary structure elements not present in EcCLC. (**B**) Surface representation of a CmCLC subunit. The TM domain, gray; CBS1 subdomain, pale blue; and CBS2, darker blue. The linker between the TM domain and CBS1 is shown as a yellow cord.

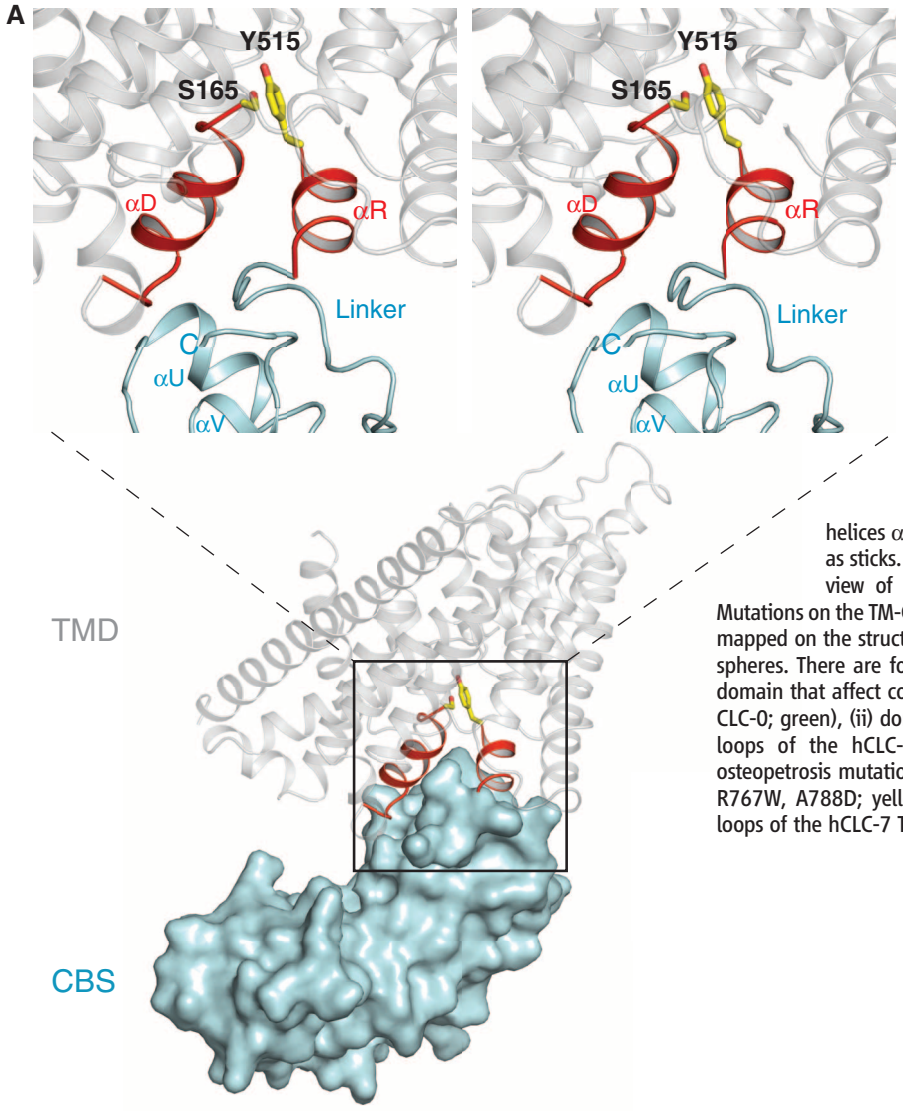

Fig. 4. The TM-CBS interface. (**A**) A CmCLC subunit highlighting the TM and CBS interface. The CBS is shown in light blue and the TM as gray ribbons with helices αR and αD highlighted in red. S165 and Y515 are shown as sticks. Yellow, carbon; red, oxygen. Top panels show the stereo view of the zoomed-in boxed area in the bottom panel. (**B**) Mutations on the TM-CBS interface. Mutations of hCLC-1, CLC-0, and CLC-7 are mapped on the structure through sequence alignment (fig. S1) and shown as spheres. There are four groups: (i) hCLC-1 and CLC-0 mutations in the CBS domain that affect common gating (H835R in hCLC-1, H736A and E763K in CLC-0; green), (ii) dominant Thomsen's disease mutations in the intracellular loops of the hCLC-1 TM (G200R, F297S, R300Q; red), (iii) dominant osteopetrosis mutations in the hCLC-7 CBS domains (F758L, R762L, G765B, R767W, A788D; yellow), and (iv) dominant osteopetrosis mutations in the loops of the hCLC-7 TM (G215R, L213F, F318L; pink).

residue (T269) is found at the proton glutamate position. We note that the side-chain hydroxyl (Oγ) of T269 is only 7.5 Å away from the carboxylate (Oε) of E210. Either this threonine residue is able to perform the H^+ transfer between the intracellular solution and the transport region in CmCLC, or, alternatively, a different amino acid performs this role.

Hypothesis for the mechanism of two Cl^-/one H^+ countertransport. Together with the prokaryotic structures, three structures are now available (Fig. 6A) (*15*, *23*). Although these structures were obtained with two different transporters and a mutant, they likely represent conformations that can occur in the transport cycle. From these structures, we put forth a hypothesis for the transport mechanism that accounts for the countertransport of two Cl^- ions against one H^+ (Fig. 6B). States (a) and (b) represent unprotonated and protonated forms, respectively, of the conformation observed in CmCLC (Fig. 6A, left); states (d) and (e) represent protonated and unprotonated forms, respectively, of the conformation observed in the mutant EcCLC-E148Q (Fig. 6A, right) (*23*); and state (f) represents the conformation observed in WT EcCLC (Fig. 6A, middle) (*15*). From state (a) to state (b), a H^+ is transferred from the intracellular solution to the carboxylate of the gating glutamate. The protonated carboxylate changes its conformation to the extracellular solution [state (c)], and two Cl^- ions enter the transport region from the external side [state (d)]. Once the H^+ dissociates from the carboxylate to the extracellular solution [state (e)], the carboxylate can enter S_{ext} [state (f)] and then S_{cen} [state (a)], in association with the movement of two Cl^- ions to the intracellular side. In S_{cen}, the glutamate is again in position to receive a H^+ from the intracellular solution. Every transition in this cycle is reversible. Net cycling can only result from the dissipation of a Cl^- or H^+ electrochemical gradient. As described here, this cycle will give rise to an exchange stoichiometry of two Cl^- ions for one H^+.

There are two apparent problems with the cycle as described. First, in the (c)-to-(d) transition, two Cl^- ions must enter from the extracellular solution, or else stoichiometric coupling and active transport will be lost. Second, (d) and (e) are "forbidden" states for a transporter, because Cl^- can move uncoupled to H^+. Both of these problems can be overcome with one assumption: that there exists a relatively large kinetic barrier to the rapid movement of Cl^- ions between S_{int} and S_{cen}. This barrier would ensure that Cl^- ions would more likely fill S_{cen} and S_{ext} from the extracellular solution. In fact, if the barriers between the transport region and the extracellular solution are small, then state (c) will exist only transiently. A sufficiently large barrier between S_{int} and S_{cen} would also permit the existence of "forbidden" states (d) and (e) without substantial loss of coupled exchange. This conclusion can be understood through a simple kinetic argument. If the transition from (d) to (e) is determined by the lifetime of the protonated carboxylate in the extracellular solution, then we expect a duration of ~10^{-6} s if the pK_a (where K_a is the acid dissociation constant) is 4.0 and we assume a H^+ association rate of 10^{10} M^{-1} s^{-1} (*55*). Therefore, if the barrier

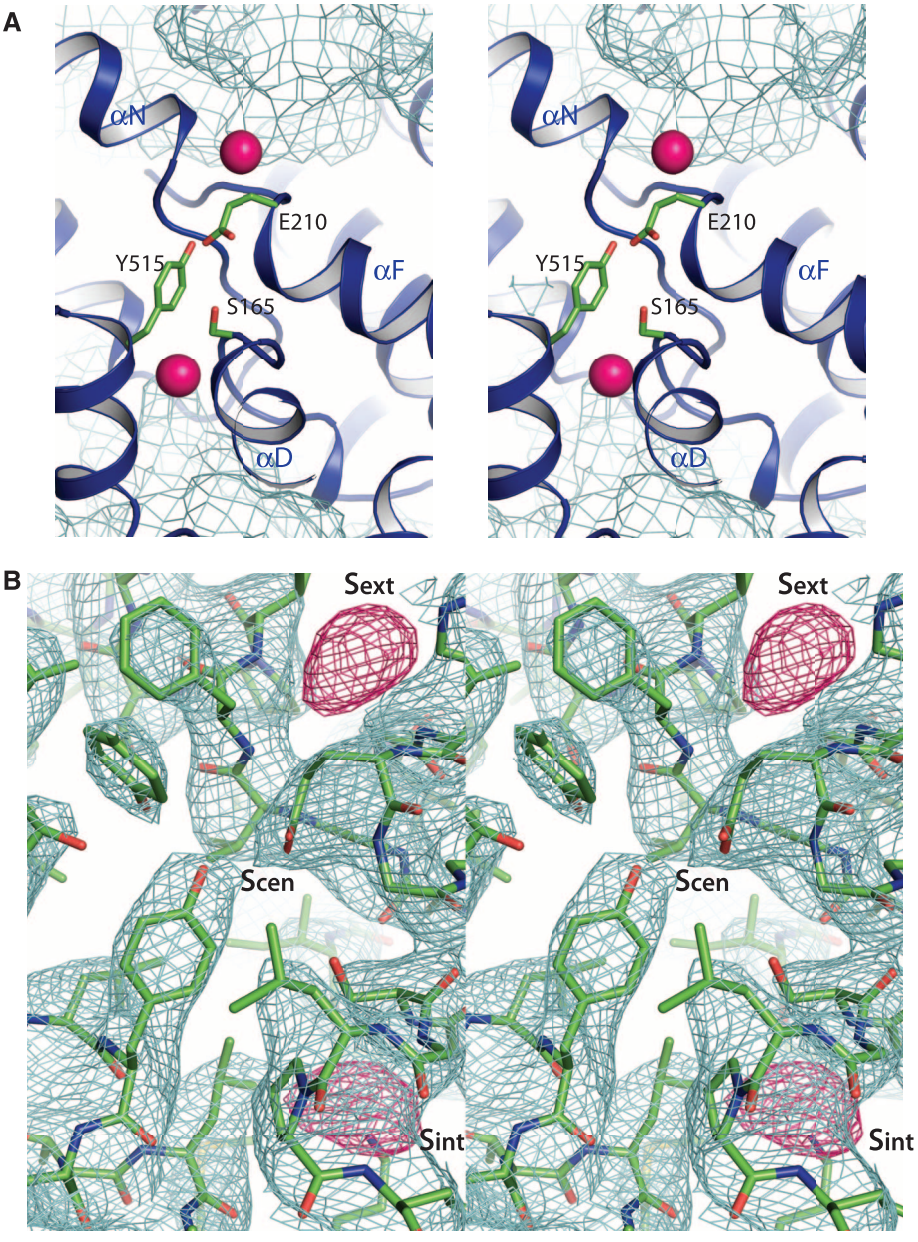

Fig. 5. Ion-transport pathway. (**A**) Stereo view of the ion-transport pathway viewed from the dimer interface. The protein is shown as a blue ribbon, with selected residues S165, E210, and Y515 shown as sticks. Aqueous cavities connecting to the Cl^- binding sites from the extracellular (top) and the intracellular (bottom) solutions are shown as pale blue mesh; Cl^- ions are shown as pink spheres. (**B**) Stereo view of the electron-density map around the ion-transport pathway. Weighted $2f_o$-f_c (where f_o is the observed structure factor amplitude, and f_c is the model structure factor amplitude) electron density at 3.5 Å, contoured at 1.35σ, is shown in pale blue. The refined model is shown as sticks. A bromine anomalous-difference Fourier map at 4.2 Å from crystals grown in Br^- is contoured at 9σ (red). (**C**) Stereo view of the ion-transport pathway. Possible hydrogen bonds between Cl^- ions (pink spheres) and protein are denoted by dashed lines, as are the possible hydrogen bonds between E210 and Y515.

were high enough to limit the Cl^- conduction rate through states (d) and (e) to 10^4 s^{-1}, then on average only one Cl^- every hundred cycles would slip through state (d) uncoupled to H^+ movement. If the transition from (e) to (f) were then rapid, little uncoupled slippage will occur during the cycle. In the EcCLC-E148Q mutant, representing a transporter caught permanently in states (d) and (e), the Cl^- conduction rate was determined to be less than 10^4 s^{-1} (*53*). We would suggest that the slow intrinsic Cl^- conductivity of mutated CLC transporters that function as channels (such as the EcCLC-E148Q mutant) results from a kinetic barrier to Cl^- that is an important aspect of the Cl^-/H^+ coupled-exchange mechanism.

Kinetic simulations corroborate the explanations above (movie S1). Simulations of the cycle—allowing Cl^- entry and exit from either side of the membrane during the transitions connecting states (c) and (d) and allowing Cl^- conduction across the membrane through states (d) and (e)—generate the experimentally observed properties of CLC exchangers: Cl^- gradients produce uphill H^+ transport, H^+ gradients produce uphill Cl^- transport, and a coupling ratio of two Cl^- ions against one H^+ is generated over conditions of membrane voltage, electrolyte, and pH under which CLC exchangers have been studied (*7*, *9*, *10*, *34*, *35*). Moreover, an adjustment of the rate at which Cl^- ions conduct through states (d) and (e) produces a loss of coupling and converts the CLC exchanger into a gated Cl^- ion channel.

The cycle also explains other more subtle features of CLC proteins. Certain mutations produce partial uncoupling (Cl^-/H^+ exchange ratios greater than two) rather than complete uncoupling (*41*). This observation is plausible if different mutations cause different rates of Cl^- conduction through states (d) and (e) or if they alter the interaction between the gating glutamate and the pore (Fig. 6B). Lowering external pH produces uncoupling

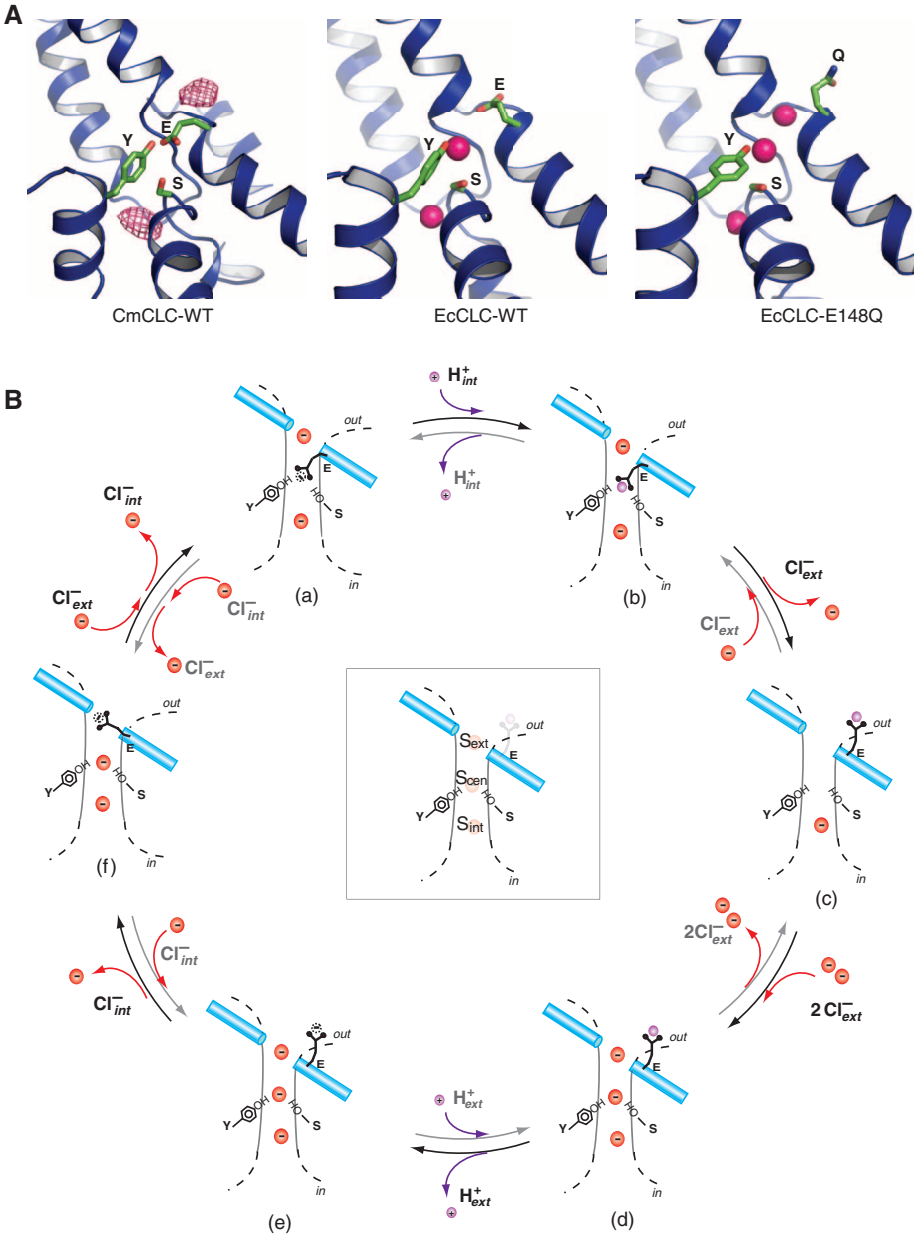

Fig. 6. A working model for ion transport. (**A**) Close-up view of the ion-transport pathway of WT CmCLC, WT EcCLC, and the E148Q mutant of EcCLC, respectively. The foreground helices were removed for clarity. Selected residues are shown as sticks and Cl^- as pink spheres. For CmCLC, a bromine anomalous-difference Fourier map contoured at 6σ is shown as red mesh. (**B**) A proposed working model for ion transport in CLC transporters. Residues corresponding to S165, E210, and Y515 in CmCLC are shown as schematic drawings. Red spheres represent Cl^- ions, and purple spheres denote protons. The negative charge on the carboxyl group of the deprotonated E210 is shown as a dashed circle. (a), (b), (c), (d), (e), and (f) are six major steps in this transport cycle, as described in the text. The illustration in the middle of the circle shows the positions that Cl^- and the carboxyl group of the gating glutamate could occupy. For an animated version of this figure, see movie S1.

in CLC-3 (*56*). This outcome is expected if, due to a high extracellular H^+ concentration, the transition rate from state (e) to state (d) becomes much greater than that from state (e) to state (f) (Fig. 6B). Finally, CLC proteins that function as channels exhibit pH-dependent gating (*16*). The cycle predicts that these channels may still mediate coupled exchange on a microscopic level that is hidden beneath uncoupled Cl^- conduction (*57*).

There may exist undiscovered conformational states of CLC transporters. Still, the mechanism of secondary active transport that we are proposing, although distinct from the classical alternating-access model (*58*), is plausible because it accounts for experimental observations. It invokes a Cl^- channel with a barrier to slow the throughput and a glutamate gate that can swing into the channel and be protonated from either side of the membrane. This mechanism explains why the CLC protein structure gives rise to both transporters and channels.

References and Notes

1. M. Maduke, C. Miller, J. A. Mindell, *Annu. Rev. Biophys. Biomol. Struct.* **29**, 411 (2000).
2. T. J. Jentsch, *Crit. Rev. Biochem. Mol. Biol.* **43**, 3 (2008).
3. K. Steinmeyer, B. Schwappach, M. Bens, A. Vandewalle, T. J. Jentsch, *J. Biol. Chem.* **270**, 31172 (1995).
4. S. Weinert *et al.*, *Science* **328**, 1401 (2010); published online 29 April 2010 (10.1126/science.1188072).
5. G. Zifarelli, M. Pusch, *Rev. Physiol. Biochem. Pharmacol.* **158**, 23 (2007).
6. C. Miller, W. Nguitragool, *Philos. Trans. R. Soc. London Ser. B Biol. Sci.* **364**, 175 (2009).
7. A. Accardi, C. Miller, *Nature* **427**, 803 (2004).
8. A. Picollo, M. Pusch, *Nature* **436**, 420 (2005).
9. O. Scheel, A. A. Zdebik, S. Lourdel, T. J. Jentsch, *Nature* **436**, 424 (2005).
10. A. R. Graves, P. K. Curran, C. L. Smith, J. A. Mindell, *Nature* **453**, 788 (2008).
11. M. F. Chen, T. Y. Chen, *J. Gen. Physiol.* **122**, 133 (2003).
12. R. Estévez, B. C. Schroeder, A. Accardi, T. J. Jentsch, M. Pusch, *Neuron* **38**, 47 (2003).
13. A. M. Engh, M. Maduke, *J. Gen. Physiol.* **125**, 601 (2005).
14. C. Miller, M. M. White, *Proc. Natl. Acad. Sci. U.S.A.* **81**, 2772 (1984).
15. R. Dutzler, E. B. Campbell, M. Cadene, B. T. Chait, R. MacKinnon, *Nature* **415**, 287 (2002).
16. T. Y. Chen, T. C. Hwang, *Physiol. Rev.* **88**, 351 (2008).
17. T. Schmidt-Rose, T. J. Jentsch, *J. Biol. Chem.* **272**, 20515 (1997).
18. M. Maduke, C. Williams, C. Miller, *Biochemistry* **37**, 1315 (1998).
19. S. Hebeisen *et al.*, *J. Biol. Chem.* **279**, 13140 (2004).
20. J. Garcia-Olivares *et al.*, *J. Physiol.* **586**, 5325 (2008).
21. B. Bennetts *et al.*, *J. Biol. Chem.* **280**, 32452 (2005).
22. S. Meyer, S. Savaresi, I. C. Forster, R. Dutzler, *Nat. Struct. Mol. Biol.* **14**, 60 (2007).
23. R. Dutzler, E. B. Campbell, R. MacKinnon, *Science* **300**, 108 (2003); published online 20 March 2003 (10.1126/science.1082708).
24. M. Pusch, *Hum. Mutat.* **19**, 423 (2002).
25. R. Estévez, M. Pusch, C. Ferrer-Costa, M. Orozco, T. J. Jentsch, *J. Physiol.* **557**, 363 (2004).
26. U. Kornak, A. Ostertag, S. Branger, O. Benichou, M.-C. de Vernejoul, *J. Clin. Endocrinol. Metab.* **91**, 995 (2006).
27. S. E. Lloyd *et al.*, *Nature* **379**, 445 (1996).
28. S. Dave, J. H. Sheehan, J. Meiler, K. Strange, *Channels (Austin)*, published online 21 July 2010 (10.4161/chan.4.4.12445).
29. Y. Jiang *et al.*, *Nature* **423**, 33 (2003).
30. M. Matsuzaki *et al.*, *Nature* **428**, 653 (2004).
31. Materials and methods are available as supporting material on *Science* Online.
32. J. Zhang, Y. Feng, M. Forgac, *J. Biol. Chem.* **269**, 23518 (1994).
33. Single-letter abbreviations for the amino acid residues are as follows: A, Ala; C, Cys; D, Asp; E, Glu; F, Phe; G, Gly; H, His; I, Ile; K, Lys; L, Leu; M, Met; N, Asn; P, Pro; Q, Gln; R, Arg; S, Ser; T, Thr; V, Val; W, Trp; and Y, Tyr.
34. A. De Angeli *et al.*, *Nature* **442**, 939 (2006).
35. G. Zifarelli, M. Pusch, *EMBO J.* **28**, 175 (2009).
36. S. Markovic, R. Dutzler, *Structure* **15**, 715 (2007).
37. A. Accardi, A. Picollo, *Biochim. Biophys. Acta* **1798**, 1457 (2010).
38. S. B. Long, X. Tao, E. B. Campbell, R. MacKinnon, *Nature* **450**, 376 (2007).
39. M. C. Lawrence, P. M. Colman, *J. Mol. Biol.* **234**, 946 (1993).
40. A. Accardi, S. Lobet, C. Williams, C. Miller, R. Dutzler, *J. Mol. Biol.* **362**, 691 (2006).
41. M. Walden *et al.*, *J. Gen. Physiol.* **129**, 317 (2007).
42. A. Picollo, M. Malvezzi, J. C. Houtman, A. Accardi, *Nat. Struct. Mol. Biol.* **16**, 1294 (2009).

43. E.-Y. Bergsdorf, A. A. Zdebik, T. J. Jentsch, *J. Biol. Chem.* **284**, 11184 (2009).
44. M. Duffield, G. Rychkov, A. Bretag, M. Roberts, *J. Gen. Physiol.* **121**, 149 (2003).
45. C. Lossin, A. L. George Jr., *Adv. Genet.* **63**, 25 (2008).
46. A. Pangrazio *et al.*, *Hum. Mutat.* **31**, E1071 (2010).
47. E. Cleiren *et al.*, *Hum. Mol. Genet.* **10**, 2861 (2001).
48. S. G. Waguespack *et al.*, *J. Bone Miner. Res.* **18**, 1513 (2003).
49. A. Frattini *et al.*, *J. Bone Miner. Res.* **18**, 1740 (2003).
50. D. H. Hryciw, G. Y. Rychkov, B. P. Hughes, A. H. Bretag, *J. Biol. Chem.* **273**, 4304 (1998).
51. S. Hebeisen, C. Fahlke, *Biophys. J.* **89**, 1710 (2005).
52. A. Accardi *et al.*, *J. Gen. Physiol.* **126**, 563 (2005).
53. H. Jayaram, A. Accardi, F. Wu, C. Williams, C. Miller, *Proc. Natl. Acad. Sci. U.S.A.* **105**, 11194 (2008).
54. H. H. Lim, C. Miller, *J. Gen. Physiol.* **133**, 131 (2009).
55. W. P. Jencks, *Catalysis in Chemistry and Enzymology* (Dover Publications, New York, 1987).
56. J. J. Matsuda, M. S. Filali, M. M. Collins, K. A. Volk, F. S. Lamb, *J. Biol. Chem.* **285**, 2569 (2010).
57. E. A. Richard, C. Miller, *Science* **247**, 1208 (1990).
58. O. Jardetzky, *Nature* **211**, 969 (1966).
59. We thank the staff at beamline X29 (National Synchrotron Light Source, Brookhaven National Laboratory) and K. R. Rajashankar and K. Perry at beamline 24ID-C (Advanced Photon Source, Argonne National Laboratory) for assistance at the synchrotron, members of the MacKinnon laboratory for helpful dicussions, and P. Yuan for comments on the manuscript. R.M. is an Investigator in the Howard Hughes Medical Institute. The x-ray crystallographic coordinates and structure factors have been deposited in the Protein Data Bank with accession identification number 3ORG.

Supporting Online Material

www.sciencemag.org/cgi/content/full/science.1195230/DC1
Materials and Methods
Figs. S1 to S6
Table S1
References
Movie S1

16 July 2010; accepted 17 September 2010
Published online 30 September 2010;
10.1126/science.1195230
Include this information when citing this paper.

Diversity of Human Copy Number Variation and Multicopy Genes

Peter H. Sudmant,[1]* Jacob O. Kitzman,[1]* Francesca Antonacci,[1] Can Alkan,[1] Maika Malig,[1] Anya Tsalenko,[2] Nick Sampas,[2] Laurakay Bruhn,[2] Jay Shendure,[1] 1000 Genomes Project,† Evan E. Eichler[1,3]‡

Copy number variants affect both disease and normal phenotypic variation, but those lying within heavily duplicated, highly identical sequence have been difficult to assay. By analyzing short-read mapping depth for 159 human genomes, we demonstrated accurate estimation of absolute copy number for duplications as small as 1.9 kilobase pairs, ranging from 0 to 48 copies. We identified 4.1 million "singly unique nucleotide" positions informative in distinguishing specific copies and used them to genotype the copy and content of specific paralogs within highly duplicated gene families. These data identify human-specific expansions in genes associated with brain development, reveal extensive population genetic diversity, and detect signatures consistent with gene conversion in the human species. Our approach makes ~1000 genes accessible to genetic studies of disease association.

Copy number–variable genes in humans tend to map to duplicated sequences (i.e., segmental duplications) (*1*–*4*), but neither the copy number nor the locus identity of these genes can be accurately assessed with existing hybridization-based experimental methods. This bias stems from the inability to discriminate subtle differences over the full range of copy number by array comparative genomic hybridization (CGH) and a lack of informative probes for these regions in single-nucleotide polymorphism (SNP) genotyping platforms (*5*). This bias is more pronounced in cases where more copies of a duplicated gene are present, because multicopy integer states are difficult to resolve proportionally, resulting in a lack of understanding of the true extent of human copy number variation. As a result, the most dynamic and variable genes are frequently excluded from genome-wide association studies (*6*). We have developed a method to survey whole-genome shotgun sequence data to accurately assay specific duplicated genes and gene families for copy number from data generated primarily from the 1000 Genomes Project (*7*).

[1]Department of Genome Sciences, University of Washington School of Medicine, Seattle, WA 98195, USA. [2]Agilent Technologies, Santa Clara, CA 95051, USA. [3]Howard Hughes Medical Institute, Seattle, WA 98195, USA.

*These authors contributed equally to this work.
†A full list of participants and institutions is available in the SOM online.
‡To whom correspondence should be addressed. E-mail: eee@gs.washington.edu

Results

Read depth can be used to predict accurately the copy number of duplicated genes within high-coverage human genomes (*8*). We applied this method to perform a copy number variant (CNV) analysis of 159 human genomes sequenced using the Illumina platform, including 15 high-coverage human genomes (12.3 to 43×) of diverse ethnicity and 141 low-coverage genomes (1.5 to 7×) from the 1000 Genomes Project representing three populations (*9*). For each genome, reads were mapped to a repeat-masked human reference genome (build 36) with the mrsFAST aligner, which returns all possible mapping locations of a read. Read depth profiles were then constructed and corrected for biases introduced in library construction. Copy number prediction was performed by regression against a standard curve of regions of known copy (*9*). Using this approach, we estimated the absolute copy number genome-wide for windows of 3000 nonrepetitive bases each and generated heatmaps displaying copy number for all 159 human genomes (Fig. 1, A and B).

Because many of these genomes (table S1) were sequenced at low coverage, we tested the accuracy of our copy number predictions using three orthogonal methods of experimental validation (Fig. 2A) (*9*). We assessed our ability to detect simple events (gains, losses, and homozygous losses) from 2270 events [median size 39.6 kilobase pairs (kbp), smallest event 1.6 kbp] across 109 common individuals. This demonstrated a concordance of 94 to 100%, dependent on the size and type of the event (fig. S20). To assess our ability to genotype multicopy number states, we performed 59 fluorescent in situ hybridization (FISH) experiments across 21 larger loci, ranging in copy from 2 to 48 (*9*). Of our copy number estimates, 93% (55 out of 59) were within ±1 of the number of FISH signals observed in interphase nuclei (e.g., Fig. 1A). Because FISH-based estimates are problematic when copy number exceeds 10, we designed a series of quantitative PCR (QPCR) assays to assess dynamic range response. These showed high correlation with our read depth–based estimates, with 7 out of 9 assays having a correlation coefficient of $r > 0.92$ (*9*). Read depth– and QPCR-based copy number estimates for the 1.9-kbp gene *CCL3L1* across 150 individuals were concordant ($r = 0.95$), with both methods capturing the population-specific distributions of copy number at this locus (fig. S26).

CNV landscape diversity. We constructed genome-wide copy number maps across 159 genomes at 3-kbp resolution (Fig. 1, A and B) to assay the full extent of large-scale copy number variation among human populations. We identified 952 large CNVs greater than 50 kbp across 159 individuals (*9*). As expected, events of increasing size occur with progressively lower frequency. We noted that the majority of large events (55%, 522 out of 952) overlapped segmental duplications. Out of all events, 47% (452 of 952) were common, being observed in more than eight individuals (>5% of genomes). Association with segmental duplications also strongly influenced CNV frequency. Events entirely outside segmental duplications were generally rare, with 71% (390 of 546) detected in three or fewer individuals (<2% of genomes). By contrast, 91% (461 of 506) of most CNVs overlapping segmental duplications were observed in more than three individuals, consistent with recurrent variation in these dynamic regions.

We identified 22 regions longer than 100 kbp that showed evidence of significant copy number differences between Asians, Europeans, and Africans [average V_{st} of >0.2; (table S9)] (*10*). These included duplications flanking the 17q21.31 *MAPT* locus, which has been associated with positive selection, rapid evolutionary turnover, and neurological

disease (*11*). Analyses of the region across populations (*9*) revealed that although the inversion of this locus and its associated duplication are largely restricted to European-Mediterranean populations with 20% allele frequency, duplications overlapping the *KIAA1267* gene were more common and definitive of populations of European origin (found in 33 out of 46 individuals at 50% allele frequency) but were nonexistent in all other ethnic groups examined (Fig. 1, B and C). Based on the extent of phased copy number change, we predicted and confirmed a short (155-kbp) duplication occurring at 20% allele frequency and a long version (205 kbp) at 30% allele frequency in Europeans (*9*). Distal to this locus, we identified a larger, more–copy number–polymorphic region (ranging from 2 to 6 copies). This more distal, population-stratified duplication encompassed the first 13 exons of the *N*-ethylmaleimide-sensitive (*NSF*) gene and shows increased copy number among Asians with the six-copy state occurring at ~25% frequency (13 out of 54 individuals) (Fig. 1, B and C). It is noteworthy that this gene is preferentially expressed in the human nervous system; reduction in its expression is associated with schizophrenia (*12*), and disruptions of its *Drosophila* ortholog lead to defective synaptic transmission (*13*).

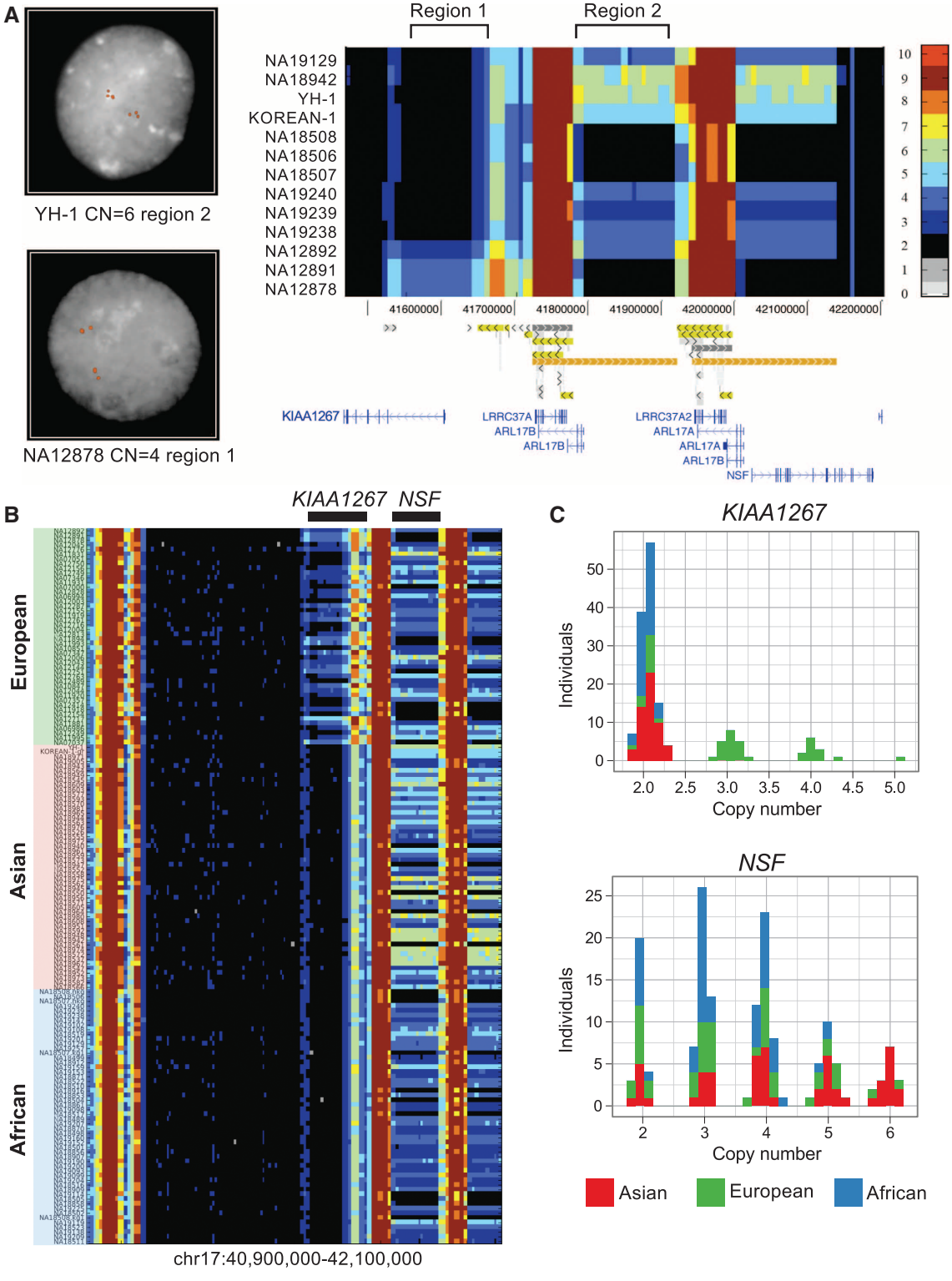

Fig. 1. Landscape of human copy number variation. (**A**) CNV heatmap of a 734-kbp duplicated region flanking the 17q21.31 *MAPT* locus in 13 individuals (11 sequenced to high coverage). Read depth–based copy number (CN) estimations (3-kbp windows) are indicated by color (scale provided to the right). FISH at two separate loci validates these absolute CN predictions across five individuals (*9*). (**B**) Copy number landscape of the 17q21.31 locus across three different populations showing marked population stratification (159 genomes analyzed). A European-enriched duplication overlaps the gene *KIAA1267* and is present on two haplotypes—a long form (205 kbp) and a short form (155 kbp). A 210-kbp duplication of the *NSF* gene ranges from two to six copies with increased copy number in Asians. For validation with array CGH, see fig. S31. (**C**) Copy number frequency histograms of the *KIAA1267* and *NSF* duplications based on median read depth predict discrete copies. Duplications of the *KIAA1267* locus are specific to Europeans at a frequency of 72%. 25% of Asians have six copies of *NSF*.

Additionally, we identified regions that are duplicated in most human individuals but previously were incorrectly classified as diploid in the reference genome, including 10 regions of >100 kbp each. We identified 173 segmentally duplicated regions for which the majority of genomes have a copy number greater than that of the reference genome. We thus have established a copy number baseline in humans, allowing more accurate genotyping from SNP microarrays. These data may be used in conjunction with single-channel intensity data from previous array CGH experiments to develop a calibration curve specifically for each region of the genome, allowing multiallelic loci to be more robustly genotyped on array-based platforms (Fig. 2A) (*9*). This CNV landscape diversity map may also be used to select an ideal reference genome (from the 1000 Genomes catalog) to maximize discriminatory power in array CGH studies, which will open more complex, copy number–polymorphic regions of the genome to further experimental characterization (Fig. 2B).

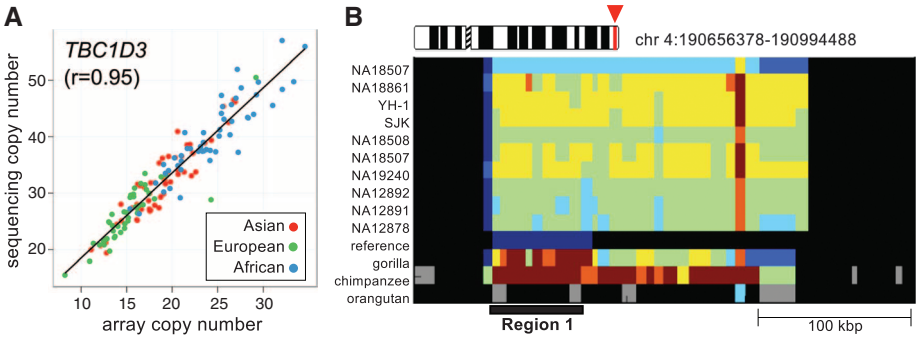

Fig. 2. Validation and application. (**A**) Single-channel array CGH data are highly correlated (r = 0.95) with read depth–based genotypes for the highly duplicated *TBC1D3* gene (copy number range 5 to 53). Note the reduced copy number of this gene family among Europeans (color coding as in Fig. 1C). (**B**) Heatmap of a 340-kbp region proximal to the fascioscapulohumeral muscular dystrophy (FSHD) region on chromosome 4 identifies a polymorphic segmental duplication ranging from 5 to 8 copies. In the human reference genome (build 36) this segment is annotated as a single copy (i.e., unique), but all humans carry duplications mapping to chromosomes 4, 13, 14, and 21.

Gene copy number diversity and evolution. To assess the impact of copy number variation specifically on the coding portion of the genome, we genotyped the absolute copy of 25,832 individual RefSeq gene models (University of California, Santa Cruz, genome browser). As expected, our read depth assessment predicts that 99.3% of hu-

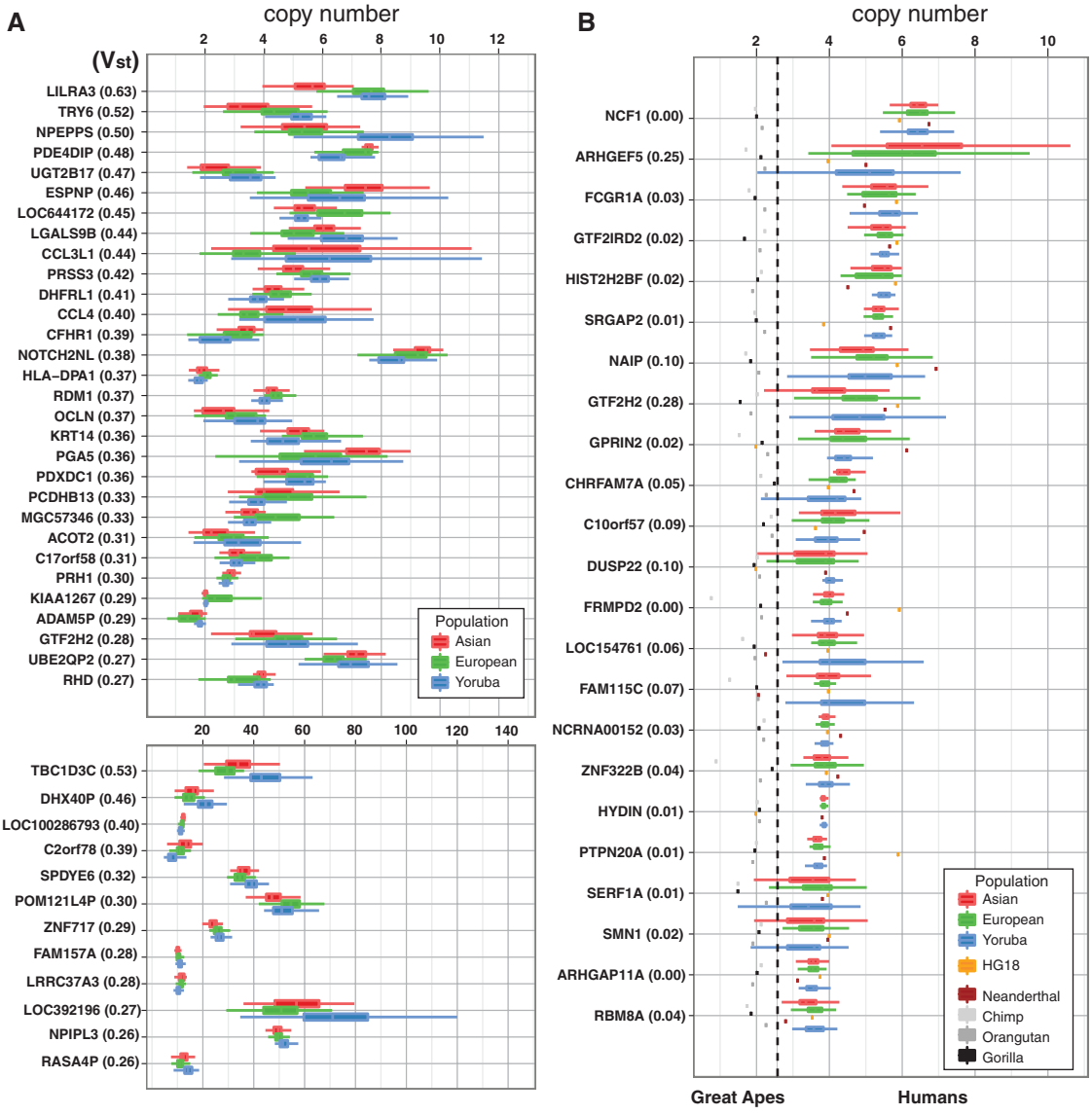

Fig. 3. Human gene family copy number diversity and evolution. (**A**) The genes most stratified by copy number in the human genome on the basis of V_{st} analysis of European, African, and Asian populations. (**B**) Human-specific gene family expansions.

man gene models outside of segmental duplications show a median copy number of two. Limiting our set to all genes greater than 10 kbp, we find that 91% of human genes are fixed as diploid in all 159 humans examined. Of the copy number–variable gene families, including those within segmental duplications, we found that 80% vary between 0 and 5 copies, which suggests that extreme variation is limited to only a few gene families. We identified the 56 most variable gene families in humans (variance >3.0 among combined populations), ranging in median copy from 5 to ~368 (fig. S33 and table S7). These genes were dramatically enriched for segmental duplications [odds ratio (OR) = 311.3, $P < 2.2 \times 10^{-16}$, Fisher's exact test]. In 19 of these cases, no individual exhibited a copy number less than or equal to that of the reference genome, which suggests that some of these gene duplicates are underrepresented in the reference. We found 44 "hidden" duplicated gene families (fig. S33 and table S6), including the rapidly evolving and high-copy *ANKRD* (about six missing haploid copies), *NBPF* (more than nine missing copies) and *NPIP* (about five missing copies) gene families. The missing members of these gene families should be targeted for sequence finishing in order to more accurately capture the architecture and diversity of the human genome.

Because significant differences in allele frequency can be a signature of selection, we searched for genes with the most extreme differences in copy among the HapMap populations. These include the Yoruba people in Ibadan, Nigeria (YRI), Utah residents with ancestry from northern and western Europe (CEU), Japanese in Tokyo, Japan (JPT), and Han Chinese in Beijing, China (CHB). We used the V_{st} statistic (*10*) and identified 64 gene families [$V_{st} > 0.2$; (Fig. 3A and table S8)]. These genes mapped almost exclusively to segmental duplications (OR = 72.0, $P < 2.2 \times 10^{-16}$) and ranged in copy from 2 to 368 (77%, 49 out of 64 with <12 copies). However, we observed no significant correlation between V_{st} and copy number ($P = 0.199$), which indicated that the differences between populations were not an artifactual product of higher copy numbers. In general, the African YRI showed greater variance in stratified gene copy number compared with either Europeans or Asians ($P < 1 \times 10^{-4}$ and $P < 1.2 \times 10^{-9}$ after multiple-testing correction; Welch's one-tailed t test), including genes with known stratification between populations, such as *LILRA3* (*14*) and *UGTB17* (*15*). One of the most stratified genes identified was *CCL3L1* (fig. S26), for which the importance of accurate multiallelic copy number genotyping has been recently highlighted because of conflicting reports of association with HIV susceptibility (*16*). In addition, we discovered stratification among several previously uncharacterized gene families, many of which show reduced copy in Europeans and Asians compared with Africans (Fig. 3A) (*9*).

We characterized the evolutionary context of human gene copy number variation by comparatively analyzing short-read depth data from a gorilla, a chimpanzee, and an orangutan (*9*). We identified 53 gene families with increased copy number within the human lineage, 23 of which were diploid in each of the great apes, and 8 of which appear to be fixed in humans (Fig. 3B, fig. S38, and tables S10 and S11). Consistent with an origin after the human-ape divergence, the human-specific duplications and expansions displayed higher sequence identity than most duplicated genes (97.0% and 98.7%, respectively; $P < 3.5 \times 10^{-5}$, Welch's one-tailed t test). Human-specific duplications include the genes *GPRIN2* and *SRGAP2*, which have been implicated in neurite outgrowth and branching (*17*, *18*); the brain-specific *HYDIN2* gene, associated with micro and macrocephaly (*19*); *DRD5*, a dopamine D5 receptor; the *GTF2I* transcription factors whose deletion has been associated with visual-spatial and sociability deficits among Williams-Beuren syndrome patients (*20*, *21*); duplication of the *SMN1* genes, at which copy increases ameliorate the severity of spinal muscular atrophy (SMA) deletions; and duplication of the *CHRNA7* locus on 15q13.2 recently implicated in cases of intellectual disability and epilepsy (*22*, *23*). We note that the fixed duplications we identified at *HYDIN* and *GPRIN2* are not annotated in the reference and thus represent "hidden" duplications (fig. S40).

A singly unique nucleotide (SUN) identifier map. Although our read depth–based genotyping provides absolute, rather than relative, copy number measurements and improved dynamic range relative to other platforms, it still lacks specificity within highly homologous segmental duplications. To discriminate among these paralogous sequences, we focused on the positions in the reference genome at which they diverge (Fig. 4A). We identified 4.07×10^6 SUN positions within high-identity duplicated regions (table S2). SUNs are a distinct class of paralogous sequence variants that uniquely tag a specific paralog. By definition, the density of these markers diminishes with increasing duplication identity, yet we estimated that ~70% of duplications contain sufficient SUN density to allow paralog-specific genotyping (*9*). Nearby SNPs or rare variants could disrupt short-read mapping at SUN positions, which could confound copy number estimation of the tagged paralog. We examined the extent of such effects among SUNs in 12 unrelated individuals sequenced to high coverage (mean = 23.4×). Reads from these individuals were mapped to SUN positions, stringently requiring perfect 36-bp matches so as to exclude contamination between paralogous sequences. Essentially all autosomal SUNs (99.7%) were present in at least one individual, with most (84.8%) present in all 12 individuals (*9*). Among these, we noted a strong enrichment for SNPs (274,245 SNPs from the dbSNP version 130, OR = 1.6, $P < 2.2 \times 10^{-16}$), which suggested that some SUNs may be misannotated as allelic variants (*1*, *24*).

Paralog-specific copy number. We used our SUN database to complement our estimates of total copy number by developing genome-wide maps of paralog-specific copy number (psCN). At locations uniquely identified by an overlapping SUN, we counted the number of reads perfectly matching and, as before, inferred copy number using a linear model trained on regions of known copy. We validated the accuracy of our psCN estimates by specifically analyzing 383 high-confidence deletion intervals that had been detected and fully resolved by capillary sequencing on the same individuals (*4*). We found that 99.4% (308 out of 310) of deletions within unique regions and 93.2% (68 of 73) of deletions within duplicated regions were accurately predicted, which underscored the specificity of this approach.

Paralog-specific copy number genotyping revealed CNVs within duplicated gene families. For

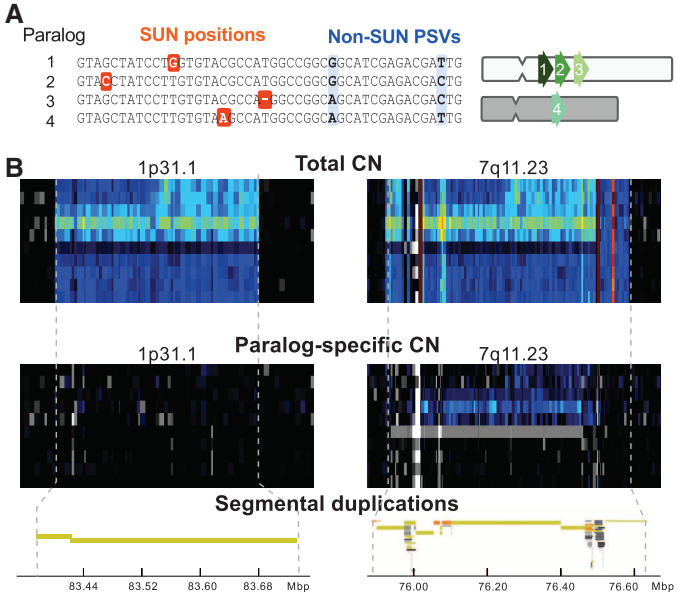

Fig. 4. Paralog-specific copy number resolution and genotyping. (**A**) Schematic showing SUN identifiers among four high-identity duplications. SUNs (orange) uniquely distinguish one duplicated copy from all others, in contrast to paralogous sequence variants (PSVs, blue), which may be shared among copies. (**B**) Resolving duplication mirror effects with paralog-specific genotyping. Total read depth and array CGH fail to distinguish the origin of copy number variation between two high-identity (98.5%) segmental duplications mapping to chromosome 1p13.1 and 7q11.23. SUN read-depth mapping, however, predicts that copy number variation is restricted to 7q11.23 and not 1p13.1. FISH on these samples confirms copy number gains and losses on 7q11.23 (fig. S51).

example, at the complement factor H (*CFH*) locus, we detected deletions in close agreement with their known boundaries (±~6 kbp on average, fig. S60) (*4*). Genotyping the resulting psCN at these intervals across all 159 samples reveals overall deletion allele frequencies for *CFHR3/1* and *CFHR1/4* of 29% and 4%, respectively, with elevated frequency among Africans at both deletions (*25*). We also identify rare genotypes, such as a reciprocal, single-copy amplification of *CFHR1/4* in a single African individual (ABT) and a deletion with novel breakpoints in a single Asian individual (NA18563).

Copy number analysis from read mapping depth can potentially lead to misassignment of CNV events to the wrong copy because of cross-mapping between highly identical sequences. Using SUNs to resolve paralogous copies, we re-genotyped 406 large (>50 kbp) CNV events overlapping segmental duplications, previously called on the basis of total read mapping depth comparisons (*9*). We find that 60% (245 out of 406) of these regions show no signature of variation using SUNs and hence represent variation at one of the homologous loci. This "mirror" effect arises from cross-mapping between highly identical sequences but can be resolved by leveraging the SUN tags (Fig. 4B). Similarly, we found that a recently reported set of CNVs identified by CGH (*2*) contained a significant fraction of calls (1547 out of 4412, 35.1%) within duplicated sequences that show no evidence of paralog-specific CNV.

Paralog-specific gene family diversity. A prerequisite to understanding the function of highly duplicated gene families is the ability to genotype them for both their copy and content. Using our psCN approach, we reassessed 990 human genes partially or completely contained within segmental duplications (Fig. 5A). This analysis allowed us to distinguish two distinct classes of paralogs: 49.2% of duplicate genes which appear largely copy-invariant within the human species, and the remainder, which show extensive variation in copy number with some bias toward gain or loss.

A particularly peculiar set of variable genes are those mapping to "core duplicons" (*26*) which have undergone recent bursts of expansion within the human lineage, including *NPIP*, *NBPF* (Fig. 5B), and others (*27*). We confirmed these genes' human-specific expansion but also observed them to be stratified among human populations (fig. S38 and Fig. 3A). We also observed more localized psCN patterns, with small patches showing reciprocal gain and loss but remaining unchanged in total copy, a signature consistent with interlocus gene conversion (i.e., unidirectional transfer of genetic information between duplicate copies) [reviewed in (*28*)]. We validated a small number of these events and confirmed this signature at the Rh blood group antigen genes *RHD* and *RHCE* (fig. S71) (*9*, *29*). A scoring metric found 78 regions with a score exceeding that of *RHD*/*RHCE* with a significant excess of this signature relative to shuffled controls ($P < 2.2 \times 10^{-16}$, one-sided Kolmogorov-Smirnov). Consistent with known examples and mechanisms of gene conversion, this was nearly exclusive to high-identity duplications (>95% ID) and was preferential to nearby tandem duplications (≤1 Mbp).

Discussion

We have leveraged next-generation sequence data to explore some of the most complex genetic variation in the human species and show that we can reliably predict absolute copy number without bias. More important, these data allowed us to assess the copy and content of specific duplicated genes. Nevertheless, several limitations remain. Some genes (~30%) show too little paralogous variation or are too small to be reliably genotyped; in other cases, the paucity of markers combined with the low sequence coverage led to uncertainty in copy number accuracy (our analysis suggests that at least 8× genome-wide sequence coverage is required to achieve copy number accuracy above 97%). Finally,

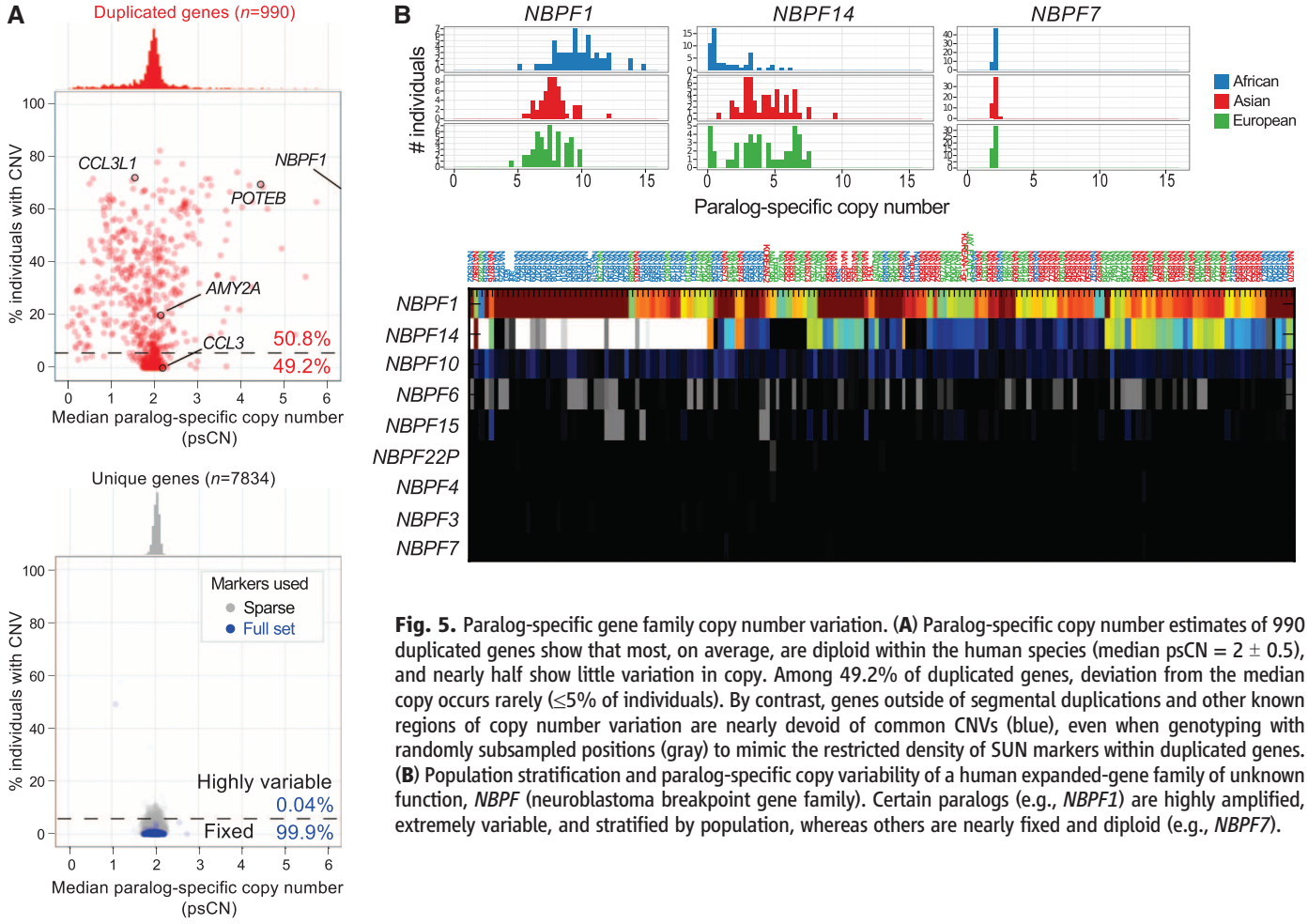

Fig. 5. Paralog-specific gene family copy number variation. (**A**) Paralog-specific copy number estimates of 990 duplicated genes show that most, on average, are diploid within the human species (median psCN = 2 ± 0.5), and nearly half show little variation in copy. Among 49.2% of duplicated genes, deviation from the median copy occurs rarely (≤5% of individuals). By contrast, genes outside of segmental duplications and other known regions of copy number variation are nearly devoid of common CNVs (blue), even when genotyping with randomly subsampled positions (gray) to mimic the restricted density of SUN markers within duplicated genes. (**B**) Population stratification and paralog-specific copy variability of a human expanded-gene family of unknown function, *NBPF* (neuroblastoma breakpoint gene family). Certain paralogs (e.g., *NBPF1*) are highly amplified, extremely variable, and stratified by population, whereas others are nearly fixed and diploid (e.g., *NBPF7*).

we found 28 large regions with such extraordinary complexity that it is difficult to interpret the underlying pattern of genetic variation (e.g., fig. S34).

Through our analysis, we identified that duplicated regions are more likely to be stratified between human populations when compared with copy number variation within unique regions of the genome. For example, 59 (92%) of the top 64 stratified gene families overlap segmental duplications ($P < 2.2 \times 10^{-16}$). Remarkably, many of these highly polymorphic genes map to duplications that promote recurrent rearrangements associated with intellectual disability, autism, schizophrenia and epilepsy. We hypothesize that the extreme polymorphism may contribute to genomic instability associated with disease and may predispose certain populations to different chromosomal rearrangements (*30*).

We have also defined the ~49% of gene duplicates that are largely invariant in copy among humans. Although this is based only on an assessment of 159 genomes from select populations, the fact that this fraction of genes remains copy number invariant in a milieu of recurrent unequal crossover suggests functional importance. Among these, we find a number of genes involved in neurological development and disease. We note that many of these duplicated genes are themselves incomplete and may represent nonprocessed pseudogenes, which may modulate the expression of the ancestral gene. The characterization of the most recently duplicated genes should facilitate identification of those that acquired new functions (neofunctionalization) versus those that have become pseudogenes or have partitioned their function among duplicate copies (*31*).

The ability to distinguish where copy number variation maps and where it does not within regions of high sequence identity facilitates breakpoint delineation within duplications, allowing us to refine the intervals associated with structural variants such as the recurrent, schizophrenia-associated deletion on 15q11.2 (fig. S70) (*32*). We anticipate that overlaying our SUN map with functional genomics data (e.g., chromatin immunoprecipitation sequencing or RNA-seq) may begin to resolve the epigenetic and expression landscape of duplicated regions and the ~1000 genes therein that have been largely inaccessible to genetic study of disease (*33*).

References and Notes

1. J. A. Bailey *et al.*, *Science* **297**, 1003 (2002).
2. D. F. Conrad *et al.*, *Nature* **464**, 704 (2010).
3. A. J. Iafrate *et al.*, *Nat. Genet.* **36**, 949 (2004).
4. J. M. Kidd *et al.*, *Nature* **453**, 56 (2008).
5. G. M. Cooper, T. Zerr, J. M. Kidd, E. E. Eichler, D. A. Nickerson, *Nat. Genet.* **40**, 1199 (2008).
6. N. Craddock *et al.*; Wellcome Trust Case Control Consortium, *Nature* **464**, 713 (2010).
7. 1000 Genomes project, *Nature,* 28 October 2010, 10.1038/nature09534.
8. C. Alkan *et al.*, *Nat. Genet.* **41**, 1061 (2009).
9. Materials and methods are available as supporting material on *Science* Online.
10. R. Redon *et al.*, *Nature* **444**, 444 (2006).
11. H. Stefansson *et al.*, *Nat. Genet.* **37**, 129 (2005).
12. K. Mirnics, F. A. Middleton, A. Marquez, D. A. Lewis, P. Levitt, *Neuron* **28**, 53 (2000).
13. L. Pallanck, R. W. Ordway, B. Ganetzky, *Nature* **376**, 25 (1995).
14. K. Hirayasu *et al.*, *Am. J. Hum. Genet.* **82**, 1075 (2008).
15. Y. Xue *et al.*, *Am. J. Hum. Genet.* **83**, 337 (2008).
16. T. J. Urban *et al.*, *Nat. Med.* **15**, 1110 (2009).
17. L. T. Chen, A. G. Gilman, T. Kozasa, *J. Biol. Chem.* **274**, 26931 (1999).
18. S. Guerrier *et al.*, *Cell* **138**, 990 (2009).
19. N. Brunetti-Pierri *et al.*, *Nat. Genet.* **40**, 1466 (2008).
20. L. Dai *et al.*, *Am. J. Med. Genet. A.* **149A**, 302 (2009).
21. L. Edelmann *et al.*, *J. Med. Genet.* **44**, 136 (2007).
22. A. J. Sharp *et al.*, *Nat. Genet.* **40**, 322 (2008).
23. M. Shinawi *et al.*, *Nat. Genet.* **41**, 1269 (2009).
24. X. Estivill *et al.*, *Hum. Mol. Genet.* **11**, 1987 (2002).
25. G. S. Hageman *et al.*; AMD Clinical Study Group, *Ann. Med.* **38**, 592 (2006).
26. Z. Jiang *et al.*, *Nat. Genet.* **39**, 1361 (2007).
27. T. Marques-Bonet *et al.*, *Nature* **457**, 877 (2009).
28. J. M. Chen, D. N. Cooper, N. Chuzhanova, C. Férec, G. P. Patrinos, *Nat. Rev. Genet.* **8**, 762 (2007).
29. H. Innan, *Proc. Natl. Acad. Sci. U.S.A.* **100**, 8793 (2003).
30. F. Antonacci *et al.*, *Hum. Mol. Genet.* **18**, 2555 (2009).
31. A. Force *et al.*, *Genetics* **151**, 1531 (1999).
32. H. Stefansson *et al.*; GROUP, *Nature* **455**, 232 (2008).
33. T. A. Manolio *et al.*, *Nature* **461**, 747 (2009).

34. We thank M. Ventura and M. Ross for sharing unpublished data; C. Lee for technical assistance; C. Campbell, J. Kidd, P. Green, and M. Hoopman for discussion; and T. Brown for manuscript preparation assistance. This work was supported by a Natural Sciences and Engineering Research Council of Canada Fellowship (P.H.S.), an NSF Graduate Research Fellowship (J.O.K.), and NIH grant HG004120 to E.E.E. E.E.E. is an Investigator of the Howard Hughes Medical Institute. E.E.E is on the scientific advisory board for Pacific Biosciences. A.T., N.S., and L.B. are employees of Agilent Technologies. J.S. is a member of the scientific advisory boards of Tandem Technologies, Stratos Genomics, Good Start Genetics, and Adaptive TCR. Sequence and array data are deposited at the NCBI under accessions SRP002878, SRP003500, SRP000031, SRP000032, and GSE24334.

Supporting Online Material

www.sciencemag.org/cgi/content/full/330/6004/641/DC1
Materials and Methods
SOM Text
Figs. S1 to S73
Tables S1 to S16
References

26 August 2010; accepted 4 October 2010
10.1126/science.1197005

REPORTS

Rate of Gas Phase Association of Hydroxyl Radical and Nitrogen Dioxide

Andrew K. Mollner,[1] Sivakumaran Valluvadasan,[2] Lin Feng,[1] Matthew K. Sprague,[1] Mitchio Okumura,[1]* Daniel B. Milligan,[2] William J. Bloss,[2] Stanley P. Sander,[2]* Philip T. Martien,[3] Robert A. Harley,[3]* Anne B. McCoy,[4]* William P. L. Carter[5]*

The reaction of OH and NO_2 to form gaseous nitric acid ($HONO_2$) is among the most influential in atmospheric chemistry. Despite its importance, the rate coefficient remains poorly determined under tropospheric conditions because of difficulties in making laboratory rate measurements in air at 760 torr and uncertainties about a secondary channel producing peroxynitrous acid (HOONO). We combined two sensitive laser spectroscopy techniques to measure the overall rate of both channels and the partitioning between them at 25°C and 760 torr. The result is a significantly more precise value of the rate constant for the $HONO_2$ formation channel, 9.2 (±0.4) × 10^{-12} cm^3 $molecule^{-1}$ s^{-1} (1 SD) at 760 torr of air, which lies toward the lower end of the previously established range. We demonstrate the impact of the revised value on photochemical model predictions of ozone concentrations in the Los Angeles airshed.

The gas phase three-body association reaction of hydroxyl radical (OH) with nitrogen dioxide (NO_2) to form nitric acid ($HONO_2$) (Eq. 1a)

$$OH + NO_2 + M \rightarrow HONO_2 + M \quad (1a)$$

(where M is N_2 or O_2 in air) is important throughout the lower atmosphere. It sequesters reactive hydrogen (HO_x, the sum of OH and peroxides) and reactive nitrogen (NO_x, the sum of NO_2 and NO) as long-lived nitric acid, shortening their atmospheric lifetimes and slowing catalytic cycles responsible for photochemically driven formation of air pollution in the troposphere and ozone depletion in the stratosphere.

The impact of the reaction in Eq. 1a is especially notable in polluted air masses, where its rate affects the formation of pollutants including ozone (O_3), nitric acid, and fine particulate nitrate. This reaction leads to lower ozone pro-

[1]Arthur Amos Noyes Laboratory of Chemical Physics, Division of Chemistry and Chemical Engineering, California Institute of Technology, Pasadena, CA 91125, USA. [2]Jet Propulsion Laboratory, California Institute of Technology, Pasadena, CA 91109, USA. [3]Department of Civil and Environmental Engineering, University of California, Berkeley, CA 94720–1710, USA. [4]Department of Chemistry, The Ohio State University, Columbus, OH 43210, USA. [5]College of Engineering, Center for Environmental Research and Technology, University of California, Riverside, CA 92521, USA.

*To whom correspondence should be addressed. E-mail: mo@caltech.edu (M.O.); stanley.p.sander@jpl.nasa.gov (S.P.P.); harley@ce.berkeley.edu (R.A.H.); mccoy@chemistry.ohio-state.edu (A.B.M.); wpcarter@ucr.edu (W.P.L.C.)

duction at elevated NO_x concentrations, because excess NO_2 removes OH. Previous sensitivity analyses (*1*) of photochemical models used to predict O_3 from inputs of precursor emissions have shown that the rate constant for this reaction, k_{1a}, ranks among the top normalized sensitivities for all chemical rate constants. Because these models are used to assess the future impact of emission reduction strategies for improving air quality, it is essential that k_{1a} be known to a high accuracy.

Determination of k_{1a} has been a long-standing problem in gas phase kinetics. It is an effective bimolecular rate constant that should depend nonlinearly on pressure according to the Lindemann-Hinshelwood mechanism, but Robertshaw and Smith found the rate constant to be anomalously high at higher pressures (*2*). They explained this behavior by proposing a second channel to form peroxynitrous acid (HOONO, in Fig. 1), a weakly bound isomer of nitric acid (Eq. 1b):

$$OH + NO_2 + M \rightarrow HOONO + M \qquad (1b)$$

HOONO formation is now believed to be a minor channel at low pressures (*3*), but the branching ratio, $\alpha(T, [M]) = k_{1b}/k_{1a}$, is expected to increase with pressure, with the two channels predicted to be comparable in the high pressure limit (*4*–*7*). Although HOONO can form initially as one of several isomers, all HOONO molecules rapidly isomerize to the lowest energy *cis-cis* conformer, which is stabilized by an intramolecular hydrogen bond (*8*).

Under conditions pertaining in the boundary layer, HOONO will redissociate rapidly to OH and NO_2 (*9*); only nitric acid is stable enough to act as a sink for HO_x and NO_x. Atmospheric models thus need k_{1a}, but experiments generally measure time-resolved loss of OH in the presence of NO_2 and hence determine the total rate constant $k_1 = k_{1a} + k_{1b}$. Deriving the rate constant needed for models, k_{1a}, therefore requires measuring α.

The difficulties in determining k_{1a} arise from two key issues. First, there are technical problems in making laboratory measurements of k_1 in air. Most previous measurements detected OH by fluorescence-based methods and suffered from poor signal-to-noise ratios at pressures above a few hundred torr of air, because collisional quenching reduced the OH fluorescence quantum yield (*10*–*12*). In addition, systematic errors in the measurements of NO_2 concentration propagate directly into measurements of k_1. This is because the experiments measure the first-order loss of OH in excess NO_2. Previous studies in nitrogen near atmospheric pressure differ by almost a factor of two (*10*–*12*). The first study by Anastasi and Smith (*10*) at N_2 pressures up to 500 torr agrees with the most recent results of D'Ottone *et al*., who have measured the rate in both air and nitrogen at pressures up to 700 torr (*11*), but Donahue *et al*. found substantially lower rates (*12*). Second, despite a large body of evidence to support the existence of the HOONO channel (*3*, *4*, *13*–*16*), there are no quantitative measurements of α at atmospheric temperature and pressure. There have been many efforts to compute k_1 and α, and the reactions in Eqs. 1a and 1b have become a test of theoretical kinetics, but reliable first principles predictions are not yet feasible (*4*, *6*).

These uncertainties make it hard for data evaluation panels to recommend a value for k_{1a} for use in atmospheric models. Recommendations for k_{1a} at 760 torr of air and 298 K by the International Union of Pure and Applied Chemistry (IUPAC) (*17*) and Jet Propulsion Laboratory (JPL) (*9*) evaluations (Table 1) differ by 14% and have large uncertainties due to the discrepancies among the laboratory results. Because predicted ozone levels in air quality models have high sensitivities to this rate constant, a reexamination of this reaction is necessary.

Here, we report the results of room temperature measurements of k_1 at pressures of N_2, O_2, and air up to 900 torr, and α at pressures up to 750 torr in N_2. A fit to both data sets yields parameters that describe k_{1a} over the range 100 to

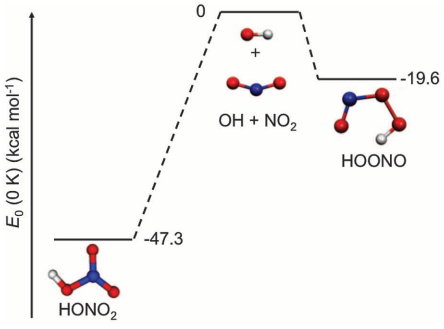

Fig. 1. Energy diagram for the reaction OH + NO_2 + M. Energies are at 0 K and include zero point energy (*3*, *29*, *30*).

Table 1. Recommended effective bimolecular rate constants at 760 torr of air and 298 K, except the IUPAC recommendation, which is for 750 torr N_2. Reported uncertainties are 1 SD and include both statistical and systematic errors.

Recommendation	$k_1/10^{-12}$ cm^3 molecule^{-1} s^{-1}	$k_{1a}/10^{-12}$ cm^3 molecule^{-1} s^{-1}
JPL 2000 (*22*)	8.9 ± 0.8	8.9 ± 0.8
JPL 2006 (*9*)	12.4 ± 3.7	10.6 ± 3.7
IUPAC 2004 (N_2) (*17*)	11.9 (+6.0/−3.0)	11.9(+6.0/−3.0)
This work	10.6 ± 0.5	9.2 ± 0.4

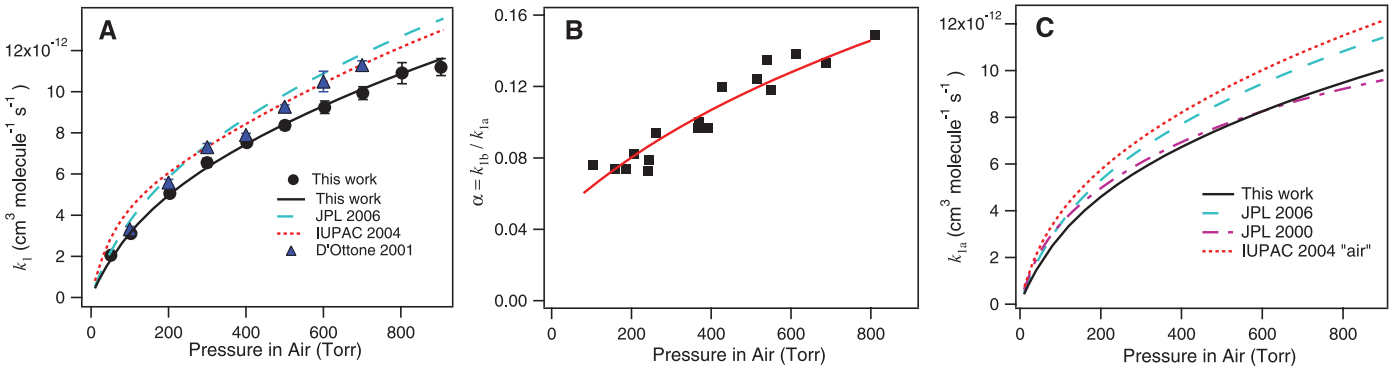

Fig. 2. Pressure dependence of rate parameters for the reaction (Eqs. 1a and 1b): OH + NO_2 + M, M = air at 298 K. Error bars represent 2 SD uncertainty. The curves are derived from fitting the data to four fall-off rate parameters; these are given in table S7. (**A**) Total effective bimolecular rate coefficient $k_1 = k_{1a} + k_{1b}$. Measurements (black circles) and fit (solid black line) from this work; previous measurements by D'Ottone *et al*. (blue triangles) (*11*); recommendations by IUPAC (dotted red line) (*17*), and NASA/JPL 2006 (dashed cyan line) (*9*). (**B**) Branching ratio $\alpha = k_{1b}/k_{1a}$. Measurements (black squares) and fit (red line). Buffer gas was predominantly N_2; nitrogen pressures were scaled by 1.063 to account for the collisional efficiency of N_2 relative to air. (**C**) Effective bimolecular rate constant k_{1a} for the nitric acid product channel. Fit to the data from this work in (A) and (B) (solid black line); recommendations by IUPAC (dotted red line) (*17*), NASA/JPL 2006 (dashed cyan line) (*9*), and NASA/JPL 2000 (dot-dashed purple line) (*22*). Pressures for the IUPAC recommendation (in N_2) were scaled by 1.063 to account for the collisional efficiency of N_2 relative to air.

760 torr. We then use an atmospheric chemistry and transport model to estimate the effect of the new results on simulated ozone levels in the Los Angeles Basin.

The total rate constant k_1 was measured with a Pulsed Laser Photolysis–Laser Induced Fluorescence (PLP-LIF) apparatus designed to overcome the experimental difficulties described above (fig. S1) (*18*). Pseudo first-order ([M] » $[NO_2]$ » $[OH]_0$) rate constants were measured in air, N_2, and O_2 buffer gases over the pressure range 20 to 900 torr at 298 K. We compensated for the reduction in OH sensitivity at higher pressures by probing the OH with a high-repetition-rate (10 kHz) laser. The high repetition rate was coupled with the use of photon counting detection and enhanced photon collection efficiency to further improve the precision of the OH kinetic decay profiles. High-sensitivity OH detection allowed data to be collected above 760 torr while keeping the $[OH]_0$ low ($\leq 10^{11}$ cm^{-3}). To better quantify NO_2 concentrations, the NO_2 was measured directly in the reaction zone by absorption spectroscopy over the wavelength range 410 to 440 nm. NO_2 concentrations were obtained by fitting the entire spectral region using cross sections measured recently by Nizkorodov *et al.* (*19*) over a wide range of pressures and temperatures relevant to the conditions of the kinetic measurements. The combination of improved OH detection sensitivity and direct NO_2 concentration measurements led to kinetics data with high precision and accuracy.

At each pressure, k_1 was determined by fitting 10 to 15 measurements of the first-order loss of OH as a function of NO_2 concentration. The observed fall-off curves of k_1 versus pressure in nitrogen, oxygen, and air from 100 to 900 torr (600 torr for O_2) are given in fig. S6. Our results support the higher range of k_1 values of D'Ottone *et al.* (*11*) for N_2 and air near atmospheric pressure, as well as those of Anastasi and Smith (*10*) for N_2, rather than the lower values of Donahue *et al.* (*12*). Our measurements in air differ slightly from a weighted linear combination of measurements in O_2 and N_2 by 3 to 4%, which we attribute to systematic errors. Our best estimate is an average of these two data sets. Our rates at 700 torr are ~10% lower than those of D'Ottone *et al.* (*11*) in air, which we attribute to improved sensitivity and to our more accurate NO_2 concentration measurements.

Experiments to determine α were performed in a second apparatus using PLP for the generation of radicals and infrared cavity ringdown spectroscopy (CRDS) for the detection of products (fig. S3). The high sensitivity of CRDS enabled detection of the ν_1(OH stretch) bands of HOONO and $HONO_2$ products in absorption (*3*). We measured relative yields of the primary products from the reaction of photolytically generated OH with excess NO_2 in the presence of predominantly (>90%) N_2 buffer gas at pressures of 100 to 750 torr. Spectra were recorded after a delay of 100 μs, sufficient to allow for complete reaction with NO_2. The ratio of product concentrations was determined from the integrated band intensities (after correcting for a small deviation in the $HONO_2$ absorption due to nonlinearities in the CRDS signal) using the ratio of ν_1 cross sections obtained from high-level ab initio calculations. These calculations include electrical and mechanical anharmonicities; furthermore, the ratio of intensities is largely invariant with respect to level of theory (*3*), because systematic errors cancel. This ratio should be accurate to 5% based on the agreement between calculated absolute intensities and experimental results for nitric acid and agreement of calculated frequencies with experimental results for both nitric acid and HOONO (*20*).

Because HOONO has an internal hydrogen bond, the OH absorption is blue-shifted when torsional vibrations, which break the hydrogen bond, are excited; the thermal population in these hot states is not fully accounted for by the measured HOONO band (*21*). To determine the fraction of the population that did not contribute to the observed HOONO band, we developed a three-dimensional (3D) potential surface as a function of the OH bond length and the HOON and OONO torsion coordinates (*18*). We extended our earlier work to include both torsions, as they were found to be strongly coupled near the potential minimum. Using the calculated energy levels, we corrected for contributions to the HOONO intensity absent from the observed band (multiplying our observed intensities by 1.2).

Experiments were performed in N_2, because the presence of O_2 would have led to the rapid formation of HO_2 and spectral interference in the region of interest. We expect the relative collisional efficiency of O_2 in the two product channels, Eqs. 1a and 1b, to be similar; the presence of O_2 would then not significantly alter the ratio α. The N_2 pressures for our α data were converted to effective air pressures by assuming the collision efficiency of air to be 94% that of N_2 (Fig. 2B).

Our measurements of k_1 and α were then fit simultaneously to obtain the four rate parameters for the two channels of the reaction, Eqs. 1a and 1b (k^0_{1a}, k^∞_{1a}, k^0_{1b}, and k^∞_{1b}), using the JPL formulation of the fall-off expression equation S1 (*9*) (see table S7 for new recommended values). Fits to both data sets were obtained, as shown in

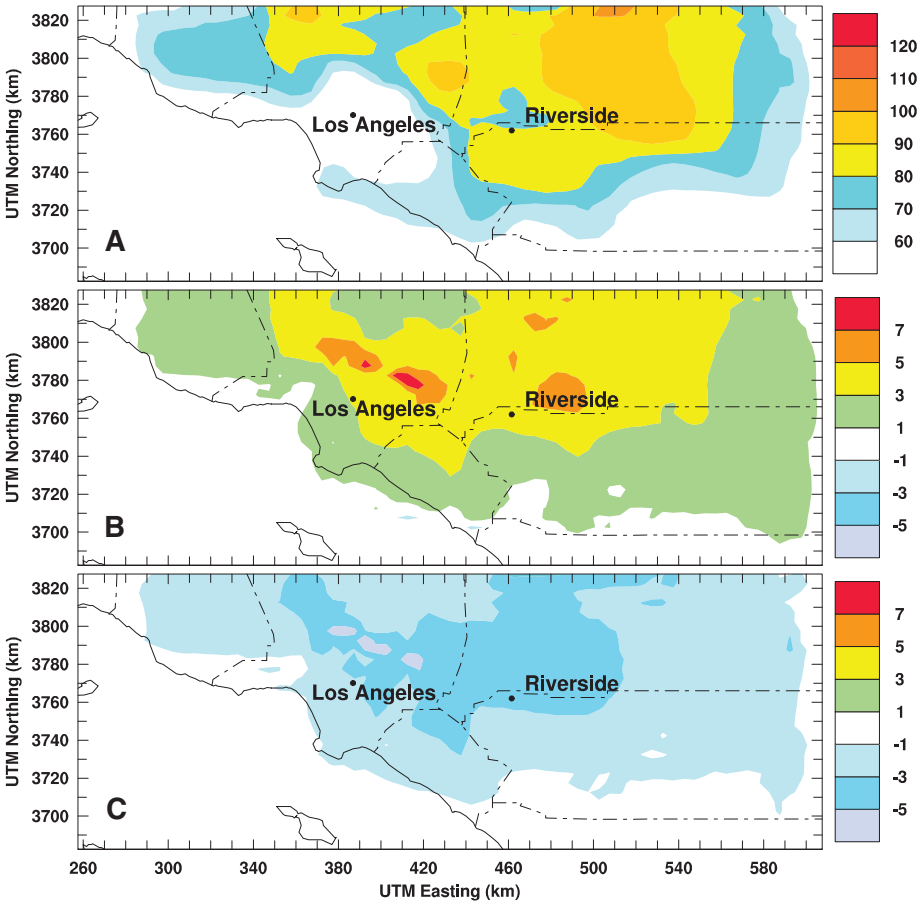

Fig. 3. Spatial distribution of predicted midday (1200 to 1300 hours) summertime ozone concentrations in parts per billion in southern California using emission inventory estimates for 2010. (**A**) defines k_{1a} as recommended by NASA/JPL 2006 (see Table 1). (**B** and **C**) show ozone changes relative to the base case for (B) lower k_{1a} measured in this work and (C) higher k_{1a} recommended by IUPAC. Apart from differences in k_{1a}, all three panels rely on the same chemical mechanism (*26*) without other adjustments to describe relevant atmospheric chemistry.

Fig. 2, A and B, and figs. S7 and S9. The pressure dependence of k_{1a} at 298 K (Fig. 2C) falls 13 to 23% below the values derived from the current recommendations over the range 100 to 760 Torr.

At 760 torr of air, we find a branching ratio of $\alpha = 0.142$ (± 0.012) (1 SD) and a rate coefficient for the formation of nitric acid of k_{1a} (298 K) = 9.2 (± 0.4) $\times 10^{-12}$ cm^3 molecule^{-1} s^{-1} (1 SD), as shown in Table 1. Our value at 1 atm air is 13% lower than the current JPL recommendation and 23% lower than the current IUPAC recommendation (which assumes $\alpha = 0$); the uncertainty in our measurement is substantially smaller than stated in the evaluations, which had to account for the large variation in k_1 among existing data sets. We anticipate that the agreement between our k_1 measurements and the higher previously reported values (*10*, *11*), in combination with quantifying the HOONO yield, will lead to a reduction in the k_{1a} uncertainty in future data evaluations. Our measurement agrees with the earlier JPL 2000 Evaluation, which has been used in many photochemical models (*22*), but the agreement is fortuitous, as this evaluation was strongly influenced by k_1 values we now believe to be too low (*12*) and did not account for reaction 1b.

Do the differences in k_{1a} shown in Table 1 imply changes in air quality predictions that are important at the policy level? To estimate the impact of our measured k_{1a}, we applied a 3D Eulerian photochemical model (*18*) to predict ozone formation in southern California under summertime conditions. Descriptions of the model, input data, and chemical mechanism are available elsewhere (*1*, *23*, *24*). Figure 3 shows the spatial distribution of ozone concentrations and changes relative to the base case (NASA/JPL 2006) when lower (this study) and higher (IUPAC) values of k_{1a} are used. The photochemical model predicts 5 to 7 parts per billion (ppb) higher O_3 concentrations when using our value of k_{1a} relative to the base case and 10 to 12 ppb higher O_3 concentrations relative to the IUPAC recommendation. In these regions of high O_3 concentrations, a 10% decrease in k_{1a} leads to a roughly 10% increase in modeled O_3 concentration. The direct effect of reducing k_{1a} is a widespread OH increase, which in turn leads to higher ozone levels. The relative changes in NO_2 and HNO_3 concentrations are smaller than for OH and vary in sign depending on location. Other measures of photochemical air pollution besides midday O_3 concentrations have large sensitivities to k_{1a} and will likewise be affected by any revision to the value of k_{1a}. In particular, the U.S. Environmental Protection Agency's health-based air quality standard for O_3 now considers daily maxima of 8-hour average rather than 1-hour peak concentrations. In the supporting online material, we show that the 8-hour average O_3 concentrations are similarly sensitive to k_{1a} (*18*).

A consideration in applying this kind of analysis is that most air pollution models use chemical mechanisms where volatile organic compound (VOC) oxidation steps that are not constrained by laboratory data are sometimes adjusted during mechanism development to improve consistency of the model predictions with O_3 measurements and other results of smog chamber experiments [see, for example, Wang *et al.* (*25*) for the case of aromatics]. To assess the extent to which a revision of k_{1a} might necessitate changes to other portions of the mechanism, we reran the simulations of all chamber experiments used in the evaluation of the mechanism used to produce Fig. 3 with the new, lower value of k_{1a} indicated by this work (*18*). Briefly, the reduction in k_{1a} required a corresponding reduction in the magnitude of the chamber radical source incorporated in the model to represent chamber effects when simulating the data (*24*, *26*), but otherwise the modified mechanism simulated the chamber data sufficiently closely to the original mechanism that no revisions are indicated, at least for the VOCs important in the ambient simulations discussed here. As a result, the mechanism we used to produce Fig. 3B is consistent with the chamber data.

We have shown that simulations using our revised value of k_{1a} lead to higher predicted ozone concentrations by as much as 5 to 10 ppb. We can assess the relevance of a change of this magnitude by putting it in the context of human health and emissions control strategies. From a health standpoint, it was recently found that a 10-ppb increase in ozone concentrations leads to a 4% increase in risk of death from respiratory causes (*27*). For emissions controls, the 2010 sensitivity of peak ozone in southern California to anthropogenic VOC has been estimated to be about 16 metric tons per day per ppb O_3 (*28*). Comparing this to the total estimated anthropogenic VOC emissions in 2010 of 740 metric tons per day, (*1*) VOC emissions would need to be roughly 10% lower to offset a 5-ppb higher predicted O_3 concentration. These two factors alone show that the magnitude of the changes in simulated ozone, caused by a revision of k_{1a}, can lead to small but noticeable differences in the predictions of photochemical models used in assessing the impact of air pollution.

Revisions to the rate of reaction 1 are likely to have an impact beyond that of air pollution. Chemical mechanisms are also used extensively in the interpretation of laboratory kinetics data, atmospheric field data, and satellite measurements for a host of issues, including derivation of rate parameters, the global HO_x budget, and stratospheric ozone depletion. For these applications, k_{1a} needs to be known precisely over a wide range of temperatures and pressures (*29*).

References and Notes

1. P. T. Martien, R. A. Harley, D. G. Cacuci, *Environ. Sci. Technol.* **40**, 2663 (2006).
2. J. S. Robertshaw, I. W. M. Smith, *J. Phys. Chem.* **86**, 785 (1982).
3. B. D. Bean *et al.*, *J. Phys. Chem. A* **107**, 6974 (2003).
4. D. M. Golden, J. R. Barker, L. L. Lohr, *J. Phys. Chem. A* **107**, 11057 (2003).
5. H. Hippler, N. Krasteva, S. Nasterlack, F. Striebel, *J. Phys. Chem. A* **110**, 6781 (2006).
6. J. Troe, *Int. J. Chem. Kinet.* **33**, 878 (2001).
7. J. Zhang, N. M. Donahue, *J. Phys. Chem. A* **110**, 6898 (2006).
8. J. L. Fry *et al.*, *J. Chem. Phys.* **121**, 1432 (2004).
9. S. P. Sander *et al.*, "Chemical Kinetics and Photochemical Data for Use in Atmospheric Studies, Evaluation Number 15" *JPL Publication 06-2* (Jet Propulsion Laboratory, California Institute of Technology, Pasadena, CA, 2006; http://jpldataeval.jpl.nasa.gov/pdf/JPL_15_AllInOne.pdf).
10. C. Anastasi, I. W. M. Smith, *J. Chem. Soc., Faraday Trans.* **72**, 1459 (1976).
11. L. D'Ottone, P. Campuzano-Jost, D. Bauer, A. J. Hynes, *J. Phys. Chem. A* **105**, 10538 (2001).
12. N. M. Donahue, M. K. Dubey, R. Mohrschladt, K. L. Demerjian, J. G. Anderson, *J. Geophys. Res. Atmos.* **102**, 6159 (1997).
13. N. M. Donahue, R. Mohrschladt, T. J. Dransfield, J. G. Anderson, M. K. Dubey, *J. Phys. Chem. A* **105**, 1515 (2001).
14. L. D'Ottone, D. Bauer, P. Campuzano-Jost, M. Fardy, A. J. Hynes, *Faraday Discuss.* **130**, 111, discussion 125, 519 (2005).
15. H. Hippler, S. Nasterlack, F. Striebel, *Phys. Chem. Chem. Phys.* **4**, 2959 (2002).
16. S. A. Nizkorodov, P. O. Wennberg, *J. Phys. Chem. A* **106**, 855 (2002).
17. R. Atkinson *et al.*, *Atmos. Chem. Phys.* **4**, 1461 (2004).
18. Materials and methods are available as supporting material on *Science* Online.
19. S. A. Nizkorodov, S. P. Sander, L. R. Brown, *J. Phys. Chem. A* **108**, 4864 (2004).
20. X. Zhang, M. R. Nimlos, G. B. Ellison, M. E. Varner, J. F. Stanton, *J. Chem. Phys.* **124**, 084305 (2006).
21. A. B. McCoy, J. L. Fry, J. S. Francisco, A. K. Mollner, M. Okumura, *J. Chem. Phys.* **122**, 104311 (2005).
22. S. P. Sander *et al.*, "Chemical Kinetics and Photochemical Data for Use in Stratospheric Modeling Supplement to Evaluation 12: Update of Key Reactions, Evaluation Number 13" *JPL Publication 00-3* (Jet Propulsion Laboratory, California Institute of Technology, Pasadena, CA, 2000); http:\\jpldataeval.jpl.nasa.gov/pdf/JPL_00-03.pdf
23. P. T. Martien, R. A. Harley, J. B. Milford, A. G. Russell, *Environ. Sci. Technol.* **37**, 1598 (2003).
24. W. P. L. Carter, "Development of the SAPRC-07 Chemical Mechanism and Updated Ozone Reactivity Scales" (Final report to the California Air Resources Board Contract No. 03-318. June 22, 2009; www.cert.ucr.edu/~carter/SAPRC).
25. L. Wang, J. B. Milford, W. P. L. Carter, *Atmos. Environ.* **34**, 4337 (2000).
26. W. P. L. Carter, R. Atkinson, A. M. Winer, J. N. Pitts Jr., *Int. J. Chem. Kinet.* **14**, 1071 (1982).
27. M. Jerrett *et al.*, *N. Engl. J. Med.* **360**, 1085 (2009).
28. "2003 Air Quality Management Plan" (South Coast Air Quality Management District, 2003; www.aqmd.gov/aqmp/docs/2003AQMP_AppV.pdf).
29. I. M. Konen *et al.*, *J. Chem. Phys.* **122**, 094320 (2005).
30. NIST Computational Chemistry Comparison and Benchmark Database, NIST Standard Reference Database 101, Release 15a, April 2010, R.D. Johnson III, Ed.; http://cccbdb.nist.gov.

31. This work was supported by National Aeronautics and Space Administration (NASA) grants NAG5-11657, NNG06GD88G, and NNX09AE21G; California Air Resources Board contracts 03-333 and 07-730; National Science Foundation grant CHE-0515627/0848242 (A.B.M.); a NASA Earth Systems Science Fellowship (A.K.M.); and a Department of Defense National Defense Science and Engineering Graduate Fellowship (M.K.S.). Research at JPL was supported by the NASA Upper Atmosphere Research and Tropospheric Chemistry Programs. This work was carried out in part at JPL, California Institute of Technology, under contract with NASA.

Supporting Online Material

www.sciencemag.org/cgi/content/full/330/6004/646/DC1
Materials and Methods
SOM Text
Figs. S1 to S16
Tables S1 to S7
References

1 June 2010; accepted 24 September 2010
10.1126/science.1193030

Direct Observation and Quantification of CO_2 Binding Within an Amine-Functionalized Nanoporous Solid

Ramanathan Vaidhyanathan,[1]* Simon S. Iremonger,[1] George K. H. Shimizu,[1]* Peter G. Boyd,[2] Saman Alavi,[2] Tom K. Woo[2]*

Understanding the molecular details of CO_2-sorbent interactions is critical for the design of better carbon-capture systems. Here we report crystallographic resolution of CO_2 molecules and their binding domains in a metal-organic framework functionalized with amine groups. Accompanying computational studies that modeled the gas sorption isotherms, high heat of adsorption, and CO_2 lattice positions showed high agreement on all three fronts. The modeling apportioned specific binding interactions for each CO_2 molecule, including substantial cooperative binding effects among the guest molecules. The validation of the capacity of such simulations to accurately model molecular-scale binding bodes well for the theory-aided development of amine-based CO_2 sorbents. The analysis shows that the combination of appropriate pore size, strongly interacting amine functional groups, and the cooperative binding of CO_2 guest molecules is responsible for the low-pressure binding and large uptake of CO_2 in this sorbent material.

The capture and storage of CO_2 emitted from industrial processes are global challenges. In many industrial processes, CO_2 is present at low partial pressures among other gases that ideally should be recycled. The currently employed capture method involves alkanolamine-based solvents that act as CO_2 scrubbers (*1*, *2*) by chemisorptive formation of N-C bonded carbamate species (bonding energies are typically 100 kJ mol^{-1}). Regeneration of the amine requires cleavage of this covalent bond by heating (at 100° to 150°C) to release CO_2. Major drawbacks of this process include the corrosive nature and volatility of the amines, their occasional decomposition, and most prominently, the high energy cost of their regeneration (*1*, *2*). The challenge is thus to couple efficient CO_2 capture with facile release in a sorbent material.

Porous systems, including zeolitic/zeotypic materials (*3*, *4*), mesoporous silica (*5*–*8*), porous carbon (*9*), and, more recently, metal-organic frameworks (MOFs) (*10*–*19*), have been investigated for CO_2 storage. Merging the inherent sorptive behavior of porous solids with less-basic amines offers a route to the sort of easy-on/easy-off materials described above. Less-basic amines would favor physisorption over chemisorption of CO_2, thus greatly reducing the energy of regeneration. This prospect has prompted research on many amine-functionalized solid materials that on the whole demonstrates that amines can enhance CO_2 uptake (*5*–*8*, *17*–*19*). Despite this conclusion, experimental insights at a molecular level on the nature of the $NH_2\cdots CO_2$ interaction are lacking (*20*). For materials such as silica and carbon, a combination of factors (lack of order, large voids, flexible amine groups, and random adsorption sites) makes the study of individual sorptive interactions virtually unfeasible. In contrast, the crystallinity of MOFs enables diffraction experiments to study structure at a molecular level. Beyond characterization of the framework, in exceptional cases, x-ray or neutron diffraction can allow direct visualization of gases within pores (*21*–*27*) to elucidate specific binding interactions and enable better sorbent design. Locating gas molecules in a MOF is challenging, but the systems typically display strong confinement effects on the guest molecules and/or specific sites of strong interaction (such as bare metal sites) that can serve as excellent models for understanding the interactions of gases in all porous systems.

We previously noted (*28*) that the MOF $Zn_2(Atz)_2(ox)$ (**1**) (Atz, 3-amino-1,2,4-triazole; ox, oxalate) showed CO_2 uptake at low pressures with an initial heat of adsorption (ΔH_{ads}) of ~40 kJ mol^{-1} (Fig. 1 and fig. S4). After manifesting the expected trend of decreased ΔH_{ads} with increased coverage, the material showed a subsequent increase in ΔH_{ads}, which remained over 35 kJ mol^{-1} during continuous gas exposure, suggesting a cooperativity effect in the binding mechanism. Here we describe a detailed study, via a combination of crystallographic and computational methods, of the nature of CO_2 binding in **1**. In a crystal structure of **1** loaded with CO_2 mol-

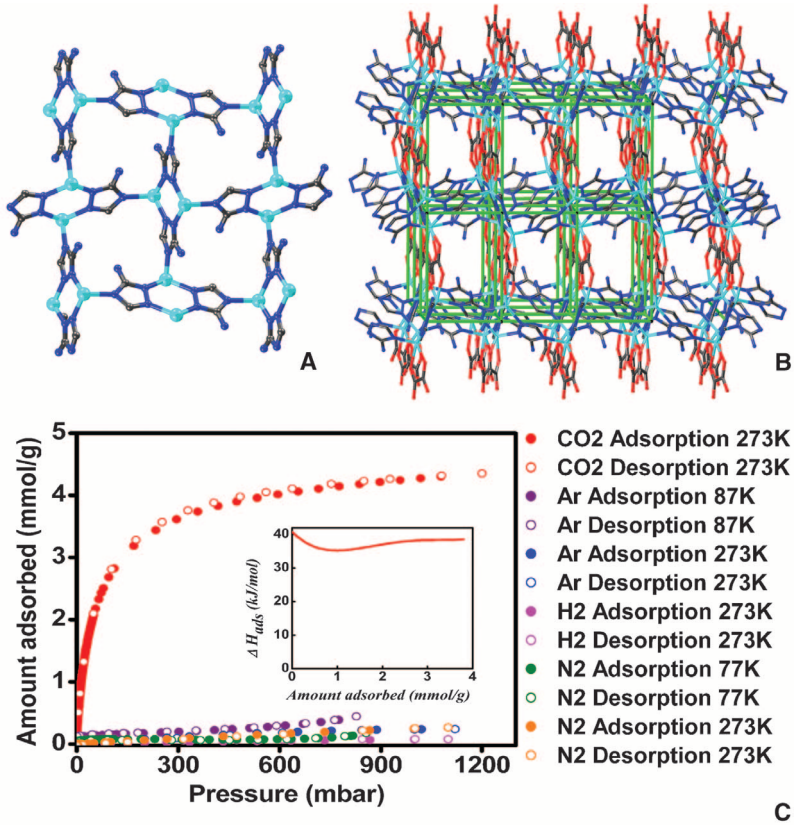

Fig. 1. (**A**) Structure of the Zn-Atz layer in **1** (Zn, cyan; C, black; N, blue; H, not shown). (**B**) Three-dimensional structure of **1**, wherein the Zn-Atz layers are pillared by oxalate moieties (O, red) to form a six-connected cubic network shown as green struts. (**C**) Adsorption isotherms for different gases carried out using **1**. The inset shows heat-of-adsorption data calculated with the CO_2 isotherms measured at 273 and 293 K (fig. S5). The zero-loading heat of adsorption was calculated, using a model based on the virial equation (figs. S6 and S7 and table S2), to be 40.8 ± 0.8 kJ mol^{-1}.

[1]Department of Chemistry, University of Calgary, Calgary T2N 1N4, Canada. [2]Department of Chemistry, Centre for Catalysis Research and Innovation, University of Ottawa, Ottawa, K1N 6N5, Canada.

*To whom correspondence should be addressed. E-mail: vvramana@ucalgary.ca (R.V.); gshimizu@ucalgary.ca (G.K.H.S.); twoo@uottawa.ca (T.K.W.)

ecules, the CO_2 binding sites are readily identified, even from room temperature diffraction data. The characteristics of CO_2 uptake in **1**, including isotherm, heat of adsorption, and location of CO_2 molecules, are modeled with high accuracy via a combination of classical grand canonical Monte Carlo (GCMC) simulations, molecular dynamics (MD) simulations, and periodic density functional theory (DFT) calculations. Thus, **1**·$(CO_2)_{1.3}$ serves to calibrate these methods for modeling gas sorption in MOFs. The modeling enables the partitioning of CO_2 binding in **1** into components based both on neighboring groups and the nature of interaction (electrostatics/dispersion).

Single crystals of **1** were prepared via a procedure modified from that previously reported (*28*), for the phases with hydrated and evacuated pores (*29*). X-ray crystallography of evacuated **1** showed no electron density in the voids, thus confirming the effectiveness of the activation procedure and the stability of the crystal. CO_2 was then loaded into evacuated crystals of **1,** and x-ray diffraction experiments conducted at 123, 173, 195, and 293 K all yielded refinable data. The CO_2 molecules could be located within the pores in all cases and were ordered except at 293 K, where the disorder could be modeled. The 173-K data set yielded the best refinement parameters [refinement factor (R) = 2.7%, weighted R (R_w) = 6.5%] and will be used for structural discussions.

The 173-K structure refinement gave a formula of **1**·$(CO_2)_{1.30}$, which agrees well with the calculated loading of 1.35 CO_2 from the adsorption isotherms at 840 mbar and 293 K (which are comparable conditions to those of single-crystal experiments). In the lattice Zn, aminotriazolate layers are pillared by oxalate ions, with free amine groups lining the pores (Fig. 1).

Within each pore, two independent CO_2 binding sites were located: CO_2-I [O(100)-C(100)-O(101)] and CO_2-II [O(200)-C(200)-O(201)] (Fig. 2 and fig. S1). CO_2-I, near the free amine group, was 80% occupied, and CO_2-II, closer to the oxalates, was 50% occupied; in filled pores, neither CO_2 molecule showed positional disorder. CO_2 could interact with an amine via N-H···O hydrogen bonding or via an interaction between the N lone pair and the C atom of CO_2. The H atoms of the amine groups were readily located in the x-ray structure of **1**·$(CO_2)_{1.30}$, enabling direct visualization of the H-bonding. CO_2-I was adjacent to the amine, with its electropositive C atom oriented toward the electronegative N atom [C(δ+)···N(δ–) = 3.151(8) Å; the C-N of monoethanolamine carbamate was modeled as 1.45 Å (*30*) and factoring C and N van der Waal radii = 3.25 Å]. The bowing of the protons on the N atoms (~21° from the mean triazole plane) confirms that the lone pair is not delocalized into the triazole ring (Fig. 2). Both O atoms of CO_2-I are within the range of longer H-bonds to the amine [N4-H···O100 = 3.039(4), O101 = 3.226(9) Å], with angles also corroborating very weak interactions [∠ N-H···O: O100 = 97.486(1)°; O101 = 95.822(1)°]. The C atom of CO_2-I also interacts with an oxalate O atom lining the pore [C(δ+)…O(δ–) = 3.155(8) Å]. The amine undergoes stronger H-bonding with oxalate O atoms [N4-H···O2 = 2.888(7), O4 = 2.122(2) Å, ∠ N-H···O = 154.718(1)° and 137.843(1)°, respectively].

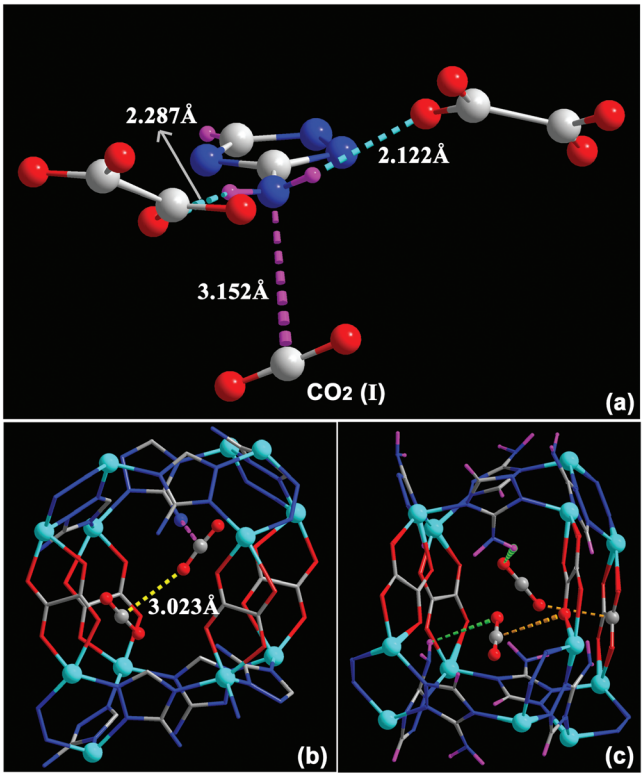

Fig. 2. X-ray structure of CO_2 binding in **1**·$(CO_2)_{1.3}$ at 173 K. (**A**) The role of the amine group of Atz in binding CO_2-I is depicted. The H atoms of the amine group (located crystallographically) H-bond to oxalate O atoms, directing the N lone pair toward the C(δ+) atom of the CO_2 molecule. H-bond distances shown are for H-acceptor interactions. (**B**) Both crystallographically independent CO_2 molecules are shown trapped in a pore, showing the cooperative interaction between CO_2-I and CO_2-II molecules. The CO_2…NH_2 interaction is represented as a dotted purple bond, and the CO_2…CO_2 interaction is indicated as a dotted yellow bond. (**C**) This panel shows the other interactions present. The CO_2-I…Ox interactions are shown in orange, and the CO_2…NH_2 hydrogen bond interactions are shown in green. For clarity, H atoms are shown in purple.

CO_2-II was located between oxalate groups along the *b* axis. The O(δ–) of CO_2-II interacts with the C(δ+) of the oxalate [$O(\delta-)_{(CO2)}$…$C(\delta+)_{(Ox)}$ = 2.961(5) Å]. In contrast to CO_2-I, CO_2-II interacts with a proximal amine via only a single H-bond [(N8-H···O200 = 2.783(8), ∠ N-H···O = 101.953(1)°]. There is an interaction between CO_2 molecules as one O atom of CO_2-I forms a contact with the C of CO_2-II [(C(δ+)…O(δ–) = 3.023(7) Å, C200···O100]. This CO_2-CO_2 interaction is highly relevant because it is most likely the origin of the observed increasing ΔH_{ads} with loading.

Regarding the geometries of the CO_2 molecules, both appear, with sizeable uncertainties, slightly bent [∠O-C-O: CO_2-I, 175.72(1.01)°; CO_2-II, 177.15(1.66)°]. Given that a 3σ range of angles approaches or includes linearity and the fact that neither chemical intuition nor the modeling studies support a nonlinear structure, the apparent bend of the CO_2 molecules probably arises from their positional distributions rather than any true distortion in bonding. The C-O bond lengths [CO_2-I: 1.137(8), 1.079(9) Å; CO_2-II: 1.141(13), 1.125(13) Å] were slightly shorter than reported [1.155(1) Å] in a 150-K/ambient pressure structure of pure CO_2 (*31*). Variable-temperature x-ray crystallography showed that although the CO_2 bond lengths and angles varied slightly with temperature, their occupancies and orientations did not appreciably change (table S1). A decrease in total gas uptake would be expected with increasing temperature; however, for **1**, this did not change between 195 and 273 K. This observation, coupled with the order of the gas molecules, reinforces the fact that the collective interactions are highly favorable for CO_2 binding. Insight regarding the specific interactions was gained through computational modeling.

To investigate the nature of the CO_2 interactions with **1** and the cooperative guest-guest binding effects, we used a combination of dispersion-corrected (*32*) periodic DFT calculations and classical GCMC simulations and MD simulations (*33*), in which the partial charge parameters were derived from the periodic DFT calculations by means of the REPEAT method (*34*). Figure 3A displays the excellent agreement between the experimental and GCMC-simulated CO_2 adsorption isotherms of **1** at 273 K. The parameters associated with the CO_2-**1** intermolecular potential were not adjusted to obtain this quality of fit. Figure 3B shows a center-of-mass probability density plot from a GCMC simulation of **1** (at 850 mbar and 273 K), where darker regions reveal a greater probability of finding CO_2. Even at 273 K, binding sites are well localized, and the symmetry of the probability clouds suggests two distinct binding sites, corroborating the crystallography. To compare the CO_2 binding sites determined computationally and crystallographically, the experimental CO_2 positions are superimposed on three-dimensional isosurfaces of the probabilities for C and O in Fig. 3C. The remarkable agreement between the simulated and experimental CO_2 positions suggests that GCMC simulations that are often used to study gas adsorption in MOFs (*33*, *35*)

not only reproduce adsorption isotherms but can also accurately reproduce specific binding sites.

The nature of the CO_2 binding was further studied with dispersion-corrected periodic DFT calculations. With all 16 binding sites in the unit cell occupied, the resulting fully optimized geometry is in excellent agreement with the x-ray structure, including the relevant CO_2-amine and CO_2-oxalate distances (fig. S8). The exception to this was the geometries of both CO_2 molecules, which, unlike their geometry in the x-ray analysis, were optimized to linear configurations, revealing that there is minimal geometric distortion from interaction with the framework. Radial distribution plots extracted from the GCMC simulations are also in agreement with the geometric parameters determined by crystallography (fig. S10). Although specific binding sites were located experimentally, the CO_2 binding is expected to be dynamic in nature. This prospect has been investigated via classical MD simulations, which show that, in a 1.4-ns time span, the CO_2 molecule can hop between several of the binding sites I and II (Fig. 3D).

The CO_2 binding energies were calculated at various occupancies at the DFT level (*29*). When **1** is empty, CO_2-I has a binding energy of 39.6 kJ mol^{-1}, which is in good agreement with the experimental zero-loading ΔH_{ads} (40.8 ± 0.8 kJ mol^{-1}). We see a strong cooperative enhancement of CO_2 binding that increases with loading. Specifically, the binding energy of CO_2-II increases by 4.6 kJ mol^{-1} to 37.0 kJ mol^{-1} when an adjacent site I is occupied. When **1** is fully occupied less one binding site, the binding energy for CO_2-II increases to 38.1 kJ mol^{-1}, whereas that of CO_2-I is 44.2 kJ mol^{-1}. Further insight into the nature of the CO_2 binding can be gained by partitioning the total binding energy. This analysis reveals that 82% of the binding energy of site I is due to dispersion, whereas 18% results from electrostatics (*29*). This contrasts with site II, where the binding energy is almost entirely (99%) due to dispersion interactions.

The cooperative binding in **1** can be attributed to a combination of dispersion and electrostatic interactions between CO_2 molecules, which can be quantified by using DFT to evaluate the interaction energy between two CO_2 molecules at sites I and II in a vacuum (*29*). This calculation gives a CO_2-CO_2 interaction energy of 3.9 kJ mol^{-1}, which accounts for most of the observed 4.6–kJ mol^{-1} binding enhancement. Of the 3.9–kJ mol^{-1} interaction between CO_2 molecules, 66% can be attributed to dispersion and 34% can be assigned to electrostatics. The same analysis, with the MOF fully loaded, attributes 61% of the interaction to dispersion and 39% to electrostatics, suggesting similar cooperativity at higher loadings.

Several key insights obtained from the detailed analysis of the binding interactions in **1** have implications for the design of future materials used for the physisorption of CO_2. The relatively high binding energies observed in the material are dominated by dispersion interactions. Because CO_2 has a substantial quadrupole moment, there is opportunity to further increase the binding energies through appropriately designed binding sites that maximize the electrostatic interactions with CO_2. The importance of the cooperative guest binding to the uptake of CO_2 in **1** is another key insight. In particular, the proper mutual orientation and high density of binding sites can be used as a strategy to increase CO_2 binding energies. Further, we believe that these strategies can be incorporated into materials with larger pores, in order to increase the overall CO_2 uptake capacity and binding energies, thereby improving the uptake properties in the important low–partial-pressure regime. In the broadest sense, via detailed modeling, this study lays the groundwork for the design of easy-on/easy-off physisorptive materials for CO_2 capture, designed from the characteristics of the guest molecules outward rather than from the host framework inward.

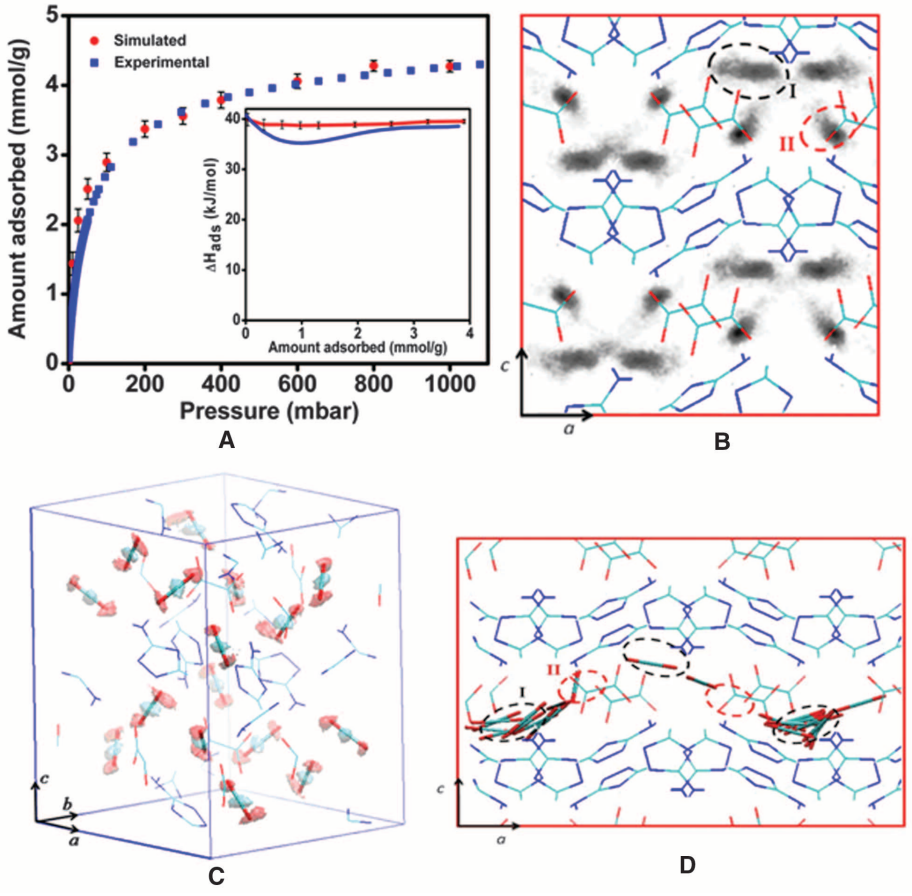

Fig. 3. (**A**) Comparison of the simulated (red) and experimental (blue) CO_2 gas adsorption isotherm of **1** at 273 K. The inset shows a comparison of experimental and simulated heats of adsorption as a function of guest loading. (**B**) Center-of-mass probability density plots of CO_2 molecules in **1** from a GCMC simulation at 850 mbar and 273 K. Probabilities along the *b* axis are summed and projected onto the *ac* plane. (**C**) Comparison of the location of the CO_2 binding sites in **1** obtained from x-ray analysis and those predicted by simulation. Probability isosurface plots of the CO_2 O atoms are shown as transparent red surfaces and those of the C atoms as transparent cyan surfaces. The 16 experimentally determined CO_2 molecule positions are shown as tubes. An isosurface value of 0.15 $Bohr^{-3}$ is used. (**D**) Trace of a single CO_2 molecule during a MD simulation of **1** with five CO_2 molecules per unit cell or a loading of 1.6 mmol g^{-1}. Shown are 23 successive snapshots, separated by 62.5 ps. Other CO_2 molecules present in the simulation are not shown. In (B) and (D), the approximate locations of binding sites I and II in a single channel are shown with dotted ellipses (site I, black; site II, red). In (B) and (C), a single unit cell of MOF **1** is shown, whereas in (D) a 2 × 1 × 1 cell is depicted. In (B) to (D), the MOF framework is shown as lines and the CO_2 molecules are shown as tubes (C, light blue; O, red; N, dark blue; Zn, not shown).

References and Notes

1. G. T. Rochelle, *Science* **325**, 1652 (2009).
2. B. Arstad, R. Blom, O. Swang, *J. Phys. Chem. A* **111**, 1222 (2007).
3. A. Zukal, I. Dominguez, J. Mayerová, J. Cejka, *Langmuir* **25**, 10314 (2009).
4. R. V. Siriwardane, M. S. Shen, E. P. Fisher, J. Losch, *Energy Fuels* **19**, 1153 (2005).
5. Y. Belmabkhout, A. Sayari, *Adsorption* **15**, 318 (2009).
6. S. Kim, J. Ida, V. V. Guliants, J. Y. S. Lin, *J. Phys. Chem. B* **109**, 6287 (2005).
7. S. N. Kim, W. J. Son, J. S. Choi, W. S. Ahn, *Microporous Mesoporous Mater.* **115**, 497 (2008).
8. J. Wei *et al.*, *Microporous Mesoporous Mater.* **116**, 394 (2008).
9. B. J. Kim, K. S. Cho, S. J. Park, *J. Colloid Interface Sci.* **342**, 575 (2010).

10. B. Wang, A. P. Côté, H. Furukawa, M. O'Keeffe, O. M. Yaghi, *Nature* **453**, 207 (2008).
11. P. K. Thallapally *et al.*, *J. Am. Chem. Soc.* **130**, 16842 (2008).
12. A. R. Millward, O. M. Yaghi, *J. Am. Chem. Soc.* **127**, 17998 (2005).
13. N. A. Ramsahye *et al.*, *J. Phys. Chem. C* **112**, 514 (2008).
14. S. R. Caskey, A. G. Wong-Foy, A. J. Matzger, *J. Am. Chem. Soc.* **130**, 10870 (2008).
15. A. Phan *et al.*, *Acc. Chem. Res.* **43**, 58 (2010).
16. K. S. Walton *et al.*, *J. Am. Chem. Soc.* **130**, 406 (2008).
17. A. Demessence, D. M. D'Alessandro, M. L. Foo, J. R. Long, *J. Am. Chem. Soc.* **131**, 8784 (2009).
18. J. An, S. J. Geib, N. L. Rosi, *J. Am. Chem. Soc.* **132**, 38 (2010).
19. B. Arstad, H. Fjellvåg, K. O. Kongshaug, O. Swang, R. Blom, *Adsorption* **14**, 755 (2008).
20. C. Villiers, J. P. Dognon, R. Pollet, P. Thuéry, M. Ephritikhine, *Angew. Chem. Int. Ed.* **49**, 3465 (2010).
21. R. Kitaura *et al.*, *Science* **298**, 2358 (2002).
22. R. Matsuda *et al.*, *Nature* **436**, 238 (2005).
23. S. Takamizawa *et al.*, *J. Am. Chem. Soc.* **132**, 3783 (2010).
24. J. P. Zhang, X. M. Chen, *J. Am. Chem. Soc.* **131**, 5516 (2009).
25. P. D. C. Dietzel *et al.*, *Chem. Commun. (Camb.)* **41**, 5125 (2008).
26. H. Wu, J. M. Simmons, G. S. Srinivas, W. Zhou, T. Yildirim, *J. Phys. Chem. Lett* **1**, 1946 (2010).
27. V. K. Peterson, Y. Liu, C. M. Brown, C. J. Kepert, *J. Am. Chem. Soc.* **128**, 15578 (2006).
28. R. Vaidhyanathan, S. S. Iremonger, K. W. Dawson, G. K. H. Shimizu, *Chem. Commun. (Camb.)* **35**, 5230 (2009).
29. Supporting material on *Science* Online includes complete details of the crystallography (crystallographic information files for all temperatures), gas sorption experiments, and computational modeling (including a movie showing the correlation of experimental and modeled CO_2 positions in **1**).
30. H. Deguchi *et al.*, *Ind. Eng. Chem. Res.* **49**, 6 (2010).
31. A. Simon, K. Peters, *Acta Crystallogr. B* **36**, 2750 (1980).
32. S. Grimme, *J. Comput. Chem.* **27**, 1787 (2006).
33. T. Düren, Y. S. Bae, R. Q. Snurr, *Chem. Soc. Rev.* **38**, 1237 (2009).
34. C. Campañá, B. Mussard, T. K. Woo, *J. Chem. Theory Comput.* **5**, 2866 (2009).
35. M. Tafipolsky, S. Amirjalayer, R. Schmid, *Microporous Mesoporous Mater.* **129**, 304 (2010).
36. T.K.W. and G.K.H.S. thank the Natural Sciences and Engineering Research Council of Canada. G.K.H.S. thanks the Institute for Sustainable Energy, Environment and Economy at the University of Calgary and the Alberta Energy Research Institute for partial financial support of this work. T.K.W. and P.G.B. thank the Canada Research Chairs Program and the High Performance Computing Virtual Laboratory for financial support. Crystallographic data for the structures reported in this paper have been deposited with the Cambridge Crystallographic Data Centre (CCDC) under reference numbers CCDC 782638 to 782642. These data can be obtained free of charge via www.ccdc.cam.ac.uk/conts/retrieving.html (or from the CCDC, 12 Union Road, Cambridge CB2 1EZ, UK).

Supporting Online Material

www.sciencemag.org/cgi/content/full/330/6004/650/DC1
Materials and Methods
SOM Text
Figs. S1 to S12
Tables S1 to S5
References
Movie S1

25 June 2010; accepted 30 September 2010
10.1126/science.1194237

The Occurrence and Mass Distribution of Close-in Super-Earths, Neptunes, and Jupiters

Andrew W. Howard,[1,2]* Geoffrey W. Marcy,[1] John Asher Johnson,[3] Debra A. Fischer,[4] Jason T. Wright,[5] Howard Isaacson,[1] Jeff A. Valenti,[6] Jay Anderson,[6] Doug N. C. Lin,[7,8] Shigeru Ida[9]

The questions of how planets form and how common Earth-like planets are can be addressed by measuring the distribution of exoplanet masses and orbital periods. We report the occurrence rate of close-in planets (with orbital periods less than 50 days), based on precise Doppler measurements of 166 Sun-like stars. We measured increasing planet occurrence with decreasing planet mass (M). Extrapolation of a power-law mass distribution fitted to our measurements, $df/d\log M = 0.39\ M^{-0.48}$, predicts that 23% of stars harbor a close-in Earth-mass planet (ranging from 0.5 to 2.0 Earth masses). Theoretical models of planet formation predict a deficit of planets in the domain from 5 to 30 Earth masses and with orbital periods less than 50 days. This region of parameter space is in fact well populated, implying that such models need substantial revision.

The architecture of our solar system, with small rocky planets orbiting close to the Sun and gas-liquid giant planets farther out, provides key properties that inform theories of planet formation and evolution. As more planetary systems are discovered, the planet occurrence fractions and distributions of mass and orbital distance similarly shape our understanding of how planets form, interact, and evolve. Such properties can be measured using precise Doppler measurements of the host stars that interact gravitationally with their planets. These measurements reveal the planetary orbits and minimum masses ($M \sin i$, due to unknown orbital inclinations i).

In the core-accretion theory of planet formation, planets are built from the collisions and sticking together of rock-ice planetesimals, growing to Earth size and beyond, followed by the gravitational accretion of hydrogen and helium gas. This process has been simulated numerically (*1*–*4*), predicting the occurrence of planets in a two-parameter space defined by their masses and orbital periods (P). These simulations predict that there should be a paucity of planets, a "planet desert" (*3*), in the mass range from ~1 to 30 Earth masses ($M_{\rm Earth}$) orbiting inside of ~1 astronomical unit (AU), depending on the exact treatment of inward planet migration.

We used precise Doppler measurements of a well-defined sample of nearby stars to detect planets having masses of 3 to 1000 $M_{\rm Earth}$ orbiting within the inner 0.25 AU. The 235 main-sequence G-, K-, and M-type dwarf stars in our NASA–University of California Eta-Earth Survey were selected from the Hipparcos catalog on the basis of brightness ($V < 11$), distance (<25 pc), luminosity ($M_V > 3.0$), low chromospheric activity ($\log R'_{\rm HK} < -4.7$), lack of stellar companions, and observability from Keck Observatory. The resulting set of stars is nearly free of selection bias; in particular, stars were neither included nor excluded based on their likelihood to harbor a planet. [The stars and planets are listed in the supporting online material (SOM).] Here we focus on the 166 G- and K-type stars, with masses of 0.54 to 1.28 solar masses and $B - V < 1.4$. We analyzed previously announced planets, new candidate planets, and nondetections on a star-by-star basis to measure close-in planet occurrence as a function of planet mass.

We measured at least 20 radial velocities (RVs) for each star, achieving 1 m s^{-1} precision (*5*) with the HIRES echelle spectrometer (*6*) at Keck Observatory. To achieve sensitivity on time scales ranging from years to days, the observations of each star were spread over 5 years, with at least one cluster of 6 to 12 observations in a 12-night span. Stars with candidate planets were observed intensively, leading to several discoveries (*5*, *7*, *8*). In total, 33 planets (Fig. 1) have been detected around 22 stars in our sample (*5, 7, 9–22*), some of which were discovered by other groups. Sixteen of these planets have $P <$ 50 days. Our analysis also includes five candidate low-mass planets from the Eta-Earth Survey with $P < 50$ days and false alarm probabilities (*5*) of <5%.

[1]Department of Astronomy, University of California, Berkeley, CA 94720, USA. [2]Space Sciences Laboratory, University of California, Berkeley, CA 94720, USA. [3]Department of Astrophysics, California Institute of Technology, Pasadena, CA 91125, USA. [4]Department of Astronomy, Yale University, New Haven, CT 06511, USA. [5]Department of Astronomy and Astrophysics, The Pennsylvania State University, University Park, PA 16802, USA. [6]Space Telescope Science Institute, 3700 San Martin Drive, Baltimore, MD 21218, USA. [7]University of California Observatories/Lick Observatory, University of California, Santa Cruz, CA 95064, USA. [8]Kavli Institute for Astronomy and Astrophysics, Peking University, Beijing, China. [9]Tokyo Institute of Technology, Ookayama, Meguro-ku, Tokyo 152-8551, Japan.

*To whom correspondence should be addressed. E-mail: howard@astro.berkeley.edu

For each star without a detected or candidate planet, we computed on a fine grid of orbital periods the maximum planet mass that would be compatible with the RV measurements. We assumed circular orbits and removed linear trends and stellar activity correlations (when appropriate) before fitting. Above this mass limit at a particular period, a planet would be detected; below it, the existence of a planet cannot be ruled out. Folding together these limits for all stars, we derived a search completeness function, $C(P, M \sin i)$. As shown in Fig. 1, C is the fraction of stars with measurements sufficient to rule out planets of a given minimum mass and orbital period.

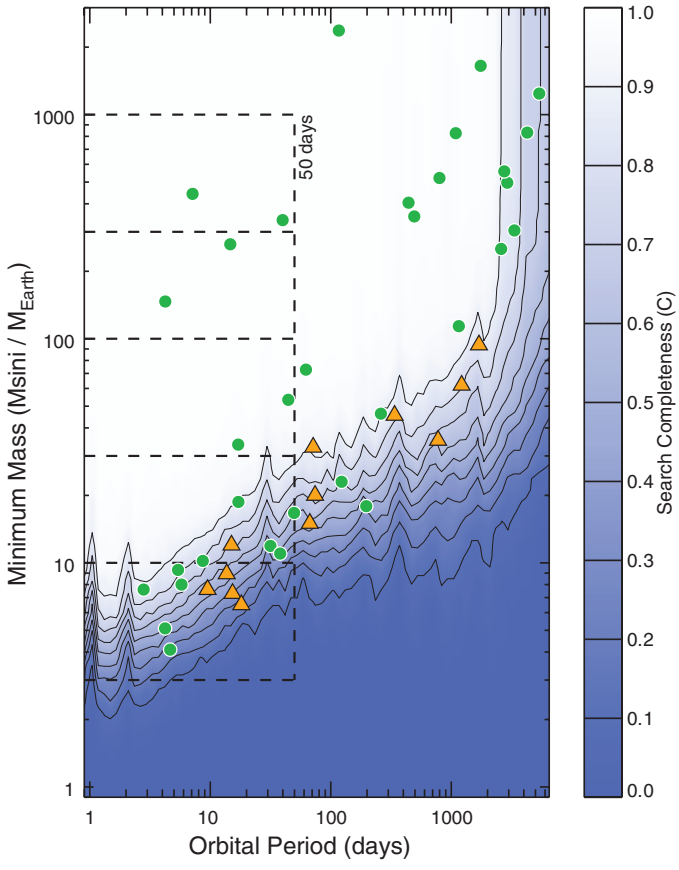

Fig. 1. Detected planets (green circles) and candidate planets (orange triangles) from the Eta-Earth Survey as a function of orbital period and minimum mass. Five mass domains (3 to 10, 10 to 30, 30 to 100, 100 to 300, and 300 to 1000 M_{Earth}) out to 50-day orbits are marked with dashed lines. Search completeness—the fraction of stars with measurements sufficient to rule out planets in circular orbits of a given minimum mass and orbital period—is shown as blue contours from 0.0 to 1.0 in steps of 0.1.

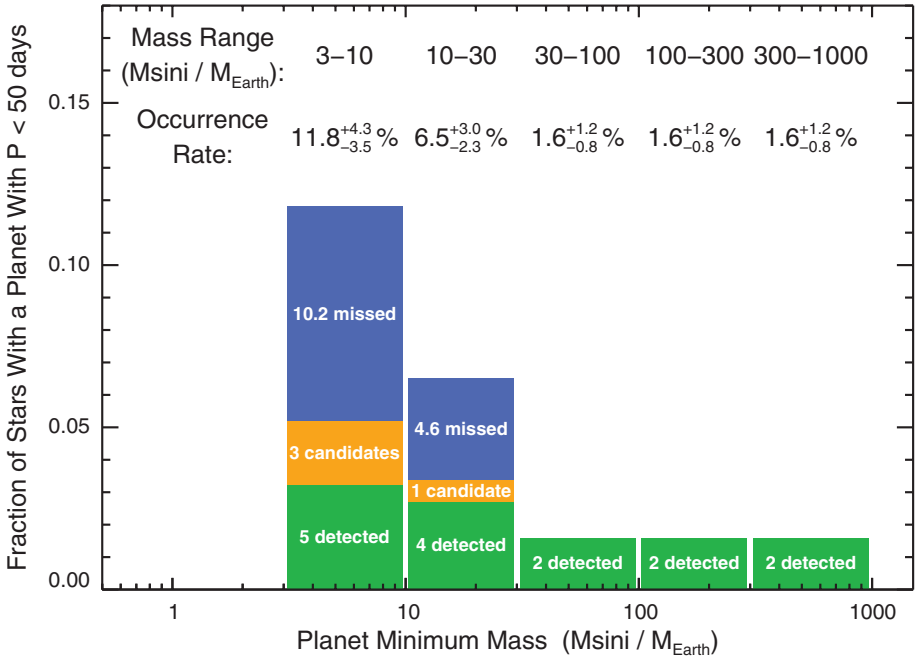

Fig. 2. Histogram of the occurrence rate of stars hosting planets with orbital periods of less than 50 days in five mass ranges. Detected (green), candidate (orange), and missed (blue) planets are depicted separately. Missed planets statistically correct for planets that are detectable by measurements at 1 m s^{-1} but were missed because of nonuniform sensitivity.

We computed the occurrence rate—the fraction of stars orbited by planets—in five planet-mass domains restricted to orbital periods of $P <$ 50 days (Fig. 2). In the three largest mass domains, our survey is complete because these planets impart easily detectable Doppler signatures ($K > 9$ m s^{-1}). In the two lowest-mass domains, there are markedly higher planet occurrence rates, despite reduced sensitivity (depicted by the shaded regions in Fig. 1). We corrected for this incompleteness by computing a "missing planet correction" by sampling $C(P, M \sin i)$ for each detected and candidate planet. The fraction of stars capable of revealing each planet is C; therefore, for each detected or candidate planet, $1/C - 1$ missed planets remain undetected. Summing over detected and candidate planets, we estimate that 10.2 and 4.6 planets were missed in the 3 to 10 and 10 to 30 M_{Earth} mass domains, respectively. Including these missed planets and using binomial statistics (SOM), we computed the planet occurrence rates shown in Fig. 2. There is a substantial increase in planet occurrence with decreasing planet mass.

We fit the planet occurrence rate in five mass domains to a power law, $df/d\log M_E = kM_E^{\alpha}$, where $df/d\log M_E$ is the occurrence rate in a $\log_{10}$ mass interval, $M = M_E \sin i/M_{Earth}$, $k = 0.39^{+0.27}_{-0.16}$, and $\alpha = -0.48^{+0.12}_{-0.14}$. Using this model, we extrapolated speculatively into two important mass domains below our detection limit. We expect planets of mass from 1 to 3 M_{Earth} to orbit 14^{+8}_{-5}% of Sun-like stars. For Earth-mass planets with $M \sin i = 0.5$ to 2 M_{Earth} and $P < 50$ days, we predict an occurrence rate of $\eta_{Earth} = 23^{+16}_{-10}$%.

Our measurements in the two largest mass domains are consistent with a 1.2 ± 0.2% occurrence rate of "hot Jupiters" within 0.1 AU ($P <$ ~12 days) for FGK dwarfs (*23*). At lower masses, our results are consistent with the two planets in the mass range $M \sin i = 5$ to 30 M_{Earth} with $P < 16$ days detected around 24 FGK dwarfs surveyed by the Anglo-Australian Telescope (*24*). Mayor *et al.* have noted a substantially higher planet occurrence rate, from 30 ± 10% (*25*) to "at least 50%" (*26*), for planets with $M \sin i = 3$ to 30 M_{Earth} and $P < 50$ days around GK stars, based on measurements with the HARPS (High Accuracy Radial Velocity Planetary Search) spectrometer. Accounting for missed planets, we find an occurrence rate of 15^{+5}_{-4}% with a 24% upper limit (95% confidence) for this range of parameters.

Our analysis extends to lower masses the work of Cumming *et al.* (*27*), who measured 10.5% of solar-type stars hosting a gas-giant planet ($M \sin i = 100$ to 3000 M_{Earth}, $P = 2$ to

2000 days), with planet occurrence varying as $df \propto M^{-0.31 \pm 0.2} P^{0.26 \pm 0.1}$ d$\log M$ d$\log P$. Although the details of planet formation probably differ for gas-giant and terrestrial planets, we can speculate that if the trend of increasing planet occurrence with longer orbital period holds down to an Earth mass, then $\eta_{\mathrm{Earth}} = 23\%$ is an underestimate for orbits near 1 AU. For orbits beyond the ice line (~2.5 AU), gravitational microlensing searches find three times as many Neptunes as Jupiters (*28*), suggesting that planet occurrence also increases with decreasing planet mass in this domain.

The distribution of planets in the mass/orbital-period plane (Fig. 1) reveals important clues about planet formation and migration. Planets with $M \sin i = 10$ to 100 M_{Earth} and $P < 20$ days are almost entirely absent. There is also an overdensity of planets starting at $P < 10$ days and $M \sin i = 4$ to 10 M_{Earth} and extending to higher masses and longer periods. These patterns suggest different formation and migration mechanisms for close-in low-mass planets as compared to massive gas-giant planets.

Population synthesis models of planet formation predict an increase in planet occurrence with decreasing planet mass (*2*, *29*). However, the bulk of their predicted low-mass planets reside near the ice line, well outside of the $P < 50$ days domains analyzed here. In fact, these models predict a "planet desert" precisely in the domain of mass and period where we detect an overdensity of planets. The desert emerges naturally in the simulations (*3*, *4*) from fast migration and accelerating planet growth. Most planets are born near or beyond the ice line, and those that grow to a critical mass of several Earth masses either rapidly spiral inward to the host star or undergo runaway gas accretion and become massive gas giants. Our measurements show that population synthesis models of planet formation are currently inadequate to explain the distribution of low-mass planets.

The Kepler mission (*30*) is currently surveying 156,000 faint stars for transiting planets as small as Earth. Our power-law model predicts that Kepler will detect a bounty of close-in small planets: an occurrence rate of 22% for $P < 50$ days and $M \sin i = 1$ to 8 M_{Earth}, corresponding to 1 to 2 Earth radii, assuming terrestrial, Earth-like density (5.5 kg m^{-3}). When the mission is complete, we estimate (see SOM) that Kepler will have detected the transits of 120 to 260 of these plausibly terrestrial worlds orbiting the ~10^4 G and K dwarfs brighter than 13th magnitude (*31*, *32*).

References and Notes

1. S. Ida, D. N. C. Lin, *Astrophys. J.* **604**, 388 (2004).
2. S. Ida, D. N. C. Lin, *Astrophys. J.* **626**, 1045 (2005).
3. S. Ida, D. N. C. Lin, *Astrophys. J.* **685**, 584 (2008).
4. C. Mordasini, Y. Alibert, W. Benz, *Astron. Astrophys.* **501**, 1139 (2009).
5. A. W. Howard *et al.*, *Astrophys. J.* **696**, 75 (2009).
6. S. S. Vogt *et al.*, *Proc. SPIE Instrum. Astron. VIII* **2198**, 362 (1994).
7. A. W. Howard *et al.*, *Astrophys. J.*, available at http://arxiv.org/abs/1003.3444 (2010).
8. J. A. Johnson *et al.*, *Proc. Astron. Soc. Pacific* **122**, 149 (2010).
9. R. P. Butler *et al.*, *Astrophys. J.* **646**, 505 (2006).
10. D. A. Fischer, G. W. Marcy, R. P. Butler, G. Laughlin, S. S. Vogt, *Astrophys. J.* **564**, 1028 (2002).
11. M. Mayor, D. Queloz, *Nature* **378**, 355 (1995).
12. D. A. Fischer *et al.*, *Astrophys. J.* **675**, 790 (2008).
13. S. S. Vogt *et al.*, *Astrophys. J.* **708**, 1366 (2010).
14. G. W. Marcy, R. P. Butler, *Astrophys. J.* **464**, L147 (1996).
15. E. J. Rivera *et al.*, *Astrophys. J.* **708**, 1492 (2010).
16. R. A. Wittenmyer, M. Endl, W. D. Cochran, H. F. Levison, G. W. Henry, *Astrophys. J. Suppl. Ser.* **182**, 97 (2009).
17. C. Lovis *et al.*, *Nature* **441**, 305 (2006).
18. D. Fischer *et al.*, *Astrophys. J.* **703**, 1545 (2009).
19. C. Mordasini *et al.*, *Astron. Astrophys.*, available at http://arxiv.org/abs/1010.0856.
20. J. T. Wright *et al.*, *Astrophys. J.* **683**, L63 (2008).
21. J. T. Wright *et al.*, *Astrophys. J.* **693**, 1084 (2009).
22. S. S. Vogt *et al.*, *Astrophys. J.* **632**, 638 (2005).
23. G. Marcy *et al.*, *Prog. Theor. Phys.* **158** (suppl.), 24 (2005).
24. S. J. O'Toole *et al.*, *Astrophys. J.* **701**, 1732 (2009).
25. M. Mayor *et al.*, *Astron. Astrophys.* **493**, 639 (2009).
26. M. Mayor, 2010, KITP Conference: Exoplanets Rising: Astronomy and Planetary Science at the Crossroads, an online presentation at the Kavli Institute for Theoretical Physics, Santa Barbara, CA, 29 March 2010, www.portaltotheuniverse.org/podcasts/eps/view/53704/.
27. A. Cumming *et al.*, *Proceedings of the Astronomical Society of the Pacific* **120**, 531 (2008).
28. T. Sumi *et al.*, *Astrophys. J.* **710**, 1641 (2010).
29. C. Mordasini, Y. Alibert, W. Benz, D. Naef, *Astron. Astrophys.* **501**, 1161 (2009).
30. W. J. Borucki *et al.*, *Science* **327**, 977 (2010).
31. N. M. Batalha *et al.*, *Astrophys. J.* **713**, L109 (2010).
32. W. J. Borucki *et al.*, *Astrophys. J.*, available at http://arxiv.org/abs/1006.2799 (2010).

33. This work was based on observations at the W. M. Keck Observatory granted by NASA and the University of California (UC). We thank the many observers who contributed to the measurements reported here and acknowledge the efforts and dedication of the Keck Observatory staff, especially S. Dahm, H. Tran, and G. Hill for support of HIRES and G. Wirth for support of remote observing. We acknowledge R. P. Butler and S. Vogt for many years of contributing to the data presented here. A.H. acknowledges support from a Townes Postdoctoral Fellowship at the UC Berkeley Space Sciences Laboratory. G.M. acknowledges NASA grant NNX06AH52G. Finally, we extend special thanks to those of Hawai'ian ancestry on whose sacred mountain of Mauna Kea we are privileged to be guests.

Supporting Online Material

www.sciencemag.org/cgi/content/full/330/6004/653/DC1
Materials and Methods
Figs. S1 to S7
Tables S1 to S3
References

8 July 2010; accepted 27 September 2010
10.1126/science.1194854

Transferable GaN Layers Grown on ZnO-Coated Graphene Layers for Optoelectronic Devices

Kunook Chung,[1] Chul-Ho Lee,[1,2] Gyu-Chul Yi[1]*

We fabricated transferable gallium nitride (GaN) thin films and light-emitting diodes (LEDs) using graphene-layered sheets. Heteroepitaxial nitride thin films were grown on graphene layers by using high-density, vertically aligned zinc oxide nanowalls as an intermediate layer. The nitride thin films on graphene layers show excellent optical characteristics at room temperature, such as stimulated emission. As one of the examples for device applications, LEDs that emit strong electroluminescence emission under room illumination were fabricated. Furthermore, the layered structure of a graphene substrate made it possible to easily transfer GaN thin films and GaN-based LEDs onto foreign substrates such as glass, metal, or plastic.

Inorganic compound semiconductors such as gallium arsenide (GaAs) and gallium nitride (GaN) provide many advantages over organic materials for optoelectronic device applications, including high carrier mobility and radiative recombination rates, as well as long-term stability and reliability (*1*, *2*). However, problems associated with high-quality inorganic film growth on large or flexible substrates represent one of the major obstacles to the use of inorganic semiconductors in foldable-display and solar-cell applications. Previous techniques such as epitaxial growth and lift-off circumvent this problem by separation of the thin film from the growth substrates (*3*–*6*), but difficulty in separating the film from a single-crystal substrate limits their use. Meanwhile, the layered structure of graphene sheets, which consist of weakly bonded layers of hexagonally arranged carbon atoms held together by strong covalent bonds, makes it easy to transfer the film to foreign substrates. Here, we describe the methods to grow a high-quality, epitaxial GaN layer and fabricate $In_xGa_{1-x}N$/GaN multi-quantum-well (MQW)–structure light-emitting diodes (LEDs) on graphene layers. Furthermore, the LEDs were transferred onto foreign substrates, such as metal, glass, and plastic, and exhibited strong light emission even under room illumination.

[1]National Creative Research Initiative Center for Semiconductor Nanorods and Department of Physics and Astronomy, Seoul National University, Seoul 151-747, South Korea. [2]Department of Materials Science and Engineering, Pohang University of Science and Technology, Pohang, Gyeongbuk 790-784, South Korea.

*To whom correspondence should be addressed. E-mail: gcyi@snu.ac.kr

Because of the excellent optical and electrical characteristics of nitride semiconductors, full-color-spectrum nitride LEDs with high efficiency and reliability and long-term stability are now commercially available (*7*). Nevertheless, problems of limited substrate size, high cost, high-resistance ohmic contacts, and poor heat dissipation remain, primarily because of the requirement of a sapphire substrate for nitride film growth. Additionally, for large-area or flexible-device applications, the device must be fabricated on glass, plastic, or metal substrates. However, high-quality, epitaxial nitride films can be grown only on a lattice-matched single-crystal substrate at a high growth temperature, above 1000°C (*1*); glass and plastic substrates have no tolerance for such high temperatures and, as amorphous materials, cannot be used for epitaxial growth of a crystalline film (*8*). For this reason, previous techniques—most notably epitaxial growth and lift-off—have separated thin films from their growth substrates to make flip-chip devices on metal substrates (*3*–*6*). However, difficulties in separating the films from a single-crystal substrate arising from strong bonding between GaN and sapphire and their high mechanical and chemical stability have limited the use of such techniques. This difficulty can be resolved readily by using substrates composed of graphene layers because the graphene-layer structure makes it possible to transfer the epitaxial film grown on graphene layers to substrates such as metal, glass, and plastic. As recently reported, large graphene films that exhibit high-temperature stability, optical transparency, mechanical flexibility, and electrical and thermal conductivities are now available (*9*, *10*).

The basic strategy for epitaxial growth of GaN on graphene layers is shown in Fig. 1 (*11*). A mirror-smooth, epitaxial GaN thin film could not be grown on pristine graphene layers, presumably because of the lack of chemical reactivity. Although GaN nucleation would not occur on the basal plane of pristine graphene, GaN islands can be grown readily along the naturally formed step-edges (fig. S1A). Accordingly, the first step is to create many step-edges, which can then act as nucleation sites. Oxygen-plasma treatment can make graphene rough (*12*). Meanwhile, although the oxygen-plasma treatment increased the GaN island density, GaN films were polycrystalline, and their surfaces were rough and irregular (fig. S1B), which is similar to the previous report on GaN films that were grown on graphite substrates (*8*). Even the typical use of a low-temperature GaN buffer layer did not improve the film crystallinity or morphology. Thus, we grew high-density zinc oxide (ZnO) nanowalls on oxygen-plasma–treated graphene layers: an intermediate layer for GaN growth. Figure 1, C and D, shows scanning electron microscopy (SEM) images of high-density, epitaxial ZnO nanowalls grown on plasma-treated graphene layers and a GaN thin film on the nanowalls, respectively. As previously reported (*13*), ZnO nanowalls are grown along naturally formed graphene step-edges, and accordingly, step-edges generated by oxygen-plasma lead to the formation of high-density ZnO nanowalls. Because of the same crystal structure and small lattice misfits with GaN, epitaxial GaN films grow on the nanowalls by means of lateral overgrowth. Although the lateral overgrowth depended on the nanowalls density (fig. S3), the SEM image in Fig. 1D shows the flat surface morphology. The high-density ZnO nanowalls play a critical role in the heteroepitaxial growth of GaN on graphene layers.

We obtained photoluminescence (PL) spectra (Fig. 2) of GaN thin films grown on graphene layers at room temperature using a continuous-wave helium-cadmium (He-Cd) or pulsed neodymium-doped yttrium aluminum garnet (Nd:YAG) laser as the optical excitation source. At a low excitation power of 1 W/cm^2 with a He-Cd laser, the dominant PL emission peak was at 3.40 eV, and a very weak deep-level emission was at 2.2 eV, which correspond to near-band-edge (NBE) emission associated with excitons and deep levels, respectively. This strong NBE emission with the extremely low deep-level emission indicates the high optical quality of GaN films on graphene layers. For low excitation power with the pulsed Nd:YAG laser [below a threshold value (I_{th}) of 0.6 MW/cm^2], the broad NBE emission peak was still observed at 3.40 eV, which is quite similar to that measured by using a He-Cd laser, although a shoulder was also seen at 3.34 eV. The integrated intensity increased linearly with the pumping power, indicating that the observed peak originated from the spontaneous emission. However, for excitation power above I_{th}, a very sharp and strong PL emission at 3.29 eV predominated that evolved from the low-energy shoulder of the spontaneous emission. Furthermore, the integrated PL intensity increased superlinearly with the pumping power, providing evidence of the stimulated emission. The threshold pumping power of 0.6 MW/cm^2, estimated from the inset in Fig. 2, is similar to the previously reported values of 0.56 to 0.70 MW/cm^2 for GaN thin films on sapphire, silicon (Si), and silicon carbide (SiC) substrates (*14*–*16*).

The heteroepitaxial growth of a high-quality thin film on graphene layers provides a hybrid heterostructure of a three-dimensional bulk single-crystal and a two-dimensional molecular material. When we use graphene layers as a substrate for the heteroepitaxial growth, a potential major advantage is that lattice mismatch may not be considered seriously because the graphene layers have weak bonding to each other. As determined with x-ray diffractometry and transmission elec-

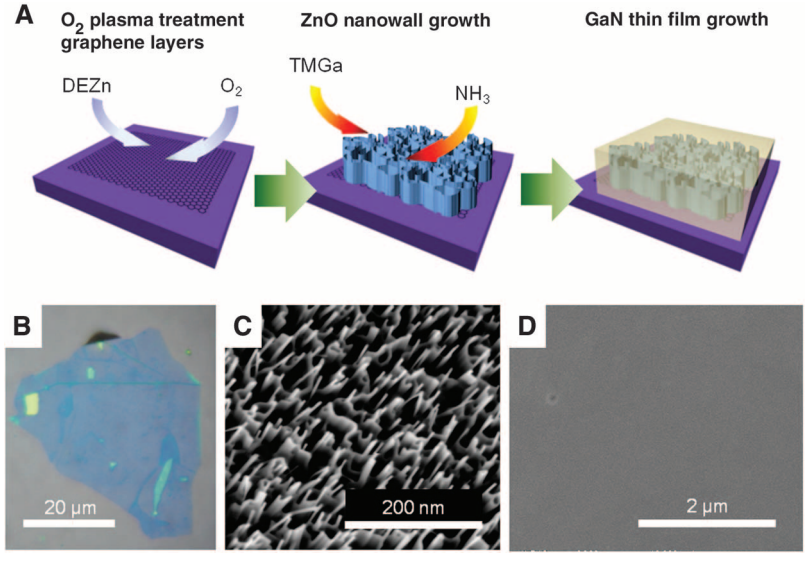

Fig. 1. (**A**) Schematic illustrations of fabrication processes for epitaxial GaN thin films. (**B**) Optical microscopic image of oxygen-plasma–treated graphene layers. (**C** and **D**) SEM images of (C) ZnO nanowalls grown on plasma-treated graphene layers and (D) GaN thin film grown on ZnO nanowalls on plasma-treated graphene layers.

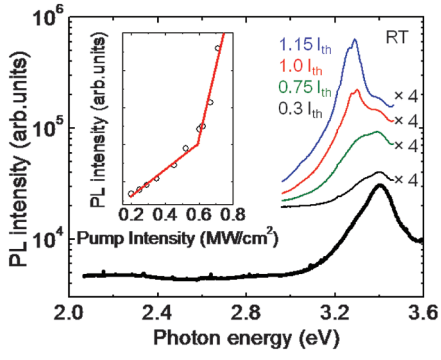

Fig. 2. Room-temperature PL spectra of GaN thin films grown on graphene layers. The thick black line and thin color lines represent the PL spectrum measured by using a continuous-wave He-Cd laser and the power-dependent PL spectra by using a pulsed Nd:YAG laser, respectively. (**Inset**) The integrated emission intensity as a function of the optical excitation.

tron microscopy, GaN films grown on graphene layers are of high crystallinity (figs. S4 and S5). The layered graphene substrates also allow transfer of the thin films onto foreign substrates and for the graphene layers to serve as electrode materials.

Schematic diagrams of the fabrication of GaN thin-film LEDs on graphene layers and their transfer onto foreign substrates are shown in Fig. 3A. To fabricate LED structures, a 2-μm-thick layer of Si-doped *n*-GaN, three-period $In_xGa_{1-x}N$/GaN MQWs, and a 350-nm-thick layer of Mg-doped *p*-GaN were deposited on the flat GaN film grown on graphene layers. For the electroluminescent (EL) devices, the metallic graphene layers underneath *n*-GaN and nickel/gold (Ni/Au) bilayers deposited on the top surface of *p*-GaN were used as *n*- and *p*-type contacts, respectively. After fabricating the devices, thin-film LEDs on the graphene layers were removed mechanically from the original substrate and transferred onto foreign substrates of metal, glass, and plastic.

All transferred devices emitted very strong blue light emissions that could be seen with unaided eyes under normal room illumination. As shown in the optical microscopy image in Fig. 3B, the light emission was fairly uniform over the area of 300 μm by 300 μm, presumably because of uniform current spreading and injection through the metallic bottom electrode—composed of graphene layers—used in this device geometry. Each substrate in Fig. 3B has benefits for LED applications. Metal substrates provide good thermal and electrical conductivity for high-power LEDs, whereas a glass or plastic substrate may allow inorganic LEDs to be fabricated as large-area, full-color LED displays in flexible or stretchable forms. Furthermore, GaN-based epitaxial films on graphene layers may readily be used as functional components of photovoltaic devices.

The EL characteristics of the LED transferred onto plastic were investigated further by measuring power-dependent EL spectra and optical images of emissions at room temperature. The EL spectra and corresponding EL images of the LED at various applied current levels are shown in Fig. 4A. The LED light emission images and the EL spectra show an increase of emission intensity with the applied current levels of 5.1, 6.4, and 8.1 mA. We also observed that the dominant peak shifted from 2.71 to 2.75 eV as the applied current level increased from 1.7 to 8.1 mA. This blue shift can be explained in terms of both a band-filling effect of the localized energy states and a screening effect by the internal polarization electric field typically observed in LEDs with GaN/$In_{1-x}Ga_xN$ MQW structures grown on a polar surface of GaN(0001) (*17*).

In addition to the EL characteristics, the electrical characteristics of the transferable LEDs were investigated by measuring their current-voltage (*I-V*) characteristic curves. The *I-V* characteristic curve of the transferred LED onto plastic in Fig. 4B shows a good rectifying behavior with a turn-on voltage of 4.5 V and a leakage current of 1×10^{-5} A at –4 V, which is similar to those of the as-fabricated LED. However, compared with conventional GaN thin-film LEDs prepared on sapphire substrates the turn-on voltage was slightly higher because of energy barriers at the junctions between the three-material system of graphene, ZnO, and GaN.

Epitaxial nitride thin films grown on graphene layers exhibit both the optical characteristics of the compound semiconductor and the electrical and mechanical characteristics of the graphene layers. The transfer of the materials and devices fabricated on graphene onto foreign substrates should provide advantages in integration and design of electronics and optoelectronic devices.

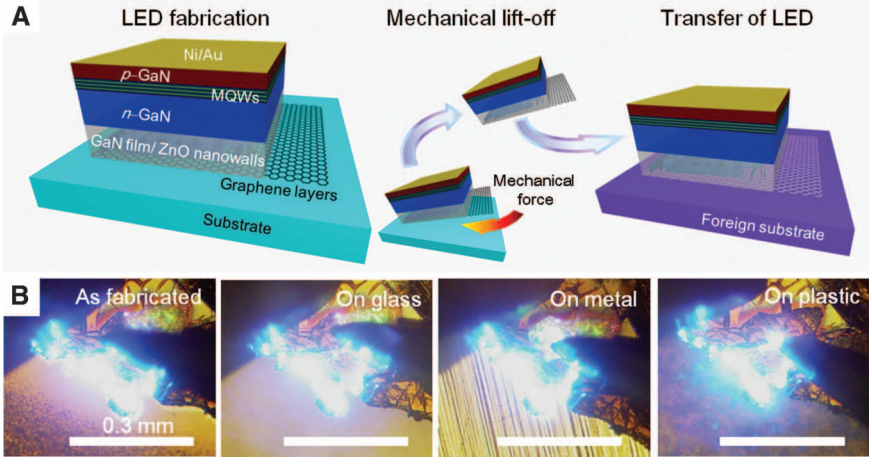

Fig. 3. (**A**) Schematic illustration of the fabrication and transfer processes for thin-film LEDs grown on graphene-layer substrates. (**B**) Optical images of light emissions from the as-fabricated LED on the original substrate and transferred LEDs on the foreign metal, glass, and plastic substrates.

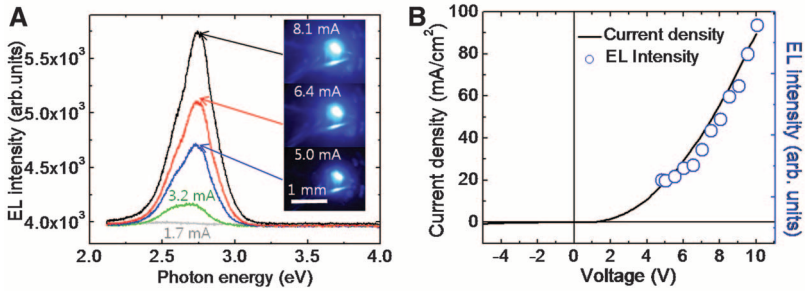

Fig. 4. (**A**) Room-temperature EL spectra of the LED transferred onto a plastic substrate. Optical microscopy images show the light emission at different applied current levels of 1.7 to 8.0 mA. (**B**) Current density and integrated EL intensity as a function of the applied bias voltage of a representative LED on a plastic substrate. The solid line and open circles correspond to the current density and integrated EL intensity, respectively.

References and Notes

1. S. Nakamura, T. Mukai, M. Senoh, *Appl. Phys. Lett.* **64**, 1687 (1994).
2. F. A. Ponce, D. P. Bour, *Nature* **386**, 351 (1997).
3. W. S. Wong, T. Sands, N. W. Cheung, *Appl. Phys. Lett.* **72**, 599 (1998).
4. W. S. Wong *et al.*, *Appl. Phys. Lett.* **75**, 1360 (1999).
5. A. David *et al.*, *Appl. Phys. Lett.* **88**, 133514 (2006).
6. H. K. Cho *et al.*, *IEEE Photon. Technol. Lett.* **20**, 2096 (2008).
7. S. Nakamura, S. Pearton, G. Fasol, *The Blue Laser Diode: The Complete Story* (Springer-Verlag, New York, ed. 2, 2000).
8. D. P. Bour *et al.*, *Appl. Phys. Lett.* **76**, 2182 (2000).
9. K. S. Kim *et al.*, *Nature* **457**, 706 (2009).
10. X. Li *et al.*, *Science* **324**, 1312 (2009).
11. Materials and methods are available as supporting material on *Science* Online.
12. X. Lu, H. Huang, N. Nemchuk, R. S. Ruoff, *Appl. Phys. Lett.* **75**, 193 (1999).
13. Y.-J. Kim, J. H. Lee, G.-C. Yi, *Appl. Phys. Lett.* **95**, 213101 (2009).
14. M. A. Khan, D. T. Olson, J. M. Van Hove, J. N. Kuznia, *Appl. Phys. Lett.* **58**, 1515 (1991).
15. S. Bidnyk *et al.*, *J. Appl. Phys.* **85**, 1792 (1999).
16. G. P. Yablonskii *et al.*, *Phys. Status Solidi A Appl. Mat.* **192**, 54 (2002).
17. E. Kuokstis *et al.*, *Appl. Phys. Lett.* **80**, 977 (2002).

18. This work was financially supported by the National Creative Research Initiative Project (grant R16-2004-004-01001-0) of the Korea Science and Engineering Foundations (KOSEF). G.-C.Y. planned the project; K.C. designed and progressed the experiments; C.-H.L. provided technical support for LED device fabrication and characterization; G.-C.Y. advised on the project; and all authors analyzed the data, interpreted the results, and wrote the manuscript. The authors declare that they have no competing financial interests.

Supporting Online Material

www.sciencemag.org/cgi/content/full/330/6004/655/DC1
Materials and Methods
Figs. S1 to S6
References

21 July 2010; accepted 27 September 2010
10.1126/science.1195403

Large $\delta^{13}C$ Gradients in the Preindustrial North Atlantic Revealed

Are Olsen[1,2]* and Ulysses Ninnemann[2,3]

The carbon isotopic composition ($^{13}C/^{12}C$, expressed as $\delta^{13}C$) of fossil foraminifera is the primary tracer used to infer changes in past ocean ventilation, and its variations are interpreted by using the modern oceanic $\delta^{13}C$ distribution as a framework. However, the present ocean $\delta^{13}C$ distribution is strongly overprinted by isotopically light anthropogenic carbon dioxide. A correction for this oceanic C-13 Suess effect in the North Atlantic (NA) shows that the pristine NA $\delta^{13}C$ distribution has a richer and more detailed structure that is more clearly related to water mass distributions. Our results revise some fundamental perceptions regarding glacial-interglacial ocean $\delta^{13}C$ differences and allow paleo-$\delta^{13}C$ variations to be understood within the context of modern climate variability.

The global distribution of carbon-13/carbon-12 (expressed as $\delta^{13}C$) of dissolved inorganic carbon in seawater as mapped during the GEOSECS (Geochemical Ocean Sections Study) surveys has been the primary frame of reference for interpretation of foraminiferal $\delta^{13}C$, the most used proxy for investigating water mass distributions and carbon cycling in paleo-oceans. Isotopically, the modern North Atlantic (NA) appears to be fairly homogenous and is dominated at depth by a single enriched (low nutrient) water mass, NA Deep Water (NADW) (*1*). Yet sedimentary $\delta^{13}C$ records commonly show values that appear inconsistent with this configuration of the NA. For example, Holocene records reveal what appears to be a much more dynamic NA, with frequent submillenial $\delta^{13}C$ oscillations (*2*), and glacial reconstructions reveal a two-layered NA, with the upper 2000 m filled by Glacial NA Intermediate Water (GNAIW), identified by its uniquely high end-member $\delta^{13}C$ value of 1.5 per mil (‰) not apparent in the modern NA (*3*, *4*).

By the principle of uniformitarianism (*5*), the specific processes determining the modern ocean $\delta^{13}C$ values and gradients are the most likely candidates for affecting past changes. Unfortunately, the details of these processes are obscured, and our perception of the ocean configuration is biased by invasion of isotopically light anthropogenic CO_2 since industrialization (*6*). This is known as the C-13 Suess effect, and, until it is quantified in sufficient detail to resolve the spatial differences of its impact, modern surveys will not provide a fully adequate context for understanding paleo-$\delta^{13}C$ changes. To circumvent this, we introduce a two-stage method that quantifies the C-13 Suess effect on a sample by sample basis in the North Atlantic (*7*) and show how it has erased the $\delta^{13}C$ signatures of key NA water masses and smoothed preanthropogenic ocean gradients, substantially complicating the interpretation of paleo-$\delta^{13}C$ records.

The distribution of $\delta^{13}C$ as observed in 1993 (Fig. 1A) appears even more homogenous than the GEOSECS distribution (*1*), demonstrating the increasing Suess effect over the two decades separating these campaigns. In stark contrast, the section of reconstructed preindustrial $\delta^{13}C$, $\delta^{13}C^{PI}$ (Fig. 1B), reveals a rich structure where the water masses [as identified in (*7*)] have much more distinct signatures (Figs. 1B and 2). Perhaps most notable is the emergence of a tongue of high $\delta^{13}C^{PI}$ associated with Labrador Sea Water (LSW) in the mid-depth NA south to about 40°N, suggesting that this water mass plays a much more important role in setting NA $\delta^{13}C$ than previously recognized (both through direct ventilation and as a potential source of high $\delta^{13}C$ water for entrainment by Nordic Seas overflows). Over recent decades, changes in the distribution of LSW have occurred in response to the North Atlantic Oscillation (NAO) (*8*); following periods of strong negative NAO forcing, the layer of LSW in the mid-depth subpolar NA thins, shifting the boundary between LSW and Northeast Atlantic Deep Water (NEADW) to shallower depths. Conversely, strong positive NAO forcing leads to thickening of the layer of LSW, shifting the boundary deeper. Such variability in the past could be an important influence on NA $\delta^{13}C$ sedimentary records and particularly on those located near the boundary of LSW, where there are strong water mass–related $\delta^{13}C^{PI}$ gradients. For example, shifts in the LSW-NEADW boundary relative to the core site designated in Fig. 1B could explain all but the largest of the Holocene $\delta^{13}C$ variations observed at this location (*2*).

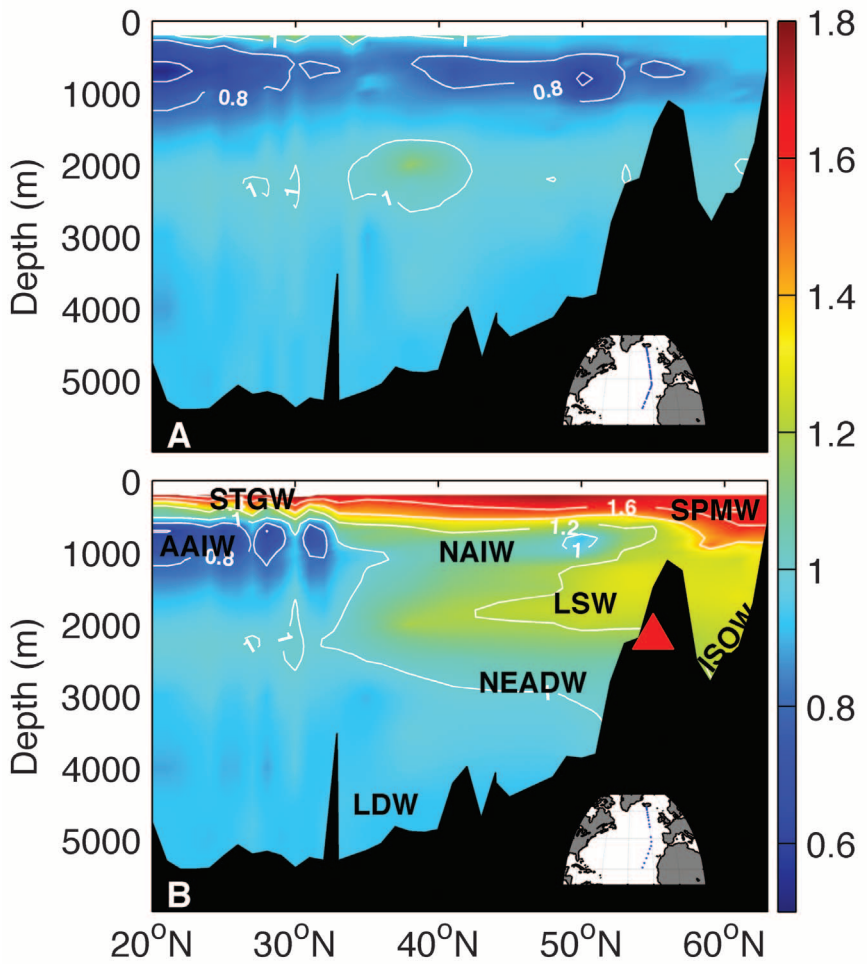

Fig. 1. Section of 1993 $\delta^{13}C$ (**A**) and $\delta^{13}C^{PI}$ (**B**) reconstructed as described in (*7*), along 20°W in the North Atlantic. The red triangle shows the location of the core used by (*2*), at 55°N, 15°W and depth of 2179 m, projected onto our section. The water masses were identified in (*7*) and have been labeled accordingly. AAIW, Antarctic Intermediate Water; see text for the other abbreviations.

[1]Uni Bjerknes Centre, Allégaten 55, N-5007 Bergen, Norway. [2]Bjerknes Centre for Climate Research, Allégaten 55, N-5007 Bergen, Norway. [3]Department of Earth Science, University of Bergen, Allégaten 41, N-5007 Bergen, Norway.

*To whom correspondence should be addressed. E-mail: are.olsen@uni.no

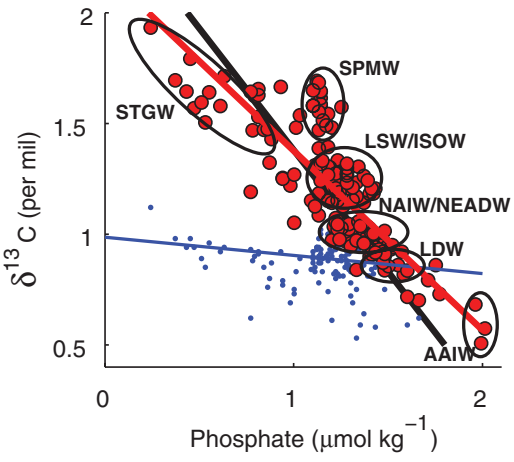

Fig. 2. Relationship between phosphate and $\delta^{13}C$ (blue) and $\delta^{13}C^{PI}$ (red) with linear regression lines as determined from samples obtained deeper than 200 m north of 20°N at the 1993 Malcolm Baldridge cruise. The black line is the –1.1 relationship expected in the absence of thermodynamic fractionation (*10*). Ellipses indicate typical $\delta^{13}C^{PI}$ and PO_4 values for the different water masses.

In addition to the LSW, other high-$\delta^{13}C^{PI}$ water masses such as Subpolar Mode Water (SPMW), Iceland Scotland Overflow Water (ISOW), and Subtropical Gyre Water (STGW) are also apparent. Indeed, accounting for the C-13 Suess effect strengthens the overall NA $\delta^{13}C$-versus-phosphate (PO_4) relationship (Fig. 2). Our preindustrial $\delta^{13}C$-PO_4 slope of –0.7‰ is essentially identical to the slope estimated through an independent approach (*9*) and close to the expected biological regression (*10*). Although there are still distinct thermodynamic isotopic signatures between southern and northern Atlantic water masses (i.e., warm STGW and cold SPMW are, respectively, depleted and enriched in $\delta^{13}C$ relative to their nutrient levels), our analysis reveals that the NA $\delta^{13}C$ is more strongly influenced by biological processes than previously appreciated.

Having defined the pristine NA $\delta^{13}C$ distribution allows us to better discern the similarities and differences between the modern and glacial oceans. NA $\delta^{13}C^{PI}$ shows notable similarities with reconstructed glacial NA $\delta^{13}C$. After correction, the SPMW end-member value (1.5 to 1.7‰) is about equal to that of the GNAIW of 1.5‰ (*3*). Thus, our reconstruction effectively removes at least one of the perceived differences between the glacial and present NA: the higher glacial northern end-member $\delta^{13}C$. Further, STGW samples have among the highest $\delta^{13}C^{PI}$ values found in our section (Fig. 2), suggesting that, just as proposed for the glacial ocean (*3*), elevated $\delta^{13}C$ in subtropical feed waters are important for achieving the high $\delta^{13}C$ of NA water masses (e.g., GNAIW). In summary, changes in water mass formation processes are not necessarily required to explain the high GNAIW end-member $\delta^{13}C$ values.

Despite these similarities, the glacial ocean was still distinct in a number of ways. The higher $\delta^{13}C$ values found in the modern deep (>2 km) NA ocean relative to glacial (*4*) cannot be a byproduct of the C-13 Suess effect. Likewise, if glacial water mass formation processes (end-member $\delta^{13}C$ values) were similar to today, other processes must be invoked to explain the geographic expansion of high $\delta^{13}C$ waters in the upper 2 km of the Atlantic (*4*). Taken together, our analysis emphasizes the role of water mass geometry and/or renewal rates (as opposed to end-member changes) in affecting glacial-interglacial $\delta^{13}C$ differences.

Our C-13 Suess effect correction elucidates the influence of individual components of NADW on ocean $\delta^{13}C$ and allows both rapid and large NA downcore $\delta^{13}C$ variability to be understood in the context of existing water masses. Comprehensive application of our C-13 Suess correction, for example, during the GEOTRACES program, would allow paleoceanographers to fully use the potential contained within the vast database of sedimentary $\delta^{13}C$ accumulated in recent decades. Ultimately, such a $\delta^{13}C^{PI}$ database is needed to provide accurate reference fields both for model evaluation and to achieve the improved proxy calibration and uncertainty estimates required to infer and quantify changes in past ocean circulation (*11*).

References and Notes

1. P. M. Kroopnick, *Deep-Sea Res.* **32**, 57 (1985).
2. D. W. Oppo, J. F. McManus, J. L. Cullen, *Nature* **422**, 277 (2003).
3. D. W. Oppo, S. J. Lehman, *Science* **259**, 1148 (1993).
4. W. B. Curry, D. W. Oppo, *Paleoceanography* **20**, PA1017 (2005).
5. C. Lyell, *The Principles of Geology* (Murray, London, 1830–1833).
6. P. D. Quay, B. Tilbrook, C. S. Wong, *Science* **256**, 74 (1992).
7. Information on material and methods, as well as water mass distribution, is available as supporting material on *Science* Online.
8. I. Yashayaev, A. Clarke, *Oceanography* **21**, 30 (2008).
9. R. Keir, G. Rehder, E. Suess, H. Erlenkeuser, *Global Biogeochem. Cycles* **12**, 467 (1998).
10. W. S. Broecker, E. Maier-Reimer, *Global Biogeochem. Cycles* **6**, 315 (1992).
11. O. Marchal, W. B. Curry, *J. Phys. Oceanogr.* **38**, 2014 (2008).

12. This work was supported by funding from the Norwegian Research Council (A-CARB) and contributes to EU-FP7 IP Past4Future. It is publication no. A305 from the Bjerknes Centre for Climate Research.

Supporting Online Material

www.sciencemag.org/cgi/content/full/330/6004/658/DC1
Materials and Methods
SOM Text
Figs. S1 and S2
References and Notes

15 June 2010; accepted 17 September 2010
10.1126/science.1193769

Early Use of Pressure Flaking on Lithic Artifacts at Blombos Cave, South Africa

Vincent Mourre,[1,2] Paola Villa,[3,4,5]* Christopher S. Henshilwood[6,7]

Pressure flaking has been considered to be an Upper Paleolithic innovation dating to ~20,000 years ago (20 ka). Replication experiments show that pressure flaking best explains the morphology of lithic artifacts recovered from the ~75-ka Middle Stone Age levels at Blombos Cave, South Africa. The technique was used during the final shaping of Still Bay bifacial points made on heat-treated silcrete. Application of this innovative technique allowed for a high degree of control during the detachment of individual flakes, resulting in thinner, narrower, and sharper tips on bifacial points. This technology may have been first invented and used sporadically in Africa before its later widespread adoption.

Pressure flaking is a retouching (*1*) technique used by prehistoric knappers to shape stone artifacts by exerting a pressure with the narrow end of a tool close to the edge of a worked piece. The earliest evidence of pressure flaking (*2*, *3*) was thought to come from the Upper Paleolithic Solutrean industry of Western Europe dating to ~20,000 years ago (20 ka) (*4*–*6*). In later times, it was used to produce Paleoindian projectile points (*7*), microlithic backed tools in the Later Stone Age of Africa (*8*), and bifacial arrowheads in the Holocene of North America and Australia (*9*, *10*). Retouch by pressure provides the flintknapper with a degree of control over the final shape, regularity, and thinness of the tool edge that cannot be achieved by direct percussion.

With the exception of obsidian, jasper, and some high-quality flint (*11*), few lithic materials

[1]INRAP Méditerranée, 561 rue Étienne Lenoir-KM Delta, 30900 Nîmes, France. [2]TRACES-UMR 5608, Université de Toulouse-Le Mirail, 31058 Toulouse, France. [3]University of Colorado Museum, Boulder, CO 80309–0265, USA. [4]Institut de Préhistoire et Géologie du Quaternaire, UMR 5199 PACEA, Université Bordeaux 1, 33405 Talence, France. [5]School of Geography and Environmental Studies, University of the Witwatersrand, Johannesburg, South Africa. [6]Institute for Archaeology, History, Culture and Religion, University of Bergen, Bergen, Norway. [7]Institute for Human Evolution, University of the Witwatersrand, Johannesburg, South Africa.

*To whom correspondence should be addressed. E-mail: villap@colorado.edu

can be pressure-flaked in their natural state, but heat treatment can improve the flaking quality of some of them (*12*). Early evidence for heat treatment of silcrete at ~164 ka comes from Pinnacle Point, southern Cape, South Africa (*13*).

Here, we show through experimental replication and microscopic study that silcrete artifacts from the ~75-ka Still Bay levels at Blombos Cave (*14*) (fig. S1) were also heat-treated before flaking and that pressure flaking was used during the final retouch phase of the Still Bay points. These bifacial points were axially hafted, and impact scars on recovered tools demonstrate that they were used as hunting weapons (*15*).

The manufacturing sequence of the Blombos Still Bay points can be divided into four production phases (*15*) (fig. S2). Direct percussion by hard hammer is used in the initial shaping (production phase 1). Advanced shaping is done by soft hammer marginal percussion (phase 2a with hard and soft hammer scars and phase 2b with only soft hammer scars). In the final phase (phase 3), retouch is applied to the edges, especially the tip. A small number of points were reworked by hard hammer percussion (phase 4). Here, we examine the finished products of production phase 3 and compare them with those from phase 2b.

Heat-treated silcrete can be recognized through the application of thermoluminescence and archeomagnetism, both destructive methods, and maximum gloss analysis that is nondestructive (*13*). We used a visual method commonly used to identify heat treatment on Paleoindian and Solutrean points [supporting online material (SOM)]. After the removal of a flake from unheated silcrete, the scar surface will have a rough, dull texture. If a silcrete piece had been heat-treated first, then the scar surface will have a smooth, glossy appearance. The contrast between the two surfaces is visible at low magnification (fig. S3). The visual method is based on contrast between the two types of surfaces; thus, it can be securely identified only on pieces where surfaces flaked before heating have not been completely removed by postheating intensive flaking (table S1). Because heating precedes the advanced flaking phases of the artifacts, it must have been a phase in the knapping process, before the final phase of retouch, and not accidental.

Different knapping techniques result in flake scar patterns with characteristic combinations of attributes (*16*–*18*). Experimental replication on the local raw material is essential to recognize the distinctive markers of different techniques. We collected silcrete from outcrops located ~30 km from Blombos Cave. Some were heat-treated following the method in (*13*). Blanks of unheated and heated silcrete were knapped with quartzite stone hammers and a wooden billet for the first phases of reduction. A bone flaker was used during the final pressure-retouching of the points.

Silcrete in its natural state can be flaked by hard hammer and can be trimmed by soft organic or soft stone hammer. However, during our experiments we found that the final phases of retouch (phase 3) observable on the Blombos bifacial points cannot be executed on unheated silcrete. For pressure flaking to be successful, the silcrete needs to be heat-treated. Regularity and parallelism of scars is considered the main trait of pressure flaking (*12*) (fig. S4). On flint, pressure will produce subparallel and rectilinear retouch scars with 10 to 15 mm of maximal length and up to 4 to 5 mm wide (*19*). However, the technical features described for flint are different from those observed on the Blombos bifacial points. It was on the basis of the flint features that we previously rejected the hypothesis of pressure retouch on the Blombos points (*15*).

Our experiments showed that wider flakes (up to 10 mm wide) can be detached by pressure retouch on heated silcrete and that the resultant scars are not always subparallel and rectilinear.

Table 1. Attributes of experimental flakes made by pressure and by marginal percussion with a soft hammer, compared to a sample of flakes from layer CC at Blombos. All flakes are ≤1 cm, to avoid differences that might be due to size.

Flake attributes	Experimental				Blombos layer CC	
	Pressure		Percussion by soft hammer			
	(*n* = 30)		(*n* = 30)		(*n* = 60)	
	n	%	*n*	%	*n*	%
Prominent bulb	28	93.3	4	13.3	21	35.0
Bulb without a lip	29	96.7	11	36.7	30	50.0
Small but not punctiform platform	29	96.7	24	80.0	49	81.7
Regular ridges	19	63.3	11	36.7	32	53.3
Hackles on the bulb	13	43.3	1	3.3	18	30.0

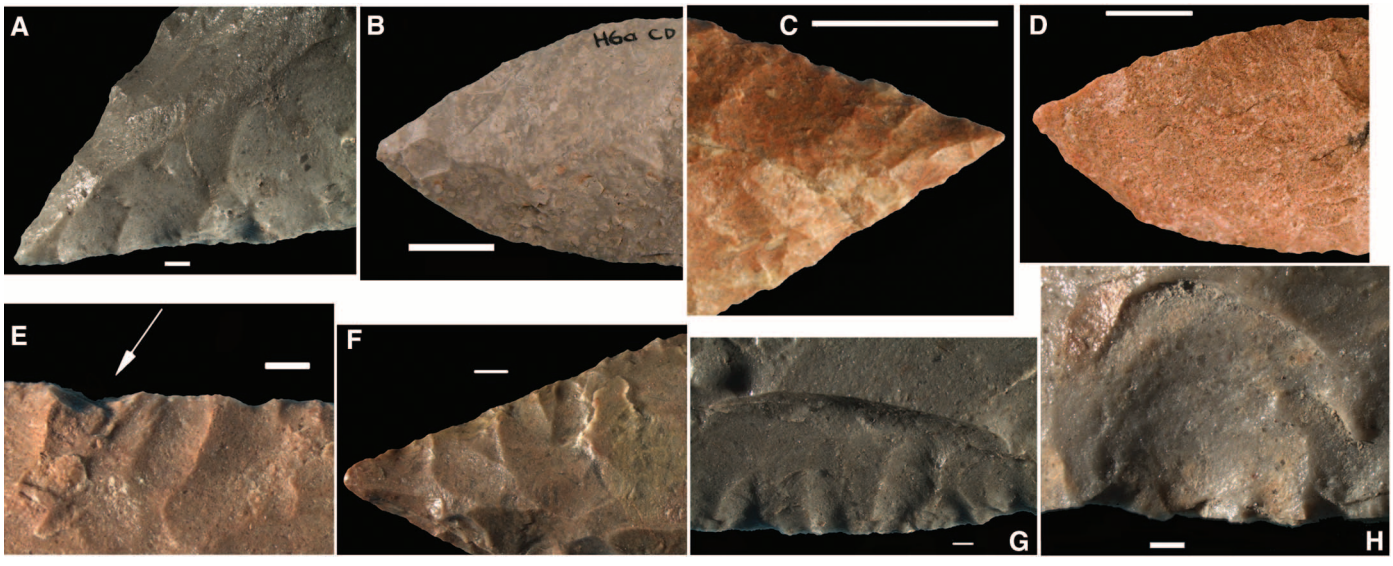

Fig. 1. Blombos Still Bay bifacial points, all production phase 3 except (D). (**A** to **D**) Examples of tip shapes; (**E** to **H**) examples of scar attributes diagnostic of pressure. (A) V-shaped tip with straight edges, PVN 45. (B) Arched tip with curved edges, PVN 66. (C) V-shaped tip with straight edges, P. 68. (D) Tip with irregular, asymmetrical sides, PVN 27, phase 2b. (E) Hackles (white arrow) on the bulb negative, PVN 84. (F) Regular ridges, PVN 68. (G) Pressure scars with deep bulb negatives inside a larger scar by direct percussion, PVN 45. (H) Deep bulb negative, Mus.2. Scale bars: (A, E to H), 1 mm; (B to D), 1 cm.

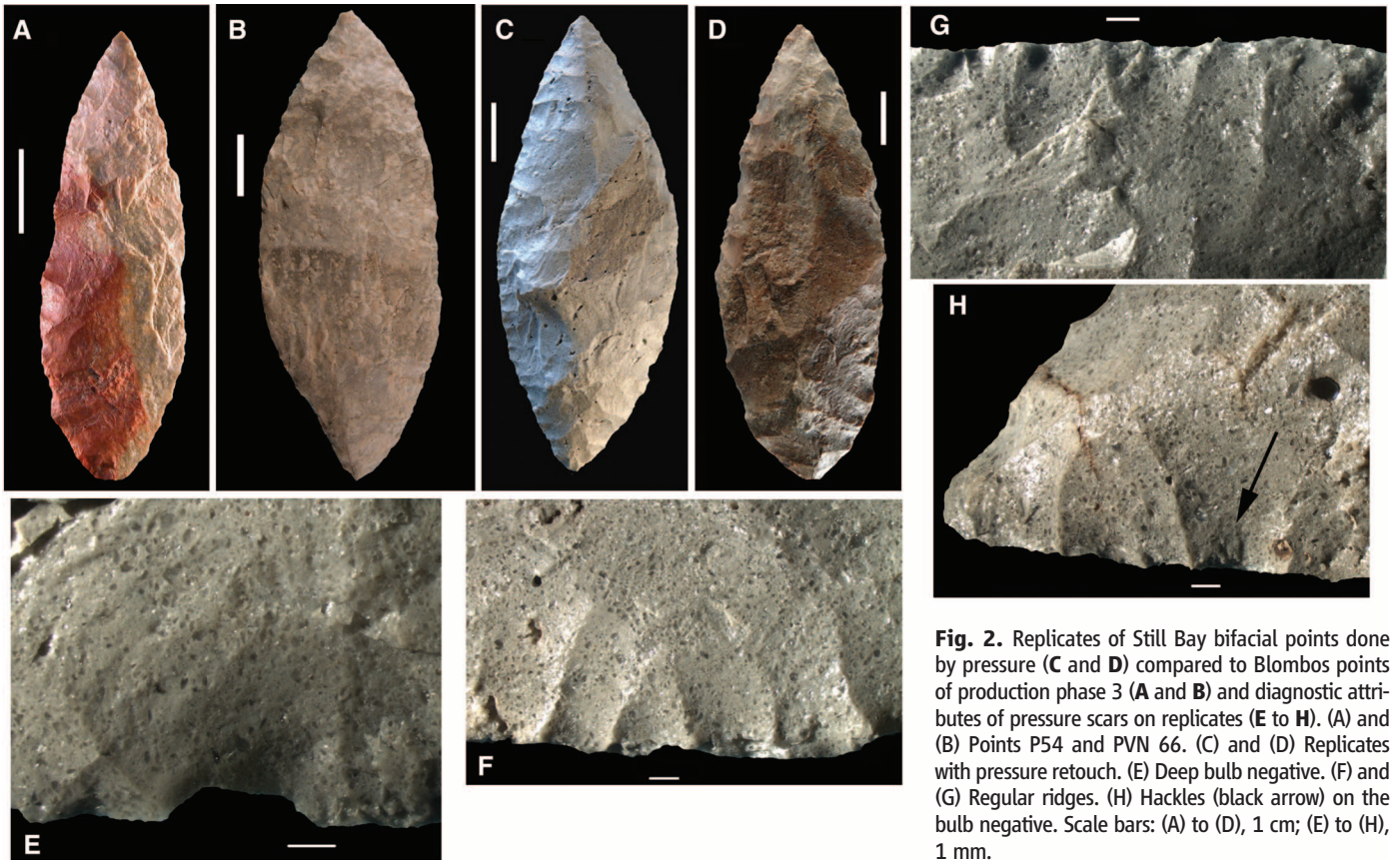

Fig. 2. Replicates of Still Bay bifacial points done by pressure (**C** and **D**) compared to Blombos points of production phase 3 (**A** and **B**) and diagnostic attributes of pressure scars on replicates (**E** to **H**). (A) and (B) Points P54 and PVN 66. (C) and (D) Replicates with pressure retouch. (E) Deep bulb negative. (F) and (G) Regular ridges. (H) Hackles (black arrow) on the bulb negative. Scale bars: (A) to (D), 1 cm; (E) to (H), 1 mm.

Table 2. Frequencies of attributes for the identification of flaking techniques and tip measurements of the Blombos Still Bay points compared to unifacial points from the post-Howiesons Poort of Sibudu (database of P. Villa).

Attributes	Phase 2b		Phase 3	
	n	%	*n*	%
Scar width ≤10 mm	24/50	48.0	55/55	100
Deep bulb negative	10/24	41.7	50/55	90.9
Regular ridges	7/24	29.2	43/55	78.2
V-shaped tip with straight edges	0/15	0	21/43	48.8
Hackles on the bulb negative	0/24	0	17/55	30.9

Tip angle (degrees)	Mean	SD	*n*
Phase 3 points			
V-shaped tip with straight edges	51.2	6.8	21
Arched tip with curved edges	63.2	6.5	20
Phase 2b points			
Tip with irregular or asymmetrical edges	65.4	7.0	11
Unifacial points from post-Howiesons Poort (HP) layers at Sibudu (RSp-MOD ~47 ka)	65.9	11.1	83

Tip thickness (mm)	Mean	SD	N
Phase 3 points	3.7	0.7	44
Phase 2b points	4.5	1.0	11
Unifacial points from post-HP layers at Sibudu (RSp-MOD ~47 ka)	5	1.4	84

Our analysis also provided a number of criteria to distinguish between pressure and soft hammer flaking (Table 1, Figs. 1 and 2, and figs. S5 to S7). Three of the attributes in Table 1 (a prominent bulb, no lip on the bulb, and hackles on the bulb) occurred in high proportions on pressure flakes, in contrast to flakes made by soft hammer. χ^2 values are high ($P < 0.001$ in all cases; SOM). Two other features (small platforms and regular ridges) seem less useful for discriminating between the two techniques. Intermediate frequency values in the Blombos flake sample show that both techniques were used by the tool makers.

The distinctiveness of the two flaking modes is also seen in the frequency distribution of scar dimensions (table S2). The mean width and length of scars on Blombos production phase 3 points are similar to those of experimental scars by pressure, whereas the scars of phase 2b points are more similar to the scars of our experimental soft hammer percussion points. To identify the flaking technique used on the Blombos bifacial points, we calculated the frequencies of five attributes (Table 2). Four of these were observed on experimental pressure scars and flakes (deep bulb negative, hackles on the bulb negative, scars ≤10 mm, and regular ridges; Figs. 1 and 2). Another attribute (V-shaped tips with straight edges) is based on expectations of rectilinear edges made by pressure (fig. S4, E and F). Two attributes, V-shaped tips with straight edges and hackles on the bulb negative, do not occur at all on phase 2b points made by soft hammer. Thus, those two features discriminate between the two techniques. On phase 3 points, these features are consistently associated with two other distinctive attributes (deep bulb negative and regular ridges). We conclude that at least half of the production phase 3 points were

finished with the pressure technique to make the tip sides straight and regular.

The penetrating angle and tip thickness of phase 3 points are significantly smaller than those of phase 2b, inferred to have been made by direct percussion. They are also smaller than the tip angle and thickness of unifacial points produced on flakes retouched by direct percussion during post-Howiesons Poort to final Middle Stone Age (MSA) times in South Africa, ~58 to 40 ka, (*20*, *21*). T tests for tip angle and tip thickness of phase 3, 2b, and unifacial points show that differences between all three samples are significant (SOM). These differences confirm the advantages of using the pressure technique to obtain points with thinner, V-shaped tips with straight edges.

There are no known antecedents to the intensively flaked Still Bay bifacial points from Blombos, or evidence for earlier pressure flaking, in the MSA (*22*). After 72 ka, bifacial technology disappears in South Africa and is replaced after 65 ka by Howiesons Poort–type backed tools (*23*). Pressure flaking adds to the repertoire of technological advances during the Still Bay (*24*–*26*) and helps define it as a time when novel ideas and techniques were rapidly introduced. This flexible approach to technology may have conferred an advantage to the groups of *Homo sapiens* who migrated out of Africa after ~60 ka (*27*).

References and Notes

1. The use of pressure to remove blades and bladelets from a core is a more complex technique that appears in Northern Asia at about 25 ka (*12*).
2. Possible evidence of heat treatment and pressure retouch has been suggested (*3*) for the Early Upper Paleolithic Streletskayan bifacial points of Kostienki 1.
3. B. A. Bradley, M. Anikovich, E. Giria, *Antiquity* **69**, 989 (1995).
4. M. Tiffagom, *Paléo* **10**, 147 (1998).
5. T. Aubry, B. Walter, E. Robin, H. Plisson, M. Ben-Habdelhadi, *Paléo* **10**, 163 (1998).
6. M.-L. Inizan, J. Tixier, *Paléorient* **26**, 23 (2001).
7. F. Sellet, *J. Archaeol. Sci.* **31**, 1553 (2004).
8. C. B. Bousman, *J. Anthropol. Archaeol.* **24**, 193 (2005).
9. G. C. Frison, *Prehistoric Hunters of the High Plains* (Academic Press, San Diego, 1991).
10. R. Harrison, *Archaeol. Oceania* **39**, 1 (2004).
11. D. E. Crabtree, *Tebiwa* **10**, 8 (1967).
12. M.-L. Inizan, M. Reduron-Ballinger, H. Roche, J. Tixier, *Technology and Terminology of Flaked Stone* (CREP, Nanterre, 1999).
13. K. S. Brown *et al.*, *Science* **325**, 859 (2009).
14. Z. Jacobs, G. A. T. Duller, A. G. Wintle, C. S. Henshilwood, *J. Hum. Evol.* **51**, 255 (2006).
15. P. Villa, M. Soressi, C. S. Henshilwood, V. Mourre, *J. Archaeol. Sci.* **36**, 441 (2009).
16. K. Ohnuma, C. Bergman, *Bull. Inst. Arch. London* **19**, 161 (1982).
17. J. Pelegrin, in *L'Europe centrale et septentrionale au Tardiglaciaire*, B. Valentin, P. Bodu, M. Christensen, Eds. (Mémoire du Musée de Préhistoire d'Ile-de-France 7, Nemours, 2000), pp. 73–86.
18. S. Soriano, P. Villa, L. Wadley, *J. Archaeol. Sci.* **34**, 681 (2007).
19. H. Plisson, J.-M. Geneste, *Paléo* **1**, 65 (1989).
20. Z. Jacobs, A. G. Wintle, G. A. T. Duller, R. G. Roberts, L. Wadley, *J. Archaeol. Sci.* **35**, 1790 (2008).
21. P. Villa, M. Lenoir, *Southern African Humanities* **18**, 89 (2006).
22. R. Singer, J. Wymer, *The Middle Stone Age at Klasies River Mouth in South Africa* (Chicago Univ. Press, Chicago, 1982).
23. P. Villa, S. Soriano, N. Teyssandier, S. Wurz, *J. Archaeol. Sci.* **37**, 630 (2010).
24. C. S. Henshilwood, F. d'Errico, I. Watts, *J. Hum. Evol.* **57**, 27 (2009).
25. F. d'Errico, C. S. Henshilwood, *J. Hum. Evol.* **52**, 142 (2007).
26. C. S. Henshilwood, F. d'Errico, M. Vanhaeren, K. van Niekerk, Z. Jacobs, *Science* **304**, 404 (2004).
27. H. Liu, F. Prugnolle, A. Manica, F. Balloux, *Am. J. Hum. Genet.* **79**, 230 (2006).

28. This research was funded by the Wenner-Gren Foundation (grant to P.V.). V.M.'s work was facilitated by a research convention between Inrap and the University of the Witwatersrand. Financial support was provided to C.S.H. by a European Research Council Advanced Grant TRACSYMBOLS (FP7 No. 249587); by a National Research Foundation/Department of Science and Technology–funded Chair at the University of the Witwatersrand, South Africa; by a Norwegian Research Council Grant; and by a PROTEA French–South Africa exchange program. We thank K. Brown for sharing information about silcrete heating and helping us in the experiments. V.M. thanks N. Schlanger for assistance. The Iziko Museum in Cape Town provided space and working facilities.

Supporting Online Materials

www.sciencemag.org/cgi/content/full/330/6004/659/DC1
Materials and Methods
Figs. S1 to S7
Tables S1 and S2
References

23 July 2010; accepted 16 September 2010
10.1126/science.1195550

Fitness Correlates of Heritable Variation in Antibody Responsiveness in a Wild Mammal

Andrea L. Graham,[1,2,3,4]* Adam D. Hayward,[2] Kathryn A. Watt,[2,3] Jill G. Pilkington,[2] Josephine M. Pemberton,[2] Daniel H. Nussey[2,4]

A functional immune system is important for survival in natural environments, where individuals are frequently exposed to parasites. Yet strong immune responses may have fitness costs if they deplete limited energetic resources or cause autoimmune disease. We have found associations between fitness and heritable self-reactive antibody responsiveness in a wild population of Soay sheep. The occurrence of self-reactive antibodies correlated with overall antibody responsiveness and was associated with reduced reproduction in adults of both sexes. However, in females, the presence of self-reactive antibodies was positively associated with adult survival during harsh winters. Our results highlight the complex effects of natural selection on immune responsiveness and suggest that fitness trade-offs may maintain immunoheterogeneity, including genetic variation in autoimmune susceptibility.

Immune systems of different individuals are notoriously heterogeneous in the strength, specificity, and efficacy of responses to infection, and much of the variation is under genetic control (*1*, *2*). Individuals likewise vary in their genetic susceptibility to generate self-targeted immune responses (autoimmunity) (*3*–*7*). The challenge is to explain why natural selection has failed to eliminate alleles that confer susceptibility to infection (*2*) or promote autoimmunity (*8*). One hypothesis is that individuals with strong immune responses experience fitness benefits of immunity (e.g., clearance of infection to promote survival or provision of maternal antibodies to promote offspring survival) but are also likely to suffer its costs (e.g., energetic drain and/or autoimmune disease) (*9*, *10*). Although wild rodents have autoimmune susceptibility genes (*3*) and higher standing antibody concentrations than their laboratory counterparts (*11*), autoimmunity is known only in people and laboratory, domestic, or captive mammals (*7*, *8*, *12*–*14*). Here, we assess the associations among antibody responses, survival, and traits associated with reproductive success in the wild.

The unmanaged population of Soay sheep (*Ovis aries*) in Village Bay, Hirta, St. Kilda, has been monitored since 1985, yielding detailed longitudinal information on both individual life histories and population dynamics (*15*). Using blood plasma samples collected during August of 11 years (1997 to 2007), we measured the concentration of antibodies that bind mammalian nuclear and cytoplasmic antigens (hereafter, antinuclear antibodies, or ANAs) (*12*, *16*, *17*). High concentrations of ANAs are indicative of high rates of division and antibody production by B and plasma cells (*18*), particularly in response to self-antigens (*6*). It is important to note that self-reactivity can represent a side effect of normal immune function (*19*, *20*). For example, although ANAs are potential markers of autoimmunity, they are also associated with useful defense mechanisms, such as natural antibodies (*20*). Only if ANAs are sustained at high titers, in combination with other markers, are they associated with autoimmune diseases like systemic lupus erythematosus in people and dogs (*12*, *16*).

ANAs were detectable in wild sheep at a prevalence comparable to that in human populations (*21*–*23*). We assayed 2622 plasma samples collected from 1476 sheep, so individual sheep were sampled 1.8 times, on average. We

[1]Department of Ecology and Evolutionary Biology, Princeton University, Princeton, NJ 08544, USA. [2]Institute of Evolutionary Biology, University of Edinburgh, Edinburgh EH9 3JT, Scotland. [3]Institute of Immunology and Infection Research, University of Edinburgh, Edinburgh EH9 3JT, Scotland. [4]Centre for Immunity, Infection and Evolution, School of Biological Sciences, University of Edinburgh, Edinburgh EH9 3JT, Scotland.

*To whom correspondence should be addressed. E-mail: algraham@princeton.edu

found that 252 samples from 170 sheep (11.5% of sheep tested) contained ANAs at concentrations that would exceed common clinical definitions for ANA positivity (*12*, *18*, *21*), as confirmed by end-point dilution analyses (*17*). Among 410 adult females [average life span, 6.0 years (*17*)], 114 (27.8%) were positive for ANA, whereas 21 out of 144 adult males [14.6%; average life span, 3.4 years (*17*)] were positive (Fig. 1A). ANA concentration increased with age from lambs to yearlings to adults ($F_{2,2342} = 416.9$, $P < 0.001$), and although sex differences were not apparent in subadult age classes, adult females had significantly higher ANAs than adult males [$F_{1,612} = 5.64$, $P = 0.018$ (figs. S1 to S3)]. The same patterns were observed if ANA positivity was analyzed instead of ANA concentration (fig. S1C). These results match trends reported in humans (*23*) and show that wild mammals experiencing food limitation and high parasite abundance (*15*), two factors hypothesized to decrease the strength and self-reactivity of immune responses (*8*), can still mount self-directed antibody responses.

To assess the overall antibody repertoire in ANA-positive sheep, we undertook further immunological analysis of that subset of samples (*17*). Concentrations of (i) total immunoglobulin G (IgG); (ii) antibodies to ribonucleoprotein, a self-antigen predictive of autoimmune disease in people (*16*); and (iii) antibodies to *Teladorsagia circumcincta,* a prevalent parasitic nematode in sheep (*15*), were all positively correlated with ANAs [correlation coefficients of 0.28, 0.30, and 0.22, respectively; all $P < 0.001$; (*17*)]. These modest but significant correlations accounted for 49% of the variation in antibody concentrations among ANA-positive sheep (*17*). This suggests that ANA concentration may reflect general antibody responsiveness.

Among-individual variation in ANA concentration was considerable, accounting for 37.4% (±4.4 SE) of the total variance (Fig. 1B and table S1). We fitted a quantitative genetic "animal model" (*17*), which uses information on relatedness among individuals from the population pedigree to estimate the contribution of additive genetic factors to variation in continuous traits (*24*, *25*). A significant proportion of ANA heterogeneity was attributed to additive genetic effects [$\chi^2(1) = 14.48$, $P < 0.001$; (table S1)], such that about one-third of the among-individual variation and one-eighth of the total phenotypic variance were genetically based (Fig. 1B) (narrow sense heritability of ANAs = 0.13 ± 0.03 SE). This was confirmed in separate age and sex subsets of the population (table S1).

We next examined the associations between ANAs and different components of fitness, including survival and fecundity in both sexes and traits associated with offspring survival (*17*). We found no evidence for associations with survival of lambs or yearlings (*17*) and so focused on adults. The population dynamics of the Soay sheep on Hirta are characterized by years of rising and high density followed by winter crashes (Fig. 2A), which account for most mortality in the population (*26*, *27*). We tested whether the strength or direction of selection on ANA varied according to whether it was a "crash" year (*17*).

We found evidence for an environment-dependent association of survival with high ANAs in adult female sheep (Fig. 2). ANAs increased linearly with age at measurement [$F_{1,798} = 21.80$, $P < 0.001$; (fig. S3A)], but this cross-sectional change was caused by females with high average ANAs living longer than females with low average ANAs (fig. S3B), rather than increases in ANAs with the age of individuals (fig. S3C) (*17*). Analyses of annual survival probability confirmed this result and further revealed that an association with survival was only apparent during crash winters [ANA-by-crash interaction: $\chi^2(1) = 4.27$, $P = 0.039$; (Fig. 2, B and C)]. There was no evidence for associations between ANAs and male survival, which could reflect true sex

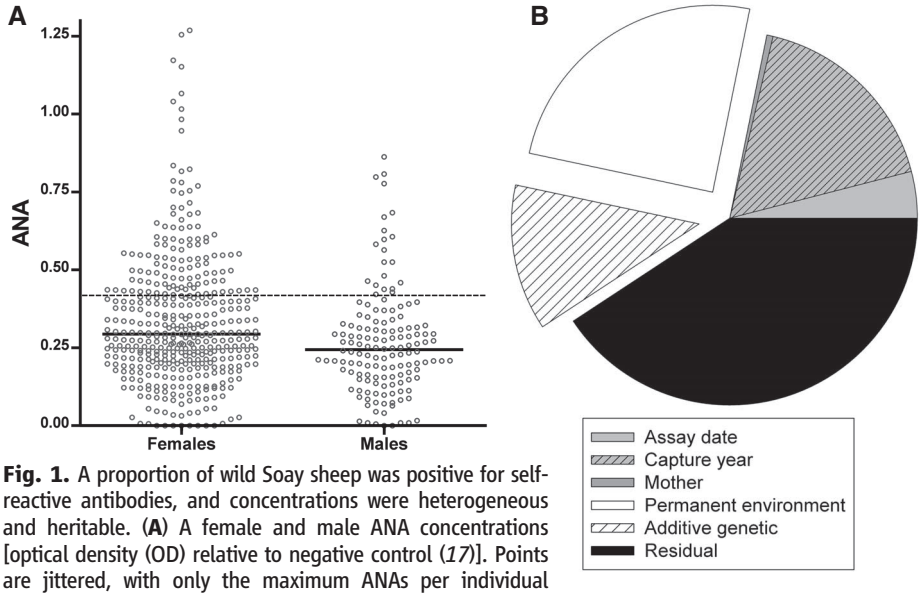

Fig. 1. A proportion of wild Soay sheep was positive for self-reactive antibodies, and concentrations were heterogeneous and heritable. (**A**) A female and male ANA concentrations [optical density (OD) relative to negative control (*17*)]. Points are jittered, with only the maximum ANAs per individual plotted. Unbroken lines represent medians, and the broken line is the 1:200 end-point dilution threshold for positivity (*17*). (**B**) Relative contributions of different components to total variance in ANAs (after controlling for age, sex, body mass, and assay background). The exploded sections represent the total among-individual variance, and the additive genetic component was significantly different from zero.

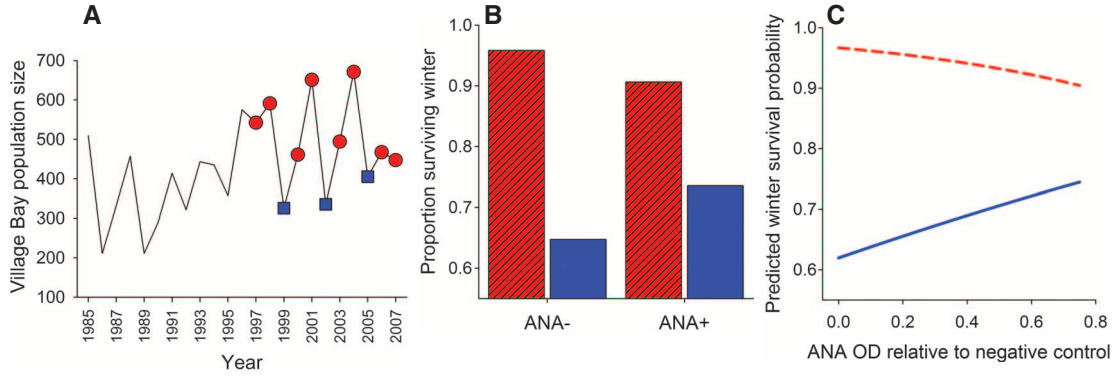

Fig. 2. Survival benefits associated with ANAs were expressed during harsh winters in adult female Soay sheep. (**A**) Population dynamics from 1985 to 2007, with years for which ANA was assayed (1997–2007) marked by red circles for years when population size was rising or stable and by blue squares for crash years. (**B** and **C**) Survival increased with ANAs in adult females, but only during crash winters. (B) Proportion below (ANA-) or above (ANA+) the positivity threshold that survived noncrash (red, hatched bar) and crash (blue bar) winters. (C) Predicted associations between overwinter survival probability and ANA OD over noncrash (red broken line) and crash (blue solid line) winters. The predictions are significant estimated effects of an ANA-by-environment interaction in a generalized linear mixed-effects model (*17*).

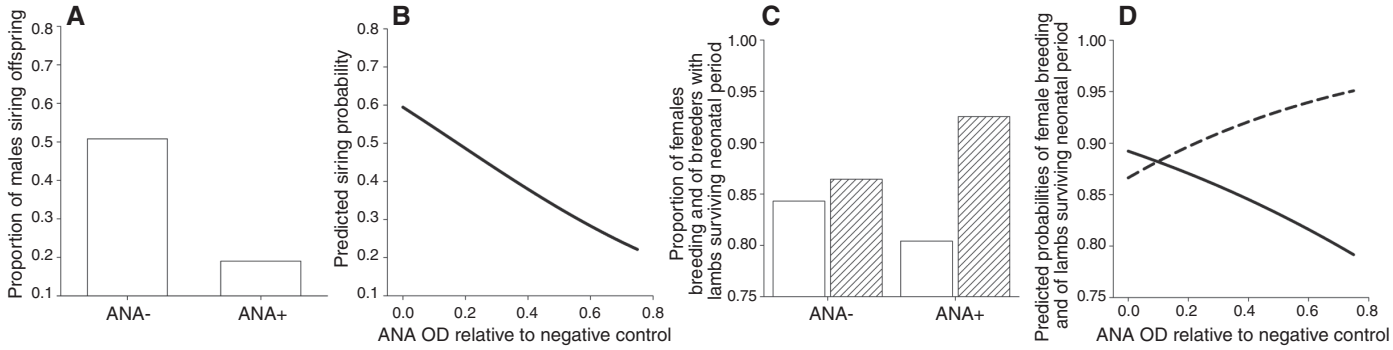

Fig. 3. High ANA concentration was associated with reduced fecundity in both sexes, but improved offspring survival among females that bred. (**A** and **B**) Male annual breeding success declined with increasing ANA. (A) The proportion of males below (ANA-) or above (ANA+) the positivity threshold that sired at least one offspring over the previous annual breeding cycle, and (B) the predicted associations between the probability of a male siring at least one offspring in the previous spring and ANA OD. (**C** and **D**) Female fecundity declined with increasing ANA, but offspring survival among breeding females increased with increasing ANA. (C) The proportion of females below (ANA-) or above (ANA+) the positivity threshold producing at least one offspring (white bars) and the proportion of breeders with at least one lamb that survived the neonatal period (hatched bars). (D) Predicted associations between probability of a female breeding (solid line) and, among females that did breed, probability of offspring surviving the neonatal period (broken line) versus ANA OD. Predictions in (B) and (D) are based on significant estimated effects of ANA in generalized linear mixed-effects models (*17*).

differences in fitness determinants (*28*) or a reduced power to detect such associations in males as a result of higher mortality and dispersal rates (*15*, *17*).

Our findings in female sheep support the rarely tested evolutionary prediction that investment in immunity, including humoral immunity, should lengthen life span in nature (*9*, *10*). Indeed, lines of laboratory mice selected for strong antibody responses exhibit striking concomitant increases in life span, relative to lines bred for weak responses, and the effect is attributable to resistance to both infection and cancer by means of a few identical or closely linked loci (*29*). However, it is possible that high ANA concentration is a consequence rather than cause of longevity (*22*, *23*).

Trade-offs between immune system function and reproduction are also predicted by evolutionary theory (*9*, *10*), and indeed, we found negative correlations between fecundity and ANAs in both sexes (Fig. 3). Males with high ANAs in August were less likely to have sired any offspring during the previous rut [$F_{1,158} = 5.74$, $P = 0.018$; (Fig. 3, A and B, and fig. S4A)], although there were no associations between ANA and the number of offspring sired among successful males [$F_{1,53} = 1.50$, $P = 0.23$; (*17*)]. Similarly, females with high ANAs in August were less likely to have produced a lamb the previous spring [$F_{1,807} = 8.15$, $P = 0.004$; (Fig. 3, C and D, and fig. S4B)], although there was no association between litter size and ANAs ($F_{1,563} = 1.46$, $P = 0.12$). Among females that did breed, those with lower ANAs gave birth to larger lambs on average [$F_{1,522} = 9.75$, $P = 0.002$; (fig. S4C)]. All of these associations were independent of whether reproduction followed a crash winter, and in neither sex did August ANAs predict reproduction in the following year (*17*). Mechanistic explanations for these results might include reproduction and immunity competing for limited resources (*9*, *10*), combined with sex-specific factors [e.g., the requirement for immunosuppression in pregnancy, lest detection of paternal antigens by the mother's immune system leads to rejection of the fetus (*30*)].

Further analysis showed that ANAs did not reflect a direct survival-fecundity trade-off. Previous studies have identified the survival costs of recent reproduction in adult females in this population (*31*–*33*). Among sheep assayed for ANAs, we likewise found that females producing offspring that survived were themselves less likely to survive the following winter [$\chi^2(1) = 5.10$, $P = 0.024$]. However, the crash-specific association of survival with high ANAs remained significant after this was accounted for [$\chi^2(1) = 4.61$, $P = 0.032$; (*17*)]. This suggests that the association of survival with elevated ANAs was independent of direct costs of recent reproduction. Furthermore, we found evidence that maternal ANAs were positively associated with offspring survival: controlling for the negative association between maternal ANAs and offspring birth weight, we found that breeding females with high ANAs had offspring that were more likely to survive the neonatal period [first 4 months of life; $F_{1,427} = 5.99$, $P = 0.015$; (Fig. 3, C and D, and fig. S4D)]. Increased provision of maternal antibody (*34*) by females with high ANAs that still bred could explain this result (*17*). Ultimately, there was no significant directional selection on ANAs through female annual reproductive success [$\chi^2(1) = 0.10$, $P = 0.75$], and average ANAs and lifetime reproductive success were not correlated at the phenotypic [correlation coefficient = –0.02, $\chi^2(1) = 0.06$, $P = 0.81$] or genetic [correlation coefficient = –0.20, $\chi^2(1) = 0.10$, $P = 0.75$] levels.

Our data indicate associations of ANAs with enhanced survival and reduced reproduction in a wild mammal. Furthermore, the survival-ANA association was environment and sex dependent, and reduced fecundity in ANA-positive females was accompanied by improved survival of their neonates. This complex and potentially balancing set of associations in a variable environment suggest a mechanism for the maintenance of immunoheterogeneity, possibly including autoimmune susceptibility genes, by natural selection.

References and Notes

1. S. A. Frank, *Immunology and Evolution of Infectious Disease* (Princeton Univ. Press, Princeton, NJ, 2002).
2. B. P. Lazzaro, T. J. Little, *Philos. Trans. R. Soc. Lond. B Biol. Sci.* **364**, 15 (2009).
3. N. Limaye *et al.*, *Genes Immun.* **9**, 61 (2008).
4. J. D. Rioux *et al.*, *Proc. Natl. Acad. Sci. U.S.A.* **106**, 18680 (2009).
5. Y. H. Lee, J. D. Ji, G. G. Song, *Lupus* **18**, 727 (2009).
6. K. R. Kumar *et al.*, *Science* **312**, 1665 (2006).
7. M. R. Clatworthy *et al.*, *Proc. Natl. Acad. Sci. U.S.A.* **104**, 7169 (2007).
8. A. L. Graham, J. E. Allen, A. F. Read, *Annu. Rev. Ecol. Evol. Syst.* **36**, 373 (2005).
9. J. Rolff, M. T. Siva-Jothy, *Science* **301**, 472 (2003).
10. M. E. Viney, E. M. Riley, K. L. Buchanan, *Trends Ecol. Evol.* **20**, 665 (2005).
11. A. P. Devalapalli *et al.*, *Scand. J. Immunol.* **64**, 125 (2006).
12. N. M. Smee, K. R. Harkin, M. J. Wilkerson, *J. Am. Vet. Med. Assoc.* **230**, 1180 (2007).
13. R. Attanasio *et al.*, *Clin. Exp. Immunol.* **123**, 361 (2001).
14. J. D. Wood *et al.*, *Dig. Dis. Sci.* **43**, 1443 (1998).
15. T. H. Clutton-Brock, J. M. Pemberton, Eds., *Soay Sheep: Dynamics and Selection in an Island Population*, (Cambridge University Press, Cambridge, 2004).
16. M. R. Arbuckle *et al.*, *N. Engl. J. Med.* **349**, 1526 (2003).
17. Materials and methods and supplementary text are available as supporting material on *Science* Online.
18. P. E. Lipsky, *Nat. Immunol.* **2**, 764 (2001).
19. G. Dighiero, N. R. Rose, *Immunol. Today* **20**, 423 (1999).
20. A. Lleo, P. Invernizzi, B. Gao, M. Podda, M. E. Gershwin, *Autoimmun. Rev.* **9**, A259 (2010).
21. R. Njemini *et al.*, *Clin. Exp. Immunol.* **127**, 99 (2002).
22. K. P. Liang, S. E. Gabriel, *J. Rheumatol.* **34**, 1203 (2007).
23. B. O. Nilsson *et al.*, *J. Autoimmun.* **27**, 281 (2006).
24. D. S. Falconer, T. F. C. Mackay, *Introduction to Quantitative Genetics* (Prentice Hall, London, ed. 4, 1996).
25. L. E. B. Kruuk, *Philos. Trans. R. Soc. Lond. B Biol. Sci.* **359**, 873 (2004).
26. B. T. Grenfell *et al.*, *Nature* **394**, 674 (1998).
27. T. Coulson *et al.*, *Science* **292**, 1528 (2001).
28. T. H. Clutton-Brock, Ed., *Reproductive Success: Studies of Individual Variation in Contrasting Breeding Systems* (Univ. of Chicago Press, Chicago, 1988).

29. V. Covelli *et al.*, *J. Immunol.* **142**, 1224 (1989).
30. J. Trowsdale, A. G. Betz, *Nat. Immunol.* **7**, 241 (2006).
31. T. H. Clutton-Brock *et al.*, *J. Anim. Ecol.* **65**, 675 (1996).
32. P. Marrow, J. M. McNamara, A. I. Houston, I. R. Stevenson, T. H. Clutton-Brock, *Philos. Trans. R. Soc. Lond. B Biol. Sci.* **351**, 17 (1996).
33. G. Tavecchia *et al.*, *J. Anim. Ecol.* **74**, 201 (2005).
34. J. L. Grindstaff, E. D. Brodie 3rd, E. D. Ketterson, *Proc. R. Soc. Lond. B Biol. Sci.* **270**, 2309 (2003).
35. This work was funded by the Biotechnology and Biological Sciences and Natural Environment Research Councils; the Wellcome Trust; and the Research and Policy for Infectious Disease Dynamics (RAPIDD) program of the Science and Technology Directorate, U.S. Department of Homeland Security, and the Fogarty International Center. Thanks to the National Trust for Scotland and Scottish National Heritage for permission to work on St. Kilda; the Ministry of Defense, QinetiQ, Amey, and Eurest Support Services staff on St. Kilda and Benbecula for logistical support; T. Clutton-Brock, M. Crawley, B. Grenfell, and many field volunteers for the data set and samples; F. Howison, N. Sanderson, K. Fairlie-Clarke, J. Matthews, and A. Nisbet for laboratory assistance; and A. Read, B. Grenfell, T. Little, D. Gray, R. Mellanby, S. Caserta, B. Craig, T. Coulson, J. Slate, R. Maizels, W. Craigens, and members of the Wild Evolution Group for discussions.

Supporting Online Material

www.sciencemag.org/cgi/content/full/330/6004/662/DC1
Materials and Methods
SOM Text
Figs. S1 to S4
Table S1
References

9 July 2010; accepted 9 September 2010
10.1126/science.1194878

Lineage Relationship Analysis of RORγt$^+$ Innate Lymphoid Cells

Shinichiro Sawa,[1,2] Marie Cherrier,[1,2] Matthias Lochner,[1,2,3] Naoko Satoh-Takayama,[4,5] Hans Jörg Fehling,[6] Francina Langa,[7] James P. Di Santo,[4,5] Gérard Eberl[1,2]*

Lymphoid tissue–inducer (LTi) cells initiate the development of lymphoid tissues through the activation of local stromal cells in a process similar to inflammation. LTi cells express the nuclear hormone receptor RORγt, which also directs the expression of the proinflammatory cytokine interleukin-17 in T cells. We show here that LTi cells are part of a larger family of proinflammatory RORγt$^+$ innate lymphoid cells (ILCs) that differentiate from distinct fetal liver RORγt$^+$ precursors. The fate of RORγt$^+$ ILCs is determined by mouse age, and after birth, favors the generation of cells involved in intestinal homeostasis and defense. Contrary to RORγt$^+$ T cells, however, RORγt$^+$ ILCs develop in the absence of microbiota. Our study indicates that RORγt$^+$ ILCs evolve to preempt intestinal colonization by microbial symbionts.

Lymphoid tissue–inducer (LTi) cells are necessary in the fetal development of lymph nodes and Peyer's patches, a lymphoid tissue of the gut (*1*), as well as in the formation of intestinal isolated lymphoid follicles after birth (*2*). They express membrane lymphotoxin (LT) α1β2 that activates local stromal cells through the receptor LTβR. Activated stromal cells in lymphoid tissue anlagen recruit and organize lymphocytes in a process resembling inflammation (*3*), involving proinflammatory cytokines, chemokines, and adhesion molecules (*1*). The nuclear hormone receptor RORγt is required for the generation of LTi cells (*4*). After birth, RORγt induces a proinflammatory program in subsets of αβ and γδ T cells, characterized by the expression of

[1]Lymphoid Tissue Development Unit, Institut Pasteur, 75724 Paris, France. [2]CNRS, URA1961, 75724 Paris, France. [3]Institute of Infection Immunology, TWINCORE, Centre for Experimental and Clinical Infection Research; a joint venture between the Medical School Hannover and the Helmholtz Centre for Infection Research, Hannover, Germany. [4]Innate Immunity Unit, Institut Pasteur, 75724 Paris, France. [5]Inserm, U668, 75724 Paris, France. [6]Institute of Immunology, University Clinics Ulm, Ulm, Germany. [7]Centre Ingénieurie Génétique Murine, Institut Pasteur, 75724 Paris, France.

*To whom correspondence should be addressed. E-mail: gerard.eberl@pasteur.fr

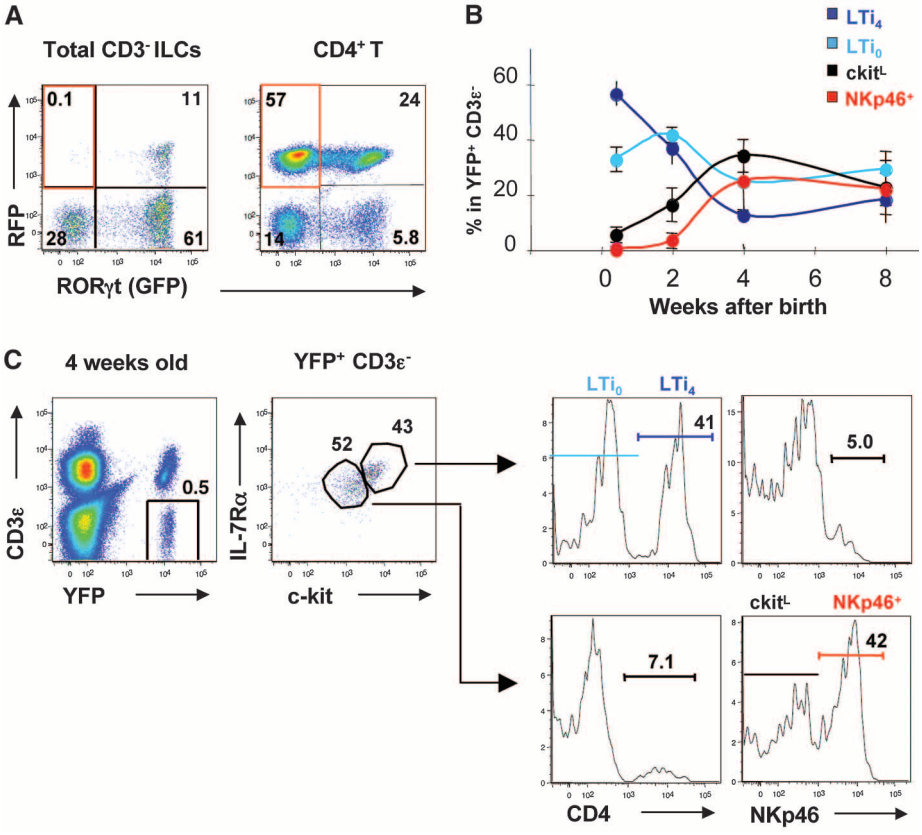

Fig. 1. Inducible fate mapping of RORγt$^+$ ILCs. (**A**) Flow cytometry analysis of cells isolated from the small intestinal lamina propria of dox-untreated 4-week-old triple transgenic mice crossed to *Rorc*(γt)-*Egfp*^{TG} reporter mice (fig. S2). The red square indicates cells that have lost RORγt expression. Numbers indicate the percentage of cells per gated type of cells. The data shown are representative of three individual experiments. (**B** and **C**) The fate of fetal and perinatal RORγt$^+$ ILCs of the small intestinal lamina propria. Triple transgenic mice (fig. S1) were given dox continuously, starting on day 3 after birth until analysis. (B) Each data point represents the mean percentage ± SD from at least five individual mice. (C) Flow cytometry analysis of 4-week-old triple transgenic mice. The data shown are representative of at least five individual mice.

interleukin-17 (IL-17) (*5*–*7*), also expressed by LTi cells (*8*). Furthermore, RORγt is required for the generation of a subset of natural killer (NK)–like NKp46^{+} cells present in the intestinal lamina propria and characterized by the production of high amounts of IL-22 (*9*–*11*), a major factor in intestinal homeostasis and defense (*12*, *13*). It is now suggested that LTi cells, NK cells, NK-like cells (*14*), and recently discovered T helper 2 (T_H2)–like innate cells involved in intestinal immunity to helminths (*15*–*17*) are members of a growing family of innate lymphoid cells (ILCs), which develop in the absence of the recombinated antigen receptors and clonal selection that are characteristic of adaptive immunity.

Recent evidence indicates that LT or LTi-like cells are not only necessary effectors for lymphoid tissue formation but also precursors to IL-22^{+}

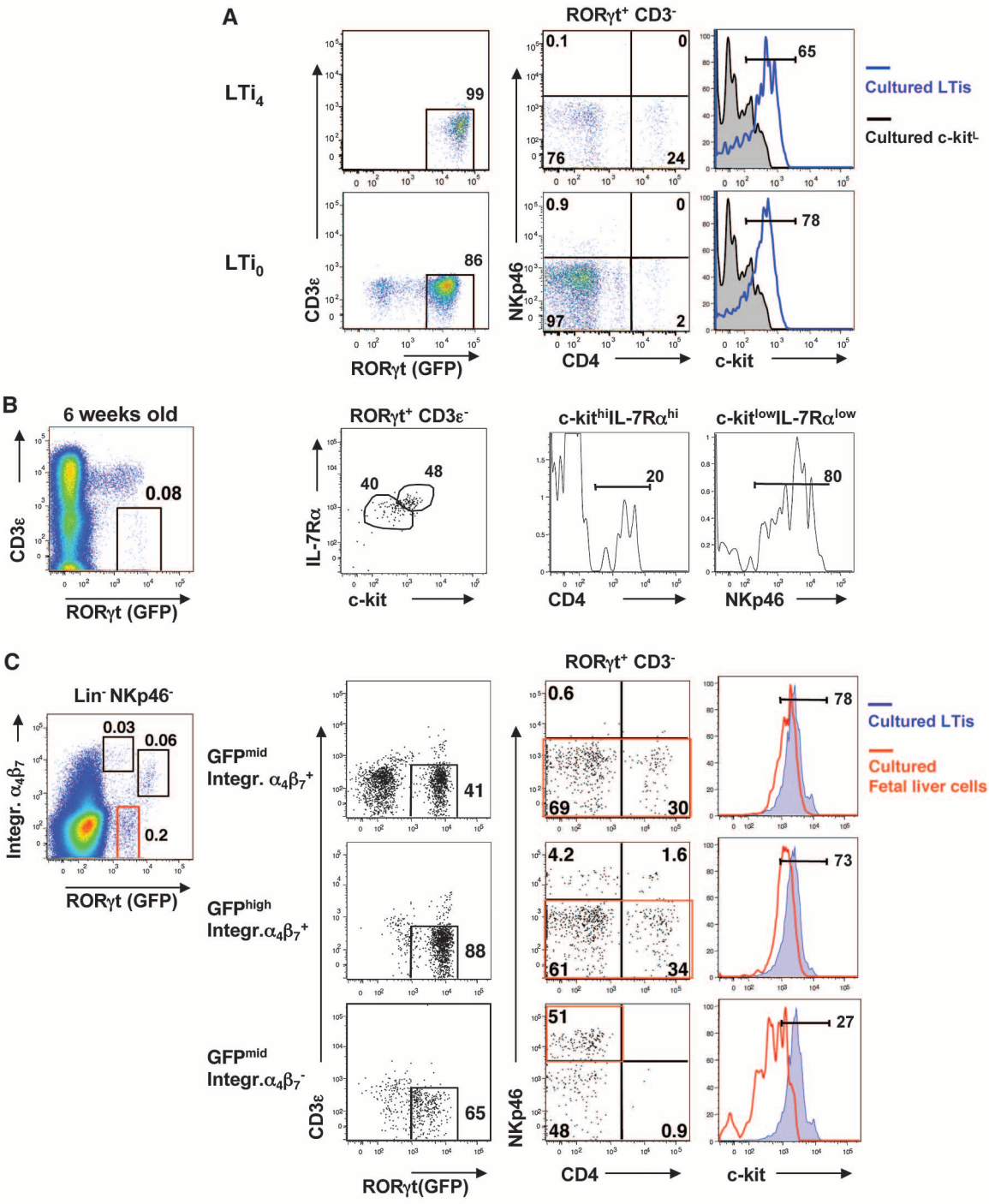

Fig. 2. The diversity of RORγt^{+} ILCs is generated by committed fetal liver RORγt^{+} precursors. (**A**) Sorted fetal LTi cells (LTi$_4$ or LTi$_0$) from the intestinal lamina propria of *Rorc*(γt)-*Egfp*^{TG} fetuses 16 days after coitus [embryonic day 16 (E16)] as well as adult c-kit^{low} RORγt^{+} ILCs were cultured on OP9 stroma cells in the presence of IL-7 and stem cell factor (SCF). Cells were analyzed by flow cytometry after 6 days. The data are representative of four independent experiments. (**B**) Reconstitution of irradiated C57BL/6 hosts was analyzed by flow cytometry 6 weeks after adoptive transfer with lineage-depleted 5 × 10^5 fetal liver cells from E16 *Rorc*(γt)-*Egfp*^{TG} mice. Data are representative of three individual mice. (**C**) Upper left: flow cytometric analysis of lineage-negative fetal liver cells from E16 *Rorc*(γt)-*Egfp*^{TG} mice. Three GFP^{+} subsets were sorted and cultured on OP-9 cells with IL-7 and SCF and analyzed by flow cytometry after 6 days. Gut mature E16 LTi$_4$ cells were used as a reference for the level of c-kit expression. Data are representative of three independent experiments.

NK-like cells (*18*, *19*). T_H2-like ILCs also have multipotent progenitor capacity and generate mast cells, basophils, and macrophages when stimulated with the T_H2-promoting cytokine IL-25 (*16*). To assess in vivo the progenitor capacity of LTi cells, we performed inducible cell fate–mapping experiments that allowed tracking of the progeny of fetal RORγt$^+$ CD3ε$^-$ cells (termed here RORγt$^+$ ILCs). Mice were generated that express the tetracycline transactivator (tTA) under control of the *Rorc*(γt) locus on a bacterial artificial chromosome (*7*, *20*) (figs. S1 and S2). The tTA induces expression of the Cre recombinase on a second transgene (*21*), which in turn induces stable expression of enhanced yellow or red fluorescent protein (EYFP or RFP) in RORγt$^+$ cells and all their progeny (*22*). Induction of genetic fate mapping can be controlled in time by the administration of doxycycline (dox), which blocks the tTA-mediated labeling cascade. Thus, the progeny of fetal RORγt$^+$ ILCs was determined by perinatal administration of dox to such triple transgenic mice. First, and in contrast to CD4$^+$ T cells that derive from RORγt$^+$ immature thymocytes and down-regulate RORγt at the mature stage (*23*), RORγt$^+$ ILCs stably expressed RORγt (Fig. 1A and fig. S2). Second, whereas fetal and perinatal RORγt$^+$ ILCs consisted mainly of c-kit^{high} IL-7Rα^{high} CD4$^+$ (LTi_4) and CD4$^-$ (LTi_0) cells (Fig. 1B and fig. S3), a phenotype consistent with LTi cells (*24*), the progeny of such cells progressively increased in complexity until 4 weeks after birth (Fig. 1B). Besides CD4$^+$ and CD4$^-$ LTi cells, the adult progeny of fetal RORγt$^+$ ILCs included c-kit^{low} IL-7Rα^{low} cells, of which 42% expressed NKp46 (*9*–*11*) (Fig. 1C). Finally, in the adult, RORγt$^+$ ILCs localized mainly to the intestinal lamina propria (fig. S4).

Even though the fate mapping of fetal RORγt$^+$ ILCs indicated that LTi cells generate the different subsets of RORγt$^+$ ILCs (Fig. 1B), it is possible that fetal RORγt$^+$ ILCs include RORγt$^+$ precursors that are distinct from LTi cells. To test whether LTi cells could generate distinct subsets of RORγt$^+$ ILCs such as NKp46$^+$ cells, LTi cells were isolated from fetal and adult intestine and transferred into irradiated newborn hosts or cultured for 6 days on OP9 stromal cells. Transferred LTi cells generated no detectable progeny, and cultured LTi cells generated no c-kit^{low}

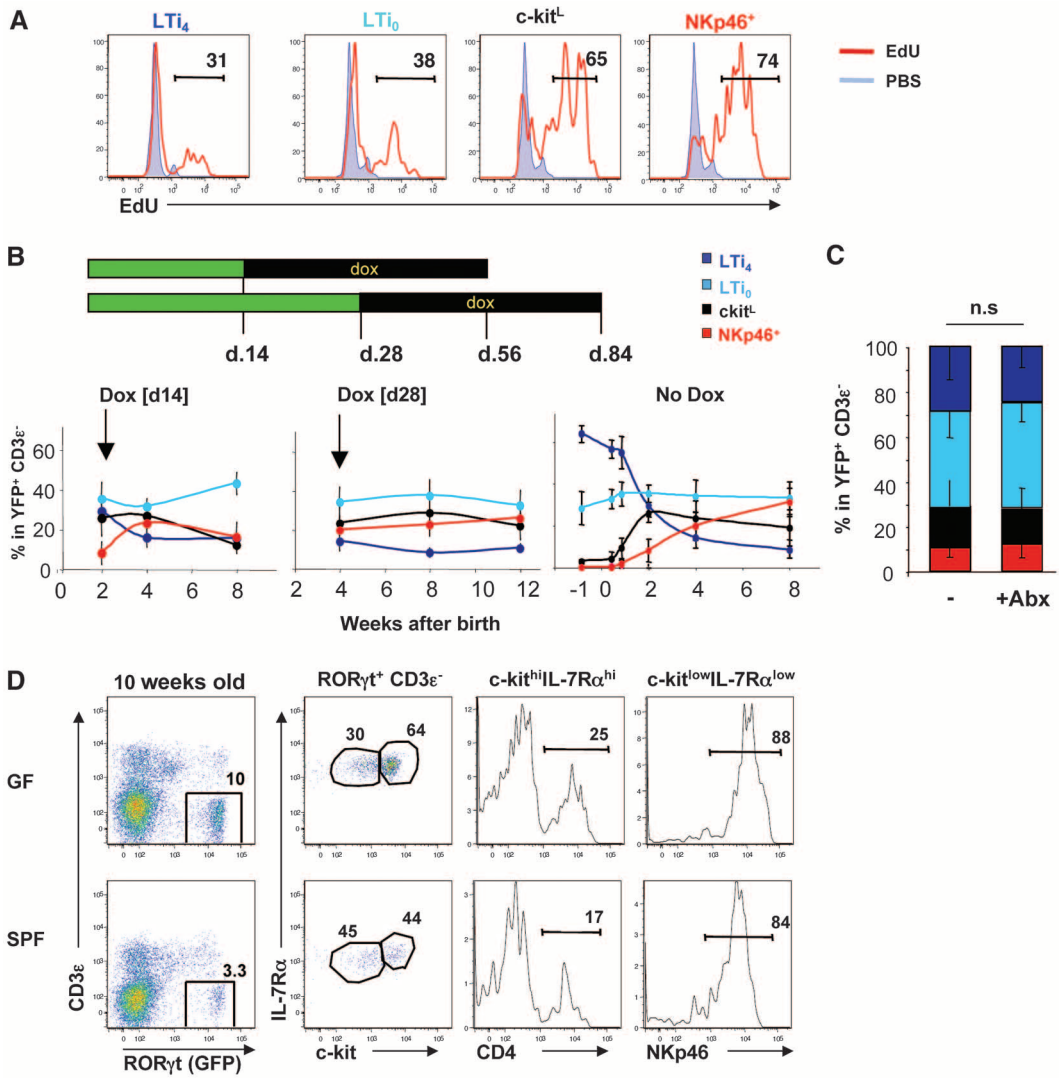

Fig. 3. The fate of RORγt$^+$ ILCs subsets is programmed. (**A**) The proliferation rates of RORγt$^+$ ILCs. Triple transgenic mice were treated with dox from day 3 after birth and injected with 5-ethynyl-2′-deoxyuridine (EdU) daily from day 7 until analysis on day 14. PBS, phosphate-buffered saline. Cells were isolated from the small intestinal lamina propria and analyzed by flow cytometry. Data are representative of three independent experiments. (**B**) Triple transgenic mice (fig. S1) were treated with dox from days 14 or 28, and cells were analyzed by flow cytometry at different time points thereafter. Each data point represents the mean percentage ± SD of at least five individual mice. (**C**) Triple transgenic mice were treated from birth with a cocktail of streptomycin, ampicillin, and colistin, as well as with dox, from day 7 after birth and analyzed at 8 weeks. Abx, antibiotics. Shown is the proportion of the distinct subsets of RORγt$^+$ ILCs within fate-mapped YFP$^+$ cells. The data are the mean of four mice per group ± SD; n.s, statistically not significant; unpaired *t* test. (**D**) Intestinal ILCs were analyzed by flow cytometry in 10-week-old germ-free (GF) or specific pathogen–free (SPF) *Rorc*(γt)-*Egfp*^{TG} mice. Data are representative of three individual mice.

IL-7Rα^{low} cells, including NKp46^{+} cells (Fig. 2A and fig. S5). Furthermore, the in vivo depletion of CD4^{+} cells affected only CD4^{+} LTi cells and no other subsets of RORγt^{+} ILCs (fig. S6), and the proportion of CD4^{+} LTi cells labeled through our fate-mapping strategy was fivefold higher than the proportion of labeled NKp46^{+} cells (fig. S2A). Collectively, these data indicate that LTi cells are not progenitor cells of other subsets of RORγt^{+} ILCs. In contrast, transfer of fetal liver lineage-negative cells into irradiated C57BL/6 mice generated LTi cells, as previously described (*25*, *26*), and the other subsets of RORγt^{+} ILCs (Fig. 2B). Examination of fetal liver cells revealed three subsets of RORγt^{+} cells characterized by distinct expression levels of RORγt and integrin α4β7 (Fig. 2C), the latter marker having been shown to define a fetal liver precursor committed to dendritic cells, NK cells, and LTi cells (*25*). Although too small to be used in transfer experiments, these populations generated all subsets of RORγt^{+} ILCs upon culture on OP9 cells: GFP^{+} α4β7^{+} cells generated CD4^{+} and CD4^{-} LTi cells, whereas GFP^{+} α4β7^{-} cells generated NKp46^{+} cells (GFP, green fluorescent protein) (Fig. 2C and fig. S7A). The presence of IL-2 favored the generation of NK cells from integrin α4β7^{+} cells, as reported (*25*), but not of RORγt^{+} NKp46^{+} cells (fig. S7B). These data demonstrate that fetal liver RORγt^{+} cells, but not LTi cells, generate the distinct subsets of RORγt^{+} ILCs. It has been reported, however, that human LTi-like cells isolated from fetal lymph nodes and adult tonsils generate RORγt^{+} NKp46^{+} cells in vitro (*18*, *19*). Thus, in humans, LTi-like cells may include RORγt^{+} precursors specific for NKp46^{+} cells.

Do fetal RORγt^{+} ILCs generate adult RORγt^{+} ILCs? To address this issue, we determined the turnover rate of RORγt^{+} ILCs from the intestinal lamina propria and found that all subsets were replaced by newly generated cells with a half-life of 22 to 26 days (fig. S8). Similar kinetics were found for RORγt^{+} ILCs in the mesenteric lymph node and spleen (fig. S9). Thus, a likely source of RORγt^{+} ILCs after birth is the bone marrow, and transfer of bone marrow cells into irradiated hosts generated all subsets of RORγt^{+} ILCs (fig. S10). The RORγt^{+} precursors in the bone marrow, however, remain to be identified.

The sharp population change occurring in RORγt^{+} ILCs after birth, characterized by a drop in the proportion of CD4^{+} LTi cells (Fig. 1B), is particularly intriguing. Because LTi cells do not generate c-kit^{low} IL-7Rα^{low} cells (Fig. 2), this population change may be partly explained by a markedly higher proliferation rate of c-kit^{low} IL-7Ra^{low} cells, including NKp46^{+} cells, as compared to LTi cells (Fig. 3A). In contrast, the progeny of RORγt^{+} ILCs from pre-weaned or adult mice showed no such sharp decrease in the proportion of LTi cells. They rather mimicked the proportions within total LTi cells found at these ages (Fig. 3B and fig. S11). These observations indicate that the proportions of the different subsets of RORγt^{+} ILCs are determined by mouse age rather than by cell-intrinsic properties of LTi cells or c-kit^{low} IL-7Rα^{low} cells.

To determine whether the symbiotic microbiota controls this age-dependent fate of RORγt^{+} ILCs, the fate of fetal and perinatal RORγt^{+} ILCs was assessed in mice treated continuously from birth with a cocktail of antibiotics that efficiently eradicates intestinal bacteria (*2*) and with dox, used for fate mapping. In such mice, the fate of fetal and perinatal RORγt^{+} ILCs remained unchanged (Fig. 3C). In accordance with these results, the proportions of the different subsets of RORγt^{+} ILCs were similar in germ-free (or dox-treated) mice as compared to mice that harbor a normal symbiotic microbiota (Fig. 3D and fig. S12); in mice recolonized with segmented filamentous bacteria that induce the generation of RORγt^{+} Th17 cells (*27*, *28*) (fig. S13); and in mice deficient in molecules involved in the recognition of microbe-associated molecular patterns, such as Nod1, Nod2, or Myd88 (fig. S14). These data demonstrate that intestinal symbionts, which induce the generation of intestinal RORγt^{+} T cells (*29*), have no impact on the development of RORγt^{+} ILCs. Furthermore, RORγt^{+} ILCs also develop independently of adaptive immunity (fig. S15).

All subsets of RORγt^{+} ILCs, with the exception of NKp46^{+} cells, expressed high amounts of both IL-17 and IL-22 (Fig. 4A). However, LTi cells differed from c-kit^{low} IL-7Rα^{low} cells in their expression of the chemokine receptor CCR6 (Fig. 4B). It has been reported that CCR6 is expressed by LTi cells clustered in cryptopatches of the lamina propria (*2*, *30*), but not by RORγt^{+} ILCs outside cryptopatches (*30*), such as NKp46^{+} cells (*9*), which expand after birth (Fig. 1B).

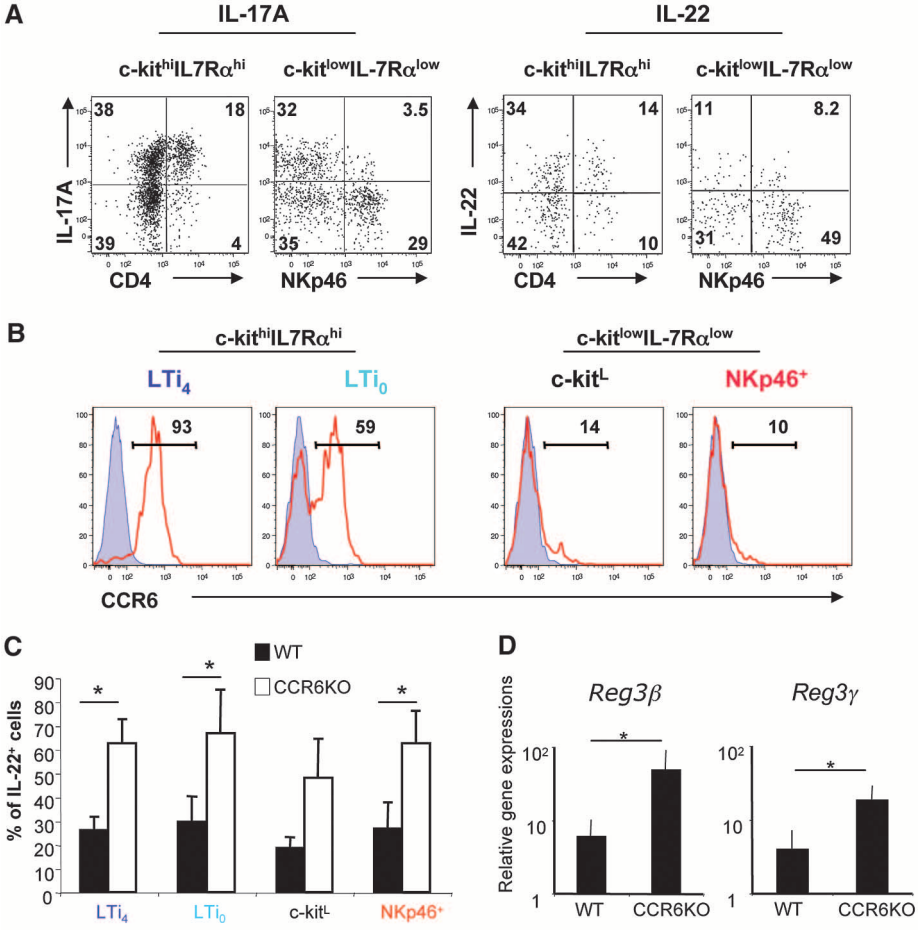

Fig. 4. Topographical and functional compartmentalization of RORγt^{+} ILCs by CCR6. (**A**) Flow cytometric analysis of intracellular expression of IL-17A and IL-22 by RORγt^{+} ILCs. Cells were isolated from the small intestinal lamina propria of 2-week-old *Rorc*(γt)-*Egfp*^{TG} mice. Data are representative of three independent experiments. (**B**) Flow cytometric analysis of CCR6 expression by LTi cells. Numbers indicate the percentage of CCR6^{+} cells as compared to cells from age-matched (6 weeks old) CCR6-deficient mice (blue histograms). Data shown are representative of results obtained in three individual mice. (**C**) Expression of IL-22 by CCR6-deficient (CCR6KO) RORγt^{+} ILCs isolated from 6-week-old mice. WT, wild type. The data are the mean of four mice per group ± SD; *$P < 0.05$, unpaired *t* test. (**D**) Antibacterial peptide expression by epithelial cells in 6-week-old CCR6-deficient mice. Transcripts for the antibacterial peptides Reg3β and Reg3γ were measured by quantitative real-time polymerase chain reaction. Data are the mean of four individual mice ± SD; *$P < 0.05$, unpaired *t* test.

CCR6 is required for the bacteria-induced generation of isolated lymphoid follicles (ILFs) from cryptopatches (*2*), and in the absence of CCR6 and ILFs, intestinal homeostasis is disrupted and the size of the microbiota is increased 10-fold (*2*). Although RORγt$^+$ ILC subsets are not altered in CCR6-deficient mice (fig. S16), the expression of IL-22 is significantly increased (Fig. 4C), and, as a consequence (*31*), the production of antibacterial peptides by epithelial cells is augmented (Fig. 4D). These data indicate that CCR6 regulates the function of RORγt$^+$ ILCs. When CCR6-dependent topographical control is lost, the lymphoid tissue-inducing function of RORγt$^+$ ILCs is ablated and their proinflammatory or epithelial defense–promoting function is abnormally expanded.

The major population change occurring in RORγt$^+$ ILCs after birth, resulting in LTi cells being numerically surpassed by c-kit^{low} IL-7Rα^{low} cells after weaning, suggested that the colonizing intestinal microbiota directed the development of RORγt$^+$ ILCs. We show, however, that this population change is independent of microbiota, indicating that RORγt$^+$ ILCs undergo a programmed development that preempts exposure to the symbiotic microbiota. Both LTi cells and NKp46$^+$ RORγt$^+$ ILCs express IL-22 (*8*–*11*), a critical cytokine for the activation and defense of epithelial cells (*13*, *31*). Whereas LTi cells are clustered in cryptopatches between crypts of the intestinal lamina propria, where they direct the formation of isolated lymphoid follicles (ILFs) (*2*), IL-22$^+$ NKp46$^+$ cells are found within villi (*9*), thus closer to epithelial cells. An important role for IL-22$^+$ NKp46$^+$ cells in epithelial defense has been shown in the case of *Citrobacter rodentium* infection (*9*) and in resistance to colitis induced by dextran sodium sulfate (*13*). Our data suggest that this topographical and functional compartmentalization of RORγt$^+$ ILCs depends on the chemokine receptor CCR6, which responds to CCL20 and β-defensins produced by epithelial cells. We have demonstrated that RORγt$^+$ ILCs, required before birth mainly for the development of lymphoid tissues, undergo a programmed population change after birth to cope with the massive microbiota and maintain intestinal homeostasis, both through the CCR6-dependent generation of ILFs and through the activation of epithelial immunity. The programmed fate of RORγt$^+$ ILCs is an example of the coevolution of the mammalian host immune system with its symbiotic microbiota in order to maintain homeostasis of the host/symbiont superorganism.

References and Notes

1. R. E. Mebius, *Nat. Rev. Immunol.* **3**, 292 (2003).
2. D. Bouskra *et al.*, *Nature* **456**, 507 (2008).
3. S. I. Nishikawa, H. Hashi, K. Honda, S. Fraser, H. Yoshida, *Curr. Opin. Immunol.* **12**, 342 (2000).
4. G. Eberl *et al.*, *Nat. Immunol.* **5**, 64 (2004).
5. I. I. Ivanov *et al.*, *Cell* **126**, 1121 (2006).
6. M. L. Michel *et al.*, *Proc. Natl. Acad. Sci. U.S.A.* **105**, 19845 (2008).
7. M. Lochner *et al.*, *J. Exp. Med.* **205**, 1381 (2008).
8. H. Takatori *et al.*, *J. Exp. Med.* **206**, 35 (2009).
9. N. Satoh-Takayama *et al.*, *Immunity* **29**, 958 (2008).
10. S. L. Sanos *et al.*, *Nat. Immunol.* **10**, 83 (2009).
11. C. Luci *et al.*, *Nat. Immunol.* **10**, 75 (2009).
12. Y. Zheng *et al.*, *Nat. Med.* **14**, 282 (2008).
13. L. A. Zenewicz *et al.*, *Immunity* **29**, 947 (2008).
14. M. Colonna, *Immunity* **31**, 15 (2009).
15. D. R. Neill *et al.*, *Nature* **464**, 1367 (2010).
16. S. A. Saenz *et al.*, *Nature* **464**, 1362 (2010).
17. K. Moro *et al.*, *Nature* **463**, 540 (2010).
18. T. Cupedo *et al.*, *Nat. Immunol.* **10**, 66 (2009).
19. N. K. Crellin, S. Trifari, C. D. Kaplan, T. Cupedo, H. Spits, *J. Exp. Med.* **207**, 281 (2010).
20. Materials and methods are available as supporting material on *Science* Online.
21. K. Schönig, F. Schwenk, K. Rajewsky, H. Bujard, *Nucleic Acids Res.* **30**, e134 (2002).
22. S. Srinivas *et al.*, *BMC Dev. Biol.* **1**, 4 (2001).
23. G. Eberl, D. R. Littman, *Science* **305**, 248 (2004).
24. H. Yoshida *et al.*, *Int. Immunol.* **11**, 643 (1999).
25. H. Yoshida *et al.*, *J. Immunol.* **167**, 2511 (2001).
26. R. E. Mebius *et al.*, *J. Immunol.* **166**, 6593 (2001).
27. V. Gaboriau-Routhiau *et al.*, *Immunity* **31**, 677 (2009).
28. I. I. Ivanov II *et al.*, *Cell* **139**, 485 (2009).
29. I. I. Ivanov *et al.*, *Cell Host Microbe* **4**, 337 (2008).
30. A. Lügering *et al.*, *Clin. Exp. Immunol.* **160**, 440 (2010).
31. K. Wolk *et al.*, *Immunity* **21**, 241 (2004).

32. We thank the members of the Lymphoid Tissue Development lab for discussions and critical reading of the manuscript and L. Polomack, S. Dulauroy, G. Chauveau-Le Friec, and the team of the Centre d'Ingénierie Génétique Murine for technical assistance. We also thank R. Varona for CCR6-deficient mice, I. Gomperts-Boneca for Nod1- and Nod2-deficient mice, and H. Bujard for LC-1-Cre mice. This work was supported by the Institut Pasteur, grants from the Mairie de Paris, the Agence Nationale de la Recherche, and an Excellence Grant from the European Commission. M.L. was supported by the Deutsche Forschungsgemeinschaft and the Schlumberger Foundation. H.J.F. is funded by the Deutsche Forschungsgemeinschaft (FE-578/3-1). The authors have no competing financial interests.

Supporting Online Material

www.sciencemag.org/cgi/content/full/science.1194597/DC1
Materials and Methods
Figs. S1 to S16
References

2 July 2010; accepted 3 September 2010
Published online 23 September 2010;
10.1126/science.1194597
Include this information when citing this paper.

Filtering of Visual Information in the Tectum by an Identified Neural Circuit

Filippo Del Bene,[1]*† Claire Wyart,[2]*‡ Estuardo Robles,[1] Amanda Tran,[1] Loren Looger,[3] Ethan K. Scott,[1]§ Ehud Y. Isacoff,[2,4]‖ Herwig Baier[1]‖

The optic tectum of zebrafish is involved in behavioral responses that require the detection of small objects. The superficial layers of the tectal neuropil receive input from retinal axons, while its deeper layers convey the processed information to premotor areas. Imaging with a genetically encoded calcium indicator revealed that the deep layers, as well as the dendrites of single tectal neurons, are preferentially activated by small visual stimuli. This spatial filtering relies on GABAergic interneurons (using the neurotransmitter γ-aminobutyric acid) that are located in the superficial input layer and respond only to large visual stimuli. Photo-ablation of these cells with KillerRed, or silencing of their synaptic transmission, eliminates the size tuning of deeper layers and impairs the capture of prey.

The optic tectum in the vertebrate midbrain, called the superior colliculus in mammals, receives visual inputs from the retina and converts this information into directed motor outputs (*1*). In larval zebrafish, the tectum is divided into two main areas: the stratum periventriculare (SPV), which contains the cell bodies of most tectal neurons, and the synaptic neuropil area, which contains their dendrites and axons as well as the axons of retinal afferents (*2*–*5*). Neurons in the SPV, called periventricular neurons (PVNs), extend a single neurite, which branches extensively and may span the entire depth of the neuropil. Retinal axons mainly target the superficial layers of the tectal neuropil [i.e., the stratum opticum (SO) and the stratum fibrosum et griseum superficiale (SFGS); fig. S1] (*5*–*8*), where they make contact with the dendrites of periventricular interneurons (PVINs) that convey the visual information to other PVINs or to periventricular projection neurons (PVPNs). The axons of PVPNs exit the tectum in the deepest neuropil layer and project to premotor regions in the midbrain and hindbrain (*2*, *5*, *6*).

The tectum is required for the localization, tracking, and capture of motile prey, such as paramecia (*9*). Other visual behaviors (e.g., optomotor and optokinetic responses) are mediated by a different pathway not involving the tectum (*10*, *11*).

[1]Department of Physiology, University of California, San Francisco, CA 94158, USA. [2]Department of Molecular and Cell Biology and Helen Wills Neuroscience Institute, University of California, Berkeley, CA 94720, USA. [3]Howard Hughes Medical Institute, Janelia Farm Research Campus, Ashburn, VA 20147, USA. [4]Materials Science Division and Physical Bioscience Division, Lawrence Berkeley National Laboratory, Berkeley, CA 94720, USA.

*These authors contributed equally to this work.
†Present address: Institut Curie, CNRS UMR3215, INSERM U934, 75724 Paris Cedex 05, France.
‡Present address: Centre de Recherche de l'Institut du Cerveau et de la Moelle Epiniere, Université Pierre et Marie Curie–Paris 6, UMR-S975, Inserm U975 and CNRS UMR 7225, CHU Pitié-Salpêtrière, 75013 Paris, France.
§Present address: School of Biomedical Sciences, University of Queensland, Queensland 4072, Australia.
‖To whom correspondence should be addressed. E-mail: ehud@calmail.berkeley.edu (E.Y.I.); herwig.baier@ucsf.edu (H.B.)

Consistent with a function in the detection of small objects, electrophysiology and optical imaging showed that single tectal neurons, in all vertebrates examined, often respond to small stimuli such as spots or bars, which occupy only a fraction of the neurons' receptive fields (*12*–*19*). To reveal the neural substrate of this size filtering, we used Gal4 enhancer-trap lines (*2*, *20*, *21*) to drive the expression of the genetically encoded Ca^{2+} indicators GCaMP1.6 (*22*) and GCaMP3 (*23*). This allowed us to record visually evoked activity in dendrites and axons of specific classes of neurons.

We used the *Atoh7:Gal4* transgenic line to drive expression of GCaMP1.6 in retinal axons, demarcating the superficial input layers in the neuropil (Fig. 1A). The fish's retina was exposed to three visual stimuli, displayed on a miniature LCD screen (fig. S1): (i) a brief (25 or 50 ms) flash that filled the entire screen (horizontal visual angle 50°), (ii) a thin black bar (2°) moving at a speed of 0.25°/ms across the screen from anterior to posterior (A→P), and (iii) a bar of the same size and speed, but moving from posterior to anterior (P→A). The responses of the retinal axons did not differ significantly in amplitude and in time to peak between the large and the small stimuli (Fig. 1, B and C; maximum $\Delta F/F$ = 2.11 ± 0.19% for flash versus 2.08 ± 0.11% for A→P and 2.16 ± 0.13% for P→A; time to peak = 0.69 ± 0.03 s for flash versus 0.72 ± 0.11 s for A→P and 0.73 ± 0.05 s for P→A; $P_{amplitude}$ = 0.31; $P_{time\text{-}to\text{-}peak}$ = 0.54; n = 5). Indeed, responses were similar in amplitude across a range of stimulus sizes (Fig. 1D).

In the *Gal4s1038t* line, a small subset of PVPNs in the posterior-ventral quadrant of the

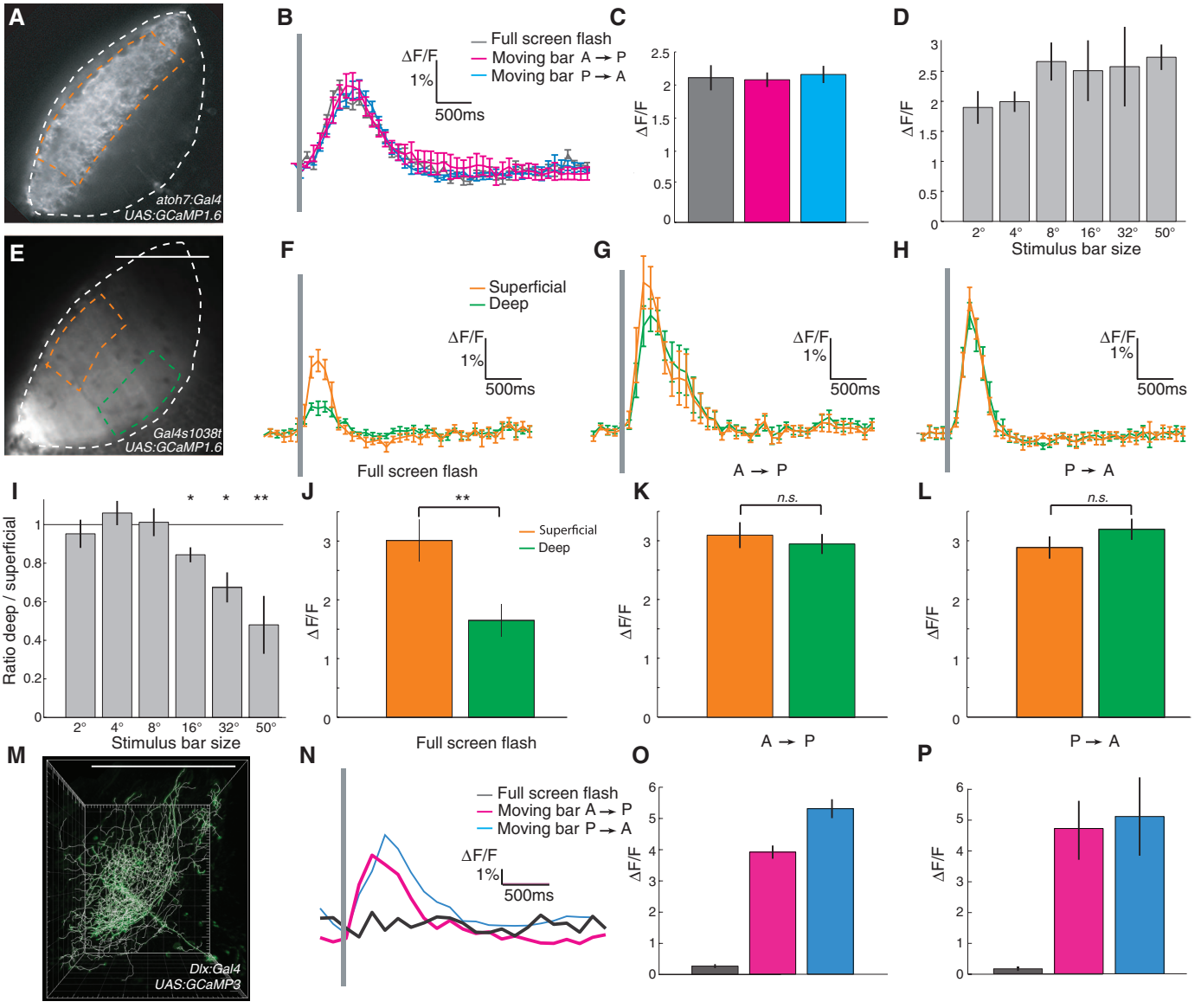

Fig. 1. Ca^{2+} responses in the tectal neuropil reveal size selectivity of deep layers. (**A**) Fluorescent signal from retinal axon terminals in the tectum of an *Atoh7:Gal4, UAS:GCaMP1.6* larva. Region of interest (ROI) is demarcated by the orange dashed line. Neuropil boundaries are indicated by white dashed lines. (**B**) Tectal responses in an *Atoh7:Gal4, UAS:GCaMP1.6* larva to a full-screen flash (50° visual angle) or to black bars (2° wide, moving A→P or P→A with a speed of 0.25°/ms). (**C**) Average maximum responses in the *Atoh7:Gal4, UAS:GCaMP1.6* larvae (n = 5). (**D**) Tuning of retinal axons in the *Atoh7:Gal4, UAS:GCaMP1.6* larvae to bars of increasing width (n = 5). (**E**) Fluorescent signal from posterior PVPNs in *Gal4s1038t, UAS:GCaMP1.6* larva. ROIs for superficial (orange) and deep (green) neuropil layers are indicated by dashed lines. Neuropil boundary is white dashed line. (**F** to **H**) Responses to three visual stimuli in a *Gal4s1038t, UAS:GCaMP1.6* larva. (**I**) Ratios of maximum responses in deep and superficial neuropil layers to bars of increasing width in *Gal4s1038t, UAS:GCaMP1.6* larvae (n = 7 for 2° and 50°; n = 3 for other stimuli). (**J** to **L**) Average maximum responses in *Gal4s1038t, UAS:GCaMP1.6* larvae (n = 7). *P < 0.05, **P < 0.01 (t test). (**M**) Reconstruction of a single PVN expressing *UAS:GCaMP3, Dlx5/6:Gal4*. (**N**) Ca^{2+} response of the PVN shown in (M). (**O**) Average maximum $\Delta F/F$ response in this cell. (**P**) Average response of bar-selective PVNs (n = 7). Error bars indicate SEM. Gray bars in (B), (F), (G), (H), and (N) indicate time of visual stimulation.

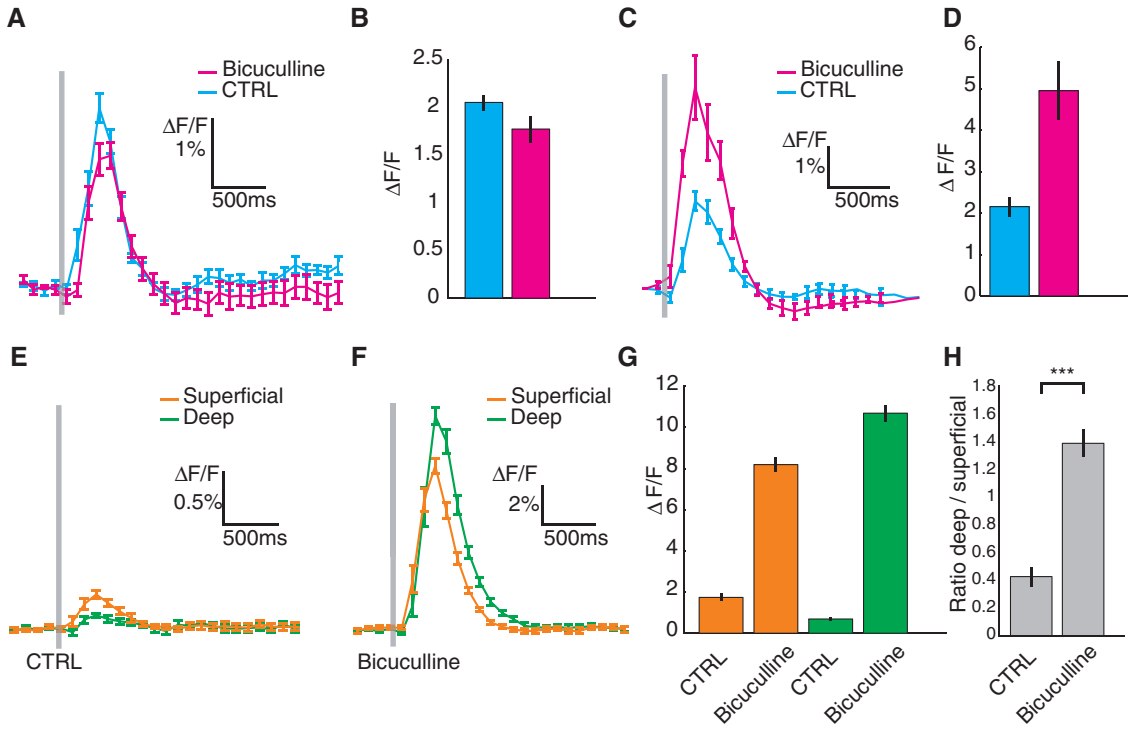

Fig. 2. The neuropil Ca^{2+} response to a large visual stimulus is shaped by tectum-intrinsic GABAergic inhibition. (**A** and **B**) Effect of bicuculline administration to the tectum in *Atoh7:Gal4, UAS:GCaMP1.6* transgenics. Response to a full-screen flash in a single larva (A) and average (n = 3) maximal response (B) before (CTRL, blue) and after bicuculline treatment (magenta). (**C** and **D**) Effect of intraocular injection of bicuculline in *Atoh7:Gal4, UAS:GCaMP1.6*. Response to a full-screen flash in a single larva (C) and average (n = 4) maximal response (D) before (CTRL, blue) and after bicuculline treatment (magenta). (**E** and **F**) Representative responses in superficial (orange) and deep (green) neuropil layers in *Gal4s1038t, UAS:GCaMP1.6* larva before (E) and after bicuculline administration to tectum (F). (**G** and **H**) Average maximal response to a full-screen flash (G) and ratios (H) of *Gal4s1038t, UAS:GCaMP1.6* larvae (n = 4) in superficial (orange) and deep (green) tectal neuropil layers before (CTRL) and after bicuculline administration. ***$P < 0.001$ (t test). Error bars indicate SEM. Gray bars in (A), (C), (E), and (F) indicate time of visual stimulation.

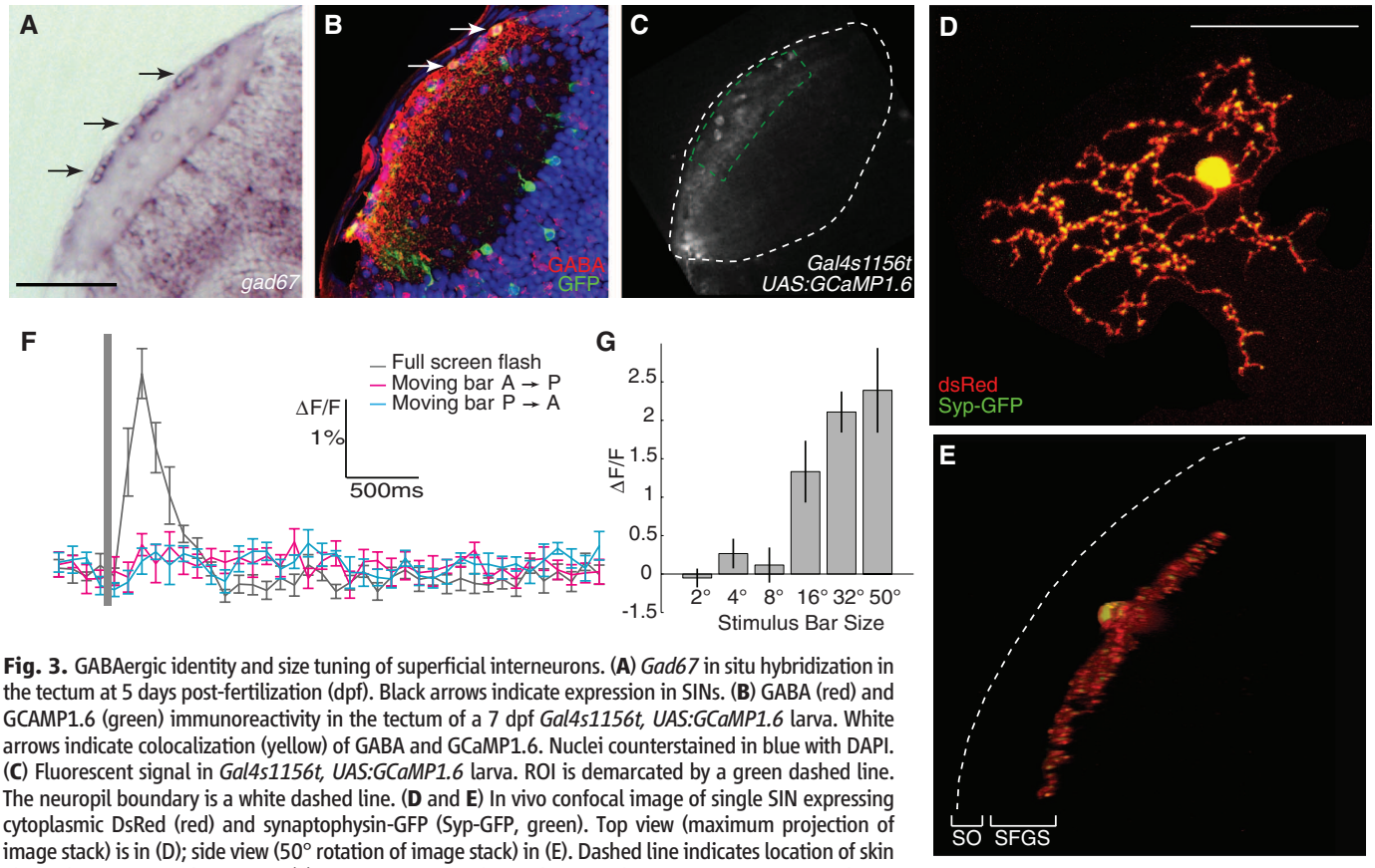

Fig. 3. GABAergic identity and size tuning of superficial interneurons. (**A**) *Gad67* in situ hybridization in the tectum at 5 days post-fertilization (dpf). Black arrows indicate expression in SINs. (**B**) GABA (red) and GCAMP1.6 (green) immunoreactivity in the tectum of a 7 dpf *Gal4s1156t, UAS:GCaMP1.6* larva. White arrows indicate colocalization (yellow) of GABA and GCaMP1.6. Nuclei counterstained in blue with DAPI. (**C**) Fluorescent signal in *Gal4s1156t, UAS:GCaMP1.6* larva. ROI is demarcated by a green dashed line. The neuropil boundary is a white dashed line. (**D** and **E**) In vivo confocal image of single SIN expressing cytoplasmic DsRed (red) and synaptophysin-GFP (Syp-GFP, green). Top view (maximum projection of image stack) is in (D); side view (50° rotation of image stack) in (E). Dashed line indicates location of skin above the surface of the tectum. (**F**) Responses to visual stimuli in a *Gal4s1156t, UAS:GCaMP1.6* larva. (**G**) Maximum average responses (n = 4). Scale bars, 50 μm in (A) and (C), 30 μm in (D) and (E). Error bars indicate SEM.

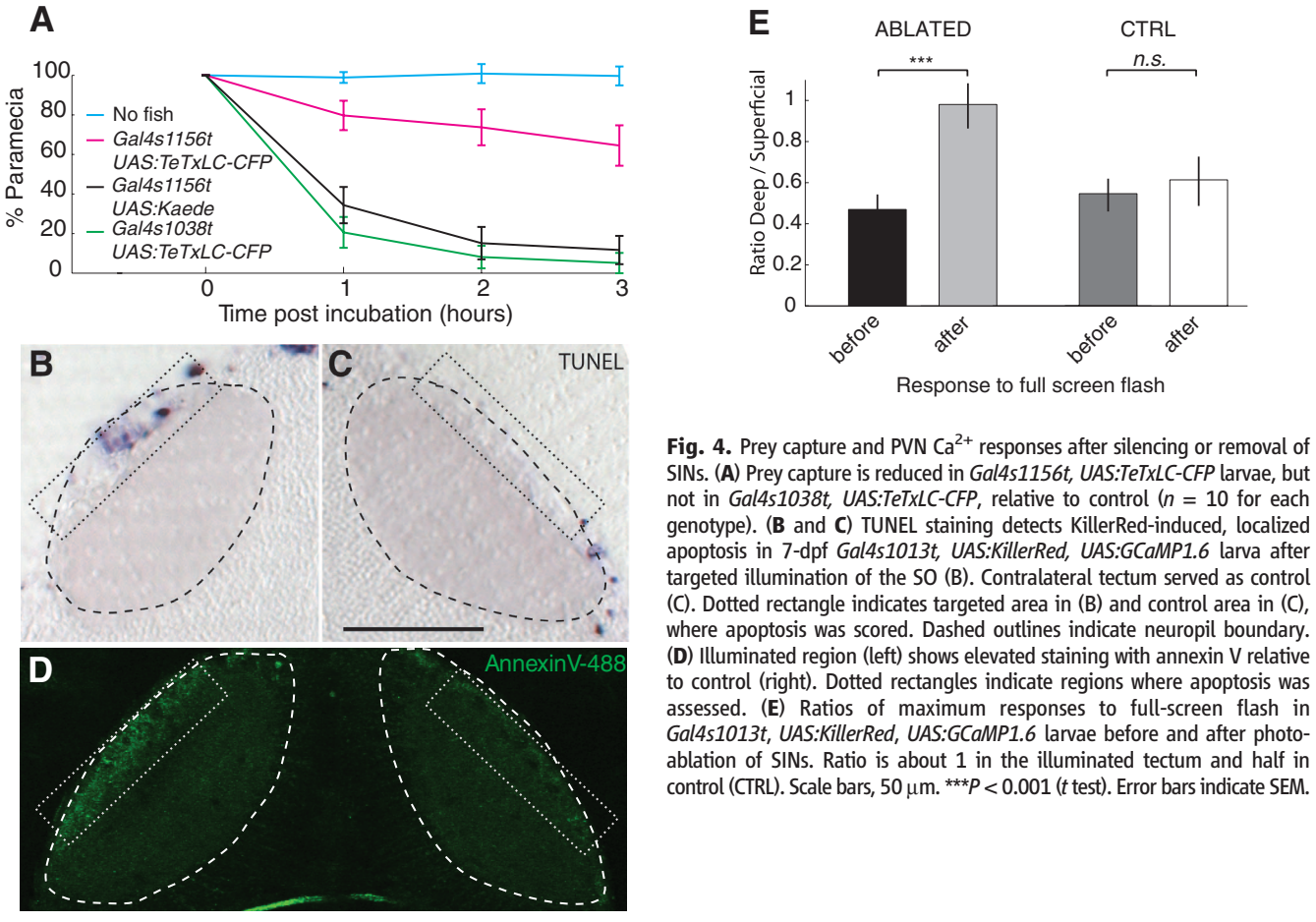

Fig. 4. Prey capture and PVN Ca^{2+} responses after silencing or removal of SINs. (**A**) Prey capture is reduced in *Gal4s1156t, UAS:TeTxLC-CFP* larvae, but not in *Gal4s1038t, UAS:TeTxLC-CFP*, relative to control (n = 10 for each genotype). (**B** and **C**) TUNEL staining detects KillerRed-induced, localized apoptosis in 7-dpf *Gal4s1013t, UAS:KillerRed, UAS:GCaMP1.6* larva after targeted illumination of the SO (B). Contralateral tectum served as control (C). Dotted rectangle indicates targeted area in (B) and control area in (C), where apoptosis was scored. Dashed outlines indicate neuropil boundary. (**D**) Illuminated region (left) shows elevated staining with annexin V relative to control (right). Dotted rectangles indicate regions where apoptosis was assessed. (**E**) Ratios of maximum responses to full-screen flash in *Gal4s1013t, UAS:KillerRed, UAS:GCaMP1.6* larvae before and after photoablation of SINs. Ratio is about 1 in the illuminated tectum and half in control (CTRL). Scale bars, 50 μm. ***$P < 0.001$ (*t* test). Error bars indicate SEM.

tectum are labeled (*2*) (Fig. 1E). This population is activated by retinal stimulation, as surgical removal of one eye eliminated GCaMP1.6 responses in the contralateral tectum (fig. S1; maximum $\Delta F/F = 2.17 \pm 0.23\%$ in ipsilateral tectum versus 0.09 ± 0.14 in contralateral tectum; $P_{I\text{-}C} < 3.16 \times 10^{-4}$; $n = 5$). However, the response to the full-screen flash was weaker in the deep output layer than in the superficial input layer (Fig. 1, F and J; $3.01 \pm 0.36\%$ for superficial versus $1.65 \pm 0.28\%$ for deep; $P < 10^{-4}$). Although the absolute fluorescence signals varied between fish, the deep-to-superficial response ratios were consistent (Fig. 1J and fig. S2; deep-to-superficial ratio = 0.48 ± 0.15; $P < 0.01$, $n = 7$). In contrast, small moving bars activated Ca^{2+} rises equally in the deep and the superficial layers (Fig. 1, G, H, K, and L; A→P: $2.95 \pm 0.17\%$ for deep versus $3.10 \pm 0.22\%$ for superficial, deep-to-superficial ratio = 0.95 ± 0.07; P→A: $3.2 \pm 0.18\%$ for deep versus $2.89 \pm 0.19\%$ for superficial, deep-to-superficial ratio = 1.10 ± 0.31; $P_{A\rightarrow P} = 0.16$ and $P_{P\rightarrow A} = 0.23$; $n = 7$). The tuning curve showed a systematic size-dependent reduction of the response (Fig. 1I), which suggests that large stimuli did not efficiently excite the cellular elements in the deep neuropil layer.

In the *Gal4s1013t* line, almost all tectal cells are labeled (*2*), allowing us to record Ca^{2+} responses across the entire visual field. The deep-to-superficial response ratios in response to a full-screen flash were not significantly different between the anterior and posterior halves of the tectum (0.41 ± 0.19 versus 0.36 ± 0.27; $n = 3$). Thus, there does not seem to be a topographic bias in size tuning across the visuotopic map.

We used a mosaic labeling strategy to image the dendritic activity of individual PVNs. Two DNA constructs encoding *UAS:GCaMP3* (*23*) and *Dlx5/6:Gal4* (*24*) were co-injected at the two-cell stage, and larvae with only one or very few labeled PVNs were used for imaging (Fig. 1M). Of 38 PVNs recorded, 7 (18%) responded to small moving bars; the remaining cells did not respond to any of the stimuli. None of the PVNs was activated by the full-screen stimulus (Fig. 1, N to P, $n = 7$). In the seven PVNs sensitive to small moving bars, we could not detect significant differences in the Ca^{2+} response between the distal (superficial) and the proximal (deep) segments of their dendritic trees ($P = 0.49$), indicating the existence of a circuit that filters out low-frequency spatial inputs before they reach the PVN dendrites.

We next showed that spatial filtering is achieved by feedforward inhibition. Local application of the $GABA_A$ receptor antagonist bicuculline (Bicu) to the tectum increased responses in the entire neuropil, but not uniformly. In the deep layers of *Gal4s1038t, UAS:GCaMP1.6*, Ca^{2+} signals rose by more than a factor of 15, whereas in the superficial layers the increase was by only a factor of 5 (Fig. 2, E to G; superficial, $8.19 \pm 0.36\%$ for Bicu versus $1.74 \pm 0.19\%$ for control; deep, $10.69 \pm 0.41\%$ for Bicu versus $0.69 \pm 0.09\%$ for control; $P_{SUP} < 1.4 \times 10^{-7}$ and $P_{DEEP} < 9.9 \times 10^{-8}$, $n = 4$), inverting the normal ratio (Fig. 2H and fig. S3; deep-to-superficial ratio for Bicu = 1.38 ± 0.10 versus 0.43 ± 0.07 for control; $P < 3.1 \times 10^{3}$; $n = 4$). Bicu administration to the tectum had no detectable effect on the strength of retinal inputs (Fig. 2, A and B; $1.99 \pm 0.18\%$ for Bicu versus $2.52 \pm 0.19\%$ for control; $n = 3$). In contrast, intraocular Bicu injection produced a robust increase in the Ca^{2+} response (Fig. 2, C and D; $4.96 \pm 0.70\%$ for Bicu versus $2.16 \pm 0.24\%$ for control; $n = 4$).

Gal4s1156t drives expression in a specific population of neurons whose cell bodies are located in the SO (Fig. 3, A to C) (*2*). Antibody staining showed that most, or all, neurons in this layer expressed the GABA markers Gad67 and Reelin (Fig. 3, A and B, and figs. S4 and S5) ($94.71 \pm 0.6\%$; 229 cells counted in $n = 3$ larvae). Furthermore, almost all *Gal4s1156t*-expressing cells were GABA-positive (54 of 56 cells in $n = 4$ larvae). Labeling of single cells by mosaic expression of cytoplasmic DsRed and synaptophysin fused to green fluorescent protein (Syp-GFP) (*25*) revealed that these cells extend a broad, regularly branched axonal arbor, containing many pre-

synaptic specializations (Fig. 3, D and E). Cells with similar morphologies have been described in other vertebrate species (*26*). Strikingly, these superficial interneurons (SINs) showed a robust response only to the full screen, not to small moving bars (Fig. 3, F and G; 2.27 ± 0.32%; $P < 1.34 \times 10^{-4}$; A→P: 0.21 ± 0.14%; P→A: 0.09 ± 0.16%; $P = 0.42$; $n = 6$). We conclude that SINs are tuned to large stimuli.

The SINs may provide feedforward inhibition of PVNs. If so, their removal from the circuit should alter the tuning of PVNs and should impair a behavior that relies on this circuit property. We blocked synaptic transmission in the SINs by driving tetanus toxin light chain fused to cyan fluorescent protein (TeTxLC-CFP) (*27*) in *Gal4s1156t*. Double-transgenic larvae captured far fewer paramecia than controls (Fig. 4A), whereas their optomotor behavior was unaffected (fig. S6). Blocking transmission from the small number of PVPNs in *Gal4s1038t* did not reduce prey capture rates. Using the pan-tectum *Gal4s1013t* line (*2*), we generated a fish expressing both the genetically encoded photosensitizer KillerRed (*28*) and GCaMP1.6 in both PVNs and SINs. To selectively kill the SINs, we illuminated the SO with an intense green laser (563 nm). Terminal deoxynucleotidyl transferase–mediated deoxyuridine triphosphate nick end labeling (TUNEL) staining and in vivo annexin V labeling showed apoptotic cells only in the targeted region (9.5 ± 1.8 $TUNEL^+$ cells per section on the ablated SO versus 1.0 ± 0.6 $TUNEL^+$ cells per section on the control side, $P < 0.05$; 4.5 ± 1.0 $TUNEL^+$ cells in the SPV of the ablated tectum versus 4.0 ± 0.4 in the control SPV, $P = 0.5$) (Fig. 4, B to D). After photo-ablation of SINs, Ca^{2+} responses in the PVNs to a full-screen flash were equalized across the neuropil layers (Fig. 4E; deep-to-superficial ratio = 0.47 ± 0.8 before illumination versus deep-to-superficial ratio = 0.98 ± 0.11 after; $P < 10^{-3}$ after illumination, $n = 4$). No significant change in response ratios was observed in the tectum contralateral to the illumination (before: deep-to-superficial ratio = 0.55 ± 0.8; after: deep-to-superficial ratio = 0.61 ± 0.12; $P = 0.38$).

Together, our findings support a contribution of SINs to the neural mechanism that filters visual inputs in the tectum. In one possible scheme (fig. S7), which is supported by the morphologies of PVN cell types (*2*, *5*), SINs make GABAergic contacts with some PVINs, which in turn convey this information to the dendritic arbors of PVPNs. Thus, the visual information flows from superficial to deep through a neural filter that subtracts low-frequency spatial information. This circuit may support prey capture by allowing the animal to track a moving object against a background that changes uniformly in brightness or is composed of low spatial frequencies. Given that the mammalian superior colliculus has similar layer-specific spatial filtering properties (*1*, *12*), it seems likely that this circuitry is evolutionarily conserved among vertebrates.

References and Notes

1. T. Isa, *Curr. Opin. Neurobiol.* **12**, 668 (2002).
2. E. K. Scott, H. Baier, *Front Neural Circuits* **3**, 13 (2009).
3. H. Vanegas, M. Laufer, J. Amat, *J. Comp. Neurol.* **154**, 43 (1974).
4. J. Meek, N. A. Schellart, *J. Comp. Neurol.* **182**, 89 (1978).
5. L. M. Nevin, E. Robles, H. Baier, E. K. Scott, *BMC Biol.* **8**, 126 (2010).
6. T. Sato, T. Hamaoka, H. Aizawa, T. Hosoya, H. Okamoto, *J. Neurosci.* **27**, 5271 (2007).
7. T. Xiao, T. Roeser, W. Staub, H. Baier, *Development* **132**, 2955 (2005).
8. L. M. Nevin, M. R. Taylor, H. Baier, *Neural Develop.* **3**, 36 (2008).
9. E. Gahtan, P. Tanger, H. Baier, *J. Neurosci.* **25**, 9294 (2005).
10. T. Roeser, H. Baier, *J. Neurosci.* **23**, 3726 (2003).
11. R. Portugues, F. Engert, *Curr. Opin. Neurobiol.* **19**, 644 (2009).
12. U. C. Drăger, D. H. Hubel, *Nature* **253**, 203 (1975).
13. C. M. Niell, S. J. Smith, *Neuron* **45**, 941 (2005).
14. P. Sajovic, C. Levinthal, *Neuroscience* **7**, 2407 (1982).
15. J. H. Bollmann, F. Engert, *Neuron* **61**, 895 (2009).
16. P. Ramdya, F. Engert, *Nat. Neurosci.* **11**, 1083 (2008).
17. P. Ramdya, B. Reiter, F. Engert, *J. Neurosci. Methods* **157**, 230 (2006).
18. G. Sumbre, A. Muto, H. Baier, M. M. Poo, *Nature* **456**, 102 (2008).
19. M. C. Smear *et al.*, *Neuron* **53**, 65 (2007).
20. E. K. Scott *et al.*, *Nat. Methods* **4**, 323 (2007).
21. H. Baier, E. K. Scott, *Curr. Opin. Neurobiol.* **19**, 553 (2009).
22. M. Ohkura, M. Matsuzaki, H. Kasai, K. Imoto, J. Nakai, *Anal. Chem.* **77**, 5861 (2005).
23. L. Tian *et al.*, *Nat. Methods* **6**, 875 (2009).
24. T. Zerucha *et al.*, *J. Neurosci.* **20**, 709 (2000).
25. M. P. Meyer, S. J. Smith, *J. Neurosci.* **26**, 3604 (2006).
26. H. Vanegas, *Comparative Neurology of the Optic Tectum* (Plenum, New York, 1984).
27. K. Asakawa *et al.*, *Proc. Natl. Acad. Sci. U.S.A.* **105**, 1255 (2008).
28. M. E. Bulina *et al.*, *Nat. Biotechnol.* **24**, 95 (2006).

29. We thank W. Staub for care of animals, T. Müller for the *gad67* probe, K. Kawakami for Tol2 and TeTxLC-CFP reagents, L. Garner for advice on the visual setup, and J. Nakai for the GCaMP1.6 vector. F.D.B. and C.W. were supported, respectively, by a Human Frontier Science Program long-term postdoctoral fellowship and a Marie Curie Outgoing International Fellowship (with CNRS UMR5020 "Neurosciences Sensorielles, Comportement Cognition," Lyon, France). E.R. was supported by an NSF postdoctoral fellowship. This work was funded by the NIH Nanomedicine Development Center for the Optical Control of Biological Function (PN2 EY018241, E.Y.I. and H.B.), NSF/FIBR 0623527 (E.Y.I.), a Sandler Opportunity Award (H.B.), the Byers Basic Science Award (H.B.), and NIH grants R01 EY012406 and R01 NS053358 (H.B.).

Supporting Online Material

www.sciencemag.org/cgi/content/full/330/6004/669/DC1
Materials and Methods
Figs. S1 to S7
References

28 May 2010; accepted 17 September 2010
10.1126/science.1192949

Visualizing Ribosome Biogenesis: Parallel Assembly Pathways for the 30*S* Subunit

Anke M. Mulder,[1] Craig Yoshioka,[1] Andrea H. Beck,[2] Anne E. Bunner,[2] Ronald A. Milligan,[1] Clinton S. Potter,[1] Bridget Carragher,[1] James R. Williamson[2]*

Ribosomes are self-assembling macromolecular machines that translate DNA into proteins, and an understanding of ribosome biogenesis is central to cellular physiology. Previous studies on the *Escherichia coli* 30*S* subunit suggest that ribosome assembly occurs via multiple parallel pathways rather than through a single rate-limiting step, but little mechanistic information is known about this process. Discovery single-particle profiling (DSP), an application of time-resolved electron microscopy, was used to obtain more than 1 million snapshots of assembling 30*S* subunits, identify and visualize the structures of 14 assembly intermediates, and monitor the population flux of these intermediates over time. DSP results were integrated with mass spectrometry data to construct the first ribosome-assembly mechanism that incorporates binding dependencies, rate constants, and structural characterization of populated intermediates.

Ribosome biogenesis in bacteria requires the coordinated synthesis and assembly of 55 ribosomal proteins and three large ribosomal RNAs (rRNAs) facilitated by ~30 assembly cofactors (*1*). Notably, both the 30*S* and 50*S* ribosomal subunits can be assembled in vitro from purified components, and most of the information required to assemble ribosomes is encoded in the sequences of the component RNAs and proteins (*2*, *3*). The 30*S* ribosomal subunit is composed of a single ~1500-nucleotide 16*S* RNA component and 20 ribosomal proteins ("r-proteins") (fig. S1). In reconstitution experiments under equilibrium conditions, 30*S*-subunit assembly is both parallel and hierarchical with primary-binding proteins binding independently to each domain, followed by secondary- and tertiary-binding proteins (*4*). As would be expected based on the cotranscriptional assembly pathway in vivo (*1*), the observed kinetic order for protein binding in vitro is that 5′-domain proteins bind fastest, followed by the central domain proteins and 3′-domain proteins (*5*, *6*). Although

[1]Department of Cell Biology, The Scripps Research Institute, La Jolla, CA 92037, USA. [2]Departments of Molecular Biology and Chemistry and The Skaggs Institute for Chemical Biology, The Scripps Research Institute, La Jolla, CA 92037, USA.

*To whom correspondence should be addressed. E-mail: jrwill@scripps.edu

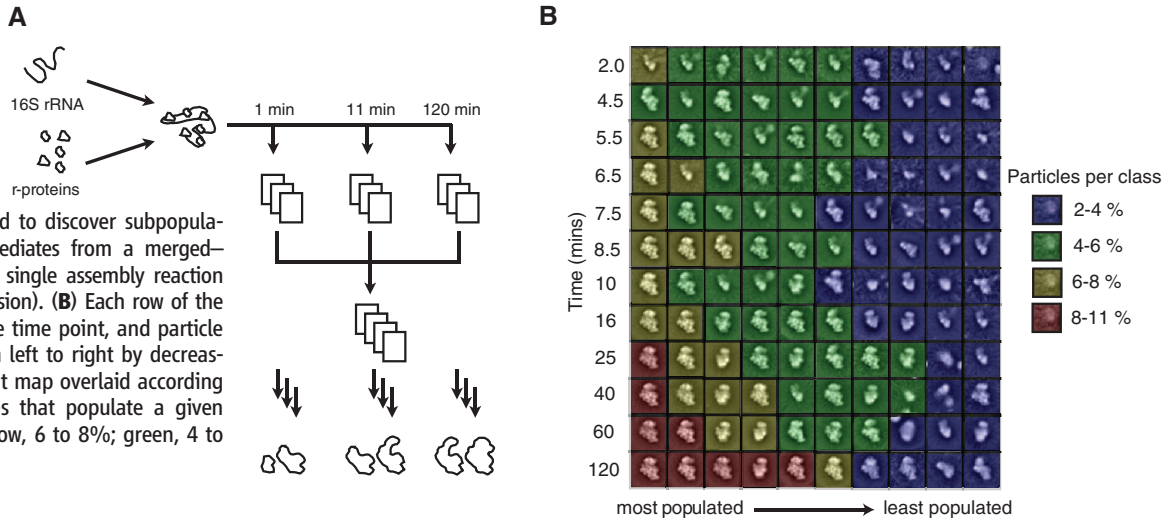

Fig. 1. Discovery single-particle profiling (DSP). (**A**) Assembly of the 30*S* subunit was initiated as described (*10*), and aliquots were prepared for negative-stain EM (*20*) at various time points. The DSP method was used to discover subpopulations of assembly intermediates from a merged–time-course data set of a single assembly reaction (see supplementary discussion). (**B**) Each row of the array results from a single time point, and particle averages are ranked from left to right by decreasing population with a heat map overlaid according to percentage of particles that populate a given class: red, 8 to 11%; yellow, 6 to 8%; green, 4 to 6%; blue, 2 to 4%.

there is evidence for parallel assembly pathways and the existence of multiple assembly intermediates, the structures of such intermediates are not known, and little mechanistic information is available for the order of their assembly.

Single-particle electron microscopy (EM) image analysis can resolve heterogeneous populations of molecules and classify them into homogenous subpopulations that can be visualized in two and three dimensions (*7*, *8*). We used single-particle reference-free alignment and classification to "discover" subpopulations of assembly intermediates within the heterogeneous assembly reaction over a time course (Fig. 1A and supplementary discussion) (*9*). After synchronous initiation of 30*S* ribosome assembly (*4*, *10*, *11*), there is a distribution of assembly intermediates at various stages of RNA folding and protein binding (*6*). Negative-stain sample preparation rapidly traps these intermediate complexes at various time points, and high-throughput EM data collection and analysis allows the visualization of these intermediates without the need for biochemical purification (*12*, *13*). Classification of the entire time-course data set allows determination of the population, conformation, and protein composition of the prevalent assembly intermediates as a function of time; this combined approach is referred to as discovery single-particle profiling (DSP).

We collected data sets at time points ranging from 0 to 120 min, and the resulting array of subpopulations indicate that, on average, particle sizes start from small structures and become increasingly 30*S*-like over time (Fig. 1B). Notably, subpopulations that are substantially populated at early time points (Fig. 1B, 2 min, column 1, yellow) are less populated at later time points (Fig. 1B, 60 min, column 9, blue), whereas subpopulations that are substantially populated at later time points (Fig. 1B, 120 min, column 1, red) are absent during early time points (Fig. 1B, 2 min). Classification of the data (figs. S2 and S3) revealed four major groups of assembly intermediates and identified 14 distinct assembly

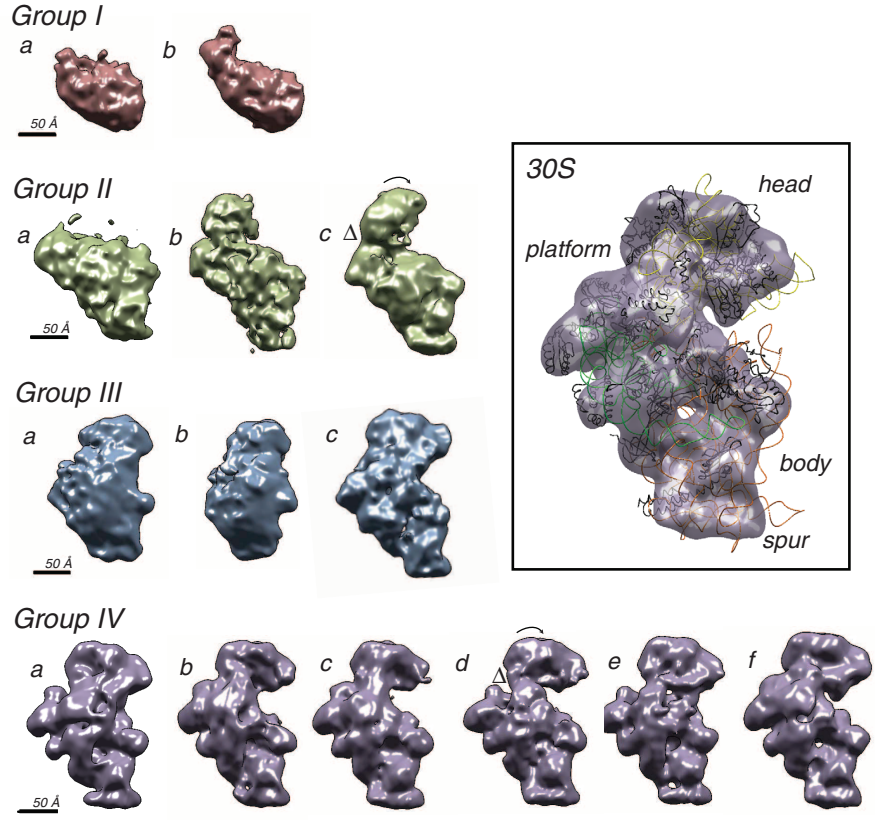

Fig. 2. Structural determination of assembly intermediates. Assembly intermediates classify into four groups based on classification of 2D data (figs. S2, S3, and S5), docking of the 30*S* subunit crystal structure (fig. S8B), and 3D difference mapping (fig. S6). RCT volumes are color coded in accordance with the state of assembly: red < green < blue < purple. A conformational change in the neck of central domain rRNA causing a rotation in the head domain is the major difference between group II and group IV intermediates (Δ symbol and arrow).

intermediates distributed among these four groups (Fig. 2). We visualized three-dimensional (3D) structures for the set of 14 intermediates and determined the compositions of individual intermediates by 3D difference mapping, comparison to the x-ray crystal structure, and subcomplex reconstitution experiments (figs. S5 to S9) (*14*, *15*). Reconstitution experiments, in which known protein components were omitted from the assembly reaction, confirmed that compositional differences between assembly intermediates were not due to negative-stain artifacts (also see supplementary discussion). The use of random conical tilt (RCT) reconstruction and 3D difference mapping also confirmed that conformational differences between assembly intermediates were real and not due to misinterpretation of 2D projection views. The structures of the set

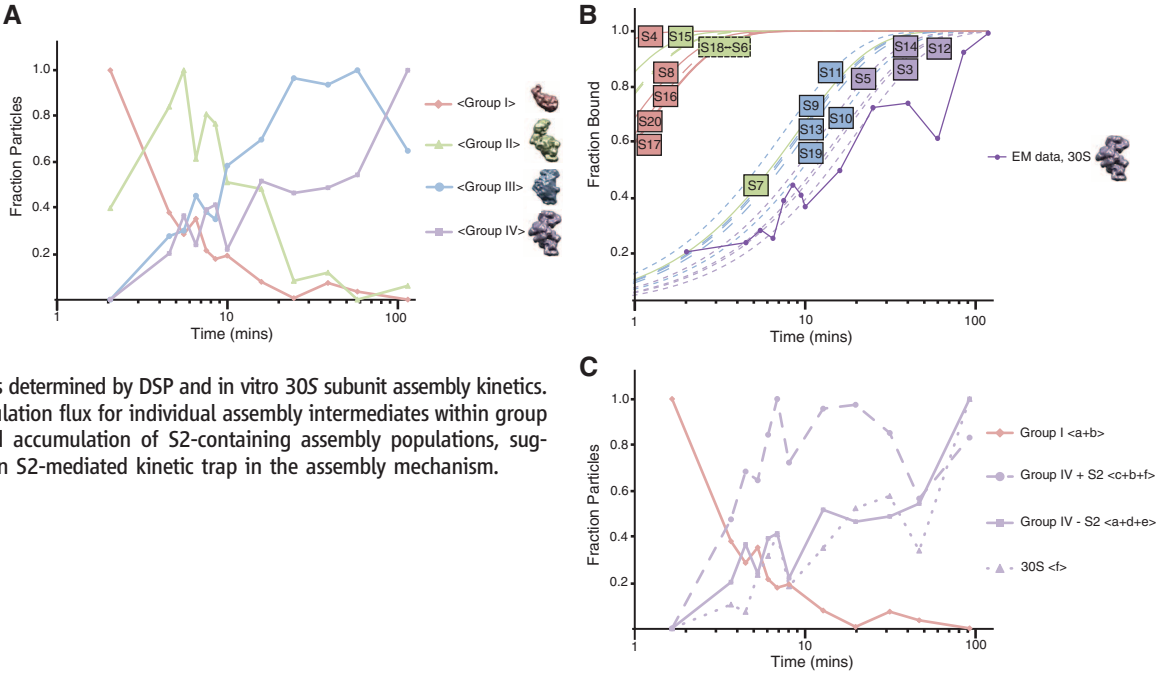

Fig. 3. Assembly intermediate population flux over time. (**A**) Classification of merged–time-point data sets allowed determination of the contribution of different time points to assembly intermediate groups I (red), II (green), III (blue), and IV (purple). (**B**) Measurement of protein binding rates by PC-QMS illustrates the correspondence between population profiles determined by DSP and in vitro 30*S* subunit assembly kinetics. (**C**) Decomposition of population flux for individual assembly intermediates within group IV (purple) revealed rapid accumulation of S2-containing assembly populations, suggesting the existence of an S2-mediated kinetic trap in the assembly mechanism.

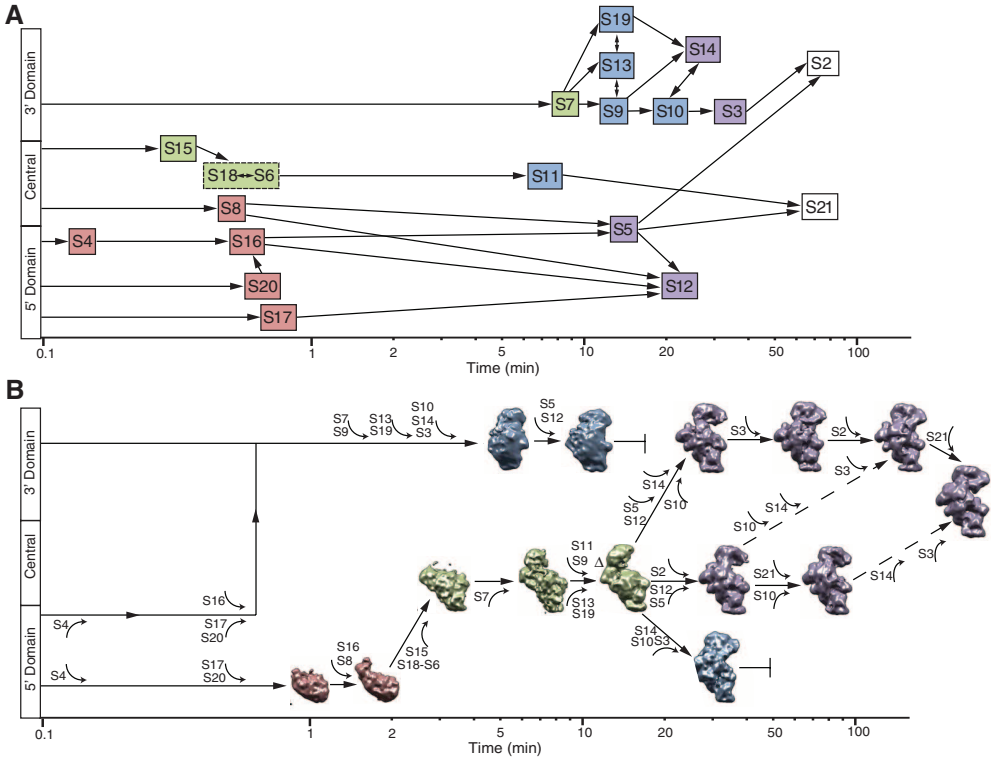

Fig. 4. A parallel mechanism for 30*S* subunit assembly. (**A**) A Nomura assembly map on a time axis that takes into account the time $t_{0.5}$ of binding for each r-protein as determined by PC-QMS. (**B**) Combination of kinetic, thermodynamic, and single-particle data allows construction of a mechanism for 30*S* subunit assembly that accounts for parallel assembly pathways.

of 14 assembly intermediates categorized into early (group I, red), middle (groups II and III, green and blue), and late (group IV, purple) stages of assembly are shown in Fig. 2.

Using DSP, we simultaneously classified the entire collection of particles from all time points and determined the fractional contribution of particles observed at each time point to the four assembly intermediate groups, resulting in single-particle profiles of subpopulation flux over time (Fig. 3A). Group I classes are primarily populated at early time points, group II and III classes are populated at middle time points, and group IV subpopulations are primarily populated at late time points. To draw a correspondence between these population profiles from DSP and protein binding kinetics in vitro, we measured the rate of binding of the 30*S* proteins under identical conditions using the pulse-chase quantitative mass spectrometry (PC-QMS) assay (Fig. 3B) (*6*). The appearance of the group IV particles exactly tracks binding of the slowest tertiary binding proteins monitored by PC-QMS (Fig. 3B, purple circles). Similarly, the depletion over time of group I subpopulations tracks binding of the fastest primary and secondary binding proteins (Fig. 3, A and B, red), with groups II and III tracking binding of the proteins with intermediate binding rates (Fig. 3, A and B, green and blue). Thus, group I subpopulations are ultimately converted into group IV subpopulations, with groups II and III bridging the assembly landscape between these two extremes. Slow

elimination for group II intermediates and slow accumulation of group III intermediates is in accordance with the lag observed after assembly of the 5′ and central domains in vitro (Fig. 3B, red versus green and blue). Thus, these subpopulations, which reflect an assembly landscape of transient intermediates, eventually converge to the native 30*S* ribosome structure.

Comparison of the 3D assembly intermediate structures to that of the fully formed 30*S* subunit readily identified known features of small ribosome subunit architecture (Fig. 2, inset). Group I fit the body domain of the 30*S* crystal structure containing primary r-proteins S4, S17, S20, and secondary r-protein S16. Diffuse density above the structure corresponds to an assembling platform domain in which the r-protein heterodimer S6-S18 is likely transiently bound, and central domain rRNA is only partially structured (Fig. 2, red, and fig. S8C). Group II intermediates include an assembled body and platform domain with various stages of early head domain assembly (Fig. 2, green, and fig. S8C). Three-dimensional difference mapping reveals a conformational change in the neck of the 16*S* rRNA central domain of group II intermediates relative to group IV intermediates (Fig. 2, arrow, and fig. S6B). This conformational change involves a rotation of the body domain relative to the platform domain, and reconstitution experiments suggest that this rRNA conformational change is stabilized, but not actively induced, by binding of 3′ domain r-proteins (fig. S7). This conformation of the head domain is also seen in volume "c" of group III intermediates, whereas group III volumes "a" and "b" have compact shapes that include partially assembled head and body domains with missing density at the spur and the platform domains (Fig. 2, blue).

Group IV subpopulations are distinctly 30*S*-like in appearance and vary primarily in the second half of the head domain and at the head-body and head-platform interfaces (Fig. 2, purple). Fitting of the 30*S* crystal structure into 3D difference maps suggests that missing density in the platform domain corresponds to S21 and/or S11 and surrounding [helix 23/helix 24 (h23/h24)] rRNA (fig. S6). Notably, the neck of the central domain for group IV intermediates has converted from that observed for group II intermediates, thereby allowing room for the additional S21/S11 density. Defined subcomplex reconstitution studies indicate that conversion from the conformation present in group II to that in group IV occurs in the presence of S21/S11, but that the associated extra density is not visible until late 3′ domain assembly (fig. S7). The structural and compositional diversity of group IV assembly intermediates is evidence for the existence of parallel assembly pathways in the 3′ domain of the 30*S* subunit.

Decomposition of the kinetic profiles for subpopulations within group IV show fast accumulation for classes with density corresponding to the S2-H44 region of the 30*S* subunit and slow accumulation for classes lacking this density (Fig. 3C and fig. S6). In contrast to the observed thermodynamic dependence of S2 binding upon earlier binding of S3 (Fig. 4A) (*4*), the S2-H44 region is able to form stably enough for EM visualization before consolidation of the S3-H34/H33 region (figs. S6 and S8). Kinetic data for S3 binding during 30*S* assembly indicate a slow-binding constant relative to primary and secondary r-proteins, but association constants for S2 have not been measurable with PC-QMS, presumably because of a weak and transient interaction (*6*, *16*). Fast protections of portions of both the S2 and S3 binding sites are observed in time-resolved hydroxyl radical foot printing experiments (*17*), consistent with formation of transient encounter complexes for these two proteins. The time-resolved EM data suggest independent binding of these two late-binding proteins, thus directly illustrating the existence of parallel assembly pathways.

The combination of thermodynamic dependency maps, ensemble kinetic data, and single-particle profiling with structural analysis allows construction of an expanded assembly mechanism that accounts for both thermodynamic and kinetic interdependencies (Fig. 4). The most populated branch of assembly starts with group I intermediates containing fast-binding primary and secondary r-proteins, proceeds to group II intermediates containing slower-binding primary and secondary r-proteins that bind in central and early 3′ domains, and culminates in the set of group IV intermediates resulting from parallel pathways for assembly of slow-binding tertiary r-proteins (Fig. 4B). In the absence of bound protein, tertiary rRNA structure is not readily visualized for early assembly intermediates, which is probably due to a combination of unfolded and/or conformationally heterogeneous rRNA structure and difficulty in directly visualizing RNA using negative stain. Nevertheless, the substantial energetic gains achieved by rRNA folding and the requirement for cooperativity with r-protein binding is illustrated by the rRNA neck conformational change that mediates transition from group II to group IV intermediates (Fig. 4B, Δ symbol). Importantly, the neck is the site of interaction for the assembly cofactor *Era*, which has been implicated in facilitation of global rRNA conformational changes during late central and early 3′ domain assembly. *Era* is thought to act in concert with cofactor *RimM*, which itself interacts with S19, an r-protein majorly implicated in kinetic cooperativity during 3′ domain assembly (*18*, *19*). We speculate that this rotated conformation is required for productive binding by slow-binding tertiary proteins such as S10, S14, S2, S3, and S21. The independent order of binding by these proteins in the group IV intermediates is evidence for parallel assembly in the 3′ domain to a much greater extent than previously appreciated. Population flux studies show rapid accumulation of S2-containing intermediates relative to S3-containing intermediates, even though S3 is thermodynamically required for S2 binding. Rapid initial binding by S2 results in kinetically trapped intermediates with slow subsequent binding rates of S3, leading to slow conversion to productively assembled 30*S* subunits (Fig. 4B, dashed arrows). Such kinetic traps are likely avoided in vivo by the participation of assembly cofactors such as *RimP*, which is thought to facilitate r-protein binding during the very late stages of assembly (*18*). Several less populated intermediates in group III consist of assembled body and head domains with unassembled platform and spur domains, likely resulting from improper assembly initiation due to the presence of the entire 16*S* rRNA. Although it is possible that these intermediates could convert to productive group IV intermediates through conformational changes or protein association and dissociation, the population profiles suggest that these subpopulations are probably dead-end intermediates in assembly reactions in vitro (fig. S4). Another potentially unproductive pathway branches from the major productive pathway at the point of conversion from group II to group IV intermediates and culminates in an end product that is compressed in structure and missing key r-proteins. The co-transcriptional nature of 30*S* assembly and the presence of cofactors likely minimize the formation of such unproductive intermediates in vivo. Nevertheless, our structural and temporal assembly map shows specific evidence for parallel assembly pathways in vitro and probably recapitulates many of the same steps undergone in vivo. The DSP method used for this work is a novel approach for understanding structure and dynamics that can be applied to a wide range of large biologically important complexes.

References and Notes

1. M. Kaczanowska, M. Rydén-Aulin, *Microbiol. Mol. Biol. Rev.* **71**, 477 (2007).
2. L. Pauling, *Proc. Natl. Acad. Sci. U.S.A.* **60**, 59 (1968).
3. K. H. Nierhaus, F. Dohme, *Proc. Natl. Acad. Sci. U.S.A.* **71**, 4713 (1974).
4. S. Mizushima, M. Nomura, *Nature* **226**, 1214 (1970).
5. T. Powers, G. Daubresse, H. F. Noller, *J. Mol. Biol.* **232**, 362 (1993).
6. M. W. Talkington, G. Siuzdak, J. R. Williamson, *Nature* **438**, 628 (2005).
7. J. Frank, *Three-Dimensional Electron Microscopy of Macromolecular Assemblies* (Oxford Univ. Press, New York, 2006).
8. W. Zhang, M. Kimmel, C. M. Spahn, P. A. Penczek, *Structure* **16**, 1770 (2008).
9. Materials and methods are available on *Science* Online.
10. I. N. Serdyuk, S. C. Agalarov, S. E. Sedelnikova, A. S. Spirin, R. P. May, *J. Mol. Biol.* **169**, 409 (1983).
11. M. Nomura, *Science* **179**, 864 (1973).
12. N. Fischer, A. L. Konevega, W. Wintermeyer, M. V. Rodnina, H. Stark, *Nature* **466**, 329 (2010).
13. A recent publication also used time series and classification to analyze a reverse translocation reaction (*12*).
14. V. Mandiyan, S. J. Tumminia, J. S. Wall, J. F. Hainfeld, M. Boublik, *Proc. Natl. Acad. Sci. U.S.A.* **88**, 8174 (1991).
15. A previous study employed reconstitution with defined subsets of ribosomal proteins combined with EM analysis to examine the structure of putative ribosome assembly intermediates (*14*).
16. A. E. Bunner, A. H. Beck, J. R. Williamson, *Proc. Natl. Acad. Sci. U.S.A.* **107**, 5417 (2010).

17. T. Adilakshmi, D. L. Bellur, S. A. Woodson, *Nature* **455**, 1268 (2008).
18. A. E. Bunner, S. Nord, P. M. Wikström, J. R. Williamson, *J. Mol. Biol.* **398**, 1 (2010).
19. M. R. Sharma *et al.*, *Mol. Cell* **18**, 319 (2005).
20. T. Ruiz, M. Radermacher, *Methods Mol. Biol.* **319**, 403 (2006).
21. This work was supported by the NIH (grants RR175173, R37-GM-53757, and GM-52468) and the NSF (graduate research fellowship to A.M.M.). The EM data collection and analysis were conducted at the National Resource for Automated Molecular Microscopy, which is supported by the NIH through the National Center for Research Resources P41 program (grants RR175173 and RR023093). We thank N. R. Voss and members of the Automated Molecular Imaging and Williamson laboratories for critical discussion of experiments. MAP, structure factors, and layer-line data have been deposited at EMDB with accession code EMD-1783.

Supporting Online Material
www.sciencemag.org/cgi/content/full/330/6004/673/DC1
Materials and Methods
SOM Text
Figs. S1 to S9
Table S1
References

3 June 2010; accepted 9 September 2010
10.1126/science.1193220

Polarized Myosin Produces Unequal-Size Daughters During Asymmetric Cell Division

Guangshuo Ou,*† Nico Stuurman, Michael D'Ambrosio, Ronald D. Vale†

Asymmetric positioning of the mitotic spindle before cytokinesis can produce different-sized daughter cells that have distinct fates. Here, we found an asymmetric division in the *Caenorhabditis elegans* Q neuroblast lineage that began with a centered spindle but generated different-sized daughters, the smaller (anterior) of which underwent apoptosis. During this division, more myosin II accumulated anteriorly, suggesting that asymmetric contractile forces might produce different-sized daughters. Indeed, partial inactivation of anterior myosin by chromophore-assisted laser inactivation created a more symmetric division and allowed the survival and differentiation of the anterior daughter. Thus, the balance of myosin activity on the two sides of a dividing cell can govern the size and fate of the daughters.

Most somatic cell divisions equally partition the cytoplasm and produce equivalent daughters. Asymmetric cell divisions are used to generate distinct daughter cells that have different fates in development and in adult stem cell lineages (*1*, *2*). Asymmetric cell division has been best studied in the first embryonic cell division in *Caenorhabditis elegans* (*3*). Here, unequal dynein-mediated pulling forces in the anterior-posterior axis displace the spindle toward the posterior pole (*3*–*5*). The cleavage furrow then forms in the middle of the elongating anaphase spindle, but because the spindle is displaced, the cell is divided into unequal-size daughters (*3*, *5*). However, in *Drosophila* neuroblasts, asymmetric cell division begins with the spindle aligned in the middle of the cell (*6*–*8*). As anaphase progresses, the spindle elongates asymmetrically and the cytokinetic furrow shifts toward one side of the cell. However, the cellular mechanism responsible for this type of asymmetric cytokinesis is unknown.

We developed fluorescence markers and live imaging methodologies to study asymmetric di-

The Howard Hughes Medical Institute and the Department of Cellular and Molecular Pharmacology, University of California, San Francisco, San Francisco, CA 94158, USA.

*Present address: National Laboratory of Biomacromolecules, Institute of Biophysics, Chinese Academy of Sciences, 15 Datun Road, Chaoyang District, Beijing 100101, China.
†To whom correspondence should be addressed. E-mail: gou@ibp.ac.cn (G.O.); vale@cmp.ucsf.edu (R.D.V.)

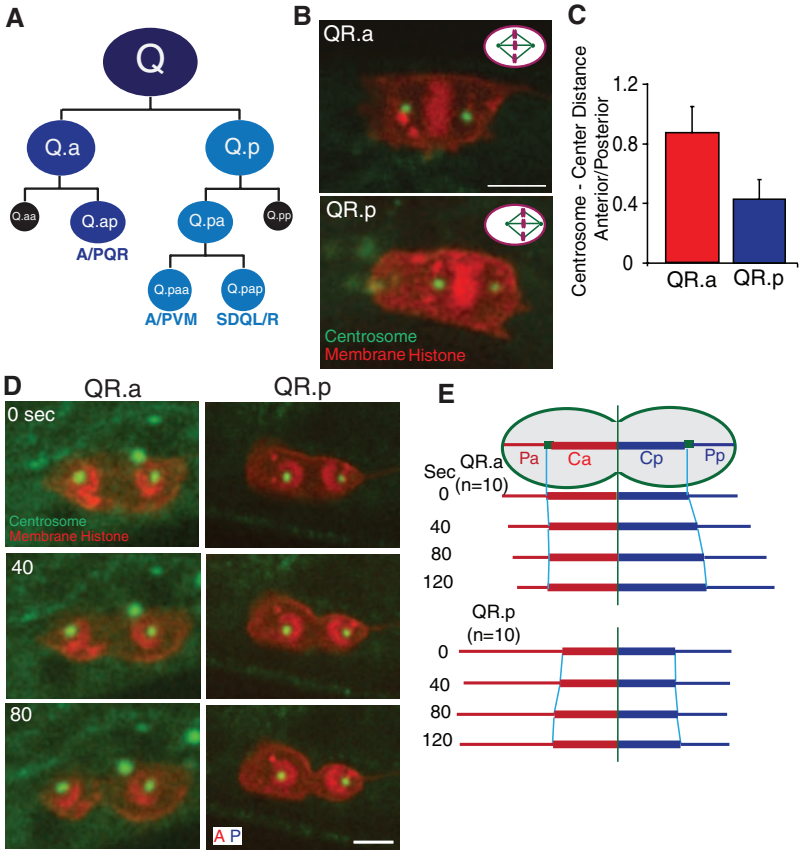

Fig. 1. *C. elegans* Q neuroblast lineage and spindle positioning in asymmetric cell division. (**A**) Three rounds of asymmetric cell divisions make three different neurons (QL generates PQR, PVM, and SDQL, whereas QR generates AQR, AVM and SDQR) and two apoptotic cells (in black). (**B**) Spindle positioning in the second-round division with centrosomes (γ-tubulin, TBG-1::GFP) in green and plasma membrane [mCherry with a myristoylation signal (*12*)] and histone (his-24::mCherry) in red. The cell anterior is toward the left. Bar, 2.5 μm. Upper right corners show a schematic summary of the results: QR.p spindle is displaced posteriorly but QR.a spindle is centered. (**C**) Centrosome–to–cell center distance ratio (anterior centrosome distance divided by posterior centrosome distance); data are shown as the mean ± SD (n = 12). Cell center is defined as the midpoint between the two cell poles. (**D**) QR.a (left) and QR.p (right) spindles during anaphase and cytokinesis. (**E**) The distance of the centrosome to the cleavage furrow (Ca, anterior; Cp, posterior) or to the cell pole (Pa, Pp). The distance is quantified from 10 movies and is normalized compared to the initial distances for each centrosome at the start of anaphase. Raw data are shown in fig. S1.

visions in the *C. elegans* Q neuroblast lineage. Q neuroblasts undergo three rounds of division to make three distinct neurons and two apoptotic cells (Fig. 1A). In the second round, asymmetric divisions give rise to a large cell that continues to divide and differentiate and a small cell that undergoes apoptosis (Fig. 1A) (*9*).

We first examined the spindle positioning of the QR.p and QR.a cells at metaphase by measuring the distances from each centrosome [marked by γ-tubulin–green fluorescent protein (GFP)] to the center of the cell. In QR.p, the metaphase spindle was displaced toward the posterior; the distance from the anterior centrosome to the cell center was 0.4 times as long as that from the posterior centrosome to the cell center (Fig. 1, B and C, and movie S1). At anaphase, the cleavage furrow formed equidistant between the two centrosomes. As the spindle elongated, the distances of the anterior and posterior centrosomes to the furrow increased in a similar manner (Fig. 1, D and E, fig. S1, and movie S1); as the spindle was displaced before anaphase, a large and a small daughter cell were produced when the cytokinetic furrow bisected the spindle. The behavior of the QL.p division was similar to that of QR.p (fig. S2, A and B). Thus, this asymmetric division appears to be similar to the first cell division in *C. elegans* embryogenesis (*3*, *5*).

The asymmetric division of the QR.a cell, however, was more similar to that described for *Drosophila* neuroblasts. In the QR.a cell, anaphase began with the two centrosomes positioned equidistant to the center [imaged with GFP–γ-tubulin (Fig. 1, B and C, and movie S2)] or GFP–α-tubulin (fig. S3 and movie S3). As anaphase progressed, the distance from the anterior centrosome to the ingressing cleavage furrow remained constant, whereas the posterior centrosome–to–furrow distance increased (Fig. 1, D and E, fig. S1, and movie S2). This progressively developing asymmetry that emerges in a cell with an initially centered spindle raises the possibility that a nonspindle factor may be driving the asymmetry in daughter cell size.

We next examined the dynamics of GFP-labeled nonmuscle myosin II in the contractile ring during cytokinesis. In the QR.p cell (posterior-displaced spindle), myosin II (NMY-2 in *C. elegans*) was equally distributed on the anterior and posterior sides of the ingressing furrow throughout cytokinesis (Fig. 2, A and B, fig. S4A, and movie S4). Myosin was depleted at both the anterior and posterior poles during telophase, as in somatic cell division (*10*). However, in the QR.a cell, where the cleavage furrow is initiated at the cell center, the distribution of myosin became asymmetric during anaphase. More cortical myosin was found at the anterior than at the posterior side of the furrow, particularly at early stages of anaphase, and cortical myosin was often found at the anterior pole of the QR.a cell, which was rarely seen in the QR.p cell (Fig. 2, A and B, movie S5, and fig. S4). We also observed a similar myosin II asymmetry during the asymmetric cell division in QL.a but not in the QL.p lineage (fig. S2, C and D).

An asymmetric distribution of myosin in the QR.a cells might create a "tense" anterior cortex that resists deformation and a "relaxed" posterior cortex that can deform and expand. To explore this idea, we examined the shape of the plasma membrane (using an mCherry-tagged plasma membrane marker) in the anterior and posterior halves of the dividing cell. For the QR.p cell, its anterior pole is the leading edge of cell migration before and after cell division (QR.pa cell). The anterior membrane of the QR.p cell was more dynamic and more ruffled than the posterior portion from metaphase and throughout cytokinesis (Fig. 2C, movie S6, and fig. S6B). As the spindle elongated in anaphase, the centrosome–to–cell pole distances decreased equally in the anterior and posterior (Fig. 1, D and E, and movie S1), and the size of the anterior half was constantly ~2.2 times as large as that of the posterior throughout cytokinesis (fig. S5). However, a very different behavior was observed for the QR.a cell. Like that of the QR.p cell, the anterior half of the QR.a cell was the leading edge of migration before division, and was more dynamic and formed more protrusions than the posterior portion through metaphase (Fig. 2C, movie S7, and fig. S6A). However, unlike that of the QR.p cell, the anterior membrane became less dynamic and protrusive at anaphase and shrunk inward, resulting in a gradual decrease of the anterior pole–to–centrosome distance and also the size of the anterior daughter (Fig. 1, D and E, figs. S1 and S5, and movies S2 and S7). Furthermore, the membrane in the posterior pole expanded outward during anaphase, resulting in an increase in the posterior pole–to–centrosome distance and the overall size of the posterior daughter (Fig. 2C, figs. S1 and S5, and movie S7). Thus, higher levels of cortical tension and contractile forces may drive the membrane toward the centrosome in the anterior half and lower cortical tension may allow the expansion of the membrane away from the centrosome in the posterior half of the QR.a cell.

To further explore whether myosin II asymmetry is involved in generating the QR.a daughter cell size asymmetry, we examined GFP–myosin II in the *pig-1* (*gm344*) mutant [PIG-1, a MELK-like kinase, is needed for asymmetric cell division in Q neuroblasts but not in the early embryo (*11*)]. In the *pig-1* mutant, GFP–myosin II was distributed symmetrically on the anterior and posterior sides of the furrow during QR.a division (Fig. 2, A and B, fig. S4, and movie S8), consistent with a role for myosin in the asymmetric cell division of the QR.a cell. However, because the *pig-1* mutant also affects the asymmetric division of the QR.p cell, which occurs by spindle displacement rather

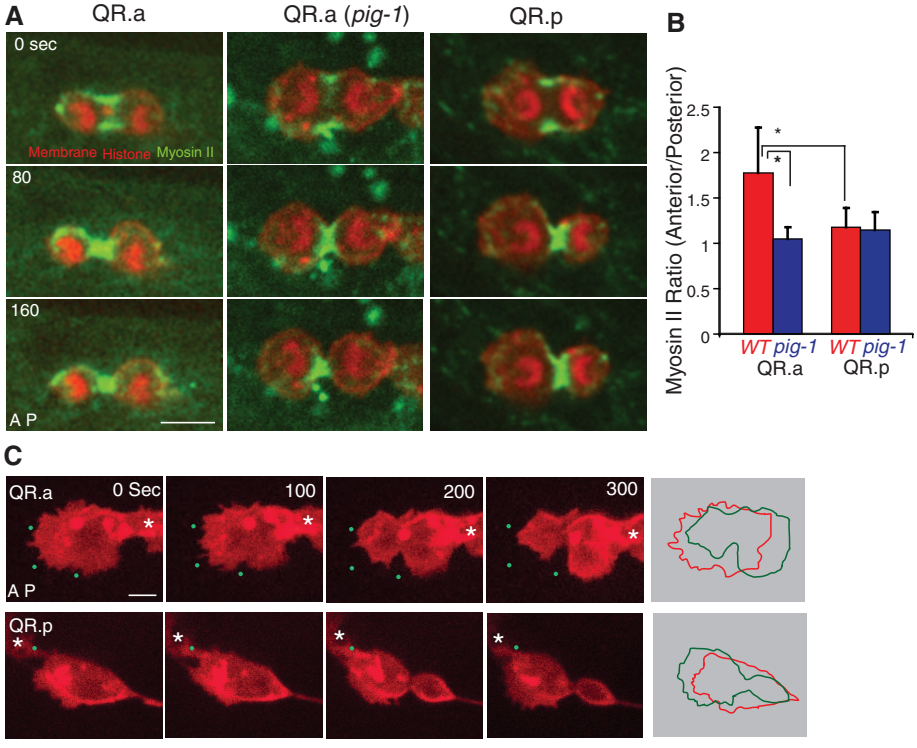

Fig. 2. Myosin II and membrane dynamics in Q neuroblasts during cytokinesis. (**A**) Still images of myosin II–GFP dynamics during cytokineses of QR.a in wild-type (WT) or QR.a in *pig-1* mutant and QR.p animals. (**B**) Myosin II–GFP fluorescence intensities ratio between the anterior and posterior parts of QR.a or QR.p cells in WT or *pig-1* (gm344) mutant (*$P < 0.001$, $n = 9$ to 11); data are shown as the mean ± SD. (**C**) Membrane dynamics of QR.a or QR.p during cytokinesis. The plasma membrane is imaged as in Fig. 1. Green dots are autofluorescent spots in the *C. elegans* body that provide fiducial marks (original image not shown). Panels on the far right show the alignment of QR.a and QR.p cell peripheries (0 s red, 300 s green) revealing the contraction and expansion of the two sides of the cell. Asters show neighboring Q cells. More examples are shown in fig. S6. Anterior of the cell is toward the left. Bar, 2.5 μm.

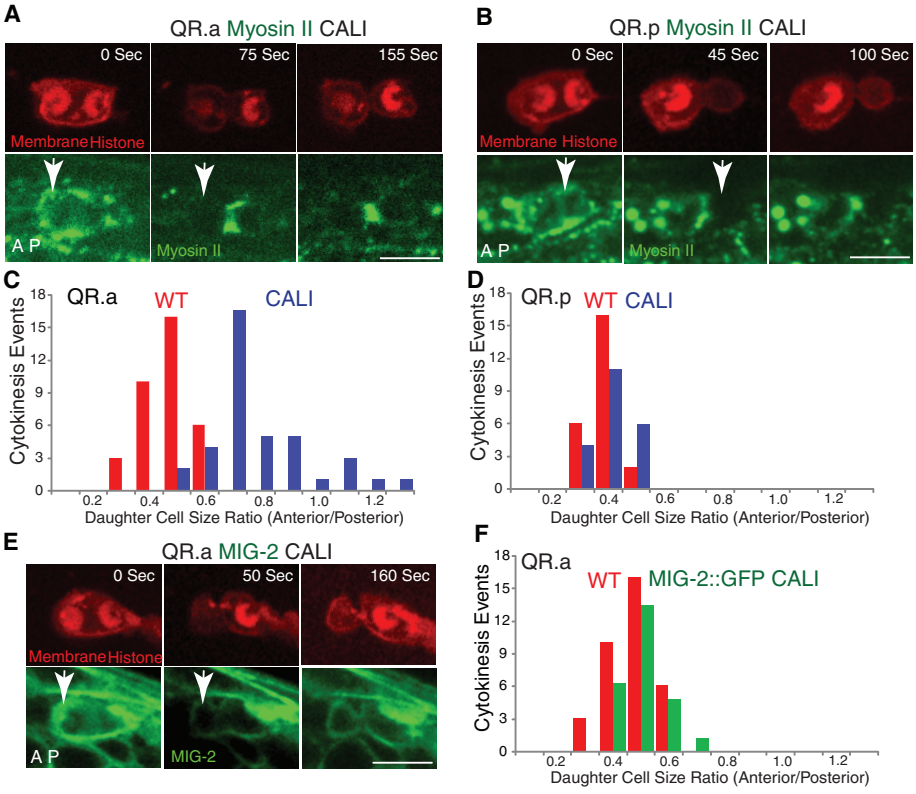

Fig. 3. Chromophore-assisted laser inactivation (CALI) of myosin II in Q neuroblasts during cytokinesis. (**A**) CALI inactivation of myosin II in the anterior of QR.a enlarges the anterior daughter cell size. Upper images show the chromosome and plasma membrane labeled with mCherry, and lower images show GFP-tagged myosin II. Arrows indicate the region that was treated with CALI at late anaphase (*12*). (**B**) CALI inactivation of myosin II in the posterior of QR.p does not change sizes of daughter cells. (**C**) and (**D**) are quantifications of the above CALI experiments. (**E** and **F**) CALI of MIG-2::GFP does not change the ratio of QR.aa and QR.ap. Anterior of the cell is toward the left. Bar, 5 μm.

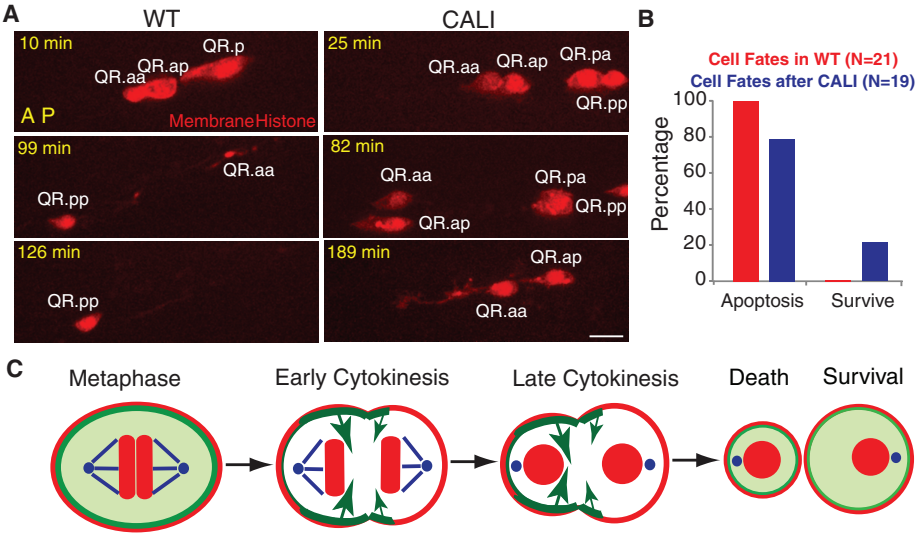

Fig. 4. Cell fate after CALI and a proposed model. (**A**) QR.aa cells normally undergo apoptosis (disappearance at 126 min). After CALI, QR.a cell migrated (82 min, the nonmotile QR.pp provides a fiduciary marker) and formed a neurite-like process (189 min). (**B**) Quantifications of QR.aa cell fates (*12*) in WT (red) and after CALI (blue) ~150 min after birth. Anterior of the cell is toward the left. Bar, 5 μm. (**C**) Proposed mechanism of QR.aa asymmetric division. Myosin II localizes evenly in QR.a cell at metaphase but distributes asymmetrically during anaphase. More myosin II at the anterior than at the posterior may generate larger cortical tension (long arrows), pushing cellular contents and resulting in a small cell in the anterior that undergoes apoptosis and a large cell in the posterior that survives. Myosin II (green); plasma membrane and chromosomes (red); centrosome and microtubules (blue).

than asymmetric myosin, this correlation does not definitively link the polarization of myosin II with asymmetric cell division. To obtain more direct evidence, we inactivated myosin II activity using chromophore-assisted laser inactivation [CALI (*12*)] in the anterior of the QR.a cell at the onset of cytokinesis and determined whether this perturbation changed the sizes of the daughters. CALI uses an intense laser irradiation of a fluorophore, including GFP, to damage proteins within ~4 nm by generating highly reactive hydroxyl radicals (*13*–*15*). GFP-based CALI of the myosin II regulatory light chain has been shown to specifically block furrow ingression during cytokinesis in *Drosophila* epithelial cells (*16*). Similarly, in the first-round division of the QR cell, we found that CALI illumination of GFP–myosin II applied to one side of the furrow caused the ingression on that side to pause while the other, nonilluminated side continued to pinch (fig. S7B, 73%, $n = 11$). Thus, CALI can inhibit the myosin II activity during cytokinesis in the Q cell.

We next applied CALI to the anterior half of QR.a cell, which had higher GFP–myosin II, and then measured the sizes of the daughters. After CALI, the anterior daughter cell QR.aa was enlarged [QR.aa/QR.ap size ratio of 0.83 ± 0.18 (mean ± SD, $n = 39$) compared to normal (0.52 ± 0.08, $n = 35$) (Fig. 3, A and C)]. Furthermore, the QR.aa cell was sometimes larger than the QR.ap cell after CALI treatment, which was not observed in the wild type (Fig. 3C). To establish that these results were due to inactivation of myosin and not to nonspecific effects of illumination, we performed a similar CALI treatment of the GFP-tagged membrane protein MIG-2, a small guanosine triphosphatase involved in Q cell migration but not in cytokinesis (*17*, *18*). Performing CALI of MIG-2::GFP in the anterior of the QR.a cell at anaphase did not significantly change the QR.aa/QR.ap cell size ratio (0.56 ± 0.07, $n = 21$) (Fig. 3, E and F). We also performed CALI of GFP-myosin II in the posterior half of the QR.p cell, whose asymmetric division appears to involve spindle displacement rather than asymmetric myosin (Figs. 1 and 2). In this case, CALI only marginally changed the QR.pp/QR.pa size ratio [(0.47 ± 0.06, $n = 21$) versus untreated (0.42 ± 0.06, $n = 24$); Fig. 3, B and D]. Thus, CALI of GFP-tagged myosin II specifically affects the daughter cell sizes of the QR.a division.

We next followed the fate of the QR.aa cell after CALI by long-term time lapse imaging. Normally, the QR.aa cell becomes engulfed and digested by neighboring cells within 150 min (Fig. 4, A and B, and movie S9) (*9*). In contrast, the QR.aa cell derived from the QR.a cell after CALI treatment sometimes escaped apoptosis (21%, $n = 19$) and could differentiate into a neuronal-like cell that extended a long process (11%) (Fig. 4, A and B, and movie S10). The larger QR.aa cells that formed after CALI were the ones that had a higher chance of survival (fig. S7C). The differentiation into a neuronal-like cell appears to be an outcome associated with survival rather than with

CALI per se, because a similar differentiation phenotype was observed when QR.aa apoptosis was blocked in a *ced-4* mutant (*n1162*) (fig. S8).

Our results show that asymmetric cortical tension, produced by an unequal distribution of myosin and perhaps other cortical proteins, produced two different-sized QR.a daughter cells. We propose that a stiffer and inward-contracting anterior pole pushes cytoplasm through the furrow toward the less contractile posterior pole, which responds by expanding like a balloon (Fig. 4C). We also demonstrate a direct connection between the size of a cell and its fate in *C. elegans* development by showing that increasing cell size by myosin II CALI can result in a rescue from apoptosis and differentiation into a neuronal-like cell.

The downstream "output" of asymmetric cortical signaling (*3*, *5*) has been thought to be the mitotic spindle, best exemplified by the displacement of mitotic spindle in the *C. elegans* embryo (*3*, *5*). Similarly, asymmetric divisions of *Drosophila* neuroblasts (which start anaphase with a symmetric, centrally positioned spindle) have been postulated to arise from the greater elongation of microtubules on one side of the spindle midzone compared with the other (*6*–*8*). We also observed asymmetric spindle elongation in the QR.a cell (Fig. 1, D and E), but propose that this occurs secondarily to myosin polarization, in which the spindle elongates preferentially toward the pole with lower cortical tension. In support of this idea, increasing cortical tension at the cell poles prevents spindle elongation and cell extension in dividing *Drosophila* S2 cells (*19*). Consequently, we propose that a polarization of myosin-based contractility is the primary driver of the QR.a cell division asymmetry, although we cannot rule out some contribution from the spindle as well. Thus, a simple organism like *C. elegans* [in which 807 out of its 949 somatic cell divisions are asymmetric (*20*)] appears to use at least two physical mechanisms (one spindle-based and one cortex-based) to generate asymmetric cell division.

Note added in proof: Cabernard *et al*. (*21*) recently showed an asymmetric distribution of myosin II during cytokinesis of *Drosophila* neuroblasts.

References and Notes

1. K. A. Moore, I. R. Lemischka, *Science* **311**, 1880 (2006).
2. R. A. Neumüller, J. A. Knoblich, *Genes Dev.* **23**, 2675 (2009).
3. S. Q. Schneider, B. Bowerman, *Annu. Rev. Genet.* **37**, 221 (2003).
4. P. Gönczy, S. Pichler, M. Kirkham, A. A. Hyman, *J. Cell Biol.* **147**, 135 (1999).
5. P. Gönczy, *Nat. Rev. Mol. Cell Biol.* **9**, 355 (2008).
6. K. H. Siller, C. Q. Doe, *Nat. Cell Biol.* **11**, 365 (2009).
7. J. A. Kaltschmidt, C. M. Davidson, N. H. Brown, A. H. Brand, *Nat. Cell Biol.* **2**, 7 (2000).
8. Y. Cai, F. Yu, S. Lin, W. Chia, X. Yang, *Cell* **112**, 51 (2003).
9. J. E. Sulston, H. R. Horvitz, *Dev. Biol.* **56**, 110 (1977).
10. R. D. Vale, J. A. Spudich, E. R. Griffis, *J. Cell Biol.* **186**, 727 (2009).
11. S. Cordes, C. A. Frank, G. Garriga, *Development* **133**, 2747 (2006).
12. Materials and methods are available as supporting material on *Science* Online.
13. T. J. Diefenbach *et al*., *J. Cell Biol.* **158**, 1207 (2002).
14. K. Jacobson, Z. Rajfur, E. Vitriol, K. Hahn, *Trends Cell Biol.* **18**, 443 (2008).
15. F. S. Wang, J. S. Wolenski, R. E. Cheney, M. S. Mooseker, D. G. Jay, *Science* **273**, 660 (1996).
16. B. Monier, A. Pélissier-Monier, A. H. Brand, B. Sanson, *Nat. Cell Biol.* **12**, 60 (2010).
17. G. Ou, R. D. Vale, *J. Cell Biol.* **185**, 77 (2009).
18. I. D. Zipkin, R. M. Kindt, C. J. Kenyon, *Cell* **90**, 883 (1997).
19. G. R. Hickson, A. Echard, P. H. O'Farrell, *Curr. Biol.* **16**, 359 (2006).
20. H. R. Horvitz, I. Herskowitz, *Cell* **68**, 237 (1992).
21. C. Cabernard, K. E. Prehoda, C. Q. Doe, *Nature* **467**, 91 (2010).

22. We thank L. Cai, D. Sherwood, J. Ziel, P. Zhang, I. Cheeseman, C. Kenyon, G. Garriga, and *Caenorhabditis* Genetics Center for reagents, equipments and strains, and thank C. Locke and W. Li for myosin quantifications. This work was supported by the Damon Runyon Cancer Research Foundation (G.O.) and the NIH and Howard Hughes Medical Institute (R.D.V.).

Supporting Online Material

www.sciencemag.org/cgi/content/full/science.1196112/DC1
Materials and Methods
Figs. S1 to S8
Table S1
References
Movies S1 to S10

5 August 2010; accepted 20 September 2010
Published online 30 September 2010;
10.1126/science.1196112
Include this information when citing this paper.

A Size Threshold Limits Prion Transmission and Establishes Phenotypic Diversity

Aaron Derdowski,[1]* Suzanne S. Sindi,[1,2]*† Courtney L. Klaips,[1] Susanne DiSalvo,[1] Tricia R. Serio[1]†

According to the prion hypothesis, atypical phenotypes arise when a prion protein adopts an alternative conformation and persist when that form assembles into self-replicating aggregates. Amyloid formation in vitro provides a model for this protein-misfolding pathway, but the mechanism by which this process interacts with the cellular environment to produce transmissible phenotypes is poorly understood. Using the yeast prion Sup35/[*PSI*$^+$], we found that protein conformation determined the size distribution of aggregates through its interactions with a molecular chaperone. Shifts in this range created variations in aggregate abundance among cells because of a size threshold for transmission, and this heterogeneity, along with aggregate growth and fragmentation, induced age-dependent fluctuations in phenotype. Thus, prion conformations may specify phenotypes as population averages in a dynamic system.

Prion proteins adopt a spectrum of conformations or strains, which create phenotypes of distinct severity and stability in vivo (*1*–*3*). These phenotypes are linked to the assembly of the protein into aggregates that, at different rates, template the conversion of newly made prion proteins to a similar state and are fragmented (*4*). But how do these biochemical events translate into distinct phenotypes? One possibility is an "abundance-based" model, in which phenotypes are linked to an equilibrium between aggregated and soluble prion protein that determines protein activity and the number of heritable prions (propagons) (*5*, *6*). However, the conversion and fragmentation reactions also create heterogeneity in aggregate size, raising the possibility of a second, "size-based" model in which a subpopulation of aggregates establishes and propagates phenotypes (*7*).

To distinguish between these models, we focused on the [*PSI*$^+$]^{Weak} and [*PSI*$^+$]^{Strong} conformations of the yeast prion protein Sup35, which create phenotypes of different stabilities in vivo (*8*). To sustain these phenotypes in a dividing culture, Sup35 protein in the prion conformation must be inherited (*7*). To test whether conformational differences affect phenotypic stability by altering protein transmissibility, we monitored Sup35–green fluorescent protein (GFP) transfer to daughter cells. Through use of fluorescence loss in photobleaching (FLIP), a [*PSI*$^+$]^{Weak} strain transferred half as much Sup35-GFP (~15% versus ~30%) (Fig. 1A) and contained ~50% fewer propagons than a [*PSI*$^+$]^{Strong} strain (Fig. 1B). Thus, conformation-based differences in protein transmission correlate with phenotypic inheritance.

Following from the models, differences in aggregate abundance and/or size may create this variation in prion protein transmission (*5*, *7*), and indeed, [*PSI*$^+$]^{Weak} strains differ from [*PSI*$^+$]^{Strong} strains by the accumulation of fewer but larger aggregates (*9*–*12*). To distinguish between these possibilities, we simulated prion propagation via each transmission mechanism (*13*). For the abundance-based model, we were unable to recapitulate the severity and stability of [*PSI*$^+$]^{Weak} and [*PSI*$^+$]^{Strong} phenotypes (fig. S5) (*13*). In contrast with a size-based model, we recapitulated all experimentally

[1]Department of Molecular Biology, Cell Biology and Biochemistry, Brown University, 185 Meeting Street, Post Office Box G-L2, Providence, RI 02912, USA. [2]Center for Computational Molecular Biology, Brown University, 115 Waterman Street, Post Office Box 1910, Providence, RI 02912, USA.

*These authors contributed equally to this work.
†To whom correspondence should be addressed. E-mail: suzanne_sindi@brown.edu (S.S.S.); tricia_serio@brown.edu (T.R.S.)

observed characteristics that distinguish these strains, including the relationship between the products of their conversion and fragmentation rates, the stabilities of their phenotypes, and their aggregate size distributions (Table 1 and figs. S6 to S10) (*11*–*13*). The latter model only captured the [*PSI*$^+$]^{Weak} and [*PSI*$^+$]^{Strong} states when the transmission size threshold was set within the range that distinguishes their aggregates (≤30 monomers/aggregate) (fig. S9) (*11*, *12*) and when fragmentation was modeled as an enzyme-limited process dependent on the catalyst for this reaction, the molecular chaperone Hsp104 (figs. S8, A and B, and S9) (*14*–*16*).

To experimentally test the hypothesis that aggregate size rather than abundance establishes conformation-based phenotypes, we altered Sup35 expression, which affected phenotypic stability differently in the two models. For the size-based model, phenotypic stability decreases with Sup35 overexpression because aggregates increase in size (Fig. 2A) and decrease in transmissibility; however, for the abundance-based model, phenotypic stability increases because more aggregates are produced (*5*, *13*). Severe overexpression of prion proteins in yeast decreases phenotypic stability (*17*–*19*), which may reflect the assembly of alternative complexes (*20*–*22*). To circumvent this potential complication, we reversibly and modestly (approximately four- to sixfold) changed Sup35-GFP expression using a tetracycline-responsive promoter (fig. S11). As predicted by the size-based model (Fig. 2A), larger aggregates appeared with Sup35-GFP overexpression (Fig. 2B), and this size shift induced a ~50% decrease in propagons (Fig. 2C), a decrease in phenotypic stability by a factor of 70 (Fig. 2D), and a ~50% decrease in Sup35-GFP transmission (Fig. 2E). Conversely, transient repression of Sup35-GFP synthesis shifted aggregates to smaller sizes (Fig. 2B) and suppressed the inheritance defects, increasing propagons and Sup35-GFP transmission by 50% (Fig. 2, C and E). These correlations between prion protein expression and heritability support the size-based model.

To further discriminate between the models, we characterized daughter-derived Sup35 directly. For the "abundance-based" model, daughters contain aggregates of similar size and abundance to their mothers (fig. S8C). However, for the size-based model, daughters contain smaller and fewer aggregates than their mothers (Table 1 and fig. S10), and the size of these aggregates is conformation-independent because of the selection imposed by transmission. Indeed, daughter-derived Sup35-GFP was transmitted with equal efficiency to mothers in [*PSI*$^+$]^{Strong} and [*PSI*$^+$]^{Weak} strains (Fig. 2F), and [*PSI*$^+$]^{Strong} daughters—isolated by means of centrifugal elutriation (fig. S12)—contained only ~17% of the aggregates in the total population (Fig. 2G), again satisfying the size-based model predictions. Thus, aggregate size rather than abundance determines phenotypic stability in vivo.

How does this framework create phenotypes of different severity? Sup35 is a translation release factor whose activity is compromised by its conformational conversion and assembly into aggregates (*23*). Thus, cell-to-cell variation in aggregate abundance created by the size-based model (Fig. 2G, Table 1, and fig. S10) raises the possibility that [*PSI*$^+$] phenotypes reflect population averages of Sup35 activities. Consistent with this idea, individual [*PSI*$^+$] cells accumulated Sup35-GFP in different physical states (Fig. 3A). This variation was more severe for the less efficiently transmitted [*PSI*$^+$]^{Weak} conformation, in which only ~67% of cells accumulated Sup35-GFP in a primarily aggregated form (punctate, less efficiently transmitted fluorescence) in contrast with ~92% of [*PSI*$^+$]^{Strong} cells (Figs. 1A and 3A). This heterogeneity in Sup35 physical state correlated with cell-to-cell variation in activity. Although the range of translation termination activities in a population of [*PSI*$^+$]^{Strong} cells expressing a stop codon read-through reporter [glutathione *S*-transferase (GST)–UGA–enhanced GFP (eGFP)–PEST] overlapped only minimally with that of a non-prion [*psi*$^-$] strain (~17%) (Fig. 3B), [*PSI*$^+$]^{Weak} activities overlapped extensively with those of [*psi*$^-$] (~53%) and [*PSI*$^+$]^{Strong} (~38%) (Fig. 3B). Thus, size-based transmission of aggregates creates phenotypic diversity within a population.

Despite these single-cell variations, [*PSI*$^+$] strains form phenotypically homogeneous rather than sectored colonies (*24*). To explore the molecular basis of this disconnect, we asked how single-cell variation is produced and maintained. According to our simulations (Table 1) and biochemical analysis (Fig. 2G), mother cells contain more aggregates than their daughters. To determine whether cell-to-cell variations in Sup35 activity (Fig. 3B) similarly correspond to replicative age, we isolated subpopulations of a [*PSI*$^+$]^{Weak} culture expressing GST-UGA-eGFP-PEST with fluorescence-activated cell sorting (FACS) and determined the number of bud scars on cells in each fraction. Young cells were strongly enriched in the fraction with the most accurate translation termination, in which 90% of the cells had produced less than two daughters (Fig. 3C). In contrast, nearly half (~48%) of the cells in the fraction with the least accurate translation termination had produced three or more daughters (Fig. 3C).

This link between replicative age and phenotypic severity suggests that cells change during aging. Indeed, when young cells were isolated and cultured to regenerate a population, cells with reduced translation termination activity reappeared (Fig. 3D). What is the mechanism underlying this phenotypic transition? According to our simulations, the limited number of aggregates inher-

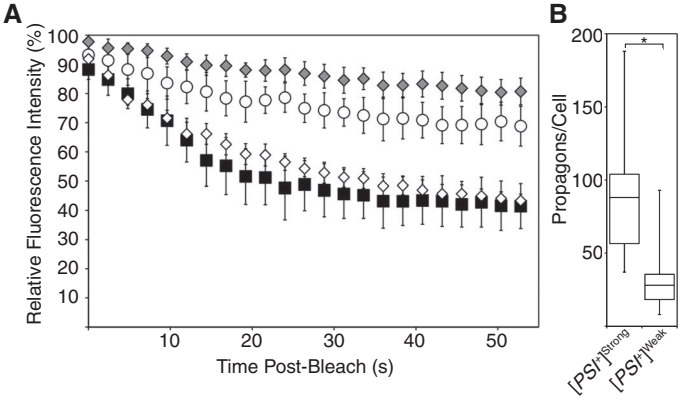

Fig. 1. Propagons correlate with transmitted Sup35. (**A**) Sup35-GFP transmission to daughters was determined by means of FLIP (mean ± SEM). [*PSI*$^+$]^{Strong} (open circles, SY81, n = 11 data sets), [*psi*$^-$] (black squares, SY85, n = 7 data sets), and [*PSI*$^+$]^{Weak} (gray diamonds, punctate SY779, n = 7 data sets; open diamonds, diffuse SY779, n = 7 data sets). (**B**) Propagons were quantified for [*PSI*$^+$]^{Strong} (SY81) and [*PSI*$^+$]^{Weak} (SY779). Horizontal lines indicate 25th, 50th, and 75th percentiles, and error bars indicate 10th and 90th percentiles; n = 12 cells ([*PSI*$^+$]^{Weak}) or 27 cells ([*PSI*$^+$]^{Strong}); *P = 0.0001.

Table 1. Comparison of [*PSI*$^+$]^{Weak} and [*PSI*$^+$]^{Strong} characteristics from simulated and experimental observations.

Strain	Prion loss		Relative product of conversion and fragmentation rates		Soluble Sup35			
					Total		Mother	Daughter
	Simulation	Experimental† (*8*, *24*)	Simulation*	Experimental† (*5*)	Simulation	Experimental† (*31*)	Simulation	Simulation
[*PSI*$^+$]^{Strong}	0%	~0%	2.5	3	15%	19%	6.8%	33.4%
[*PSI*$^+$]^{Weak}	1.6%	1 to 3%	1	1	31.3%	35%	12.8%	87.9%

*Simulated conversion rates for [*PSI*$^+$]^{Strong} and [*PSI*$^+$]^{Weak} are 2.45×10^{-5} and 6.45×10^{-5} (molecules min)$^{-1}$, respectively, and simulated fragmentation rates for [*PSI*$^+$]^{Strong} and [*PSI*$^+$]^{Weak} are 1.3×10^{-2} and 0.2×10^{-2} min^{-1}, respectively (*13*). †Experimental values are reported in the cited references.

Fig. 2. A size threshold limits aggregate transmission. (**A**) Aggregate size distributions for [*PSI*$^+$]^{Strong} with (dotted line) wild-type, (solid line) 4X Sup35, or (dashed line) the latter after repression of Sup35 synthesis for one generation were determined by means of stochastic simulation (*13*). (**B**) Lysates from [*PSI*$^+$]^{Strong} (+; p35, SY81 or ptet, SY1607) or [*psi*$^-$] (–; SY85) in the presence (+) or absence (–) of doxycycline (Dox) for the indicated generations were analyzed by means of semidenaturing agarose gel electrophoresis (SDD-AGE) and immunoblotting with antibody to GFP. (**C**) Propagons were quantified in [*PSI*$^+$]^{Strong} cells (p35, SY81; ptet, SY1607) in the absence (–) or presence (+) of Dox for one-generation. Box plots, as in Fig. 1B. p35, $n = 27$ cells; p35+Dox, $n =$ 13 cells; ptet, $n =$21 cells; ptet+dox, $n = 16$ cells; *$P = 0.02$; **$P = 0.001$ (**D**) The frequency of prion loss was determined for [*PSI*$^+$]^{Weak} (w, SY779) and [*PSI*$^+$]^{Strong} (s) strains in (B). (**E**) Sup35-GFP transmission to daughters was determined with FLIP (mean ± SEM; $n = 3$ data sets) in [*PSI*$^+$]^{Strong} (circles, SY81; squares, SY1607) in the (open) absence or (black) presence of Dox for one generation. (**F**) Sup35-GFP transmission to mothers was determined with FLIP (mean ± SEM; $n = 3$ data sets) in [*PSI*$^+$]^{Strong} (open circles, SY81) and [*PSI*$^+$]^{Weak} (gray diamonds, SY779). (**G**) [*PSI*$^+$]^{Strong} (SY1607) total (lane 1, solid line) and daughter (lane 2, dashed line) fractions were analyzed with SDD-AGE and immunoblotting with antibody to GFP. (Right) Densitometry traces are provided.

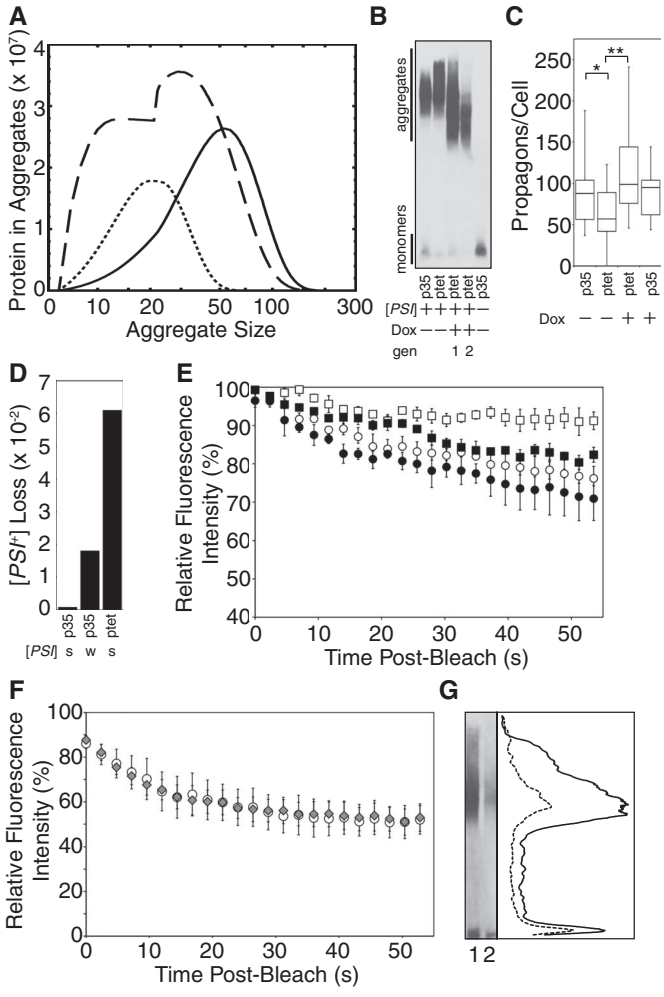

Fig. 3. Size-based transmission of aggregates creates population heterogeneity and fluctuations. (**A**) (Left) Sup35-GFP fluorescence pattern (punctate, white; diffuse, black) was (right) quantified (mean ± SD; $n =$ 3 experiments) in [*PSI*$^+$]^{Strong} (SY81), [*PSI*$^+$]^{Weak} (SY779), and [*psi*$^-$] (SY85). Scale bar, 5μm. (**B**) [*PSI*$^+$]^{Strong} (solid black line, SY1635), [*PSI*$^+$]^{Weak} (pink filled, SY1636), and [*psi*$^-$] (red line, SY1637; dotted black line, 74D-694) were analyzed by means of flow cytometry. Vertical dotted lines indicate least and most fluorescent 20%. (**C**) Bud scars were quantified in the fractions marked in (B) (SY1636; $n = 3$ data sets). (**D**) [*PSI*$^+$]^{Weak} (SY1636) cultures after (dotted line) FACS and (solid line) regrowth were analyzed by means of flow cytometry. (**E**) Aggregate size distributions were simulated for a mother cell before its (red) first, (orange) fourth, (green) seventh, (blue) 10th, and (purple) 12th divisions (*13*). (**F**) Propagons were quantified ($n \geq 3$ cells) in successive daughters from a [*PSI*$^+$]^{Strong} strain (74D-694). Box plots are as in Fig. 1B; *$P = 0.0081$.

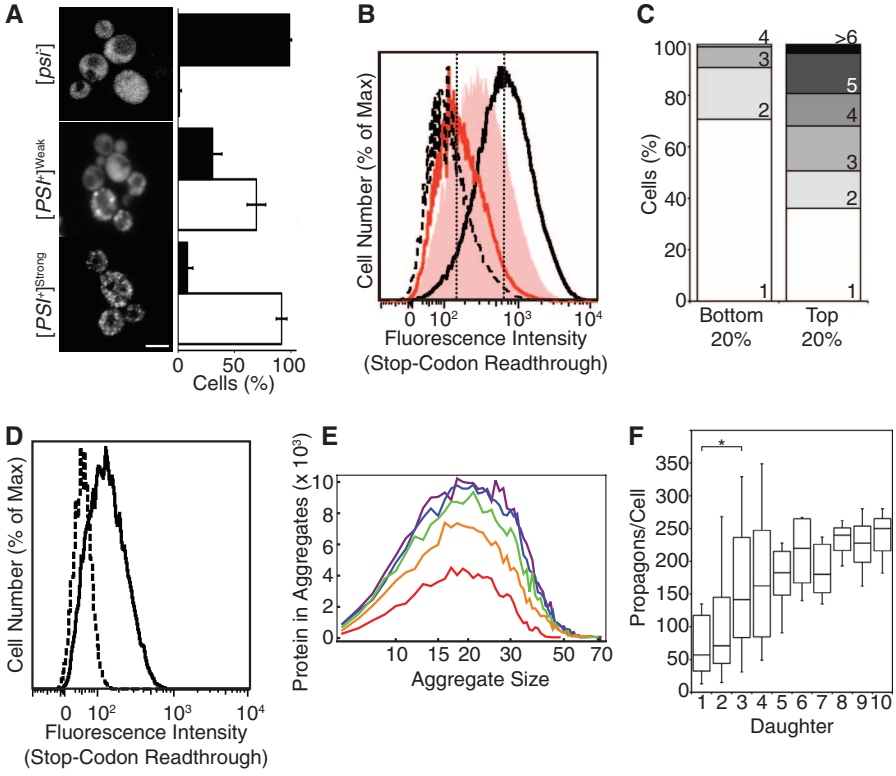

ited by a daughter progressively amplifies to a steady-state plateau as that cell ages (Fig. 3E). Thus, early daughters will inherit fewer aggregates than later daughters. Indeed, propagons transmitted to successive daughters increased through the third generation and then remained relatively constant (Fig. 3F). Our observations provide a mechanistic explanation for previously observed cell-to-cell variability in propagons (*6*, *25*) and reveal age-dependent [*PSI*$^+$] phenotypes at the single-cell level.

Thus, the seemingly static phenotypes associated with prion protein conformations may actually reflect highly dynamic pathways of prion protein biogenesis in dividing cells. For any given cell, the complement of aggregates and the phenotype fluctuate in response to the interplay between the protein-misfolding pathway and its cellular environment, creating a self-regenerating system that settles to a stable population average for each conformation. Thus, the cellular environment has profound effects on the phenotypic manifestations of prion protein conformations.

The dynamic size-based system that we have uncovered may contribute to the physiological consequences of protein misfolding in ways that are not possible for an abundance-based process. The phenotypic variation established and maintained through the events described here strengthens the argument that the prion mechanism, like other epigenetic processes, facilitates selection in new environments and consequently evolution (*26*). According to our model, access to an advantageous state may not require a [*prion*$^-$]/[*PRION*$^+$] phenotypic switch (*27*) but instead may always be present within a population. In mammals, variation in aggregate size may similarly affect protein transmissibility between nondividing cells and the spread of pathology in prion and perhaps other protein-misfolding disorders, such as Parkinson's, Alzheimer's, and Huntington's diseases (*28*–*30*). Indeed, prion protein conformation and expression—parameters that alter aggregate size—are more reliable predictors of the clinical course of disease than is the presence of protease-resistant aggregates (*1*).

References and Notes

1. J. Collinge, A. R. Clarke, *Science* **318**, 930 (2007).
2. L. Benkemoun, S. J. Saupe, *Fungal Genet. Biol.* **43**, 789 (2006).
3. S. B. Prusiner, *Science* **216**, 136 (1982).
4. J. A. Pezza, T. R. Serio, *Prion* **1**, 36 (2007).
5. M. Tanaka, S. R. Collins, B. H. Toyama, J. S. Weissman, *Nature* **442**, 585 (2006).
6. B. Cox, F. Ness, M. Tuite, *Genetics* **165**, 23 (2003).
7. S. S. Sindi, T. R. Serio, *Curr. Opin. Microbiol.* **12**, 623 (2009).
8. I. L. Derkatch, Y. O. Chernoff, V. V. Kushnirov, S. G. Inge-Vechtomov, S. W. Liebman, *Genetics* **144**, 1375 (1996).
9. S. M. Uptain, G. J. Sawicki, B. Caughey, S. Lindquist, *EMBO J.* **20**, 6236 (2001).
10. P. Zhou *et al.*, *EMBO J.* **18**, 1182 (1999).
11. D. S. Kryndushkin, I. M. Alexandrov, M. D. Ter-Avanesyan, V. V. Kushnirov, *J. Biol. Chem.* **278**, 49636 (2003).
12. S. N. Bagriantsev, V. V. Kushnirov, S. W. Liebman, *Methods Enzymol.* **412**, 33 (2006).
13. Materials and methods are available as supporting material on *Science* Online.
14. F. Ness, P. Ferreira, B. S. Cox, M. F. Tuite, *Mol. Cell. Biol.* **22**, 5593 (2002).
15. P. Satpute-Krishnan, S. X. Langseth, T. R. Serio, *PLoS Biol.* **5**, e24 (2007).
16. T. Haslberger, B. Bukau, A. Mogk, *Biochem. Cell Biol.* **88**, 63 (2010).
17. H. K. Edskes, V. T. Gray, R. B. Wickner, *Proc. Natl. Acad. Sci. U.S.A.* **96**, 1498 (1999).
18. K. D. Allen *et al.*, *Genetics* **169**, 1227 (2005).
19. M. Crapeau, C. Marchal, C. Cullin, L. Maillet, *Mol. Biol. Cell* **20**, 2286 (2009).
20. A. B. Salnikova, D. S. Kryndushkin, V. N. Smirnov, V. V. Kushnirov, M. D. Ter-Avanesyan, *J. Biol. Chem.* **280**, 8808 (2005).
21. E. G. Rikhvanov, N. V. Romanova, Y. O. Chernoff, *Prion* **1**, 217 (2007).
22. V. V. Kushnirov, A. B. Vishnevskaya, I. M. Alexandrov, M. D. Ter-Avanesyan, *Prion* **1**, 179 (2007).
23. T. R. Serio, S. L. Lindquist, *Annu. Rev. Cell Dev. Biol.* **15**, 661 (1999).
24. B. Cox, *Heredity* **20**, 505 (1965).
25. L. J. Byrne *et al.*, *PLoS ONE* **4**, e4670 (2009).
26. R. Halfmann, S. Alberti, S. Lindquist, *Trends Cell Biol.* **20**, 125 (2010).
27. A. K. Lancaster, J. P. Bardill, H. L. True, J. Masel, *Genetics* **184**, 393 (2010).
28. J. R. Silveira *et al.*, *Nature* **437**, 257 (2005).
29. B. Frost, M. I. Diamond, *Nat. Rev. Neurosci.* **11**, 155 (2010).
30. P. Brundin, R. Melki, R. Kopito, *Nat. Rev. Mol. Cell Biol.* **11**, 301 (2010).
31. J. A. Pezza *et al.*, *Mol. Biol. Cell* **20**, 1068 (2009).

32. We thank N. Rhind, M. Duennwald, J. Sherley, and members of their groups for assistance with centrifugal elutriation, and the Center for Computation and Visualization, the Leduc Bioimaging Facility, and the Flow Cytometry and Sorting Facility at Brown University for instrumentation and the assistance of the respective support staffs. We thank J. Bender, J. Laney, M. Tuite, and members of the Serio and Laney labs for helpful discussions and comments on the manuscript. This research was supported by grants from NIH (GM069802 to T.R.S., GM085976 to A.D., GM089049 to S.S.S., AG034754 to C.K., and AG032818 to S.D.) and NSF/ADVANCE (0548311 to T.R.S.).

Supporting Online Material

www.sciencemag.org/cgi/content/full/330/6004/680/DC1
Materials and Methods
Figs. S1 to S12
Tables S1 and S2
References

14 September 2010; accepted 5 October 2010
10.1126/science.1197785

Cognitive Illusions of Authorship Reveal Hierarchical Error Detection in Skilled Typists

Gordon D. Logan* and Matthew J. C. Crump

The ability to detect errors is an essential component of cognitive control. Studies of error detection in humans typically use simple tasks and propose single-process theories of detection. We examined error detection by skilled typists and found illusions of authorship that provide evidence for two error-detection processes. We corrected errors that typists made and inserted errors in correct responses. When asked to report errors, typists took credit for corrected errors and accepted blame for inserted errors, claiming authorship for the appearance of the screen. However, their typing rate showed no evidence of these illusions, slowing down after corrected errors but not after inserted errors. This dissociation suggests two error-detection processes: one sensitive to the appearance of the screen and the other sensitive to keystrokes.

Errors are ubiquitous in human performance (*1*, *2*). Their consequences can be costly, ranging from mild annoyance to global-scale disaster. Errors are common in the early stages of skill acquisition, when learning is based on trial and error, but they still prevail in expert performance, when skills are automatic and fluent. Detecting and correcting errors are important components of executive control at high skill levels (*3*, *4*). The control processes that manage errors are evident in behavioral measures of post-error slowing and conscious reports of errors (*1*), as well as in neural measures of error-related potentials in the electroencephalogram (*5*) and activation of the anterior cingulate cortex in functional brain imaging (*6*, *7*). Several theories have been proposed to account for these measures. Some assume a post hoc comparison of intended and actual actions (*5*). Others suggest that conflict between competing responses may be sufficient to trigger error detection and correction (*4*). Researchers often view these accounts as mutually exclusive and perform experiments intended to decide between them, as if there were a single error-detection mechanism and the goal of their research was to determine its properties. That may be possible in simple tasks with single responses, but it is unlikely to apply to complex tasks, like typewriting, that involve hierarchical processing and extended interaction with the environment (*8*–*10*). Here, we report the induction of cognitive illusions of authorship (*11*–*14*) in skilled typists and provide evidence for two separate error-detection mechanisms nested in a hierarchical control process (*10*).

Skilled typewriting engages many processes, from perception to cognition and action (*9*, *15*). The processes can be divided into two nested

Department of Psychology, Vanderbilt University, Nashville, TN 37203, USA.

*To whom correspondence should be addressed. E-mail: gordon.logan@vanderbilt.edu

feedback loops: (i) an outer loop that begins with language comprehension and generation and produces a series of words to be typed and (ii) an inner loop that begins with the words the outer loop provides and produces a series of keystrokes (*9*, *10*, *15*–*17*). The two loops are relatively autonomous: The outer loop commands the inner loop but knows little about how the inner loop carries out its commands (*10*, *17*). Our research was guided by the hypothesis that the two loops are driven by different kinds of feedback: The outer loop is sensitive to the appearance of the output on the screen, whereas the inner loop is sensitive to feedback from the fingers and the keyboard (*9*, *17*, *18*). Thus, the two loops should detect errors with different mechanisms (*19*, *20*).

We created illusions of authorship by introducing mismatches between errors in the inner and outer loops. We corrected errors that typists made, so the output matched their intentions when their motor behavior did not, and we inserted errors into the output that the typists produced, so that their motor behavior matched their intentions when the output did not. We hypothesized that the outer loop would evaluate the match between intended and actual actions, claiming authorship for the appearance of the screen. The outer loop decides that the response is correct if the screen looks right and incorrect if the screen looks wrong. Thus, the outer loop would treat corrected errors like actual, typist-produced correct responses and inserted errors like actual, typist-produced errors, creating illusions of authorship (*11*–*14*). We hypothesized that the inner loop would monitor keystrokes, evaluating proprioceptive and kinesthetic feedback (*17*–*20*), and so would respond differently to inserted errors and actual errors and to corrected errors and correct responses. The inner loop would know the truth behind the illusion.

We tested these hypotheses in three experiments in which skilled typists typed single words presented one at a time on a computer screen, with their responses echoed on the screen below the word to be typed (*21*). We measured outer-loop error detection by asking for explicit reports of errors. The three experiments varied in the intrusiveness of explicit error detection. The first was the least intrusive, asking for retrospective reports after the experiment finished. The second asked participants to judge whether each word was correct or erroneous as soon as they typed it. The third told participants about corrected and inserted errors at the outset and asked them to judge whether each word was correct, erroneous, a corrected error, or an inserted error. We measured inner-loop error detection by evaluating post-error slowing. Skilled typists typically slow down immediately after an error, prolonging the interkeystroke interval between the error and the next keystroke (*18*). We predicted post-error slowing after actual errors and corrected errors and no slowing for inserted errors and correct responses.

We assessed the illusion of authorship by comparing explicit error detection with post-error slowing. If outer- and inner-loop error detection are accomplished by a single process, then typists should report errors in conditions that produce post-error slowing (actual errors and corrected errors), and they should report correct responses in conditions that do not produce post-error slowing (correct responses and inserted errors). If outer- and inner-loop error detection involve separate, hierarchically nested processes, then typists should report "correct" whenever the screen looks right (correct responses and corrected errors) and "error" whenever the screen looks wrong (actual errors and inserted errors), whether or not those conditions produce post-error slowing.

In each experiment, we inserted errors on 6% of the trials. On the remaining 94% of trials, we corrected ~45% of actual errors by echoing the correct response on the computer screen regard-

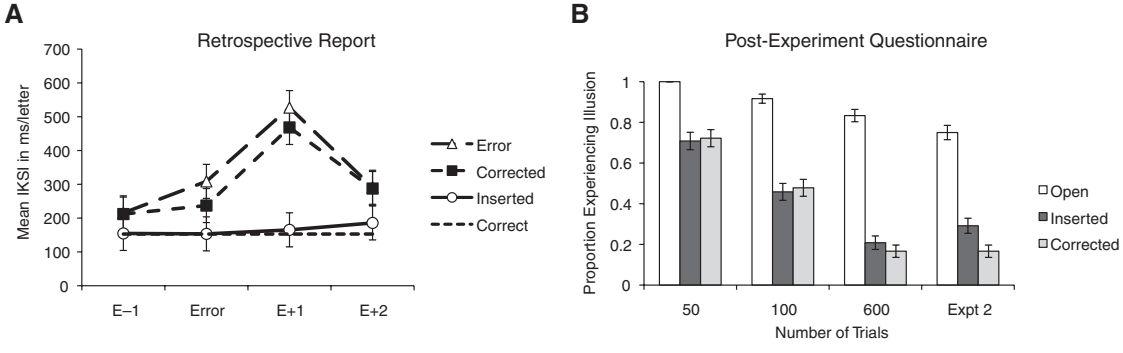

Fig. 1. (**A**) Mean interkeystroke interval in milliseconds per letter for the trial preceding an error (E–1), the error trial (Error), and the two trials after the error (E+1, E+2) for the 600-word group in experiment one, which used retrospective error reports gathered in a questionnaire administered after the experiment. Error bars are the 95% confidence intervals for the means based on Fisher's least significant difference test, calculated from the interaction between response type (error, inserted, corrected) and error position (E–1, Error, E+1, E+2). The data for correct responses are averaged over positions. (**B**) Proportions of participants who experienced illusions of authorship (did not report noticing inserted and corrected errors in question two, which was open-ended, in question three, which addressed inserted errors, and in question four, which addressed corrected errors) in the 50-, 100-, and 600-word groups and in experiment two. Error bars are 95% confidence intervals for the proportions calculated from the binomial distribution.

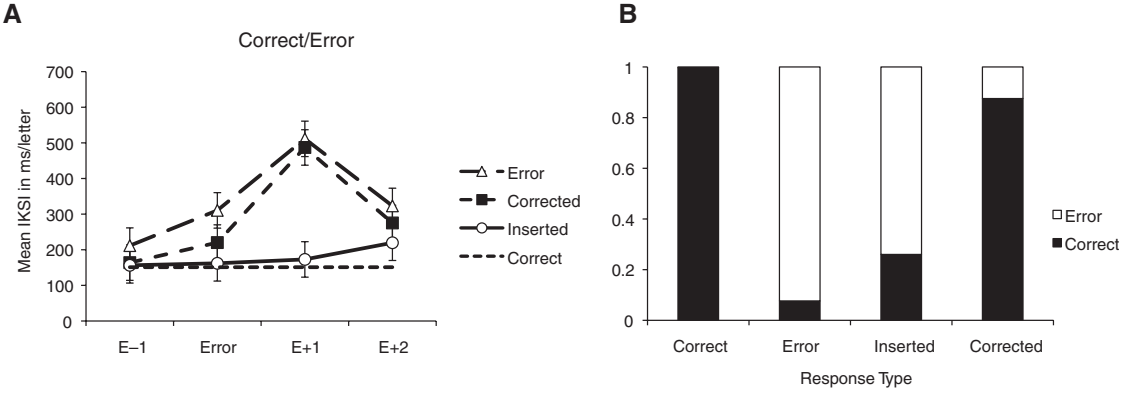

Fig. 2. (**A**) Mean interkeystroke interval in milliseconds per letter for the trial preceding an error (E–1), the error trial (Error), and the two trials after the error (E+1, E+2) in the second experiment, which used post-trial error reports in which participants said whether the preceding response was correct or incorrect. The data for correct responses are averaged over positions. Error bars indicate 95% confidence intervals based on Fisher's least significant difference test calculated from the interaction between response type and error position. (**B**) Mean probabilities of reporting correct or error for correct responses (correct), actual errors (error), inserted errors (inserted), and corrected errors (corrected).

less of what participants typed on 45% of the trials. We quantified skill as words per minute (WPM) on a typing test administered at the end of the experiment, reporting mean WPM ± standard deviation for each experiment. The typists were predominantly of college age, had 12.86 ± 5.35 years of experience, and typed at speeds comparable to professional typists.

The first experiment used retrospective error-detection reports, varying the number of words that were typed (50, 100, or 600) between participants to manipulate the opportunity to detect corrected and inserted errors. We tested three different groups of 24 skilled typists (WPM = 61.6 ± 16.9, 70.6 ± 20.6, and 68.6 ± 20.7 words, respectively); they typed 91.0, 89.9, and 91.0% of the words correctly, respectively. We assessed post-error slowing by examining interkeystroke interval for the trial before and two trials after an error. Twenty-two typists in the 600-word group provided sufficient data for this analysis. Their results, plotted in Fig. 1A, show slowing immediately after the error for incorrect responses ($F_{1,126}$ = 150.8, $p < 0.01$) and corrected errors ($F_{1,126}$ = 114.8, $p < 0.01$), but no slowing for inserted errors ($F < 1.0$). Thus, the inner loop responds differently to actual and inserted errors, as predicted. Interkeystroke intervals were longer for corrected errors and actual errors than for inserted errors and correct responses. This difference may reflect early error detection in the inner loop (*20*) or differences between words typed correctly and incorrectly. Errors are more likely to occur in words that are more difficult to type, and so are typed more slowly (*21*).

We assessed illusions of authorship with a post-experiment questionnaire, which consisted of six questions. The second, third, and fourth questions were most relevant. The first question asked for an estimate of the number of correct and incorrect responses. The second was open-ended, asking, "Did you notice anything about the kind of errors that you made?" Responses to this question were scored as illusions of authorship if typists made no mention of inserted or corrected errors. The third and fourth questions were direct, asking, "Did you notice that on some proportion of the trials the computer may have inserted errors, even if you correctly typed the word?" and "Did you notice that on some proportion of the trials the computer may have correctly typed a word even though you made an error?" Responses to these questions were scored as illusions of authorship if typists said "no."

The proportions of typists showing illusions of authorship are plotted in Fig. 1B. The proportions were significantly greater than zero for each question in each group (that is, the 95% confidence intervals constructed from the binomial distribution did not include 0). Illusions of authorship were stronger in the open-ended question than in the more direct questions, perhaps because typists were less willing to admit they had not noticed inserted and corrected errors when they were told they had occurred. Illusions of authorship were about the same for inserted and corrected errors. Illusions of authorship declined as typists experienced more inserted and corrected errors. There were 3, 6, and 36 inserted errors in the 50-, 100-, and 600-word versions of the experiment, respectively. Corrected errors were generated by randomly correcting 45% of all responses. The average numbers of corrected errors for the 18, 23, and 24 typists who experienced one or more in the 50-, 100-, and 600-word versions of the experiment were 2.4, 4.3, and 24, respectively.

The post-error–slowing data and retrospective reports show a dissociation between inner- and outer-loop error detection. Typists slowed after corrected errors but not after inserted errors, yet many of them accepted corrected errors as correct responses and inserted errors as errors. This analysis of post-error slowing collapses over typists who did and did not show illusions of authorship. We analyzed post-error slowing separately for typists who did and did not show illusions and found the same pattern in both groups (fig. S1) (*21*). Thus, the pattern in Fig. 1A is representative of all typists.

The second experiment asked 24 skilled typists (WPM = 68.2 ± 11.0) to type 600 words. After each word, they were asked to report errors explicitly, indicating whether they typed the word correctly or incorrectly. There was no mention of corrected and inserted errors. Typists typed 88.4% of the words correctly. Mean interkeystroke intervals from 23 typists who provided sufficient data for analysis are plotted in Fig. 2A. There was post-error slowing for incorrect responses ($F_{1,132}$ = 125.0, $p < 0.01$) and corrected errors ($F_{1,132}$ = 169.6, $p < 0.01$), but not for inserted errors ($F < 1.0$), suggesting again that inner-loop error detection distinguishes between actual errors and correct responses.

Explicit error-detection probabilities, plotted in Fig. 2B, show good discrimination between correct and incorrect responses. For correct responses, typists said "correct" more than "error" [$t(23) = 41.61$, $p < 0.01$]; for incorrect responses, typists said "error" more than "correct" [$t(23) = 10.40$, $p < 0.01$]. Typists showed illusions of authorship for inserted errors, saying "error" more than "correct" [$t(23) = 5.33$, $p < 0.01$]. They also showed illusions of authorship for corrected errors, saying "correct" more than "error" [$t(23) = 5.26$, $p < 0.01$].

The post-error slowing and post-trial report data reveal a dissociation between inner- and outer-loop error detection. We assessed the dissociation further by comparing trials in which typists did and did not experience illusions of authorship (*21*). The pattern of post-error slowing was the same for both sets of trials (fig. S5), suggesting that the pattern in Fig. 2A is representative of all trials.

The explicit report task did not allow typists to distinguish between actual errors and inserted errors or between correct responses and corrected errors. Nevertheless, typists chose responses that reflected the appearance of the screen instead of the keys they struck, consistent with their experience with computers and with our hypothesis that explicit error detection reflects outer-loop control processes. We administered the post-experiment questionnaire from experiment one and found that typists did not seem to be confused about the requirement to classify inserted and corrected errors. The proportions of typists showing illusions of authorship were about the same as those of the typists in the 600-word group in experiment one, who were not required to report errors after each trial (Fig. 1B).

We conducted a third experiment that included four response categories in the explicit detection

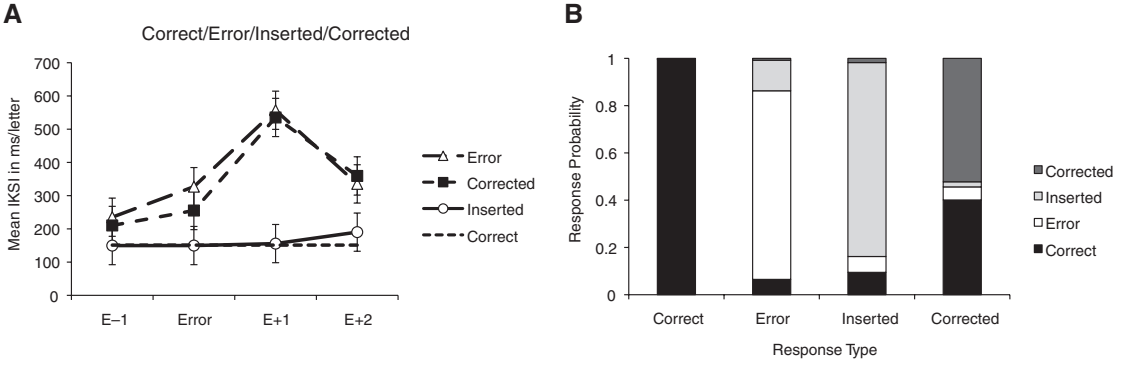

Fig. 3. (**A**) Mean interkeystroke interval in milliseconds per letter for the trial preceding an error (E–1), the error trial (Error), and the two trials after the error (E+1, E+2) in the third experiment, which used post-trial error reports in which participants said whether the preceding response was correct, error, inserted error, or corrected error. The data for correct responses are averaged over positions. Error bars indicate 95% confidence intervals based on Fisher's least significant difference test calculated from the interaction between response type and error position. (**B**) Mean probabilities of reporting correct, error, inserted error, or corrected error for correct responses (correct), actual errors (error), inserted errors (inserted), and corrected errors (corrected).

task (correct, error, inserted error, and corrected error) to allow typists to distinguish sources of errors and correct responses and, therefore, provide a stronger test of illusions of authorship. We asked 24 skilled typists (WPM = 70.7 ± 16.4) to type 600 words, each of which was followed by a four-alternative explicit report screen. Typists typed 91.8% of the words correctly. Mean interkeystroke intervals, plotted in Fig. 3A, show post-error slowing for incorrect responses ($F_{1,138} = 117.7$, $p < 0.01$) and corrected errors ($F_{1,138} = 120.0$, $p < 0.01$), but not for inserted errors ($F < 1.0$), indicating that inner-loop detection distinguishes between actual errors and correct responses.

Explicit detection probabilities, plotted in Fig. 3B, show good discrimination between correct and error responses. For correct responses, typists said "correct" more than "error" [$t(23) = 97.29$, $p < 0.01$]; for error responses, typists said "error" more than "correct" [$t(23) = 8.22$, $p < 0.01$]. Typists distinguished actual errors from inserted errors well, avoiding an illusion of authorship. They said "error" more than "inserted" for actual errors [$t(23) = 7.06$, $p < 0.01$] and "inserted" more than "error" for inserted errors [$t(23) = 14.75$, $p < 0.01$]. However, typists showed a strong illusion of authorship with corrected errors. They were just as likely to call them correct responses as corrected errors [$t(23) = 1.38$].

The post-error slowing and post-trial report data show a dissociation between inner- and outer-loop error detection. We assessed the dissociation further by comparing post-error slowing on trials in which typists did and did not experience illusions of authorship (*21*). The pattern of post-error slowing was the same for both sets of trials (fig. S6), suggesting that the pattern in Fig. 3A is representative of all trials.

The three experiments found strong dissociations between explicit error reports and post-error slowing. These dissociations are consistent with the hierarchical error-detection mechanism that we proposed, with an outer loop that mediates explicit reports and an inner loop that mediates post-error slowing. This nested-loop description of error detection is consistent with hierarchical models of cognitive control in typewriting (*9*, *10*, *15*–*17*) and with models of hierarchical control in other complex tasks (2, *8*, *22*). Speaking, playing music, and navigating through space may all involve inner loops that take care of the details of performance (e.g., uttering phonemes, playing notes, and walking) and outer loops that ensure that intentions are fulfilled (e.g., messages communicated, songs performed, and destinations reached). Hierarchical control may be prevalent in highly skilled performers who have had enough practice to develop an autonomous inner loop. Previous studies of error detection in simple tasks may describe inner-loop processing. The novel contribution of our research is to dissociate the outer loop from the inner loop.

The three experiments demonstrate cognitive illusions of authorship in skilled typewriting (*11*–*14*). Typists readily take credit for correct output on the screen, interpreting corrected errors as their own correct responses. They take the blame for inserted errors, as in the first and second experiments, but they also blame the computer, as in the third experiment. These illusions are consistent with the hierarchical model of error detection, with the outer loop assigning credit and blame and the inner loop doing the work of typing (*10*, *17*). Thus, illusions of authorship may be a hallmark of hierarchical control systems (*2*, *11*, *22*, *23*).

References and Notes

1. P. M. A. Rabbitt, *J. Exp. Psychol.* **71**, 264 (1966).
2. D. A. Norman, *Psychol. Rev.* **88**, 1 (1981).
3. C. B. Holroyd, M. G. H. Coles, *Psychol. Rev.* **109**, 679 (2002).
4. N. Yeung, M. M. Botvinick, J. D. Cohen, *Psychol. Rev.* **111**, 931 (2004).
5. W. J. Gehring, B. Goss, M. G. H. Coles, D. E. Meyer, E. Donchin, *Psychol. Sci.* **4**, 385 (1993).
6. S. Dehaene, M. I. Posner, D. M. Tucker, *Psychol. Sci.* **5**, 303 (1994).
7. C. S. Carter *et al.*, *Science* **280**, 747 (1998).
8. K. S. Lashley, in *Cerebral Mechanisms in Behavior*, L. A. Jeffress, Ed. (Wiley, New York, 1951), pp. 112–136.
9. T. A. Salthouse, *Psychol. Bull.* **99**, 303 (1986).
10. G. D. Logan, M. J. C. Crump, *Psychol. Sci.* **20**, 1296 (2009).
11. T. I. Nielsen, *Scand. J. Psychol.* **4**, 225 (1963).
12. M. M. Botvinick, J. D. Cohen, *Nature* **391**, 756 (1998).
13. D. M. Wegner, *The Illusion of Conscious Will* (MIT Press, Cambridge, MA, 2002).
14. G. Knoblich, T. T. J. Kircher, *J. Exp. Psychol. Hum. Percept. Perform.* **30**, 657 (2004).
15. D. E. Rumelhart, D. A. Norman, *Cogn. Sci.* **6**, 1 (1982).
16. L. H. Shaffer, *Psychol. Rev.* **83**, 375 (1976).
17. X. Liu, M. J. C. Crump, G. D. Logan, *Mem. Cognit.* **38**, 474 (2010).
18. A. M. Gordon, J. F. Soechting, *Exp. Brain Res.* **107**, 281 (1995).
19. J. Long, *Ergonomics* **19**, 93 (1976).
20. P. Rabbitt, *Ergonomics* **21**, 945 (1978).
21. Materials and methods are available as supporting material on *Science* Online.
22. M. M. Botvinick, *Trends Cogn. Sci.* **12**, 201 (2008).
23. R. Cooper, T. Shallice, *Cogn. Neuropsychol.* **17**, 297 (2000).

24. We thank J. D. Schall for comments on the manuscript. This research was supported by grants BCS 0646588 and BCS 0957074 from the NSF.

Supporting Online Material

www.sciencemag.org/cgi/content/full/330/6004/683/DC1
Materials and Methods
SOM Text
Figs. S1 to S6
References

5 April 2010; accepted 13 September 2010
10.1126/science.1190483

Evidence for a Collective Intelligence Factor in the Performance of Human Groups

Anita Williams Woolley,[1]* Christopher F. Chabris,[2,3] Alex Pentland,[3,4] Nada Hashmi,[3,5] Thomas W. Malone[3,5]

Psychologists have repeatedly shown that a single statistical factor—often called "general intelligence"—emerges from the correlations among people's performance on a wide variety of cognitive tasks. But no one has systematically examined whether a similar kind of "collective intelligence" exists for groups of people. In two studies with 699 people, working in groups of two to five, we find converging evidence of a general collective intelligence factor that explains a group's performance on a wide variety of tasks. This "*c* factor" is not strongly correlated with the average or maximum individual intelligence of group members but is correlated with the average social sensitivity of group members, the equality in distribution of conversational turn-taking, and the proportion of females in the group.

As research, management, and many other kinds of tasks are increasingly accomplished by groups—working both face-to-face and virtually (*1*–*3*)—it is becoming ever more important to understand the determinants of group performance. Over the past century, psychologists made considerable progress in defining and systematically measuring intelligence in individuals (*4*). We have used the statistical approach they developed for individual intelligence to systematically measure the intelligence of groups. Even though social psychologists and others have studied for decades how well groups perform specific tasks (*5*, *6*), they have not attempted to measure group intelligence in the same way individual intelligence is measured—by assessing how well a single group can perform a wide range of different tasks and using that information to predict how that same group will perform other tasks in the future. The goal of the research reported here was to test the hypothesis that groups, like individuals, do have characteristic levels of intelligence, which can be measured and used to predict the groups' performance on a wide variety of tasks.

Although controversy has surrounded it, the concept of measurable human intelligence is based on a fact that is still as remarkable as it was to Spearman when he first documented it in 1904

[1]Carnegie Mellon University, Tepper School of Business, Pittsburgh, PA 15213, USA. [2]Union College, Schenectady, NY 12308, USA. [3]Massachusetts Institute of Technology (MIT) Center for Collective Intelligence, Cambridge, MA 02142, USA. [4]MIT Media Lab, Cambridge, MA 02139, USA. [5]MIT Sloan School of Management, Cambridge, MA 02142, USA.

*To whom correspondence should be addressed. E-mail: awoolley@cmu.edu

(*7*): People who do well on one mental task tend to do well on most others, despite large variations in the tests' contents and methods of administration (*4*). In principle, performance on cognitive tasks could be largely uncorrelated, as one might expect if each relied on a specific set of capacities that was not used by other tasks (*8*). It could even be negatively correlated, if practicing to improve one task caused neglect of others (*9*). The empirical fact of general cognitive ability as first demonstrated by Spearman is now, arguably, the most replicated result in all of psychology (*4*).

Evidence of general intelligence comes from the observation that the average correlation among individuals' performance scores on a relatively diverse set of cognitive tasks is positive, the first factor extracted in a factor analysis of these scores generally accounts for 30 to 50% of the variance, and subsequent factors extracted account for substantially less variance. This first factor extracted in an analysis of individual intelligence tests is referred to as general cognitive ability, or *g*, and it is the main factor that intelligence tests measure. What makes intelligence tests of substantial practical (not just theoretical) importance is that intelligence can be measured in an hour or less, and is a reliable predictor of a very wide range of important life outcomes over a long span of time, including grades in school, success in many occupations, and even life expectancy (*4*).

By analogy with individual intelligence, we define a group's collective intelligence (*c*) as the general ability of the group to perform a wide variety of tasks. Empirically, collective intelligence is the inference one draws when the ability of a group to perform one task is correlated with that group's ability to perform a wide range of other tasks. This kind of collective intelligence is a property of the group itself, not just the individuals in it. Unlike previous work that examined the effect on group performance of the average intelligence of individual group members (*10*), one of our goals is to determine whether the collective intelligence of the group as a whole has predictive power above and beyond what can be explained by knowing the abilities of the individual group members.

The first question we examined was whether collective intelligence—in this sense—even exists. Is there a single factor for groups, a *c* factor, that functions in the same way for groups as general intelligence does for individuals? Or does group performance, instead, have some other correlational structure, such as several equally important but independent factors, as is typically found in research on individual personality (*11*)?

To answer this question, we randomly assigned individuals to groups and asked them to perform a variety of different tasks (*12*). In Study 1, 40 three-person groups worked together for up to 5 hours on a diverse set of simple group tasks plus a more complex criterion task. To guide our task sampling, we drew tasks from all quadrants of the McGrath Task Circumplex (*6*, *12*), a well-established taxonomy of group tasks based on the coordination processes they require. Tasks included solving visual puzzles, brainstorming, making collective moral judgments, and negotiating over limited resources. At the beginning of each session, we measured team members' individual intelligence. And, as a criterion task at the end of each session, each group played checkers against a standardized computer opponent.

The results support the hypothesis that a general collective intelligence factor (*c*) exists in groups. First, the average inter-item correlation for group scores on different tasks is positive (r = 0.28) (Table 1). Next, factor analysis of team scores yielded one factor with an initial eigenvalue accounting for more than 43% of the variance (in the middle of the 30 to 50% range typical in individual intelligence tests), whereas the next factor accounted for only 18%. Confirmatory factor analysis supported the fit of a single latent factor model with the data [χ^2 = 1.66, P = 0.89, df = 5; comparative fit index (CFI) =.99, root mean square error of approximation (RMSEA) = 0.01]. Furthermore, when the factor loadings for different tasks on the first general factor are used to calculate a *c* score for each group, this score strongly predicts performance on the criterion task (r = 0.52, P = 0.01). Finally, the average and maximum intelligence scores of individual group members are not significantly correlated with *c* [r = 0.19, not significant (ns); r = 0.27, ns, respectively] and not predictive of criterion task performance (r = 0.18, ns; r = 0.13, ns, respectively). In a regression using both individual intelligence and *c* to predict performance on the criterion task, *c* has a significant effect (β = 0.51, P = 0.001), but average individual intelligence (β = 0.08, ns) and maximum individual intelligence (β =.01, ns) do not (Fig. 1).

In Study 2, we used 152 groups ranging from two to five members. Our goal was to replicate these findings in groups of different sizes, using a broader sample of tasks and an alternative measure of individual intelligence. As expected, this study replicated the findings of Study 1, yielding a first factor explaining 44% of the variance and a second factor explaining only 20%. In addition, a confirmatory factor analysis suggests an excellent fit of the single-factor model with the data (χ^2 = 5.85, P = 0.32, df = 5; CFI = 0.98, NFI = 0.89, RMSEA = 0.03).

In addition, for a subset of the groups in Study 2, we included five additional tasks, for a total of ten. The results from analyses incorporating all ten tasks were also consistent with the hypothesis that a general *c* factor exists (see Fig. 2). The scree test (*13*) clearly suggests that a one-factor model is the best fit for the data from both studies [Akaike Information Criterion (AIC) = 0.00 for single-factor solution]. Furthermore, parallel analysis (*13*) suggests that only factors with an eigenvalue above 1.38 should be retained, and there is only one such factor in each sample. These conclusions are supported by examining the eigenvalues both before and after principal axis extraction, which yields a first factor explaining 31% of

Table 1. Correlations among group tasks and descriptive statistics for Study 1. n = 40 groups; *$P \leq$ 0.05; **$P \leq$ 0.001.

	1	2	3	4	5	6	7	8	9
1 Collective intelligence (*c*)									
2 Brainstorming	0.38*								
3 Group matrix reasoning	0.86**	0.30*							
4 Group moral reasoning	0.42*	0.12	0.27						
5 Plan shopping trip	0.66**	0.21	0.38*	0.18					
6 Group typing	0.80**	0.13	0.50**	0.25*	0.43*				
7 Avg member intelligence	0.19	0.11	0.19	0.12	−0.06	0.22			
8 Max member intelligence	0.27	0.09	0.33*	0.05	−0.04	0.28	0.73**		
9 Video game	0.52*	0.17	0.38*	0.37*	0.39*	0.44*	0.18	0.13	
Minimum	−2.67	9	2	32	−10.80	148	4.00	8.00	26
Maximum	1.56	55	17	81	82.40	1169	12.67	15.67	96
Mean	0	28.33	11.05	57.35	46.92	596.13	8.92	11.67	61.80
SD	1.00	11.36	3.02	10.96	19.64	263.74	1.82	1.69	17.56

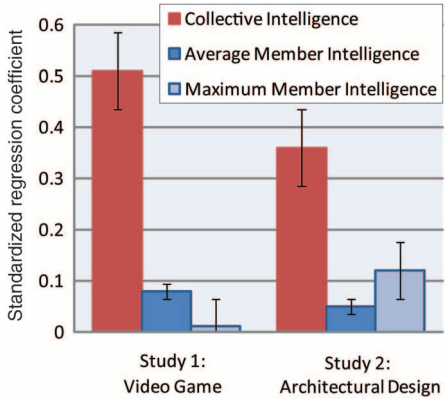

Fig. 1. Standardized regression coefficients for collective intelligence (*c*) and average individual member intelligence when both are regressed together on criterion task performance in Studies 1 and 2 (controlling for group size in Study 2). Coefficient for maximum member intelligence is also shown for comparison, calculated in a separate regression because it is too highly correlated with individual member intelligence to incorporate both in a single analysis (r = 0.73 and 0.62 in Studies 1 and 2, respectively). Error bars, mean ± SE.

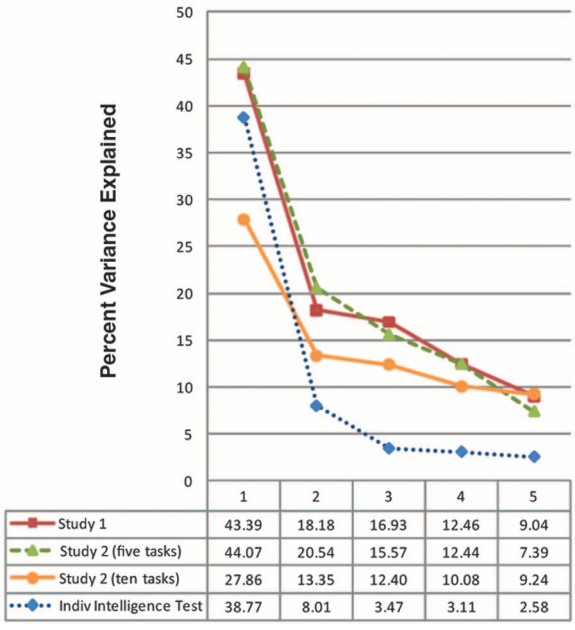

	1	2	3	4	5
Study 1	43.39	18.18	16.93	12.46	9.04
Study 2 (five tasks)	44.07	20.54	15.57	12.44	7.39
Study 2 (ten tasks)	27.86	13.35	12.40	10.08	9.24
Indiv Intelligence Test	38.77	8.01	3.47	3.11	2.58

Fig. 2. Scree plot demonstrating the first factor from each study accounting for more than twice as much variance as subsequent factors. Factor analysis of items from the Wonderlic Personnel Test of Individual intelligence administered to 642 individuals is included as a comparison.

the variance in Study 1 and 35% of the variance in Study 2. Multiple-group confirmatory factor analysis suggests that the factor structures of the two studies are invariant ($\chi^2 = 11.34$, $P = 0.66$, df = 14; CFI = 0.99, RMSEA = 0.01). Taken together, these results provide strong support for the existence of a single dominant *c* factor underlying group performance.

The criterion task used in Study 2 was an architectural design task modeled after a complex research and development problem (*14*). We had a sample of 63 individuals complete this task working alone, and under these circumstances, individual intelligence was a significant predictor of performance on the task ($r = 0.33$, $P = 0.009$).

When the same task was done by groups, however, the average individual intelligence of the group members was not a significant predictor of group performance ($r = 0.18$, ns). When both individual intelligence and *c* are used to predict group performance, *c* is a significant predictor ($\beta = 0.36$, $P = 0.0001$), but average group member intelligence ($\beta = 0.05$, ns) and maximum member intelligence ($\beta = 0.12$, ns) are not (Fig. 1).

If *c* exists, what causes it? Combining the findings of the two studies, the average intelligence of individual group members was moderately correlated with *c* ($r = 0.15$, $P = 0.04$), and so was the intelligence of the highest-scoring team member ($r = 0.19$, $P = 0.008$). However, for both studies, *c* was still a much better predictor of group performance on the criterion tasks than the average or maximum individual intelligence (Fig. 1).

We also examined a number of group and individual factors that might be good predictors of *c*. We found that many of the factors one might have expected to predict group performance—such as group cohesion, motivation, and satisfaction—did not.

However, three factors were significantly correlated with *c*. First, there was a significant correlation between *c* and the average social sensitivity of group members, as measured by the "Reading the Mind in the Eyes" test (*15*) ($r = 0.26$, $P = 0.002$). Second, *c* was negatively correlated with the variance in the number of speaking turns by group members, as measured by the sociometric badges worn by a subset of the groups (*16*) ($r = -0.41$, $P = 0.01$). In other words, groups where a few people dominated the conversation were less collectively intelligent than those with a more equal distribution of conversational turn-taking.

Finally, *c* was positively and significantly correlated with the proportion of females in the group ($r = 0.23$, $P = 0.007$). However, this result appears to be largely mediated by social sensitivity (Sobel $z = 1.93$, $P = 0.03$), because (consistent with previous research) women in our sample scored better on the social sensitivity measure than men [$t(441) = 3.42$, $P = 0.001$]. In a regression analysis with the groups for which all three variables (social sensitivity, speaking turn variance, and percent female) were available, all had similar predictive power for *c*, although only social sensitivity reached statistical significance ($\beta = 0.33$, $P = 0.05$) (*12*).

These results provide substantial evidence for the existence of *c* in groups, analogous to a well-known similar ability in individuals. Notably, this collective intelligence factor appears to depend both on the composition of the group (e.g., average member intelligence) and on factors that emerge from the way group members interact when they are assembled (e.g., their conversational turn-taking behavior) (*17*, *18*).

These findings raise many additional questions. For example, could a short collective inteligence test predict a sales team's or a top management team's long-term effectiveness? More importantly, it would seem to be much easier to raise the intelligence of a group than an individual. Could a group's collective intelligence be increased by, for example, better electronic collaboration tools?

Many previous studies have addressed questions like these for specific tasks, but by measuring the effects of specific interventions on a group's *c*, one can predict the effects of those interventions on a wide range of tasks. Thus, the ability to measure collective intelligence as a stable property of groups provides both a substantial economy of effort and a range of new questions to explore in building a science of collective performance.

References and Notes

1. S. Wuchty, B. F. Jones, B. Uzzi, *Science* **316**, 1036 (2007).
2. T. Gowers, M. Nielsen, *Nature* **461**, 879 (2009).
3. J. R. Hackman, *Leading Teams: Setting the Stage for Great Performances* (Harvard Business School Press, Boston, 2002).
4. I. J. Deary, *Looking Down on Human Intelligence: From Psychometrics to the Brain* (Oxford Univ. Press, New York, 2000).
5. J. R. Hackman, C. G. Morris, in *Small Groups and Social Interaction*, Volume 1, H. H. Blumberg, A. P. Hare, V. Kent, M. Davies, Eds. (Wiley, Chichester, UK, 1983), pp. 331–345.
6. J. E. McGrath, *Groups: Interaction and Performance* (Prentice-Hall, Englewood Cliffs, NJ, 1984).
7. C. Spearman, *Am. J. Psychol.* **15**, 201 (1904).
8. C. F. Chabris, in *Integrating the Mind: Domain General Versus Domain Specific Processes in Higher Cognition*, M. J. Roberts, Ed. (Psychology Press, Hove, UK, 2007), pp. 449–491.
9. C. Brand, *The g Factor* (Wiley, Chichester, UK, 1996).
10. D. J. Devine, J. L. Philips, *Small Group Res.* **32**, 507 (2001).
11. R. R. McCrae, P. T. Costa Jr., *J. Pers. Soc. Psychol.* **52**, 81 (1987).
12. Materials and methods are available as supporting material on *Science* Online.
13. R. B. Cattell, *Multivariate Behav. Res.* **1**, 245 (1966).
14. A. W. Woolley, *Organ. Sci.* **20**, 500 (2009).
15. S. Baron-Cohen, S. Wheelwright, J. Hill, Y. Raste, I. Plumb, *J. Child Psychol. Psychiatry* **42**, 241 (2001).
16. A. Pentland, *Honest Signals: How They Shape Our World* (Bradford Books, Cambridge, MA, 2008).
17. L. K. Michaelsen, W. E. Watson, R. H. Black, *J. Appl. Psychol.* **74**, 834 (1989).
18. R. S. Tindale, J. R. Larson, *J. Appl. Psychol.* **77**, 102 (1992).

19. This work was made possible by financial support from the National Science Foundation (grant IIS-0963451), the Army Research Office (grant 56692-MA), the Berkman Faculty Development Fund at Carnegie Mellon University, and Cisco Systems, Inc., through their sponsorship of the MIT Center for Collective Intelligence. We would especially like to thank S. Kosslyn for his invaluable help in the initial conceptualization and early stages of this work and I. Aggarwal and W. Dong for substantial help with data collection and analysis. We are also grateful for comments and research assistance from L. Argote, E. Anderson, J. Chapman, M. Ding, S. Gaikwad, C. Huang, J. Introne, C. Lee, N. Nath, S. Pandey, N. Peterson, H. Ra, C. Ritter, F. Sun, E. Sievers, K. Tenabe, and R. Wong. The hardware and software used in collecting sociometric data are the subject of an MIT patent application and will be provided for academic research via a not-for-profit arrangement through A.P. In addition to the affiliations listed above, T.W.M. is also a member of the Strategic Advisory Board at InnoCentive, Inc.; a director of Seriosity, Inc.; and chairman of Phios Corporation.

Supporting Online Material

www.sciencemag.org/cgi/content/full/science.1193147/DC1
Materials and Methods
Tables S1 to S4
References

2 June 2010; accepted 10 September 2010
Published online 30 September 2010;
10.1126/science.1193147
Include this information when citing this paper.

NEW PRODUCTS: STRUCTURAL GENOMICS

NANOLITER LIQUID HANDLING

The mosquito provides precise and repeatable nanoliter dispensing of any liquid down to 25 nL, irrespective of liquid viscosity. The liquid handler is available in three standard formats, each of which is flexible enough to address a range of applications, including high throughput screening (HTS), 'hit picking', and protein crystallography. Making protein crystallography exceptionally fast and cost effective, the mosquito Crystal automates crystallography setups (hanging drop, sitting drop, and microbatch techniques) and additive screening. Mosquito LCP offers an additional fully automated solution to lipidic cubic phase (LCP) screening. Mosquito HTS miniaturizes screening applications, such as assay-ready plate preparation, reformatting, and serial dilutions to make more efficient use of valuable compounds. Finally, mosquito X1 is a single tip 'hit picking' instrument, which offers precision nanoliter sampling of any individual well or location. This enables researchers to transfer nanoliter volumes of hits from primary screening plates directly to hit validation without cross-contamination or further dilution.

TTP LabTech Ltd.
For info: 617-494-9794 | www.ttplabtech.com

PROTEIN EXTRACTION

The Universal Protein Extraction (UPX) Kit is designed for unbiased, high-yield detergent extraction of proteins from cells and tissue. The kit extracts both soluble and insoluble proteins at high efficiency, enabling subsequent analysis of membrane proteins and other hydrophobic proteins. Designed to solubilize the whole proteome, including difficult membrane proteins, the UPX Kit gives researchers more protein from their tissues to work with and opens opportunities for researchers to analyze specific insoluble proteins, or to obtain a more encompassing understanding of the proteome. The UPX Kit provides high-yield, unbiased protein extraction results from mammalian tissue, mammalian-derived cell lines, bacteria, and other samples commonly used for protein research. Starting material can be frozen or freshly harvested.

Protein Discovery
For info: 865-521-7400 | www.proteindiscovery.com

GENE DELIVERY

A new range of expression-ready lentiviral particles allow easy gene delivery into hard-to-transfect cells, including primary cells, nondividing cells, and cells in suspension. The particles are supplied ready-to-use, eliminating the need for any lipids or transfection reagents. The range of premade lentiviral particles deliver genes in a highly reproducible and controllable manner for the expression of greater than 250 human proteins, mouse proteins, enzymes, and fluorescent markers. These particles can also be used to easily and cost-effectively create stable cell lines for long-term high constitutive or Tet inducible expression applications in the presence of TetR (a repressor protein). Further, lentiviral particles can also be used in vivo for the generation of transgenic animals and for inducing pluripotent stem cells. Custom lentiviral particles for the expression of your own gene of interest or shRNA can also be generated.

AMSBIO
For info: +44-(0)-1235-828200 | www.amsbio.com

PROTEIN PURIFICATION

The Glutathione Agarose family of products is designed for cost-effective purification of glutathione S-transferase (GST)-tagged proteins from cellular lysates. Pierce Glutathione Agarose consists of glutathione linked to agarose beads though a 12-atom spacer which minimizes steric hindrance effects during purification. The six percent beaded agarose and highly purified glutathione limit nonspecific binding and result in a high binding capacity of greater than 25 mg of GST per milliliter of settled resin. The purification resin can be reused at least five times without loss in functionality. The affinity purification of GST-tagged proteins using Pierce Glutathione Agarose is a simple, one-step process. Bound GST-tagged proteins are easily eluted with a buffer containing Thermo Scientific Reduced Glutathione. If the GST fusion protein contains a Factor Xa protease site, then the protein can be cleaved from the GST tag with Thermo Scientific Factor Xa. Pierce Glutathione Agarose is available in numerous formats and as a standalone resin.

Thermo Scientific/Pierce
For info: 815-968-0747 | www.thermoscientific.com/pierce

PLASMID DNA EXTRACTION

The GET Plasmid DNA kits are spin column purification kits for the isolation of high quality plasmid from bacterial cultures. These kits are available in different formats: Maxiprep, Mediprep, Miniprep, and a 96-well kit. The different formats allow you to isolate various yields of plasmid. The GET Plasmid kits use an extraction method based on alkaline lysis of bacteria and uses our high affinity GET Plasmid columns to bind and purify plasmid DNA. This quick and easy protocol eliminates toxic phenol/chloroform extractions or ethanol precipitations. The extracted plasmid is ready for further DNA manipulation such as restriction enzyme digestion, ligation, transformation, transfection, and sequencing.

G-Biosciences/Genotech
For info: 314-991-6034 | www.GBiosciences.com

Electronically submit your new product description or product literature information! Go to **www.sciencemag.org/products/newproducts.dtl** for more information.

Newly offered instrumentation, apparatus, and laboratory materials of interest to researchers in all disciplines in academic, industrial, and governmental organizations are featured in this space. Emphasis is given to purpose, chief characteristics, and availability of products and materials. Endorsement by *Science* or AAAS of any products or materials mentioned is not implied. Additional information may be obtained from the manufacturer or supplier.

POSITIONS OPEN

Northeastern University

FACULTY POSITION in FISHERIES BIOLOGY Northeastern University

The Department of Biology invites applications for a tenure-track position at the rank of **ASSISTANT PROFESSOR** to start as early as September 2011. While we seek a junior faculty member at the Assistant Professor level, exceptionally qualified candidates could be considered at a higher level. Qualifications include a Ph.D. in Marine Biology or a related discipline, postdoctoral/professional experience, and evidence of outstanding research and academic potential. Candidates are expected to have or to develop an independently funded research program of national caliber and participate in undergraduate and graduate teaching. Expertise in all areas of biology will be considered, especially those in molecular biology, physiology, ecology, and evolution. We are particularly interested in applicants whose research involves economically important fisheries species, including resource management, sustainability, conservation, and policy. Although the successful candidate's appointment is within the Department of Biology, the primary office and laboratory space will be at Northeastern University's Marine Science Center (MSC) located in Nahant, Massachusetts. Hence, the successful candidate is expected to complement and strengthen existing research and teaching efforts within the MSC (**website: http://marinesciencecenter.yolasite.com/**) and the Department of Biology (**website: http://www.biology.neu.edu**).

To apply, visit "Careers at Northeastern" at **website: https://psoft.neu.edu/psc/neuhrprdpub/EMPLOYEE/HRMS/c/NEU_HR.NEU_JOBS.GBL.** Click on "Faculty Positions" and search for the current position under the College of Science. Applications can also be submitted by visiting the College of Science **website: http://www.northeastern.edu/cos/** and clicking on the Faculty Positions button. A complete application should include curriculum vitae; a statement of research interests and plans; a statement describing the applicant's teaching experience, interests, and philosophy; and three letters of recommendation. For questions about the search or to submit external references, call the Search Committee Chair, **Dr. Geoffrey C. Trussell,** at **telephone: 781-581-7370** (**ext. 300**). Review of applications will begin December 1, 2010, and will continue until the position is filled. *Northeastern is an Equal Opportunity/Affirmative Action Title IX University. Women and minority candidates are especially encouraged to apply.*

THREE TENURE-TRACK POSITIONS (Rank Open)—The Department of Anatomy at the University of Mississippi Medical Center wishes to fill two positions with a research emphasis, and one with a teaching emphasis, as part of its aggressive program to expand Neurobiology research. For more information about the department, go to **website: http://anatomy.umc.edu.** Successful candidates for the research positions need a strong funding history. Candidates for the teaching position need to demonstrate experience in teaching in the anatomical sciences. Applicants should electronically send their curriculum vitae, personal statement about research and teaching, and the names and e-mail addresses of three references to **Dr. Paul J. May,** Search Committee Chair, at **e-mail: pmay@anatomy.umc.edu.** *The University of Mississippi Medical Center is an Equal Opportunity Employer, Minorities/Females/Persons with Disabilities/Veterans.*

POSTDOCTORAL ASSOCIATE Mouse Models of Cancer

Position available immediately at Fox Chase Cancer Center for newly funded project involving mouse models of malignant mesothelioma. Experience in the use of transgenic or knockout mouse models desired. Strong background in molecular genetics and/or carcinogenesis required. Campus located in park-like setting in Philadelphia, Pennsylvania. Submit curriculum vitae and names of two references to **e-mail: joseph.testa@fccc.edu.**
Equal Opportunity Employer.

POSITIONS OPEN

Northeastern University

ASSISTANT PROFESSOR Developmental Biology or Neurobiology, with Focus on Adult Stem Cells

The Department of Biology at Northeastern University, Boston, Massachusetts invites applications for a tenure-track appointment in the area of Developmental Biology or Neurobiology, with specific focus on adult stem cells, and on the role of such cells in tissue regeneration or behavioral plasticity. Although appointment at the assistant professor level is preferred, applications at the associate professor level will be considered for candidates with a particularly strong track record. The anticipated start date is fall 2011. A competitive startup package will be provided.

Responsibilities will include teaching undergraduate and graduate courses and conducting an independent, externally funded research program. The Department has 28 full-time faculty members and administers programs in biology, biochemistry, behavioral neuroscience, and marine biology for over 1100 undergraduates, and currently hosts 61 students in the Biology Ph.D. program. In addition to facilities at Northeastern's main campus in the Back Bay area of Boston, the department has faculty and facilities nearby at Northeastern's Marine Science Center in Nahant, Massachusetts.

Applicants should have a Doctorate in biology or related field, a strong record of publication, and strong potential for external research funding. Candidates must have experience in, or a demonstrated commitment to, working with diverse student populations and/or in a culturally diverse work and educational environment.

Application materials should be submitted to "Careers at Northeastern" at **website: https://psoft.neu.edu/psc/neuhrprdpub/EMPLOYEE/HRMS/c/NEU_HR.NEU_JOBS.GBL.** Click on "Faculty Positions" and search for the current position under the College of Science. You can also apply by visiting the College of Science **website: http://www.northeastern.edu/cos/** and clicking on the Faculty Positions button. A complete application includes a cover letter, curriculum vitae, research statement, teaching statement, and a list of three references. The applicant should ask each reference to submit a letter directly to: **Chair, Department of Biology, 134 Mugar Building, 360 Huntington Avenue, Boston, MA 02115.** Review of applications will begin immediately. For full consideration, all application materials, including the reference letters, should be submitted by December 15, 2010.

Northeastern University, founded in 1898 and widely recognized for its success in Cooperative Education, is an Equal Opportunity, Affirmative Action Educational Institution and Employer, Title IX University. It is a participant in the National Science Foundation ADVANCE program (Advancement of Women in Academic Science and Engineering Careers). Candidates from groups underrepresented in science are especially encouraged to apply.

FACULTY POSITION in Organic and Bioorganic Materials Chemistry University of California, Irvine

The Department of Chemistry at the University of California, Irvine invites applications for a tenure-track position at the **ASSISTANT PROFESSOR** level in the field of experimental Organic and Bioorganic Materials Chemistry. We are seeking a Ph.D.-level scientist who will establish a vigorous research program involving any aspect of organic polymers/soft materials (special attention will be given to applicants with interests in soft materials related to biology, energy, environment, and catalysis); a strong commitment to teach at the undergraduate and graduate levels is also required. Applications should contain a cover letter, curriculum vita, list of publications, and a description of research plans. Applicants should also arrange to have at least three letters of recommendation submitted electronically on their behalf. Completed applications should be sent electronically, online at **website: https://recruit.ap.uci.edu.** To ensure full consideration, applications and supporting materials should be received by November 15, 2010. *The University of California, Irvine is an Equal Opportunity/Affirmative Action Employer committed to excellence through diversity. UC Irvine has an active ADVANCE Gender Equity Program.*

Senior Lecturer/ Associate Professor in Biomedical Research

The Faculty of Medicine at Linköping University runs the most highly rated MD program in Sweden, as well as a number of other strong educational programs in Health Care and Life Sciences. It trains a large number of health care professionals and researchers, and has strong research within several areas of modern medical sciences.

The Department of Clinical and Experimental Medicine hosts several strategic research centers, i.e. neuroscience, infectious disease, and regenerative medicine. The Department is now seeking a Senior Lecturer/Associate Professor in Biomedicine. The position is primarily focused on research, and the successful applicant is expected to establish an independent research group conducting research within his or her area of choice.

For more details please go to: **www.liu.se/en/job/**

Linköping University
expanding reality

10-0910

BIOLOGY DEPARTMENT CHAIR

Brookhaven National Laboratory (BNL) seeks a Biology Department Chair to lead the continued development of nationally and internationally competitive core biology and biotechnology capabilities at BNL. In addition to maintaining his/her own active research program, the successful candidate will be expected to: provide intellectual leadership for the Department; work with the staff to recruit, mentor and develop new members, and to maintain an interactive environment supportive of creative scientific research; develop a scientific vision for the Department in a leading national laboratory, and participate actively in accomplishing this vision; build strategic partnerships that significantly enhance BNL bioscience R&D capabilities and the impact of our programs. The goal is to develop a premier biosciences program consistent with the missions of the U. S. Department of Energy and, where possible, leveraging the unique multi-disciplinary capabilities and facilities at BNL.

Qualified candidates will have a doctorate degree in the biosciences or related disciplines, an internationally recognized record of accomplishment, and an active effort in one or more of the following areas: plant and/or microbial biology, metabolic biology, plant epigenetics, structural biology, synthetic biology, quantitative biology relevant to the U. S. Department of Energy missions in Energy and Environment. Successful candidates will have experience in developing integrated multi-disciplinary research programs and leading highly successful R&D teams. We believe that a comprehensive employee benefits program is an important and meaningful part of the compensation employees receive. Our programs offer medical and dental; life insurance, 401(k) plan, retirement plan, on-site day care, exercise facility, tennis courts, and other employee perks and benefits.

For consideration, please apply online at **www.bnl.gov** and click Jobs, then click Search Job List and apply to job **#15519** listed under Management. If you have questions, email **BiologyChair@bnl.gov**.EOE

BROOKHAVEN NATIONAL LABORATORY
a passion for discovery.

www.bnl.gov

MIAMI UNIVERSITY
OXFORD OHIO

PHYSIOLOGY/NEUROSCIENCE

Miami University is seeking to fill a tenure-track assistant professor position in an area that will complement research activities of the faculty. The successful applicant will be expected to maintain an active research program, acquire extramural funding, supervise student research, and participate in teaching graduate and undergraduate courses. In addition, s/he will participate in the new interdepartmental Cellular, Molecular, and Structural Biology PhD program as well as interdisciplinary minors in neuroscience and/or molecular biology. The University has state-of-the-art facilities for using molecular, cellular and whole organism techniques and offers competitive start-up funds. The Department has 32 faculty, over 60 PhD/MS students, and approximately 1,000 majors (**http://zoology.muohio.edu/**). Miami University (enrollment 24,000) is rated nationally as a highly selective public university.

Send letter of application, curriculum vitae, statements of teaching and research interests, and three letters of recommendation to: **Dr. Paul James, Search Committee Chair, Department of Zoology, 212 Pearson Hall, Miami University, Oxford, OH 45056**. Review of applications will begin on **7 December 2010** and continue until the position is filled. PhD required. Telephone **513-529-3100** or e-mail **biosearch@muohio.edu** for more information. For information regarding campus crime and safety, visit **www.muohio.edu/righttoknow**. Hard copy upon request.

Miami University is an EOE/AA Employer with smoke-free campuses.

Assistant/Associate Professor of Immunology and Infectious Diseases

The Department of Immunology and Infectious Diseases at the Harvard School of Public Health seeks candidates for the position of assistant or associate professor of immunology and infectious diseases. This is a tenure-ladder position, with academic rank to be determined in accordance with the successful candidate's experience and productivity.

Applicants must have a PhD, MD, DVM, or equivalent degree with extensive training and experience in vector-borne disease systems. The successful candidate will build and maintain an internationally recognized extramurally funded research program, with a special emphasis on malaria. The candidate should possess the ability to work collaboratively with other scientists and the scholarly qualities required to mentor doctoral students in the graduate program in the Division of Biological Sciences.

Please send a letter of application, including a statement of current and future research interests; curriculum vitae, including current and past grant support; sample publications; and the names of four referees to the address below. Applicants should ask their four referees to write independently to this address. The electronic submission of application documents to the e-mail below is welcome.

Dr. Dyann Wirth
Chair, Search Committee for
Assistant/Associate Professor of Immunology and Infectious Diseases
c/o Stephen Heim
Department of Immunology and Infectious Diseases
665 Huntington Avenue, SPH1-807
Harvard School of Public Health
Boston, MA 02115
E-mail: sheim@hsph.harvard.edu

Harvard University is committed to increasing representation of women and minority members among its faculty and particularly encourages applications from such candidates.

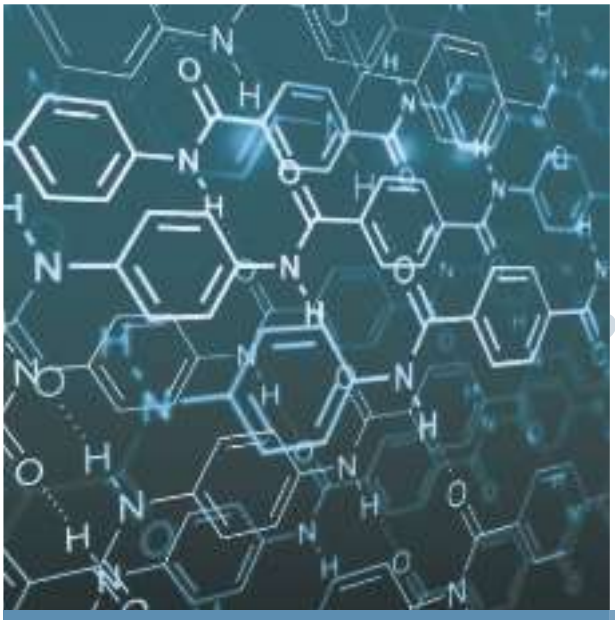

Help Us Help Millions

Division of Intramural Research
Laboratory of Molecular Immunology

NIAID

Postdoctoral positions are available in the Inflammation Biology Section of the Laboratory of Molecular Immunology, NIAID. The section uses the chemokine system to understand T-cell biology in humans and mouse models related to effector/memory cell function and differentiation, inflammation, host defense, and cancer. Principal, current projects focus on characterizing long-lived populations of memory cells in humans, understanding pathways for the differentiation of human CD4+ T cells, investigating the roles for chemokines/chemokine receptors in models of Th17-type inflammatory disease and host defense, understanding chemokine receptor signaling in lymphocytes, and using chemokine receptors as targets of novel probes for *in vivo* imaging. In consultation with the principal investigator, new members of the section will design independent projects related to these areas.

Application for these positions requires an interview. Contact Joshua M. Farber at **jfarber@niaid.nih.gov**. For more information about NIAID's available training and career opportunities, visit **www.niaid.nih.gov/careers/DLIS**.

National Institute of Allergy and Infectious Diseases

U.S. DEPARTMENT OF HEALTH AND HUMAN SERVICES
National Institutes of Health

National Institute of Allergy and Infectious Diseases

Proud to be Equal Opportunity Employers

Scientific Director

NIH Center For Translational Therapeutics, National Human Genome Research Institute

The National Human Genome Research Institute (NHGRI), a major research component of the National Institutes of Health (NIH) and the Department of Health and Human Services (DHHS), seeks to identify an outstanding Scientific Director to lead the newly created NIH Center for Translational Therapeutics (NCTT), located in Rockville, Maryland. The NCTT Scientific Director leads a program that discovers and translates novel targets into viable therapeutic compounds aimed to treat rare and neglected diseases. The NCTT brings together diverse and unique scientific expertise to develop and deploy reagents and technologies to translate physiological and genomic insights into functional and therapeutic innovations. The NCTT Scientific Director has the responsibility for an annual budget exceeding $60 million and a staff of ~150. In addition to providing scientific and administrative leadership of this premier research enterprise, the Scientific Director is expected to be an internationally recognized and highly accomplished researcher in drug development, and genetics and/or genomics.

This position offers a unique and exciting opportunity to develop and implement an overall vision for the NCTT that is consistent with the mission and strategic objectives of the NIH. The Scientific Director is responsible for the recruitment and professional development of NCTT staff. S/he plays a key role in creating and maintaining a nurturing research environment that encourages creativity, collaboration among scientists from different disciplines and organizations, effective training of students and postdoctoral fellows, and efficient utilization of resources. The ability to develop productive interactions among NCTT investigators, other NIH Institutes, non-profit and for-profit organizations, and the broader research community is critical, as is the ability to serve as a spokesperson for translational therapeutic research.

Applicants must possess an M.D. and/or Ph.D. or equivalent degree in the biomedical sciences, as well as academic and drug development experience. The applicant must have a broad knowledge of the field of human genetics, genomics, pharmacology including high-throughput screening, and pre-clinical drug development, in addition to having a compelling vision for the future of the field, including novel therapeutic technology development. The applicant must also have demonstrated experience working with biotech/pharma, disease advocacy groups, and research foundation organizations. S/he must have proven experience in directing and managing a scientific research program, with well-honed administrative and interpersonal skills to meet the demands of both research and program direction.

Salary is competitive and will be commensurate with candidate's experience. A full Federal benefit package is available, including retirement, health and life insurance, long-term care insurance, annual and sick leave, and the thrift savings plan (401K equivalent). Appropriate support for this program will be provided. Interested applicants should submit a cover letter that includes a brief description of research and administrative experience, a current curriculum vitae and bibliography, names and contact information of five references, and a brief written vision for leading the NCTT. Questions about the position and applications themselves should be sent to Ms. Ellen Rolfes via email at ellenr@exchange.nih.gov. All information provided by the candidates will remain confidential and will not be released outside the NHGRI search process without a signed release from the candidate.

Applications will be reviewed starting December 1, 2010, and will be accepted until the position is filled.

DHHS and NIH are Equal Opportunity Employers and encourage applications from women and minorities.

NATIONAL HUMAN GENOME RESEARCH INSTITUTE
U.S. DEPARTMENT OF HEALTH AND HUMAN SERVICES | NATIONAL INSTITUTES OF HEALTH | genome.gov

Director, National Institute of Dental and Craniofacial Research (NIDCR),

National Institutes of Health

The NIH is the center of medical and behavioral research for the Nation

----making essential medical discoveries that improve health and save lives.

The mission of the National Institute of Dental and Craniofacial Research (NIDCR) is to improve and promote oral, dental, and craniofacial health through research, research training, and the dissemination of health information.

Are you an exceptional candidate who can provide leadership to one of the preeminent Institutes for oral, dental, and craniofacial health research in the world? This position offers a unique opportunity to serve as the chief visionary for the Institute, actively engaging others to create a shared vision of the purpose and direction of the organization. The Director, NIDCR, works collaboratively within the Institute and across the NIH to generate and gain commitment for organizational goals and has a keen awareness of how to navigate through the workings of the public sector to effectively promote and reach NIDCR and NIH objectives. The Director optimizes organization performance by developing strategic priorities, setting and communicating clearly defined expectations, and promoting accountability for results. Serving as a role model for the institute, the Director, NIDCR, demonstrates integrity and fairness, adhering in work and behavior to the highest ethical, scientific research, and business practices standards.

We are looking for applicants with a D.D.S., M.D. and/or Ph.D. who have senior-level research experience and knowledge of research programs in one or more scientific areas related to oral, dental, and craniofacial health. Applicants should be known and respected within their profession, both nationally and internationally, as individuals of outstanding scientific competence.

The successful candidate for this position will be appointed at a salary commensurate with experience and accomplishments, and full Federal benefits, including leave, health and life insurance, retirement and savings plan (401K equivalent) will be provided.

If you are ready for an exciting leadership opportunity, please see the detailed vacancy announcement at http://www.jobs.nih.gov (under Executive Jobs). ***Applications are due by 11:59 p.m., Friday, December 10, 2010.***

NIDCR, NIH AND DHHS ARE EQUAL OPPORTUNITY EMPLOYERS

WWW.NIH.GOV

Tenure/Tenure Track Investigator Position
Laboratory of Immunology

The Laboratory of Immunology (LI), Division of Intramural Research, National Institute of Allergy and Infectious Diseases, National Institutes of Health, invites applications for a tenure/tenure-track investigator position in immunology. Applicants should have a Ph.D., M.D., or equivalent degree; an outstanding record of postdoctoral accomplishment; and an interest in any area of biomedical research related to immunology.

Specifically, we seek a highly creative individual who will establish an independent, world-class research program that takes full advantage of the special opportunities afforded by the stable, long-term funding of the intramural research program at NIH. Applicants should be interested in developing and applying novel approaches to the study of problems of major biological and/or medical importance, which could include a significant clinical or translational effort in addition to bench research. The successful candidate would have access to the NIH Clinical Center, a state-of-the-art research hospital on the NIH campus in Bethesda, MD, and would have ample opportunity to participate in the activities of the Center for Human Immunology and other trans-NIH initiatives involving technology development, translational investigation, and multidisciplinary science.

Generous ongoing support for salary, technical personnel, postdoctoral fellows, equipment, and research supplies will be provided. Available cores or collaborative facilities include flow cytometry, advanced optical imaging, microarray generation and analysis, high throughput sequencing, computational biology, production of transgenic and gene-manipulated mice, biosafety level (BSL)-3 facilities, chemical genomics, and support for projects involving RNAi screening. In addition to an outstanding, international postdoctoral community, a superior pool of graduate and undergraduate students is available to the successful applicant.

NIAID's Laboratory of Immunology has a distinguished history of accomplishment in immunology. We strongly encourage application by outstanding investigators who can continue and enhance this record of achievement. Current LI investigators are Ronald Germain, Michael Lenardo, David Margulies, Stefan Muljo, William Paul, Ethan Shevach, and Tsan Xiao.

To apply, e-mail your curriculum vitae, bibliography, and an outline of a proposed research program (no more than two pages) in PDF format to Ms. Bao-Hanh Ngo at **LIT-TTSearch@niaid.nih.gov**. In addition, three letters of reference must be sent directly from the referee to Drs. Giorgio Trinchieri and Dan Kastner, Co-Chairs, NIAID Search Committee, c/o Ms. Bao-Hanh Ngo at **LIT-TTSearch@niaid.nih.gov** or 10 Center Drive, MSC 1356, Building 10, Room 4A22, Bethesda, MD 20892-1356. E-mail is preferred.

Applications will be reviewed starting **December 13, 2010**, and will be accepted until the position is filled. For further information about this position, contact Dr. William Paul at 301-496-5046 or **wpaul@niaid.nih.gov**.

A full package of benefits (including retirement and health, life, and long-term care insurance) is available. Women and minorities are especially encouraged to apply. U.S. citizenship is not required.

Further information on working at NIAID is available on our Web site at **www.niaid.nih.gov/careers/LIS**.

NIAID

National Institute of Allergy and Infectious Diseases

University of Massachusetts Lowell
UMASS Lowell

Associate Professor Positions
Department of Biological Sciences

The University of Massachusetts Lowell is a comprehensive university with a national reputation in science, engineering and technology, and committed to educating students for lifelong success in a diverse world and conducting research and outreach activities that sustain the economic, environmental and social health of the region. In February 2009 a campus-wide strategic planning initiative was launched to reposition UMass Lowell as a world-class institution over the next decade. A major component of that initiative is to ensure that diversity and inclusion are in every aspect of our strategic plan. We seek a diverse, talented candidate pool to be part of our mission and achievements.

Position Description:
The University of Massachusetts Lowell Department of Biological Sciences invites applications for full-time tenure-track faculty positions, rank negotiable, to start September 2011 or thereafter. The successful candidate will be expected to have a vigorous, externally funded research program, and collaboration within this and other departments is encouraged.

Current faculty research interests include genetics, neurobiology, cancer biology, invertebrate biology, developmental biology, virology, microbial ecology, evolution, and biogeochemistry. Our campus is located very near the vibrant academic and commercial biotechnology centers of Boston, Cambridge and Worcester.

We are seeking established mid-career individuals with expertise in one or more of the following areas: molecular/cell biology, plant science, integrative zoology, vertebrate physiology, comparative vertebrate structure/biomechanics, and/or evolutionary developmental biology. Teaching obligations include development of upper-level undergraduate/graduate courses in his/her area of expertise and participation in the teaching of core undergraduate courses as needed.

Minimum Qualifications:
- Earned doctorate
- Demonstrated teaching ability at the undergraduate and graduate levels
- Evidence of a sustainable externally funded research program
- Demonstrated publication record in scholarly journals
- Excellent communication and interpersonal skills
- Demonstrated ability to work with diverse student and faculty population

How to apply: Interested applicants should apply online at https://jobs.uml.edu. Applications must be submitted by November 19, 2010. Thank you for considering the University of Massachusetts Lowell as an employer of choice. We look forward to receiving your application.

The University of Massachusetts Lowell is committed to increasing diversity in its faculty, staff, and student populations, as well as curriculum and support programs, while promoting an inclusive environment. We seek candidates who can contribute to that goal and encourage you to apply and to identify your strengths in this area.

UHealth | University of Miami Miller School of Medicine

FACULTY POSITION
MOLECULAR AND CELLULAR PHARMACOLOGY

The Department of Molecular and Cellular Pharmacology at the University of Miami Miller School of Medicine is seeking applications for a **TENURE-TRACK FACULTY POSITION** (rank open). Candidates must have a Ph.D. and/or M.D. degree and have an established record of research excellence. Applicants from all areas of molecular/cellular biology and biomedical research are welcome, but we are particularly interested in research relating to the cardiovascular system to complement existing research efforts in this field. Rank and salary will be commensurate with experience. Competitive laboratory space and start-up funds will be offered.

Applicants should send electronic copies of their CV, statement of current and future research interests and the names and addresses of three references to **ELalor@med.miami.edu** and hard copies to **Ms. Elba M. Lalor, Asst. to the Chairman, Department of Molecular and Cellular Pharmacology, University of Miami Miller School of Medicine, P.O. Box 016189, Miami, FL 33101**.

An Equal Opportunity/Affirmative Action Employer.

Promega is Hiring Due to Growth in Research & Applied Markets

With strong corporate growth and double digit investment in R&D, Promega continues to expand its scientific staff to develop new technological capabilities for the life sciences.

Promega is seeking additional scientific expertise across multiple areas, including **analytical methods in cellular biology and proteomics, nucleic acid isolation and analysis, high throughput assays, laboratory automation, toxicology, and human identity.**

Requirements include:

- Desire to innovate new tools for advancing basic research, drug discovery, human identity, and molecular diagnostics
- Willingness to work in a dynamic team environment engaged in diverse disciplines.
- Interest in sharing scientific achievements and collaborating with innovators from other companies, universities, and institutes.

Promega is located in Madison, WI, a community of international scientists, beautiful natural settings and an award winning quality of life.

Established in 1978, Promega is a privately held company supplying 2000+ products to over 100 countries.

Visit www.promega.com/RDjobs

Promega Corporation is an equal opportunity/affirmative action employer.

Promega

JAAS 江苏省农业科学院

Jiangsu Academy of Agricultural Sciences

Seeking Distinguished Scientists in Various Agriculture Areas

Jiangsu Academy of Agricultural Sciences (JAAS) is a professional agricultural research and extension institution that has been established since 1932. JAAS ranks at the top of provincial agricultural academies in China in terms of the comprehensive strength in agriculture. JAAS's headquarter and main research facilities are located in Nanjing, Jiangsu, China.

Currently, there are 3 distinguished full professor positions available for application in the following areas: breeding, food processing, bioenergy, facility agriculture, and large-scale farming for modern animal husbandry. Applicants should have a faculty position already beyond the assistant professor level in a university or the equivalent position in a research institution. In addition, all candidates should demonstrate excellent records of research accomplishment and have a command of bilingual language for English and Chinese, both in spoken and written.

Successful applicants will be offered a competitive package, including sufficient laboratory space, startup funding, relocation fee and competitive salary commensurate with experience, in addition to a housing allowance, and other employee benefit. Applicants can go to www.jaas.ac.cn for application details.

In addition, more information for other regular faculty positions from JAAS relevant to a variety of disciplines in agriculture is also available at www.jaas.ac.cn.

Contact information
E-mail: rsc-gbk@jaas.ac.cn; Tel: 086-25-84390037

J. Craig Venter Institute

Faculty Positions

La Jolla, CA and Rockville, MD

For nearly two decades our scientists have been at the forefront of the genomic revolution. Now, we want you to join us in our quest!

J. Craig Venter Institute scientists have been unraveling and understanding the complexities of life as contained in the genomes of thousands of microbes, plants, and mammals, including humans. Our scientific success is built on the philosophy of conducting science boldly in new interdisciplinary ways, using new tools and with the best scientist. The ever increasing amounts of genomic data and new avenues of research to explore, mean we need additional scientists with unique skills and ideas that will help us better understand the world around us.

JCVI is seeking qualified applicants for positions at all levels at our La Jolla, California and Rockville, MD facilities particularly in the following research focus areas:

- Human genomics
- Environmental genomics, including human microbiome research
- Synthetic genomics
- Bioenergy
- Bioinformatics and computational biology
- Vaccine Development

Successful candidates will conduct innovative, independent research, obtain extramural funding, take advantage of interactions with our interdisciplinary, highly collegial group of scientists within JCVI, and complement existing strengths within the organization. Candidates must have a Ph.D. or M.D. and a record of accomplishment in one or more of the targeted areas. The level of appointment will be commensurate with experience.

JCVI offers an excellent working environment and a competitive benefits package. Interested applicants should apply directly in our career center by submitting their CV and a cover letter which includes a description of research interests and contact information for three references. JCVI's Career Center is located on our web site at www.jcvi.org.

Equal Opportunity Employer M/F/D/V

J. Craig Venter®
INSTITUTE

University of Connecticut Health Center

Chair of the Department of Immunology

The University of Connecticut Health Center's School of Medicine is seeking to recruit a highly qualified individual with an outstanding record of accomplishments in research, education and an excellent record of sustained NIH funding to become Chair of the Department of Immunology. We particularly encourage individuals with a current track record in human or translational immunology. The position is ideal for an energetic and visionary individual who is presently at the Associate or Full Professor level and shows evidence of the leadership skills required to ensure the health and growth of the department and to recognize the importance of interpersonal relationships and team building. The department is the academic home to faculty with nationally and internationally known research programs that focus on the cellular, molecular, and regulatory processes of the immune system. The scope of the department's research is from the most fundamental mechanisms to therapeutic applications. Departmental faculty are educational leaders in the graduate and preclinical medical and dental school curriculum.

The Chair will be responsible for oversight of all research, educational, and administrative activities involving the department. The Chair will work to enhance the funded research portfolio of the department emphasizing basic and translational research; develop and support the education of medical and graduate students and serve as a mentor for trainees at multiple levels; assure the professional development and mentoring of faculty engaged in research, education, and administration; play a major role in active governance at the institutional and departmental levels; be involved in faculty recruiting; and develop a comprehensive budget, which promotes departmental and institutional financial integrity.

The University of Connecticut Health Center is a vibrant organization composed of the School of Medicine, the School of Dental Medicine, the Graduate School of Biomedical Science, the John Dempsey Hospital, and the UCONN Medical Group. The Health Center's campus is situated on 162 acres of wooded hilltop in the beautiful, historic community of Farmington, Connecticut.

Candidates should apply by submitting a curriculum vita via email to the search committee chair, Dr. Paul Dworkin c/o Stephanie Holden, **immuchair@uchc.edu** or via the University of Connecticut Health Center Employment Services website, **https://jobs.uchc.edu**, Search Code No. 2011-065.

UCHC is an Equal Opportunity Employer M/F/V/PwD

KU THE UNIVERSITY OF KANSAS

The Department of Pharmaceutical Chemistry, University of Kansas (**http://www.pharmchem.ku.edu/**) invites applications for a full-time tenure-track faculty position at the **Assistant or Associate Professor** level in Protein and Macromolecular Design and Analysis for the 2011-2012 academic year. The candidate should demonstrate a strong potential for research and scholarship for appointment at the rank of Assistant Professor or a proven record of research and scholarship, commensurate with rank, for appointment at the level of Associate Professor.

Applications include a letter of interest, a concise summary of past research and future research plans, a resume, and the names and addresses of three references. For position details and to apply go to **https://jobs.ku.edu**, search for position **00208822**. Screening of applications will begin **December 15, 2010**. Applications will be accepted until the position is filled.

EO/AA Employer.

UF FLORIDA
The Foundation for The Gator Nation

Molecular Immunology

The Department of Infectious Diseases and Pathology at the University of Florida College of Veterinary Medicine is seeking a tenure-track faculty member, at an academic rank commensurate with experience, to join our team of highly productive senior faculty. The successful candidate will be expected to establish a research program that can enhance our ongoing clinical and basic immunology programs in T-cell based vaccine development, immune-modulating drug development, and MHC-based immunology of vaccines and transplantation.

The candidate must have expertise in MHC/T-cell immunology and interest in specializing in vaccine, transplantation, or cancer immunology with emphasis in one or more of the following areas: Vaccine, adjuvant, and delivery system; Immune-modulating drugs and immunotherapy for diabetes, neurological diseases, and cancer; MHC-peptide presentation and cytokine interaction in antigen-specific TCR activation; Immunoinformatics, antigen presentation, and T-cell regulation; Companion animal or non-human primate models.

The Department (http://www.vetmed.ufl.edu/college/departments/patho/) has strong ties to the UF Emerging Pathogens Institute (EPI) (http://epi.ufl.edu), which coordinates a multidisciplinary research program in infectious diseases across eight UF Colleges. In addition to the EPI, the close proximity of the UF College of Medicine (with a CTSI award currently in place) and the Veteran's Affairs Medical Center provide unique opportunities for collaborations. Applicants must have an advanced degree (PhD, DVM, MD) and a record of accomplishment in conducting extramurally-funded (NIH or equivalent) research. Preference will be given to candidates with demonstrated leadership skills as well as expertise in immunology research and development. The ideal candidate would possess a passion and vision for improving human and animal health, together with the skills required to share this vision with other scientists.

Applicants should submit: a letter outlining professional goals, curriculum vitae, and list of three professional referees to: Dr. John B. Dame, Search Committee Chair, Department of Infectious Diseases & Pathology, College of Veterinary Medicine, PO Box 110880, University of Florida, Gainesville, FL 32611-0880; e-mail: **damej@ufl.edu**; fax: 352-392-9704. Review of applications will begin **December 6, 2010** and continue until the position is filled. The University of Flordia is an equal opportunity employer·

GRANTS

€ 70,000
GRANTS AVAILABLE

The Wings for Life Spinal Cord Research Foundation is a grant giving charity funding research aimed at resolving spinal cord injury–induced impairments. We invite applications for project grants in basic sciences, applied basic sciences, and clinical sciences. Proposals should have a view to translation from the laboratory to the clinical setting and have the likelihood of providing real benefits to human patients.

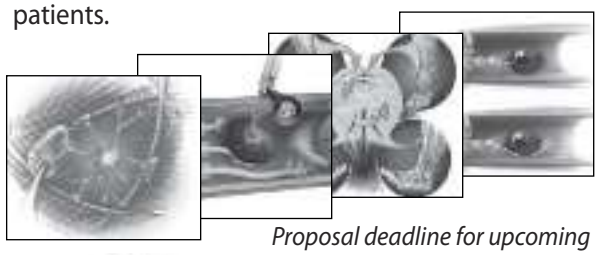

Proposal deadline for upcoming grant round is ***December 1, 2010***

WINGS for LIFE

www.wingsforlife.com

Job Opportunities at the Centre for Computational Science

UCL

The Centre for Computational Science (http://ccs.chem.ucl.ac.uk/) at UCL is seeking high quality applicants for a range of new projects described below. Several of these are aligned with the activities of the new UCL Computational Life and Medical Sciences Network (http://www.clms.ucl.ac.uk/). The successful candidates will join a very active inter-disciplinary group, working on international projects in fields ranging from condensed matter physics and chemistry to life sciences and medicine.

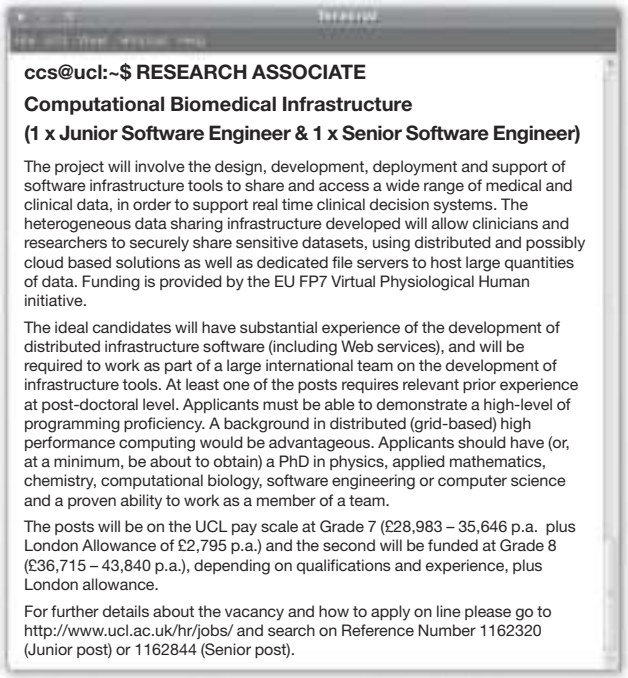

ccs@ucl:~$ RESEARCH ASSOCIATE

Computational Biomedical Infrastructure

(1 x Junior Software Engineer & 1 x Senior Software Engineer)

The project will involve the design, development, deployment and support of software infrastructure tools to share and access a wide range of medical and clinical data, in order to support real time clinical decision systems. The heterogeneous data sharing infrastructure developed will allow clinicians and researchers to securely share sensitive datasets, using distributed and possibly cloud based solutions as well as dedicated file servers to host large quantities of data. Funding is provided by the EU FP7 Virtual Physiological Human initiative.

The ideal candidates will have substantial experience of the development of distributed infrastructure software (including Web services), and will be required to work as part of a large international team on the development of infrastructure tools. At least one of the posts requires relevant prior experience at post-doctoral level. Applicants must be able to demonstrate a high-level of programming proficiency. A background in distributed (grid-based) high performance computing would be advantageous. Applicants should have (or, at a minimum, be about to obtain) a PhD in physics, applied mathematics, chemistry, computational biology, software engineering or computer science and a proven ability to work as a member of a team.

The posts will be on the UCL pay scale at Grade 7 (£28,983 – 35,646 p.a. plus London Allowance of £2,795 p.a.) and the second will be funded at Grade 8 (£36,715 – 43,840 p.a.), depending on qualifications and experience, plus London allowance.

For further details about the vacancy and how to apply on line please go to http://www.ucl.ac.uk/hr/jobs/ and search on Reference Number 1162320 (Junior post) or 1162844 (Senior post).

C:\ RESEARCH ASSOCIATE

Biomedical molecular dynamics

This post will involve the development of patient specific molecular models, using established molecular dynamics codes such as NAMD and GROMACS, to investigate and rank available drugs in order to inform the clinical decision making process. This work will build on and extend the Binding Affinity Calculator system developed at the Centre for Computational Science.

Applicants must have substantial experience of biological molecular simulation and related proven programming expertise. Experience of high performance visualisation and distributed (grid-based) high performance computing would be advantageous. Applicants should have (or be about to obtain) a PhD in physics, applied mathematics, chemistry, computational biology or computer science and a proven ability to work as a member of a team.

For further details about the vacancy and how to apply on line please go to http://www.ucl.ac.uk/hr/jobs/ and search on Reference Number 1163163.

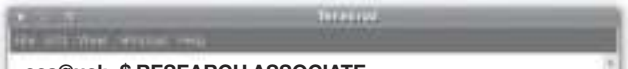

ccs@ucl:~$ RESEARCH ASSOCIATE

Multiscale Lattice-Boltzmann methods for complex fluids

The project will involve development, deployment and application of advanced computational methods including optimisation of high performance parallel lattice-Boltzmann codes for use in turbulence, complex fluid and blood flow research domains, in order to be able to run these codes on a range of evolving petascale and exascale architectures. The research will involve close collaborations with other personnel at CCS, across UCL, and within a number of international collaborations.

Applicants should have substantial experience of the use of lattice-Boltzmann methods within a high performance computing environment. Experience of high performance visualisation and grid computing would be

advantageous. A proven ability to programme large scale parallel applications is essential. Applicants should have (or be about to obtain) a PhD in physics, applied mathematics, chemistry, computational biology or computer science and a proven ability to work as a member of a team.

For further details about the vacancy and how to apply on line please go to http://www.ucl.ac.uk/hr/jobs/ and search on Reference Number 1163161.

C:\ RESEARCH ASSOCIATE

Evolution and Assessment of Biomedical Informatics & the Virtual Physiological Human

The post holder will be responsible for coordinating UCL's activity in a newly funded EU FP7 Virtual Physiological Human (VPH) project (INBIOMEDVision) which aims to monitor and assess the evolution of the Biomedical Informatics field, including the impact of VPH, and to address the scientific challenges and opportunities by means of collaborative work performed by a broad group of international experts having complementary perspectives on the field. In addition, the post holder will be involved in the administration and management of other VPH projects currently underway.

Applicants should have substantial experience of biological and/or biomedical informatics, including computational biology/biomedicine. Experience in project management and administration would be an advantage. Applicants should have (or be about to obtain) a PhD in physics, applied mathematics, chemistry, bioinformatics, computational biology or computer science, or an MSc in a relevant discipline, and a proven ability to work as a member of a team.

The post is initially funded for 18 months

For further details about the vacancy and how to apply on line please go to http://www.ucl.ac.uk/hr/jobs/ and search on Reference Number 1163171.

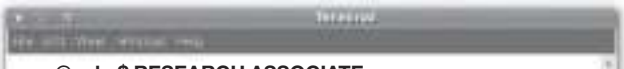

ccs@ucl:~$ RESEARCH ASSOCIATE

Quantum and classical molecular dynamics in life and materials science

The post holder will be responsible for developing molecular and multiscale models in two distinct research domains: biomolecular simulation and materials simulation. In the biomolecular domain, the post holder will be responsible for developing molecular models for use across a number of different biomedical research projects, concerned with drug binding efficacy in diseases such as HIV and cancer. In the materials domain the post holder will be responsible for developing quantum chemical methods to model chemical reactions of organic compounds within clay based layered materials, as well as course grained models for clay-polymer nanocomposites.

Applicants must have substantial experience of molecular simulation and proven programming expertise. Experience of high performance visualisation, distributed (grid) high performance computing and/or multiscale modelling would be advantageous. Applicants should have (or be about to obtain) a PhD in physics, applied mathematics, chemistry, computational biology or computer science and a proven ability to work as a member of a team.

The post is partly funded by the Qatar National Research Foundation, and the postholder will be expected to spend between 12 to 18 months at Qatar University in Doha where accommodation and certain living expenses will be provided in addition to salary.

For further details about the vacancy and how to apply on line please go to http://www.ucl.ac.uk/hr/jobs/ and search on Reference Number 1163169.

Positions are initially funded for 2.5 years from 1 February 2011, except where otherwise stated . The posts will be on the UCL pay scale at Grade 7 (£28,983 – 35,646 p.a. plus London Allowance of £2,795 p.a.), unless otherwise stated. The closing date for applications is 5pm on November 22nd.

Further particulars including job description and person specification are available at http://www.ucl.ac.uk/hr/jobs/ where you can apply online. Informal inquiries may be addressed to Professor Peter Coveney, Director of the Centre for Computational Science, University College London, 20 Gordon Street London WC1H 0AJ U.K. email: P.V.Coveney@ucl.ac.uk.

UCL Taking Action for Equality

SIGNAL TRANSDUCTION
DEPARTMENT OF SURGERY

The Department of Surgery in the College of Human Medicine at Michigan State University seeks candidates for an academic-year position at a Faculty Rank to be determined in signal transduction. Applicants are sought with demonstrated expertise in cellular signal transduction, with preference toward those with a background in mechanotransduction and physical force effects or intestinal epithelial biology. In addition to individual research efforts, the person who fills this position will be expected to collaborate actively with and mentor clinical surgical faculty and trainees as well as other MSU faculty. A strong record of research accomplishment and an independent externally funded research program are required. The position includes competitive salary and startup package, academic rank commensurate with previous experience, and the possibility of a co-appointment in one of the basic science department at MSU.

MICHIGAN STATE UNIVERSITY

Applications will only be accepted from candidates with current NIH funding or the equivalent. Applicants should submit a letter of interest, CV including complete publication list, history of research funding, statement of current and future research plans, and contact information (address, email and phone) for three referees to **Dr. Marc D. Basson, Professor and Chair, Department of Surgery, Michigan State University, Suite 655, 1200 East Michigan Ave, Lansing, MI 48912.** We would prefer electronic submission to **marc.basson@hc.msu.edu**. Applications will be accepted until the position is filled.

MSU is committed to achieving excellence through cultural diversity. The university actively encourages applications and/or nominations of women, persons of color, veterans and persons with disabilities.

THE UNIVERSITY OF CHICAGO

The Department of Biochemistry and Molecular Biology at The University of Chicago invites applications from outstanding candidates who will develop independent and creative research programs focused on fundamental problems in biochemistry and molecular biophysics. The position will be filled at the Assistant Professor level. We are especially interested in individuals who value teaching and whose interests bridge fields within the department or ongoing initiatives with other departments involving biomedical research. Ph.D. or M.D./Ph.D. or equivalent terminal degree with postdoctoral experience required. Successful candidates will be provided a generous startup package and will be expected to develop a well-funded, robust research program.

Applicants must include curriculum vitae, list of publications, summary of past accomplishments and plan for future research. Please submit application materials to **academiccareers.uchicago.edu/applicants/Central?quickFind=51342** by **December 10, 2010**. Applicants must also arrange for three letters of reference to be sent to:

Chair, Search Committee
Department of Biochemistry and Molecular Biology
929 E. 57th Street, Room W225
Chicago IL 60637

The University of Chicago is an Affirmative Action / Equal Opportunity Employer.

Tenure-track/Tenured Faculty Positions – Department of Genetics

University of Texas MD Anderson Cancer Center

The Department of Genetics is recruiting two tenure-track/tenured faculty positions at the Assistant or Associate levels to establish an outstanding research program in the area of genetics. We are particularly interested in individuals working in genomics and bioinformatics, and/or in human, mouse or other genetic systems that relate to human disease and biology. The department has strong ongoing programs in tumor suppressor genes, mechanisms of DNA repair, mouse and human genetics, and developmental and stem cell biology. We offer a very attractive recruitment package, active graduate and postdoctoral training programs, and the unmatched scientific environment of the Texas Medical Center. Applicants should hold a Ph.D. and/or M.D. degree and should be able to demonstrate their potential as independent scientists. Those interested should send a curriculum vitae, a three page research summary, and the names and addresses of at least three references before December 31, 2010, to:

Guillermina (Gigi) Lozano, Ph.D.
Chair, Department of Genetics
The University of Texas MD Anderson Cancer Center
1515 Holcombe Blvd., Unit 1010
Houston, Texas 77030

THE UNIVERSITY OF TEXAS
MD Anderson Cancer Center

MD Anderson Cancer Center is an equal opportunity employer and does not discriminate on the basis of race, color, national origin, gender, sexual orientation, age, religion, disability or veteran status, except where such distinction is required by law. All positions at MD Anderson are considered security sensitive; drug screening and thorough background checks will be conducted. The University of Texas MD Anderson Cancer Center values diversity in its broadest sense. MD Anderson is a smoke-free environment.

Career opportunities *in the tropics*

James Cook University is one of Australia's most distinctive universities with a focus on creating a brighter future for life in the tropics worldwide. The University is located in the vibrant regional community of tropical Queensland, which has one of the fastest growing economies in Australia adjacent to the Great Barrier Reef and Wet Tropics World Heritage Areas. The University's internationally recognised research is matched by strong commitment to its region, partners and teaching. A broad range of career opportunities are available at the University including the following recent vacancy:

Lecturer – Physiology
School of Veterinary & Biomedical Sciences

Ref. No. 10211 – Townsville

Employment Type: Full-time, continuing

Academic Level B - A$73,814 - A$87,096 per annum

Applications close: 3 December 2010

Staff Benefits include a generous superannuation scheme with up to 17% employer contributions, five weeks annual recreation leave, flexible working arrangements and attractive options for salary packaging.

For more information go to: **www.jcu.edu.au/jobs**, enter the Reference Number in the search field and follow the links.

www.jcu.edu.au/jobs

JAMES COOK UNIVERSITY AUSTRALIA

Celebrating 40 YEARS 1970–2010

sustainable.living.learning.research - at the Health University!

Medical University of Graz

Medical University of Graz in Austria is seeking to fill the position of an

Associate Professor (f/m) for Experimental Cardiology

at the Department of Cardiology/University Heart Center

Professional Requirements:

- Ph.D. or other doctorate, or equivalent scientific qualification in natural sciences or medicine
- Established record of excellence in cardiac cellular research with emphasis on ion homeostasis, arrhythmogenesis, cardiac remodeling and heart failure
- Excellent skills in the methodology of visualizing subcellular processes (confocal microscopy, FRET imaging, etc.) and in molecular biology techniques

Detailed job description: www.medunigraz.at/jobs (Wissenschaftliches Universitätspersonal)

Please submit your application with the reference number **W325ex2009/10**, preferably by e-mail to personal@medunigraz.at or to the following postal address: **Medizinische Universität Graz**, Abteilung Personaladministration, Universitätsplatz 3, A-8010 Graz. The application deadline is **30th of Nov. 2010**.

www.medunigraz.at

UNIVERSITY OF LOUISVILLE

James Graham Brown Cancer Center and the Owensboro Cancer Research Program (OCRP) Endowed Chair Position

The University of Louisville James Graham Brown Cancer Center and the Owensboro Cancer Research Program (OCRP) invite nominations and applications for a Helmsley Charitable Trust funded Endowed Chair position. The Endowed Chair will hold the rank of Professor in an appropriate department in the University of Louisville School of Medicine and will be affiliated with the James Graham Brown Cancer Center. It is expected that the successful candidate will be an internationally recognized scientist with a M.D., and/or Ph.D., an established and funded research program, and a strong track record of publications. The Endowed Chair will join the OCRP and be located in newly constructed laboratory space at the Mitchell Memorial Cancer Center, Owensboro, Kentucky. The OCRP represents a new translational research program focused on combining the field of plant-made pharmaceuticals with the prevention and treatment of cancer and serious infectious diseases. The OCRP is currently comprised of four faculty members and is expected to expand to eight faculty members over the next 5 years. It is expected that the Endowed Chair will conduct collaborative research with faculty at the OCRP and contribute to the future development of the OCRPC as it establishes itself as a leader in the area of plant-made pharmaceutical research. Candidates with research interests in any area relevant to plant-based expression of protein therapeutics for cancer and infectious disease are welcome. Candidates working in the areas of molecular target discovery, cancer vaccines, innate immunity, and cancer virus research are particularly encouraged to apply. Applications must include a curriculum vitae that includes a summary of previous and current funding, a synopsis of current and future research interests, and the contact information for at least three references to: **Donald Miller, MD, PhD, Chair, Search Committee and Keith R. Davis, PhD, Co-Chair, Search Committee, James Graham Brown Cancer Center, 529 South Jackson Street, Louisville, KY 40202 or by Email: sairama@ulh.org**. Review of applications will begin immediately and continue until the position is filled.

The University of Louisville is an Affirmative Action, Equal Opportunity Employer.

IST AUSTRIA IS LOOKING FOR

Professors and Assistant Professors

IST Austria (Institute of Science and Technology Austria) is a new Institute located on the outskirts of Vienna, dedicated to cutting-edge basic research. The Institute invites applications and nominations for Professors and Assistant Professors in all fields of the natural sciences and related disciplines. Outstanding scientists in the Physical Sciences, Neurosciences, and Mathematics are especially encouraged to apply.

The Institute, established by the Austrian Government, opened its campus in 2009. Its funding is substantial, allowing for over 500 employees and graduate students by 2016. IST Austria is entitled to award PhD degrees and includes an English-language Graduate School. It aims to achieve an international mix of scientists and recruits them solely on the basis of their individual excellence and potential contribution to research.
The Institute is recruiting leaders of independent research groups. Professors have indefinite contracts and Assistant Professors have fixed-term contracts for an initial period of five years, with a possible, but not automatic, renewal for two additional years. Before the end of this period, the scientist will be considered for an indefinite appointment as a Professor at IST Austria, the decision being based on merit only (as is the case for a "Tenure-Track Assistant Professor" at US universities).
The selected candidates will receive a competitive salary and a substantial annual research budget, covering operating expenses and the cost of PhD students, postdoctoral fellows, and technical staff. Additional costs of starting a new laboratory, including instruments and infrastructure, will be offered separately. Scientists are also expected to apply for external research grants.

Applications or nominations to: professor@ist.ac.at or assistant.professor@ist.ac.at (depending on position). Applications must include a CV, list of publications, and research plan. Nominations should include an appraisal of the achievements and scientific qualifications of the nominee. IST Austria is committed to Equality and Diversity. In particular female researchers are encouraged to apply. More information: www.ist.ac.at

IST AUSTRIA
Institute of Science and Technology

WPI

Worcester Polytechnic Institute

Department of Biology and Biotechnology
Tenure-Track Assistant Professor in Neuroscience

The Biology and Biotechnology Department of WPI invites applications for a tenure-track Assistant Professor position to begin in the fall of 2011. WPI is committed to further strengthening its capabilities in the life sciences and bioengineering arena.

U.S. News and World Report consistently ranks WPI among the top national universities and recently placed WPI in its top 30 for faculty resources. To learn more about the Biology and Biotechnology Department, which offers BS, MS, and PhD degrees, research at the LSBC, and WPI visit http://www.wpi.edu/+BBT, www.wpi.edu/research, www.gatewayparkworcester.com, and www.wpi.edu

Applicants should submit an application (pdf-formatted) including a cover letter, curriculum vitae, a statement of accomplishments and future priorities in research and teaching, and a list of five references (with contact information). Applications should be sent to Professor J.B. Duffy, Department of Biology and Biotechnology at Faculty-searchBBT@wpi.edu . Review of applications will be conducted on a rolling basis and continue until the position is filled.

To enrich education through diversity, WPI is an affirmative action, equal opportunity employer.
– A member of the Colleges of Worcester Consortium. –

UAF UNIVERSITY OF ALASKA FAIRBANKS

TENURE-TRACK FACULTY POSITION
Assistant or Associate Professor of Wildlife Biology

The Department of Biology and Wildlife and the Institute of Arctic Biology, University of Alaska Fairbanks, seek an individual with broad training in wildlife biology for a joint appointment to a tenure-track position available in August 2011. The appointment will be a 9-month, 50% teaching and 50% research appointment with full benefits. We seek to complement current wildlife faculty expertise in genetics, nutrition, population biology and spatial ecology. Candidates with expertise with meso-carnivores, furbearers, or predator-prey dynamics are especially encouraged to apply. Salary and level of appointment are negotiable and dependent on experience. Applicants must have an earned PhD in biology or ecology of vertebrate animals with training or experience in application of research to management of populations. Applicants should have the ability to work with wildlife managers and other stakeholders on issues of local, regional, and national interest. The successful candidate will be expected to develop a research program that trains MS and PhD students with extramural support and contribute to courses and student activities in Wildlife Biology and Conservation. Instructional responsibilities include undergraduate advising and two semester-length courses per year (e.g. at least one course in the wildlife core curriculum and a graduate course in the candidate's area of expertise). Applicants should apply online at UAKJobs (**www.uakjobs.com**). Application materials will include a cover letter, CV, statement of teaching philosophy and interests, statement of research philosophy and interest, and 3 letters of recommendation. Applicants can have letters of recommendation sent directly to **fyuaflob@alaska.edu** and reference listing number 0060812. Recruitment will remain open until the position is filled; review of applications will commence on **8 November 2010**. For inquiries contact **Kris Hundertmark** (**khundert@alaska.edu**).

Our department has a rich history of training wildlife managers, which is facilitated by the Alaska Cooperative Fish and Wildlife Research Unit (**http://www.akcfwru.uaf.edu/about.php**) and faculty in related departments such as fisheries, and natural resource management. The Institute of Arctic Biology (**http://www.iab.uaf.edu**) provides administrative and logistical support for implementing research on animals in the field and in captivity through facilities such as Animal Quarters, Large Animal Research Station, DNA Core Lab, Spatial Ecology Lab and the Toolik Field Station. University of Alaska Fairbanks (http://www.uaf.edu) is a research-intensive university (10.5k students) with a focus on circumpolar issues. Fairbanks has a vibrant cultural life and unparalleled wilderness access and outdoor recreational opportunities (**http://www.fairbankschamber.org/**).

University of Alaska Fairbanks is an Equal Employment Opportunity/Affirmative Action Employer and Educational Institution.

Visit our ENHANCED WEBSITE!

Revealing your vision to employers is our job. We're your source for connecting with top employers in industry, academia, and government. We're the experts and entry point to the latest and most relevant career information across the globe.

Our newly designed website offers a set of tools that reveal career opportunities and your personal potential. Whether you're seeking a new job, career advancement in your chosen field, or ways to stay current on industry trends, *Science* Careers is your window to a limitless future.

Improved Website Features:

- Relevant Job E-mail Alerts
- Improved Resume Uploading
- Content Specific Multimedia Section
- Facebook Profile

Job Search Functionality:

- Save and Sort Jobs
- Track Your Activity
- Search by Geography
- Enhanced Job Sorting

Your Future Awaits.

Science Careers

From the Journal *Science* AAAS

ScienceCareers.org

AAAS is here – helping scientists achieve career success.

Every month, over 400,000 students and scientists visit ScienceCareers.org in search of the information, advice, and opportunities they need to take the next step in their careers.

A complete career resource, free to the public, *Science* Careers offers a suite of tools and services developed specifically for scientists. With hundreds of career development articles, a grants and scholarships database, webinars and downloadable booklets filled with practical advice, a community forum providing real-time answers to career questions, and thousands of job listings in academia, government, and industry, *Science* Careers has helped countless individuals prepare themselves for successful careers.

As a AAAS member, your dues help AAAS make this service freely available to the scientific community. If you're not a member, join us. Together we can make a difference.

To learn more, visit **aaas.org/plusyou/sciencecareers**

AAAS + U = Δ

Post-Doctoral Fellowship
to study
Hematopoietic Stem/ Progenitor Cell Trafficking and Engraftment in the Bone Marrow Microenvironment.
Children's Hospital Boston
Harvard Medical School,
Boston MA

The goal of our research program is to better define the mechanisms by which normal and neoplastic hematopoietic stem/progenitor cells home to the bone marrow and take up residence in supportive niches. A multidisciplinary approach combining biochemistry, cell biology, animal studies, and imaging is employed.

For more information, please see the following website: **http://www.childrenshospital.org/cfapps/research/data_admin/Site188/mainpageS188P0.html**

To apply, e-mail a cover letter, curriculum vitae, statement of research experience and career goals, and contact information for three references addressed to **Dr. Leslie Silberstein, Director of the Joint Program in Transfusion Medicine.** E-mails should be sent to **Lauren Smith, Administrative Associate: Lauren.Smith@childrens.harvard.edu**.

Children's Hospital Boston is an Equal Opportunity, Affirmative Action Employer.

UNIVERSITY of HAWAI'I
MĀNOA

Dean, College of Natural Sciences
Honolulu, Hawai'i

The University of Hawai'i at Mānoa (UH Mānoa) seeks an innovative, motivational and experienced leader to serve as Dean of the College of Natural Sciences (CNS). Building upon the many strengths of the University, as well as the unique attributes of the Hawaiian Islands, the successful candidate has an exciting opportunity to lead CNS to a stronger intellectual presence in Hawai'i, the Asia Pacific region and around the globe.

The College of Natural Sciences is comprised of the following departments: Biology, Botany, Chemistry, Information and Computer Science, Mathematics, Microbiology, Physics and Astronomy, and Zoology. The Dean serves as the top academic and administrative leader for the College, and is expected to develop a vision and strategic plan to guide and lead the College's members to achieve new levels of excellence by pursuing an integrated, comprehensive academic program that balances scholarship, instruction and service. The Dean should be a committed, collaborative, and engaging advocate for the College within the University, across the state, and beyond. For more information about the UH Mānoa and the College, please go to **www.manoa.hawaii.edu** and **www.hawaii.edu/natsci**.

UH Mānoa is the premier institution of higher learning in the Pacific Basin and belongs to an international community of research universities. It is the flagship campus of the UH System and enrolls more than 20,000 students. Ten percent (10%) of UH Mānoa students are majoring in programs within the CNS. These students comprise 11% of the undergraduates and 7% of the graduate students. There are approximately 130 instructional faculty members in the College.

UH Mānoa is one of the nation's few land-, sea- and space-grant institutions, and plays a unique role in serving Hawaiian, Asian and Pacific cultures through education, research, extension/outreach and service. Many of the university's fields of study relate directly to the distinctive geographical and cultural setting of Hawai'i, an island community with diverse eco-systems and exceptional diversity of cultures.

Nominations, inquiries, and application information: Nominations, inquiries, and applications are being accepted for the position. Review of applications will begin on Monday, **December 6, 2010**, and will continue until the position is filled. Candidates must submit a cover letter summarizing the candidate's interest and qualifications for the position, a current resume, and the names of six (6) professional references, including title and contact information. For a job description and search information, please go to **www.manoa.hawaii.edu/executivesearch/natsci**. **E-mail correspondence is strongly encouraged.** Please send materials to:

University of Hawai'i at Mānoa CNS
Dean Search
Attn: Michele Tom,
Executive Search Coordinator
University of Hawai'i at Mānoa
2500 Campus Road, Hawai'i Hall 209
Honolulu, Hawai'i 96822
Phone: 808-956-9396 / Fax: 808-956-7115
E-mail: tomm@hawaii.edu

The University of Hawai'i is an Equal Opportunity/Affirmative Action Institution and encourages applications from and nominations of women and minority candidates.

FELLOWSHIPS

POSITIONS OPEN

POSTDOCTORAL POSITION in Computational Systems Biology

The Guda laboratory at University of Nebraska Medical Center (UNMC, **website: http://www.unmc.edu/genetics/index.cfm?conref=57**) is seeking a self-motivated individual to pursue exciting research in Computational Systems Biology. The incumbent will develop novel computational methods using machine learning and data mining techniques for functional annotation of biological systems. Related research projects in the PI's laboratory include prediction of subcellular localization, inferring potential protein domain-domain interactions, and alignment of cancer protein interaction networks.

UNMC offers state-of-the-art computational facilities to carry out cutting edge research in systems biology. The new center for Bioinformatics and Systems Biology at UNMC will provide enriching opportunities for teaching and professional development. Initial appointment will be for one year with a possibility of continuation for three years. UNMC offers competitive salary with excellent healthcare and retirement benefits.

Requirements: A recent Ph.D. in Bioinformatics and/or computational biology, computer science, or in a quantitative discipline with an aptitude for life sciences research is required. A thorough training in machine learning algorithms, graph theory, and strong programming skills in C/C++/Java with some working knowledge in statistics and relational databases is required. Experience in analyzing large-scale genomic and/or proteomic datasets is considered a plus.

POSTDOCTORAL POSITIONS Viruses, Telomeres, and Drug Discovery The Wistar Institute

Positions for postdoctoral trainees are available in several areas, both in mammalian cells and human tumor-associated viruses. (1) Telomere and Cell Growth Regulation by TERRA RNA. The role of non-coding telomere RNA in regulating telomere chromatin and cell growth (*Mol Cell.* 2009; *Cell Cycle*. 2010). (2) Viral and Cellular Genome Maintenance. Mechanisms regulating genome stability and chromosome organization, including factors controlling chromatin insulators and origins of DNA replication (*J Virol.* 2009a, 2009b, 2009c; *EMBO J.* 2008). (3) Small molecule inhibitors of latent viral infection. Identification of natural and synthetic inhibitors of viral regulatory proteins at the newly established Center for Chemical Biology and Translational Medicine at Wistar Institute.

Applicants should have a Ph.D. and experience in molecular biology, virology, and/or biochemistry. Highly competitive salary and benefits package. Forward curriculum vitae to: **Paul M. Lieberman, Ph.D., Gene Expression and Regulation Program, The Wistar Institute, 3601 Spruce Street, Philadelphia, PA. 19104; e-mail: lieberman@wistar.org.**

STONY BROOK UNIVERSITY Bioinformatics and Biostatistics

Stony Brook University's Department of Applied Mathematics and Statistics seeks a tenure-track **ASSISTANT PROFESSOR** in biostatistics or computational statistics, with a priority for the area of bioinformatics. For full position description and/or application procedures, visit **website: http://www.stonybrook.edu/jobs** (Reference **#F-6547-10-10**). *Stony Brook University/SUNY is an Equal Opportunity/Affirmative Action Employer.*

ASSISTANT PROFESSOR of BIOLOGY—The Biology Department of Whitworth University invites applications for a tenure-track position as Assistant Professor of Biology with a primary focus on Environmental Biology, Field Biology, Wildlife Biology, and/or Conservation Biology. Earned Doctorate in an appropriate area of biology or environmental science by August 2011, and demonstrated teaching ability required. Go to **website: http://www.whitworth.edu/jobs** for further details and information on how to apply.

POSITIONS OPEN

The Department of Chemistry and Biochemistry (CBC) at The University of Arizona is seeking a tenure-track faculty position. We expect to fill this position at the **ASSISTANT PROFESSOR** level. The successful candidate is expected to develop an outstanding research program that will lead to external support. Although the particular research interests are open, the candidate is expected to contribute to the interdisciplinary efforts of our Drug Design Center, which is administered by BIO5, a consortium of researchers at the University of Arizona that is focused on the issues of health and disease. Outstanding candidates will also be considered at the level of Associate and Full Professor. To apply, please submit a letter of application, curriculum vitae, and statements of research and teaching interests online at **website: http://www.uacareertrack.com** (**position #46326**). Candidates for the Assistant Professor position should also have three letters of recommendation sent to: **Drug Design Center Search Committee, c/o Margaret Gomez, Department of Chemistry and Biochemistry, University of Arizona, P.O. Box 210041, Tucson, AZ 85721-0041.** *The University of Arizona is an Equal Employment Opportunity/ADA/Affirmative Action Employer. Women and minorities are especially encouraged to apply. The Immigration Reform and Control Act requires you to have proof of authorization to work in the United States.*

MOLECULAR GENETICS Reed College

The Biology Department at Reed College invites applications for a tenure-track position at the **ASSISTANT PROFESSOR** level, to begin fall semester, 2011. A Ph.D. and postdoctoral experience are required. The successful candidate will develop a competitive research program involving undergraduates. The research area within genetics should complement the expertise of the existing faculty. A renovated research laboratory and startup funds are available. Formal teaching duties include a lecture-laboratory course in general genetics, an advanced seminar in the candidate's specialty, participation in the team-taught introductory biology sequence, and supervision of year-long senior research theses. We seek an individual committed to the pursuit of science in an undergraduate environment. Reed College is a highly selective liberal arts institution with a distinguished record of educational accomplishment and a strong commitment to scholarship (**website: http://web.reed.edu**).

Electronic applications are required and must be sent as PDF (preferred) or Word attachments. Please send a cover letter, curriculum vitae, statement of research interests, and three letters of recommendation to **e-mail: biology.search@reed.edu.** If letters of recommendation must be sent as hard copy, please submit to: **Dr. Janis Shampay, Search Committee Chair, Reed College, 3203 SE Woodstock Boulevard, Portland, OR 97202.** Deadline for receipt of applications is 15 December 2010.

An Equal Opportunity Employer, Reed values diversity and encourages applications from underrepresented groups.

FACULTY POSITION Experimental Biological Physics University of Illinois, Urbana-Champaign

The Department of Physics invites applicants for a tenured or tenure-track faculty position in experimental biological physics with an emphasis in cellular biophysics, beginning as early as August 16, 2011. The UIUC Department of Physics has strong programs in both theoretical and experimental biological physics. The successful candidate is expected to teach effectively at both the undergraduate and graduate levels, have a strong record of publication, and to lead a vigorous research program. For full consideration, application materials must be received by December 1, 2010. Please visit **website: http://jobs.illinois.edu** to view the complete position announcement and application instructions.

The University of Illinois is an Affirmative Action/Equal Opportunity Employer.

POSITIONS OPEN

UNIVERSITY OF MINNESOTA FACULTY POSITION in MICROBIOLOGY

The Department of Microbiology at the University of Minnesota Medical School invites applications for a faculty position to be filled at the tenure-track **ASSISTANT PROFESSOR** level. The successful applicant will be expected to establish a competitive research program in bacterial pathogenesis (broadly defined, to include bacterial physiology, genetics, genomics, molecular biology, and/or the bacterial basis for host-pathogen interactions), and to contribute to departmental teaching. The department and affiliated units at the University have broad research strengths in microbiology and immunology, including immunity and host defense, microbial pathogenesis, virology, microbial physiology, genetics, genomics, environmental microbiology, and biotechnology. More information about the Department of Microbiology, affiliated institutes and centers, and the graduate training program, can be found on the department **website: http://www.microbiology.med.umn.edu.**

Minimum qualifications: Ph.D., M.D., or equivalent in a relevant field of study, plus applicable postdoctoral or faculty experience. Review of applications will continue until suitable candidates are identified. To apply, please upload a curriculum vitae and concise summary of current and planned research in response to requisition number **169013** at **website: http://employment.umn.edu.** Please also arrange to have three letters of recommendation sent to **e-mail: microbiology@umn.edu** or to: **Sandra K. Armstrong, Ph.D., Search Committee Chair, Department of Microbiology, University of Minnesota, MMC 196, 420 Delaware Street S.E., Minneapolis, MN 55455.**

The University of Minnesota shall provide equal access to and opportunity in its programs, facilities, and employment without regard to race, color, creed, religion, national origin, gender, age, marital status, disability, public assistance status, veteran status, sexual orientation, gender identity, or gender expression.

FACULTY POSITION in Pharmacological Chemistry Department of Chemistry and Biochemistry at UC San Diego

The Department of Chemistry and Biochemistry within the Division of Physical Sciences at University of California, San Diego (UCSD, **website: http://www-chem.ucsd.edu**) is committed to academic excellence and diversity within the faculty, staff, and student body. We invite applications for a tenure-track position in Pharmacological Chemistry. Candidates must have a Ph.D. in one of the chemical/biological sciences and a demonstrated ability or potential for a recognized program of excellence in both teaching and research. Candidates with research interests in the biochemical and molecular mechanisms of drug metabolism and or development are encouraged to apply. A successful candidate will be judged on teaching and research accomplishments as well as potential for demonstrated leadership in areas contributing to diversity. Salary is commensurate with qualifications and based on University of California pay scale. Candidates should submit online their curriculum vitae, list of publications, reprints of up to five representative papers, and a personal statement that includes a summary of research plans as well as their past or potential contributions to diversity at **website: https://apol-recruit.ucsd.edu/.** Please select the following job opening: Chemistry and Biochemistry **ASSISTANT PROFESSOR** in Pharmacological Chemistry (10-178) **JPF000xx.** Candidates should also arrange to have three letters of reference addressing research, teaching, and any contributions to diversity submitted at the above-mentioned URL. Prompt response is recommended. For full consideration, applicants are encouraged to submit applications by November 29, 2010. *UCSD is an Equal Opportunity/Affirmative Action Employer with a strong institutional commitment to excellence through diversity.*

TEXAS TECH UNIVERSITY
Health Sciences Center
Paul L. Foster School of Medicine

Basic Science Medical Educators;
Department of Medical Education
(Immunology, Microbiology, Neurophysiology, Anatomy)

The Paul L. Foster School of Medicine at El Paso is seeking highly qualified biomedical scientists to serve as full time medical educators in the Department of Medical Education. This is an extraordinary opportunity for basic scientists to pursue a career in medical education in a scholarly environment that encourages biomedical science and medical education scholarship.

The medical education commitment shall be approximately 80% time and effort, primarily delivering the first and second year medical student curriculum. Basic Scientist Medical Educators have approximately 20% time and effort for scholarly activity. A special feature of our curriculum is a scholarly project requirement that is supported in part by an advanced "Laboratory for Education in Molecular Medicine" (LEMM). The LEMM is accessible for scholarly work directly involving the instruction of medical students in the processes and procedures of biomedical science.

Minimum Qualifications: Ph.D., M.D., or equivalent terminal degree in the biomedical sciences (M.D. candidates without a Ph.D. in a relevant biomedical science must have additional credentials related to advanced scientific training and scholarship); A substantial record of success as a biomedical science educator; A relevant and substantial record of scholarship (including abstracts, publications and presentations).

Preferred Qualifications: See website for full details.

All basic science medical educator positions are salaried and fully funded. Salary, academic rank and tenure option are commensurate with experience. A comprehensive benefits package is included. All candidates must apply online at **http://jobs.texastech.edu**, requisition number **82125**. For further information please contact: **Tanis Hogg, Ph.D.; Search Committee Chair, Associate Professor and Vice-Chairman, Department of Medical Education, TTUHSC; Paul L. Foster School of Medicine, 5001 El Paso Drive, El Paso, Texas 79905; tanis.hogg@ttuhsc.edu; (915) 783-1700 ext. 226 (Brenda Mead).**

Texas Tech University Health Sciences Center is an Equal Opportunity/ Affirmative Action Employer.

MEETINGS

SMART TRACK

CAREER CHOICES IN SCIENCE

ROYAL SOCIETY LONDON 19 NOVEMBER 2010

Planning and implementing your career progression

Today, more than ever, scientists are at the forefront of our economic and environmental survival!
But where do you fit? What direction should your career path take? Who should you talk to?
Find out at SMART TRACK 2010 at the Royal Society, London 19 November.
It is free of charge to attend the networking sessions and only £15 to listen to our exciting range of speakers.
For further information **www.smart-track.co.uk.**

For any enquiries about this event, please email anita@ya-ya.co.uk or call 0207 989 2424

Supported by

Organised by ya-ya

Department of Cellular Biology
University of Georgia

Faculty Position: Cell Biology

The Department of Cellular Biology at the University of Georgia invites applications for a tenure-track Assistant Professor. The candidate's research must address fundamental problems in cell biology. Individuals whose research bridges cell biology with other disciplines are also encouraged to apply. Successful applicants will be expected to develop a strong extramurally funded research program and contribute to instruction in cell biology or related disciplines. A competitive package of startup funds and salary will be offered. Visit **www.uga.edu/cellbio/newfaculty** for further detail. Applicants should send a cover letter, curriculum vitae, research statement, statement of teaching philosophy, and arrange to have 3 letters of references sent to: **cbsearch@uga.edu**. Applications received by **January 10, 2011**, are assured of full consideration.

Endowed Faculty Position: Infectious Diseases

The Department of Cellular Biology at the University of Georgia invites applications for an endowed tenure-track faculty position at the associate professor level in the area of **Infectious Diseases**. Candidates with an established research program focusing on novel approaches to understanding the interaction between pathogen/parasite and host at the cellular, metabolic, or immunological level are particularly encouraged to apply. The Department has strong representation in the Center for Tropical and Emerging Global Diseases, one of the world's leading centers for parasite research. The position includes a very competitive salary, excellent laboratory space and a generous startup package and is further enhanced by an endowment. Visit **www.uga.edu/cellbio/newfaculty** for further detail. Applicants should send a cover letter, curriculum vitae, research statement and teaching philosophy and arrange to have 3 letters of reference sent to: **idsearch@uga.edu**. Applications received by **January 10, 2011**, are assured of full consideration.

The Franklin College of Arts and Sciences, its many units, and the University of Georgia are committed to increasing the diversity of its faculty and students, and sustaining a work and learning environment that is inclusive. Women, minorities and people with disabilities are encouraged to apply. The University is an EEO/AA Institution.

POSITIONS OPEN

CHAIR
Microbiology and Immunology

The College of Medicine of The Pennsylvania State University invites applications and nominations of outstanding candidates for the Chair of the Department of Microbiology and Immunology. In addition to leading an established and exceptional department with nationally recognized research programs in virology and immunology, this individual will play a key role in a large, cross-campus endeavor to build University programs in genomics and systems biology. The new Chair will serve as an important link to the international microbiology, virology, and immunology community and advance the position of the department scientifically. In addition to leading an active research program, the new Chair will embrace the education of our medical and graduate students, as well as postdoctoral and resident trainees. The successful candidate will be an internationally recognized scientist who has a record of leadership and experience in the administrative, teaching, and research activities of an academic department. The College is part of a large, growing, and fiscally stable academic health care center, which includes the Penn State Milton S. Hershey Medical Center, Penn State Hershey Cancer Institute, Penn State Hershey Children's Hospital, an outpatient surgery center, and multiple nearby research and clinic facilities. For more information regarding the position, please visit **website: http://med.psu.edu/web/microbiology/home.** Electronic applications are preferred and should be sent to **e-mail: jdunkinson@hmc.psu.edu** and addressed to: **Thomas P. Loughran, Jr., M.D. Director, Penn State Hershey Cancer Institute, Professor of Medicine, Mail Code CH72, 500 University Drive, Hershey, PA 17033.**

Penn State is committed to Affirmative Action, Equal Opportunity, and the diversity of its workforce.

POSTDOCTORAL POSITION(S) available in the laboratory of **Dr. Venigalla Rao,** Biology Department, The Catholic University of America, Washington, D.C., to work on (i) the structure and mechanisms of virus assembly and DNA packaging in bacteriophage T4, or (ii) development of novel multi-component vaccines using bacteriophage T4 display (**website: http://faculty.cua.edu/rao/**). Research involves recombinant DNA construction, protein purification, and mutagenesis. Candidate will have Ph.D. in Biological Sciences and strong background in molecular biology and biochemistry. Experience in bioinformatics and structural biology will be an asset. Electronically send curriculum vitae and names of three references to **e-mail: rao@cua.edu.** *Catholic University is an Equal Opportunity Employer.*

POSTDOCTORAL ASSOCIATES

The Institute of Marine and Coastal Sciences at Rutgers, The State University of New Jersey, is seeking Postdoctoral Associates for one-year renewable appointments in the areas of biological, chemical, geological, and physical oceanography. To apply, please electronically send your resume, a statement of research interest, and the names of three references by January 15, 2011, to **Dr. Francisco E. Werner, e-mail: postdoc2011@marine.rutgers.edu.** *Rutgers is an Equal Opportunity/Affirmative Action Employer. Employment verification required.*

POSITIONS OPEN

ASSISTANT PROFESSOR of Applied Mathematics or Statistics

The Science Programs at the Vancouver Campus, with the Departments of Mathematics and/or Statistics at Washington State University (WSU), announces a full-time, tenure-track Assistant Professor position in applied mathematics, applied probability, and/or statistics. The successful candidate will be a dynamic and collaborative individual who applies mathematical or statistical techniques to biological, physical, and/or environmental problems. Area of specialization is open. Exceptional scholars who complement the strengths of existing science faculty in Vancouver are encouraged to apply. Applicants must have a Ph.D. in mathematics, statistics, or closely related field by date of hire, and demonstrate high potential to establish an externally funded research program in mathematics/statistics, as well as an ability to contribute to the diversity goals of the university. Position responsibilities include teaching at the undergraduate and graduate levels, research and service, with research expectations and teaching loads consistent across the four WSU campuses. WSU Vancouver is located in Vancouver, Washington, across the Columbia River from Portland, Oregon and offers significant opportunities for research and an excellent quality of life. For additional information, see **website: http://science.vancouver.wsu.edu/.**

To view complete information and to apply, please visit **website: http://www.wsujobs.com** and search postings by location: Vancouver, **position #111650.**

Review of completed applications begins December 1, 2010.

Washington State University is an Equal Opportunity/Affirmative Action Educator and Employer. Members of groups underrepresented in quantitative disciplines are strongly encouraged to apply.

POSITIONS OPEN

MARKETPLACE